JOURNAL
OF
THE PHYSICAL SOCIETY
OF JAPAN

Being a continuation of
"Proceedings of the Physico-Mathematical Society of Japan"

Volume 3 Number 1

January~February, 1948.

Office of the Society:
Faculty of Science, University of Tokyo.

Thermionic Constants of Polycrystalline Metal.

Tetsuya ARIZUMI

Research Laboratory, Kawanishi Machine Works Co.

(Received December 26, 1946)

§ 1. Introduction.

Thermionic emission current from a pure, clean metal is represented in the form,

$$i = AT^2 \varepsilon^{-\frac{e\varphi}{kT}} \tag{1}$$

or in the logarithmic form,

$$\log \frac{i}{T^2} = \log A - \frac{e\varphi}{kT}, \tag{1'}$$

per unit area of the cathode, where φ is the work function characteristic of the metal and A is the Richardson constant which is independent of the metal. For the experimental determination of thermionic constants, the relation (1′) is used as follows. When $\log(i/T^2)$ is plotted against $1/T$ from measured values of i and T, the inclination of the straight line is equal to φ and the cross point of this line with the ordinate gives $\log A$. The experimental values of Richardson constant thus obtained are in most cases smaller than the theoretical value even in the case of pure metal, showing a characteristic dependence upon the metal used. To explain such discrepancy between the theoretical value and the experimental one, the following mechanism has been postulated.

(1) Existence of microscopic pits on the surface of metals,

(2) Effect due to impurities and surface contamination,

(3) The transmission coefficient of electrons at the surface potential barrier being smaller than unity,

(4) Effect of positive temperature coefficient of work function.

(1) and (2) should be excluded, because it is too artificial to assume the existence of su h pits or surface contamination enough to explain the discrepancy observed in the recent accurate experiments, carried out under great cares. Since the value of transmission coefficient of very slow electrons has been confirmed to be almost equal to 1, both in theory and in experiments[1)], the hypothesis (3) also is not enough. Krüger and Stabenow[2)], and Potter[3)], found experimentally to be 6.3×10^{-5} e.v./deg for the temperature coefficient of work function of the pure tungsten. The actual Richardson constant calculated from this value was 58A/cm^2, deg^2, in good accordance with the experimental value. Thus Potter and others considered that the discrepancy between the theory and experiments was well explained only by the temperature coefficient. There remains, however, some ambiguities in the fact that their experiments were carried out on polycrystalline wires.

In the case of composite cathode, such as thoriated tungsten[4)] or oxide-coated cathode[5)], the observed Richardson constants are of extraordinarily small order of magnitude ranging from 1/100 to 1/10,000 of the theoretical one. On the other hand, the experimental Richardson constant of oxydized tungsten[6)] is abnormally large, being of 5×10^{11} A/cm^2, deg^2. Up to the present, the theory to explain such abnormal Richardson constants has never been successfully proposed. In this paper and in subsequent several papers such problems will be treated and the content of the present paper will be limited to the qualitative discussion.

§ 2. Cryatal Orientation and Work Function.

It has been well known since several ten years ago that each of orystallographic faces has its own work function different from the others. Many qualitative results have been obtained by means of various kinds[7)] of electron microscope. For the quantitative determination, photoelectric method and contact potential differnce method have been applied.

For example, Rose[8] found the contact potential difference between (100)- and (111)-planes of copper was 0.46 e. v., while Anderson[9] found that that between (100)-plane and polycrystalline surface of silver was 0.32 e. v. According to Farnsworth and Winch[10], the photoelectric work function of (100)- and (111)-planes of silver was 4.81 e. v. and 4.75 e, v. respectively, their diffecnce being 0.06 e. v. Nichols' result[11] obtained thermionically on a tungsten single crystal wire is shown in the Table I. Here, the maximum differnce of the work function was 0.3 e. v.

Table I

Work function of pure tungsten

Crystal face	(111)	(112)	(116)	(001)	(110)
φ (e. v.)	4.36	4.66	4.36	4.53	4.65
A(A/cm², deg²)	36	125	56	117	15

In almost all thermionic experiments the polycrystalline wire composed of many small crystal faces with their own work functions and thus their own emission has been used. The original thermionic emission formula (1) can naturally be applied to a uniform surface of a single crystal, but it is questionable to apply the formula in its original form to a polycrystalline wire composed of many small crystal surfaces with different work functions. Thus it is of primary importance to make clear the physical meaning of the so-called thermionic constants determined experimentally by applying the formula (1) to the polycrystalline wire.

§ 3. Average Thermionic Constants of Polycrystalline Wire.

On dividing the cathode surface into small regions in which the work function is uniform, the formula (1) holds for each of the divided regions. The total emission current per unit areas, therefore, is represented by summing up the emission current from each small region,

$$i=\sum_n i_n=\sum_n p_n A_n T^2 \varepsilon^{-\frac{e\varphi_n}{kT}}. \tag{2}$$

where p_n is the ratio of the divided small region n to the total cathode surface (1 cm²). Assuming that A_n in the formula (2) is an universal constant 120 A/cm², deg², independent of the kind of metals and the crystal orientation, the total emission current per unit area of cathode is written in the form

$$i=AT^2\sum_n p_n \varepsilon^{-\frac{e\varphi_n}{kT}}. \tag{2'}$$

On the other hand, the average Richardson constant A^* and the average work function φ_t^* are determined by means of the Richardson line method and thus the total emission ourrent is expressed by

$$i=A^*T^2\varepsilon^{-\frac{e\varphi_t^*}{kT}}, \tag{3}$$

per unit surface area. Thus equating (2′) and (3), we get

$$\varphi_t^*=\frac{kT}{e}\log\left[\frac{A^*}{A}\cdot\frac{1}{\sum_n p_n\varepsilon^{-\frac{e\varphi_n}{kT}}}\right], \tag{4}$$

showing that the average work function is a function of temperature. In the special case of $n=2$,

$$\varphi_t^*=\varphi_1+\frac{kT}{e}\log\left[\frac{A^*}{A}\frac{1}{p+(1-p)\varepsilon^{-\frac{e}{kT}(\varphi_1-\varphi_1)}}\right],$$

$$\varphi_2>\varphi_1 \tag{4'}$$

According to whether almost all emission currents come from regions with lower work function φ_1 or those with higher one φ_2, we have

$$\varphi_t^*\fallingdotseq\varphi_1 \qquad A^*\fallingdotseq pA \tag{5}$$

or

$$\varphi_t^*\fallingdotseq\varphi_2 \qquad A^*\fallingdotseq(1-p)A \tag{6}$$

respectively. The relations (5) and (6) show that the measured value of the work function is approximately equal to the work function of regions giving the predominant emission and the measured Richardson constant is equal to the value the true Richardson constant multiplied by the fraction of the area with predominant emission. As p and $(1-p)$ are smaller than unity, the experimental Richardson constant is always smaller than the theoretical value, when more than two work functions co-exist on the cathode surface.

§ 4. Exact Expression of Thermionic Constants.

For the experimental determination of work function, the Richardson line is plotted from experimental value of i and T and thus, if the line is straight, the work function is determined simply from the inclination of this straight line, but, if the line is curved, it is determined from the tangent to this line at a definite temperature. So the work function, when it is expressed in e. v., is given by

$$\varphi_t^* = -\frac{k}{e}\frac{\partial \log(i/T^2)}{\partial(1/T)}$$

$$\doteqdot \frac{\sum_n p_n\left(\varphi_n - T\frac{\partial\varphi_n}{\partial T}\right)\varepsilon^{-\frac{e\varphi_n}{kT}}}{\sum_n p_n \varepsilon^{-\frac{e\varphi_n}{kT}}}. \qquad (7)$$

The Richardson constant is given by the intersection of the tangent to the Richardson line at $T = T_0$ with the ordinate. The equation of the tangent at (i, T_0) is given by

$$-\frac{e}{k}\varphi_t^* = \frac{\log(i/T^2) - [\log(i/T^2)]_{T=T_0}}{(1/T)-(1/T_0)} \qquad (10)$$

As $\log(i/T^2)$ is equal to $\log A^*$ at $1/T = 0$,

$$\log A^* = \left[\log\frac{i}{T^2}\right]_{T=T_0} + \frac{e}{k}[\varphi_t^*]_{T=T_0}\cdot\frac{1}{T_0} \quad (10')$$

When (2) and (9) are substituted into the above formula

$$\log\frac{A^*}{A} = \log\left(\sum_n p_n\varepsilon^{-\frac{e\varphi_n}{kT}}\right)$$

$$+\frac{e}{kT}\frac{\sum_n p_n\left(\varphi_n - T\frac{\partial\varphi_n}{\partial T}\right)\varepsilon^{-\frac{e\varphi_n}{kT}}}{\sum_n p_n\varepsilon^{-\frac{e\varphi_n}{kT}}} \qquad (11)$$

Especially, when there co-exist only two different work functions, and moreover i_1 is larger than i_2

$$\varphi_t^* = \varphi_1 - T\frac{\partial\varphi_1}{\partial T}, \quad \log\frac{A^*}{A} = \log p + \frac{e}{k}\frac{\partial\varphi_1}{\partial T}. \quad (12)$$

If $i_1 \ll i_2$, we get

$$\varphi_t^* = \varphi_2 - T\frac{\partial\varphi_2}{\partial T}, \quad \log\frac{A^*}{A} = \frac{e}{k}\frac{\partial\varphi_2}{\partial T}. \qquad (13)$$

So, when

$$\frac{\partial\varphi_1}{\partial T} = \frac{\partial\varphi_2}{\partial T} = 0,$$

these results are in accordance with those obtained in the previous paragraph.

It is difficult to calculate the value of $\log(A^*/A)$ form the most general formula, but when there exist only two different kinds of work functions on the cathode, the calculation of its extreme value is easy, because $\log(i/T^2)$ is the uniform function of p and the extreme value, p_m is calculated from

$$\frac{\partial}{\partial p}\log\frac{A^*}{A} = 0.$$

Thus we obtain;

$$p_m = \frac{e}{kT}\frac{\varphi_2 - \varphi_1 - T\left(\frac{\partial\varphi_2}{\partial T} - \frac{\partial\varphi_1}{\partial T}\right)}{\left(\varepsilon^{-\frac{e\varphi_1}{kT}} - \varepsilon^{-\frac{e\varphi_2}{kT}}\right)^2}\varepsilon^{-\frac{e}{kT}(\varphi_1+\varphi_2)}$$

$$-\frac{\varepsilon^{-\frac{e\varphi_2}{kT}}}{\varepsilon^{-\frac{e\varphi_1}{kT}} - \varepsilon^{-\frac{e\varphi_2}{kT}}} \qquad (14)$$

If $\varepsilon^{-\frac{e\varphi_1}{kT}} \gg \varepsilon^{-\frac{e\varphi_2}{kT}}$, p_m is given as follows;

$$p_m \doteqdot \left\{\frac{e}{kT}(\varphi_2 - \varphi_1) - 1\right\}\varepsilon^{-\frac{e}{kT}(\varphi_2-\varphi_1)}, \quad (14')$$

where $\partial\varphi_1/\partial T$ and $\partial\varphi_2/\partial T$ are neglected. (14′) may be written in the logarithmic form,

$$\text{lop}\, p_m = -\frac{e}{kT}(\varphi_2 - \varphi_1) + \log\left\{\frac{e}{kT}(\varphi_2 - \varphi_1) - 1\right\}$$

$$(14')$$

The value of A at the extreme value is given by

$$\log\frac{A^*}{A} = \log\left[\frac{e}{kT}(\varphi_2 - \varphi_1)\right] - \log\left(\varepsilon^{-\frac{e\varphi_1}{kT}} - \varepsilon^{-\frac{e\varphi_2}{kT}}\right)$$

$$+\frac{e}{kT}\frac{\varphi_1\varepsilon^{-\frac{e\varphi_1}{kT}} - \varphi_2\varepsilon^{-\frac{e\varphi_2}{kT}}}{\varepsilon^{-\frac{e\varphi_1}{kT}} - \varepsilon^{-\frac{e\varphi_2}{kT}}} + 1. \qquad (15)$$

If $\varepsilon^{-\frac{e\varphi_1}{kT}} \gg \varepsilon^{-\frac{e\varphi_2}{kT}}$, $\log\frac{A^*}{A}$ is written in the simple form,

$$\log\frac{A^*}{A} \doteqdot \log\left[\frac{e}{kT}(\varphi_2 - \varphi_1)\right] - \frac{e}{kT}(\varphi_2 - \varphi_1) + 1 \quad (15')$$

or

$$\log\frac{A^*}{p_m A} = 1 - \log\left\{1 - \frac{kT}{e}\frac{1}{\varphi_2 - \varphi_1}\right\}. \qquad (15'')$$

As $(kT/e)(1/\varphi_2 - \varphi_1)$ is in general less than unity, so long as $\varphi_4 - \varphi_1$ is larger than 0,5 e. v., the third term in (15″) is expanded in series and thus approximately

$$\log\frac{A^*}{p_m A} = 1 + \frac{kT}{e}\frac{1}{\varphi_2 - \varphi_1}. \qquad (15''')$$

Thus p_m and A_m also are functions of T, and the former becomes the smaller, while the latter becomes the larger, the higher the temperature becomes.

§ 5. An Example.

In this paragraph numerical calculation will be carried out, assuming, for simplicity, $\varphi_1 = 3.0$ e. v. and $\varphi_2 = 4.0$ e. v. In Fig. 1 the Richardson lines are shown with p is as a paremeter. The curves (1) and (2) are Richardson lines for

$$i_1 = AT^2 \varepsilon^{-\frac{e\varphi_1}{kT}}$$

and

$$i_2 = AT^2 \varepsilon^{-\frac{e\varphi_2}{kT}} .$$

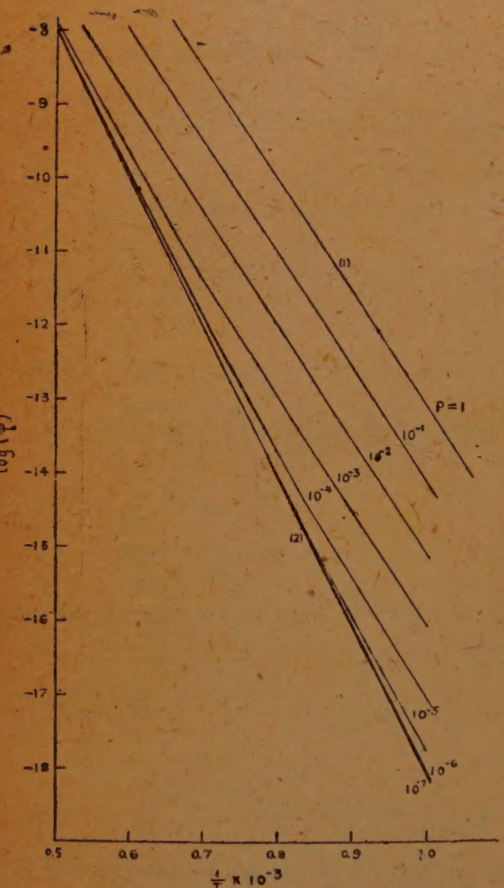

(Fig. 1. Richardson diagram)

The lower part of the calculated Richardson lines in which i_1 is much greater than i_2 is parallel to (1) and the higher part to (2), as the contribution of i_2 is much greater than i_1. The intercept of the lower straight part with the ordinate gives the value of $\log (1-p)A$. As seen from the theoretical formula or Fig. 1 both the work function and the Richardson constant do vary with temperature. The variation of φ_t^* and A^* are shown in Fig. 2 and Fig. 3 with parameter p. The variation of φ_t^* and A^* against p are shown in Fig. 4 and Fig. 5, where $\log p$ is used instead of p and $\log A^*/A$ instead of A^*. φ_t^* is almost constant in the range $P > 10^{-2}$ and then gradually increases with the decrease in p. In the range $10^{-2} > p > 10^{-5}$ it increases rather sharply and, beyond this region, approximates to 4.0 e. v. A^* decreases linearly with the decrease of p at first, and after passing through the minimum value, increases to a large amount until it finally tends to A.

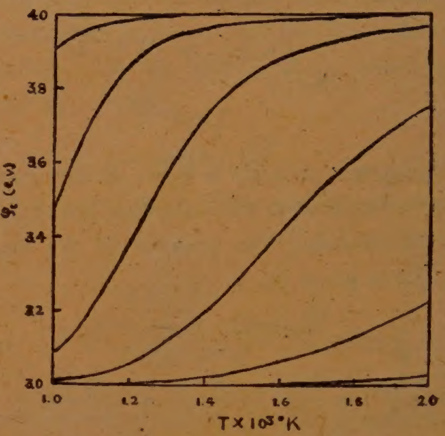

Fig. 2. The relation between the work function φ_t and temperature.

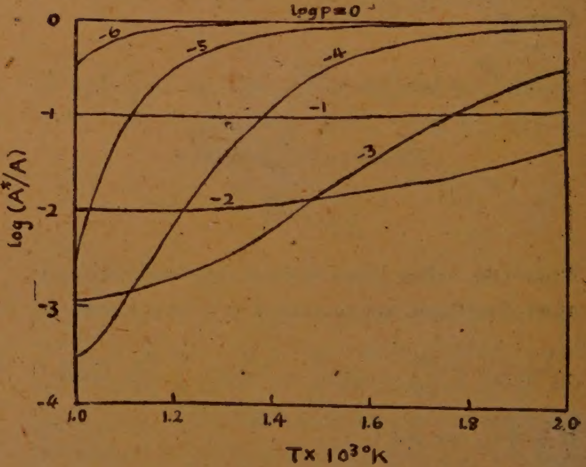

Fig. 3. The relation between the Richadson constant and temperature.

When there co-exist many work functions on the same cathode, the process of such calculation is much more difficult than in the case mentioned above, but it is of no question that A^* is smaller than the theoretical value.

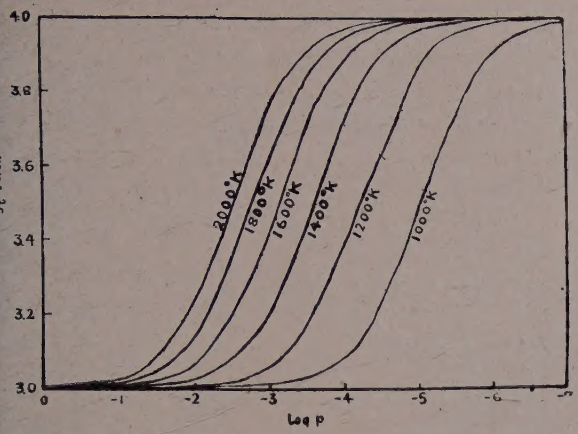

Fig. 4. The relation be'ween the work function and p.

Table II

Thermionic constants of pure metals.

metal	A^*	φ_t^*	metal	A^*	φ_t^*
Ba	60	2.11	W	60	4.54
Zr	330	4.12	Re	200	5,1
Th	70	3.38	Pd	60	4.91
Ta	60	4.1	Pt	35	5.32
Mo	55	4.15			

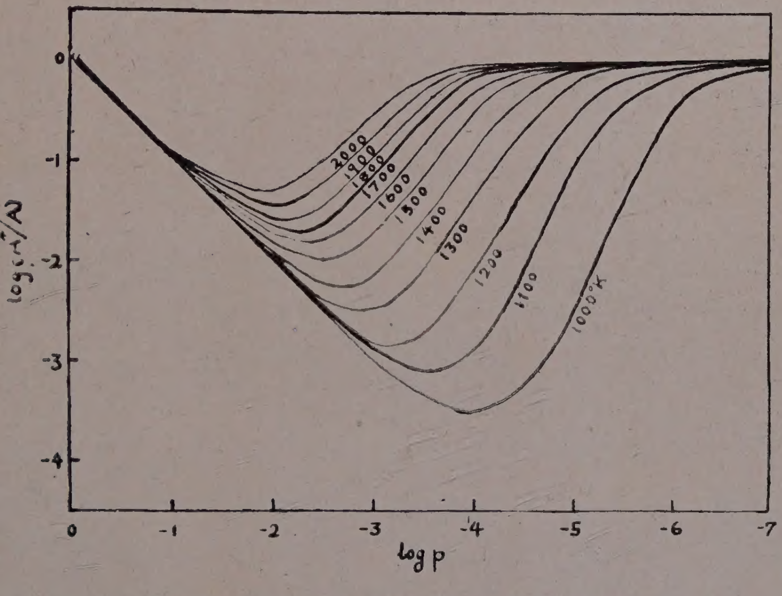

Fig. 5. The relation between the work function and p.

§ 6. Thermionic Constants of Pure Metals.

For experimental determination of the thermionic constants, polycrystalline wires have been used. The Richardson constant, thus determined, is of course smaller than the theoretical value, as shown in the above paragraphs. Many experimental results have shown that the Richardson constants of ordinary metals are always smaller than the theoretical values, supporting the present theory. Main results are shown is Table II, reprinted from Reimann's[12] and other's papers[13].

The metals whose Richardson constants are larger than the theoretical value, are only two, Zr and Re, which have not only great affinities to oxygen and other gases, but their purification are also difficult. The higher Richardson constants of these metals are probably resulted from the imcomplete treatment of the materials. In the case of matals with adsorbed layer of electronegative gases such as oxygen on their surface, the greater Richardson constant will be expected to appear if p is a function of temperature. The abnormally large Richardson constant, obtained in the case of oxydized tungsten, will be explained in this way. Such special cases will be discussed in detail in future papers.

As seen from the Nichols' paper on the single crystal tungsten wire, the Richardson constants of (112)-and (001)-planes are almost equal to the theoretical value within experimental error, while those of (110)-, (116)- and (111)-planes are much smaller than the theoretical value. Fig. 6 shows the microscopic photographs of both (100)- and (110)- planes,

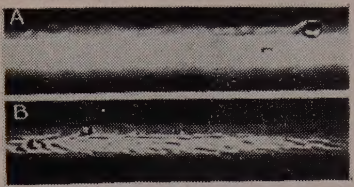

Fig. 6 A, photomicrograph of single crystal wire looking down the (001) direction; B, ten degrees off the (110) directien.

cited from Nichols' paper. On (100) and in its neighbourhood the purity of the crystal surface is worse, showing existence of microcrystals. In the former the observed Richardson constant has been found to be almost equal to the theoretical value, because the work function is uniform, while in the latter the observed values are smaller because on these surfaces there still exist many different work functions. Nichols' view is in coincidence with the present explanation. The result obtained by Nichols is of much interest, for it gives a direct support to the author's theory. The quantitative discussion on pure tungsten will be carried out in a following paper.

§ 7. Thermionic Constants of Complex Cathodes.

The monomolecular layered cathodes such as thoriated tungsten and oxide-coated cathode are found to have anomalously smaller Richardson constants than the theoretical value or that for the pure metal. In the case of the thoriated tungsten(14) it is 3.0 A/cm^2, deg^2, while that of the oxide-coated cathode is of the order of 10^{-2} to 10^{-4} A/cm^2, deg^2, in the best activated state. The explanation of such anomaly has never been proposed with success. As A^* is the function of p in the present theory, qualtative explanation on such anomaly is very easy. For the thoriated tungsten the experimental result as seen in the Fig. 7 has been obtained. A^* decreases linearly at first with the decrease in the work function, i.e. with the progress of the activation, and then it increases when the activation proceeds further. Such behaviour will be understood from Fig. 5, where there are assumed to be only two different kinds of work functions. When the activation proceeds to some degree, the Richardson constant increases, while the work function remains nearly constant. Such range corresponds to $\varphi_t^* \doteqdot 3.0$ e. v. in Fig. 8 showing the relation between φ_t^* and A^*. In the case of thoriated tungsten, there are many work functions as shown by the electron microscope, the relation should not be so simple as the case shown in Fig. 8, but its qualitative aspects will be understood.

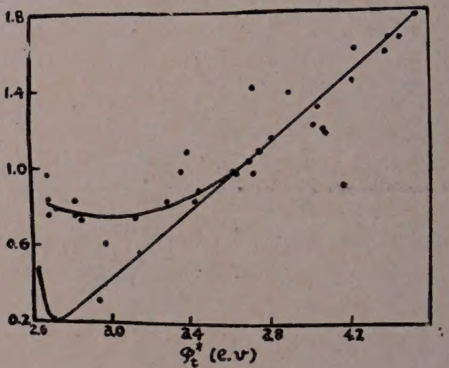

Fig. 7. The relation between the work Function and the Richardson constant of the thoriated tungsten.

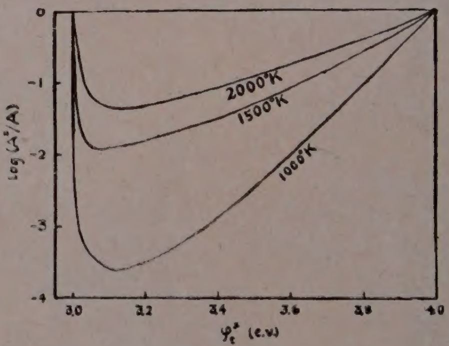

Fig. 8. The theoretical relation between the work function and the Richardson constant.

In the case of the oxide-coated cathode, it is still of question that there co-exist more than two different work fnnctions. Its exxceedingly small Richardson constant, however, is well explained by assuming $p = 10^{-4}$, in good accordance with Prescott and Morrison's(15) estimation of the amount of reduced barium in the oxide layer. The development of the present theory to the complex cathodes shall be published in the following papers.

§ 8. Conclusion.

Experimental determination of the thermionic constants has been carried out on the assumption that there exists only one work function even in the polycrystalline cathode. In the actual cathode, however, there co-exist many work functions even in the pure metal, beuause the work function depends upon the crystallographic direction. When the theoretical formula in its original form is applied to such a cathode with many work functions, the average thermionic constant should be obtained. The present paper was an answer for this ploblem. According to the results, the average work fuuction approximates to that of the portion of maximum emission, and the average Richardson constant is equal to the value of the real Richardson constant multiplied by the ratio of the portion of maximum emission to the total surface area of the cathode. This results in the relation $A > A^*$, that is satisfied qualitatively in the case of pure metals. Numerical calculation on tungsten, in which the dependance of work function upon the crystallographic direction has been comparatively well known, will be carried out ,after the complete theory will be presented,

References.

(1) L. Nordheim: Proc, Roy. Soc. **121**, (1928), 626. H. E, Farnsworth: Phys. Rev., **20**, (1922), 358. R. L. Retry: Phys. Rev., **28**, (1926), 362.

(2) F. Krüger & G. Stabenow: Ann. d. Phys. **22**, (1935), 713.

(3) J. G, Potter: Phys. Rev., **58**, (1940), 623.

(4) S. Dushmann & J. W. Ewald: Phys. Rev., **26**, (1927), 857. W. H. Brattain & J, A. Becker: Phys. Rev.. **43**, (1935), 428.

(5) L. R. Koller: Phys. Rev., **25**, (1925), 671.

(6) K. H. Kingdom: Phys. Rev., **24**, (1924), 510.

(7) Johnson & Schockley: Phys. Rev., **49**, (1936), 439. Martin: Phys. Rev. **59**, (1939), 947. Müller: Zeits. f. Phys., **106**, (1937), 541.

(8) I. Rose: Phys. Rev., **44**, (1933), 585.

(9) P. A. Anderson: Phys. Rev., **59**, (1934), 1034.

(10) H. E. Farnsworth & R. P. Winch. Phys. Rev,, **58**, (1940), 818.

(11) Nichols: Phys. Rev., **57**, (1940), 297.

(12) A. L. Reimann: Thermionic Emission, London, (1934).

(13) L. V. Whittny: Phps. Rev., **50**, (1936), 1154.

(14) S. Dushmann & J. W. Ewald: Phys. Rev., **29**, (1927), 857. K. H. Kingdom: Phys. Rev., **24**, (1924), 510.

(15) Prescott & Morrison: J. A. Chem. Soc., **60**, (1938), 3047.

The Dispersion of the Dielectric Constant in Rochelle Salt Crystal at Low Frequencies.

By Heiji KAWAI and Masakazu MARUTAKE.

Kobayasi Institute of Physical Research, Kokubunji, Tokyo, Japan.

(Received June 11, 1947)

§ 1. Introduction.

The dielectric constant ε of Rachelle salt crystal along the a-axis is noted for its anomalous characters, and numerous measurements have been reported[1]. Recently one of the writers found out effects of humidity on physical properties of Rochelle salt and sufficiently reproducible values of dielectric constant were measured with 1000 Hz. a. c.[2]. Nevertheless there is a great difference between the values measured with 1000 Hz. and that measured statically with ballistic galvanometer[3]. R. D. Schulwas-Sorokin and M. V. Posnov investigated the behavior of the dielectric constant at low frequencies (from 1000 to 0.5 Hz.), and found that there is an anomalous dispersion which depends on the strength of the field and on the thickness of the crystal in a rather complicated manner[4].

The purpose of this experiment is to study the dispersion in the weak field together with the effects of humidity. The dielectric constant was measured at frequencies from 1000 to 1/4 Hz., and two dispersions were found out below the Curie point. One is a normal dispersion, independent of the field, and exists at 10~100 Hz., the value of dispersion of ε being about 300. The other is very large (more than thousands) and exists at lower than 10 Hz.

§ 2. Experiments.

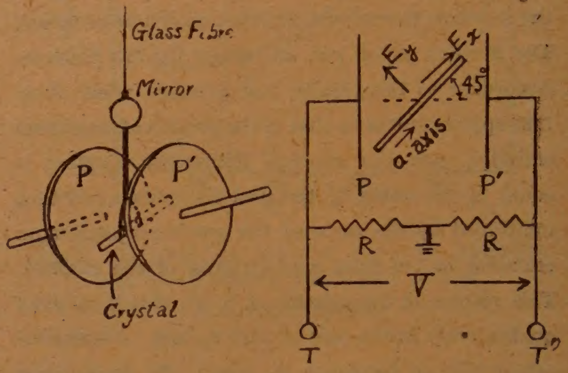

Fig. 1. The apparatus of measurement.

As shown schematically in Fig. 1, the thin long bar of the Rochelle salt crystal cut aloug the a-axis (length: 28.6 mm; the section: a circle of diameter of 1.1 mm) is hung horizontally with thin fibre of glass between two electrodes P, P′ (distance: about 2.6 cm) wlth the angle of 45°. When voltage of various frequencies is applied, the bar of Rochelle salt crystal is polarized and rotates until the torque is balanced by the torsion of fibre. The angle of rotation is measured with the mirror attached to the bar. The natural period of the rotation of bar is about 8 seconds. In order that the voltage may be applied symmetrically with regard to the centre of the bar, two equal resistances R (100 $K\Omega$) are connected in parallel and the middle point is earthed. The apparatus is set in the case of brass, which is earthed and kept in constant humidity using H_2SO_4 of proper density. The case is placed in an air thermostat.

For the source of a. c. voltage, from 1000 to 30 Hz. the valve oscillator was used. From 30 to 1/4 Hz. the following device was used. As shown schematically in Fig. 2, many (about one hundred)

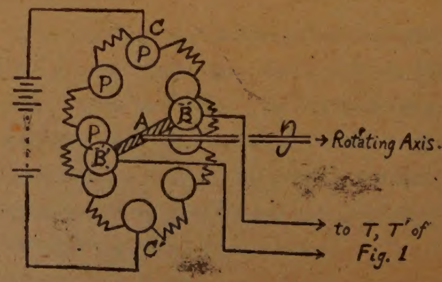

Fig. 2. The low-frequency oscillator.

poles P are arranged on the circumference of the circle (the diameter: about 5 cm). Between poles are connected proper resistance (from 0 to 50 ohms) and the d. c. voltage is applied on the two antipoles C, C′. To the two ends of the arm A brushes B, B′ are attached, and electric motor makes the arm A rotate with various frequencies. When resistances are properly taken, the voltage difference between two brushes can be made sinusoidal. Of course minute higher harmonics are included, but as (5) shows the rotation being proportional to the square of applied voltage, even harmonics of 1/10 of fundamental are out of question.

It is readily seen that

$$\theta \infty PE_y \qquad (1)$$

where θ: the angle of rotation, P: polarization along the a-axis, E_y: the y-component of the field. As the dielectric constant is much larger in the direction of the a-axis than in other directions, the polarization in other directions need not be considered.

Now if E_x' is the x-component of the effective field in the interior of the bar, (For brevity, it is assumed that the crystal is uniformly polarized.)

$$P = \kappa E_x' \qquad (2)$$

$$E_x' = E_x - NP \qquad (3)$$

where κ is the susceptibility and N is the depolarization factor depending on the shape of the bar.

From (2) (3), $$P = \frac{\kappa}{1+N\kappa} E_x \qquad (4)$$

And E_x, E_y being proportional to V,

$$\theta = K \frac{\kappa}{1+N\kappa} V^2 \qquad (5)$$

where K is a constant. The proportionality of θ to the square of the applied voltage V was confirmed experimentally from 0 to 70 Volts. This means that in this range ε does not depend on the magnitude of the field.

Fig. 3 and Fig. 5 show the angle of rotation reduced to 50 Volts in the arbitrary scale. Circles and cross-points show respectively the values measured in about 45 % and 57 % humidity. (H_2SO_4 of density 1.360 and 1.400 at 20°C. was used.) It was found that above the upper Curie point (24°C.) the dielectric constant is independent of frequency from 1000 to 1/4 Hz., and observed values are situated on the curve A of Fig. 3. On the other hand, below the Curie point, the dispersion takes place. As Fig. 5 shows, two dispersions are ob-

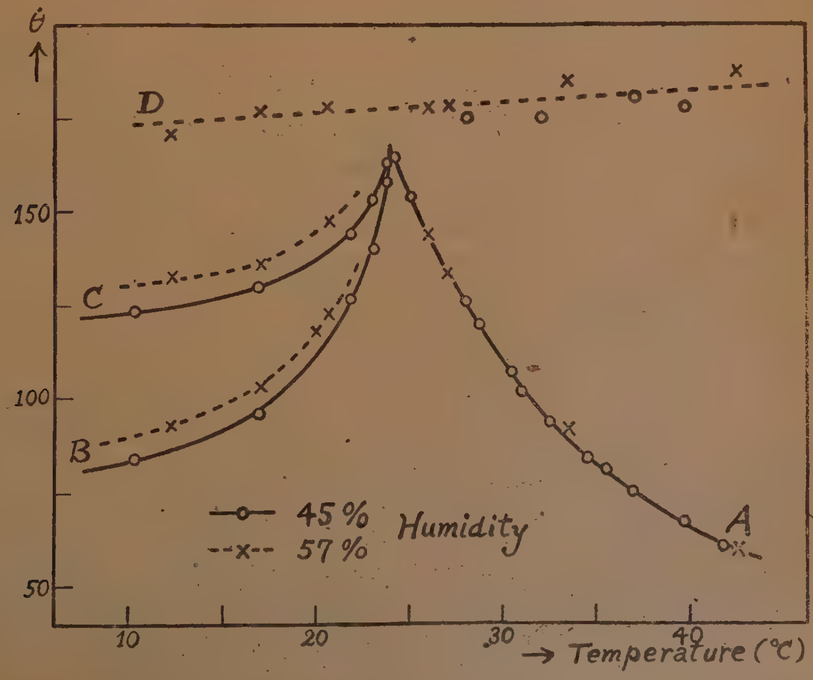

Fig. 3.

served. In Fig. 3 curves B and D show the values measured with 1000 Hz. and with d. c., respectively, and curve C shows the stationary values between two dispersions.

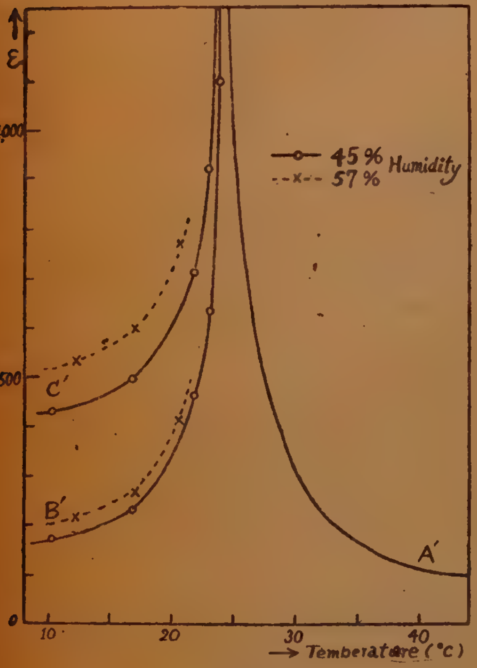

Fig. 4.

The values of ε for 1000 Hz. being well known (curve A′ of Fig. 4)⁽²⁾, the sensitivity of the experiment can be determined, and the corresponding values of ε to the curves B and C can be evaluated which are shown on curves B′ and C′ of Fig. 4.

As it is apparent from (5), that the sensitivity decreases as κ increases, d. c. values of curve D correspond to very large values of ε (perhaps more than several thousand). This means that the second dispersion is very large below the Curie point. Above the Curie point, however, the large d. c. values seem to be not due to the dispersion but to the surface leakage of the caystal as will be explained below.

Now taking account of the first dispersion only, let polarization P be devided into two parts P_1 and P_2, P_1 being a part with negligible relaxation time and P_2 having a time of relaxation τ.

Then $$P = P_1 + P_2. \qquad (6)$$

$$P_1 = \kappa_1 E_x', \qquad (7)$$

and the real part of $P_2 = \dfrac{\kappa_2 E_x'}{1+\omega^2\tau^2}$ (8)

In (8), ω is the angular frequency of the applied a. c. voltage.

P_2 considered as a complex quantity satisfies the following differential equation

$$\tau\dot{P}_2 = \kappa_2 E_x' - P_2 \qquad (9)$$

Then if E_x varies as $e^{j\omega t}$, the angle of rotation θ can be readily solved from (3) (5) (6) (7) (9).

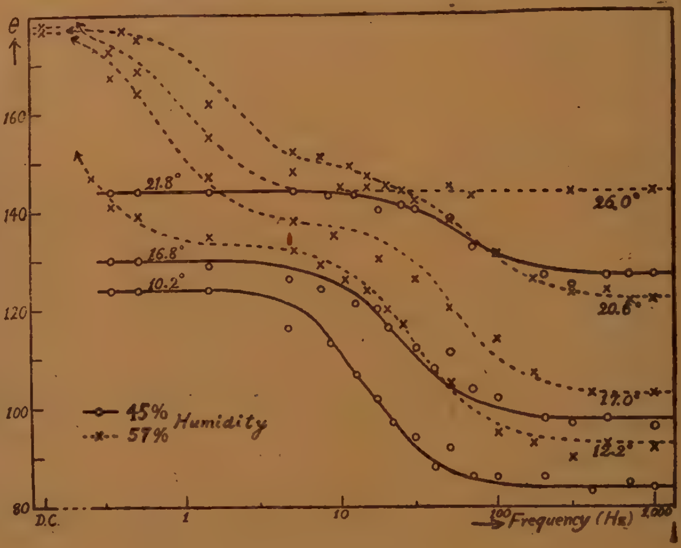

Fig. 5.

$$\theta-\theta_1 = K\frac{\kappa_2}{(1+N\kappa_1)\{1+N(\kappa_1+\kappa_2)\}} \times \frac{1}{1+\left\{\dfrac{1+N\kappa_1}{1+N(\kappa_1+\kappa_2)}\right\}^2\omega^2\tau^2}V^2 \qquad (10)$$

where θ_1 is the angle of rotation which corresponds to P_1. When (10) is compared with (8), it is known that θ has an apparent relaxation time τ' which is $(1+N\kappa_1)/\{1+N(\kappa_1+\kappa_2)\}$ times the true relaxation time τ.

Or $$\theta-\theta_1 \propto \frac{1}{1+\omega^2\tau'^2} \qquad (11)$$

τ' is determined from Fig. 5 so that measured values may fit the equation (11) best. In Fig. 5 the true and dotted lines show the calculated values using τ' thus determined. The correction factor $(1+N\kappa_1)/\{1+N(\kappa_1+\kappa_2)\}$ can be calculated, as κ_1, κ_2 are already known (Fig. 4) and N is determined experimentally as 0.057 (by comparing Fig. 3 with the equation (5), above the Curie point). This factor lies between 0.5 and 0.8.

Fig. 6 shows the first disphrsion calculated from

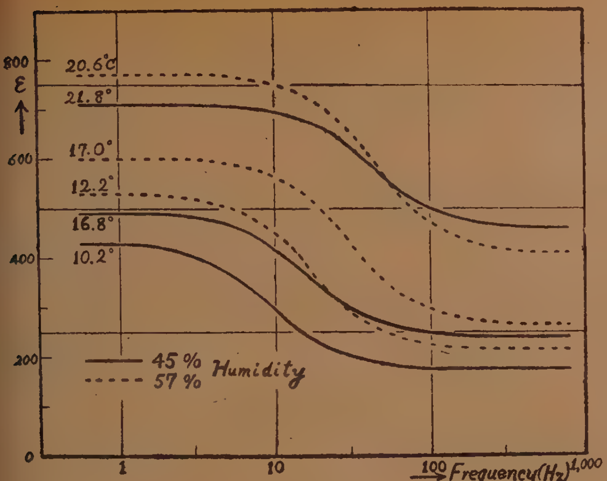

Fig. 6.

the next equation by evaluating the true relaxation time τ.

$$\varepsilon = 1+4\pi\kappa, \quad \kappa = \kappa_1 + \frac{\kappa_2}{1+\omega^2\tau^2} \tag{12}$$

In Fig. 7 dotted lines show the values of ε_2 ($=1+4\pi\kappa_2$) of the first dispersion, which are almost independent of temperature but increase as the humidity. On curves (a) are plotted the logarithm of the time of relaxation τ, which decreases linearly as temperature rises and depends upon humidity.

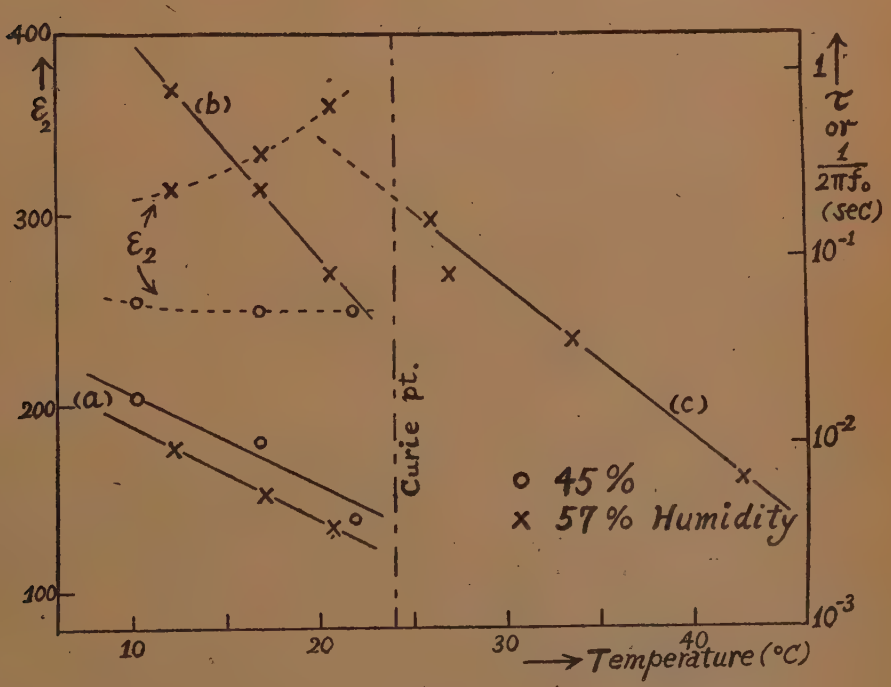

Fig. 7.

Next, let us consider the second dispersion. In Fig. 7 on curves (b) and (c) are plotted log $1/2\pi f_0$, where f_0 means the frequency at which the second dispersion occurs apparently in Fig. 5. Curves (b) and (c) do not coincide with each other at the Curie point, and it seems that below the Curie point there exists the second dispersion but above it, the dispersion is fictitious one due to the surface leakage. This is confirmed also by the fact that when the Rochelle salt condenser is discharged, the discharging current observed with oscillograph shows that there are at least two times of relaxation below the Curie point, but that the time of relaxation is almost zero above it. This experiment with oscillograph is now in progress, though quantitative results have not yet obtained. As explained above, this experiment has poor accuracy for larger values of κ, and it is inconvenient for the characters of the second dispersion. In 45 % humidity the second dispersion could not be observed, perhaps on account of the fact that the dispersion occurs at lower frequency than 1/4 Hz. and the measurment with d. c. is quite difficult because of the pyroelectricity and spontaneous polarization.

§ 3. Results.

From this experiment the following results were found:

(1) Above the Curie point, there exists no dispersion.

(2) Below the Curie point, there are at least two dispersions. The behavior of the first dispersion is shown in Fig. 6.

(3) The second dispersion is very large, but in this experiment its characters could not be determined quantitatively.

The facts that dispersions occur only below the Curie point, indicates that these phenomena have some relation with spontaneous polarization and the rotation of the domains, but the writers have not yet succeeded to explain them.

References.

(1) H. Mueller: Phys. Rev., **47**, (1935), 175; **57**, (1940), 829; **58**, (1940), 565; **58**, (1940), 805.
(2) H. Kawai: In printing in this Journal.
(3) J. Valasek: Phys., Rev. **17**, (1921), 475; **24**, (1924), 560.
(4) R. D. Schulwas-Sorokin and M. V. Posnov: Phys. Rev. **47**, (1935), 166.

Collective Electron Ferromagnetism, I.

By Hiroshi WATANABE.

Research Institute for Iron, Steel and other Metals, Tohoku University.

(Received July 3, 1947)

§ 1. Criticism of Stoner's Theory.

Stoner[1] has developed a theory of ferromagnetism based on collective electron model and obtained many valuable results. On the other hand Hirone[2] has used Bloch-Slater's satistics which is somewhat different from Stoner's. According to Hirone the condition for the occurrence of ferromagnetism is given by the following formula

$$J/L > \frac{1}{\nu(\varepsilon_0)}, \qquad (1.1)$$

where J denotes the mean of the exchange integral between the electrons in the energy band responsible for ferromagnetism, ν the density of levels of the energy band, ε_0 the Fermi energy and L the number of atoms. Stoner has shown that if this condition is satisfied, saturation magnetization at the absolute zero of temperature M_0 is not necessarily equal to the number of electrons or of holes times the Bohr magneton. Stoner named $M_0/n\mu$ as the relative magnetization ζ_0, where n denotes the number of electron and μ the Bohr magneton and showed that ζ_0 becomes 1 only when the following condition

$$J/L > \frac{3}{2}\, 2^{-\frac{1}{3}} \frac{1}{\nu(\varepsilon_0)} \qquad (1.2)$$

is satisfied and when $J\nu(\varepsilon_0)/L$ increases from 1 to $\frac{3}{2} \cdot 2^{-\frac{1}{3}}$ and then the relative magnetization ζ_0 from 0 to 1 continuously. In actual metals, for example Ni, Fe or Co, ζ_0 seems to lie between 0.9 and 1. In many ferromagnetic alloys, therefore, it will perhaps not necessarily be equal to unity. As is pointed out by Hirone, in many of the alloys of Ni the characteristic relationships among the measured saturation value, the Curie point, the Curie-Weiss constant and the atomic percentage can be explained by assuming that the relative magnetization is equal to unity, but Fallot's[3] measurements on alloys of Fe do not always show such regularity as shown by Hirone. It will not be unreasonable to consider that this irregularity follows from the fact that in these alloys the exchange integral is not sufficiently large to satisfy (1.2), so that the relative magnetization cannot reach the value 1. (Pauling's[4] postulate becomes the necessary requirement if we assume that ζ_0 equals to 1, but as Niessen(5) has showed it is not reasonable.)

Stoner's method has many advantages compared with that of using tightly bound electron model, but, as it takes the free electron (or hole) model, it requires too large exchange integral to be ferromagnetic and leads to too small low-temperature specific heat. So we shall use an alternative model, assuming the density of levels in the energy band is constant with respect to the energy of electrons. This model is not of course a better approximation to actual alloys than Stoner's but by its simplicity, it enables us to show to what extent and in which manner the band form and the exchange integral play an essential roll in ferromagnetic properties.

On adopting general band form it is difficult to discuss magnetic properties in an analytical form, and then we are confined to calculate only the saturation magnetization at the absolute zero and hence ζ_0.

§ 2. The Saturation Magnetization at the Absolute Zero.

A simple method for obtaining ζ_0 or the quantity x defined by

$$x=\begin{cases}\dfrac{n}{N}\zeta_0=\dfrac{M_0}{N\mu}, & 0\leqq\dfrac{n}{N}\leqq 1/2\\[2ex] \dfrac{1-n}{N}\zeta_0=\dfrac{M_0}{N\mu}, & 1/2\leqq\dfrac{n}{N}\leqq 1\end{cases}\tag{2.1}$$

has been given by Miyahara[6] in the following form

$$x=\frac{L}{JN}(\varepsilon_+-\varepsilon_-)\tag{2.2}$$

where $\int_{\varepsilon_0}^{\varepsilon_+}\nu(\varepsilon)d\varepsilon=\int_{\varepsilon_-}^{\varepsilon_0}\nu(\varepsilon)d\varepsilon=\frac{N}{2}x$, N being the total number of levels in the band and ε_+ and ε_- the maximum energies of electrons having + and − spins respectively.

As the above formulae follow from the condition of extremum of the energy of the system, we have to exclude those x's which correspond to maxima.

We shall be able to obtain the values of x in actual metals or alloys if we had a detailed information of their electronic structures. We shall show only in several simple, idealized cases how it is related to the band form and exchange integral.

Case I. $\nu(\varepsilon)=a+b\varepsilon$.

Fig. 1 shows the case of $a=0$. In Fig. 1b the abscissa represents N and the ordinate x. $x=0$ corresponds to the critical value of J for the occurrence of ferromagnetism. $x=\frac{n}{N}$ or $\frac{1-n}{N}$ corresponds to $\zeta_0=1$. Illustrated curves represent $x\left(\frac{n}{N},\ J\frac{\bar{\nu}}{L}\right)$, the numbers on the curves giving the values of $\frac{J\bar{\nu}}{L}$ where ν denotes the mean density of levels. As seen from the figure, ferromagnetism can occur most easily at $\frac{n}{N}=1$, where ν is highest, and as ν decreases it requires large value of J to make the metal ferromagnetic, until at $\frac{n}{N}=0$ infinitely large J is required. The values of x's of several observed alloys are inserted in the figure.

Case II. $\nu(\varepsilon)=a+b\varepsilon$, where $b=-\frac{a}{2}$.

In this case the slopes of the curves are negative, contrary to the case I, because of $b<0$, Since b is smaller than in I. curves are steeper. As $a\neq 0$ infinitely large value of J is not required for the occurrence of ferromagnetism.

Case III. $\nu(\varepsilon)$ increases in the range $\frac{n}{N}\leqq\frac{1}{2}$ and decreases in the range $\frac{n}{N}\geqq\frac{1}{2}$.

The whole figue is symmetrical with respect to the ordinate axis of $\frac{n}{N}=\frac{1}{2}$, the signs of the slopes of the curves coinciding with the case I in the left hand side and to the case II in the right hand side.

Each of values of x in the figures (1), (2) and (3) is realizable, corresponding to minima of the energy of the system.

Case IV. $\nu(\varepsilon)$ decreases in the range $\frac{n}{N}\leqq\frac{1}{2}$ and increases in the range $\frac{n}{N}\geqq\frac{1}{2}$.

In this case there are unrealizable values of x derived from (2.2) which are contained within the upper region above the dotted lines in the figure.

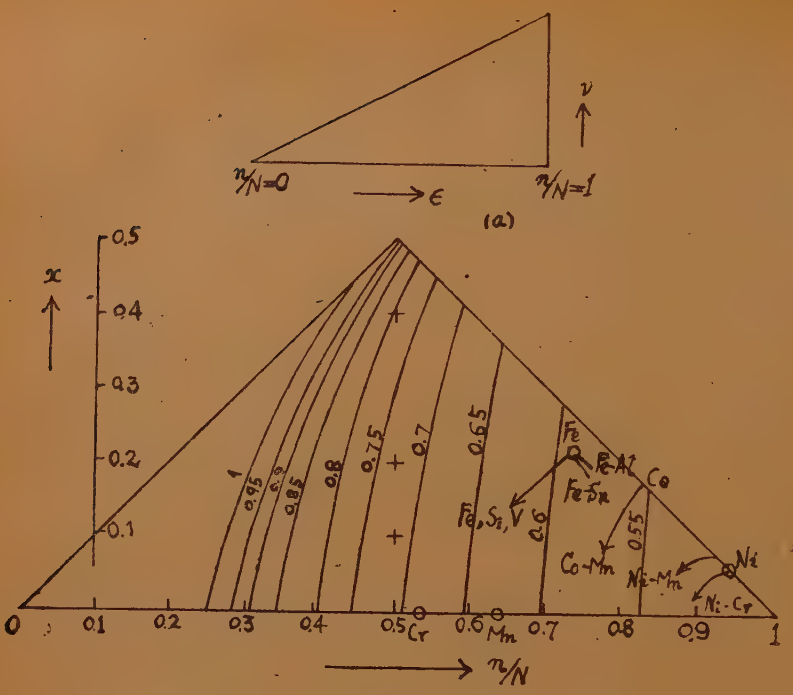
ν
n/N=0
→ ε
n/N=1
(a)
x
0.5
0.4
0.3
0.2
0.1
1
0.95
0.9
0.85
0.8
0.75
0.7
0.65
0.6
0.55
Fe
Fe-Al
Co
Fe-Sn
Fe, Si, V
Co-Mn
Ni-Mn
Ni
Ni-Cr
0
0.1
0.2
0.3
0.4
0.5 Cr
0.6 Mn
0.7
0.8
0.9
1
n/N

Fig. 1.

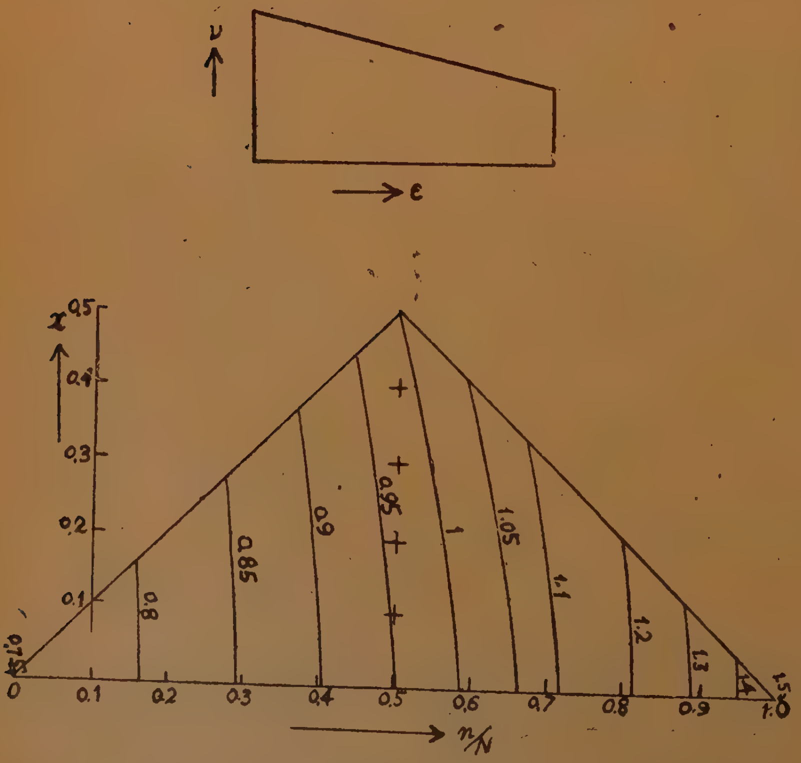
ν
ε
x
0.5
0.4
0.3
0.2
0.1
0.75
0.8
0.85
0.9
0.95
1
1.05
1.1
1.2
1.3
1.4
1.5
0
0.1
0.2
0.3
0.4
0.5
0.6
0.7
0.8
0.9
1.0
n/N

Fig. 2.

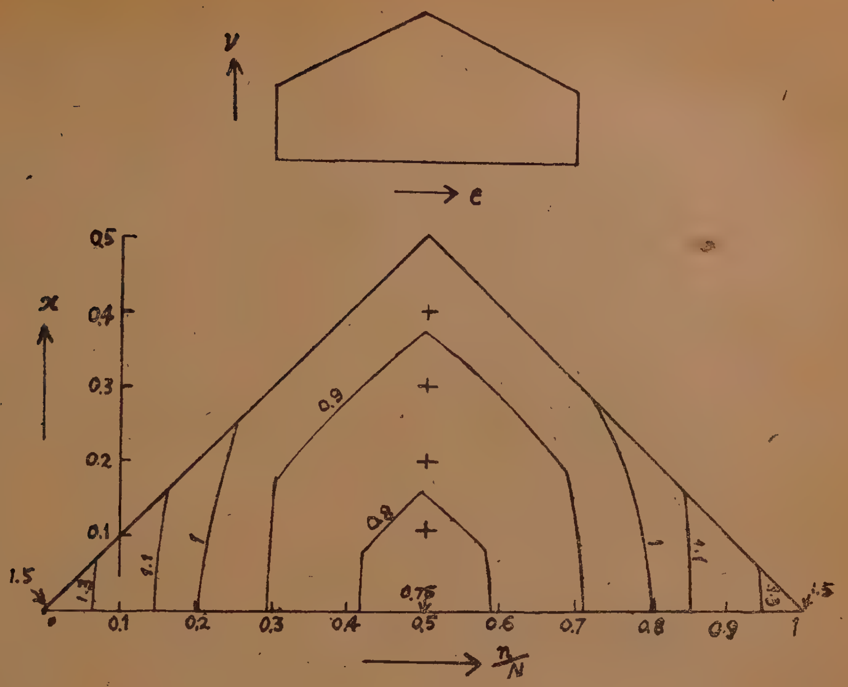
v
ε
x
0.5
0.4
0.3
0.2
0.1
1.5
1.3
1.1
1
0.9
0.8
0.75
0
0.1
0.2
0.3
0.4
0.5
0.6
0.7
0.8
0.9
1
1.5
n/N

Fig. 3.

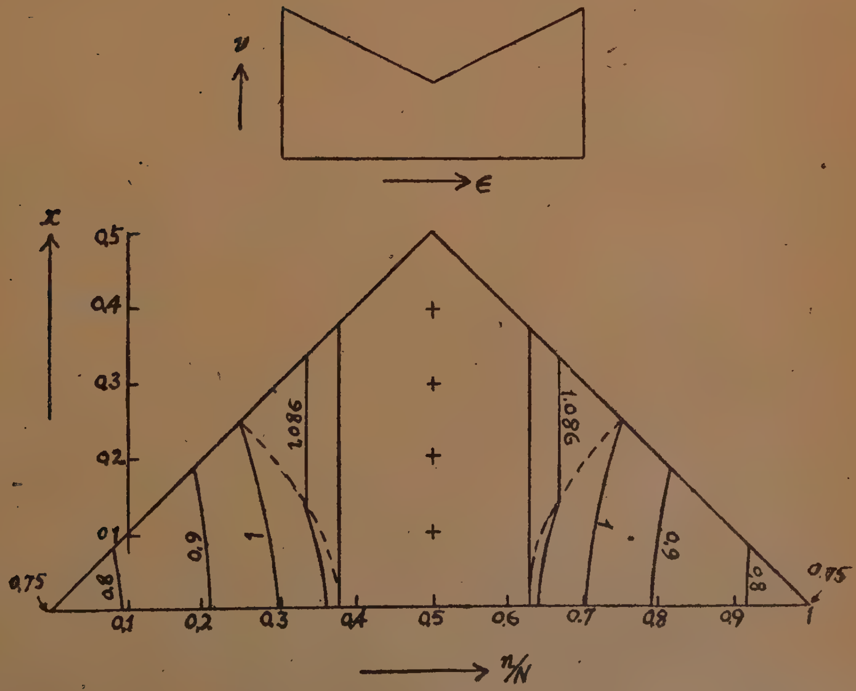
v
ε
x
0.5
0.4
0.3
0.2
0.1
0.75
0.8
0.9
1
1.086
1.086
1
0.9
0.8
0.75
0.1
0.2
0.3
0.4
0.5
0.6
0.7
0.8
0.9
1
n/N

Fig. 4.

When $\frac{J\bar{\nu}}{L} < 1$ curves are similar to those of the cases I or III. On the other hand, when $\frac{J\bar{\nu}}{L} > 1$, and $J = \text{const}$, say, 1.086, x increases continuously with n to its certain value, and then it jumps abruptly to the point corresponding to $\zeta_0 = 1$.

So far we are merely concerned with the idealized, simple models, from which we have actually shown that the values of [illegible] are much sensitive to the value of J and the form of the band. So we can expect that the regularity in Ni alloys, as mentioned in § 1, of does not hold in general. The writer wishes to study some simple cases that may be considered to approximate fairly well to the general one, and point out that some data are required to be measured experimentally for the interpretation of complicated experimental facts about the saturation values of alloys.

§ 3. Magnetic Properties in the Simplest Case where $\nu(\varepsilon) = \text{const.}$

One of the simplest cases is that $\nu = \text{const}$, which case shall be worked out in detail. This model is realized approximately fairly well in the ease of Ni and its alloys, as we shall see below. Following Stoner's satistics, x may be determined by the following simultaneous equations:

$$x = \frac{kT}{2E_0}[F(\eta+\beta) - F(\eta-\beta)] \tag{3 1}$$

$$\frac{n}{N} = \frac{kT}{2E_0}[F(\eta+\beta) + F(\eta-\beta)] \tag{3.2}$$

where $$\beta = \frac{JNx}{2LkT}, \tag{3.3}$$

and $$F(\eta) = \int_0^{\frac{E_0}{kT}} \frac{d\xi}{1+\exp(\xi-\eta)}. \tag{3.4}$$

E_0 denoting the energy at the top of the band.

Simple calculation yields, in the limit $\beta \to 0$ ($T \to \theta$, θ; Curie point),

$$\exp\left(\frac{nE_0}{Nk\theta}\right) = \frac{1+\exp(\eta)}{1+\exp\left(\eta - \frac{E_0}{k\theta}\right)}, \quad \text{and}$$

$$\frac{2LE_0}{JN} = \frac{1}{1+\exp(-\eta)} - \frac{1}{1+\exp\left(-\eta + \frac{E_0}{k\theta}\right)}. \tag{3.5}$$

and then we can determine θ by solving those simultaneous equations for θ and η.

In the case $\frac{n}{N} = \frac{1}{2}$, (3.3) reduces to

$$\frac{k\theta}{E_0} = 1 \Big/ \left[\log\left(\frac{1+(2LE_0/JN)}{1+(2LE_0/JN)}\right)\right]. \tag{3 6}$$

In Tab. I and Fig. 5, θ is reprerented as a function of $\frac{n}{N}$ and $\frac{2LE_0}{JN}$. We can see from (3.5) that Hirone's formula $\theta = \frac{nJ}{2kL}$ is valid when $(1+\exp(-\eta))^{-1} \sim \frac{2LE_0}{JN} \ll 1$, so that the exchange integral is sufficiently large.

In the following discussion, we shall assume that $E_0/kT \gg 1$ which is valid for most cases. Hence, from (3.4), it follows

$$F(\eta) \simeq \int_0^{\infty} \frac{d\xi}{1+\exp(\xi-\eta)} = \log(1+\exp(\eta)). \tag{3.7}$$

If we eliminate η from (3.1) and (3.2) we obtain

$$\exp\left(\frac{JNx}{LkT}\right) = \frac{\exp\left\{\frac{E_0}{kT}\left(\frac{n}{N}+x\right)\right\}-1}{\exp\left\{\frac{E_0}{kT}\left(\frac{n}{N}-x\right)\right\}-1}. \tag{3.3}$$

In the case where $\frac{nE_0}{NkT}$ or $\frac{(1-n)E_0}{NkT} \ll 1$ (3.8) reduce to Hirone's:

$$x = nN\,\text{tgh}\left(\frac{JNx}{2LkT}\right). \tag{3.9}$$

We shall call this case "the classical limit."

In the opposite case where $\frac{nE_0}{NkT}$ or $\frac{(1-n)E_0}{NkT} \gg 1$ it reduces to

$$J = \frac{2LE_0}{N}, \tag{3.10}$$

and x cannot be determined. This limit may be called "Fermi-Dirac" limit and (3.10) represents the critical value of J for the occurrence of ferromagnetism.

If we denote the Curie-Weiss constant by C, we obtain

$$C = \frac{n\mu^2}{k}\left(\frac{\theta}{Jn/2kL}\right)(1+\exp(\eta_0)), \tag{3.11}$$

where η_0 denotes the value of η at $T = \theta$. In the classical limit $\theta \to \frac{Jn}{2kL}$, $\eta \to -\infty$ and $C \to C_H = \frac{n\mu^2}{k}$, so that

$$\frac{C}{C_H} = (1+\exp(\eta_0))\left(\frac{\theta}{Jn/2kL}\right)^2. \tag{3.12}$$

From the observed value of C we can obtain the value of the right hand side of (3.12), which is merely a function of η_0 or $\frac{2LE_0}{Jn}$ represented in Fig. 6. Consulting with the computed curves in Fig. 6

Tab. I.

The value of $\frac{k\theta}{E_0}$ as a function of $\frac{n}{N}$ and $\frac{2LE_0}{JN}$

$\frac{2LE_0}{JN}$ \ $\frac{n}{N}$	0.1	0.2	0.3	0.4	0.5	0.6	0.7	0.8	0.9
0.1	0.892	1.584	2.091	2.392	2.492	2.392	2.091	1.584	0.892
0.2	0.434	0.783	1.033	1.183	1.233	1.183	1.033	0.783	0.434
0.3	0.284	0.509	0.674	0.763	0.806	0.763	0.674	0.509	0.284
0.4	0.197	0.363	0.490	0.565	0.590	0.565	0.490	0.363	0.197
0.5	0.144	0.276	0.375	0.435	0.455	0.435	0.375	0.276	0.144
0.6	0.109	0.213	0.294	0.352	0.361	0.352	0.294	0.213	0.109
0.7	0.083	0.168	0.232	0.274	0.288	0.274	0.232	0.168	0.083
0.8	0.062	0.125	0.179	0.216	0.228	0.216	0.179	0.125	0.062
0.9	0.043	0.087	0.131	0.159	0.170	0.159	0.131	0.087	0.043

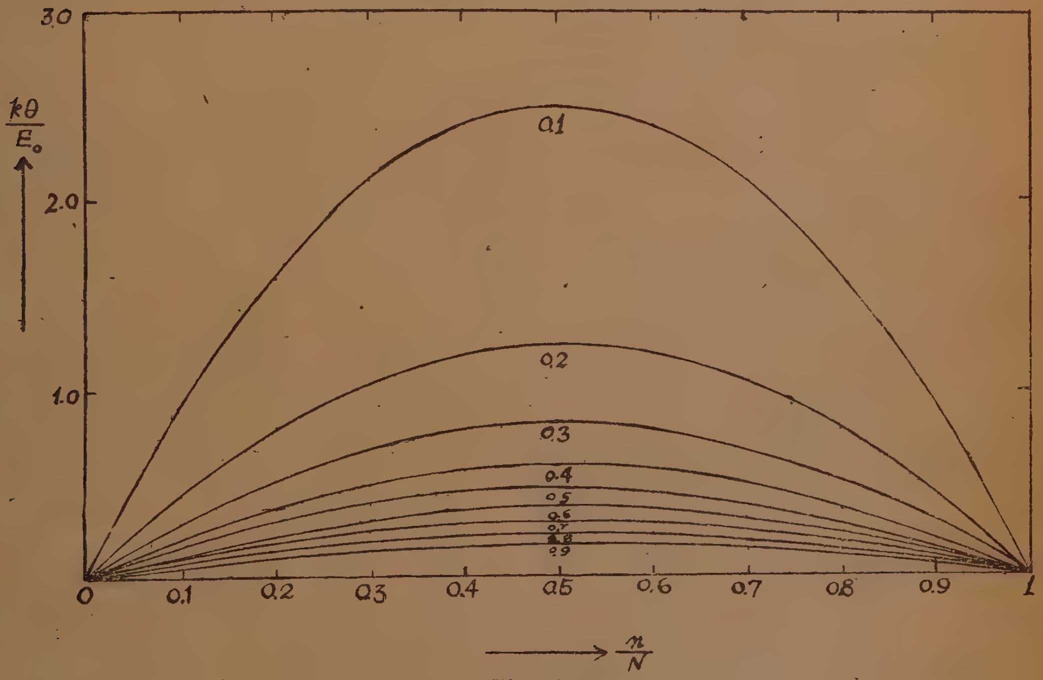

Fig. 5.

Tab. II.

Process of obtaiding E_0 and J from C and θ.

	C_H	C	$(1+\exp(\eta_0))\left(\frac{\theta}{Jn/2kL}\right)^2$	$\frac{2LE_0}{JN}$	$\frac{Nk\theta}{nE_0}$	$\left(\frac{Nk\theta}{n}\right)_{obs}$	E_0	J
Ni	0.227	0.321	1.414	0.88	0.50	1.44×10^{-12}	2.83×10^{-12}	6.63×10^{-13}
Co	0.646	1.23	1.904	0.925	0.37	$1.12\times$,,	$3.03\times$,,	$6.48\times$,,
Fe	0.839	1.27	1.513	0.89	0.45	$0.53\times$,,	$1.18\times$,,	$2.64\times$,,

we can now determine the values of $\frac{2LE_0}{JN}(A)$ inversely, from which we can obtain $\frac{k\theta}{n}$ by using (3.12) again. On the other hand $\frac{k\theta}{E_0}(B)$ is given by the curves in Fig. 5 and from (A) and (B) we can obtain the band-width and J simultaneously. Several examples are shown in Tab. II.

§ 4. Conclusion.

As shown above we can evaluate the width of the band and the exchange integral from the measurements of θ and C, and hence derive the characteristic properties that are associated with the saturation magnetization and n. Unfortunately, there are available data of C only for Ni-alloys. The writer wishes to emphasize the importance of such measurements of C for other materials since the results obtained above will be much affected by the shape of the energy band, we have not to overestimate the reliability of our results mentioned above for the theoretical discussion of the experimental data. When the detailed informations about the shape of the band will be obtained in the future, then we will be able to give more complete account of the phenomena under consideration.

Finally the writer wishes to express his sincere thanks to Dr. Honda and Dr. Hirone for their generous guidance for this work and to Dr. Miyahara for his valuable advices.

References.

(1) Stoner, E. C.: Proc. Roy. Soc. A **165** (1938), 372; Proc. Roy. Soc. A **169** (1939), 339.

(2) Hirone, T.: Sci. Rep. Tohoku. Imp. Univ. **21** (1938), 101.

(3) Fallot. M.: Ann. d. Phys. 10. Ser. **6** (1936), 305.

(4) Pauling, L.: Phys, Rev. **54** (1938), 899.

(5) Niessen, K. F.: Physica. **3** (1941), 377.

(6) Miyahara, S.: Progress in Quantum Physics. 1. Ser. 1946 (in Japanese) 484. Progress of Theoretical Physics **2** (1947), 25.

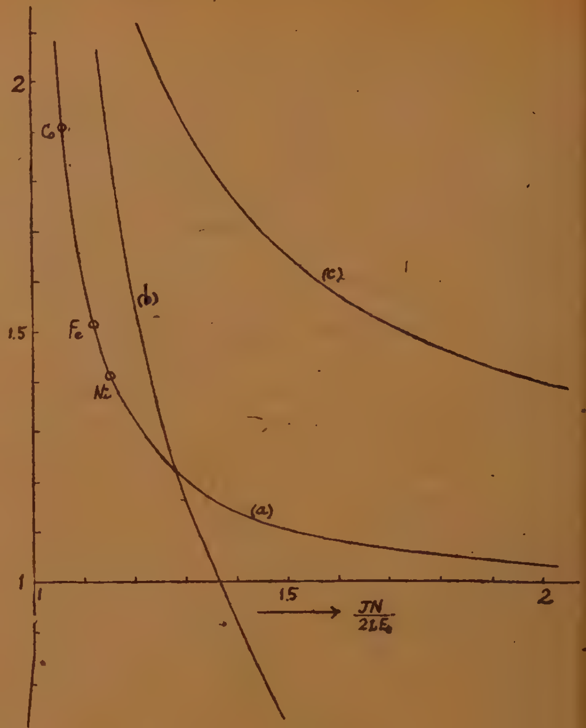

Fig. 6.

Several constants as functions of $JN/2LE_0$.

(a) $(1\times\exp(\eta_0))\left(\frac{\theta}{Jn/2kL}\right)^2$. (b) η_0.

(c) $\frac{Jn/2kL}{\theta}$.

On Abnormal Melting of Raw Rubber.

By Akira ISIHARA.

Department of Physics, University of Tokyo.

(Received July 4, 1947)

Abstract.

The experimental results on the abnormal melting of crystallized raw rubber by Wood and Bekkedahl are theoretically studied. The effect can be explained by the fact that the relaxation time for the thermal expansion of the crystalline particles differs from that of the amorphous particles. At the point where the melting begins, the time interval of observation becomes comparable to the relaxation time of amorphous particles. The point will become higher when the time rate of heating increases, and also when the relaxation time itself becomes larger. The point at which the melting completes itself is determined by the relaxation times of amorphous and crystallized state, heating rate and previous history. This effect will become remarkable at a suitable heating rate, and will be more remarkale in natural rubber than vulcanized rubber.

§ 1. Introduction.

It is a well known fact that the amorphous state of raw rubber exists as a supercooled metastable state even at a considerable low temperature[1), 2)], and this fact was already explained by us using statistical mechanics[3)]. But N. Bekkedahl and others[4), 5)] found recently a very peculiar fact on the raw rubber in this state; that is, not only the time rate of crystallization but also the melting range is different according to the temperature at which crystallization occurs. They suggest that the reason why the melting points previously determined by various investigators spread widely, and that the β-anomaly of Ruheman and Simon[6)], and other queer facts may have their origin in this fact.

As this phenomenon is so strange and it seems no explanation has been offered as yet, I wish to offer some interpretation in the next paragraph. In this paper I wlll discuss only the abnormal melting, because the main properties of eryctallization of super-cooled raw rubber seems to be the same as in other substances, even if the details are different between them.

§ 2. The Melting of Crystallized Raw Rubber.

A sample of raw rubber annealed at 55°C is brought quickly to a temperature of crystallization (in Fig. 1, −32°C, −17°C, 1°C, 14°C) and crystallized there: its specific volume decreases about 2 present. When the crystallization is completed, the temperature is raised at the rate of about 0.5°C per minute, then its specific volume increases first linearly along the straight line characteristic to the crystalline state (Fig. 1)[5)].

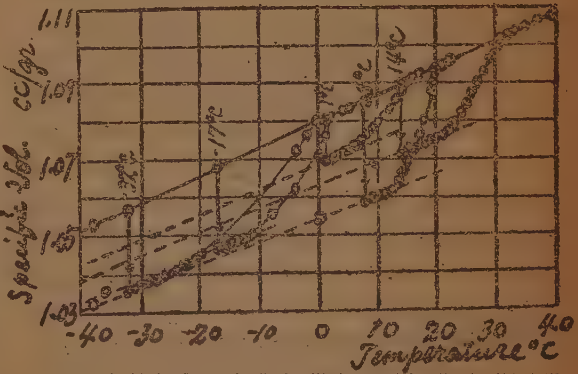

Fig. 1. Melting of crystallized raw rubber.

At about 5 degrees above the crystallization temperature, almost suddenly it deviates upward from the straight line. Finally when it reaches the upper straight line characteristic to the amorphous state, melting comes to the end.

The poits where the melting starts and is completed are the function of the temperature of crystallization, and independent of the degree of crystallization. This relation is shown in Fig. 2[5)].

The cause of this phenomena which is immediately noticed is the existence of many crystal grains in the crystalline state whose size and melting points are different according to the temperature at which they were formed.

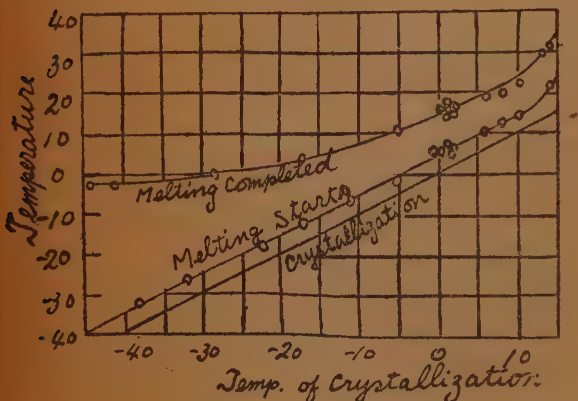

Fig. 2. The melting range of crystallized raw rubber as a function of the temperature of crystallization.

But this does not seem to be the case; because when we cease to raise the temperature recrystallization occurs. This shows that the true thermodynamical equilibrium state is not the partially melted state but the completely crystallized state. Moreover, the experiment of Ruheman and Simon[6] shows that the β-anomaly, which is clearly associated with this abnormal melting as indicated by L. A. Wood[7], is not reproducible. The authors state: "In contrast to the α-anomaly the β-anomaly was not strictly reproducible. Depending on the speed of heating as well as the previous cooling the curve is steeper or flatter. Also the energy, that is the area under the curve, was different in different measurements." In this concern, it may be noticeable that the melting curves in Fig. 1 do not resemble the typical S curve of crystallization (even if the abscissa is changed), and the melting points of paraffin homologues converge about 400°K at relatively low polymerization.

§ 3. Theory of Abnormal Melting.

The first problem concerning the melting phenomena is whether they are the thermodynamical equilibrium phenomena or some rate effects. Bekkedahl states: "It was found in preliminary experiment that at a heating rate of 0.5°C per minute or less no observable differences from the equilibrium values of the volume could be noted, and there was found to be no evidence of time lag or delay in melting of the crystals after the establishment of thermal equilibrium. For example, at any constant temperature in the melting range the volume was not observed to increase with time. In this range if the temperature is lowered, the volume-temperature relation is observed to be linear and intermediate between the amorphous and crystalline volumes. Rubber in the partially-melted state, however, can undergo additional crystallization with a resulting decrease of volume."

We can not see under what kind of conditions the preliminary experiment was performed, but it can be understood that the true thermodynamical equilibrium state is not in the partially-melted state but in the crystalline state in this range. In the previous paper[1] the volume temperature curve of amorphous state deviates from the straight line at the heating rate of 0.02–0.03° per minute, at about —25°C and approaches to that of the crystalline state. On the other hand the experiment of Ruheman and Simon shows the influence of heating rate as stated above. In the experiment of Bekkedahl and others the heating rate seems to be about 0.5°/min. (The whole time needed to cover the 10°C of melting range was about 20–30 minutes.)

But a high polymer shows relaxation in thermal expansion. For example the relaxation time of polystyrene is about 5 minutes, and the approach to the equilibrium value is nearly exponential.[8] Accordingly the relaxation effect must be taken into consideration in the present subject.

Now there may exist amorphous particles or amorphous nuclei in crystalline particles—the kinetic units of crystallization and melting are not molecules themselves but "segments", here we call them simply particles—similarly as we consider the crystalline nuclei in the amorphous particles, and the relaxation times of both states must be different; the former may be smaller, as the state of it resembles that of a gas.

Then if we raise the temperature at a suitable heating rate a the amorphous particles denoted by A_1, A_2, in Fig. 3 may expand more rapidly than the other crystalline parts C_1, C_2, C_3 and compress at that moment such parts as C_2 held between A_1 and A_2 and will "buckle" them, and consequently melting takes place. The force acting there is of course not isotropic pressure. If we keep the temperature constant at that point, this scheme of melting stops and they will fall into equilibrium crystalline state. At first, melting may be very slow, as the amorphous particles in crystalline state or amorphous nuclei are very small in number, and therefore the recrystallization is comparatively predominant over the expansion of volume. But it will become more remarkable according as the temperature rises and the number of amorphous particles as well as their mobility (in comparison with that of crystalline particles) increases. But when the melting is nearly completed, the stress will become very small again as the outer surface is free, and the volume approaches asymptotically to that of the amorphous state.

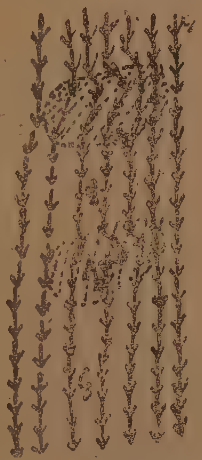

Fig. 3. Schematic representation of amorphous nuclei in crystallized particles.

To treate these phenomena quantitatively, we denote by v_0 the average volume of an amorphous nucleus at crystallization temperature T_c, and by α its thermal expansion coefficient. Then its equilibrium volume at temperature T is given by $(1+\alpha(T-T_c))v_0$. But when we raise the temperature at a suitable heating rate its volume does not reach this value when the temperature becomes T. We denote this actual volume by v. Then, thereafter, it approaches the above equilibrium value with relaxation time λ nearly exponentially. Therefore, the volume-increase δv after the moment when the temperature reaches T is given by

$$\{1+\alpha(T-T_c)v_0-v(T-T_0)\}\{1-e^{-\frac{\delta t}{\lambda}}\}=\delta v. \quad (1)$$

Here λ may be represented as follows:

$$\lambda=\lambda_0 e^{\frac{Fa}{kT}}. \quad (2)$$

For convenience we denote:

$$\left.\begin{aligned} T-T_c&=\tau, \\ a&=\frac{dT}{dt}. \end{aligned}\right\} \quad (3)$$

Then the differential equation determining the volume-temperature relation is (by expanding exp $\left(-\frac{\delta t}{\lambda}\right)$)

$$\frac{dv}{d\tau}=\frac{1+\alpha\tau}{a\lambda}v_0-\frac{v}{a\lambda}. \quad (4)$$

This equation resembles ordinary relaxtion equation, but not exactly, because in this case the final volume continuously changes with temperature or with time.

To integrate this equation we assume that the variation of λ with temperature is small compared with that of $\frac{\tau}{a}$, and take it constant for the moment. Such an approximation may be sufficiently accurate at least when the temperature is high enough. As the heating rate is constant, we obtain

$$v=v_0\{1+\alpha\tau-\alpha a\lambda(1-e^{-\frac{\tau}{a\lambda}})\}. \quad (5)$$

The meaning of this equation is obvious.

Then we consider a hole in orystalline particles surrounding these amorphous volume v as in Fig. 4.

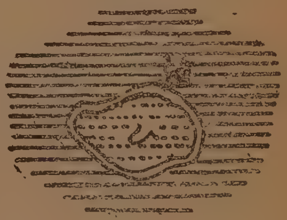

Fig. 4. Amorphous nucleus and the surrounding crystalline hole. The volume of each state is designated by v and v_h respectively.

It expands with relaxation time μ:

$$\mu=\mu_0 e^{\frac{Fc}{kT}}. \quad (6)$$

The equilibrium volume of the hole is attained when its volume reaches that of the amorphous nucleus. Then we obtain, as in the case of eq. (4), the differential equation determining the volume of the hole:

$$\frac{dv_h}{d\tau}=\frac{1+\alpha\tau}{a\mu}v_0-\frac{v}{a\mu}. \quad (7)$$

If the expansion of hole were not rapid enough, it may be overcome by the expansion of the amorphous particles. But in reality there takes place the melting before such events occur. This process of "invasion" by amorphous particles is perhaps a rapid reaction and reveals no time lag. We assume the rate is proportional to the difference between the time rates of thermal expansions of two states, that is

$$\frac{dn}{d\tau} = Kn\left\{\frac{dv}{dt} - \frac{dv_h}{dt}\right\}, \qquad (8)$$

where n is the total number of amorphous particles, K is a proportional constant. In this equation we also have assumed that the melting becomes more effective as the amorphous particles increases. Then to the same approximation as in equation (5), we obtain

$$n = n_c \exp\left[K\left(1-\frac{\lambda}{\mu}\right)v_0\{\tau - a\lambda(1-e^{-\frac{\tau}{a\lambda}})\}\right]. \qquad (9)$$

Here n_c is the number of amorphous particles at T_c.

If $\lambda=\mu$ or $K=0$, $n=n_c$ as naturally expected. Particularly, if τ is small

$$v = v_0\left(1+\frac{a\tau^2}{2a\lambda} - \frac{a\tau^3}{6(a\lambda)^2} + \cdots\right), \qquad (10)$$

$$n = n_c\left\{1+K\left(1-\frac{\lambda}{\mu}\right)v_0\left(\frac{\tau^2}{2a\lambda} - \frac{\tau^3}{6(a\lambda)^2} + \cdots\right)\right\}. \qquad (11)$$

The point T_i where the melting starts can be obtained by equating the second derivative of the right hand member of equation (11) to zero:

$$\tau_i = T_i - T_c = a\lambda, \qquad (12)$$

or

$$\frac{T_i - T_c}{a} = \lambda. \qquad (13)$$

That is, the melting starts when the time interval of observation approaches the relaxation time λ. In this equation the temperature contained in the expression of λ must be taken to be the mean value of T_c and T_i, but the difference may be negligible even if we take it for T_c. Then

$$\log(T_i - T_c) = \log a\lambda_0 + \frac{E_a}{kT_c}. \qquad (14)$$

This relation is shown in Fig. 5.

From this figure we obtain:

$$a\lambda_0 = 5.3. \qquad (15)$$

Accordingly if the heating rate a is 05°/.min.,

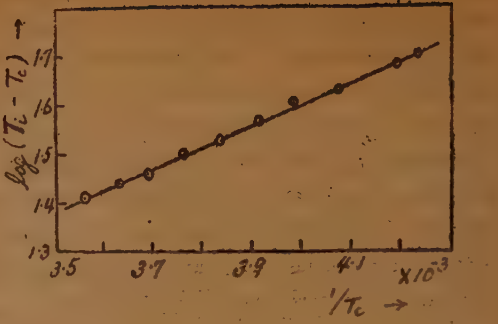

Fig. 5. Relation between the temperature of crystallization and the point where the melting starts. The circles show the experimental data from Fig. 2.

$$\lambda_0 = 10.6 \text{ min.} \qquad (16)$$

This value seemes to be plausible. Also the activation energy E_a is found to be 4.4 k, but this value in not reliable since we used the approximation that the variation of λ with temperature is small.

It is said that the apparent second order transitions of polystyrene[3] and other high polymers occur when the time interval of observation becomes comparable to the relaxation time[5]. In this case only one state comes into the question and only the relation (10) is necessary, and the conclusion analogous to the above statement can be deduced.

The point T_f where melting completes itself is determined by the condition that the number of amorphous particles becomes equal to N—the total number of particles. In this case the last term of the equation (9) can be neglected, and if we put

$$A = K\left(1-\frac{\lambda}{\mu}\right)v_0, \qquad (17)$$

then the temperature is given by

$$N = n_c \exp[A(\tau_f - a\lambda)], \qquad (18)$$
$$\tau_f = T_f - T_c.$$

In these equations v_0 is the volume at temperature T_c, but the error will be negligible even if we take it to be independent of T_c.

To determine the explicit dependence of τ_f on T_c, we must determine n_c as a function of crystallization temperature. This dependence can be obtained as follows.

The amorphous particles or nuclei are oscillating of course with frequencies different from those of crystalline particles surrounding them. For simplicity we take Einstein model for each state and designate the characteristic frequencies of the amorphous and crystalline state as ν', and ν respectively. If we denote by W the work to be done to produce an amorphous particle in crystalline state, then the partition function Z of the whole system can be written down as follows:

$$Z = e^{-\frac{nW}{kT}} \frac{1}{(1-e^{-\frac{h\nu}{kT}})^{3(N-n)}} \frac{1}{(1-e^{-\frac{h\nu'}{kT}})^{3n}} \frac{N!}{n!(N-n)!}; \tag{19}$$

From this we can determine the equilibrium value of n as a function of temperature by minimising the free energy calculated from the above equation. If the temperature is high we can thus obtain approximately,

$$\frac{n}{N} = \gamma e^{-\frac{W}{kT}}, \tag{20}$$

where $\gamma = \nu/\nu'$.

The amorphous particles increases according to equation (20) as the temperature increases. But when we raise it at some heating rate they will not immediately reach this value, especially in such substances as rubber. Because, for the occurence of it, molecules must move as a whole, and this is difficult particularly in high polymers. Accordingly, we can express in this case equation (20) as follows:

$$n = n_0 e^{-\frac{W}{kT_c}}, \tag{21}$$

where n_0 is a constant independent of T_c.

From equations (18) and (21) we obtain

$$T_f = T_c + a\lambda + \frac{W}{AkT_c} + \frac{1}{A} \log \frac{N}{n_0}, \tag{22}$$

where A is a function of temperature according to equation (17) but we can neglect this variation according to the above assumption. Therefore, $(T_f - T_c - a\lambda)$ vs. $1/T_c$ must be linear (Fig. 6). This linearity is in accordance with experiment particularly at higher temperatures. The deviation at lower temperature is legitimate. As in this case the melting range is very wide (cf. Fig. 2) and the variation of the relaxation time with temperature is great; the above assumption fails. Also the determination of the end-point itself is rather difficult owing to the recrystallization, and the experimental error due to this fact may give some influence upon the result. At any rate the theory is more accurate at higher temperature, and the calculated melting curve is shown by heavy curve in Fig. 7 as an example. The calculated curve represents the experimental one fairly well, although this seems rather unimportant.

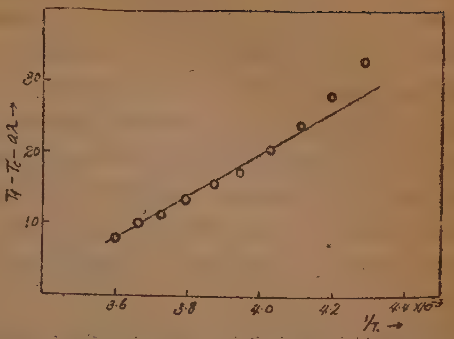

Fig. 6. Relation between the crystallization temperature and the point where the melting completes. Circles show the experimental data from Fig. 2.

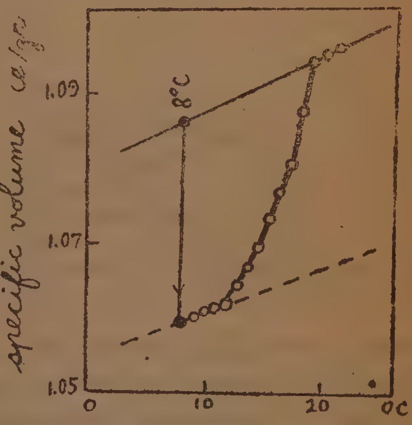

Fig. 7. Melting curve of the sample crystallized at 8°C. The heavy curve is the theoretical.

It must be noted that we have determined the end-point in a somewhat different way compared with the starting point. It was determined by using equation (21), and the temperature in this equation represents that which gives the equilibrium number of amorphous nuclei. If we crystallize a sample of amorphous rubber at some temperature or cease the crystallization by the way and bring it to another temperature and keep there for a time interval comparable to the time needed for the first crystallization, then the distribution of amorphous nuclei may be a function of both temperatures. In other words it has a hysteresis character. Also the starting point itself may become more complicated in such a treatment. Because the deviation from equilibrium value sets in when the time interval of observation becomes comparable to the relaxation time, but there may be various kinds of relaxation time in the case of such a treatment. The "stark rubber" may be the case.

As the last explanation shows, the end-point was not merely the point where the time interval of observation becomes comparable to the relaxation time of hole μ, but it is determined by this quantity at any rate, and the melting range itself seems to be the domain between the curve λ and μ—the shaded part in Fig. 8. In the figure the straight line passing through T_c represents the time of observation.

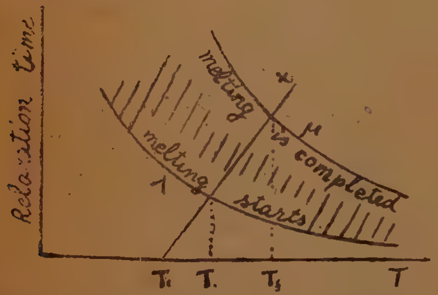

Fig. 8. Physical meaning of the melting range shown in Fig. 2.

Another attention may be drawn: Firstly, the right hand side of equation (13) does not depend on the degree of crystallization, and this is also approximately true for the end-point, in accordance with the experimental result. Secondly, if we raise the heating rate, the starting point will become higher and the melting curve itself will become steeper. Thirdly, if these ideas are correct, these phenomena may be more remarkable in raw rubber than in vulcanized rubber, as the difference of the two relaxation times and the relaxation times themselves in the former may be greater than those in the latter. Finally, it is not suitable to the actual situation that we have neglected the recrystallization, particularly when the heating rate is very small. When we raise the temperature very slowly the sample may expand merely with the expansion coefficient of crystalline state (the effect of amorphous nuclei is very small) and the "invasion" by amorphous nuclei will not appear. If the heating rate is very large and the crystalline sample is brought as it was to the range in which the state of amorphous rubber is more stable than the crystalline, i. e. to the range above the "true melting point," the sample will melt there independently of its crystallization temperature. In other words the phenomena discovered by Bekkedahl take place most remarkably at a suitable heating rate.

I hope that these conclusions will be put into experimental test.

In conclusion, I wish to express my hearty thanks to Professor T. Sakai for his kind guidance, and also T. Saito, R. Kikuchi and K. Ichimura for the valuable discussion on the present subject.

References.

(1) N. Bekkedahl: J. Res. Nat. Bur. Stand., **13** (1934), 411.
(2) Ibid. **15** (1935), 503.
(3) T. Sakai and A. Isihara: Ōyobuturi, **15**, (Showa 21), 1.
(4) N. Bekkedahl and L. A. Wood: Jour. Chem. Phys. **9** (1941), 193.
(5) L. A. Wood and N. Bekkedahl: Jour. App. Phys. **17** (1946), 362.
(6) M. Ruheman und F. Simon: Zeits. Phys. Chem. A. **138** (1928), 1.
(7) L. A. Wood: Jour. Chem. Phys. **10** (1942), 403.
(8) R. S. Spencer and R. F. Boyer: Jour. App. Phys. **17** (1946), 398.
(9) T. Alfrey, G. Goldfinger and H. Mark: Jour. App. Phys. **14** (1943), 700.
R. F. Boyer and R. S. Spencer: Jour. App. Phys. **15** (1944), 398; **16** (1945), 594.

High Precision Nomogram.

By Isao Osida.

Department of Dynamics, Faculty of Engineering, University of Nagoya.

(Received July 11, 1947)

Part I.

(This part was read on Nov. 18, 1944 at the monthly meeting of the Physico-Mathematical Society of Japan).

In spite of the great easiness of the use, the application of alignment charts is still restricted on account of their low precision. In general, it is very difficult to get a precise result exceeding three significant figures from the reading. Of course, the preparation of a very large nomogram or of many charts each corresponding to a narrow range of variation of the presenting quantities is unquestionably effective to obtain higher precision, but both of them are awkward in practice. The present author will show in the following that a nomogram belonging to a certain type can be transformed into far more precise one expressed by a single, handy chart, which enables us to have even five significant figures.

At first, we consider an alignment chart consisting of three parallel straight lines a, b and c, which is shown in Fig. 1. The base line g intersects them at points A_0, B_0 and C_0 respectively, satisfying $A_0C_0 : C_0B_0 = m : n$. The chart remains equivalent when a, b and c are moved parallel to themselves on the line g and when A_0C_0 and B_0C_0 are changed in their length keeping the ratio $m : n$ constant.

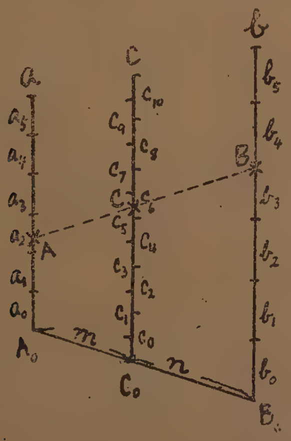

Fig. 1

We divide a, b and c into equal sections, beginning at the origins A_0, B_0 and C_0 having the lengths ms, ns and $\frac{mn}{m+n}s$ respectively, where s is an appropriate length, and name the segments in order $a_0, a_1, a_2, \cdots\cdots;\ b_0, b_1, b_2, \cdots\cdots;\ c_0, c_2, c_4, \cdots\cdots$, respectively. As for the scale c, we designate by c_1 the part extending from the middle of c_0 to the middle of c_2, and by c_3 the part from the middle of c_2 to that of c_4 etc.

Now we draw a straight line AB intersecting the scale c at point C. If A is on segment a_i and B is on b_j, then the point C is obviously on segment c_{i+j}. Then we cut off each segment $a_0, a_1, \cdots\cdots;\ b_0, b_1, \cdots\cdots;\ c_0, c_1 \cdots\cdots$, arrange them parallel to each other with one of the ends on a straight line (Fig. 2) and denote the spacing between a-scales $m\tau$, that between b-scales $n\tau$ and that between c-scale $\frac{mn}{m+n}\tau$ respectively, where τ is any length, as shown in Fig. 2. Moreover let the distance between the scales a_0 and c_0 be mp, and that between c_0 and b_0 be np, where p is any length, then (distance between a_i and c_{i+j}):(distance between c_{i+j} and b_j)

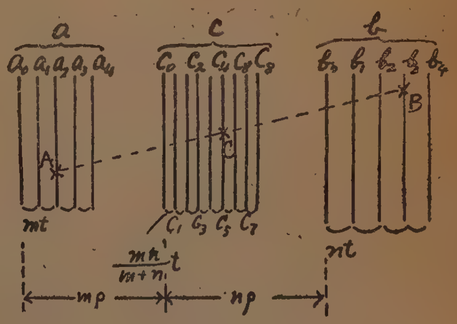

Fig. 2

$$= \left[mp+\frac{mn(i+j)\tau}{m+n}-im\tau\right] : \left[(m+n)p+jn\tau-pm-\frac{mn(i+j)\tau}{m+n}\right]$$

$$= m\left[p+\frac{jn\tau-im\tau}{m+n}\right] : n\left[p+\frac{jn\tau-im\tau}{m+n}\right]$$

$$= m : n$$

Thus, the operation reading the needed quantity, in the rearranged figure, from the intersection point of the scale c_{i+j} and a straight line combining one point on a_i and another on b_j is justified.

Accordingly, as far as we obey the rule "If one of given quantities falls on a_i and another on b_j, then the reading must be done on c_{i+j}", Fig. 1. can be replaced by Fig. 2.

Such transformation enables us to take a very long alignment chart consisting of three parallel straight lines of convinient size. For instance, it is not easy task to make or use a nomogram of 10 metre long, but if we divide it into 20 segments, each of them being 50 cm. long, it can be received into an ordinary graph paper. If we can distinguish the position of a point up to 0.3 mm., the relative error of this diagram becomes $\frac{0.3\text{ mm}}{10000\text{ mm}}=3\times10^{-5}$, which is comparable to that of five-place logarithmic tables.

Fig. 3. shows a multiplication chart $uv=w$. The logarithmic scales a, b and c of the three variables u, v and w each being of 1 metre long are divided into six sections of 17 cm. long, under the conditions $m=n$, $\tau=1$ cm and $p=6.5$ cm. We can apply the above method to all the chart of the same type, expressing the relation $f(u)+g(v)=(w)$ among three variables u, v and w. The method are also applicable to the alignment chart expressing the relation between more than four

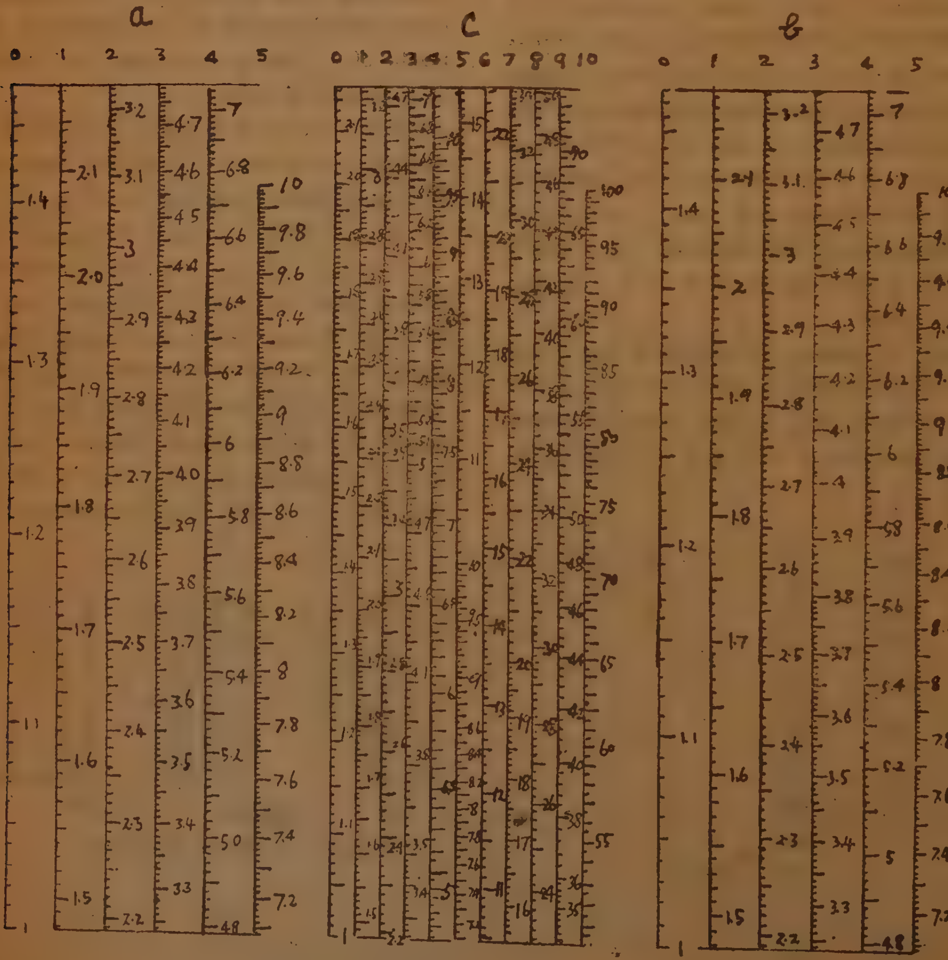

Fig. 3

quantities, if it can be resolved to the three-parallel-straight-line type.

The writer expresses his thanks the Hattori Hōkō Kai for the financial support, and also to Miss. M. Fukazu for her help to prepare the diagrams.

Part II.

(This part was read on May 11, 1947 at the annual meeting of the Physical Society of Japan).

The writer has reported in the previous part on a new type of high precision nomograms. In the following, the result of the test of the real accuracy of a such a nomogram are reported, which will serve as a reference for constructing such a sort of nomograms.

As an example, we took Fig. 3. and carried out 30 multiplications of two numbers both of them being of four figures and being arbitrarily chosen, and have compared the result w' with the precise one w_0 computed by an arithmometer. The mean and the standard deviation of the relative errors $\frac{w'-w_0}{w_0}$ were fonnd to be

$$(-4.3\pm63.3)\times10^{-5}$$

respectively. The former is very small compared with the latter, the systematic error seems to be negligible. The standard deviation corresponds to the linear dimension about 0.3 mm. on the c scales.

The same calculations were put forth by a 10″ (25 cm) slide rule, and

$$(-5.0\pm63.0)\times10^{-5}$$

was found as the corresponding figure. This is almost equal to the above result, but the unit of the scale of such a slide rule is one-half of the c-scale of Fig. 3, the standard deviation 63×10^{-5} corresponds to 0.16 mm in length on the sliding scale.

For the sake of comparison, the same multiplications were performed by the four place logarithmic table. The mean and the standard deviation were found to be

$$(+1.3\pm16.5)\times10^{-5}.$$

Neglecting the small value $+1.3\times10^{-5}$ which comes from the accidental fluctuations, the standard deviation is about one-fourth of the above two cases. Thus we know, if the accuracy of a nomogram is proportional to its length, that we must prepare such a nomogram of 4 metres in its total length to have the same accuracy as the four decimal logarithmic tables, and that of 40 metres as the five decimal logarithmic tables. The latter is not impossible to realize if the scale divided for instance into 50 sections, each of them being 80 cm. long.

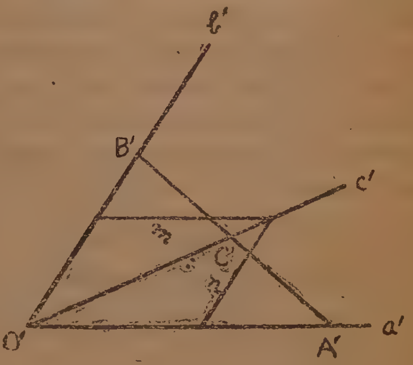

Fig. 4

The application of our method is not confined to the nomograms which consist of three parallel lines, but is also available for the other types of nomograms which can be derived from the above mentioned type by a projective transformation. This is obvious because by a projective transformation a straight line is always transformed to a straight line. We consider an example in the following.

Suppose that Fig. 1. is a nomogram expressing the relation

$$f(u)+g(v)=h(w)$$

and take the point C_0 as the origin, the line g as the X-axis and the c-scale as the Y-axis, so that they generally form oblique coordinates. If A, B and C are the points representing the quantities u, v and w respectively, the coordinates of them are

$$\mathrm{A}\begin{cases}x=-mp\\ y=mf(u),\end{cases}\quad \mathrm{B}\begin{cases}x=+np\\ y=ng(v),\end{cases}\quad \mathrm{C}\begin{cases}x=0\\ y=\dfrac{mn}{m+n}h(w)\end{cases}$$

respectively, where p means a length such that $p=\frac{A_0B_0}{m+n}$. Trying the projective transformation

$$x'=\frac{np-x}{(m+n)py},\qquad y'=\frac{x+mp}{(m+n)py}$$

we have

$$A'\begin{cases} x' = \dfrac{1}{mf(u)} \\ y' = 0 \end{cases} \quad B'\begin{cases} x' = 0 \\ y' = \dfrac{1}{ng(v)} \end{cases} \quad C'\begin{cases} x' = \dfrac{1}{mh(w)} \\ y' = \dfrac{1}{nh(w)} \end{cases}$$

respectively. These form a nomogram of three crossed straight line type and are shown in Fig. 4.

If the same procedure is applied to Fig. 2., the high precision type is obtained in the following way.

In Fig. 2., take the origin at the lower end of c_0 scale, combining the lower ends of the scales by x-axis ann make y axis coincide with c_0. Then the coordinates of the points A on a_i, B on b_j and C on c_k become

$$A\begin{cases} x = -mp + im\tau \\ y = mf(u) \end{cases} \qquad B\begin{cases} x = np + jn\tau \\ y = ng(v) \end{cases}$$

$$C\begin{cases} x = \dfrac{mn}{m+n}k\tau \\ y = \dfrac{mn}{m+n}h(w) \end{cases}$$

respectively. Applying the above projective transformation, these transform into

$$A'\begin{cases} x' = \dfrac{(n+m)\,p - im\tau}{m(m+n)\,pf(u)} \\ y' = \dfrac{im\tau}{m\,(m+n)\,pf(u)} \end{cases}$$

$$B'\begin{cases} x' = \dfrac{-jn\tau}{n\,(m+n)\,pg(v)} \\ y' = \dfrac{(m+n)\,p + jn\tau}{n(m+n)\,pg\,(v)} \end{cases}$$

$$C'\begin{cases} x' = \dfrac{np - \dfrac{mn}{m+n}k\tau}{mnph(w)} \\ y' = \dfrac{mp + \dfrac{mn}{m+n}k\tau}{mnph(w)} \end{cases}$$

respectively. These form together a nomogram of radial type. As an illustrative example, we take the relation

$$\frac{1}{u} + \frac{1}{v} = \frac{1}{w},$$

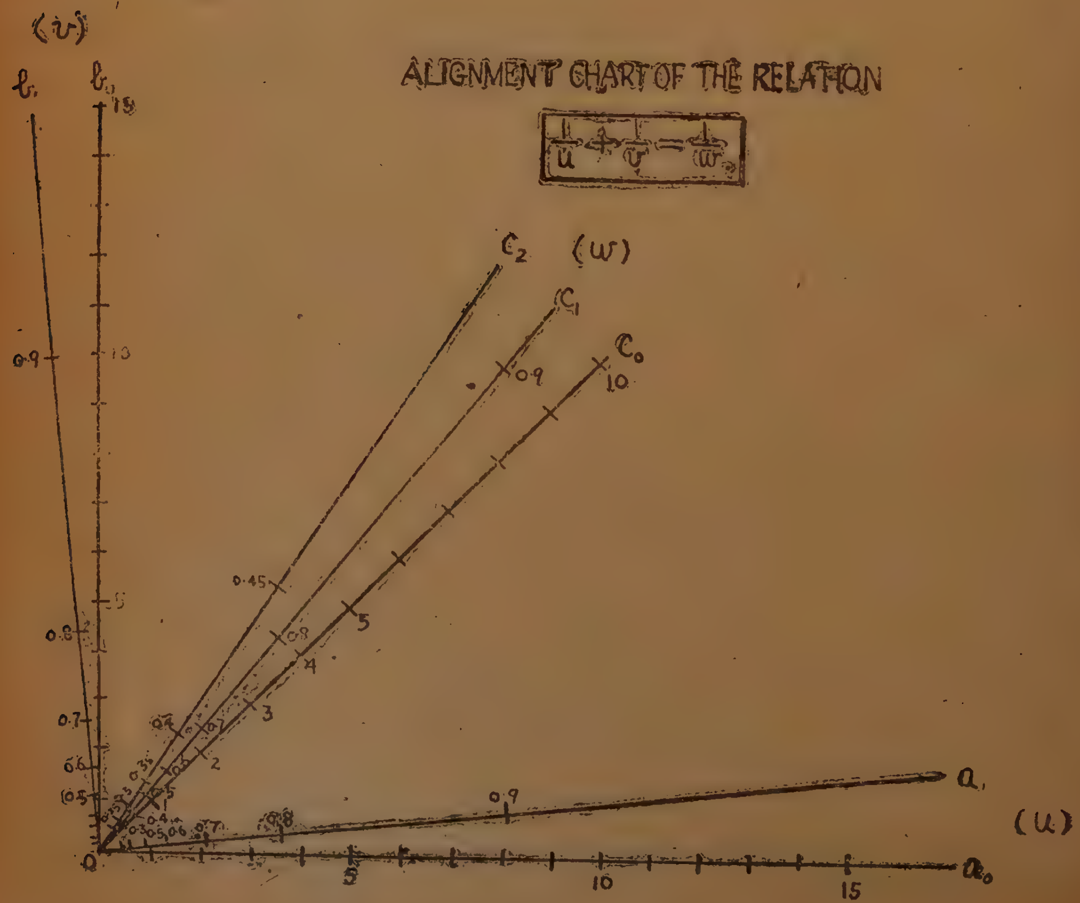

Fig. 5

namely $f(u)=\frac{1}{u}$, $g(v)=\frac{1}{v}$, $h(w)=\frac{1}{w}$. Let $m=n$ and

a_0 scale has the coordinates

$$x=-p,\qquad y=\frac{1}{u}$$

a_1 ,, ,,

$$x=-p+\tau,\qquad y=\frac{1}{u}-a$$

b_0 ,, ,,

$$x=p,\qquad y=\frac{1}{v}$$

b_1 ,, ,,

$$x=p+\tau,\qquad y=\frac{1}{v}-a$$

c_0 ,, ,,

$$x=0,\qquad y=\frac{1}{w}$$

c_1 ,, ,,

$$x=\frac{1}{2}\tau,\qquad y=\frac{1}{w}-a$$

c_2 ,, ,,

$$x=\tau,\qquad y=\frac{1}{w}-2a,\qquad \text{etc.}$$

these transform into

$$a_0'\begin{cases}x'=u\\ y'=0\end{cases}$$

$$a_1'\begin{cases}x'=\dfrac{2p-\tau}{2p}\,\dfrac{u}{1-au}\\[2ex] y'=\dfrac{\tau}{2p}\,\dfrac{u}{1-au}\end{cases}$$

$$b_0'\begin{cases}x'=0\\ y'=v\end{cases}$$

$$b_1'\begin{cases}x'=-\dfrac{\tau}{2p}\,\dfrac{v}{1-a\tau}\\[2ex] y'=\dfrac{2p+\tau}{2p}\,\dfrac{v}{1-av}\end{cases}$$

$$c_0'\begin{cases}x'=w\\ y'=w\end{cases}$$

$$c_1'\begin{cases}x'=\dfrac{2p-\tau}{2p}\,\dfrac{w}{1-aw}\\[2ex] y'=\dfrac{2p+\tau}{2p}\,\dfrac{w}{1-aw}\end{cases}$$

$$c_2'\begin{cases}x'=\dfrac{p-\tau}{p}\,\dfrac{w}{1-2aw}\\[2ex] y'=\dfrac{p+\tau}{p}\,\dfrac{w}{1-2aw}\end{cases}$$

respectively, Putting $p=5$, $\tau=1$ and $a=1$ we have Fig. 5. Its usage is the same as that of Fig. 3. This is somewhat advantageous if we deal with quantities less than unity, by the aid of a_1, b_1, c_1 and c_2 scales.

Unfortunately, our device is not applicable when the chart contains at least one curved line. It is eagerly hoped that a mighty method which transforms any type of nomograms into a high precision type will be found.

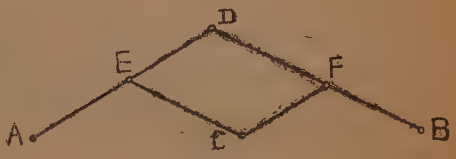

Fig. 6

Notes.

(1) Prof. Katuhiko Morita, Mathematical Institute, Kanazawa Higher Normal School, kindly called my attention to d'Ocagne's "fractionizing" method, dealing with similar problem, of which I was not aware at the time when the present work was done, D'Ocagne's method is cited in his famous book "Traité de Nomographie" published in 1899, and, on referring to the original text, his method, consisting of the use of doubly graduated scales and the mere superposition of the constituent. Accordingly, his method is, as he recognized, hardly applicable when the nomogram resolved into more than three parts owing to the appearance of so many supports, some of them being graduated in many folds, so that we are embarassed in construction or application. Moreover, he has never allude to the application of a projective transformation to them. However, strange to say, for a long time since the first touch of the great pioneer to the nomography no fundamental progress has been made in such an important problem. (cf. M. d'Ocagne, Traité de Nomographie, Paris 1988, pp. 150–157.)

(2) On reading the high precision nomograph of this type, there might occur some confusions that we may take wrong scales, for there are so many of them. In order to avoid the confusion and the trouble of adding the suffixes, the following apparatus can be conveniently used.

Two rods AD and BD are combined at D. Let the points dividing AD and DB in the ratio of $m:n$, be E and F respectively, that is

$$\frac{\mathrm{AE}}{\mathrm{ED}}=\frac{\mathrm{DF}}{\mathrm{FB}}=\frac{m}{n}.$$

Then we take two more rods EC and CF, being combined at their ends C and being equal to DF and ED respectively, and attach them to ADB so as to DECF becomes a parallelogram, as shown in Fig 6. It is easy to prove that A, C and B lie on a straight line and the ratio AC and CB equals to $m:n$. Thus, if A and B are laid on the right position of the nomogram such as shown in Fig. 2, then C comes also to the right position where we read the answer.

On Schaefer-Bergmann's Diffraction Diagrams of Vibrating Quartz Crystals, produced when they are observed in Directions not parallel to any of the Crystallographic Axes.

By Otohiko NOMOTO.

Kobayashi Insitute of Physical Research, Kokubunji, Tokyo.

(Read May 11, 1947; Received July 16, 1947)

1. Introduction.

It was found by Schaefer and Bergmann(1), that parallelepipedes of transparent crystals or amorphous solids vibrating at ultrasonic frequencies, produce peculiar diagrams corresponding to each kind of solid and direction of observation, when they are observed in the arrangement of the Fraunhofer's diffraction experiment with a point source of monochromatic light. This diagram was explained by Fues and Ludloff(2) as the phenomenon of the diffraction of light by elastic waves in solids of various directions of propagation and of three directions of vibration (polarisation) in each direction. These plane waves have particular velocities of propagation determined by the elastic constants of the solid, the directions of propagation, and the directions of polarization. All the waves which are effective for the production of diffraction diagrams have their directions of propagation perpendicular to the direction of incident light.

The author(3) formerly made an experiment on the Schaefer-Bergmann's diffraction diagrams of vibrating quartz crystals and showed a method for obtaining the elastic constants of quartz from the diffraction diagrams obtained along three crystallographic axes*. He also calculated the diffraction curves from the elastic constants of Koga(4) for the thickness vibrations of quartz plates with various orientations, and found them to be in good agreement with the observed diagrams.

This paper, being a supplement of the former one, reports some observations on the Schaefer-Bergmann's diffraction diagram of quartz crystals, corresponding to directions of observation other than the crystallographic symmetry axes, and the results of calculation made by using the numerical values of the elastic constants for thickness vibrations of Koga.

2. Results of the Experiment and Comparison with the Calculated Curves.

The three elastic constants c for three plane waves with mutually perpendicular directions of polarization and common direction of propagation (l, m, n) relative to the crystallographic axes x, y, z are given by the equation

---

* The term "three crystallographic axis" is inaccurate, for the mechanical axis y, is not a symmetry axis. But the term is used for brevity in this paper.

$$\begin{vmatrix} L-c & H & G \\ H & M-c & F \\ G & F & N-c \end{vmatrix} = 0, \qquad (1)$$

in which L, M, N, F, G, H are the functions of elastic constants and the direction of propagatiun, and takes the following form for quartz:

$$\left.\begin{aligned} L &= c_{11}l^2+\frac{1}{2}(c_{11}-c_{12})m^2+c_{44}n^2+2c_{14}mn, \\ M &= \frac{1}{2}(c_{11}-c_{12})l^2+c_{11}m^2+c_{44}n^2-2c_{14}mn, \\ N &= c_{44}(l^2+m^2)+c_{33}n^2, \\ F &= c_{14}(l^2-m^2)+(c_{13}+c_{44})mn, \\ G &= (c_{13}+c_{44})nl+2c_{14}lm, \\ H &= 2c_{14}nl+\frac{1}{2}(c_{11}+c_{12})lm. \end{aligned}\right\} \qquad (2)$$

The three elastic constants for the thickness vibrations of quartz plates of the direction cosines (l, m, n) are also given by the same equations (1) and (2). The equation (1) was numerically solved by Koga for various directions (θ, φ) of propagation

$$l = \sin\theta\cos\varphi, \quad m = \sin\theta\sin\varphi, \quad n = \cos\theta,$$

with the use of Voigt's values of elastic constants with necessary corrections for adiabatic processes.

The velocity of propagation in any direction and polarization is given by

$$V = \sqrt{c/\rho}, \qquad (3)$$

where ρ means the density of the crystal and c the root of equation (1), The diffraction patterns are considered to lie on the theoretical diffraction curves, when the latters are given by the expression

$$r = A\lambda/\Lambda = A\nu\lambda/V \qquad (4)$$

in polar coordinates about the image of the point light source, where A means the focal length of the objective lens (or the distance between the crystal and the image in case of the application of convergent beam of light), λ the light wave-length in air, ν the frequency, and Λ the elastic wave-length in the medium.

As the lengths of the radius vectors r of the diffraction curves are proportional to $1/\sqrt{c}$ by (3) and (4), the calculations are made on the $1/\sqrt{c}$-curves corresponding to various directions of observations (l', m', n'), i. e. in planes perpendicular to these directions.

The experiment was made on a quartz sample of cubic form cut in an orientation as illustrated in Fig. 1, which have one pair of surfaces perpendicular to the z-axis, and the other two pairs making angles of -10° and 20° with x-axis respectively. By observations made on this cubic sample in the two directions (A, B) of incident light, perpendicular to the two pairs of surfaces parallel to the z-axis respectively, we obtained the two photographs reproduced in Fig. 2. Of the many calculated curves, we reproduce here only the two corresponding to the observed directions (Fig. 3). The latters coincide with the observed diagrams quite well. By comparing these photographs or curves with the photographs (Fig. 2) or curves (Fig. 6) of the previous paper, we can see the gradual change of the diffraction image between x and y directions. (From the symmetry of the quartz crystals, the diffraction curves for the directions of observations $\pm\alpha$ are common and the curves for the directions $\alpha = \pm 50°$ and $\pm 40°$ are the mirror images of the curves for the directions $\alpha = \pm 10°$ and $\pm 20°$ respectively.

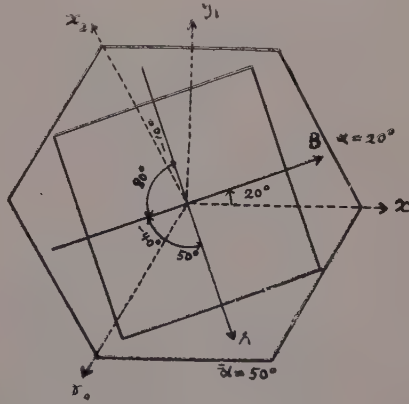

Fig. 1. Orientation of the quartz cube.

The analytical solutions of (1) are cumbersome and not practicable for general directions of observations, so that the photographs as here reproduced are not useful for obtaining the elastic constants. But they may be of some use for knowing the detailed changes with directions of the elastic constants, or the vibration frequencies of the plates, especially in cases, when the calculations are made only in discrete directions, and when there is some ambiguity as to the existence of crossing of the curves or any such details.

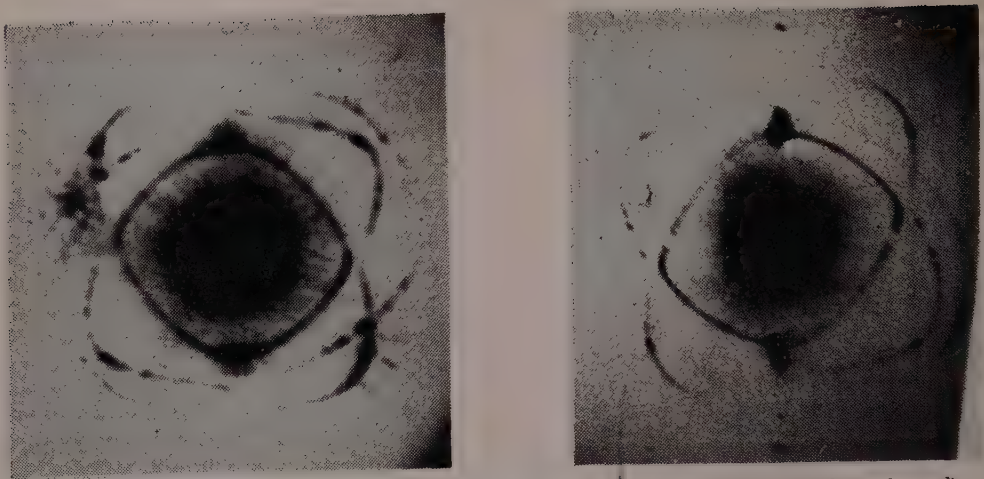

Fig. 2. Schaefer-Bergmann's diffraction diagrams of a quartz crystal. (15 Mc. enlarged)

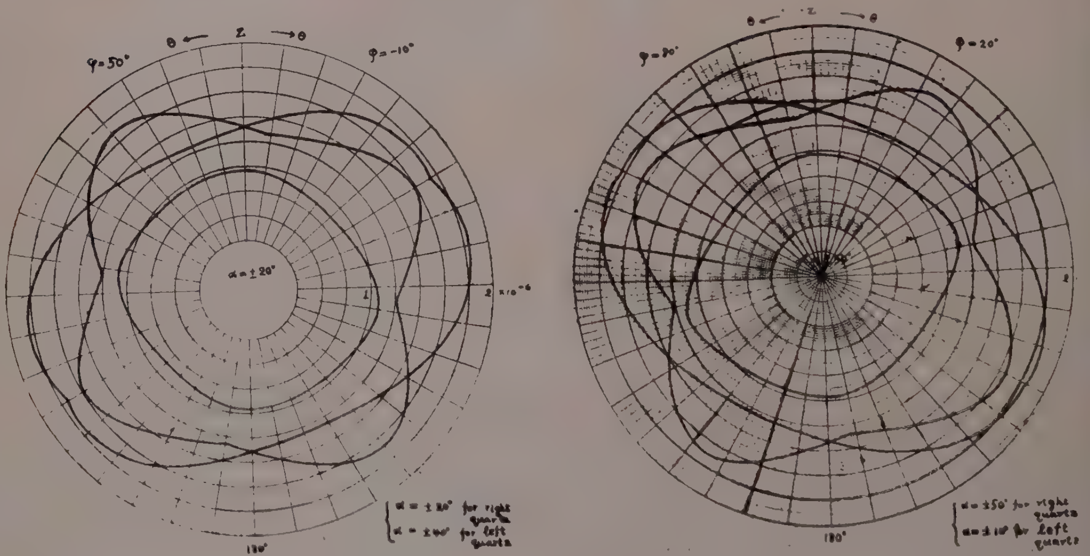

Fig. 3. $1/\sqrt{c}$-curves of quartz crystals

References.

(1), (2) Cl. Schaefer and L. Bergmann, E. Fues and L. Ludloff, Sitz.-Ber. Berliner Akad. Phys.-Math. Klasse, (1935), 222.

(3) O. Nomoto, Proc. Phys.-Math. Soc. Japan, **25** (1943), 240.

(4) I. Koga. Proc. I. R. E., **24** (1936), 510.

A New Approximate Solution in Boundary Value Problems by the Use of Orthogonal Curvilinear Coordinates.

Shigeo Uchida.

Institute of Science and Technology, University of Tokyo.

(Received July 8, 1947)

I. General Remarks.

§ 1. Introduction.

The purpose of this paper is to give a new approximate method for solving partial differential equations in boundary value problems. Taking suitable curvilinear coordinates the author transforms the partial differential equations approximately to the ordinary ones, and, as in many cases the terms of the equations are simplified, this method will be advantageous particularly in complicated non-linear problems. The author will state two ways for getting solutions.

§ 2. The Method of Fixed Axes.

We consider a partial differential equation $D=0$, the independect variables of which are curvilinear coordinates, α, β, γ.

$$D\left[\psi, \frac{\partial\psi}{\partial\alpha}, \frac{\partial\psi}{\partial\beta}, \frac{\partial\psi}{\partial\gamma}, \frac{\partial^2\psi}{\partial\alpha^2}, \frac{\partial^2\psi}{\partial\beta^2}, \frac{\partial^2\psi}{\partial\gamma^2}, \frac{\partial^2\psi}{\partial\alpha\partial\beta}, \frac{\partial^2\psi}{\partial\beta\partial\gamma}, \frac{\partial^2\psi}{\partial\gamma\partial\alpha}, \cdots\cdots\right]=0 \quad (1)$$

When there is no singular point in the region concerned, the derivatives of ψ with respect to α and γ, and thus, the terms by which

$$\frac{\partial\psi}{\partial\alpha}, \frac{\partial\psi}{\partial\gamma}, \frac{\partial^2\psi}{\partial\alpha^2}, \frac{\partial^2\psi}{\partial\gamma^2}, \frac{\partial^2\psi}{\partial\alpha\partial\beta}, \frac{\partial^2\psi}{\partial\beta\partial\gamma}, \frac{\partial^2\psi}{\partial\gamma\partial\alpha}, \frac{\partial^3\psi}{\partial\alpha^3}, \frac{\partial^3\psi}{\partial\gamma^3},$$

$$\frac{\partial^3\psi}{\partial\alpha^2\partial\beta}, \frac{\partial^3\psi}{\partial\alpha\partial\beta^2}, \frac{\partial^3\psi}{\partial\beta^2\partial\gamma}, \frac{\partial^3\psi}{\partial\beta\partial\gamma^2}, \frac{\partial^3\psi}{\partial\gamma^2\partial\alpha}, \frac{\partial^3\psi}{\partial\gamma\partial\alpha^2}, \text{etc.}$$

are multiplied may be made infinitely small by taking a coordinate $\beta=$ constant sufficiently near the group of curves $\psi=$ constant, which must be solved hereafter. We separate the terms of the differential equation into two parts, a part which involves ψ and its derivatives with respect to β only, that is, $\frac{\partial\psi}{\partial\beta}, \frac{\partial^2\psi}{\partial\beta^2}, \frac{\partial^3\psi}{\partial\beta^3}, \cdots\cdots$ etc., and another part which involves the terms mentioned above.

Denoting the two parts by D and D' respectively, we write the differential equation as,

$$D\equiv D\left[\psi, \frac{\partial\psi}{\partial\beta}, \frac{\partial^2\psi}{\partial\beta^2}, \cdots\cdots\right]+D'\left[\frac{\partial\psi}{\partial\alpha}, \frac{\partial\psi}{\partial\gamma}, \frac{\partial^2\psi}{\partial\alpha^2}, \frac{\partial^2\psi}{\partial\gamma^2}, \frac{\partial^2\psi}{\partial\alpha\partial\beta}, \frac{\partial^2\psi}{\partial\beta\partial\gamma}, \frac{\partial^2\psi}{\partial\gamma\partial\alpha}, \cdots\cdots\right]=0 \quad (2)$$

where $\quad D \gg D'$

If we neglect the small term D' at first, an ordinary differential equation

$$D\left[\psi, \frac{\partial\psi}{\partial\beta}, \frac{\partial^2\psi}{\partial\beta^2}, \cdots\cdots\right]=0$$

is obtained. This is integrated by the methods of ordinary differential equations, and as the first approximation we take the solution ψ_1 of this equation. Substituting the first approximation ψ_1 into the term D', which has been neglected at first, we have again the second differential equation involving only β as an independent variable. The integration of this equation gives the second approximate solution ψ_2. This result is substituted into D' and gives the next approximation. These processes must be contiuned to obtain a converging solution.

Denoting the degree of approximation by suffix m, the differential equations in each stage are

$$\left.\begin{aligned}
&\psi_1:\ D_1\left[\psi_1, \frac{\partial\psi_1}{\partial\beta}, \frac{\partial^2\psi_1}{\partial\beta^2}, \cdots\cdots\right]=0\\
&\psi_2:\ D_2\left[\psi_2, \frac{\partial\psi_2}{\partial\beta}, \frac{\partial^2\psi_2}{\partial\beta^2}, \cdots\cdots\right]+D_1'\left[\frac{\partial\psi_1}{\partial\alpha}, \frac{\partial\psi_1}{\partial\gamma}, \frac{\partial^2\psi_1}{\partial\alpha^2}, \frac{\partial^2\psi_1}{\partial\gamma^2}, \frac{\partial^2\psi_1}{\partial\alpha\partial\beta}, \cdots\cdots\right]=0\\
&\qquad\cdots\cdots\cdots\cdots\cdots\cdots\\
&\psi_m:\ D_m\left[\psi_m, \frac{\partial\psi_m}{\partial\beta}, \frac{\partial^2\psi_m}{\partial\beta}, \cdots\cdots\right]+D'_{m-1}\left[\frac{\partial\psi_{m-1}}{\partial\alpha}, \frac{\partial\psi_{m-1}}{\partial\gamma}, \frac{\partial^2\psi_{m-1}}{\partial\alpha^2}, \frac{\partial^2\psi_{m-1}}{\partial\gamma^2}, \frac{\partial^2\psi_{m-1}}{\partial\alpha\partial\beta}, \cdots\cdots\right]=0\\
&\qquad\cdots\cdots\cdots\cdots\cdots\cdots
\end{aligned}\right\} \quad (3)$$

The integration constantsin each process must be detecmined by the boundary conditions step by step and generally are given as functions of α and γ.

§3. The Method of Correcting Axes.

This method is based on the Flügel's idea1)2) who has taken the lengths of curves as the independent variable, but it is not correct as these lengths have some functional relations with each other.

Taking a coordinate $\beta =$ constant sufficiently near the curves of solution, the first approximate solution ψ_1 is obtained as before. Then for the second approximation, take a new coordinate axis, which is corrected in the first approximation. That is, we take the curves $\psi_1 =$ constant for the coordinate $\beta =$ constant. Then the term D' in (2) will become smaller than that of the first approximation. Therefore, the differential equation for the second approximation is obtained also by neglecting this term. Further approximations are made in this way.

Other coordinates α=constant and γ=constant must be determined by their conditions of orthogonality. As the analytical calculations of such groups of curves are difficult, graphical solutions will be more convenient.

The differential equations giving each approximate solution are

$$\left.\begin{array}{l}
\psi_1:\quad D_1\left[\psi_1, \dfrac{\partial\psi_1}{\partial\psi_0}, \dfrac{\partial^2\psi_1}{\partial{\psi_0}^2}, \cdots\cdots\right]=0 \\
\psi_2:\quad D_2\left[\psi_2, \dfrac{\partial\psi_2}{\partial\psi_1}, \dfrac{\partial^2\psi_2}{\partial{\psi_1}^2}, \cdots\cdots\right]=0 \\
\qquad\cdots\cdots\cdots\cdots\cdots\cdots \\
\psi_m:\quad D_m\left[\psi_m, \dfrac{\partial\psi_m}{\partial\psi_{m-1}}, \dfrac{\partial^2\psi_m}{\partial\psi^2_{m-1}}, \cdots\cdots\right]=0 \\
\qquad\cdots\cdots\cdots\cdots\cdots\cdots
\end{array}\right\} \quad (4)$$

The integration constants in each stage are determined by the boundary conditions as in the last paragraph.

II. Differential Equation in Flow of Compressible Fluids.

§4. Fundamental Equations Referred to the Orthogonal Curvilinear Coordinates.

We wish to illustrate these methods by an example in the flow of a compressible fluid which has no viscosity and is in a steady-state flow in a two dimentional field under the condition of adiabatic change, namely, an irrotational flow.

The orthogonal curvilinear coordinates, α=constant and β=constant, are taken and their components of velocity vector V are denoted by u, v and density of fluid by ρ. Introducing the parametric function,

$$h_\alpha = \sqrt{\left(\frac{\partial x}{\partial\alpha}\right)^2+\left(\frac{\partial y}{\partial\alpha}\right)^2}, \quad h_\beta = \sqrt{\left(\frac{\partial x}{\partial\beta}\right)^2+\left(\frac{\partial y}{\partial\beta}\right)^2}, \tag{5}$$

the conditions of continuity and irrotationality are represented as follows.

$$\operatorname{div}(\rho V) \equiv \frac{1}{h_\alpha h_\beta}\left\{\frac{\partial(h_\beta \rho u)}{\partial\alpha}+\frac{\partial(h_\alpha \rho v)}{\partial\beta}\right\}=0 \tag{6}$$

$$\operatorname{rot} V \equiv \frac{1}{h_\alpha h_\beta}\left\{\frac{\partial(h_\beta v)}{\partial\alpha}-\frac{\partial(h_\alpha u)}{\partial\beta}\right\}=0 \tag{7}$$

As a function which satisfies (6) a stream function ψ can be introduced. This is defined by the relations

$$u = \frac{1}{\rho}\frac{1}{h_\beta}\frac{\partial\psi}{\partial\beta}, \quad v = -\frac{1}{\rho}\frac{1}{h_\alpha}\frac{\partial\psi}{\partial\alpha}, \tag{8}$$

Substituting (8) into (7) the non-linear partial differential equation for ψ is obtained;

$$\frac{\partial}{\partial\alpha}\left(\frac{h_\beta}{h_\alpha}\frac{1}{\rho}\frac{\partial\psi}{\partial\alpha}\right)+\frac{\partial}{\partial\beta}\left(\frac{h_\alpha}{h_\beta}\frac{1}{\rho}\frac{\partial\psi}{\partial\beta}\right)=0 \tag{9}$$

The density ρ has the following relation which is obtained from the equation of energy and the condition of adiabatic change:

$$\frac{\rho}{\rho_0}=\left[1-\frac{\kappa-1}{2{c_0}^2}\left\{\left(\frac{1}{h_\alpha}\frac{1}{\rho}\frac{\partial\psi}{\partial\alpha}\right)^2+\left(\frac{1}{h_\beta}\frac{1}{\rho}\frac{\partial\psi}{\partial\beta}\right)^2\right\}\right]^{\frac{1}{\kappa-1}} \tag{10}$$

where ρ_0 and c_0 are the density and the velocity of sound in still air. κ is the ratio of specific heats for constant pressure and constant volume, $\kappa = \dfrac{c_p}{c_v}$.

Representing the boundaries by $\alpha =$ constant (α_c, α_d) and β=constant (β_a, β_b) the boundary conditions are, for example,

$$\psi=\psi_a \quad \text{at } \beta=\beta_a, \qquad \psi=\psi_b \quad \text{at } \beta=\beta_b; \tag{11}$$

$$\frac{\partial\psi}{\partial\alpha}=0 \quad \text{at } \alpha=\alpha_c, \qquad \frac{\partial\psi}{\partial\alpha}=0 \quad \text{at } \alpha=\alpha_d. \tag{12}$$

The problem is reduced to solving (9) so as to satisfy (11) and (12).

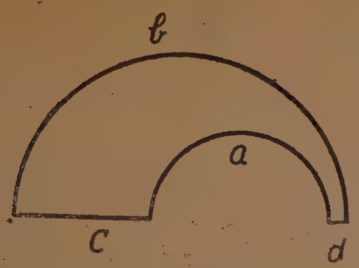

Fig. 1. Boundary.

§ 5. The Method of Fixed Axes.

We take a coordinate axis $\beta = \text{constant}$ sufficiently near the curves of the expected solution, for example, the streamline of the incompressible solution. Then, if there is no singular point in the field concerned, $\frac{\partial \psi}{\partial \alpha}$, $\frac{\partial^2 \psi}{\partial \alpha^2}$ become sufficiently small as compared with $\frac{\partial \psi}{\partial \beta}$, $\frac{\partial^2 \psi}{\partial \beta^2}$, and therefore the differential equation obtained by neglecting the first term of (9) will be taken for the first approximation ψ_1:

$$\frac{\partial}{\partial \beta}\left(\frac{h_\alpha}{h_\beta}\frac{1}{\rho_1}\frac{\partial \psi_1}{\partial \beta}\right) = 0$$

Substituting this result into the term which is omitted at first, the differential equation for the second approximation ψ_2 is obtained as:

$$\frac{\partial}{\partial \beta}\left(\frac{h_\alpha}{h_\beta}\frac{1}{\rho_2}\frac{\partial \psi_2}{\partial \beta}\right) = -\frac{\partial}{\partial \alpha}\left(\frac{h_\beta}{h_\alpha}\frac{1}{\rho_1}\frac{\partial \psi_1}{\partial \alpha}\right).$$

In the same way the differential equation for the mth approximation is obtained as follows:

$$\frac{\partial}{\partial \beta}\left(\frac{h_\alpha}{h_\beta}\frac{1}{\rho_m}\frac{\partial \psi_m}{\partial \beta}\right) = -\frac{\partial}{\partial \alpha}\left(\frac{h_\beta}{h_\alpha}\frac{1}{\rho_{m-1}}\frac{\partial \psi_{m-1}}{\partial \alpha}\right). \qquad (13)$$

As the right hand side is a known function, this is an ordinary differential equation and can be integrated at once.

$$\frac{h_\alpha}{h_\beta}\frac{1}{\rho_m}\frac{\partial \psi_m}{\partial \beta} = \int_{\beta_a}^{\beta} -\frac{\partial}{\partial \alpha}\left(\frac{h_\beta}{h_\alpha}\frac{1}{\rho_{m-1}}\frac{\partial \psi_{m-1}}{\partial \alpha}\right) d\beta + F_m(\alpha), \qquad (14)$$

$F_m(\alpha)$ is a function of α only and gives the velocity distribution on the boundary a. Integrating (14) once more

$$\psi_m = \int_{\beta_a}^{\beta} \frac{h_\beta}{h_\alpha}\rho_m d\beta \int_{\beta_a}^{\beta} -\frac{\partial}{\partial \alpha}\left(\frac{h_\beta}{h_\alpha}\frac{1}{\rho_{m-1}}\frac{\partial \psi_{m-1}}{\partial \alpha}\right) d\beta + \int_{\beta_a}^{\beta} \frac{h_\beta}{h_\alpha}\rho_m F_m(\alpha) d\beta + G_m(\alpha) \qquad (15)$$

$F_m(\alpha)$, $G_m(\alpha)$ are determined by the boundary condition (11), the first condition of which gives $G_m(\alpha) = \psi_a$ (general constant) and $F_m(\alpha)$ is determined by the relation $\psi = \psi_b$ at $\beta = \beta_b$. Namely, by the relation

$$\psi_b = \int_{\beta_a}^{\beta_b} \frac{h_\beta}{h_\alpha}\rho_m d\beta \int_{\beta_a}^{\beta} -\frac{\partial}{\partial \alpha}\left(\frac{h_\beta}{h_\alpha}\frac{1}{\rho_{m-1}}\frac{\partial \psi_{m-1}}{\partial \alpha}\right) d\beta + \int_{\beta_a}^{\beta_b} \frac{h_\beta}{h_\alpha}\rho_m F_m(\alpha) d\beta + \psi_a \qquad (16)$$

$F_m(\alpha)$ is found as a function of α and $\psi_b - \psi_a$. Substituting this value in (15) the mth approximation is obtained.

The mth approximation of density in these calculations is represented by the following relation:

$$\frac{\rho_m}{\rho_0} = \left[1 - \frac{\kappa - 1}{2c_0^2}\left\{\left(\frac{1}{h_\alpha}\frac{1}{\rho_{m-1}}\frac{\partial \psi_{m-1}}{\partial \alpha}\right)^2 + \left(\frac{1}{h_\beta}\frac{1}{\rho_m}\frac{\partial \psi_m}{\partial \beta}\right)^2\right\}\right]^{\frac{1}{\kappa - 1}}. \qquad (17)$$

Another boundary condition is valid for the calculation of the right hand side in (13).

§ 6. The Method of Correcting Axes.

The method which has been stated in § 3 is based on the conception that the curve of the step before the approximation $\psi_{m-1} = \text{constant}$ can be taken as the coordinate axis $\beta_m = \text{constant}$ in the mth approximate calculation. As the terms $\frac{\partial \psi}{\partial \alpha}$, $\frac{\partial^2 \psi}{\partial \alpha^2}$ are always considered to be small enough, the author advances the calculation neglecting these terms and, if the solution converges, it can be adopted for the required solution. As the streamlines are modified in accordance with the progress of approximation, the function h_α and h_β are also corrected step by step. The corrections are carried out graphically.

The differential equation which gives the mth approximate solution ψ_m is

$$\frac{\partial}{\partial \psi_{m-1}}\left(\frac{h_{\alpha \cdot m-1}}{h_{\beta \cdot m-1}}\frac{1}{\rho_m}\frac{\partial \psi_m}{\partial \psi_{m-1}}\right) = 0. \qquad (18)$$

This can be integrated easily:

$$\frac{h_{\alpha \cdot m-1}}{h_{\beta \cdot m-1}}\frac{1}{\rho_m}\frac{\partial \psi_m}{\partial \psi_{m-1}} = F_m(\alpha). \qquad (19)$$

$F_m(\alpha)$ is a function of α only and gives the velocity distribution of the boundary, and integrating again

$$\phi_m = \int_{\psi_a}^{\psi_{m-1}} \frac{h_{\beta\cdot m-1}}{h_{\alpha,m-1}} \rho_m F_m(\alpha) d\phi_{m-1} + G_m(\alpha). \tag{20}$$

$F_m(\alpha)$ and $G_m(\alpha)$ are determined by the boundary conditions (11). Obviously, $G_m(\alpha) = \phi_a$ and $F_m(\alpha)$ can be calculated from the condition $\phi = \phi_b$ at $\beta = \beta_b$, namely at $\phi_{m-1} = \phi_b$, as follows:

$$\phi_b = \int_{\psi_a}^{\psi_b} \frac{h_{\beta\cdot m-1}}{h_{\alpha\cdot m-1}} \rho_m F_m(\alpha) d\phi_{m-1} + \phi_a. \tag{21}$$

The density ρ_m in the formulae above cited is given by

$$\frac{\rho_m}{\rho_0} = \left[1 - \frac{\kappa-1}{2c_0^2}\left(\frac{1}{h_{\beta\cdot m-1}} \frac{1}{\rho_m} \frac{\partial \phi_m}{\partial \phi_{m-1}}\right)^2\right]^{\frac{1}{\kappa-1}}. \tag{22}$$

§ 7. Flow of Compressible Fluid Past Circular Walls.

As a practical example the flow of a compressible fluid past circular walls has been calculated The same problem was solved by G. I. Taylor[4] expanding the solution in a double power series in x and y.

a. Calculation by the meteod of fixed axes.

For the coordinate curves the author takes the streamlines and equipotential lines of incompressible solution. This is the bipolar coordinate and represented by the complex function as follows.

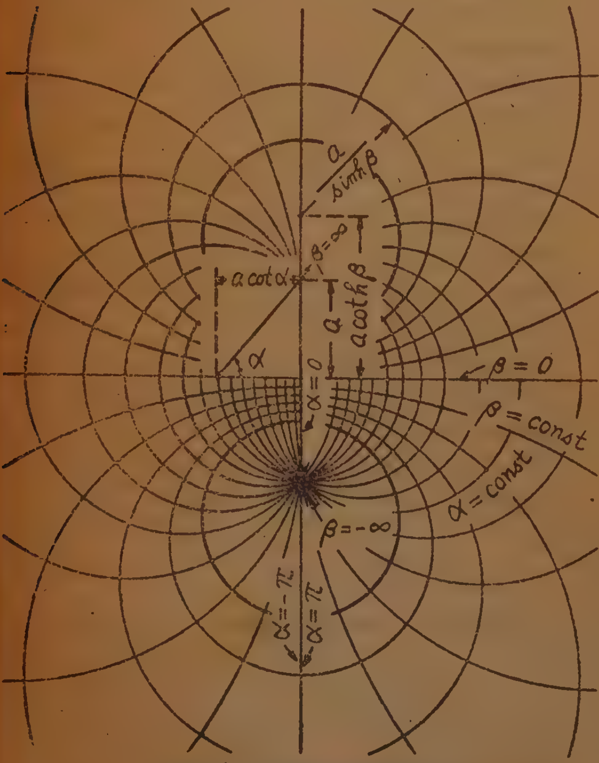

Fig. 2. Bipolar Coordinate.

$$Z = a \tan\frac{\zeta}{2} \quad \text{where} \quad z = x+iy,\ \zeta = \alpha + i\beta$$

$$\text{hence,}\ h_\alpha = h_\beta = h = \left|\frac{dz}{d\zeta}\right| = \frac{a}{\cos\alpha + \cosh\beta}.$$

Denoting the radius of boundary b by R, the author calculates the case where $\frac{R}{a} = 1$; then, $\beta_a = 0$, $\beta_b = \log(\sqrt{2}+1)$. Taking the 10 streamlines, he performs numerical calculation at intervals of $\frac{1}{10}\log(\sqrt{2}+1)$, by means of Simpson's rule for the integration and Collatz's method for the differentiation.

The results of the maximum flow are shown in Table I. The value of correcting term D' substituted by the first approximation ϕ_1 is less than 0.01 and therefore the calculation at four effective figures as in this case will be almost convergent by the 3rd approximation.

Table I. Velocity distribution on the circular wall (maximum flow)

	α	Method of Fixed Axis		Method of Correcting Axis		Expts.
		1st ap-prox.	2nd ap-prox.	1st ap-prox.	2nd ap-prox.	
$\frac{w_b}{c_0}$	−.2644	.9144		.916	.912	.89
	−.1763	.9534		.954	.948	.92
	−.0881	.9928	.9839	.994	.985	.97
	0	1.0829	1.0204	1.034	1.022	1.00
	.0881	1.0734	1.0600	1.074	1.060	1.03
	.1763	1.1146		1.114	1.096	1.06
	.2644	1.1564		1.155	1.134	1.10
$\psi_b - \psi_a/\rho_0c_0a$		.23880	,23900	.23880	.23916	

b. Calculation by the method of correcting axes.

The velocity distribution is shown in Fig. 3 and Table II, and the corrected streamlines in Fig. 4. In order to compare with another method the results are listed also in Table I. In spite of the low accuracy in graphical calculation, the obtained values are close to those of the method of fixed axes.

The convergency of the method is very good in all subsonic regions and in a part of the supersonic region, for the section No. 2. But behind the section No. 6 there exists a tendency for divergence, and about here will be the boundary of the convergent region. With increasing value of θ_1

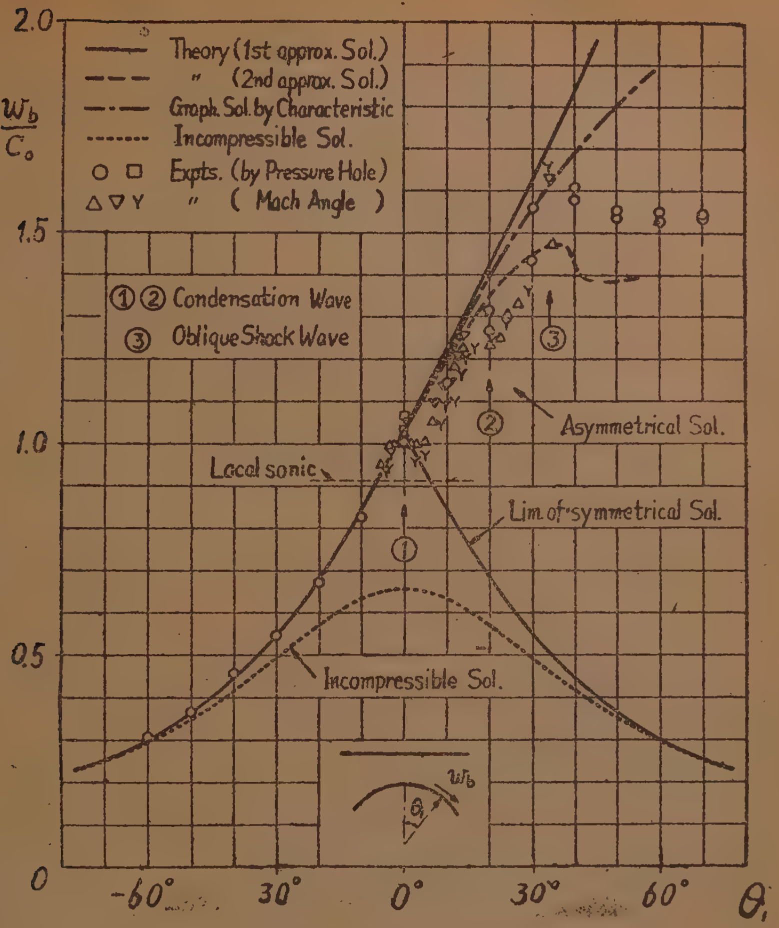

Fig. 3. Velocity distribution on the circular wall.

the velocity on the circular walls builds up to the maximum speed, which is attained at the vacuum state and the streamline leaves the curved surface as shown in Fig. 4. As the pressure and density both vanish and are constant along this streamline, the flow becomes a kind of discontinuous motion and the free streamline stretches to the vacuum state at infinity. For the most part, calculated results are in good agreement with experimental results. The chain line in Fig. 3 is the velocity distribution gained by Busemann's characteristic method, the calculation of which is started by connecting the sonic line with that which is obtained by the second approximation. From this calculation the streamlines in the supersonic region is obtained graphically, and a more convergent solution will be gained by taking these as the coordinate curves.

c. Experimental result.

The experiment here cited was carried out by the author in February, 1945 and has been reported in a previous paper[3]. He measured the pressure distribution on the curved surface by means of the small wooden channel as shown in Fig. 5, and converted into the velocity $\frac{w}{c_0}$, neglecting the loss of total head pressure.

The velocity distribution in maximum flow (Fig. 3 and Table II) shows good agreement with theory up to the middle section. By virtue of the sudden condensation of the moisture two stepped deviations take place in the supersonic region.

The limit of symmetrical flow was investigates by experiments varying the back pressure. The results are shown in Fig. 6. Excepting the asymmetry caused by the separation, there exists a symmetrical state, in the lower velocity. In accordance with the reduction of back pressure, at first, the velocity on the surface increases as a

Table II. Velocity dustribution on the circular wall (maximum flow)

(a) Theory

Calculated by the Method of Correcting Axis					
No.	θ_1	Incomp.	1st approx.	2nd approx.	by Charac-teristic
-12	-71° 19′	.2481	.252	.252	
-11	-61° 13′	.2909	.298	.298	
-10	-52° 33′	.3366	.349	.349	
- 9	-45° 0′	.3837	.405	.405	
- 8	-38° 20′	.4308	.464	.464	
- 7	-32° 21′	.4765	.526	.526	
- 6	-26° 45′	.5194	.591	.592	
- 5	-21° 52′	.5581	.659	.660	
- 4	-17° 9′	.5916	.730	.730	
- 3	-12° 40′	.6187	.803	.802	
- 2	- 8° 21′	.6387	.879	.875	
- 1	- 4° 9′	.6510	.955	.949	
0	0°	.6551	1.034	1.022	1.022
1	4° 9′	.6510	1.113	1.096	1.098
2	8° 21′	.6387	1.196	1.169	1.177
3	12° 40′	.6187	1.282	1.241	1.259
4	17° 9′	.5916	1.374	1.310	1.342
5	21° 52′	.5581	1.467	1.372	1.425
6	26° 54′	.5194	1.569	1.423	1.509
7	32° 21′	.4765	1.679	1.463	1.591
8	38° 20′	.4308	1.804	1.468	1.669
9	45° 0′	.3837	1.950	1.382	1.748
10	52° 33′	.3366	2.132	1.387	1.828
11	61° 13′	.2909	2.380		
12	71° 19′	.2481	2.756		

(b) Experiments

by Pressure Holes		
θ_1	⊙ 1	⊙ 2
-60°	.309	.304
-50°	.367	.364
-40°	.458	.450
-30°	.548	.547
-20°	.673	.673
-10°	.827	.830
0°	1.002	1.005
10°	1.146	1.144
20°	1.314	1.268
30°	1.557	1.437
40°	1.578	1.612
50°	1.534	1.557
60°	1.528	1.555
70°	1.531	1.550

θ_1	⊡ 1	⊡ 2
0°	1.011	1.031

from observed Mach Angle					
θ_1	△	θ_1	▽	θ_1	Y
-5.5°	.947			-4.2°	.925
-3 4°	.985			-3.8°	.941
-2.5°	.997			-3.3°	.977
-0.8°	.990			-2.4°	.987
0.2°	.993			2.7°	.956
1.4°	1.000			5.0°	.970
3.0°	.997			8.6°	1.044
5.0°	1.003	7.0°	1.098	9.8°	1.086
6.6°	1.048	9.0°	1.132	12.0°	1.098
11.7°	1.180	11.0°	1.146	13.3°	1.162
13.6°	1.225	12.3°	1.210	14.5°	1.195
20.0°	1.233	14.0°	1.256	16.5°	1.225
22.3°	1.251			20.7°	1.242
24.2°	1.304			22.4°	1.249
26.5°	1.333			23.9°	1.284
				24.8°	1.293
				26.5°	1.325
				29.0°	1 368

from the Angle of oblique Shock Waves					
θ_1	△	θ_1	▽	θ_1	Y
34.7°	1.48	34.0°	1.64	33.6°	1.66

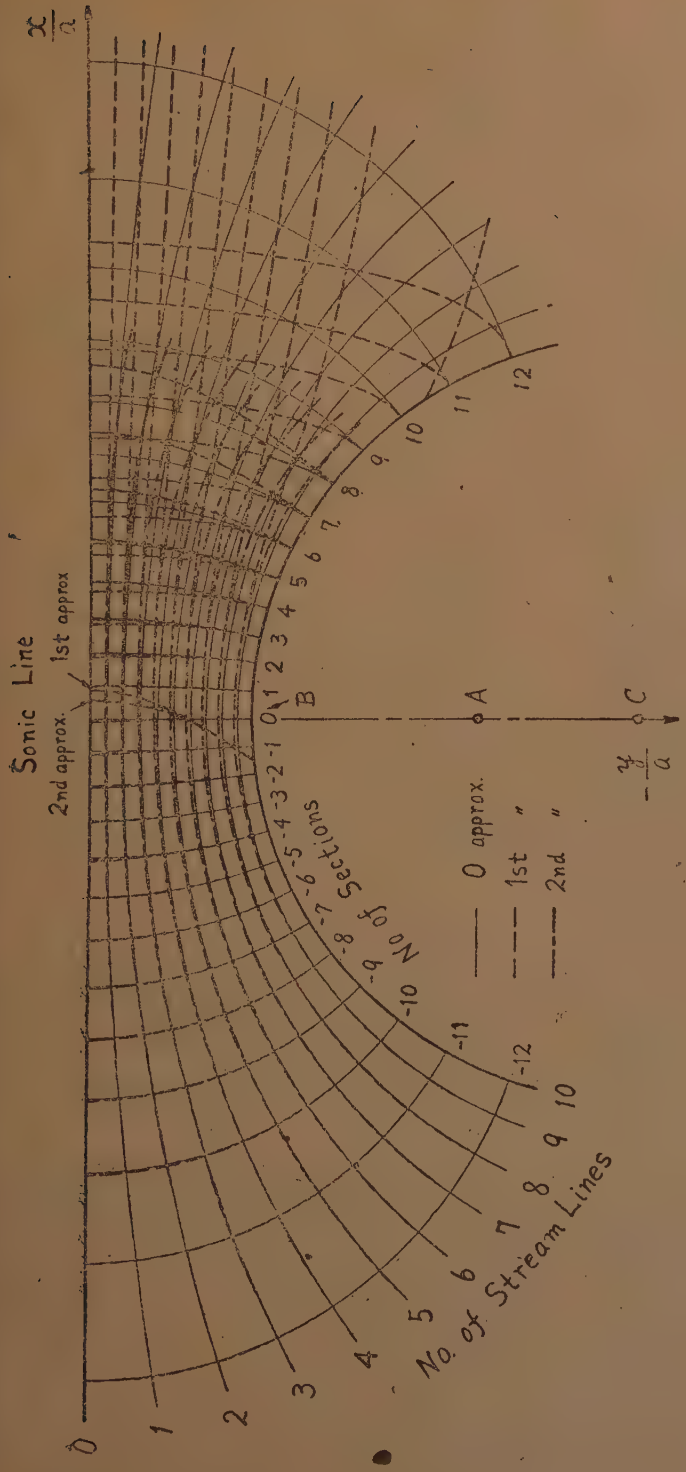

Fig. 4. Stream Lines.

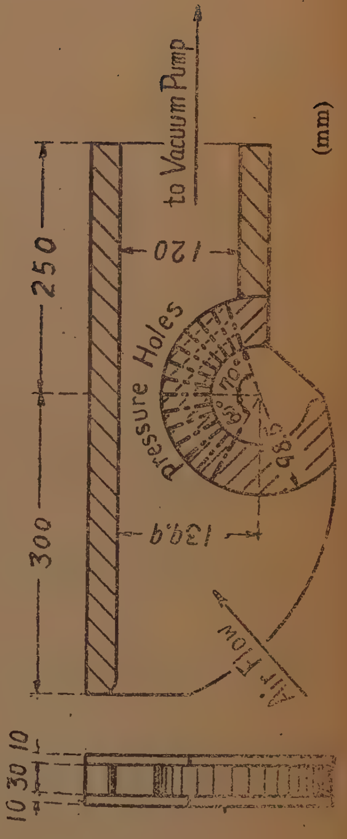

Fig. 5. Model of the circular wall.

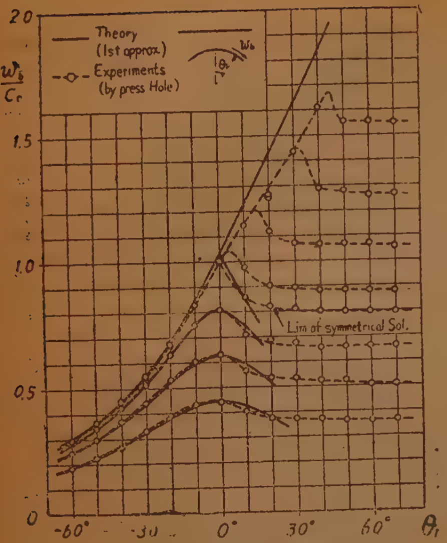

Fig. 6. Velocity distribution on the cricular wall.

whole. Further reduction produces a limiting state in which the velocity distribution becomes fixed in the forward region ($\theta<0$) and with still further reduction, the velocity in rearward region ($\theta>0$) begins to increase rapidly. In this state, loud noise of high frequency, caused by the vibrations of fluid and shockwaves at the throat of tube, are usually produced. In this limiting case the velocity on the wall becomes $\frac{w}{c_0}=0.997$ at the centre section and almost coincides, within experimental error, with that of asymmetrical flow $\frac{w}{c_0}=1.002$ or 1.005. The velocity distribution at the limit of the symmetrical solution in Fig. 6 shows an experimental result in which the velocity distribution has an abrupt break at this limiting case.

The full lines in the figure is the first approximation by our method and shows good agreement with the observed values.

§ 8. A Relation between the Maximum Velocity Obtained in a Circular Walled Intake and the Radius of Inlet Circle.

The calculation in the preceding paragraph shows that the maximum flow obtained changes with the radius R of the minimum section. With an inlet channel consisting of circular intakes and parallel walls as is shown in Fig. 7, the maximum flow obtained will be limited by the radius R. If we equate this flow quantity to the uniform flow downstream, the maximum velocity gained in such an inlet channel will be approximately found; the calculated result is given in Fig. 7. It shows that even a radius ten times larger than the minimum section gives only $M=0.95$.

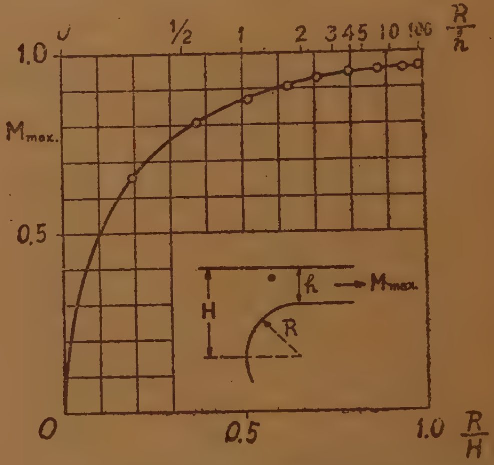

Fig. 7. The relation between the maximum velocity and the radius of circular walls.

Bibliography.

(1) G. Flügel: Ein neues Verfahren der graphischen Integration, angewandt auf Strömungen idealer Flüssi keit in Kreiselräder, Ztschr. f. des gesamte Turbinenwesen 12 (1915) S. 73.
(2) G. Flügel: Mehrdimensionale Strömung von Gasen, Ztschr. f. das gesamte Turbinenwesen 16 (1919) S. 161.
(3) S. Uchida: An approximate solution in compressible fluid problems (flow past circular walls), Jour. Aero. Res. Inst., Univ. Tokyo No. 246 (1945) p. 67.
(4) G. I. Taylor: The flow of air at high speeds past curved surfaces, R. & M. No. 1381 (1930) p. 328.

On the Crystal Rectifiers

By Akio KOBAYASHI.

Research Laboratory, Tokyo Shibaura Electric Co., Kawasaki.

(Received July 18, 1947)

Abstract.

The temperature-dependence of rectifying action of silicon and iron pyrite detectors was measured between –183°C and 300°C. The maximum rectification ratio for Si-W detector occurs at about 60°C, while for some iron pyrites a kink appears at about –60°C in the rectification-ratio versus temperature curves, although we have no maximum in the measured range of temperatures. Mott's and Davydov's theories on the reetification are insufficient o explain these results. The author proposes a theory based on the tunnel effect of electrons through the upper part of a blocking layer. in which the calculation was made for the thickness 20 Å∼30 Å of the blocking layer. It is expected from our theory that there exists a critical temperature at which the inversion of rectification occurs and that the rectifylng action is a function of the thickness of layer and the conductivity of the crystal in bulk. The inversion of rectification at different places on the surface of the crystal can also qualitatively be explained by our theory,

§ 1. Introduction.

It is well known that the rectifying action occurs on the contact surface between a metal and a semi-conductor, although the nature of contact is somewhat ambiguous and no convincing explanation has been given for the different rectifying action at different places on the surface of the same crystal.

Although the temperature-dependence of rectification was measured by several authors[1)2)3)] so far, these measurements were carried out within rather small range of temperature so that they do not agree with each other regarding the question whether the rectification-ratio increases with temperature or not. The author, therefore, measured the rectifying action of silicon and pyrite detectors in a wide range of temperature, i. e. –183°C to 300°C, which results shall be reported here. The details of experiments have already been described in Japanese in the other publication[4)].

§ 2. Sign of the Current Carriers.

According to the recent theory of crystal rectification [5)6)7)] the sign of charge of current carriers in semi-conductors has been shown to play an important role for deciding the sense of the rectification, It can be easily determined experimentally by the sign of the thermo-electromotive force of the crystal.

The observed values of T. E. M. F. for silicon used were about –450 μV per degree at room temperatures and –350 μV per deg. above 60°C, while those for pyrite changed from 100 μV to 150 μV per deg, between room temperatures and 150°C. So it was turned out that clean silicon is the semiconductor with positive holes, where as pyrite the one with electrons.

§ 3. Dependence of Rectification on Temperature.

The detector was mounted in a sealed glass vessel filled with dry nitrogen gas to protect the crystal surface against moisture and oxidation. For the metal point a tungsten filament of 0.1 mm dia. was used under a lead weight of 10 g which maintains a constant contact-pressure throughout all measurements. The current through the contact of the crystal was measured for several values of the applied voltage between the range from –183 °C to 300°C.

Some of the results are shown in Figs. 1a and b in which rectification ratios, obtained by dividing an easy flow current by a hard flow one, are

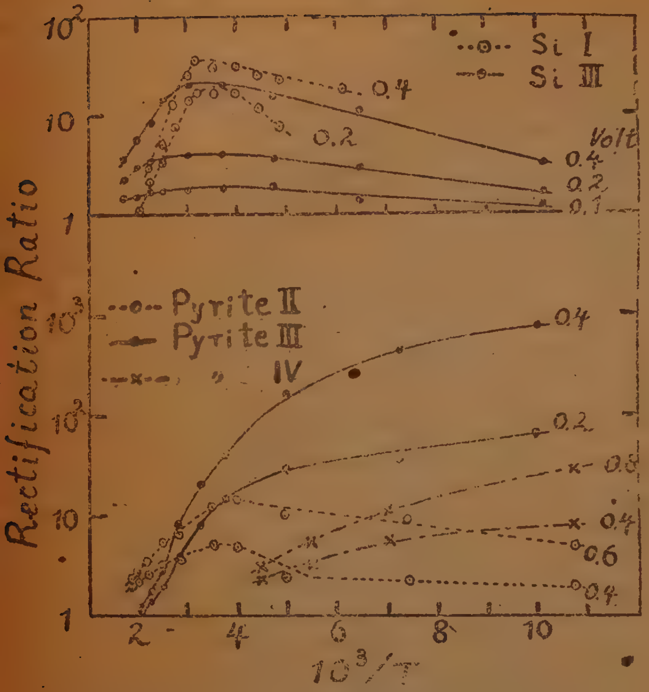

Fig. 1 a & 1 b. The rectification rations versus $1/T$ curves for various values of applied voltages.

plotted against reciprocals of absolute temperatures. The curves for all the silicon detectors have a maximum at about 60°C and those for pyrite have a maximum at about -20°C or a small curvature without maximum at low temperatures. When the logarithms of current are plotted against $1/T$, we get curves shown in Figs. 2 to 4, in which the applied voltage is taken as a parameter. There are kinks on the curves of the easy flow direction as well as the hard flow direction corresponding to the kink of the curves of the rectification-ratio. In both cases, the parts the curves on the left side of the kinks follow Mott's and Davydov's theory of crystal rectifier, but on the right hand side they do not. Let us call the left hand part of the kinks in these curves a thermionic region, and the right hand part of them a tunnel region[8].

When a semi-conductor is brought in contact with a metal, an electrical double layer occurs as shown in Fig. 5a. In this figure A is the region within the metal, BC that of an adsorbed film of water or ice, condensed from moisture between two materials, or a tarnished film such as oxide on the semi-conductor, and CD the double layer produced by ionization of impurity centres in the semi-conductor. If the thickness of BC is negligible as compared with that of CD, then we can assume the potential at the contact to be the one shown in Fig. 5b. In the figure V_0 denotes the contact potential difference, E_0 the activation energy of impurity centres. Then the thickness of the double layer is given by

$$d = \sqrt{\kappa V_0/2\pi Ne}, \qquad (1)$$

where N is the number of the impurity atoms per cc. and κ the dielectric constant of the layer.

If the thickness d is of the order of the mean free path of electrons, we have the thermionic current of rectification at applied voltage V,

$$i = S\frac{4\pi mek^2T^2}{h^3}e^{\frac{-e(V_0-\Delta V_0)}{kt}}\left(e^{\frac{eV}{kT}}-1\right), \qquad (2)$$

where ΔV_0 is a value reduced by image force effect,

$$\Delta V_0 = e^{\frac{1}{2}}\sqrt{(V_0-V)/\kappa d}$$

and S is the area of the contact surface.

Applying the formula (1) to the thermionic region of the curves of easy flow, we get for V_0 0.8 Volt and 0.4~0.6 Volt for Si and FeS_2 respectively and for ΔV_0 at $V = 0$ about 0.4 Volt and 0.2 Volt respectively. It is, therefore, expected that d and N must be of the order of $m\mu$ and 10^{19} respectively using $\kappa \sim 10$. As the applied voltage V increases, the spreading resistance $\rho/4r$ through the contact point, where ρ is the specific resistance of the crystal in bulk and r the radius of the whisker, must exceed that of the blocking layer, then the temperature dependence of the conductivity may be said as that of the specific one in bulk. Thus from the slope of these curves, E_0 for both crystals are found to have values 0.007 to 0.025 eV.

§ 4. Rectification in the Tunnel Region.

If the temperature of the crystal, whose blocking layer is of a few $m\mu$ thick, is lowered, the so-called thermionic current will decrease exponentially, but the current passing through the upper part of

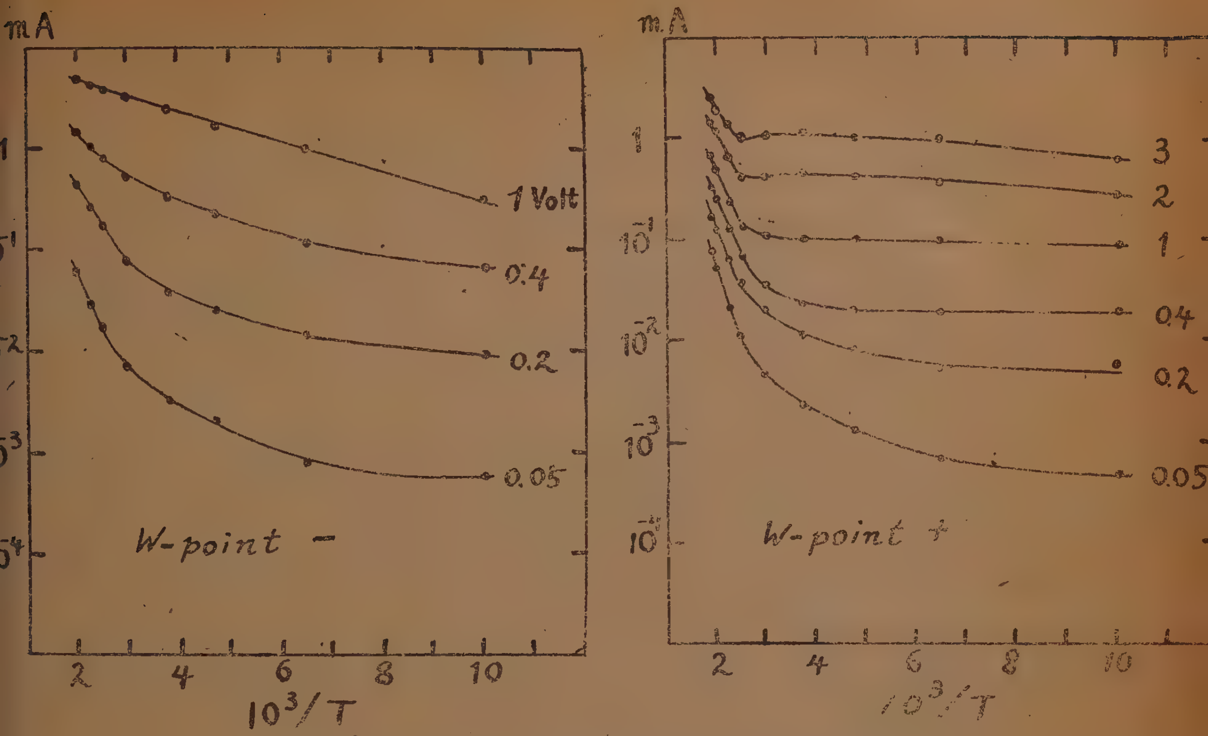

Fig. 2. The current versus $1/T$ curves of a silicon detector,

A for easy flow, B for hard flow.

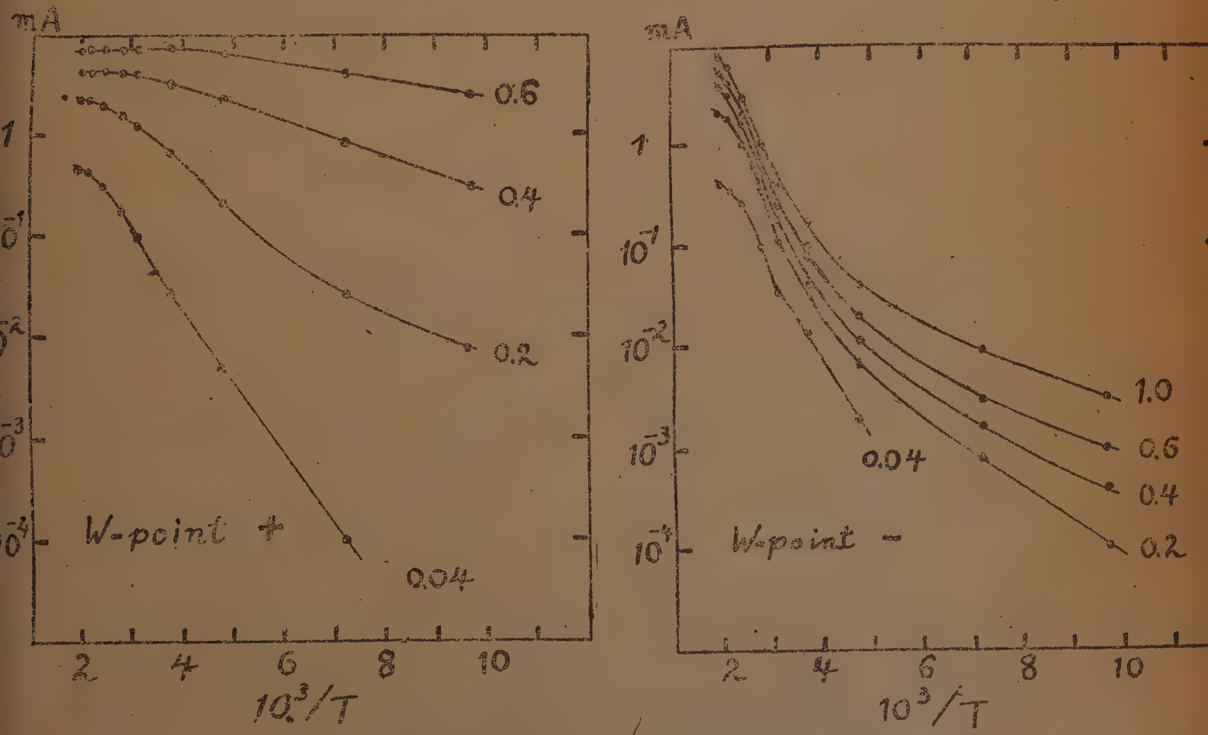

Fig. 3. The current versus $1/T$ curves of a pyrite detector,

A for easy flow currents, B for hard flow.

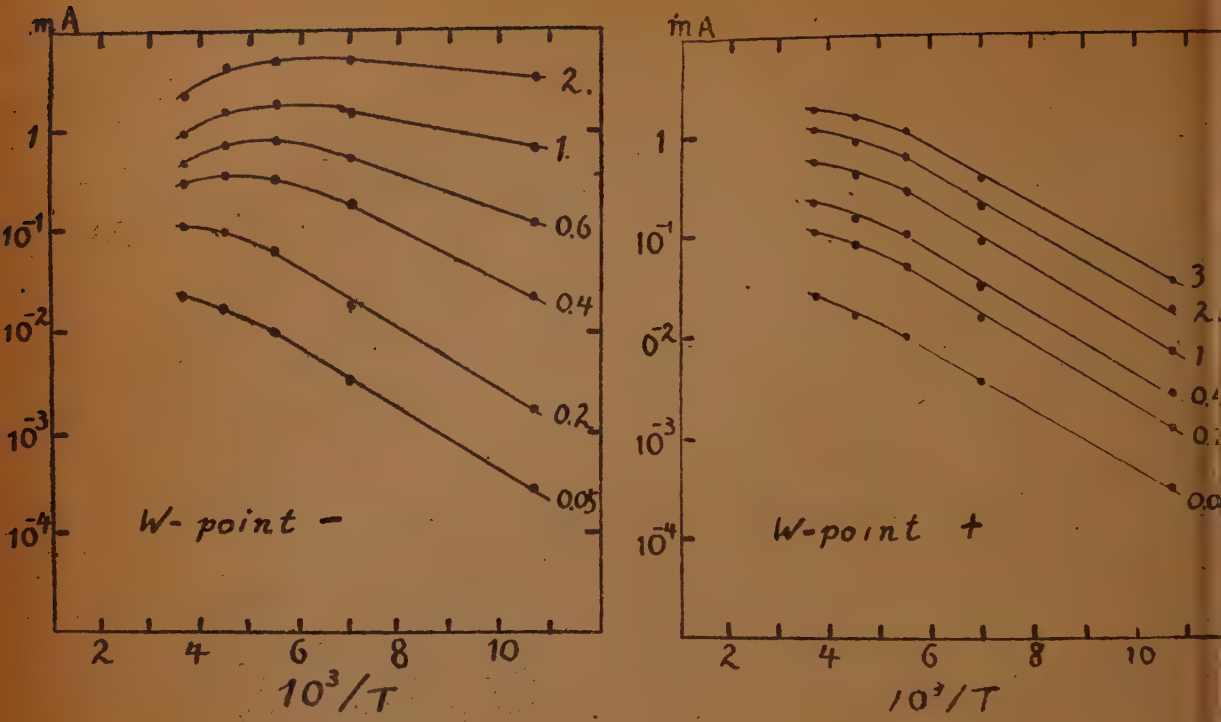

Fig. 4, The current versus $1/T$ curves of a pyrite detector,
A for easy flow, B for hard flow.

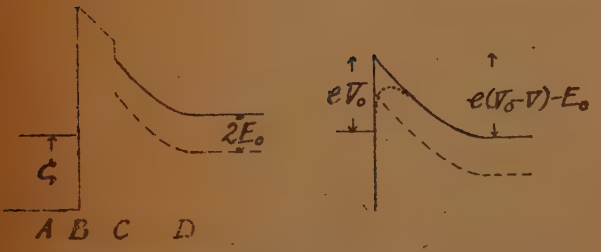

Fig. 5. The potential barrier of the contact between a semi-conductor and a metal.

the potential hump will not decrease so rapidly. The temperature coefficient of the latter current attributed to the tunnel may be considered to be much smaller than in the case of the thermionic region, because for the tunnel electrons it is not necessary to have such an energy to pass over the potential hump.

The current from the semi-conductor to the metal is given by

$$i_s = SA\int_0^{\varepsilon_0-e\Delta V_0} D(\varepsilon)\log\left\{1+Ce^{-\frac{E_0+\varepsilon}{kT}}\right\}\cdot d\varepsilon, \tag{3}$$

where

$$A = \frac{4\pi mekT}{h^3}, \quad C = \frac{N^{\frac{1}{2}}}{2}\left(\frac{h^2}{2\pi mkT}\right)^{\frac{3}{4}},$$

and $D(\varepsilon)$ is a transmission coefficient,

$$D(\varepsilon) = \frac{4\{E(W-E)\}^{\frac{1}{2}}}{W}\exp\{-\alpha(\varepsilon_0-\varepsilon)^{\frac{3}{2}}\varphi(y)\},$$

where

$$\alpha = \frac{8\pi}{3}\frac{\sqrt{2m}}{ehF}, \quad F = \left(V_0-V-\frac{E}{e}\right)/d,$$

$$E = \zeta+eV+E_0+\varepsilon, \quad \varepsilon_0 = eV_0-E_0,$$

$\varphi(y)$ is a correction term calculated for the image force by Nordheim[9] and $y = \frac{e}{V_0}\sqrt{\frac{F}{\kappa}}$, ε the energy of the motion normal to the blocking layer and ζ Gibbs' free energy of an electron.

If we expand the logarithm in (3) by neglecting the degeneration of electrons and assume $\varphi(y) = 1$, we get

$$i_s = SAC\int_0^{\varepsilon_0}\frac{4\{E(W-E)\}^{1/2}}{W}\exp\left\{-\alpha(\varepsilon_0-\varepsilon)^{3/2}-\frac{(\varepsilon+E_0)}{kT}\right\}d\varepsilon. \tag{4}$$

When $\varepsilon_0 \leqq \left(\frac{2}{3\alpha kT}\right)^2$ or V, T is samll, we have[10]

$$i_s = SAC\,\frac{4\{(\zeta+eV)\varepsilon_0\}}{W}\,\frac{\alpha\varepsilon_0^{3/2}}{\frac{1}{kT}-\frac{3}{2}\alpha\varepsilon_0^{1/2}}\,e^{-\frac{E_0}{kT}}. \tag{5}$$

When $\varepsilon_0 > \left(\frac{2}{3\alpha kT}\right)^2$ or V, T is large, we have

$$i_s = SAC\sqrt{\frac{\pi}{2\beta}}\left\{1+\Phi\left(\sqrt{\frac{\beta}{2}}\cdot\varepsilon^*\right)\right\}\frac{4\{E^*(W-E^*)\}}{W}$$

$$\cdot\exp\left\{\frac{e_0}{kT}+\frac{4}{\alpha^2}\left(\frac{1}{2kT}\right)^3-\frac{E_0}{kT}\right\} \qquad (6)$$

where $\beta = 9\alpha^2kT/8$, $\varepsilon^* = \varepsilon_0 - \left(\frac{2}{3\alpha kT}\right)^2$

and Φ is the error function.

Using (5) and (6), the resultant current for $V>0$ may be given by

$$i = i_s(1-e^{-\frac{eV}{kT}}). \qquad (7)$$

When negative small voltage is applied, the temperature dependence of the current may be similar to that of Eq. (7). As the bias increases however, the cold emission current from the metal to the semicoductor may become larger because α is of the order $m\mu$, and its temperature-dependence may become very small, thus the current in the hard flow direction at large voltage

$$i_c = -\frac{Se}{2\pi h}\frac{\zeta^{1/2}}{W(W-\zeta)^{1/2}}eF^2\exp\{-\alpha(eV_0)^{5/2}\varphi(y)\} \qquad (8)$$

§ 5. Discussion of the Results.

If $-eV \gg 2E_0$ and kT, we have $i \approx i_c$. Taking the logarithm of the hard flow current, therefore, it follows

$$\log\{i_c/(V_0+|V|)^2\} \approx \text{const.} - \frac{8\pi}{3}\frac{\sqrt{2m}}{eh}(eV_0)^{3/2}\frac{d}{(V_0+|V|)}. \qquad (9)$$

the curve of $\log\{i/(V_0+|V|^2\}$ vs. $1/(V_0+|V|)$ for large voltage in the hard flow direction must be a straight line independent of temperatures and thus d can be evaluated from the slope of the curves. The curves for silicon and pyrite are shown in Figs. 6a and b. In these figures, the slope of the curves becomes steeper as the temperature is lowered. On the curves below about –100°C, the slope for small value of $1/(V_0+|V|)$ becomes nearly constant.

According to the above-mentioned consideration we get the values of d from the slope of these high field part of the curves. The values of d are of the order of a few $m\mu$, as seen in Table. I.

Numerical results of the formulae (5) and (6) are graphically shown in Fig. 7, where it is assumed to be $d = 20$ Å, $V_0 = 0.8$ Volt, $W = 5\,eV$, $E = 0$, $S = 10^{-1}\,\text{cm}^2$ and $N = 10^{19}$, and in Fig. 8 where $d = 30$ Å, $V_0 = 0.4$ Volt and the other quantities remain unchanged. The calculated curves in these figures are very similar to the observed ones of Si- and FeS_2-detectors respectively, except the cases for $V \approx V_0$ at which the spreading resistance begins to exceed the blocking one.

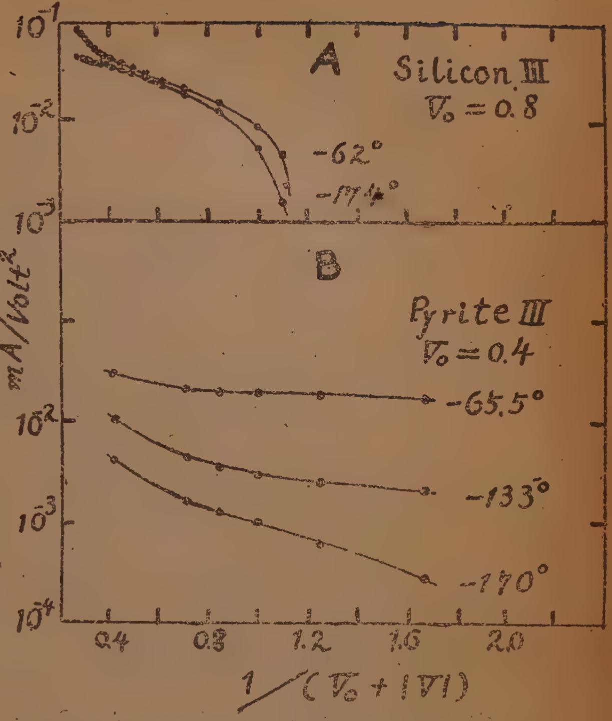

Fig. 6. A-The field emission curves for a silicon detector, B-That for a pyrite detector.

The capacity is approximately given by

$$C = \frac{\kappa S}{4\pi d} \approx 0.2\,pF.$$

Of course the value of capacity will vary with applied voltage and with temperatures, owing to the variation of d.*

Table I. The calculated values of d from eq. (9) for the silicon and pyrite detectors.

	V_0 \ Temp.	–9°C	–62°C	–117°C	–174°C
Si	0.4 volt	15 Å	17 Å	15 Å	**
	0.8	10	12	10	

---

* The voltage and temperature dependence of the capacity are now in study by a bridge operated at 1 MC to 5 MC.

** The effect was disturbed by the adsorbed layer.

	Temp. / V_0	$-135°C$	$-170°C$
FeS_2	0.4 volt	18 Å	18 Å
	0.6	13	13

§ 6. Inversion of Rectification.

If the temperature is lowered, the currents for $V>0$, calculated by Eq. (5), decrease gradually, but the reverse currents for $V<0$ show less decrease in comparison with former and may finally approach the value i_c at absolute zero. At a very low temperature, therefore, the direction of easy flow must reverse. The calculated values of i_c for $V=0$ become equal to the values of i from Eq. (7) at not so low temperatures in Figs. 7 and 8, on account of which the inversion of rectification may bn expected to be observed in the experimental observations according to our theory.

El Sherbini and Yousef[3] have already found such inversion with detectors of molybdenite and bornite, but their results have somewhat ambiguous points to check our theoretical expectation, since we could not found experimentally such an effect in the mentioned detectors. But for some pyrite detectors, which rectify in the reverse direction at room temperatures except small value of applied voltage, the easy flow currents vary with exponential of $1/kT$, as shown in Fig. 4, whereas the hard flow curreuts do not vary so steeply. This is a qualitative and indirect verification of the theory, the result being similar to the case of the cold emission theory by Frenkel and others,[11] in which the activation energy has a small value of 0.06 eV. The theory, therefore, may explain the phenomenon of the region between Frenkel's cold emission theory and Mott's thermionic one.

In the above discussion we have neglected the adsorbed layers of moisture which affect the rectification strongly[12], and further the tarnished layer which always exists as silica on the surface of silicon. Moreover, we have assumed $\varphi(y)=1$ by ignoring the image force and effective mass of current carriers is equal to the electronic one, but in reality m varies with the level in the band. These situations may be the causes of the quantitative discrepancy between the experiments and the theory.

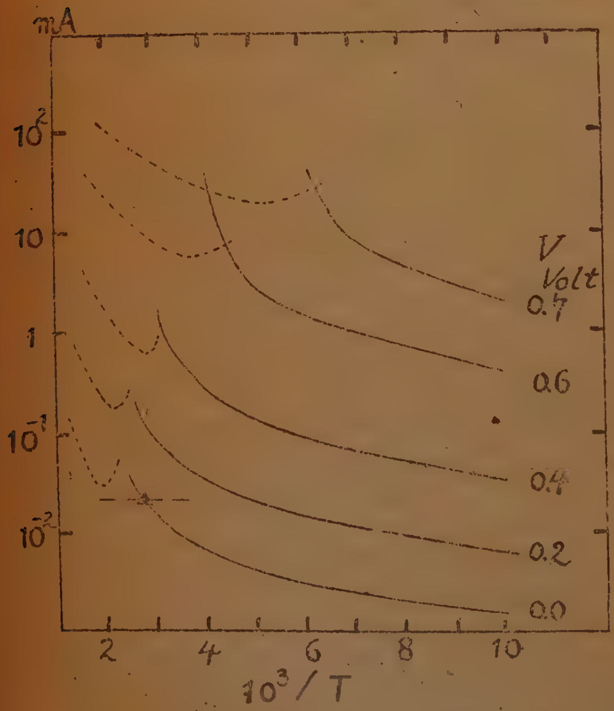

Fig. 7. The calculated curves; the dotted lines for equation (6) and the real lines for equation (5) with the values $d=20$ A and $V_0=0.8$ volt.

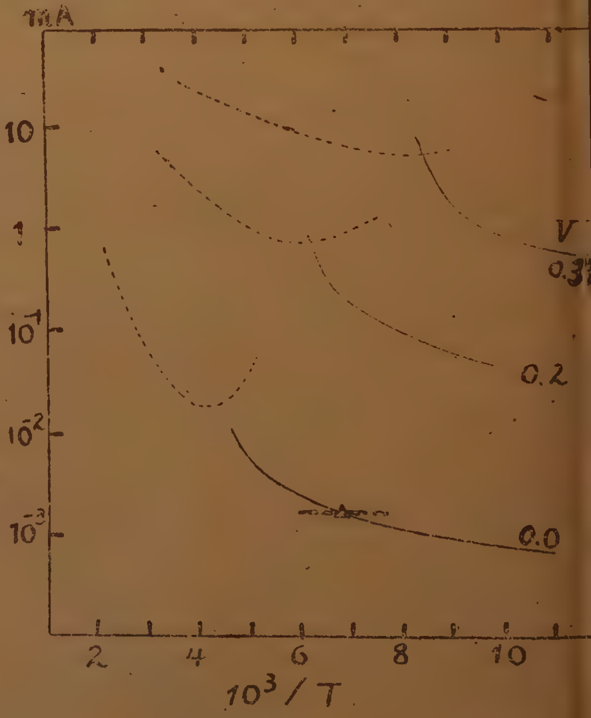

Fig. 8. The calculated curves; the dotted lines for equation (6) and the real lines for equation (5) with the values $d=30$ A and $V_0=0.4$ volt.

This effect explains qualitatively the reason why the inversion of rectification can take place at different places on the same surface of crystals at room temperature.

References.

(1) S. R. Khastigir and A. K. D. Gupta: Phil. Mag. 19, 557 (1935).
(2) B. K. Sen: Ind. Jour. of Phys. 10, 91 (1937).
(3) M. A. El Sherbini and Y. L. Yousef: Proc. Phys. Soc. London, 51, 449 (1939), 53, 120 (1941).
(4) A. Kobayasi: Toshiba Review. 1, 33 (1946).
(5) N. F. Mott: Proc. Roy. Soc. London A 171. 27 (1939).
(6) B. Davydov: Jour. of Phys. 1, 166 (1939), 4, 335 (1941).
(7) W. Schottky: Zeits. f. Phys. 131, 367 (1939), W. Schottky and E. Spenke, Wiss. Veroeff. Siemens-Werken 18, 225 (1939).
(8) A similar effect appears to be observed in Schottky and Deutschmann's experiment, Phys. Zeits. 30, 839 (1929), if the resistance be plotted against $1/T$.
(9) L. W. Nordheim: Proc. Roy. Soc. London A 121, 626 (1928).
(10) A similar formula was obtained by I. W. Kurtschatow, T. Z. Kostina and L. I. Rusinow, Phys. Zeits. d. Sowjetuion, 7, 129 1935), in the paper on silicon carbide.
(11) J. Frenkel and A. Joffe: Phys. Zeits. Sowj. 1, 60 (1932), L. Nordheim: Zeits. f. Phys. 75, 434 (1932), A. H. Wilson: Proc. Roy. Soc. London A 136, 487 (1932), W. Ch. van Geel: Phil. Tech. Rev. 4, 100 (1939).
(12) F. Heineck: Phys. Zeits. 35, 113 (1934), H. Geismann: Phys. Zeits. 36, 132 (1935).

The Relation between the Intensity and the Action of Ultrasonic Waves.

By Otohiko NOMOTO and Seiichi OKUI.

Kobayashi Institute of Physical Research, Kokubunji, Kokunjimachi, Tokyo

Institute of Pharmacy, Faculty of Medicine, University of Tokyo

(Read May 11, 1947; Received July 29, 1947)

§ 1. Introduction.

It was observed by Kusano[1] that the isolation of iodine from acidic solutions of potassium iodide under the action of ultrasonic waves takes place with the maximum rate at some particular ultrasonic intensity. But he did not measure the intensity itself. Beuthe, Furbach and Sörensen[2] observed that the quantity of hydrogen peroxide formed in distilled water by ultrasonic waves becomes maximum at the acoustical power dissipation of 0.09—0.10 watt/gr., which they measured calorimetrically, and that the maximum of the chemical action coincides with the maximum of the expulsion of air bubbles by cavitation caused by ultrasonic radiation. Paounoff[3] observed that the remainder of air or oxygen in water, saturated by air or oxygen respectively, showed the minima at ultrasonic intensity corresponding to the radiation pressure of 170 bar/cm² after ultrasonic treatment. The intensity of the sono-luminescence of water, on the other hand, became perceptible at 140 bar/cm², and had the maximum rate of increase at 170 bar/cm², and saturated gradually beyond 230 bar/cm². Oyama, Ogata and others[4)-6)] observed that the expulsion of air bubbles decreased remarkably at the ultrasonic intensity where the formation of fogs on the liquid surface begins. They observed that chemical reactions such as the decrease of pH, the formation of H_2O_2, and the oxydation of birilubin, have their maximum rate at some ultrasonic intensity, corresponding to the maximum of cavitation, though they did not measure the intensity absolutely.

As these facts are related, as we think, to the basic points of the action of ultrasonic waves, it is intended to investigate the chemical action of the ultrasonic wave in dependence upon its intensity in irradiated liquids themselves.

§ 2. Apparatus.

The arrangement of the experimental apparatus is illustrated schematically in Fig. 1. Two quartz plates Q_1, Q_2, 50 mm in diameter and 6 mm thick (470 kHz), are piled with their x-axes antiparallel, and are connected with three wire-mesh electrodes to an pick-up circuit, which is inductively coupled to the tank circuit of an Hartley circuit oscillator, of the maximum impput 1 kW using a 205 A tube. The output was regulated by adjusting the plate voltage of the vacuum tube, and partly by changing the state of resonance of the quartz plates by adjusting the variable condenser C of the tank circuit. A hollow plane reflector, of adjustable distance, helps to increase the upward radiation. The waves are produced within transformer oil in vertical direction, and, by penetrating the bottom of the reacting vessel V, they reach the liquid sample in it. The vessel is made of Terex glass with an inner diameter 1.9 cm, and is equipped with a water-jacket to cool the treated liquid. With this arrangement, the temperature-rise of the liquid was suppressed within 2—3°C. Sometimes we used a non-cooled vessel with a greater diameter 4.3 cm. In this case the temperature after ultrasonic treatment reached often to 45–60°C.

For the measurement of ultrasonic intensities we used a radiation pressure meter of the balance-type, as is illustrated in the figure. This one consists of an ordinary balance (sensitivity 7 mm per gram), equipped with the pressure vane, P. V., which is suspended beneath the one of the arms. The diameter of the vane is 1.5 cm for use of the vessel of diameter 1.9 cm, and 3 cm for use of the vessel of diameter 4.3 cm. They are of glass or of brass.

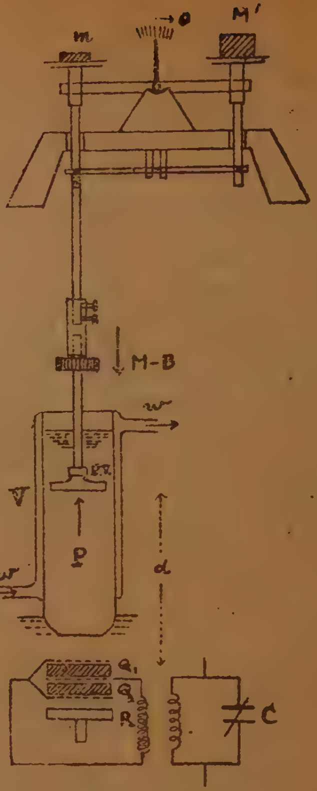

Fig. 1. Apparatus.

The weight M′ is the counter-poise to balance the weight M of the pressure-apparatus minus the bouyancy B when the ultrasonic waves are switched off. The weight m measures the sound radiation-pressure in gram-weights. This pressure with plane pressure-vane showed a peculiar behaviour by the formation of the standing wave between the pressure vane and the quartz transmitter. There were found many positions of stable equilibrium for the same weight m. This is illustrated in Fig. 2. The curve A illustrates schematically the variation of the intensity of ultrasonic radiation pressure on P. V., when it is moved away from the quartz transmitter. It shows maxima and minima of the periodicity of half wave-length as is supposed from the case of acoustic interferometers. The sensitivity curve in working condition of the balance is represented by the straight line B. The descending intervals a_1b_1', a_2b_2, etc. of the curve A are stable, because any small increase in ultrasonic intensity pushes the pressure vane upwards, thus resulting in an increase of the distance d between the vane and the quartz. This in turn reduces the intensity of the ultrasonic wave by its reaction on the quartz plate, and a new equilibrium is attained. On the contrary, the ascending intervals b_0a_1, b_1a_2, etc. are unstable. The intercepts of both curves c_0, c_1', c_2', c_3', etc. give the equilibrium positions for the same weight m.

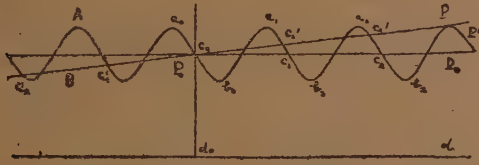

Fig. 2. Explanation of the multiplicity of the positions of equilibrium of the pressure vane.

The sensitivity of the apparatus for small variations of the radiation pressure ΔP is easily calculated. By a small increase of the output, the curve A becomes the curve A' in Fig. 3. The intercept E of the new curve A' with the sensitivity curve B gives the new position of equilibrium. Thus the sensitivity is

$$k' = \frac{\Delta\theta}{\Delta P} = \frac{\Delta\theta}{\Delta d}\,\frac{\Delta d}{\Delta P} = c\,\frac{\Delta d}{\Delta P}, \tag{1}$$

where $c = \Delta\theta/\Delta d$ means the ratio of the variation of the reading of the balance (in cm) to the displacement of the pressure vane. This is the same with the ratio of the length of the pointer to that of the arm of the balance. On the other hand, we obtain

$$\begin{aligned} \Delta P = P_0 - P &= \rho S(d-d_0) + \frac{1}{k}\,\theta \\ &= \left(\rho S + \frac{c}{k}\right)\cdot \Delta d \end{aligned} \tag{2}$$

from the equilibrium conditions of the force, where $k = \partial\theta/\partial m$ means the sensitivity of the balance, ρ the density of the liquid in which the pressure is measured, and S the sectional area of the shaft of the pressure vane. Thus from (1) and (2), we obtain the sensitivity

$$k' = i\,\frac{k}{c+\rho Sk}. \tag{3}$$

For the balance here used k was 0.7 cm/gr., and the diameter of the shaft of the pressure vane was 3 mm (brass vane) or 6 mm (glass vane), so that $k' = 0.95\,k$ or $k' = 0.83\,k$ respectively. Thus the sensitivity is somewhat lower than that of the balance itself.

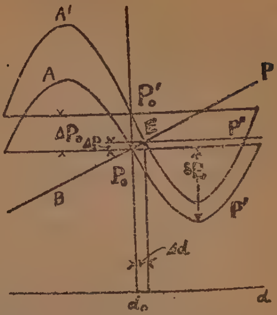

Fig. 3. Shift of the equilibrium position of balance by small change of the radiation pressure.

§ 3. Methods and Result of the Experiment.

(i) *The fading of the colour of the 2,6-dichlorphenol-indophenol sodium* ($O : C_6H_2Cl_2N\ C_6H_4ONa$) *solution (an reducing reaction).*

This substance (in the following simply termed as "dyestuff") is blue in colour in normal or alkaline solutions and red in acidic solutions. When irradiated by ultrasonic waves, it becomes red and then colourless. The red-change is the result of the HNO_2-formation in water by the action of ultrasonic waves. The fading is explained by the formation of NO in water under ultrasonic treatment. This substance reacts with the dyestuff, and becomes HNO_2 by the reaction

$$2NO + H_2O + O \rightarrow HNO_2,$$

while the dyestuff is reduced by losing its oxygen.

Fig. 4 shows the time of fading of 50 cc of the normal dyestuff solution (10^{-5}) in uncooled vessel A. The pressure vane was a disc of diameter 3 cm. It is seen that on the average, 1.2 gr-wt. corresponds to the minimum of the time of fading, or the maximum of the reaction rate. Fig. 5 shows the same for alkaline solutions of this substance of 50 cc (curve a) and 80 cc (curve b). The maximum reaction rates are found at the same radiation pressure 1.2 gr-wt., but the time required is longer for greater amounts of the liquid. This means that not the whole volume of the liquid is effective in producing the reaction. This was verified by observing the sonic chemiluminescence of luminol (3

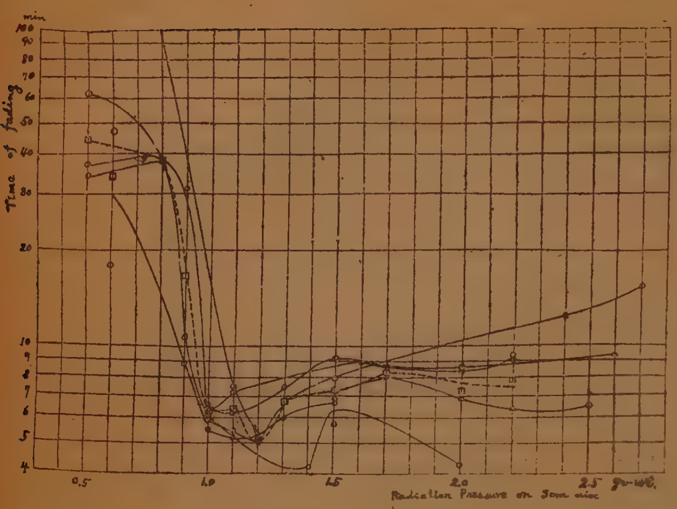

Fig. 4. Time of fading of 2, 6-dichlorphenol -indophenol sodium solution as a function of the ultrasonic intensity.

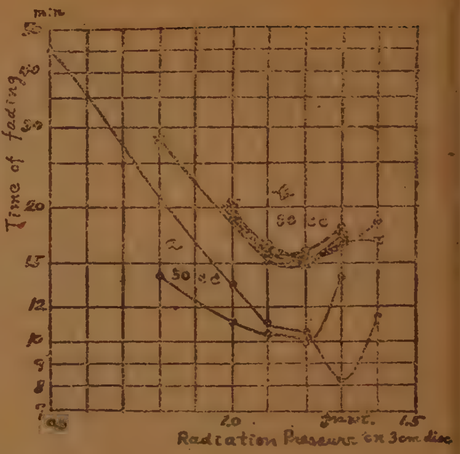

Fig. 5. Fading of colour of the alkaline solution of 2.6-dichlorphenol-indophenol sodium.

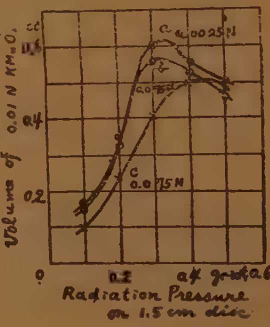

Fig. 6 Consumed amount of $KMnO_4$ per 10 cc in 5 minutes treatment by ultrasonic waves.

aminophthalhydrazide) in Na_2CO_3 solution. The roughly hemispherical volume in front of the pressure plate was found to be the most intense region of luminescence. This may be said also in other chemical reactions produced by ultrasonic waves. It is also explained by this that, in the case of curbe *b*, the result is the same whether the pressure vane is in the upper part of the liquid (points marked with o) or it is in the middle of the liquid (points marked with ×). If all parts of the liquid except the shadow of the vane were equally effective, the increase of dead space behind the pressure plate might decrease the rate of reaction in the latter case.

(ii) *Fading of colour of the acidic solution of potassium permanganate* ($KMnO_4$) (*a reducing reaction.*)

In this case we obtain the maximum reaction rate at 0.32 gr-wt. for the pressure disc of 1.5 cm in diameter. Fig. 6, curve *a* (0.0025 N solution) and curve *b* (0.075 N solution) show this result. The ordinate is the volume of $KMnO_4$ when reduced to 0.01 N solution, consumed in 5 minutes. The consumed amount is independent of the concentration. Curve *c* gives the result for 0.075 N solution, but when the pressure vane is lowered to the middle of the liquid vessel. The increase of ultrasonic intensity for the maximum reaction rate in this case is explained as that, in this narrower vessel, the whole volume is effective except the shadow of the pressure plate, and that, the sound intensity in side volumes of the liquid attains the optimum when the volume directly beneath the pressure plate becomes more intense. The decrease of the maximum height also tells the effect of increased dead space. The optimum intensity in this case of 0.32 gr-wt. on 1.5 cm disc nearly coincides with 1.2 gr-wt. on 3 cm disc of the experiment (i), but is slightly higher.

(iii) *Separation of iodine from acidic solutions of potassium iodide and other reactions* (*oxidizing reactions*).

Fig. 7 shows the result for the separation of I_2 from acidic solutions of potassium iodide in the cooled vessel. The abscissa shows the radiation pressure on 1.5 cm disc, and the ordinate the volume of 0.01 N hypo ($Na_2S_2O_3$)- solution necessary to titrate the I_2, isolated in 10 cc of the solution in 5 minutes treatment. Curve *a* is the titration value immediately after switching off the ultrasonic wave, and curve *b* is the total value obtained by adding the separated amount during 1 hour after the first titration. Both curves have the maxima at 0.4 gr.-wt. on 1.5 cm disc. This value is higher than the optimum intensities for the two reducing reactions (i) and (ii).

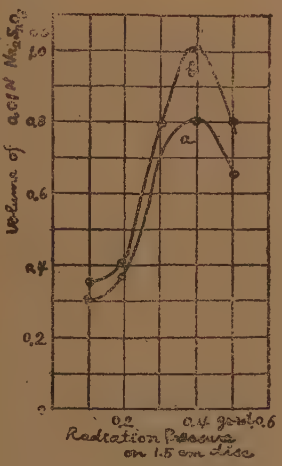

Fig. 7. Isolation of I_2 from KI by ultrasonic treatment.

The same results were obtained for the separated quantity of I_2 from KI, when it is added to distilled water, which is treated with ultrasonic radiation, and also for the quantity of HNO_2 formed in distilled water by ultrasonic treatment. The quantity of HNO_2 was measured by the colour reaction which takes place by adding sulphanilac d and 1-(β-diethylamino-ethylamino) naphthalene. These oxidizing actions of ultrasonic waves showed the maxima at 0.4 gr.-wt. of radiation pressure on 1.5 cm disc. The separation of I_2 from KI is produced by both HNO_2 and H_2O_2, and not stoichiometric, but the chief agent is HNO_2, particularly in short time treatments. These oxidizing reactions are supposed to have their maximum rate at the maximum quantity of HNO_2 in water.

§ 4. Summary and Discussion of the Results.

Since the radiation pressure *P* of the sound in open media is equal to the energy density *E* of the sound, as is known from the theoretical investigations of Langevin and Brillouin, we can calculate the pressure amplitude δp of the ultrasonic wave by the equation

$$P = E = \frac{(\delta p)^2}{2\rho c^2},$$

where ρ is the density and c the velocity of sound in the medium. The observed results are summarized in Table 1, which gives the optimum intensity of ultrasound for various chemical reactions in terms of the energy density and the corresponding pressure amplitude. It is seen that the reducti n of 2,6-dichlorphenol-indophenol sodium attains its maximum rate at an ultrasonic energy density of about 166 erg/cm³, or at a pressure amplitude of 2.64 atm. This is supposed to correspond to the maximum quantity of NO formed in water. The oxidizing reactions are found to be optimum at the ultrasonic intensity of about 215 erg/cm³ or at the pressure amplitude of 3.00 atm. And this corresponds to the maximum quantity of NO_2'-ion formed in water. The reduction of $KMnO_4$ solution by ultrasonic waves takes place rate with maximum rate at about 177 erg/cm³ energy density, or 2.73 atm. pressure amplitude. This value is roughly the same as in the case of the reducing action of 2,6-dichlorphenol-indophenol sodium solution, though perhaps slightly higher. $KMnO_4$ acts on NO, giving up 1.5×O to change the latter to NO_3', while it acts on NO_2', giving up 1×O to form NO_3', so that the optimum reaction rate of the fading of $KMnO_4$ corresponds to the maximum of $1.5 \times NO + NO_2'$ in water. This is found between the maxima of NO and NO_2', and perhaps nearer to the former. This is not in contradiction with the result of the experiment. The maximum of NO coincides with the maximum of the expulsion of dissolved gases observed by Paounoff (170 erg/cm³), while the maximum of NO_2' corresponds nearly to the beginning of the saturation of the intensity of sono-luminescence of water observed by Paounoff.

The errors of observations are perhaps about 10 % in energy densities and about 5 % in presure amplitudes. Why these particular intensities are found for the maximum reaction rates of ultrasonic reactions are not concluded as yet.

Table I. Optimum intensity of ultrasonic waves for sono-chemical reactions.

Reactions (Mainly concerned processes)	Radiation Pressure			Energy density erg/cm³	Pressure amplitude M bar (atm.)
	on 1.5 cm disc gr.-wt.	on 3 cm disc gr.-wt.	dyne/cm²		
Reducing reactions of 2,6-dichlorphenol-indophenol sodium ($NO \rightarrow NO_2'$)	0.32	1.2	166	166±10 %	2.64±5 %
$KMnO_4$ ($NO \rightarrow NO_3'$, $NO_2' \rightarrow NO_3'$, and $H_2O \rightarrow H_2O_2$			177	177	2.73
Oxidizing reactions, HNO_2 in dist. water (NO_2')					
$KI \rightarrow I_2$ (directly)					
$KI \rightarrow I_2$ (by irradiated dist. water) ($NO_2' \rightarrow NO$, $H_2O_2 \rightarrow H_2O$)	0·4	(1.6)	215	215	3.00

In conclusion, the authors express their hearty thanks to Professor Dr. Hichiro Akiya of the Institute of Pharmacy, Faculty of Medicine, Tokyo University, for his kind guidance and support throughout the work.

References.

(1) S. Kusano: Tohoku J. Exp. Med., **30** (1936), 175.

(2) H. Beuthe, E. Furbach, Ch. Sörensen: Akus-Zeits., **4** (1939), 2.9.

(3) Petre Paounoff: C. R., **209** (1939), 33.

(4) H. Oyama, G. Kusumoto: Denkigakkai Zasshi (J. Instn. Electr. Eng. Japan, in Japanese), **62** (1942), 549.

(5) H. Oyama, S. Ogata, T. Nakajima, S. Banno, G. Furukawa: ibid. **62** (1942), 546.

(6) H. Oyama, S. Ogata: Denkigakkai, Denkitsushingakkai, Shomeigakkai 19-kai Rengotaikai Yoko (Proceedings of the 19. joint meeting of Instn. Electr. Eng. Japan, Instn. Electr. Comm. Eng. Japan. and Instn. Electr. Lighting Eng. Japan, in Japanese), (1941), 24-2, 323.

On the Structure of Silver Sulphide and Silver-Arsenic Alloy grown on Silver Crystals.

By Mituo MIWA and Yasuyoshi WATANABE.

Department of Physics, Tokyo University of Literature and Science.

(Read May 9, 1947; Received July 28, 1947)

§ 1. Introduction.

The structure of oxide crystals grown on single crystals of a number of metals was studied by several investigators[1] by means of electron diffraction and it was found that crystals of oxides in most cases grew in particular orientation on the metal crystals. No examination on the growth of metal sulphide, however, seems to have been made except by Uyeda[2], who studied the sulphuration of silver mirror, finding that acanthite, a modification of Ag_2S stable below 180°C, is formed at some particular, not yet analysed, orientation.

The present writers have investigated the structure of silver sulphide crystal formed by sulphuration on single crystals of silver, which were in turn prepared on cleavage faces of molybdenite and rock salt by evaporation in vacuo. In some instances silver-arsenic alloy has been found instead of silver sulphide when hydrogen sulphide was used without being purified, and its structure has also been studied.

§2. Experimental Procedure.

Single crystals of silver were prepared as usual by evaporating silver in vacuo onto fresh cleavage faces of molybdenite at about 50°C and of rock salt at about 200°C, the thickness of silver films being about 50 mμ in either case. The film thus obtained always gave elongated diffraction spots when examined by reflection method, showing that the surface of silver crystal is smooth.

The hydrogen sulphide gas was prepared from mineral iron sulphide and sulphuric acid or hydrochloric acid and washed at first by passing through water only. The gas thus prepared was found to contain arsine as impurity. In the later experiment, therefore, the gas was purified further by passing through calcium chloride, solid iodine and then water in turn. Water vapor was not removed, because it had been known that the dry gas at room temperature did not change silver surface at all. Moreover, the gas was not free from air for the same reason[3].

The silver film formed on molybdenite was exposed to the gas for the duration varying from half an hour to five, without removing from the base, and then examined by the reflection method of electron diffraction, while the film formed on rock salt was treated in the same way after dissolving off the rock salt in water and receiving the film on a brass plate with small holes, and then examined by transmission method. The treated film always gave a faint diffraction pattern with strong background, when examined by reflection method.

§3. Experimental Results and Interpretation.

A. Silver Sulphide grown on Silver Crystal.

1) *Sulphuration of the silver crystal formed on molybdenite.* It has been well known that silver film of moderate thickness deposited on molybdenite cleavage face by evaporation crystallizes in flat plates and takes up complete orientation with (111)-plane parallel to the substrate surface, giving rise to elongated diffraction spots in reflection photograph. Such an aggregate of completely orientated crystals may be considered as a single crystal film with predominant (111)-face.

The film, when exposed to hydrogen sulphide gas, was found to give a complicated and rather diffuse spot pattern with strong background, as shown in Fig. 1, and the product was identified as acanthite in particular crystalline orientation. But there was some inevitable ambiguity in the determination of crystalline orientation for the following reasons: According to X-ray data,(4) acanthite belongs to the orthorhombic system and the lattice constants are 4.77, 6.92 and 6.88 A respectively. Therefore, the lattice type is very close to tetragonal one. Moreover, it will be found that in Fig. 2

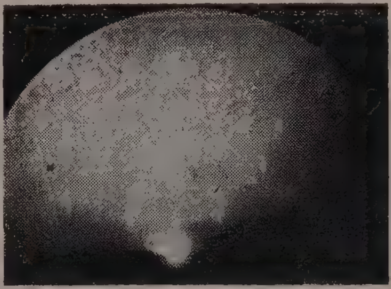

Fig. 1. Pattern of sulphurated silver.

$$AD \simeq 2\,OA,$$

and

$$AS \simeq SE \simeq OA = a.$$

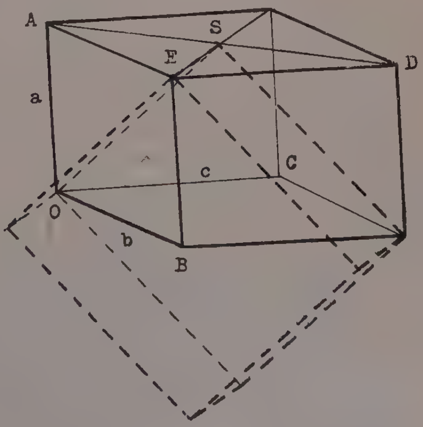

Fig. 2. Unit cell of acanthite.

Hence OS is nearly normal to the (111)-plane and

$$OS \simeq b \simeq c,$$

and the spacings of three net planes (111), (002) and (020) are nearly equal to each other, the values being 3.41, 3.44 and 3.46 Å respectively. Because of these facts and the diffuse nature of diffraction pattern, the two parallelepipeds illustrated in Fig. 2 could not be distinguished from each other in the analysis of diffraction pattern. Thus there were three probable orientations of acanthite on the (111)-face of silver. The result of analysis can be summarized as follows:

a p-plane of acanthite // $(111)_{Ag}$,

and a p-axis of acanthite // $[0\bar{1}1]_{Ag}$,

where p-axis is b-, c-, or OS-axis and p-plane the plane perpendicular to one of the axes. Coexistence of two or three of these orientations is also very probable.

One of these orientations is illustrated in Fig. 3 by making use of reciprocal lattice. In the figure the plane of paper is (111)-plane of the reciprocal lattice of silver, and solid circles represent reciprocal lattice points of silver and crosses those of acanthite. The photograph reproduced in Fig. 1 was obtained with electron beam incident at the azimuth perpendicular to [I] direction. In these orientations, however, no simple relation seems to exist among the atomic distances in the (111)-plane of silver and those in the p-plane of acanthite, although the coincidence of the atomic distances is fairly good in the normal direction. Thus there will be little chance for the growth of large acanthite crystals, and this will partly explain the diffuse nature of the diffraction pattern.

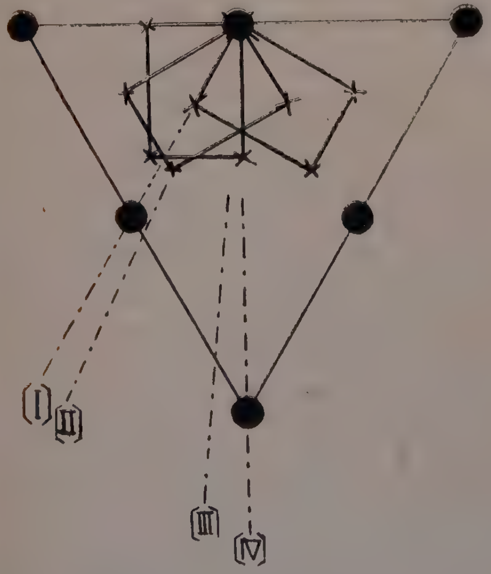

Fig. 3. Reciprocal lattice diagram of possible orientations of acanthite on silver crystal. [I], [II], [III] and [IV] are the azimuths at which the reflection photographs were taken.

2) *Sulphuration of the silver crystals formed on rock salt.* The silver film formed on the cleavage face of rock salt also crystallizes in flat plates and takes up complete orientation with their (001)-plane, instead of (111)-plane in the previous case, parallel to the cleavage face of substrate crystal. When these silver crystals were exposed to hydrogen sulphide gas, acanthite was again found to grow on them in a particular crystalline orientation, though different from that in the previous case, as is seen in the transmission pattern shown in Fig. 4 schematically.

The diffraction spots due to the acanthite, in this case, were fairly sharp, though faint, and the orientation of the acanthite could be determined with considerable certainty. The spacings determined on the basis of the lattice constant of silver agree fairly well with X-ray data (Table I). The assignment of indices to the spots is given in Fig. 4. Another possibility of assigning (131) instead of (113) to the most intense spot seems to be excluded, because the calculated value of the spacing 1.99 Å is too far from the observed one. The final result can be summarized as follows:

Table I.

Indices	Spacings (A)	
	Electron	X-ray
(002)	3.4_3	3.44
(111)	3.4_0	3.41
(113)	1·969	1.98

$$[110]_{Ag_2S} \perp (001)_{Ag}$$

and $$[001]_{Ag_2S} \,//\, [100]_{Ag}$$

It will be noticed that there is no simple lattice plane of acanthite parallel to (001) plane of silver or the surface of the film, although (001) plane of

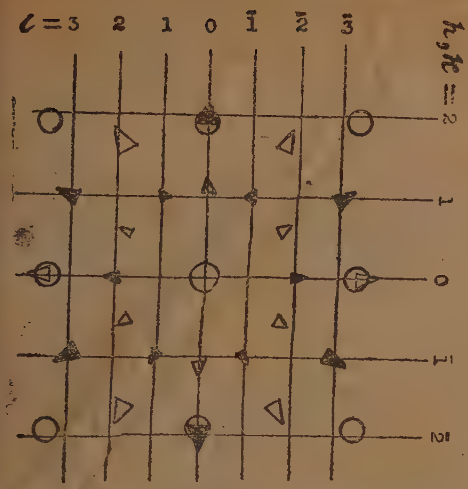

Fig. 4. Schema of the transmission pattern of sulphurated silver on rock salt. Open circles belong to silver and triangles to acanthite, solid and open ones corresponding to two different orientations. In the one orientation c-axis is normal to (100)-plane of silver and in the other to (010)-plane. The size of triangles gives a measure of intensities of spots.

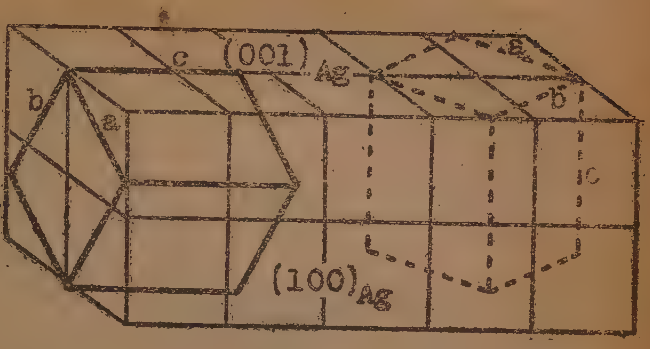

Fig. 5. The orientation of acanthite on silver deposited on rock salt.

acanthite is parallel to (100)- or (010)-plane of silver, as is illustrated in Fig. 5. It must be also emphasized that there is no acanthite crystal whose (001)-plane is parallel to (001)-plane of silver crystal (the orientation illustrated with dotted lines in Fig. 5). Thus it is highly probable that crystal nuclei of acanthite are formed not on smooth (001)-face but on (100)- or (010)-face of silver crystal. Finally it will be worth mentioning that the pattern given in Fig. 4 is not explained by the acanthite crystals that might grow on (111)-faces of silver existing probably along the periphery of predominant (001)-face. The pattern should have a four-fold symmetry in that case.

B. Silver-Arsenic Alloy grown on Silver Crystal.

In the course of the study described above, the silver film exposed to hydrogen sulphide gas was often found to give a pattern having simple structure which could not be explained by the structure of acanthite. It was a curious fact that such a pattern was generally obtained only after the treated specimen was kept in a desiccator for a few days. The elongation of diffraction spots of silver always faded away after the appearance of the new spots. However, it was soon found that the hydrogen sulphide gas contained arsine as impurity and the pattern was probably due to a kind of alloy of silver and arsenic or silver arsenide, having a closest packing hexagonal lattice with $a = 2.89$ A and $c/a = 1.63$.

According to Broderick and Ehret(5), $5 \sim 20\,\%$ arsenic alloy of silver, when quenched from high temperature, has closest packed hexagonal lattice with $a = 2.89$, A and $c/a = 1.63_3$, and belongs to so-called ε-phase, the ideal composition of which for this combination is Ag_3As(6). In bulk state, however, the phase is unstable below 390°C and the alloy decomposes into two phases, i. e. pure arsenic and silver containing a few atomic percent of arsenic as solute. The latter has the same crystal lattice as pure silver, which is quite different from the observed one. But the observed lattice constants are very close to the ones found by Broderick and Ehret and it is not a rare case that the phase usually unstable in bulk state comes out to be stable in thin film state. The encroachment of smooth (111)-surface of silver suggested by the disappearance of the elongation of diffraction spots is also favourable for the theory of the formation of alloy. The composition of the alloy, however, is difficult to be determined on the basis of the electron diffraction data.

The orientation of the supposed alloy grown on (111)-face of silver (deposited on a cleavage face of molybdenite) was

$$(0001)_{\text{alloy}} // (111)_{\text{Ag}},$$

and

$$[11\bar{2}0]_{\text{alloy}} // [110]_{\text{Ag}}.$$

The atomic arrangements and distances in both lattices of silver and alloy are very close to each other, as is seen in Fig. 6. Therefore, the arsenic

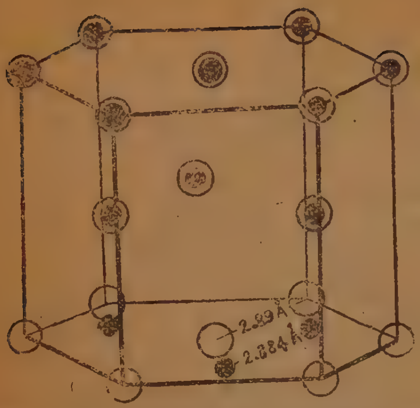

Fig. 6. Atomic arrangements and relative orientation of silver (solid circle) and silver-arsenic alloy (open circle).

atom will be able to diffuse into the lattice of silver crystal without disturbing it violently. This will be one of the reasons why arsenic atoms captured by the silver crystal migrate in it, forming alloy crystals of moderate size within a few days, and thus, give rise to well defined diffraction spots.

In conclusion the writers wish to express their gratitude to the Department of Education for the financial support.

References.

(1) Mehl, M'Candless and Rhines: Nature, **134** (1934), 1009. Burgers and von Amstel: Physica, **3** (1936), 1057. Nelson: Jour. Chem. Phys., **5** (1937), 252. Yamaguchi: Proc. Phys.-Math. Soc. Japan, **20** (1938), 230.
(2) Uyeda: Kagaku (in Japanese), **11** (1941), 482.
(3) Meller: A Comprehensive Treatise on Inorganic and Theoretical Chemistry, Vol 3, P 439, P 349. Gmelin-Krant: Handbuch der Anorganischen Chemie, Bd. **5**, S 73.
(4) J. Palacious and S, Salvia: An. Soc. Esp. Fisica Qim., **29** (1931), 269, cited in Zeit. f. Krist. Referatenteil, **4** (1933), R 38.
(5) S. Broderick and W. F. Ehret: Jour. Chem. Phys., **35** (1931), 3322.
(6) Glocker: Materialprüfung mit Röntgenstrahlen unter besonderer Berücksichtigung der Röntgenmetallkunde, (1936), S 246.

Theory of Split-Anode Magnetrons. I.

By Sin-itiro TOMONAGA.

Tokyo Bunrika Daigaku.

(Received July 30, 1947.)

§ 1. Introduction.

In order to clarify the oscillation mechanism of a magnetron it is necessary to know how electrons move in the inner space of the magnetron and especially how energy is transported from electrons to the electric oscillation taking place in the resonant circuit attached to the split anode of the magnetron. It is further necessary for the understanding of the nature of the magnetron oscillation to know how the phases of electrons' motions which are, without some special cause, distributed with equal probability over all values between zero and 2π, are regulated in such a way that these electrons have the tendency of moving in phase making several clusters of space charge in the magnetron and thus inducing electric oscillation in the split anode.

In studying the motion of electrons for this purpose two distinct methods have been thus far used, a particle-mechanical method on one hand and a hydrodynamical method on the other. Although the latter method seems to be preferable since it contains no difficulty of many body problem, it must be noted that the swarm of electrons in the magnetron is far too rare to allow the application of the hydrodynamical method except in some special cases.

We are thus forced to use a particle-mechanical method for our perpose. In this treatment the difficulty of the many body problem can be overcome if one replaces the influence upon one electron of other electrons by a suitably chosen electrostatic force caused by the space charge distributed in the magnetron.

There are strong presumptions that this electrostatic force has the potential of the from

$$U(r) = U_a(r/r_a)^2, \tag{1}$$

where r is the distance from the central axis of the magnetron, U_a the anode voltage, r_a the radius of the anode.

If one assumes that the potential of this form really exists in the magnetron, it is comparatively easy to develop a theory of the magnetron oscillation. A detailed report of this problem is now in preparation and a comprehensive discription of the theory as well as the experimental results obtained by members of the Technical Institute of Japanese Navy will soon be published, so we shall give in the present report only a brief account of the theory.

§ 2. Unperturbed Motion of Electrons.

We investigate first the motion of an electron in a magnetron when no electric oscillation is taking place in the split anode. We assume, for simplicity, that the magnetron is infinitely long along its axis. Let U_a be the anode voltage and H the impressed magnetic field, the latter being assumed to be exactly parallel to the axis of the magnetron. The potential energy of the electron at the position (r, θ) is then, according to our assumption (1),

$$V(r, \theta) = -eU_a(r/r_a)^2, \tag{2}$$

where $-e$ denotes the charge of the electron.

The Hamiltonian function of the electron is then

$$H = \frac{1}{2m}\left(p_r^2 + \frac{1}{r^2}p_\theta^2\right) + \omega_H p_\theta + \frac{m}{2}(\omega_H^2 - \omega_c^2)r^2, \tag{3}$$

where ω_H and ω_c are defined by

$$\begin{cases} \omega_H = \dfrac{eH}{2mc}, \text{ (Larmor frequency)} \\ \omega_c = \sqrt{\dfrac{2eU_a}{mr_a}}, \text{ (critical frequency)} \end{cases} \tag{4}$$

m being the mass of the electron.

The motion is now obtained by introducing the action variables J_r, J_θ and the angle variables w_r, w_θ. This process, which is familiar to us in the atomic physics, gives

$$re^{i\theta} = \sqrt{\frac{1}{m\sqrt{\omega_H^2 - \omega_c^2}}}\left(\sqrt{J_r - J_\theta} - i\sqrt{J_r}\, e^{iw_r}\right)e^{iw_\theta}, \tag{5}$$

Where J_r and J_θ are constants independent of time, and w_r and w_θ increase linearly with time:

$$\begin{cases} w_r = \omega_r t + \delta_r, \\ w_\theta = \omega_\theta t + \delta_\theta. \end{cases} \tag{6}$$

The frequencies ω_r and ω_θ in (6) are found to be

$$\begin{cases} \omega_r = 2\sqrt{\omega_H^2 - \omega_c^2}, \\ \omega_\theta = \omega_H - \sqrt{\omega_H^2 - \omega_c^2}. \end{cases} \tag{7}$$

In (6) δ_r and δ_θ are two phase constants independent of time. The four constants J_r, J_θ, δ_r and δ_θ are determined if one specifies the initial condition. As is well known, the energy of the motion expressed in terms of the action variables is given by

$$E = \omega_r J_r + \omega_\theta J_\theta, \tag{8}$$

From (5) it is seen that the motion of the electron is a superposition of two uniform circular motions. The electron performs thus an epicyclic motion, in which the revolutional motion has the radius

$$R_{\text{rev}} = \sqrt{\frac{1}{m\sqrt{\omega_H^2 - \omega_c^2}}}\sqrt{J_r - J_\theta}, \tag{9}$$

and the rolling motion the radius

$$R_{\text{rol}} = \sqrt{\frac{1}{m\sqrt{\omega_H^2 - \omega_c^2}}}\sqrt{J_r}. \tag{10}$$

The distance of the electron from the center when it is most distant from the center is given by

$$R_{\text{aph}} = \sqrt{\frac{1}{m\sqrt{\omega_H^2-\omega_c^2}}}\left(\sqrt{J_r}+\sqrt{J_r-J_\theta}\right). \tag{11}$$

We shall call this distance "aphelion radius".

It is seen from (5) that for an electron which starts from the center we have to put

$$J_\theta = 0, \tag{12}$$

and the energy is given by

$$E_0 = J_r\omega_r. \tag{13}$$

The aphelion radius for this electron will be denoted by R_0. It is given by

$$R_0 = 2\sqrt{\frac{1}{m\sqrt{\omega_H^2-\omega_c^2}}}\sqrt{J_r}. \tag{14}$$

It is to be noted that J_r is always positive and J_θ is positive or negative according to the initial condition for the motion. It is further proved that J_r must be larger than J_θ when J_θ is positive.

§ 3. General Theory of Motion Perturbed by an electric Oscillation.

We shall now develop the theory of motion perturbed by the electric oscillation taking place in the anode segment. When an electric oscillation is excited in the split anode, there exists in the inner space of the magnetron an alternating field due to this oscillation. The potential of this field will be denoted by $\Phi(r, \theta, t)$. Then, as we shall show later, it can be expressed in the form of a Fourier expansion:*

$$\Phi(r, \theta, t) =$$

$$\mathrm{Re}\left[\sum_{\sigma=1}^{\infty} A_\sigma r^\sigma e^{i(\sigma\theta-\omega t)} + \sum_{\sigma=1}^{\infty} B_\sigma r^\sigma e^{i(\sigma\theta+\omega t)}\right], \tag{15*}$$

where the Fourier coefficients A_σ and B_σ, $\sigma = 1, 2, 3, \cdots$, are determined later. Further ω in (15) denotes the frequency of the oscillation.

In the unperturbed motion the variables J_r, J_θ, δ_r and δ_θ are constant throughout the motion. But, being perturbed by the potential $\Phi(r, \theta, t)$, they are no longer constant when oscillation is taking place. Since these variables form a set of canonical coordinates and momenta, their dependence on time are given by the canonical equations

$$\left\{\begin{aligned} \dot{J}_r &= -\frac{\partial V}{\partial \delta_r}, & \dot{J}_\theta &= -\frac{\partial V}{\partial \delta_\theta}, \\ \dot{\delta}_r &= \frac{\partial V}{\partial J_r}, & \dot{\delta}_\theta &= \frac{\partial V}{\partial J_\theta}, \end{aligned}\right. \tag{16}$$

in which V is the potential energy of the electron due to the alternating potential Φ:

$$V(J_r, J_\theta, \delta_r, \delta_\theta) = -e\Phi(r, \theta, t). \tag{17}$$

On the right-hand side of (17) r and θ are considered as functions of J_r, J_θ, δ_r and δ_θ according to (5) and (6).

From (15) we can see that V is expressed in the form

$$\begin{aligned} V = \mathrm{Re}\sum_{\sigma,\tau}\big[&X_{\sigma,\tau}\exp\{i(\sigma\delta_\theta+\tau\delta_r)+i(\sigma\omega_\theta+\tau\omega_r-\omega)t\} \\ &+Y_{\sigma,\tau}\exp\{i(\sigma\delta_\theta+\tau\delta_r)+i(\sigma\omega_\theta+\tau\omega_r+\omega)t\}\big], \end{aligned} \tag{18}$$

in which the coefficients X and Y are functions of J_r and J_θ only. The equations for the perturbed motion become then

$$\left\{\begin{aligned} \dot{J}_\theta &= -\mathrm{Re}\sum_{\sigma,\tau}[i\sigma X_{\sigma,\tau}\exp\{i(\sigma\delta_\theta+\tau\delta_r)+i(\sigma\omega_\theta+\tau\omega_r \\ &\quad -\omega)t\}+i\sigma Y_{\sigma,\tau}\exp\{i(\sigma\delta_\theta+\tau\delta_r)+i(\sigma\omega_\theta+\tau\omega_r+\omega)t\}], \\ \dot{J}_r &= -\mathrm{Re}\sum_{\sigma,\tau}[i\tau X_{\sigma,\tau}\exp\{i(\sigma\delta_\theta+\tau\delta_v)+i(\sigma\omega_\theta+\tau\omega_r \\ &\quad -\omega)t\}+i\tau Y_{\sigma,\tau}\exp\{i(\sigma\delta_\theta+\tau\delta_r)+i(\sigma\omega_\theta+\tau\omega_r+\omega)t\}], \\ \dot{\delta}_\theta &= \mathrm{Re}\sum_{\sigma,\tau}\Big[\frac{\partial X_{\sigma,\tau}}{\partial J_\theta}\exp\{i(\tau\delta_\theta+\tau\delta_r)+i(\sigma\omega_\theta+\tau\omega_r \\ &\quad -\omega)t\}+\frac{\partial Y_{\sigma,\tau}}{\partial J_\theta}\exp\{i(\sigma\delta_\theta+\tau\delta_r)+i(\sigma\omega_\theta+\tau\omega_r+\omega)t\}\Big], \\ \dot{\delta}_r &= \mathrm{Re}\sum_{\sigma,\tau}\Big[\frac{\partial X_{\sigma,\tau}}{\partial J_r}\exp\{i(\sigma\delta_\theta+\tau\delta_r)+i(\sigma\omega_\theta+\tau\omega_r \\ &\quad -\omega)t\}+\frac{\partial Y_{\sigma,\tau}}{\partial J_r}\exp\{i(\sigma\delta_\theta+\tau\delta_r)+i(\sigma\omega_\theta+\tau\omega_r+\omega)t\}\Big]. \end{aligned}\right. \tag{19}$$

Since the right-hand sides of (19) are sums of periodic functions of t with small amplitudes, they give rise to, in general, merely small fluctuations of J_r, J_θ, δ_r and δ_θ, because they give at some instant of time positive and at some other instant of time negative changes to these variables, so that, averaged over a long time, they cause no marked changes of J and δ.

But when the condition

$$\sigma\omega_\theta+\tau\omega_r-\omega = 0 \tag{20}$$

is satisfied for some positive integral values of σ and τ, an exceptional case occurs. In such a case some term on the right hand side is no longer periodic and hence causes one-sided changes of the variables. In such a case secular changes of J and δ take place.

---

* The symbol Re in (15) and in the following equations is to be read as "real part of".

When the "resonance condition" (20) is satisfied, the electron orbit will thus deforms gradually and it becomes possible that the orbit of the electron, having started from the center and remained initially in its neighbourhood expands outwards until the electron reaches the anode.

Approximate equations for snch secular changes of J and δ are obtained by neglecting all terms in (19) which cause merely small fluctuations of the variables. In this way we obtain

$$\left\{\begin{aligned} \dot{J}_\theta &= -\mathrm{R_e} i\sigma X_{\sigma,\tau}(J_r, J_\theta)\exp\{i(\sigma\delta_\theta+\tau\delta_r)\}, \\ \dot{J}_r &= -\mathrm{R_e} i\tau X_{\sigma,\tau}(J_r, J_\theta)\exp\{i(\sigma\delta_\theta+\tau\delta_r)\} \\ \dot{\delta}_\theta &= \mathrm{R_e}\frac{\partial X_{\sigma,\tau}(J_r, J_\theta)}{\partial J_\theta}\exp\{i(\sigma\delta_\theta+\sigma\delta_r)\} \\ \dot{\delta}_r &= \mathrm{R_e}\frac{\partial X_{\sigma,\tau}(J_r, J_\theta)}{\partial J_r}\exp\{i(\sigma\delta_\theta+\tau\delta_r)\}. \end{aligned}\right. \tag{21}$$

The equations (21) are now sufficiently simple to give insight on the general feature of the secular change of the electron orbit. One can see using these equations in what manner the energy is transported from the electron to the oscillation and how the phase regulation of the electron's motion will take place. But before entering to the general treatment it is preferrable to give typical examples of such considerations.

§ 4. Example of a Four-split Push-pull Magnetron.

In a four-split push-pull magnetron the oscillating voltages on four anode segments are given by

$$\frac{\Phi(r_a, \theta, t)}{=\cos\omega t}\left\{\begin{array}{ll} \phi, & \text{for } 0<\theta<\frac{\pi}{2} \\ -\phi, & \text{for } \frac{\pi}{2}<\theta<\pi \\ \phi, & \text{for } \pi<\theta<\frac{3\pi}{2} \\ -\phi, & \text{for } \frac{3\pi}{2}<\theta<2\pi. \end{array}\right. \tag{22}$$

In (22) we have assumed that the gaps between neighbouring anode segments are infinitely narrow.

When the voltage on the anode segments is given by (22), the alternating potential in the inner space can be determined if we assume that the potential satisfies the Laplace equation in this space. We obtain this potential in the form of a Fourier expansion:

$$\Phi(r, \theta, t) = \frac{4\phi}{\pi}\cos\omega t\cdot\sum_{n=0}^{\infty}\frac{1}{2n+1}\left(\frac{r}{r_a}\right)^{2(2n+1)}\sin 2(2n+1)\theta$$

$$= \mathrm{R_e}\frac{2\phi}{\pi}\sum_{n=0}^{\infty}\left\{\frac{-i}{2n+1}\frac{1}{r_a^{2(2n+1)}}r^{2(2n+1)}\cdot\exp[i\{2(2n+1)\theta-\omega t\}] + \frac{-i}{2n+1}\frac{1}{r_a^{2(2n+1)}}r^{2(2n+1)}\exp[i\{2(2n+1)\theta+\omega t\}]\right\}. \tag{23}$$

one notices that in this expansion only terms of $\sin 2\theta$, $\sin 6\theta$, $\sin 10\theta$, $\cdots\cdot$ appear. This fact results in that in the series on the right-hand sides of (18), (19) and (21) only terms with

$$\sigma = 2, 6, 10, \cdots\cdot, 2(2n+1), \cdots\cdot \tag{24}$$

appear.

Using (23) the coefficients $X_{\sigma,\tau}$ can be calculated. We obtain, for example,

$$\left\{\begin{aligned} X_{2,0} &= \frac{2e\phi}{\pi r_a^2 m}\frac{i}{\sqrt{\omega_H^2-\omega_c^2}}(J_r-J_\theta), \\ X_{2,1} &= \frac{4e\phi}{\pi r_a^2 m}\frac{1}{\sqrt{\omega_H^2-\omega_c^2}}\sqrt{J_r(J_r-J_\theta)}, \\ X_{2,2} &= -\frac{2e\phi}{\pi r_a^2 m}\frac{i}{\sqrt{\omega_H^2-\omega_c^2}}J_r, \\ X_{2,\tau} &= 0, \quad \text{for } \tau\neq 0,\ 1 \text{ nor } 2. \end{aligned}\right. \tag{25}$$

In general we have

$$\left\{\begin{aligned} &X_{\sigma,\tau} = 0, \quad \text{for other values of } \tau \text{ than} \\ &\qquad \tau = 0, 1, 2, \cdots\cdot, \sigma. \end{aligned}\right. \tag{26}$$

As mentioned in the preceding section the secular change of the orbit takes place when the condition $\omega=\sigma\omega_\theta+\tau\omega_r$ is satisfied. But in our case σ must have one of the values given by (24) and τ must be zero or positive and not greater than σ according to (26).

We shall now see how J and δ behave when the resonace condition is satisfied. As typical examples we shall discuss the three cases with $\sigma=2$ corresponding each to the three values of τ: $\tau=0$, 1 and 2.

(i) Case of $\sigma=2$ and $\tau=0$.

In this case (21) is

$$\left\{\begin{aligned} &\dot{J}_\theta = 2\Omega(J_r-J_\theta)\cos 2\delta_\theta, \qquad \dot{J}_r = 0, \\ &\dot{\delta}_\theta = \Omega\sin 2\delta_\theta, \qquad \dot{\delta}_r = -\Omega\sin 2\delta_\theta, \\ &\Omega = \frac{2e\phi}{\pi r_a^2 m}\frac{1}{\sqrt{\omega_H^2-\omega_c^2}}. \end{aligned}\right. \tag{27}$$

These equation can be intgrated easily, giving

$$\left\{\begin{aligned} J_\theta &= J_{\theta_0}+(J_{\theta_0}-J_{r_0})\{\sin^2\delta_{\theta_0}\cdot e^{2\Omega(t-t_0)} + \cos^2\delta_{\theta_0}\cdot e^{-2\Omega(t-t_0)}\} \\ J_r &= J_{r_0}, \\ \cos 2\delta_\theta &= -\frac{\sin^2\delta_{\theta_0}\cdot e^{2\Omega(t-t_0)}-\cos^2\delta_{\theta_0}\cdot e^{-2\Omega(t-t_0)}}{\sin^2\delta_{\theta_0}\cdot e^{2\Omega(t-t_0)}+\cos^2\delta_{\theta_0}\cdot e^{-2\Omega(t-t_0)}} \\ \cos 2(\delta_r-\delta_{r_0}+\delta_{\theta_0}) &= \cos 2\delta_\theta. \end{aligned}\right. \tag{28}$$

The quantities with the suffix zero mean the initial values. As the electron starts initially from the center we have to put

$$J_{\theta_0} = 0. \tag{29}$$

Having found the solutions (28) we can now see how the orbit deforms. Introducing (28) into (10) we obtain

$$R_{\mathrm{aph}} = \frac{R_0}{2}\left[1+\{\sin^2\delta_{\theta_0}\cdot e^{2\Omega(t-t_0)} + \cos^2\delta_{\theta_0}\cdot e^{-2\Omega(t-t_0)}\}^{\frac{1}{2}}\right], \tag{30}$$

which means that the aphelion radius either increases immediately or decreases first, reaches the minimum and then increases. In any case it increases ultimately until the electron arrives at the anode. It is to be noted that this ultimate increase of R_{aph} occurs independently of the initial value of the phase of the motion. All electrons will thus reach the anode independently of their initial conditions.

We can also calculate how the energy of the electron changes. It is given by

$$\begin{aligned} E &= E_0+\omega_\theta J\mathrm{s}_0[1-\{\sin^2\delta_{\theta_0}\cdot e^{2\Omega(t-t_0)} \\ &\qquad +\cos^2\delta_{\theta_0}\cdot e^{-2\Omega(t-t_0)}\}] \\ &= E_0-4\omega_\theta J_{r_0}\frac{R_{\mathrm{aph}}}{R_0}\left(\frac{R_{\mathrm{aph}}}{R_0}-1\right). \end{aligned} \tag{31}$$

This equation shows that the energy *decreases* as the electron approaches the anode. The net change of the electron during the travel from cathod to anode is given by

$$\Delta E = -4\omega_\theta J_{r_0}\frac{r_a}{R_0}\left(\frac{r_a}{R_0}-1\right), \tag{32}$$

which is evidently negative. This latter fact means that work is done by the electron on the alternating potential during this travel. Since the energy must be conserved, this amount of energy is supplied to the oscillation by the electron.

By means of this energetic consideration we can conclude in the following way: When in the oscillation circuit attached to the split anode a minute germ of oscillation is generated by some chance, it will grow by this energy supply from the electrons, if the anode voltage and the impressed magnetic field have such suitable values that the resonance condition $\omega = 2\omega_\theta$ is satisfied.

It is to be noted here that all electrons contribute to this energy supply, because (32) holds for all electrons independently of their initial conditions.

From the third equation of (28) a remarkable result is obtained: When a sufficiently long time has elapsed, $\cos 2\delta_\theta$ tends to -1 independently of the initial value of δ_θ. This means that the phases of electrons' motions, which have had initially quite random values, are regulated and tend to either $\pi/2$ or $3\pi/2$ according as their initial values. If the initial value of δ_0 lies in the first or second quadrant, it tends to $\pi/2$ and if it is initially in the third or fourth quadrant, it tends to $3\pi/2$. In this way the electrons are gathered gradually into the positions given by

$$re^{i\theta} = re^{i\left(\omega_\theta t+\frac{\pi}{2}\right)} \quad \text{or} \quad re^{i\left(\omega_\theta t+\frac{3\pi}{2}\right)} \tag{33}$$

as they approach the anode. They form thus two rotating clusters of space charge rotating with the angular velocity ω_θ. It can be shown that the phase of rotation of these clusters is such that they induce positive charges in the anode segments whose voltages are rising and negative charges in the anode segments whose voltages are sinking. Thus the rising voltage of the anode segment has the tendency of being still more raised and the sinking voltage of the anode segment the tendency of being still more lowered. In this way the oscillation in the circuit is enforced by the rotating clusters of electrons and the minute germ of oscillation will grow until it obtaines an observable intensity. This is the mechanism of self-excitation of oscillation by the magnetron.

As is obvious, this mechanism of oscillation by rotating clusters of electrons resembles very much the mechanism of generation of alternating current by an alternator. In the latter machine the alternating current is generated by the electromagnetic induction by rotating magnetic poles, while in the magnetron the oscillation is excited by the electrostatic induction by the rotating clusters of electrons. This analogy has suggested the member of the Naval Technical Institute to call the rotating cluster "electron pole" and the existence of such rotating poles in the magnetron had been expected by them already befere the present mathematical theory was established.

(ii) Case of $\sigma = 2$ and $\tau = 2$.

In this case (21) becomes,

$$\left\{\begin{aligned} \dot{J}_\theta &= -2\Omega J_r \cos(2\delta_\theta+2\delta_r), \\ \dot{J}_r &= -2\Omega J_r \cos(2\delta_\theta+2\delta_r), \\ \dot{\delta}_\theta &= 0, \\ \dot{\delta}_r &= \Omega \sin(2\delta_\theta+2\delta_r), \end{aligned}\right. \tag{34}$$

which gives rise to

$$\left\{\begin{aligned} J_\theta &= J_{\theta_0}-J_{r_0}+J_{r_0}\{\sin^2(\delta_{\theta_0}+\delta_{r_0})\cdot e^{2\Omega(t-t_0)} \\ &\quad +\cos^2(\delta_{\theta_0}+\delta_{r_0})\cdot e^{-2\Omega(t-t_0)}\}, \\ J_r &= J_{r_0}\{\sin^2(\delta_{\theta_0}+\delta_{r_0})\cdot e^{2\Omega(t-t_0)} \\ &\quad +\cos^2(\delta_{\theta_0}+\delta_{r_0})\cdot e^{-2\Omega(t-t_0)}\} \\ \delta_\theta &= \delta_{\theta_0}, \\ \cos 2(\delta_r+\delta_{\theta_0}) &= \\ &\frac{\sin^2(\delta_{\theta_0}+\delta_{r_0})\cdot e^{2\Omega(t-t_0)}-\cos^2(\delta_{\theta_0}+\delta_{r_0})\cdot e^{-2\Omega(t-t_0)}}{\sin^2(\delta_{\theta_0}+\delta_{r_0})\cdot e^{2\Omega(t-t_0)}+\cos^2(\delta_{\theta_0}+\delta_{r_0})\cdot e^{-2\Omega(t-t_0)}}. \end{aligned}\right. \tag{36}$$

If one calculates R_{aph} by using (36), one finds that it is given by (30) also in the present case. But now the energy of the electron is given by

$$\begin{aligned} E &= E_0+(\omega_r+\omega_\theta)J_{r_0}[\{\sin^2(\delta_{\theta_0}+\delta_{r_0})\cdot e^{2\Omega(t-t_0)} \\ &\quad +\cos^2(\delta_{\theta_0}+\delta_{r_0})\cdot e^{-2\Omega(t-t_0)}\}-1] \\ &= E_0+4(\omega_r+\omega_\theta)\frac{R_{aph}}{R_0}\left(\frac{R_{aph}}{R_0}-1\right), \end{aligned} \tag{36}$$

so that this energy *increases* as the electron approaches the anode. The net change of the energy is then given by

$$\varDelta E = 4(\omega_r+\omega_\theta)\frac{r_a}{R_0}\left(\frac{r_a}{R_0}-1\right), \tag{37}$$

which is positive, so that work is done by the alternating potential upon the electron. The electron will thus brake the oscillation in the circuit even if an oscillation is one generated in the circuit. In this way it becomes clear that when the resonance condition $\omega = 2(\omega_\theta+\omega_r)$ is satisfied no self-excitation of oscillation is possible.

Also in this case the formation of electron poles takes place. But the calculation shows that the phase of their rotation is shifted by 90° from that in the former case. Thus the poles induce negative charges in the anode segments whose voltages are rising and positive charges in the anode segments whose voltages are sinking. As the consequence, the oscillation in the circuit is weakened by the electron poles.

(iii) Case of $\sigma = 2$ and $\tau = 1$.

In this last case it is easily shown that the electron never reach the anode, so that, of course, no energy is supplied from the electrons to the oscillation. No self-excitation of oscillation is possible in this case:

The above three typical examples show how the secular change of the electron orbit takes place, how the energy is supplied to or absorbed from the oscillation by the electrons and how the electron poles are formed in the magnetron. Moreover, these three examples cover all posibilities of the resonance phenomena: (i) all electrons reach the anode by supplying energy to the oscillation, (ii) all electrons reach the anode by absorbing energy from the oscillation and (iii) the electrons never reach the anode so that, of course, no energy exchange takes place between electrons and oscillation. That no further cases can occur will be shown in the general treatment which will be given in the second report. The self-excitation of oscillation is expected only in the first case (but see the section 6 of the seeond report).

It is a remarkable feature of the self-excitation of oscillation by a magnetron that all electrons contribute to the oscillation. No electron-selecting process is thus necessary in this oscillator. It may be the main ground for the evidence that by a magnetron very intense oscillation can be more easily obtained than with any other devices such as B. K.-tube and Osaka-tube. In these tubes only such electrons which starts from the cathode with favorable phases can contribute to the oscillation, and other electrons with unfavorable phases must be removed by some selecting process since these latter will hinder the growth of oscillation if they are left in the tube.

Generalization of our treatments to multi-split magnetrons as well as the comparison of theoretical results with experimental evidences will be given in the second report.

Theory of Split-Anode Magnetrons II.

By Sin-itiro TOMONAGA

Tokyo Bunrika Daigaku.

(Received July 30, 1947)

§ 1. Introduction.

In the first report⁽¹⁾ we have developed a general theory of secular change of electron motion in a magnetron caused by the electric oscillation taking place in the attached oscillation circuit. We have then illustrated by referring to a simple example of a four-split magnetron how energy is supplied by the electron to the oscillation and how the minute germ of oscillation grows until it obtains an observable intensity.

In this second report the considerations of the first report will be generalized so as to include multi-split magnetrons in which, in general, also various polyphase oscillations can be excited. In the last section of the present report also the comparison of the theory with experiments is given to show how our theory gives results which agree satisfactorily with experimental evidences.

§ 2. Alternating Field in the Magnetron.

Imagine an N-split magnetron. Owing to the structure of the oscillation circuit attached to the split anode, there belong $N-1$ possible modes of oscillation to the proper oscillation of the circuit. When u_1, u_2, u_3, $\cdots\cdot u_N$ denote the alternating voltages of the anode segments 1, 2, 3, $\cdots\cdot N$ respectively, then these anode voltages for $N-1$ possible sequences of oscillations are represented by

$$\left\{\begin{aligned} u_1 &= \phi\cos\omega t, \\ u_2 &= \phi\cos\left(\omega t-\frac{2\pi}{N}Z\right), \\ u_3 &= \phi\cos\left(\omega t-2\frac{2\pi}{N}Z\right), \\ &\vdots \\ u_\nu &= \phi\cos\left(\omega t-\overline{\nu-1}\frac{2\pi}{N}Z\right), \\ &\vdots \\ u_N &= \phi\cos\left(\omega t-\overline{N-1}\frac{2\pi}{N}Z\right), \end{aligned}\right. \tag{1}$$

where Z takes $N-1$ integral values:

$$Z=1,\,2,\,3,\,\cdots\cdot N-1; \tag{2}$$

each value of Z corresponding to each mode of oscillation. This specifies thus the mode of oscillation taking place in the circuit. Among various modes the oscillation with $Z=N/2$ (provided that N is even) is called of push-pull type.

When the alternating voltage on the anode is given by (1), the alternating potential in the inner space of the magnetron can be calculated, if one assumes that this satisfies the Laplace equation in this space. We obtain thus the potential $\Phi(r,\theta,t)$ for the case in which the Z-th sequence of N-phase oscillation is taking place on the split anode:

$$\begin{aligned} \Phi(r,\theta,t) = \\ \mathrm{Re}\,C\Bigg[&\sum_{n=0}^{\infty}\frac{1}{Z+nN}\left(\frac{r}{r_a}\right)^{Z+nN} \\ &\cdot\exp\left\{i\left[(Z+nN)\theta-\omega t-\frac{\pi Z}{N}\right]\right\} \\ &-\sum_{n=0}^{\infty}\frac{1}{(N-Z)+nN}\left(\frac{r}{r_a}\right)^{(N-Z)+nN} \\ &\cdot\exp\left\{i\left[(N-Z+nN)\theta+\omega t+\frac{\pi Z}{N}\right]\right\}\Bigg], \end{aligned} \tag{3}$$

with the abbreviation

$$C=\frac{N\phi}{\pi}\sin\left(\frac{\pi Z}{N}\right). \tag{4}$$

The relation (3) means that A_σ and B_σ in (I, 15) are given by

$$A_\sigma=\begin{cases}\dfrac{C}{Z+nN}\,\dfrac{1}{r_a{}^{Z+nN}}\,e^{\frac{-i\pi Z}{N}}, & \text{for } \sigma=Z+nN, \\ 0, & \text{otherwise;}\end{cases} \tag{5}$$

and

$$B_\sigma=\begin{cases}\dfrac{C}{(N-Z)+nN}\,\dfrac{1}{r_a{}^{(N-Z)+nN}}\,e^{\frac{i\pi Z}{N}}, & \\ & \text{for } \sigma=(N-Z)+nN. \\ 0, & \text{otherwise.}\end{cases} \tag{6}$$

---

(1) S. Tomonaga: J. Phys. Soc. Japan, 3 (1948), p. 56. This first report will be referred to as I.

§ 3. Generalized Resonance Conditions.

Having thus obtained the alternating potential Φ in the inner space of the magnetron, we can now apply the general theory of secular change of electron orbits described in section 3 of I to study the resonance phenomena in our general cases.

Using $\Phi(r, \theta, t)$ of (3) we calculate the Fourier coefficients X and Y occurring in (I, 18). We can then show that among various $X_{\sigma, \tau}$ only those with

$$\begin{cases} \sigma = Z+nN, & n = 0, 1, 2 \cdots, \\ \tau = 0, 1, 2 \cdots \sigma, \end{cases} \tag{7}$$

do not vanish, and among various $Y_{\sigma, \tau}$ only those with

$$\begin{cases} \sigma = (N-Z)+nN, & n = 0, 1, 2, \cdots, \\ \tau = 0, 1, 2 \cdots \sigma, \end{cases} \tag{8}$$

do not vanish.

It can be noted that some term of the series on the right-hand sides of (I, 19) becomes aperiodic in time when the condition

$$\omega = \sigma\omega_\theta + \tau\omega_r, \tag{9}$$

is fulfilled by some values of σ and τ occurring in (7). The secular change of the orbit takes place in such a case. The cosdition (9) with (7) is thus to be regarded as the generalized resonance condition for our multi-split magnetron.

§ 4. G-type Oscillations.

Among various possible resonance cases, those in which the resonance condition (9) is fulfilled by vanishing τ are important. We have then

$$\omega = \sigma\omega_\theta, \quad \sigma = Z+nN, \quad n = 0, 1, 2, \cdots. \tag{10}$$

In these cases the equations (I, 21) for the secular change become

$$\begin{cases} \dot{J}_\theta = -\mathrm{Re}\, i\sigma X_{\sigma,0} \exp\{i\sigma\delta_\theta\}, \\ \dot{J}_r = 0, \\ \dot{\delta}_\theta = \mathrm{Re} \dfrac{\delta X_{\sigma,0}}{\delta J_\theta} \exp\{i\sigma\delta_\theta\}, \\ \dot{\delta}_r = \mathrm{Re} \dfrac{\delta X_{\sigma,0}}{\delta J_r} \exp\{i\sigma\delta_\theta\}. \end{cases} \tag{11}$$

Now on calculating X using (5) and (6) in (I. 17) we see that X has the form

$$X_{\sigma,0} = \Omega i (J_r - J_\theta)^{\frac{\sigma}{2}}. \tag{12}$$

It is not necessary for the following to give the explicit form of Ω except that it is real and positive. The equations (11) become thus

$$\begin{cases} \dot{J}_\theta = \sigma\Omega (J_r - J_\theta)^{\frac{\sigma}{2}} \cos\sigma\delta_\theta, \\ \dot{J}_r = 0, \\ \dot{\delta}_\theta = \dfrac{\sigma}{2} \Omega (J_r - J_\theta)^{\frac{\sigma}{2}-1} \sin\sigma\delta_\theta, \\ \dot{\delta}_r = \dfrac{\sigma}{2} \Omega (J_r - J_\theta)^{\frac{\sigma}{2}-1} \sin\sigma\delta_\theta. \end{cases} \tag{13}$$

These equations are the generalization of (I, 27) to our case.

The equation (13) can be solved in an elementary way. We shall give here only the conclusions obtained in this way:

(i) All electrons reach the anode idependently of their initial conditions.

(ii) Net change of energy of electrons during the travel from cathode to anode is negative, so that the energies of these electrons diminish when they arrive at the anode. These energies are supplied to the oscillation in the circuit. All electrons contribute equally to this energy supply independently of their initial conditions.

(iii) As these electrons approach the anode they are gathered into the positions given by

$$re^{i\vartheta} = re^{i\left\{\omega_\theta t + \frac{\pi}{\sigma}\left(\frac{Z}{N}+\frac{1}{2}\right) + m\frac{\pi}{\sigma}\right\}},$$
$$m = 0, 1, 2, \cdots \text{ or } \sigma-1. \tag{14}$$

These electrons form σ clusters which rotate with the angular velocity ω_θ. The phases of rotation of these rotating clusters of electrons are such that they enforce the oscillation in the split anode.

From these conclusions it becomes clear that the self-excitation of oscillation is possible when the resonance condition

$$\omega = \sigma\omega_\theta \tag{15}$$

is fulfilled, where σ is equal to $Z+nN$, N being the split-number, Z the number specifying the mode of oscillation and n a positive integer including zero.

Oscillations excited in this way are called "G-type oscillation". These are the most important kind of oscillations which occur in the magnetron.

§ 5. Selection Rules.

The fulfilment of the resonance condition is the necessary but not sufficient condition for the self-excitation of oscillation. This can be seen by the typical examples given in I. We have shown there that when the resonance condition is fulfilled by $\sigma = 2$ and $\tau = 0$ the self-excitation does really occur, but when it is fulfilled by $\sigma = 2$ and $\tau = 1$ or by $\sigma = 2$ and $\tau = 2$ no self-excitation is possible. In this section we shall give rules for deciding whether or not the self-excitation is possible when σ and τ have some specified values.

From the equation (I, 21) we obtain

$$\frac{dJ_\theta}{dJ_r} = \frac{\sigma}{\tau} \qquad (16)$$

which gives, on integration,

$$J_r = \frac{\tau}{\sigma} J_\theta + J_{r0}\,. \qquad (17)$$

Substituting this J_r into (I, 11) and (I, 8) we obtain $R_{\rm aph}$ and E as functions of J_0:

$$\left\{\begin{aligned} R_{\rm aph} &= \frac{1}{m\sqrt{\omega_H^2-\omega_c^2}}\Big[\Big(\frac{2\tau}{\sigma}-1\Big)J_0+2J_{r0} \\ &\quad +2\sqrt{\Big(\frac{\tau}{\sigma}-1\Big)\Big\{\Big(\frac{\tau}{\sigma}-1\Big)J_\theta+J_{r0}\Big)}\,\Big], \\ E &= E_0+\Big\{\Big(\frac{2\tau}{\sigma}-1\Big)\sqrt{\omega_H^2-\omega_c^2}+\omega_H\Big\}J_\theta\,. \end{aligned}\right. \qquad (18)$$

Now, by eliminating J_θ from these two equations we obtain the energy as function of $R_{\rm aph}$:

$$\begin{aligned} E = E_0+m\sqrt{\omega_H^2-\omega_c^2}\Big\{\Big(\frac{2\tau}{\sigma}-1\Big)\sqrt{\omega_H^2-\omega_c^2}+\omega_H\Big\} \\ \cdot\Big\{\Big(\frac{2\tau}{\sigma}-1\Big)\pm\sqrt{\Big(\frac{2\tau}{\sigma}-1\Big)^2-\Big(1-\frac{R_0^2}{R_{\rm aph}^2}\Big)}\Big\}, \end{aligned} \qquad (19)$$

where the double sign should be taken in the following manner:

$$\left\{\begin{array}{lll} \text{upper sign} & \text{for} & \dfrac{2\tau}{\sigma}-1<0 \\ \text{lower sign} & \text{for} & \dfrac{2\tau}{\sigma}-1>0\,. \end{array}\right. \qquad (20)$$

As

$$m\sqrt{\omega_H^2-\omega_c^2}\Big\{\Big(\frac{2\tau}{\sigma}-1\Big)\sqrt{\omega_H^2-\omega_c^2}+\omega_H\Big\} = m\sqrt{\omega_H^2-\omega_c^2}\,\frac{\omega}{\sigma}$$

in (20) is always positive, we can draw the following conclusion as to the sign of the net change of the energy

$$\Delta E = m\sqrt{\omega_H^2-\omega_c^2}\,\frac{\omega}{\sigma} \cdot\Big\{\Big(\frac{2\tau}{\sigma}-1\Big)\pm\sqrt{\Big(\frac{2\tau}{\sigma}-1\Big)^2-\Big(\frac{R_0^2}{r_a^2}\Big)}\Big\}. \qquad (21)$$

(i) In case of $\frac{2\tau}{\sigma}-1<1$, the net change of the energy is negative, so that the energy of electrons arriving at the anode is smaller than its initial value.

(ii) In case of $\frac{2\tau}{\sigma}-1>1$, the net change of the energy is positive, so that the energy of electrons arriving at the anode is larger than its initial value.

(iii) In case of $\frac{2\tau}{\sigma}-1=0$, (21) gives an imaginary value. This means that the electrons do never arrive at the anode. See below. (22)

The self-excitation of oscillation is evidently possible only in the case (i). We can in this way conclude that for the possibility of the self-excitation it is necessary that the resonance condition $\omega = \sigma\omega_\theta + \tau\omega_r$ is fulfilled by σ and τ satisfying

$$\frac{2\tau}{\sigma} < 1\,; \qquad (23)$$

It must be noticed here that this conclusion is valid only when the electrons do really arrive at the anode. In order to see whether or not the electrons really arrive at the anode, we must carry out the integration of the equations of motion and it will be a rather tedious problem. We shall take here an easier way:

From (20) it is seen that for

$$R_{\rm aph} < \frac{R_0}{2}\,\frac{\sigma}{\sqrt{\tau(\sigma-\tau)}} \qquad (24)$$

E becomes imaginary. This means that the electrons can at most recede from the center by the distance

$$R_{\rm max} = \frac{R_0}{2}\,\frac{\sigma}{\sqrt{\tau(\sigma-\tau)}}, \qquad (25)$$

so R_0 of the electron should not too much smaller than the anode radius r_a in order that the electron can really reach the anode. (in case of $\tau = 0$ or

$\tau = \sigma$ (25) gives infinite value, so that the electron can reach the anode, no matter how large the anode radius may be).

Now, according to (I, 14), R_0 can be made arbitrarily large when the applied anode voltage and the impressed magnetic field are such that the difference between ω_H and ω_c is sufficiently small. This means that H and U_a are not so much different from their "critical values" which satisfy the equation

$$U_a = \frac{r_a}{8mc^2}\,. \tag{25}$$

Summarizing these facts we obtain the following conclusions:

(I) When the resonance condition $\omega = \sigma\omega_\theta + \tau\omega_r$ is fulfiled by some σ and $\tau = 0$, electrons can always reach the anode supplying energy to the oscillation. The self-excitation is thus always possible in this case.

(II) When the resonance condition $\omega = \sigma\omega_\theta + \tau\omega_r$ is fulfilled by σ and τ satisfying $0 < \frac{\tau}{\sigma} < \frac{1}{2}$, electrons can supply energy to the oscillation. But in order that the electrons can really reach the anode it is necessary that H and U_a do not differ too much from their critical values defined by (25).

(III) When the resonance condition $\omega = \sigma_\theta + \tau\omega_r$ is fulfilled by σ and τ satisfying $\frac{1}{2} < \frac{\sigma}{\tau} \leqq 1$, electrons absorb energy from the oscillation, so that no self-excitation is possible in this case (but see (III′) in the next section).

(IV) When the resonance condition $\omega = \sigma\omega_\theta + \tau\omega_r$ is fulfilled by σ and τ satisfying $\frac{\sigma}{\tau} = \frac{1}{2}$, electrons never reach the anode, so that, of course, no self-excitation is possible in this case.

In any of these cases σ must have values $\sigma = Z + nN$, where N is the split number, Z the number specifying the mode of oscillation which takes $N-1$ values $1, 2, 3, \cdots, N-1$, and n is a positive integer including zero.

We have thus obtained the rules to decide whether or not the excitation is possible for some specified values of σ and τ. We shall call these rules "selection rules".

§ 6. Perfect and Imperfect Oscillations.

We have mentioned above that, when the resonance condition is fulfilled by σ and τ satisfying $\frac{1}{2} < \frac{\sigma}{\tau}$, no self-excitation is possible. But it must be noticed that under special conditions the excitation of a weak oscillation is still possible also in this case.

We shall illustrate this situation referring to the simple example of a four split magnetron considered in I.

It has been shown in section 4 of I that in case of $\sigma = 2$, $\tau = 2$ the electron absorb energy from the oscillation during the travel from cathode to anode. But if one observes the equation (I, 36), one can see that the energies of those electrons whose $\delta_{\theta_0} + \delta_{r_0}$ satisfies $\tan(\delta_{\theta_0} + \delta_{r_0}) < 1$ decrease first, so that such electrons can meanwhile supply energy to the oscillation. The orbits of these electrons contract according to (I, 35) during this time. On the other hand, the energies of those electrons whose $\delta_{\theta_0} + \delta_{r_0}$ satisfies $\tan(\delta_{\theta_0} + \delta_{r_0}) < 1$ increase immediately after leaving the cathode, so that these electrons brake the oscillation as soon as they start from the cathode. But since the orbits of these electrons expand outwards according to (I, 35) immediately after the starts, these electrons will be caught by the anode as soon as they leave the cathode provided that the magnetron is working at the condition near the critical state in which H and U_a do not differ so much from their critical values defined by (25). This is because R_0 of the electrons are in such a case so large that a little expansion of the orbits by resonance suffices the electrons to be caught by the anode.

Under such a working condition there will remain in the magnetron only those electrons which can supply energies to the oscillation. But the energies of these electrons will sooner or later begin to increase so that the braking action will set in. When, however, these electrons can be removed from the inner space of the magnetron at a suitable time, there will be in the space always only those electrons which supply energies to the oscillation. Then the self-excitation will be possible.

Such an electron-removing process will be performed when the magnetron is set in such a way that the direction of its axis is a little inclined with respect to the direction of the magnetic field.

Since in such an oscillation mechanism only those electrons which start from the cathode with favorable phases contribute to the oscillation, no intense oscillation can be expected. We shall call such oscillations to which only little part of electrons contribute "imperfect oscillations", while the oscillations to which all the electrons emitted from the cathode contribute will be called "perfect oscillation". According to this classification G-type oscillation in a magnetron is perfect, while oscillations by means of a B. K-tube are imperfect.

The above consideration can be generalized to the case of multi-split magnetrons. Then we see that in the case of (III) such inperfect oscillation will be possible when the working condition is such that H and U_a lie in the neighbourhood of the critical values and the magnetron is set in such a way that its axis is a little inclined with respect to the impressed magnetic field. We obtain thus instead of (III) the following conclusion:

(III′) When the resonance condition $\omega = \sigma\omega_\theta + \tau\omega_r$ is fulfiled by σ and τ satisfying $\frac{1}{2} < \frac{\sigma}{\tau} \leqq 1$, the self-excitation is still possible when H and U_a do not too much differ from their critical values defined by (25) and the axis of the magnetron is a little inclined with respect to the direction of the magnetic field. In this case the oscillation is imperfect and will be weak as compared with the oscillations in the case (I) or (II) where the oscillations are perfect.

§ 7. Relations Existing between H, U_a and λ.

We shall now find the relations which must be satisfied by H, U_a and λ in order that the magnetron can self-excite, where λ denotes the wave length of the oscillation.

We have shown that the condition of self-excitation is

$$\omega = \sigma\omega_\theta + \tau\omega_r, \tag{26}$$

where σ and τ are

$$\begin{cases} \sigma = Z + nN, \\ \tau = 0, 1, 2, \cdots \sigma, \end{cases} \tag{27}$$

N being the split-number, Z the number specifying the mode of oscillation, and n a positive integer including zero.

Further we have shown that the oscillation is perfect when we have

$$\tau < \frac{\sigma}{2}, \tag{28}$$

and it is imperfect when

$$\tau > \frac{\sigma}{2}. \tag{29}$$

Now, the relation (26) imposes the following relation upon U_a, H and λ, as one sees by using (I, 3) and the relation $\lambda = 2\pi c/\omega$,

$$\lambda(\sigma, \tau) = \frac{4\pi mc^2/e}{\sigma H\left\{1 + \left(\frac{2\tau}{\sigma} - 1\right)\sqrt{1 - \frac{8mc^2 U_a}{e r_a H^2}}\right\}}. \text{(2)} \tag{30}$$

On solving (30) with respect to U_a, considering thereby the wave length λ as a parameter, we obtain a formula which is used more conveniently for a fixed-wavelength magnetron:

$$U_a^{(\sigma,\tau)} = \frac{r_a^2}{\left(\frac{2\tau}{\sigma} - 1\right)^2}\left\{\frac{4\pi}{\sigma}\left(\frac{\tau}{\sigma} - 1\right)\frac{e}{8mc^2}H^2 + \frac{\pi}{\sigma\lambda}H - \frac{\pi^2}{(\sigma\lambda)^2}\frac{mc^2}{e}\right\}. \tag{31}$$

When one measures U_a in volt, H in Gauss, and r_a and λ in cm, this gives

$$U_a^{(\sigma,\tau)} = \frac{r_a^2}{\left(\frac{2\tau}{\sigma} - 1\right)^2}\left\{\frac{4\tau}{\sigma}\left(\frac{\tau}{\sigma} - 1\right)0{,}0221 H^2 + 942\frac{H}{\sigma\lambda} - 10020000\frac{1}{(\sigma\lambda)^2}\right\}. \tag{31′}$$

For the G-type oscillation, viz. for the oscillation with $\tau = 0$, we obtain from (31′)

$$U_a^{(\sigma,0)} = r_a^2\left\{942\frac{H}{\sigma\lambda} - 10020000\frac{1}{(\sigma\lambda)^2}\right\}. \text{(2)} \tag{31″}$$

For the purpose of comparing the theory with experiments it is convenient to plot the above relation between U_a and H on the H-U_a plane. Then the equation (31) gives parabolas. One sees that a group of parabolas having the same σ and

---

(2) Before the present theory was established, a half empirical formula $H = \frac{4\pi mc^2/e}{\sigma\lambda(1+\xi)}$ had been used by Yamasaki in analysing the experimental results, where ξ is a constant to be determined experimentally. Then Takao proposed the formula of the same form as (31″), which he had obtained from the angular velocity of the rotating charge cloud supposed to exist in the magnetron according to his hydrodynamical consideration.

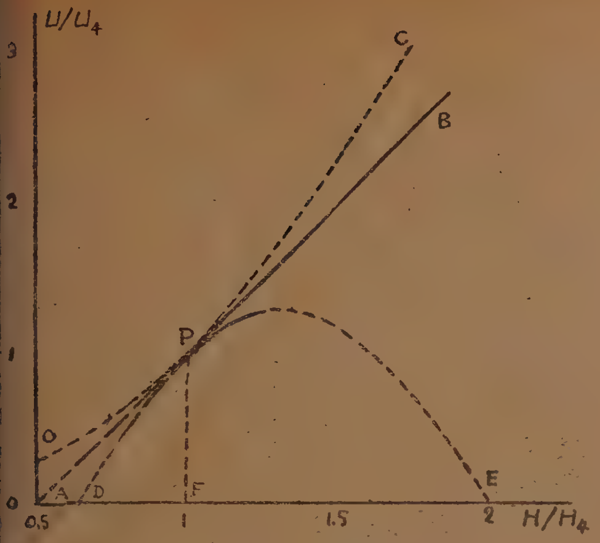

Fig. 1. Working parabolas for $\sigma = 4$.

OPC: Critical parabola
PB: $\tau = 0$, PE: $\tau = 1$, PF: $\tau = 2$,
PD: $\tau = 3$, PA: $\tau = 4$.
——: Part on which perfect oscillations are possible.
- - -: Part on which imperfect oscillations are possible.
· · · ·: Part on which no oscillations are possible.

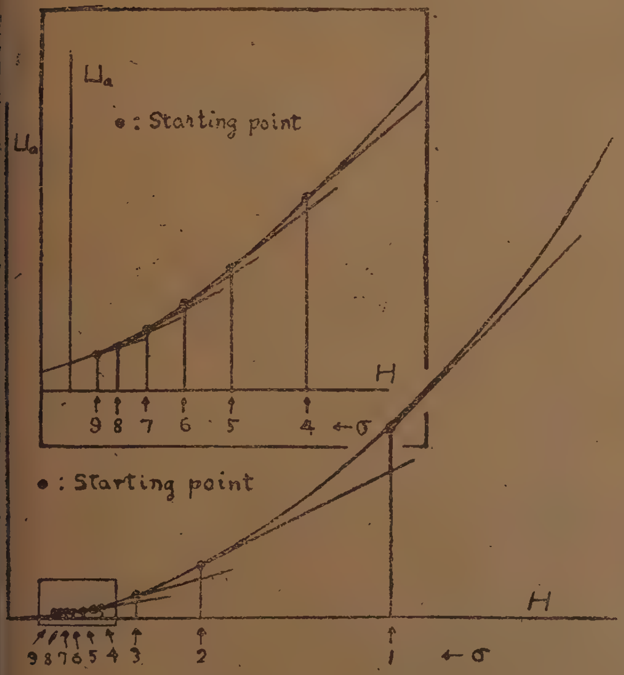

Fig. 2. Arrangement of starting points with various values of σ.

various possible τ touch with each other and with the parabola representing the critical relation (25) at a common point of contact. The ordinate and the abscissa of this point are given by

$$\begin{cases} H_\sigma = \dfrac{4\pi mc^2/e}{\sigma\lambda} = \dfrac{21300}{\sigma\lambda}, \\ U_\sigma = \dfrac{\pi^2 mc^2 r_a^2/e}{(\sigma\lambda)^2} = \dfrac{10020000 r_a^2}{(\sigma\lambda)^2} \end{cases} \tag{32}$$

In Fig. 1 is given an example of such plots. In this figure are drawn five parabolas with $\sigma = 4$ and $\tau = 0, 1, 2, 3, 4$ respectively. On the diagram the critical parabola is also added. The common point of contact is denoted by P.

We call the parabolas representing (31) "working parabolas". Among them the parabola with $\tau = 0$ or $\tau = \sigma$ degenerates into a straight line, which will be called "working straight line". The equation for the working straight line is given by (31″). The common point of contact with a specified value of σ is called "starting point for the oscillation with this specified value of σ", since the perfect oscillation with this value of σ sets in at this point when H is increased along a working parabola (see below).

We see that $U^{(\sigma,\tau)}$ given by (31) do not change when we replace τ by $\sigma-\tau$. So, at first sight, it might be thought that two parabolas representing $U^{(\sigma,\tau)}$ and $U^{(\sigma,\sigma-\tau)}$ coincide with each other. But this is not true. We have from (30)

$$H = \frac{4\pi mc^2/e}{\sigma\lambda\left\{1+\left(\dfrac{2\tau}{\sigma}-1\right)\sqrt{1-\dfrac{8mc^2 U_a}{er_a H^2}}\right\}}, \tag{33}$$

which indicates that H must be larger or smaller than H_σ according as $\left(\dfrac{2\tau}{\sigma}-1\right)$ is negative or positive. This means that, if σ and τ satisfy, for instance, $\dfrac{2\tau}{\sigma}-1<0$, only that part of the parabola which lies on the side of $H > H_\sigma$ belongs to $U^{(\sigma,\tau)}$, and the other part belongs to $U^{(\sigma,\sigma-\tau)}$.

This fact, combined with the selection rules (I), (II) on one hand and (III′) on the other, will give the following result: (i) when σ and τ are specified, a perfect oscillation is possible on that part of the working parabola with these σ and τ which lies on the side of $H > H_\sigma$, and (ii) an imperfect oscillation is possible on that part of the working parabola which lies on the side of $H < H_\sigma$. Further (iii) the oscillations with $\tau \neq 0$ are possible only on those parts of the working parabolas which do not lie too much apart from the critical para-

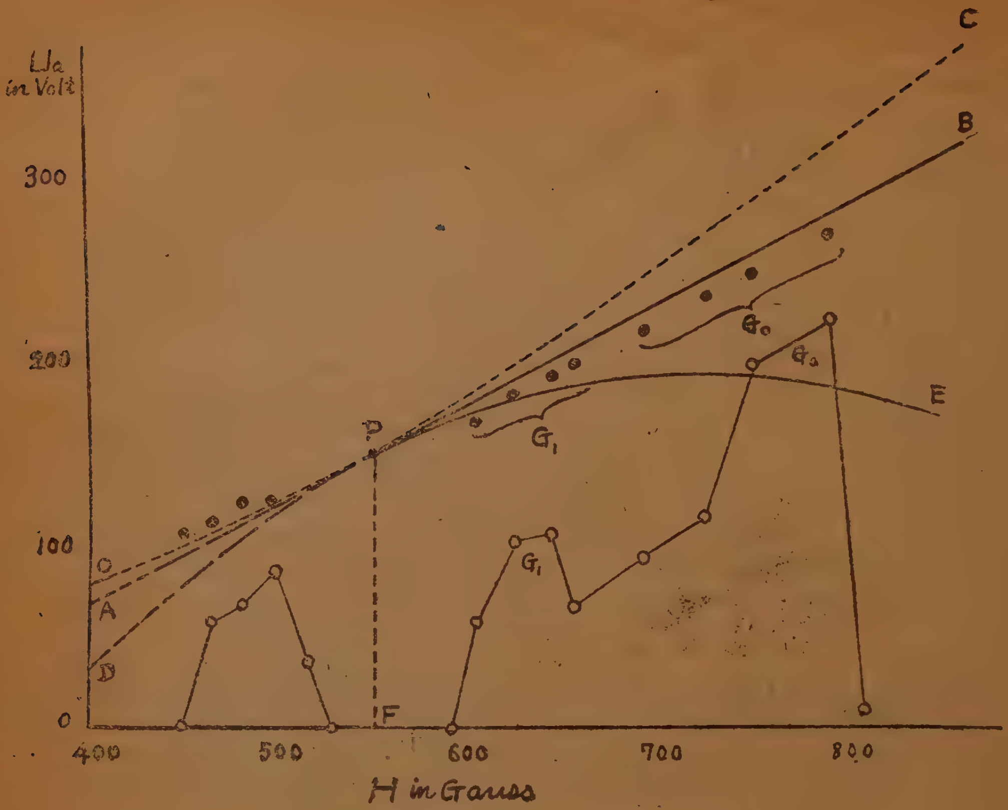

Fig. 3. Experimental optimum points and intensities. ($N = 8$).
●: Optimum points, ○: Intensity.
Note that optimum points are really arranged along the working straight line.

bola. In Fig. 1 full lines are used to indicate those parts of the working parabolas on which the perfect oscillations are possible, and broken lines are used to indicate those parts on which the imperfect oscillrtions are possible. On the parts drawn with dotted lines no oscillations at all are possible.

When the split-number N of the magnetron is given, the possible values for σ are determined by (27) in which Z can take $N-1$ values 1, 2, 3, $\cdots$, $N-1$, and n can be any positive integer including zero. Now, for a fixed-wave-length magnetron the wave length λ is a characteristic constant of the magnetron. Then, if one plots on the H-U_a plane the starting points for various possible values of σ, one obtains a remarkablly regular arrangement of the points. Fig. 2 shows this arrangement of the starting points.

§ 8. Comparison with Experiments.

In Fig. 3 we reproduce the result of the experiment which has been carried out in 1942 by Yamasaki and Sato at the Japan Wireless Telegram and Telephone Company. The magnetron used was an eight-split push-pull magnetron with the anode redius 0.15 cm. The oscillation wave length was 9.7 cm.

In this experiment one measured the oscillation intensity for various (fixed) values of H changing U_a. One determined thus the anode voltage at which the oscillation intensity became maximum for every value of H. The black points on the diagram give these "optimum points". The small circles in the figure give the relative intensity at these optimum points. The oscillations marked by the letter R was far weaker than that marked by the letter G, so the scale for the intensities of R-oscillations is enlarged about ten times as compared with that for the intensities of G-oscillations.

Since the magnetron used was a push-pull magnetron, we have to put

$$Z = N/2 = 4.$$

The possible values for σ is then, according to (27)

$$\sigma = 4,\ 12,\ 20,\ \cdots.$$

Now, in order to compare the experimental results with the theory, we plot on the diagram the curve representing the critical relation (25). Then we obtain the parabola OC. Next we calculate the coordinates of the starting point P by means of (32). This gives

$$\begin{cases} H_i = \dfrac{21300}{4\times 9.7} \approx 550 \text{ Gauss} \\ U_i = 10020000 \times \dfrac{0.15^2}{4^2\times 9.7^2} \approx 150 \text{ Volt.} \end{cases}$$

This point is marked on the diagram.

We then plot five working parabolas belonging each to $\sigma = 4$ and $\tau = 0, 1, 2, 3, 4$ according to (31′). Thus we get the curves PB, PE, PF, PD and PA.

Now, according to our theory, perfect oscillations will occur along those parts of the working parabolas which are drawn in the diagram with full lines, and imperfect oscillations will occur along those part which are drawn with broken lines.

Our experimental result shows that the black points are in fact arranged along the straight lines PB and PA. Several points marked by the letter G_1 may also be regarded as arranged along the parabola PE. Whether the points G_1 belong to the straight line PB or to the parabola PE can not be decided by this experiment, but the fact that the intensity curve has two maxima at G_1 and G_0 seems to imply that these oscillations are of different kinds: the black points marked by the letter G_1 belong to the parabola PE while the points marked by the letter G_0 to the straight line PB.

In this way we may assign $\sigma = 4$, $\tau = 0$ to the oscillations belonging to the group G_0 and assign $\sigma = 4$, $\tau = 1$ to the oscillations belonging to the group G_1. The former oscillations are thus of G-type.

Weak oscillations marked by the letter R appear on the side of $H < H_G$. These oscillations are to be interpreted as belonging to the imperfect oscillations with $\sigma = 4$, $\tau = 4$ or eventually with $\sigma = 4$, $\tau = 3$.

The agreement of the experimental results with our theory is thus quite satisfactory.

In Fig. 4 we give a further experimental result obtained at the same place by Nakajima, Matsumoto and Nukushina by means of a 12-split magnetron. In the diagram the optimum points are given by dotted lines and the intensities at these points by full lines. The anode radius of the magnetron used was 0.5 cm. The wave length

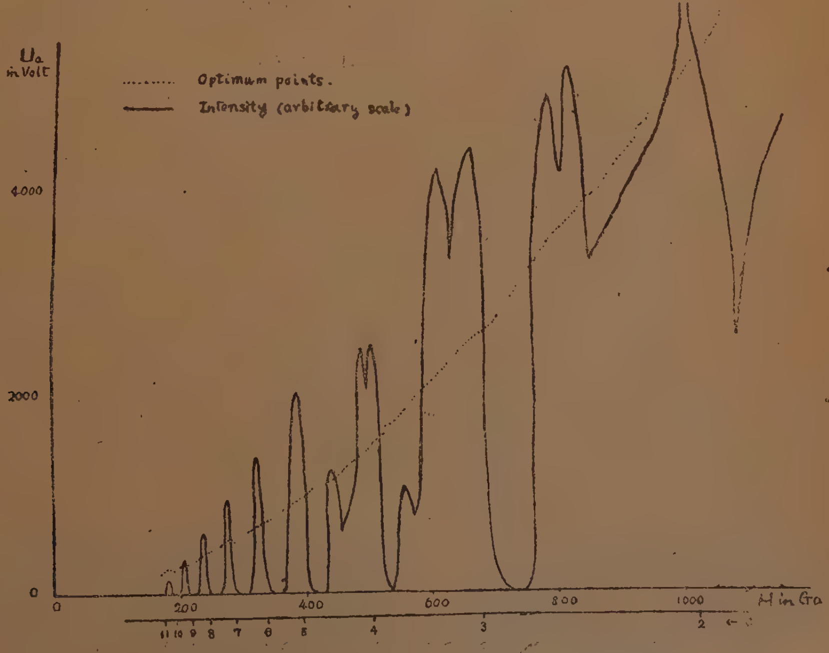

Fig. 4. Experimental optimum points and intensities ($N = 12$). Note the band structure of oscillating interval of H.

was found to be about 10 cm.

The attached oscillation circuit of this magnetron was so constructed that all 11 modes of polyphase oscillations are possible. Thus Z can have values 1, 2, 3, 4, 5, 6, 7, 8, 9, 10, and 11. Then σ can take any positive integral values except the multiples of 12.

Observing the diagram, one notices that the oscillation occurs in several separate bands of H. The arrangement of these bands has a very marked regularity. Comparing this arrangement of bands with the arrangement of the starting points given in Fig. 2, one finds a remarkable similarity.

Suggested by this similarity, we calculate the starting magnetic field intensity for various possible values of σ. We mark these field intensity on the H-axis of the diagram. Then we find that the left end of each oscillating band coincides with one of these starting fields.

According to our theory the perfect oscillation belonging to some specified value of σ starts from the starting point belonging to this σ. Thus we can conclude that the oscillations in each band have a definite value of σ, which can be determined by reading the left end of the band and seeing with what H_σ this end point coincides.

The beautiful agreement of these arrangement of the oscillation bands with the arrangement of the theoretical starting points is to be regarded as a powerful support of our theory.

Acknowledgement. This work was established in 1943 by the requirement of the electromagnetic-wave division of the former Technical Institute of Japanese Navy and carried out by the collaboration of Prof. Y. Hagihara, Prof. M. Kotani, Assist. Prof. T. Miyazima and the present author (S. T.). The detailed contents of this and the foregoing reports were presented in a limited circle in January 1944. Although this and the foregoing reports have been written by the present author, many important parts were contributed by these colleagues, to whom the author wishes to express his sincere thanks. Thanks are also due to Mr. S. Mizuma and Dr. I. Takao of the former Naval Technical Institute and Mr. S. Nakajima and Mr. S. Yamasaki of the Japan Wireless Telegram and Telephone Company for many valuable discussions. They have also supplied many experimental data, without which so rapid development of the theory was hardly possible.

Application of Celestial Mechanics to the Theory of a Magnetron. I.

By Yusuke HAGIHARA.

Astronomy Department, University of Tokyo.

(Received July 31, 1947)

§ 1. We suppose a magnetron as a circular cylinder with the cathode along its axis and the anode of the surface of the cylinder with a number of splits of equal spacings parallel to the cylinder axis. The electrostatic field between the anode and the cathode is assumed to be proportional to the square of the distance from the cathode in conformity with the hypothesis of Tomonaga. An oscillating electric potential is supposed to be superposed upon this electrostatic potential with alternating signs on the consecutive anode pieces. The applied magnetic field is assumed to be uniform and parallel to the cylinder axis. In order to discuss the excitation mechanism of a magnetron Kotani has studied the motion of an electron under such electrostatic and oscillating electric field together with this magnetic field and explained the formation of the rotating electron pole in the case of a magnetrons with two split anode. The present series of notes are for summarising the author's more detailed work on the theory of the mechanism of magnetron excitation based on the discussion of the electronic motion in a magnetron with its anode with several divisions by the author's method(2) for solving a system of linear differential equations with periodic coefficients in celestial mechanics.

In the present Note the author proposes to deal with the domain—which we call the resonance domain—for both the applied electrostatic and the magnetic field in which the magnetron oscillation takes place for a magnetron with four split anode. The equations of motion for an electron are solved by matrix method with the applied electrostatic potential and applied magnetic field as two parameters and the resonance domain is defined with these two parameters as the domain where we have the non-periodic solution of the equations of motion. The formation, the shape and the behavior of the rotating electron poles are deduced both for the inside of, and for the transition to and from, such resonance domains. The idea in the theory of adiabatic inveriants is applied for the last discussion. The magnetron oscillation treated in the present Note is the so-called mono-phase oscillation. For a further study on the mechanism of magnetron oscillation we shall have to consider the external circuit at the same time.

The author aknowledges his indebtedness to Dr. Kotani and Dr. Tomonaga for continual discussions.

§ 2. Consider a plane section of the circular cylinder forming a magnetron with $2s$ split anodes and let the radius of the circle of the section be R and the coordinates of a point in the circle be $x = r\cos\theta$, $y = r\sin\theta$. The potential difference between a point r and the cathode be denoted by $U = U_a\,(r/R)^2$, where U_a is the potential difference between the anode and the cathode for electrostatic potential. The oscillating electric potential can be shown to be expressed by

$$
(1)\quad \begin{cases} \mathfrak{V}(r,\theta,t) = V(r,\theta)\sin\omega t, \\ V(r,\theta) = \dfrac{4\varphi}{\pi}\displaystyle\sum_{j\ 0}^{\infty}\dfrac{z^{(2j+1)s}-\bar{z}^{(2j+1)s}}{2i(2j+1)R^{(2j+1)s}}, \end{cases}
$$

with $z = x+iy$, $\bar{z} = x-iy$, $i = \sqrt{-1}$. The amplitude φ, is ssumed to be small compared with U_a. We define

$$
(2)\quad \begin{cases} U = -\dfrac{m}{2}\,\omega_c^2 z\bar{z}, & \omega_c^2 = -\dfrac{2U_a}{mR^s}, \\ W = \dfrac{4e\varphi}{m\pi}, & \omega_H = \dfrac{eH}{2mc}, \end{cases}
$$

where e, m, c and H denote respectively the electron charge, the electron mass, the light velocity and the applied magnetic field, and ω_c and ω_H the cut-off frequency and the Larmor frequency.

In order to be able to discuss the resonance domain we write the equations of motion of an electron in the following form with two small parameters h and k.

$$
(3)\quad \begin{cases} \ddot{z}-2i\left(\omega_H+\dfrac{h}{R^s}\right)\dot{z}-\left(\omega_c^2+\dfrac{k}{K^s}\right)z \\ \qquad = isW\sin\omega t\cdot\displaystyle\sum_{j=0}^{\infty}\dfrac{\bar{z}^{(2j+1)s-1}}{R^{(2j+1)s}}, \\ \ddot{\bar{z}}+2i\left(\omega_H+\dfrac{h}{R^s}\right)\dot{\bar{z}}-\left(\omega_c^2+\dfrac{k}{R^s}\right)\bar{z} \\ \qquad = -isW\sin\omega t\cdot\displaystyle\sum_{j=0}^{\infty}\dfrac{z^{(2j+1)s-1}}{R^{(2j+1)s}}. \end{cases}
$$

§ 3. We take the first degree terms in z and $\bar{z}$ from (3) and consider the case $s = 2$, then we get a system of linear differential equations with periodic coefficients which is a generalisation of Mathieu equation in mathematical physics. This system is written in matrix notation

$$
(4)\quad \frac{d\mathbf{x}}{dt} = (\mathfrak{A}+\mathfrak{B})\cdot\mathbf{x},
$$

with $\quad \mathbf{x} = (z, \dot{z}, \bar{z}, \dot{\bar{z}})$,

$$
\mathfrak{A} = \begin{pmatrix} 0 & 1 & 0 & 0 \\ \omega_c^2 & 2i\omega_H & 0 & 0 \\ 0 & 0 & 0 & 1 \\ 0 & 0 & \omega_c^2 & -2i\omega_H \end{pmatrix}
$$

$$
\mathfrak{B} = \begin{pmatrix} 0 & 0 & 0 & 0 \\ \dfrac{k}{R^2} & 2i\dfrac{h}{R^2} & \dfrac{2iW}{R^2}\sin\omega t & 0 \\ 0 & 0 & 0 & 0 \\ -\dfrac{2iW}{R^2}\sin\omega t, & 0 & \dfrac{k}{R^2} & -2i\dfrac{h}{R^2} \end{pmatrix}
$$

The roots of the characteristic equation $|\mathfrak{A}-\chi 1|$

$= 0$, where 1 denotes the unit matix, are $\chi = \pm i\nu_1$, $\pm i\nu_2$ with

$$\nu_1 = \omega_H + \sqrt{\omega^2{}_H - \omega^2{}_c}\,,\quad \nu_2 = \omega_H - \sqrt{\omega^2{}_H - \omega^2{}_c}\,.$$

Put

$$\mathfrak{C} = \begin{pmatrix} i\nu_1 & 0 & 0 & 0 \\ 0 & i\nu_2 & 0 & 0 \\ 0 & 0 & -i\nu_2 & 0 \\ 0 & 0 & 0 & -i\nu_1 \end{pmatrix},$$

$$\Omega(\mathfrak{C}) = \begin{pmatrix} e^{i\nu_1 t} & 0 & 0 & 0 \\ 0 & e^{i\nu_2 t} & 0 & 0 \\ 0 & 0 & e^{-i\nu_1 t} & 0 \\ 0 & 0 & 0 & e^{-i\nu_1 t} \end{pmatrix},$$

then $\mathfrak{T}$ such that $\mathfrak{T}\mathfrak{A}\mathfrak{T}^{-1} = \mathfrak{C}$ is

$$\mathfrak{T} = \begin{pmatrix} \omega_c^2 & i\nu_1 & 0 & 0 \\ \omega_c^2 & i\nu_2 & 0 & 0 \\ 0 & 0 & \omega_c^2 & -i\nu_2 \\ 0 & 0 & \omega_c^2 & -i\nu_1 \end{pmatrix}$$

and

$$(5)\quad \mathfrak{T}\mathfrak{B}\mathfrak{T}^{-1} = \frac{-i}{2\omega_c^2\sqrt{\omega_H^2 - \omega_c^2}} \cdot \begin{pmatrix} \nu_1\nu_2 k - 2\nu_1\omega_c^2 h & -\nu_1^2 k + 2\nu_1\omega_c^2 h & -2i\nu_1^2 W\sin\omega t & 2i\nu_1\nu_2 W\sin\omega t \\ \nu_2^2 k - 2\nu_2\omega_c^2 h & -\nu_1\nu_2 k + 2\nu_2\omega_c^2 h & -2i\nu_1\nu_2 W\sin\omega t & 2i\nu_2^2 W\sin\omega t \\ 2i\nu_2^2 W\sin\omega t & -2i\nu_1\nu_2 W\sin\omega t & \nu_1\nu_2 k - 2\nu_2\omega_c^2 h & -\nu_2^2 k + 2\nu_2\omega_c^2 h \\ 2i\nu_1\nu_2 W\sin\omega t & -2i\nu_1^2 W\sin\omega t & \nu_1^2 k - 2\nu_1\omega_c^2 h & -\nu_1\nu_2 k + 2\nu_1\omega_c^2 h \end{pmatrix}$$

The coefficient Γ_1 of t in the matrix $Q[\Omega^{-1}(\mathfrak{C})\mathfrak{T}\mathfrak{B}\mathfrak{T}^{-1}\Omega(\mathfrak{C})]$ is called the matrix of the characteristic exponents, where Q denotes the operation of integrating each element of the matrix from $t = 0$ to $t = t$ and $\Omega = 1 + Q + Q^2 + \cdots$. We call the terms with the j-th power of W as of the j-th order.

§ 4. When there is no commensurability relation among ν_1, ν_2 and ω, we get

$$(6)\quad \Gamma_1^{(0)} = \frac{iW}{\nu_1\nu_2(\nu_1-\nu_2)R^2} \cdot \begin{pmatrix} -\nu_1 L_2 & 0 & 0 & 0 \\ 0 & \nu_2 L_1 & 0 & 0 \\ 0 & 0 & -\nu_2 L_1 & 0 \\ 0 & 0 & 0 & -\nu_1 L_2 \end{pmatrix},$$

with

$$L_1 = \frac{\nu_1 k}{W} - \frac{2\nu_1\nu_2 h}{W}, \quad L_2 = \frac{\nu_2 k}{W} - \frac{2\nu_1\nu_2 h}{W},$$

$$\beta = \frac{W}{\nu_1\nu_2(\nu_1-\nu_2)\,k^2}.$$

The solution with the initial condition that the electron starts from the cathode in the direction θ_0 with speed v_0 is

$$(7)\quad \begin{cases} \dfrac{\nu_1-\nu_2}{v_0}\,x = -\sin[\nu_1(1-L_2\beta)t+\theta_0] \\ \qquad\qquad + \sin[\nu_2(1+L_1\beta)t+\theta_0], \\ \dfrac{\nu_1-\nu_2}{v_0}\,y = \cos[\nu_1(1-L_2\beta)t+\theta_0] \\ \qquad\qquad - \cos[\nu_2(1+L_1\beta)t+\theta_0]. \end{cases}$$

The complete solution for (4) with the initial condition $x = x^0$ is

$$(8)\qquad x(t) = \Omega(\mathfrak{A}+\mathfrak{B})\cdot x^0,$$

$$\Omega(\mathfrak{A}+\mathfrak{B}) = \mathfrak{T}^{-1}\Omega(\mathfrak{C})\mathfrak{T}\Omega[\mathfrak{T}^{-1}\Omega^{-1}(\mathfrak{C})\mathfrak{T}\mathfrak{B}\mathfrak{T}^{-1}\Omega(\mathfrak{C})\mathfrak{T}],$$

and is (7) superposed with periodic oscillations of short periods of the order $\nu_1/2\pi$ or $\nu_2/2\pi$, coming from the terms omitted in $Q[\Omega^{-1}(\mathfrak{C})\mathfrak{T}\mathfrak{B}\mathfrak{T}^{-1}\Omega(\mathfrak{C})]$.

§ 5. When there is a linear relation of the form

$$(i\kappa+1)\omega \pm 2\nu_2 = 0, \quad (2\kappa+1)\omega \pm (\nu_1+\nu_2) = 0,$$

$$(2\kappa+1)\omega \pm 2\nu_1 = 0,$$

or

$$2\kappa\omega \pm (\nu_1-\nu_2) = 0,$$

then the matrix of the characteristic exponents is different from (6). The left hand sides of these relations are called the resonance arguments and each of these resonance arguments appears in the terms of order indicated by the coefficient of ω. We consider the most important case of the first order $\omega = \pm 2\nu_2$, $\omega = \pm(\nu_1+\nu_2)$, $\omega = \pm 2\nu_1$.

(i) $\omega = 2\nu_2$:

$$(9)\quad \Gamma_1^{(c)} = \frac{iW}{2\omega_c^2\sqrt{\omega_H^2 - \omega_c^2}\,R^2} \cdot \begin{pmatrix} -\nu_1 L_2 & 0 & 0 & 0 \\ 0 & \nu_2 L_1 & \nu_1\nu_2 & 0 \\ 0 & -\nu_1\nu_2 & -\nu_2 L_1 & 0 \\ 0 & 0 & 0 & \nu_1 L_2 \end{pmatrix}.$$

The roots of the characteristic equation formed of this matrix are $\pm\nu_1 L_2$, $\pm\sqrt{\nu_2^2 L_1^2 \quad \nu_1^2\nu_2^2}$. Thus the motion is periodic outside the hatched domain in Fig. 1, which we call the resonance domain. In the resonance domain the solution has exponential factors showing the electron streaming from the cathode to the anode and hence the occurence of magnetron oscillation. When $\omega = 2\nu_2$ exactly, we call it the exact resonance. h and k show the deviation of the values of H and U_a respectively from these values corresponding to the exact resonance.

The thickness of the resonance domain is

$$(10) \quad \varDelta\omega = \frac{4W}{(\nu_1-\nu_2)R^3} \quad \text{for } h = \text{const.,} \quad \text{i.e. for } H = \text{const.}$$

$$(10)' \quad \varDelta\omega = \frac{2(\nu_1+\nu_2)W}{\nu_2(\nu_1-\nu_2)R^2} \quad \text{for } k = \text{const.,} \quad \text{i.e. for } U_a = \text{const.}$$

This type of magnetron oscillation is called of B type. Fig. 1 is nothing but the (H, U_a)-diagram usually drawn by experimentalists.

(ii) $\omega = \nu_1+\nu_2$:

$$\varGamma_1^{(c)} = i\beta\begin{pmatrix} -\nu_1 L_2 & 0 & \nu_1^2 & 0 \\ 0 & \nu_2 L_1 & 0 & -\nu_2^2 \\ \nu_2^2 & 0 & -\nu_2 L_1 & 0 \\ 0 & -\nu_1^2 & 0 & \nu_1 L_2 \end{pmatrix}.$$

The motion is periodic and the magnetron oscillation does not occur.

(iii) $\omega = 2\nu_1$:

$$\varGamma_1^{(c)} = i\beta\begin{pmatrix} -\nu_1 L_2 & 0 & 0 & \nu_1\nu_2 \\ 0 & \nu_2 L_1 & 0 & 0 \\ 0 & 0 & -\nu_2 L_1 & 0 \\ -\nu_1\nu_2 & 0 & 0 & \nu_1 L_2 \end{pmatrix}.$$

The characteristic exponents are

$$\pm\nu_2 L_1, \quad \pm\sqrt{\nu_1^2 L_2^2 - \nu_1^2\nu_2^2}.$$

The resonance domain is the hatched area of Fig. 2. This type of magnetron oscillation is called of quasi-A type. The thickness of the resonance domain is

$$\varDelta\omega = \frac{4W}{(\nu_1-\nu_2)R^2} \quad \text{for } h = \text{const., i.e. for } H = \text{const.}$$

$$\varDelta\omega = \frac{2(\nu_1+\nu_2)W}{\nu_1(\nu_1-\nu_2)R^2} \quad \text{for } k = \text{const.,} \quad \text{i.e. for } U_a = \text{const.}$$

§ 6. The coefficient of t in the matrix $\{Q[\Omega^{-1}(\mathfrak{S})\mathfrak{T}\mathfrak{B}\mathfrak{T}^{-1}(\mathfrak{S})\Omega]\}^2$ subtracted by $\varGamma_1^2 t^2$ forms the second order matrix for the characteristic exponents. The only resonance argrument is $2\omega\pm(\nu_1-\nu_2)$. It can be shown that this argument does not give rise to any new resonance domain and that the condition $2\omega\pm(\nu_1-\nu_2) = 0$ does not modify the resonance character of the first order terms.

The magnetron oscillations deduced in this manner are only those for which $s = p$, where p is the so-called phase number. No oscillation for which $s > p$ does not take place even if we consider the higher order terms. If we adopt

$$\varphi_1 \sin\omega t + \varphi_2 \sin 2\omega t + \varphi_3 \sin 3\omega t + \cdots,$$

instead of $\varphi \sin \omega t$ in (1), then magnetron oscillations for which $s > p$ appear. It is in this way that Tomonaga has explained the poly-phase magnetron oscillations. The resonance domains for such oscillations can be similarly treated.

§ 7. The matrix (9) is transformed by $\varGamma_1^{(c)} = S\mathfrak{D}^{-1}S$ with

$$\mathfrak{D} = \begin{pmatrix} i\nu_1 L_2\beta & 0 & 0 & 0 \\ 0 & f\beta & 0 & 0 \\ 0 & 0 & -f\beta & 0 \\ 0 & 0 & 0 & -i\nu_1 L_2\beta \end{pmatrix},$$

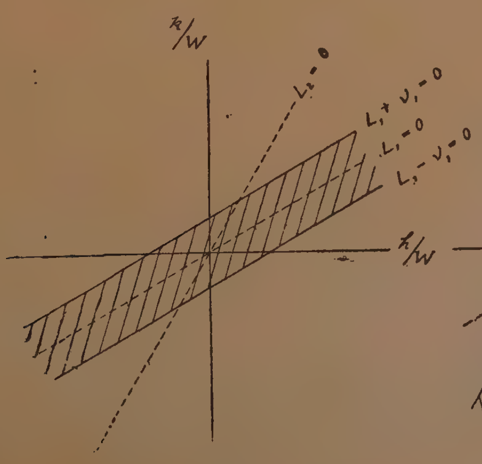

Fig. 1

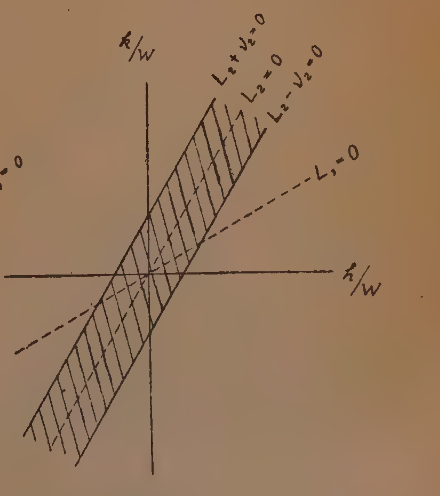

Fig. 2

$$S = \begin{pmatrix} 1 & 0 & 0 & 0 \\ 0 & i\nu_1\nu_2\beta & f\beta+i\nu_2 L_1\beta & 0 \\ 0 & i\nu_1\nu_2\beta & -f\beta+i\nu_2 L_1\beta & 0 \\ 0 & 0 & 0 & 1 \end{pmatrix},$$

to a diagonal form $\mathfrak{T}$. Our solution with our initial condition, free from periodic terms with short periods, is

$$\begin{aligned} \frac{z}{c} &= e^{\nu_1(1-L_2\beta)it+\left(\theta_0-\frac{\pi}{2}\right)i} \\ &+e^{f\beta t}\cdot e^{\left\{\nu_2 t+\left(\frac{\pi}{2}-\frac{\delta}{2}\right)\right\}i}\cdot\frac{\cos\left(\theta_0+\frac{\pi}{2}-\frac{\delta}{2}\right)}{\sin\delta} \\ &+e^{-f\beta t}\cdot e^{\left\{\nu_2 t-\left(\frac{\pi}{2}-\frac{\delta}{2}\right)\right\}i}\cdot\frac{\cos\left(\theta_0+\frac{\pi}{2}+\frac{\delta}{2}\right)}{\sin\delta}, \end{aligned} \tag{11}$$

where $\nu_1 L_1 = \nu_1\nu_2\cos\delta$, $f = \nu_1\nu_2\sin\delta$, $c = \dfrac{v_0}{\nu_1-\nu_2}$. This can be written in the case of exact resonance

$$\left\{ \begin{aligned} & z = r_1 e^{\theta_1 i}+r_2 e^{\theta_2 i}, \\ & r_2^2 = c^2[\cosh(2f\beta t)-\sinh(2f\beta t)\sin 2\theta_0], \\ & \theta_2 = \nu_2 t+\frac{\pi}{2}+\theta_0+\chi, \\ & \tan\chi = -\frac{(e^{2f\beta t}-1)\cos 2\theta_0}{(e^{2f\beta t}+1)-(e^{2f\beta t}-1)\sin 2\theta_0}, \\ & r_1 = c, \qquad \theta_1 = \nu_1 t+\theta_0-\frac{\pi}{2}. \end{aligned} \right. \tag{12}$$

Although the motion is asymptotic to a periodic solution of the second genus in the sense of Poincaré[3] as viewed from space, it can be understood more clearly if we look it in the rotating reference frame with angular speed $d\theta/dt = \nu_2$. Then the split anodes charged positively by the oscillating part of tne electric field lie in $-\frac{\pi}{4} < \theta_2-\nu_2 t < \frac{\pi}{4}$ and $\frac{3\pi}{4} < \theta_2-\nu_2 t < \frac{5\pi}{4}$, and those charged negatively lie in $\frac{\pi}{4} < \theta_2-\nu_2 t < \frac{3\pi}{4}$ and $\frac{5\pi}{4} < \theta_2-\nu_2 t < \frac{7\pi}{4}$. In exact resonance (12) the electron beam is elongated in the directions $\theta_2-\nu_2 t = \frac{\pi}{4}$ and $\frac{5\pi}{4}$, and contracted in the directions $\theta_2-\nu_2 t = \frac{3\pi}{4}$ and $\frac{7\pi}{4}$. The electrons in $-\frac{\pi}{4} < \theta_2-\nu_2 t < \frac{3\pi}{4}$ move towards $\theta_2-\nu_2 t = \frac{\pi}{4}$ and those in $\frac{3\pi}{4} < \theta_2-\nu_2 t < \frac{7\pi}{4}$ towards $\theta_2-\nu_2 t = \frac{5\pi}{4}$. The speed of electron streaming is $dr_2/dt = f\beta r_2$. Hence, if we suppose that $2\pi N$ electrons are emitted from the cathode per unit length per unit time, then the electric current from the cathode to the anode per unit length is

$$I_a = -2\pi N f\beta\frac{Re}{\nu_1-\nu_2} = -\frac{2\pi N W e}{(\nu_1-\nu_2)^2 R}. \tag{13}$$

Let the X-axis of the rotating frame lie in $\theta_2 = \nu_2 t+\frac{\pi}{4}$, then

$$\left\{ \begin{aligned} & X = X_1+X_2, \qquad Y = Y_1+Y_2, \\ & X_1 = c\cos\left[(\nu_1-\nu_2)t+\theta_0-\frac{3\pi}{4}\right], \\ & \qquad\qquad X_2 = ce^{f\beta t}\cos\theta_0, \\ & Y_1 = c\sin\left[(\nu_1-\nu_2)t+\theta_0-\frac{3\pi}{4}\right], \\ & \qquad\qquad Y_2 = ce^{-f\beta t}\sin\theta_0. \end{aligned} \right. \tag{14}$$

If we neglect terms of short period, then the locus of electrons emitted simultaneously from the cathode is an ellipse

$$e^{-2f\beta t}X_2^2+e^{2f\beta t}Y_2^2 = c^2. \tag{15}$$

It is more and more elongated as $t-t_0$ becomes greater and tends to the X_2-axis. The envelope for all such ellipses for different $t-t_0$ is two hyperbolas

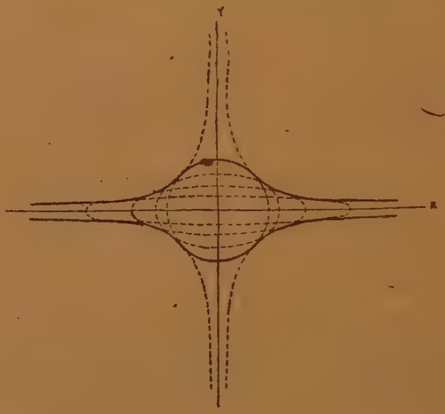

Fig. 3

$$X_2^2 Y_2^2 = \frac{1}{4}c^4. \tag{16}$$

Fig. 3 shows the (X_2, Y_2)-motion and Fig. 4 the (X, Y)-motion, which is a superposition of a circular motion on the (X_2, Y_2)-motion. The electrons emitted from time to time by the cathode are limited in the spindle-shaped region of Fig. 4. This forms the rotating electron poles which are often spoken of but have never been proved to exist.

The boundary shape of the rotating electron poles for (X, Y)-motion in Fig. 4 is formed of the envelope of all circles with radius c and with the centers at every point of the spindle-shaped area of Fig. 1 for (X_2, Y_2)-motion. It can be obtained by eliminating X_2, Y_2 from

$$(X-X_2)X_2 = -(Y-Y_2)Y_2, \quad 2X_2Y_2 = c^2,$$
$$(X-X_2)^2+(Y-Y_2)^2 = c^2.$$

The result is⁽¹⁾

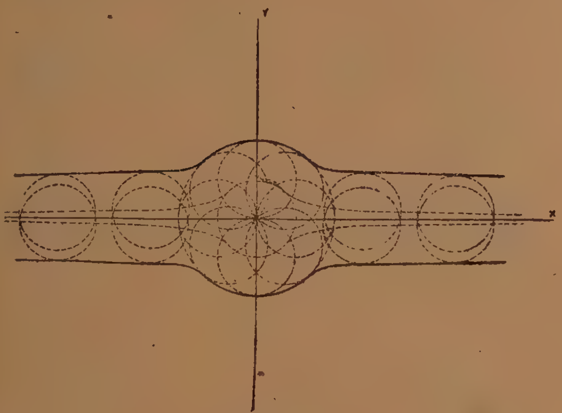

Fig. 4.

$$\begin{aligned} \Theta \equiv\ & X^2Y^2(X^2+Y^2)^2 \\ & -(X^2+Y^2)^3c^2-XY(X^2+Y^2)^2c^2 \\ & -2X^2Y^2(X^2+Y^2)c^2-8X^3Y^3c^2 \\ & +\frac{13}{4}(X^2+Y^2)^2c^4+11XY(X^2+Y^2)c^4 \\ & \qquad +13X^2Y^2c^4 \\ & -\frac{1}{8}(X^2+Y^2)c^6-16XYc^6 \\ & = 0, \end{aligned} \tag{17}$$

or

$$\begin{aligned} & r^6(1-\cos 4\theta) \\ & -2c^2r^4(5+5\sin 2\theta-\cos 4\theta-\sin 6\theta) \\ & +e^4r^2(39+44\sin 2\theta-13\cos 4\theta) \\ & -64c^6(1+\sin 2\theta) = 0, \end{aligned} \tag{17'}$$

in polar co-ordinates, $VX = r\cos\theta$, $Y = r\sin\theta$.

For $\frac{\pi}{4} < \theta < \frac{3\pi}{4}$ and $\frac{5\pi}{4} < \theta < \frac{7\pi}{4}$ the boundary curve is $r = 2c$ or $X^2+Y^2 = 4c^2$.

§ 8. When $h \neq 0$ and $k \neq 0$ but still in the resonance domain, we get from (11)

$$z = r_1 e^{\theta_1 i}+r_2e^{\theta_2 i}$$

$$\left\{\begin{aligned} & \frac{r_2^2}{c^2}\sin^2\delta = e^{2f\beta t}\sin^2\left(\theta_0-\frac{\delta}{2}\right)+e^{-2f\beta t} \\ & \quad \cdot\sin^2\left(\theta_0+\frac{\delta}{2}\right)-2\sin\left(\theta_0-\frac{\delta}{2}\right)\sin\left(\theta_0+\frac{\delta}{2}\right) \\ & \qquad\qquad \cdot\cos\delta, \\ & \theta_2 = \nu_2 t+\frac{3\pi}{2}-\frac{\delta}{2}-\xi-\varDelta\xi, \\ & \quad \sin(\xi+\varDelta\xi) = \frac{c}{r_2}\sin\left(\theta_0+\frac{\delta}{2}\right)e^{-f\beta t}, \\ & r_1 = c. \quad \theta_1 = \nu_1(1-L_2\beta)t+\theta_0+\frac{3\pi}{2}. \end{aligned}\right. \tag{18}$$

The rotating electron pole is situated by an angle $\frac{\delta}{2}$ backwards compared with the case of exact resonance and is of a similar form. We call this case the semi-resonance.

The case of the resonance $\omega = 2\nu_1$ can be treated similarly.

§ 9. We now discuss the transitions from and to the resonance domain by supposing δ as a slowly varying parameter in the theory of adiabatic invariants. We consider the B type oscillation. In the (H, U_a)-diagram of Fig. 1 the line $L_1 = 0$ corresponds to $\delta = \frac{\pi}{2}$, and the lines $L_1-\nu_1 = 0$ and $L_1+\nu_1 = 0$ bounding the resonance domain correspond respectively to $\delta = 0$ and $\delta = \pi$. As $\delta \to 0$ we get

$$\left\{\begin{aligned} & r_2 \to c[1-\nu_1\nu_2\beta t\sin 2\theta_0], \\ & \theta_2 \to \nu_2 t+\frac{\pi}{2}-\theta_0+2\nu_1\nu_2\beta t\sin^2\theta_0. \end{aligned}\right.$$

Thus the electron stream tends to rotate in the positive sense with regard to the rotating frame, except the directions $\theta_2 = \nu_2 t+\frac{\pi}{2}$ and $\theta_2 = \nu_2 t+\frac{3\pi}{2}$, which are directed towards the middle points of the split anodes positively charged by the oscillating field. For $\delta \to \pi$ the electron stream tends to rotate in the negative sense except $\theta_2 = \nu_2 t$ and $\theta_2 = \nu_2 t+\pi$, which are directed towards the middle points of the split anodes negatively charged by the oscillatng field. Thus the motion of electrons becomes periodic as we get out of the resonance domain from inside.

In order to see the behavior as we get into the resonance domain from outside, we put

$$f_1 = \nu_1\nu_2\sinh\delta_1, \qquad \nu_2 L_1 = \nu_1\nu_2\cosh\delta_1.$$

Then $\delta_1 = 0$ corresponds to the boundary of the resonance domain. $\delta_1 \to +0$ corresponds to $\delta \to 0$ and $\delta_1 \to -0$ to $\delta \to \pi$. When $\delta_1 \neq 0$, the motion is periodic, but when δ_1 tends to 0 the motion becomes more and more elongated in the specified directions and the rotating electron poles appear.

The deviation of the electrostatic potential from the law $U = U_a(r/R)^2 = -\frac{m}{2}\omega_c^2 r^2$ can be expressed by $\varDelta\omega_c^2$, which is supposed to be a function of r. $\varDelta\omega_c^2 > 0$ corresponds to $\frac{\pi}{2} > \delta > 0$ and $\varDelta\omega_c^2 < 0$ to $\pi > \delta > \frac{\pi}{2}$. Hence the deviation is translated to the variation of δ along r. The magnetron oscillation takes place if the condition $\varDelta\omega_c^2 = \pm W/R^2$, which can be obtained from (10), is satisfied all through $0 < r < R$.

This theory can be applied to the case when we vary slowly either H or U_a and make transitions to and from the resonance domain. Thus we see the reason for existence of the domains for magnetron oscillations obtained by experiments in the (H, U_a)-diagram by varying H or U_a slowly.

Reference.

(1) This work was done from October 1943 to March 1945.

(2) Hagihara: Elis Strömgren Commemoration Volume, Copenhagen 1940 p 58; Jap. J. Astr. Geophys., **5** (1927), 81; Proc. Phys.-Math. Soc. Japan. **10** (1928), 1, 34, 87, 127, 61; **12** (1930), 22. *Cf.*, Ince, *Ordinary Differential Equations*. 1927, p. 408; Frazer, Duncan, Collar: *Elementary Matrices*. 1938, Chap. IX; Strutt: *Lamésche-, Mathieusche- und verwandte Funktionen in Physik und Technik*. 1932; Brillouin, Quantenstatistik. 1931.

(3) Poincaré: *Methodes Nouvelles de la Mecanique Céleste* III.

(4) The method of elimination is described in Serret: Cours d'algèbre supérieur. Tome I, pp. 168–173;

Application of Celestial Mechanics to the Theory of a Magnetron. II.

By Yusuke HAGIHARA.

Astronomy Department, University of Tokyo.

(Received July 31, 1947)

§ 1. In the First Note the author has obtained the formation, the shape and the behavior of rotating electron poles on the basis of the assumption of quadratic form law $U = U_a(r/R)^2$ on the electrostatic potential by discussing the motion of electrons inside a magnetron with four split anodes. In this Second Note I propose to compute the electron density distribution inside the magnetron by using the result of the First Note and deduce the electrostatic potential by solving Poisson's equation and see whether our last assumption on U is correct. The motion of electrons under this modified field is next discussed and the electron density and the electrostatic potential modified by one step further ought to be obtained. We may be able to arrive at the correct electrostatic potential in this manner, provided that the convergence of the process is not taken into our consideration. This is what is called the method of self-consistent field in quantum mechanics.

In the present Note only the second approximation is treated. The computation of the electrostatic potential even in this second approximation is tremendously complicated, so an approximate theory for that part of the electron motion which is free from all purely periodic oscillations, that is, for the (X_2, Y_2)-motion defined in the First Note, is described, although the computation by considering the (X, Y)-motion has been actually carried out after great labor. In the discussion of the approximate theory we are able to get relations between the radius of the anode and the dimension of the cathode, and those between the applied magnetic field H, the anode electrostatic potential U_a, the direct anode current I_a and the amplitude of the alternating electric potential φ, necessary for the excitation of the magnetron oscillation. The cause of the so-called virtual cathode is explained, together with other outcomes from experiments. It is shown that the modified electrostatic potential can not give rise to any new resonance domain in the (H, U_C)-diagram.

§ 2. From I (14) of the expression for X_2 and Y_2 we have

$$dX_2 = cf\beta e^{f\beta t}\cos\theta_0 dt - ce^{-f\beta t}\sin\theta_0 d\theta_0 ,$$
$$dY_2 = -cf\beta e^{-f\beta t}\sin\theta_0 dt + ce^{-f\beta t}\cos\theta_0 d\theta_0 .$$

Hence the Jacobian

$$\frac{D(X_2, Y_2)}{D(t, \theta_0)} = c^2 f\beta\cos 2\theta_0 ,$$

or, by the relation $2X_2Y_2 = c\sin 2\theta_0$ obtainable from I (14),

$$\left|\frac{D(X_2, Y_2)}{D(t, \theta_0)}\right| = f\beta\sqrt{c^4 - 4X_2^2Y_2^2}. \tag{1}$$

We assume that $2\pi N$ electrons are emitted from the cathode per unit length per unit time unformly in all directions with the same initial speed v_0, the motion parallel to the magnetron cylinder axis being neglected. Then the number of electrons with the initial direction $(\theta_0, \theta_0 + d\theta_0)$ and with the time elapsed from the emission $(t, t+dt)$ is $Ndt\, d\theta_0$. On the other hand such electrons are considered at present to be inside an infinitesimal rectangular area defined by the coordinates (X_2, X_2+dX_2) and (Y_2, Y_2+dY_2). Let the number of electrons in this infinitesimal area be $\rho_2(X_2, Y_2)dX_2dY_2$, where $\rho_2(X_2, Y_2)$ denotes the electron density at (X_2, Y_2). Hence by equating those two expressions we get

$$\rho_2(X_2, Y_2) = N\Big/\frac{D(X_2, Y_2)}{D(t, \theta_0)} ,$$

or

$$\rho_2(X_2, Y_2) = \frac{N}{f\beta\sqrt{c^4 - 4X_2^2Y_2^2}} . \tag{2}$$

The (X, Y)-electron motion described in I (14) is the (X_1, Y_1)-motion superposed on this (X_2, Y_2)-motion. Thus the electron revolves on a circle $(X - X_2)^2 + (Y - Y_2)^2 = c^2$ with frequency $\nu_1 - \nu_2$, of which the centre (X_2, Y_2) performs the (X_2, Y_2)-motion. The linear electron density at a point (X, Y) on this circle is $1/(2\pi c)$. The contribution to the electron density at this point due to the electrons at (X_2, Y_2) in its (X_2, Y_2)-motion with density $\rho_2(X_2, Y_2)$ is $\rho_2(X_2, Y_2)/(2\pi c)$. The contribution to the electron density $\rho(X, Y)$ at (X, Y) due to the electrons at all points (X_2, Y_2) in its (X_2, Y_2)-motion at distance c from the point (X, Y) is

$$\rho(X, Y) = \int\frac{1}{2\pi c}\rho_2(X_2, Y_2)ds(X_2, Y_2),$$

where

$$[ds(X_2, Y_2)]^2 = dX_2^2 + dY_2^2 = \frac{c^2 dX_2^2}{(Y_2 - Y)^2}.$$

Hence

$$\rho(X, Y) = \frac{N}{2\pi f\beta}\int\frac{dX_2}{(Y_2 - Y)\sqrt{c^4 - 4X_2^2Y_2^3}} \tag{3}$$
$$= \frac{N}{2\pi f\beta}$$
$$\times\int\frac{dX_2}{\sqrt{c^2 - (X_2 - X)^2}\sqrt{c^4 - 4X_2^2\{Y - \sqrt{c^2 - (X_2 - X)^2}\}^2}}.$$

The integration is to be extended to the values of X_2 corresponding to those parts of the circular arcs of $(X - X_2)^2 + (X - Y_2)^2 = c^2$ which are inside the rotating electron poles for the (X_2, Y_2)-motion. The actual computation even of the integral in (3) is very much complicated. We have to divide the inside of the rotating electron poles for the (X, Y)-motion into 28 areas and obtain different expression for the electron density in each of those areas. The solution of Poisson's equation is different for each of these areas and we ought to consider, in order to determine the integration constants, so many boundary conditions as the number of the boundaries of these 28 areas, and of the electron poles and of its outside area, together with the boundary conditions at the cathode and on the anode. Although the complicated expressions for the density have been actually computed, we consider here only the density $\rho_2(X_2, Y_2)$ for the non-periodic part of the electron motion and solve Poisson's equation for the modified electrostatic potential by duly taking the boundary conditions into account.

§ 3. Thus we consider exclusively (X_2, Y_2)-motion of electrons and omit the unnecessary suffix 2. Carry out the transformation

$$P + iQ = (X + iY)^2,$$

then

$$\begin{cases} P = c^2e^{2f\beta t}\cos^2\theta_0 - c^2e^{-2f\beta t}\sin^2\beta_0 , \\ Q = c^2\sin 2\theta_0 , \end{cases}$$

and

$$\frac{D(P, Q)}{D(t, \theta_0)} = \frac{4f\beta}{c^2}\sqrt{c^4 - Q}\cdot\sqrt{P^2 + Q^2},$$

$$\rho_2(P, Q) = \frac{Nc^2}{4f\beta\sqrt{c^4 - Q}\sqrt{P^2 + Q^2}} . \tag{4}$$

The electron pole in this transformed (P, Q)-plane has the boundaries $Q=\pm c^2$ for $P>0$ and $P^2+Q^2=c^4$ for $P<0$, as shown in Fig. 5. It is of the same form as for a magnetron with two split anodes.

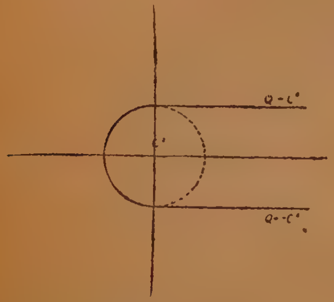

Fig. 5.

Poisson's equation

$$\left(\frac{\partial^2}{\partial X^2}+\frac{\partial^2}{\partial Y^2}\right)\Psi=-4\pi\rho,$$

is in the (P, Q)-plane transformed into

$$\text{(5)}\qquad \left(\frac{\partial^2}{\partial P^2}+\frac{\partial^2}{\partial Q^2}\right)\Psi=\frac{\pi Nc^2e}{4f\beta}\,\frac{1}{(P^2+Q^2)\sqrt{c^4-Q^2}}.$$

Put

$$P=\sigma\cos\tau,\quad Q=\sigma\sin\tau,\quad h=\frac{\pi Nc^2e}{4f\beta},$$

then (5) takes the form

$$\text{(6)}\qquad \frac{\partial^2\Psi}{\partial\sigma^2}+\frac{1}{\sigma}\,\frac{\partial\Psi}{\partial\sigma}+\frac{1}{\sigma^2}\,\frac{\partial^2\Psi}{\partial\tau^2}=f(\sigma,\tau),$$

with

$$f(\sigma,\tau)=\begin{cases}\dfrac{h}{\sigma^2\sqrt{c^4-\sigma^2\sin^2\tau}}, & \text{for } \begin{cases}\sigma\leqq c^2,\ |\tau|\leqq\sin^{-1}\dfrac{c^2}{\sigma},\\ \sigma\geqq c^2,\end{cases}\\[2ex] 0, & \text{for } \sigma\geqq c^2,\ |\tau|\geqq\sin^{-1}\dfrac{c^2}{\sigma}.\end{cases}$$

We expand $f(\sigma,\tau)$ in Fourier series

$$f(\sigma,\tau)=\sum_{j=0}^{\infty}\Phi_j(\sigma)\cos j\tau,$$

$$\Phi_j(\tau)=\int_0^{2\pi}f(\sigma,\tau)\cos j\tau\frac{d\tau}{2\pi}=\frac{h}{2\pi\sigma^2}\int_0^{2\pi}\frac{\cos j\tau d\tau}{\sqrt{c^4-\sigma^2\sin^2\sigma}}.$$

Although the integral can be expressed by complete elliptic integrals of both kinds, we had better to expand it in powers of σ/c^2 or of c^2/σ according as $\sigma<c^2$ or $\sigma>c^2$.

We divide the area inside $P^2+Q^2=R^4$ or $\sigma=R^2$ into three separate regions: $\sigma>c^2$, $|\tau|<\sin^{-1}\dfrac{c^2}{\sigma}$; $\sigma\leqq c^2$; and $\sigma>c^2$, $|\tau|>\sin^{-1}\dfrac{c^2}{\sigma}$, the last being the outside of the electron pole. Denote the solution of Poisson's equation for these three regions by Ψ, Ψ' and Ψ'' respectively. The boundary conditions are

$$\text{(7)}\qquad \begin{cases}\Psi=\Psi',\quad \dfrac{\partial\Psi}{\partial r}=\dfrac{\partial\Psi'}{\partial r},\ \text{or}\ \dfrac{\partial\Psi}{\partial\sigma}=\dfrac{\partial\Psi'}{\partial\sigma}, \\ \qquad\qquad \text{for } r=c \ \text{or}\ \sigma=c^2;\\ \Psi=\Psi''=0,\quad \text{for } r=R\ \text{or}\ \sigma=R^2;\\ r\dfrac{\partial\Psi'}{\partial r}\ \text{or}\ \sigma\dfrac{\partial\Psi'}{\partial\sigma}\ \text{is finite for } r=0\\ \qquad\qquad \text{or}\ \sigma=0.\end{cases}$$

The last condition expresses the vanishing of the electrostatic field on the cathode. The logarithmic infinity of $\dfrac{\partial\Psi'}{\partial r}$ or $\dfrac{\partial\Psi'}{\partial\sigma}$ at $r=0$ or $\sigma=0$ is permitted for convenience.

The solution has been obtained after some labor. We give here only the principal terms.

$$\begin{aligned}\frac{c^2}{h}\Psi\sim{}&2.519\log\frac{r}{R}\\ &+\left\{-\left(0.466-1.151\log\frac{c}{R}\right)\frac{c^2}{r^2}\right\}\cos 2\theta\\ &-0.124\left(\frac{c}{r}\right)^2\cos 4\theta,\qquad \text{for } r>c,\end{aligned}$$

(8)

$$\begin{aligned}\frac{c^2}{h}\Psi'\sim{}&10.604(\log r)^2\\ &+\left\{\left[0.1325+\left(0.466-1.152\log\frac{c}{R}\right)\frac{c^4}{R^4}\right]\frac{r^2}{c^2}\right.\\ &\qquad\qquad\qquad \left.-0.637\right\}\cos 2\theta\\ &+\left\{\left(-0.0621-0.0238\frac{c^2}{R^2}+0.1240\frac{c^6}{R^6}\right.\right.\\ &\quad\left.\left.-0.0367\frac{c^{10}}{R^{10}}-0.0057\frac{c^{14}}{R^{14}}\right)\frac{r^4}{c^4}\right\}\cos 4\theta\\ &\qquad\qquad\qquad \text{for } r\leqq c,\end{aligned}$$

where log is expressed with the base 10. The potential Ψ'' can be obtained from Ψ by taking $|\tau|>\sin^{-1}\dfrac{c^2}{\sigma}$ or $|\theta|>\dfrac{1}{2}\sin^{-1}\dfrac{c^2}{r^2}$ and $|\pi-\theta|>\dfrac{1}{2}\sin^{-1}\dfrac{c^2}{r^2}$, because we have expanded Ψ in Fourier series with regard to τ or θ, so that $\rho_2(X_2, Y_2)=0$ is satisfied automatically outside the electron poles.

The numerical computation for $\Psi(r)$ and $\Psi'(r)$ has been carried out for various values of c/R. The logarithmic term in (8) predominates and the potential can not be considered as proportional to r^2, but rather to $\log r$. However the term $1/r^2$ predominates near the anode and the potential is nearly of the assumed form. For $r>c$ the electron is attracted to the anode and for $r < c$ to the cathode. If v_0 is small, then c is small and the point $r = c$, where the potential attains its minimum, approaches the cathode. Thus the so-called virtual cathode appears for electrons with sufficiently small initial speed of emission. So far as the present theory is concerned the virtual cathode becomes inefficient if we make the speed of emitted electrons greater by heating more the cathode with electric current.

§4. In order to avoid the difficulty of the boundary condition at the cathode we suppose the cathode to be a circular cylinder of radius $r = r_c$ parallel to the axis of the cylinder of the magnetron. Further assume $v_0 = 0$ at $r = r_c$, $\theta = \theta_0$ initially. The electrostatic potential in this case is assumed to be

$$U_a' = \left(1-\frac{r_c^2}{R^2}\right) U_a. \tag{9}$$

That these two assumptions are nearly true can be ascertained by experiments.

The method of procedure is very much the same as in the previous case. We get for exact resonance in place of I (11)

$$\begin{aligned}\frac{\nu_1-\nu_2}{r_c} z &= \nu_2 e^{i\nu_1 t+i\theta_0}\\ &+\nu_1 e^{f\beta t}.e^{\left(\nu_2 t+\frac{\pi}{4}\right)i}\cos\left(\theta_0-\frac{5\pi}{4}\right)\\ &+\nu_1 e^{-f\beta t}.e^{\left(\nu_2 t-\frac{\pi}{4}\right)i}\cos\left(\theta_0-\frac{3\pi}{4}\right).\end{aligned} \tag{10}$$

For the (X_2, Y_2)-motion of the electron in the rotating coordinate system the only difference is the substitution of $c' = \dfrac{\nu_1 r_c}{\nu_1-\nu_2}$ for c. The principal terms for the modified electrostatic potential are

$$\left\{\begin{aligned}\frac{c'^2}{h}\Psi &\sim \left\{1.1714\left(\frac{c'}{r}\right)^2+C_1\times 4.605\log\frac{r}{c'}+C_0\right\}\\ &+\left\{B\left(\frac{c'}{r}\right)^2-\frac{c'^2}{8r^2}\left(1+4.605\log\frac{r}{c'}\right)\right\}\cos 2\theta\\ &-0.1243\left(\frac{c'}{r}\right)^2\cos 4\theta; \qquad \text{for } r > c',\\ \frac{c'^2}{h}\Psi' &\sim \left\{10.604\left(\log\frac{r}{c'}\right)^2+C_1'\times 4.605\log\frac{r}{c'}\right.\\ &\left.+C_0'\right\}+\left\{B'\left(\frac{c'}{r}\right)^2-0.6366\right\}\cos 2\theta\\ &+0\times\cos 4\theta, \qquad \text{for } r < c',\end{aligned}\right. \tag{11}$$

where

$$\begin{aligned}C_1'\times 4.605\log\frac{R}{r_c} &= 10.604\left(\log\frac{r_c}{c'}\right)^2-\overline{U}+1.1133\\ &-1.171\left(\frac{c'}{R}\right)^2-6.3418\log\frac{R}{c'},\end{aligned}$$

$$\begin{aligned}C_0\times 4.605\log\frac{R}{c} &= -\left\{10.604\left(\log\frac{r_c}{c'}\right)^2-\overline{U}+1.1133\right\}\\ &\times 4.605\log\frac{R}{c'}+\left\{1.171\left(\frac{c'}{R}\right)^2+6.3418\log\frac{R}{c'}\right\}\\ &\times 4.605\log\frac{r_c}{c'},\end{aligned}$$

$$C_1 = C_1'+1.3771, \qquad C_0' = C_0+1.1133.$$

$$\begin{aligned}B'\times\left(\frac{R^2}{r_c^2}-\frac{r_c^2}{R^2}\right) &= 0.6366\left(\frac{R}{c'}\right)^2\\ &-\left[0.1323\left(\frac{R}{c'}\right)^2+0.3408\left(\frac{c'}{R}\right)^2\right.\\ &\left.+\frac{c'^2}{8R^2}\left(1+4.605\log\frac{R}{c'}\right)\right]\left(\frac{r_c}{c'}\right)^2,\end{aligned}$$

$$B = B'-0.3408,$$

$$\overline{U} = \frac{c'^2}{h}\left(1-\frac{r_c^2}{R^2}\right)U_a.$$

For $c' > R$ we get a different expression but omit to rewrite here.

After numerical computation with several values of r_c/R, c'/R and ν_1/ν_2 we see that the logarithmic term in (11) still predominates and the virtual cathode appears for $r < c' = \dfrac{\nu_1 r_c}{\nu_1-\nu_2}$. The point $r = c'$ is always outside the cathode and $c' \to \infty$ corresponds to the cut-off condition. It is remarked that ν_1/ν_2 fixes a relation between H and U_a. With a number of numerically computed tables and diagrams for the potential we get the following conclusion.

For a sufficiently large cathode the minimum of the curve for Ψ gets into the inside of the cathode and the potential curve approaches the assumed quadratic form r^2. If I_a increases, if φ decreases, or if $\nu_1-\nu_2$ decreases, that is, if we opproach the cut-off condition, then the potential approaches the quadratic form. Fig. 6 shows clearly the circumstance that the potential curve approaches the quadratic form as r_c increases. The dotted line represents the quadratic form law and the small circles on this line show the positions of the cathode. The full curves show the parts $\mathfrak{A}_0$ of Ψ independent of θ in e. s. u. for $\nu_1/\nu_2 = 2$, $H = 250$ Gauss,

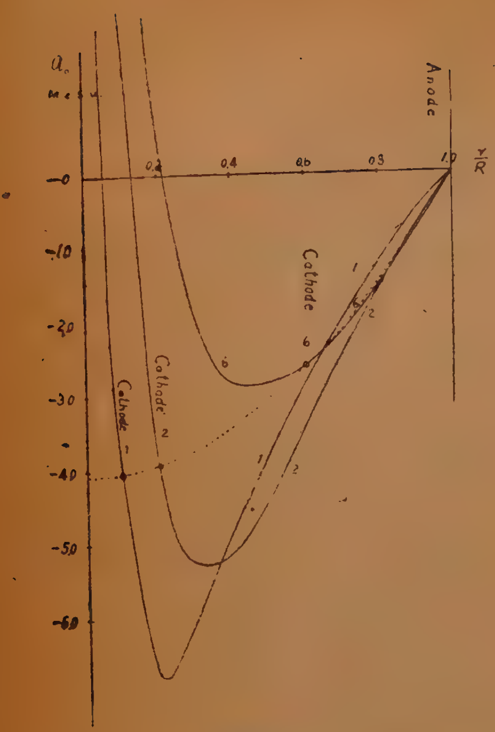

Fig. 6.

$I_a = 50\,\text{mA}$, $\varphi = 5$ volt, $R = 1$ cm, and respectively for $r_c = 0.1$, 0.2, 0.6 cm and $U_a' = 1210$, 1173, 781 volts.

§ 5. In the First Note we have obtained the thickness of the resonance domain to be

$$|\varDelta\omega_c^2| \leqq \frac{W}{eR^2}.$$

Hence the condition for being in the resonance domain is

$$\left|\frac{\Psi(r)}{r^2} - \frac{U_a}{R^2}\right| \leqq 0.6366\,\frac{\varphi}{R^2}, \tag{12}$$

the unit being volt and cm. On the other hand we have

$$\frac{h}{c'^2} = \frac{\pi m I_a}{32 e\varphi}\,(\nu_1 - \nu_2)R^2. \tag{13}$$

Thus, if φ increases, then the resonance domain is enlarged by (12) and the circumstance becomes more favorable for the magnetron oscillation. But, if φ increases, then h/c'^2 decreases according to (13) and $\overline{U}$ which appears in (11) as a factor in C_1 increases, and accordingly the potential curve approches the logarithmic. Hence there ought to be an optimum value of φ which is the most favorable for magnetron oscillations. Further it can be shown that a sufficiently large electron density, and accordingly a sufficiently large value of I_a, is necessary for magnetron oscillations. This is in conformity with the experimental fact that the magnetron oscillation starts at a value very near the saturation of I_0. Fig. 7 shows the behavior of the potential curve as we vary φ continuously. It represents the function Ψ for $\theta = 0$ in e. s. u. for $r_c/R = 0.4$, $R = 1$ cm, $I_a = 50$ mA, $H = 250$ Gauss, and $\nu_1/\nu_2 = 4/3$ with various values of a parameter κ:

$$\kappa = \frac{\varphi/5}{\dfrac{I_a}{50}\cdot R^2\cdot\dfrac{H}{250}},$$

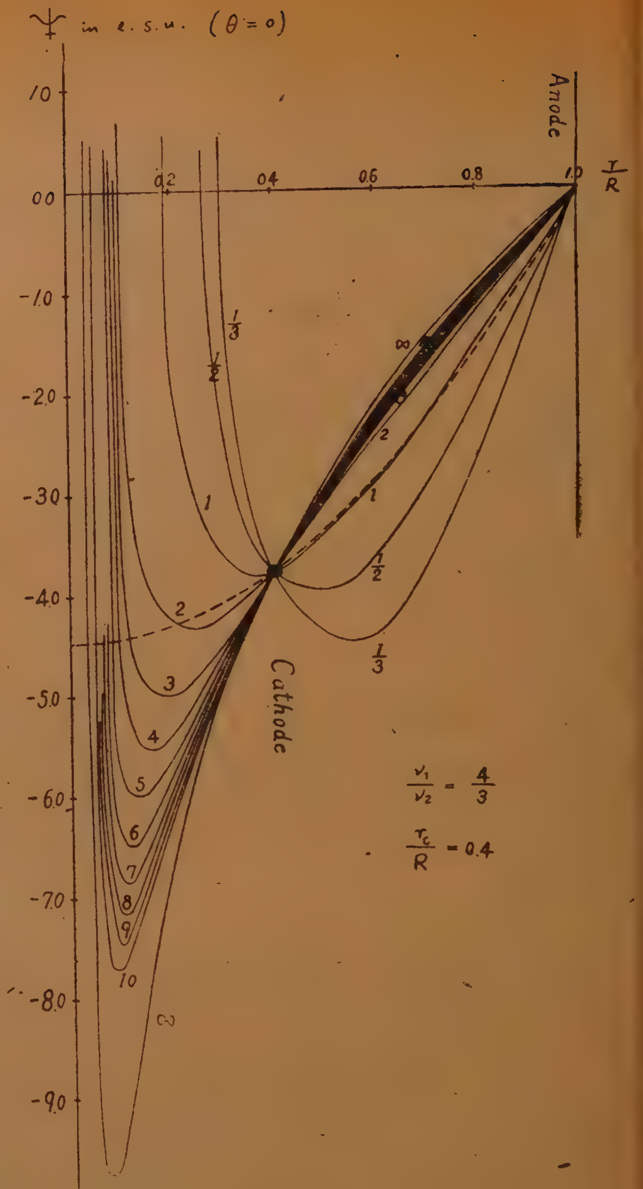

Fig. 7.

where φ is expressed in volt, I_a in mA, R in cm, H in Gauss. The values of κ are written along the various curves. There is a curve for $\kappa = 1$ nearly coincident with the dotted curve representing the quadratic form law. We have a firm conviction that the quadratic form law $U \infty r^2$ of the electrostatic potential is necessery for the type of magnetron oscillation under consideration. Hence, it is evident that there is an optimum value of φ favorable for the magnetron oscillation. The circumstance has been ascertained by drawing several similar diagrams by varying ν_1/ν_2 and r_c/R. It can also be shown that this optimum value of φ is proportional to I_a and to R^2. Hence decrease of R is the most effective in increasing φ and in enlarging the resonance domain. Unfortunately the experiments have not yet provided us with enough data for testifying our present theory. The numerical data in the present Note may be a little bit inaccurate owing to our omission of purely periodia parts of the electron motion in computing the electron density in the magnetron and to our exclusion of the external circuit from our consideration which might cause the displacement of this optimum value due to its coupling with the magnetron as an internal circuit.

§ 6. Instead of starting with zero speed from the cathode the electron is now supposed to be ejected from the cathode in the direction θ_0 with a non-zero speed v_0 at (r_c, θ_0). Then the whole result in the above is valid except only we have to replace $\nu_1 r_c/(\nu_1-\nu_2)$ by $\sqrt{\nu_1^2 r_c^2+v_0^2}/(\nu_1-\nu_2)$ and $\nu_2 r_c/(\nu_1-\nu_2)$ by $\sqrt{\nu_2^2 r_c^2+v_0^2}/(\nu_1-\nu_2)$ in (10) and in the subsequent expressions. Further the fluctuation in the value of v_0 has been studied. There has been found any essential difference with the above conclusion.

§ 7. The effect of the modified electrostatic potential (11) on the electron motion has been studied by a method similar to the one in the First Note by considering the deviation from the quadratic form law as the perturbation. After complicated computation it has been seen that no new resonance domain appears by this effect either in the direct current part independent of θ or in the alternating current part depending on θ.

Application of Celestial Mechanics to the Theory of a Magnetron. III.

By Yusuke HAGIHARA.

Astronomy Department, University of Tokyo.

(Received July 31. 1947)

§ 1. In the two preceding Notes the author treated a magnetron with four split anodes and deduced the modified electrostatic potential due to the formation of rotating electron poles on the view-point of the self-consistent field method in quantum mechanics, together with the physical consequences to be compared with experiments. In the present Note he proposes to discuss similar problems for magnetrons with more than four split anodes. The equations of motion for an electron are now of non-linear character and the author's method1) in celestial mechanics for treating the differential equations for secular perturbation of higher degrees is applied. The method gives the correct answer for the resonance domains and the direction of the rotating electron poles. Thus the domains for all types of resonance capable of being generated in magnetrons with any number of split anodes are classified into five separate kinds according to the behavior of the solution for the electron moiton in the neighborhood of the exact resonance. Among others the sharpness of the resonance can be judged for each of these kinds of resonance domains. The behavior of the exponents in the exponential factors of the solution is studied in detail over the entire resonance domain, as this exponent is correlated closely with the direct anode current I_a. However the shape of the electron poles, especially for the semi-resonance case, comes out to be somewhat misleading owing to the inaccuracy of our approximation method for the solution of the non-linear differential equations, because of the presence of the exponential factors, although the method has been successful for the problems of celestial mechanics for which the solution contains no exponential factor but exclusively purely trigonometrical functions.

§ 2. Consider the system of equations (3) of the First Note and put, with integration constants a_1, a_2, $\bar{a}_1$ and $\bar{a}_2$,

$$\begin{cases} z = a_1 e^{i\nu_1 t} + a_2 e^{i\nu_2 t} + \zeta, \\ \bar{z} = \bar{a}_1 e^{-i\nu_1 t} + \bar{a}_2 e^{-i\nu_2 t} + \bar{\zeta}, \end{cases}$$

then we get

$$(1)\quad \begin{cases} \ddot{\zeta} - 2i\omega_H \dot{\zeta} - \omega_c^2 \zeta = 2i \dfrac{h}{R^s} \dot{\zeta} + \dfrac{k}{R^3} \zeta \\ \qquad - \dfrac{s(s-1)W}{2R^s} \cdot \displaystyle\sum_{j=0}^{s-2} \binom{e-2}{j} \bar{a}_1^{s-2-j} \bar{a}_2^{j} \\ \qquad \times \left[e^{-(\omega - \overline{s-2-j}\,\nu_1 - j\nu_2)it} \right. \\ \qquad \left. - e^{(-\omega - \overline{s-2-j}\,\nu_1 - j\nu_2)it} \right] \zeta + \cdots, \\ \ddot{\bar{\zeta}} + 2i\omega_H \dot{\bar{\zeta}} = -2i \dfrac{h}{R^s} \dot{\bar{\zeta}} + \dfrac{k}{R^s} \bar{\zeta} \\ \qquad + \dfrac{s(s-1)W}{2R^s} \cdot \displaystyle\sum_{j=0}^{s-2} \binom{s-2}{j} a_1^{s-2-j} a_2^{j} \\ \qquad \times \left[e^{(\omega + \overline{s-2-j}\,\nu_1 + j\nu_2)it} \right. \\ \qquad \left. - e^{(-\omega + \overline{s-2-j}\,\nu_1 + j\nu_2)it} \right] \zeta + \cdots. \end{cases}$$

These equations are linear for ζ and $\bar{\zeta}$. By a method similar to the one in the First Note we form the matrix $Q[\Omega^{-1}(\mathfrak{S})\mathfrak{T}\mathfrak{V}\mathfrak{T}^{-1}\Omega(\mathfrak{S})]$ and pick out the matrix Γ_1 formed by the terms linear in t in this matrix. Then the resonance arguments are seen to be

$$\pm\omega + (s-2-j)\nu_1 + (j+2)\nu_2,$$

$$\pm\omega + (s-1-j)\nu_1 + (j+1)\nu_2,$$

$$\pm\omega + (s-j)\nu_1 + j\nu_2, \quad (j = 0, 1, 2, \cdots, s-2).$$

From the terms of higher orders with respect to W in the same matrix we get the resonance arguments

$$\pm 2l\omega + (\nu_1 - \nu_2), \quad \pm 2l\omega, \quad (l = 0, 1, 2, \cdots, m)$$

for an even order $2m$, and

$$\pm(2l+1)\omega + [(s-2--j)\nu_1 + (j+2)\nu_2],$$

$$\pm(2l+1)\omega + [(s-1-j)\nu_1 + (j+1)\nu_2],$$

$$\pm(2l+1)\omega + [(s-j)\nu_1 + j\nu_2],$$

$$(l = 0, 1, \cdots, m;\ j = 0, 1, \cdots, s-2)$$

for an odd order $2m+1$.

We now study the resonance domains. We denote by Z the square of the imaginary part of the characteristic root for the matrix Γ_1. The behavior of Z in the entire resonance domain has been discussed in each case carefully in order to examine the sharpness of the resonance. The quantity $\pm Z^{\frac{1}{2}}\beta_s$ with

$$\beta_s = \frac{s(s-1)W}{4\omega_c^2 \sqrt{\omega_H^2 - \omega_c^2} \cdot R^s}$$

represents the coefficient of t in the exponents, which corresponds to the outward or the inward stream motion of electrons from or to the cathode, and hence controls the direct anode current I_a. Only the main results of the discussion are briefly given in the present Note.

§ 3. Resonance $\omega = s\nu_2$:

The characteristic roots are

$$\pm\nu_1 L_2, \quad \pm\sqrt{\nu_2^2 L_1^2 - (a_2\bar{a}_2)^{s-2}\nu_1^2\nu_2^2}.$$

The resonance domain is of a similar character as shown in Fig. 1 of the First Note, the boundaries in tne present case being $L_1 \pm (a_2\bar{a}_2)^{\frac{s-2}{2}}\nu_1 = 0$. The thickness of the resonance domain is

$$(2)\quad |\varDelta\omega_H| = (a_2\bar{a}_2)^{\frac{s-2}{2}} \frac{1}{2\nu_2} \frac{W}{R^s}, \qquad \text{for } U_a = \text{const.},$$

$$|\varDelta\omega_c^2| = (a_2\bar{a}_2)^{\frac{s-2}{2}} \frac{W}{R^s}, \qquad \text{for } H = \text{const.},$$

$$Z = [(a_2\bar{a}_2)^{s-2}\nu_1^2\nu_2^2 - \nu_2^2 L_1^2].$$

Z has a maximum at the origin $h = k = 0$ and is zero on the boundaries of the resonance domain.

---

(1) See the foot-note (2) of the First Note.

The resonance is thus very sharp.

§ 4. Resonance $\omega=(s-1)\nu_2+\nu_1$:

The domain is bounded by two hyperbolas

$$L_1L_2-\nu_1\nu_2(a_2\bar{a}_2)^{s-2}\pm\nu_1L_2\cdot(s-2)\sqrt{(a_1\bar{a}_1)(a_2\bar{a}_2)^{s-3}}=0.$$

Fig. 8 shows the domain for $(a_2\bar{a}_2)<\frac{1}{4}(s-2)^2(a_1\bar{a}_1)$ and Fig. 9 that for $(a_2\bar{a}_2)>\frac{1}{4}(s-2)^2(a_1\bar{a}_1)$. In the first case the origin is inside two hyperbolas

$$L_1L_2-\nu_1\nu_2(a_2\bar{a}_2)^{s-2}\pm\nu_1L_2\cdot(s-2)\sqrt{(a_1\bar{a}_1)(a_2\bar{a}_2)^{s-3}}=0,$$

and in the second case it is inside an ellipse

$$\nu_1{}^2L_2{}^2+\nu_2{}^2L_1{}^2+2\nu_1{}^2\nu_2{}^2(a_2\bar{a}_2)^{s-2}$$
$$-(s-2)^2(a_1\bar{a}_1)(a_2\bar{a}_2)^{s-3}=0.$$

In the first case Z shows a maximum at the origin, but in the second case it has two values of which the one is a maximum while the other is a minimum. The resonance is not sharp in the second case.

Let D denote the discriminant of the quardatic equation for the square of the characteristic root. The regions for $D>0$ and for $D<0$ are marked in Fig. 8 and Fig. 9. The pairs of symbols $++$, $+-$, $-+$, $--$ mean the signs of the pair of the characteristic root squares in the case $D>0$. The symbol $++$ corresponds to domains for periodic solutions, and the other symbols to resonance domains for which $D>0$. The region for which $D<0$ is obviously a resonance domain.

Especially for $s=4$ and $(a_1\bar{a}_1)=(a_2\bar{a}_2)$ the origin is contained at the same time in the ellipse and in the hyperbolas both representing the boundaries of the resonance domains. It is remarked that the condition $(a_1\bar{a}_1)=(a_2\bar{a}_2)$ corresponds to the initial condition given in the First Note for the motion of electrons under consideration. Apart from this circumstance the explicit formulation of the integration constants does not concern us in the scope of the discussion of the present Note, so we do not bother about them and leave them just as they stand.

§ 5. Resonance $\omega=(s-2)\nu_2+2\nu_1$:

(i) $s=3$. $\omega=\nu_2+2\nu_1$.

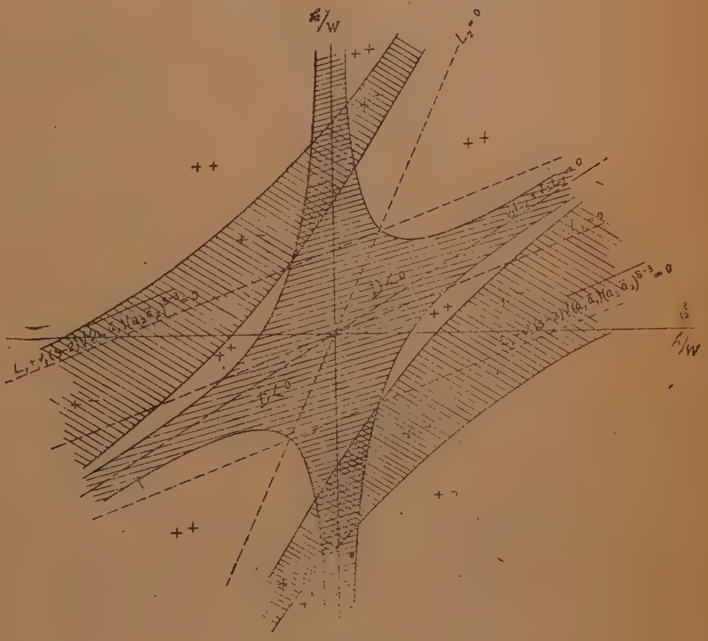

Fig. 8

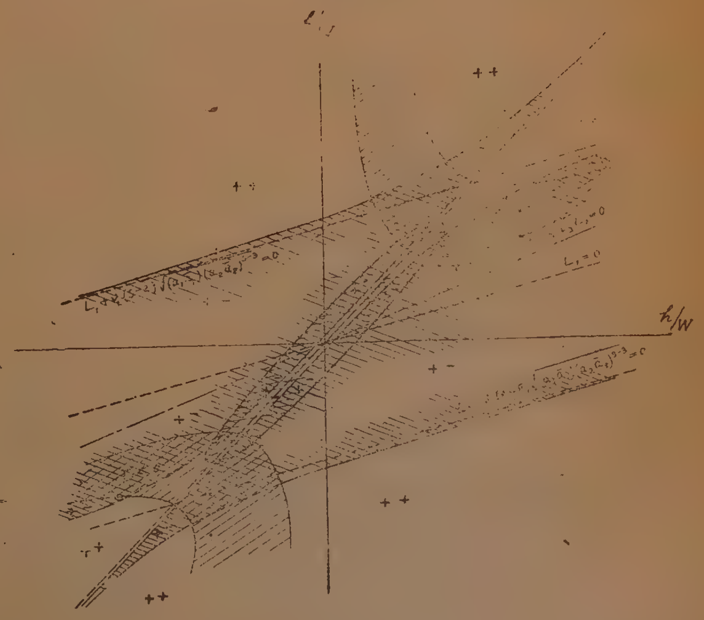

Fig. 9

The resonance domain is bounded by

$$\nu_1 L_2+\nu_2 L_1 \pm (a_2\bar{a}_2)^{\frac{1}{2}}\nu_1\nu_2 = 0$$

surrounding the origin, for which $D<0$. Similarly to the case $\omega = 2\nu_2$ the quantity Z has a maximum at the origin and decreases to zero on the boundary. The resonance is sharp.

(ii) $s = 4$. $\omega = 2\nu_2+2\nu_1$.

The solution is periodic near the origin. The magnetron oscillation does not take place.

(iii) $s = 5$. $\omega = 3\nu_2+2\nu_1$,

The resonance domain is bounded by

$$\nu_1 L_2+\nu_2 L_1 \pm (a_2\bar{a}_2)^{\frac{1}{2}}\{(a_2\bar{a}_2)^2-6(a_1\bar{a}_1)(a_2\bar{a}_2)$$
$$+9(a_1\bar{a}_1)^2\}^{\frac{1}{2}}\nu_1\nu_2 = 0.$$

The situation is similar to the case $s = 3$.

(iv) $s = 6$. $\omega = 4\nu_2+2\nu_1$.

The region near the origin is contained in an ellipse

$$\nu_1^2 L_2^2+\nu_2^2 L_1^2-(a_2\bar{a}_2)^2\{(a_2\bar{a}_2)^2-32(a_1\bar{a}_1)(a_2\bar{a}_2)$$
$$+36(a_2\bar{a}_2)^2\}\nu_1^2\nu_2^2 = 0,$$

and at the same time in

$$\{\nu_1 L_2 \pm (a_2\bar{a}_2)^2\nu_1\nu_2\}\{\nu_2 L_1 \pm 6(a_1\bar{a}_1)(a_2\bar{a}_2)\nu_1\nu_2\}$$
$$= 16(a_1\bar{a}_1)(a_2\bar{a}_2)^3\nu_1^2\nu_2^2,$$

for which $D<0$. Z has a maximum at the origin and decreases to zero on the circumference of the ellipse.

(v) $s = 7$. $\omega = 5\nu_2+2\nu_1$.

The resonance domain is very much complicated. The origin is inside an ellipse for which $D>0$ but the characteristic roots are purely imaginary, and hence the region surrounding the origin is a resonance domain. The maximum of Z at the origin is very weak and the resonance is not sharp.

§ 6. Resonance $\omega = (s-k)\nu_2+k\nu_1$, $(k = 2, 3, \cdots, s-2)$:

For $s =$ an even integer and $k = s/2$, the solution is periodic. The condition for $D>0$ at the origin is

$$\frac{s-k}{k-1}-\sqrt{\left(\frac{s-k}{k-1}\right)^2-\frac{(s-k)(s-k-1)}{k(k-1)}}$$

$$<\sqrt{\left(\frac{a_2\bar{a}_2}{a_1\bar{a}_1}\right)}<\frac{s-k}{k-1}+\sqrt{\left(\frac{s-k}{k-1}\right)^2-\frac{(s-k)(s-k-1)}{k(k-1)}}.$$

The condition for the presence of two pairs of real characteristic roots in the case of $D>0$ is

$$\left(\frac{s-k}{k-1}\right)^2-\frac{s-k}{k-1}\sqrt{\left(\frac{s-k}{k-1}\right)^2-\left(\frac{s-k-1}{k}\right)^2}.$$

$$<\left(\frac{a_2\bar{a}_3}{a_1\bar{a}_1}\right)<\left(\frac{s-k}{k-1}\right)^2+\frac{s-k}{k-1}\sqrt{\left(\frac{s-k}{k-1}\right)^2-\left(\frac{s-k-1}{k}\right)^2};$$

We get Table I by assuming $(a_2\bar{a}_2) = (a_1\bar{a}_1)$ which corresponds to the same initial condition for the motion of electrons as in the First Note.

Table I

$s =$	3	4	5	6	7	8
$k = 2$	$+\times$	$+\bigcirc p$	$+\times$	$-\times$	$-\bigcirc$	$-\bigcirc$
3		$-\bigcirc$	$+\times$	$+\bigcirc p$	$+\times$	$+\times$
4			$-\bigcirc$	$-\times$	$+\times$	$+\bigcirc p$
5				$-\bigcirc$	$-\bigcirc$	$+\times$
6					$-\bigcirc$	$-\bigcirc$
7						$-\bigcirc$

The table shows the nature of the resonance domain surrounding the origin. The case of $D>0$ is indicated by $+$ and the case of $D<0$ by $-$. The case in which all characteristic roots are real is designated by the symbol $\bigcirc$ and the other cases by the symbol $\times$. The symbol p denotes the case in which only periodic solutions are obtained, which is denoted by the double symbol $+\bigcirc$. Thus there are five separate kinds of resonance domains with regard to their behavior near the origin, that is, the four combinations of the above two sets of two symbols in the table and the fifth kind consisting of the case $\omega = s\nu_2$. In the cases with the symbol $-$ the origin is surrounded by a real ellipse, the inside of which is a resonance domain. In the cases with symbols $-\bigcirc$ and $-\times$ the resonance domain near the origin is wide and the resonance is not sharp. In the case with symbol $+\times$ and in the case $\omega = s\nu_2$ the resonance is very sharp. The behavior of Z inside each of these resonance domains has been studied in detail but the description is omitted in the present Note. The diagrams showing the behavior of the resonance domains in each of these cases are omitted to save the space.

§ 7. Now we are in the position to be able to carry out the synthetic discussion of the resonance domain for every type of magnetron oscillations. We consider the situation in the (ω_H, ω_c^2)-diagram, which is nothing but the (H, U_a)-diagram frequently employed by experimentalists. Now

$$\begin{aligned}\omega &= (s-k)\nu_2+k\nu_1\\ &= s\omega_H-(s-2k)\sqrt{\omega_H^2-\omega_c^2}.\end{aligned}$$

The curve $\omega = s\nu_2$ is a straight line which touches a parabola $(\omega_c^2) = \omega_H^2$ representing the cut-off curve in the (ω_H, ω_c^2)-diagram. As a matter of fact the part of this straight line above the point of contact A in Fig. 10 corresponds to $\omega = s\nu_2$, the B type magnetron oscillation, and the part below the point A corresponds to $\omega = s\nu_1$, the quasi-A type oscillation. The cut-off parabola $(\omega_c^2) = \omega_H^2$ is the envelope of $\omega = s\nu_2$ and $\omega = s\nu_1$ for all values of ω. The curve for the other types of resonances $\omega = (s-k)\nu_2+k\nu_1$ are represented by parabolas touching the cut-off parabola at the same point A for all values of $k = 0, 1, 2, \cdots, s-2$. The situation is shown in Fig. 10 for $s = 4$ as an example. The resonance domains are hatched. The thickness of the resonance domain is taken from (2) and from a similar formula for $\nu = 3\nu_2+\nu_1$:

$$\Delta\omega_c^2 = c^2\frac{W}{R^4}, \qquad \text{for } H = \text{const.},$$

$$|\Delta\omega_H| = c^2\frac{W}{2\nu_2 R^4}, \qquad \text{for } U_a = \text{const.}$$

As we have seen in the Second Note that the modified electrostatic potential does not give rise to any new resonance domain, the area between the cut-off curve and the straight line ought to be free from resonance domains. The types of resonance

$$\omega = (s+k')\nu_2-k'\nu_1$$

and

$$\omega = (s+k')\nu_1-k'\nu_2$$

are expected to lie in this area. But such types can not be thought physically to exist. If any resonance occurs in this area in the result of experiments, it must be attributed to a poly-phase magnetron oscillation. A double resonance such as

$$\omega = s\nu_2 = (i-\sigma\mu)\nu_2+\kappa\mu\nu_1$$

or

$$\omega = s\nu_1 = \mu\kappa\nu_1-(\sigma\mu-s)\nu_2$$

with a positive or a negative integer μ and two positive integers σ and κ, as will be touched upon in § 9, corresponds to a point of intersection of the straight line for $\omega = s\nu_2$ or $\omega = s\nu_1$ with a parabola touching the cut-off parabola at the origin and lying in the upper half of the (ω_H, ω_e^2)-diagram. If such double resonances are actually to occur with several values of μ, then, as we vary H or U_a, we may encounter a zig-zag maximum for the intensity of the magnetron oscillation such as observed by experimentalists. However a double resonance of this character can hardly be believed to take place actually.

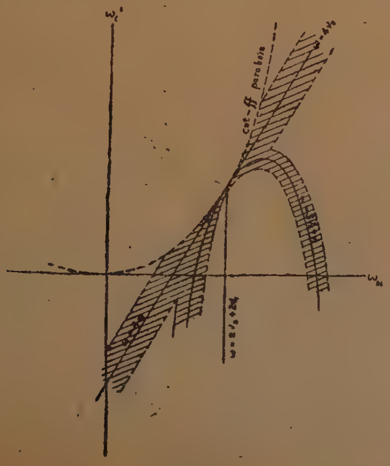

Fig. 10

§ 8. The solution of the differential equations free from periodic oscillations of short periods, putting

$$\nu_1\nu_2 = \nu_1 L_2\cos\delta, \qquad f = (a_1\bar{a}_1)^{\frac{s-2}{2}}\nu_1\nu_2\sin\delta,$$

$$f\beta_s = (a_2\bar{a}_2)^{\frac{s-2}{2}}\frac{W\sin\delta}{(\nu_1-\nu_2)R^s},$$

is

$$\begin{aligned}\frac{\nu_1-\nu_2}{v_0}z &= e^{\nu_1 it+\left(\theta_0-\frac{\pi}{2}\right)i}\\ &\quad+e^{f\beta_s t}e^{\nu_2 it-\left(\frac{s-2}{2}\theta_0+\frac{s\pi}{4}-\frac{3}{4}\pi\right)i}\\ &\qquad\times\cos\left(\frac{s\theta_0}{2}+\frac{s\pi}{4}-\frac{\pi}{4}\right)\\ &\quad+e^{-f\beta_s t}e^{\nu_2 it-\left(\frac{s-2}{2}\theta_0+\frac{s\pi}{4}-\frac{\pi}{4}\right)i}\\ &\qquad\times\cos\left(\frac{s\theta_0}{2}+\frac{s\pi}{4}+\frac{\pi}{4}\right)\end{aligned}$$

for exact resonance, and

$$\frac{\nu_1-\nu_2}{v_0}z = e^{\nu_1(1-L_2\beta_s)it+\left(\theta_0-\frac{\pi}{2}\right)i}$$

$$+e^{f\beta_s t}e^{\nu_2 it-\left(\frac{s-2}{2}\theta_0+\frac{\delta}{2}+\frac{s\pi}{4}-\pi\right)i}$$

$$\times\frac{\cos\left(\frac{s\theta_0}{2}-\frac{\delta}{2}+\frac{s\pi}{4}\right)}{\sin\delta}$$

$$+e^{-f\beta_s t}e^{\nu_2 it-\left(\frac{s-2}{2}\theta_0-\frac{\delta}{2}+\frac{s\pi}{4}\right)}$$

$$\times\frac{\cos\left(\frac{s\theta_0}{2}+\frac{\delta}{2}+\frac{s\pi}{4}\right)}{\sin\delta}$$

for semi-resonance. The electron poles appear in the direction $\theta-\nu t=\frac{\pi}{2s}-\frac{2L\pi}{s}$, $L=0,\ 1,\ 2,\ \cdots$. For the semi-resonance case the electron poles develope in the direction $\theta_2-\nu_2 t=\frac{\pi}{2s}+\frac{2L\pi}{s}+\frac{\pi}{2s}-\frac{\delta}{s}$. Here $\delta=\frac{\pi}{2}$ corresponds to the exact resonance.

Our method of solving the non-linear differential equations is apt to be inaccurate owing to the presence of real exponential factors in the solution. Hence the shape of the electron poles in general cases $s>2$, especially for semi-resonance, is not touched upon at this stage, although it has been obtained with an artifice.

Transitions to and from the resonance domain can be discussed similarly to the case $s=2$. The deviation of the electrostatic potential from the quadratic form law can also be treated similarly, but our method is not suitable for the computation of the modified electrostatic potential.

§ 9. The higher order terms with regard to z and $\bar{z}$, for which $j\geqq 1$, on the right hand sides of the equation I(3) in the case $s=2$ are treated by a similar method. From the terms $j=1$ we get resonance arguments $\omega\pm 6\nu_2$, $\omega\pm(5\nu_2+\nu_1)$, $\omega\pm(4\nu_2+2\nu_1)$, $\omega\pm(3\nu_2+3\nu_1)$. The resonance domains for $\omega=6\nu_2$, $\omega=5\nu_2+\nu_1$ and $\omega=4\nu_2+2\nu_1$ are similar respectively to those for $\omega=s\nu_2$, $\omega=(s-1)\nu_2+\nu_1$ and $\omega=(s-2)\nu_2+2\nu_1$ discussed in §§ 3, 4 and 5.

The double resonance can be supposed to occur for a magnetron with $s=2$ of the resonance due to the fundamental harmonics $j=0$ and of the resonance due to the first harmonics $j=1$ just described. The only possible combinations are $\omega=6\nu_2=\nu_1+\nu_2$, $\omega=5\nu_2+\nu_1=2\nu_1$ and $\omega=6\nu_2=2\nu_1$. The resonance domains for each of these double resonance have been studied on the supposition stated at the end of § 7. However, we omit to report it here because the supposition is hardly considered to be tenable.

On the Oscillation Mechanism of the Magnetron.

By Masao KOTANI.

Physical Institute, University of Tokyo.

(Received July 31, 1947.)

In this paper a theory of the oscillation mechanism of a split-anode magnetron is presented. This theory was developed during the War, in collaboration with Dr. Y. HAGIWARA and Dr. S. TOMONAGA. Although most of the results described here are already contained in the recent papers of these authors, the following discussion would be of some interest, since the analytical method used here is quite simple and is applicable to the study of other hyper-frequency vacuum tubes such as "BK-tube."

The inner surface of the anode of a common magnetron forms a circular cylinder of finite length, which is split into several segments separated by narrow longitudinal gaps. We neglected the thickness of the cathode, and assumed that it is stretched along the axis of the cylinder.

Take rectangular axis xyz in such a way that the z axis coincides with the axis of the cylinder (cathode). Parallel to the z axis a magnetic field of uniform intensity H is applied.

Main part of the electric field is an axial-symmetric static one, with the corresponding potential $U(r)$, where $r = \sqrt{x^2+y^2}$. In an oscillating condition a weaker alternating field with potential $V(x, y, t)$ is superposed due to the oscillation of potentials of the anode segments. We neglect the dependence of these potentials on z, and are interested mainly in the motion of electrons in planes parallel to xy.

Neglecting relativistic effects the equation of motion of an electron is

$$\left.\begin{aligned} m\frac{d^2x}{dt^2} &= -eH\frac{dy}{dt}+e\frac{\partial}{\partial x}(U+V), \\ m\frac{d^2y}{dt^2} &= eH\frac{dx}{dt}+e\frac{\partial}{\partial y}(U+V), \end{aligned}\right\} \qquad (1)$$

where $-e$ is the charge, and m the mass, of an electron. It is convenient for the following calculation to introduce the complex coordinate

$$\zeta = x+iy$$

and combine the two equations (1) into the following form

$$\frac{d^2\zeta}{dt^2}-\frac{ieH}{m}\frac{d\zeta}{dt} = \frac{2e}{m}\frac{\partial}{\partial\bar{\zeta}}(U+V). \qquad (2)$$

In (2), U and V are regarded as function of ζ and its complex conjugate $\bar{\zeta}$.

Concerning the form of the electrostatic potential $U(r)$ we introduce here an assumption, which plays a rather essential role in our theory; i. e., we assume that $U(r)$ is proportional to r^2. This means that in the anode space a space charge is formed with uniform density. If we choose the potential of the cathode as zero and denote the anode voltage by U_a, our assumption is expressed by

$$U(r) = U_a\cdot\left(\frac{r}{r_a}\right)^2, \qquad (3)$$

where r_a is the radius of the anode surface. The physical grounds—experimental as well as theoretical—favorable to this form of $U(r)$ were already fully discussed by S. TOMONAGA, and will not be repeated here.

In the absence of oscillation, we have from (2), (3) the following equation of motion

$$\frac{d^2\zeta}{dt^2}-2i\omega_H\frac{d\zeta}{dt}-\omega_c^2\zeta = 0, \qquad (4)$$

where we have introduced

$$\omega_H = \frac{eH}{2m} \text{ (LARMOR's circular frequency)},$$

$$\omega_c = \sqrt{\frac{2eU_a}{mr_a^2}}.$$

Now the solution of (4) is simply given by—

$$\zeta = C_1e^{i\Omega_1t}+C_2e^{i\Omega_2t}, \qquad (5)$$

where Ω_1 and Ω_2 are two characteristic frequencies defined by

$$\left.\begin{aligned} \Omega_1 &= \omega_H+\sqrt{\omega_H^2-\omega_c^2}, \\ \Omega_2 &= \omega_H-\sqrt{\omega_H^2-\omega_c^2}, \end{aligned}\right\} \qquad (6)$$

and C_1, C_2 are complex constants. If ω_H is $<\omega_c$, Ω_1 and Ω_2 have imaginary parts, and (5) shows that in this case all electrons emitted from the cathode flow outwards indefinitely, and thus contribute to a steady anode current. But if ω_H is $>\omega_c$, the general motion of the electron is described as a superposition of two circular motions with angular velocities Ω_1 and Ω_2, and of radii $|C_1|$ and $|C_2|$ respectively. Thus, as H increases gradually, the anode current is "cut off" at the critical field $H = H_c$, for which ω_H is equal to ω_c. In this sence ω_c may be called the "critical LARMOR frequency".

In the following we limit our consideration to the case $\omega_H > \omega_c$, which is realized in the oscillating condition.

For later use, we give here the formula for the total (kinetic + potential) energy E of the electron whose motion is given by (5):

$$\begin{aligned} E &= \frac{m}{2}v^2-eU(r) \\ &= \frac{m}{2}(\Omega_1-\Omega_2)(\Omega_1|C_1|^2-\Omega_2|C_2|^2). \end{aligned} \qquad (7)$$

Thus the energy of the circular motion with angular velocity Ω_1 increases with the radius of the circle, while the motion with angular velocity Ω_2 decreases with it.

In order to study the motion of electrons in the condition when the oscillation is generated, we have to take the alternating potential V also into account. For the sake of simplicity we restrict ourselves to the case of oscillations of "push-pull" type, and the oscillating potentials of anode segments are assumed to be

$$(V)_{r=r_a}$$
$$=\begin{cases} \dfrac{\phi_0}{2}\cos\omega t, & \dfrac{2m\pi}{N}<\theta<\dfrac{(2m+1\,\pi}{N}, \\ -\dfrac{\phi_0}{2}\cos\omega t, & \dfrac{(2m+1)\pi}{N}<\theta<\dfrac{(2m+2)\pi}{N}, \end{cases}$$
$$m=0,1,\cdots,N-1 \qquad (8)$$

where $2N$ means the number of splits of the anode. If we assume that the dependence of V on the spatial coordinates can be determined by solving LAPLACE's equation $\Delta V=0$ with (8) as boundary conditions, V must have the following form

$$V=\frac{\phi_0}{\pi}\tan^{-1}\frac{2r_a^N r^N\sin N\theta}{r_a^{2N}-r^{2N}}\cos\omega t$$
$$=\frac{\phi_0}{\pi}\cos\omega t\left\{\sum_{n=0}^{\infty}\frac{i^{-(2n+1)}}{2n+1}\left(\frac{\zeta}{r_a}\right)^{(2n+1)N}\right.$$
$$\left.+\text{ complex conjugate}\right\}. \qquad (9)$$

The experiments seem to indicate that the amplitude ϕ_0 of the oscillating anode voltage is small as compared with the static one U_a, and nevertheless the efficiency of the oscillation is fairly large (sometimes close to unity). But this is possible only when some "resonance condition" holds, and electrons emitted from the cathode change their "static" orbits slowly and continually, and finally impinge on the anode with less kinetic energy than eU_a. The following analysis shows that these situations do really occur.

Retaining the first term in (9) only, the equation of motion is written as

$$\frac{d^2\zeta}{dt^2}-2i\omega_H\frac{d\zeta}{dt}-\omega_c^2\zeta=\frac{2Ne\phi_0}{i\pi m r_a^N}\bar{\zeta}^{N-1}\cos\omega t. \qquad (9)$$

Since the right side is small, it is convenient to express the motion of electrons in the form

$$\zeta=\mathfrak{A}_1e^{i\Omega_1t}+\mathfrak{A}_2e^{i\Omega_2t} \qquad (10)$$

similar to (5), but with slowly varying coefficients $\mathfrak{A}_1$, $\mathfrak{A}_2$. Further it is allowed to assume one arbitrary condition between $\mathfrak{A}_1$, $\mathfrak{A}_2$, which we shall take as follows:

$$\frac{d\mathfrak{A}_1}{dt}e^{i\Omega_1t}+\frac{d\mathfrak{A}_2}{dt}e^{i\Omega_2t}=0. \qquad (11)$$

From (9), (10), (11) we have easily

$$\left.\begin{aligned}\frac{d\mathfrak{A}_1}{dt}&=\frac{Ne\phi_0}{\pi m(\Omega_1-\Omega_2)r_a^N}(\bar{\mathfrak{A}}_1e^{-i\Omega_1t}\\&\quad+\bar{\mathfrak{A}}_2e^{-i\Omega_2t})^{N-1}e^{-i\Omega_1t}(e^{i\omega t}+e^{-i\omega t}),\\ \frac{d\mathfrak{A}_2}{dt}&=-\frac{Ne\phi_0}{\pi m(\Omega_1-\Omega_2)r_a^N}(\bar{\mathfrak{A}}_1e^{-i\Omega_1t}\\&\quad+\bar{\mathfrak{A}}_2e^{-i\Omega_2t})^{N-1}e^{-i\Omega_2t}(e^{i\omega t}+e^{-i\omega t})\end{aligned}\right\} \qquad (12)$$

Now, since ϕ_0 is assumed to be small, $\mathfrak{A}_1$ and $\mathfrak{A}_2$ undergo usually only small periodic variations. Only when a term which does not explicitly involve time appears in the expansion of the right side, the amplitude $\mathfrak{A}_1$ or $\mathfrak{A}_2$ changes secularly, and consequently, the electron orbits are influenced largely in spite of the smallness of ϕ_0. This "resonance" condition holds when

$$\omega=\tau\Omega_1+(N-\tau)\Omega_2,$$
$$\tau=0,1,2,\cdots,N \qquad (13)$$

Assuming that this "resonance" condition is satisfied for any one of these values of τ, the secular variation of $\mathfrak{A}_1$, $\mathfrak{A}_2$ can be determined by

$$\left.\begin{aligned}\frac{d\mathfrak{A}_1}{dt}&=\frac{Ne\phi_0}{\pi m(\Omega_1-\Omega_2)r_a^N}\binom{N-1}{\tau-1}\bar{\mathfrak{A}}_1^{\tau-1}\bar{\mathfrak{A}}_2^{N-\tau},\\ \frac{d\mathfrak{A}_2}{dt}&=-\frac{Ne\phi_0}{\pi m(\Omega_1-\Omega_2)r_a^N}\binom{N-1}{\tau}\bar{\mathfrak{A}}_1^{\tau}\bar{\mathfrak{A}}_2^{N-\tau-1},\end{aligned}\right\}$$
$$(14)$$

in which terms on the right side of (12) have been dropped except the resonant term.

First let us take the case $\tau=0$, i. e.

$$\omega=N\Omega_2 \qquad (15)$$

In this case (14) reduces to

$$\left.\begin{aligned}\frac{d\mathfrak{A}_1}{dt}&=0,\\ \frac{d\mathfrak{A}_2}{dt}&=-\frac{Ne\phi_0}{\pi m(\Omega_1-\Omega_2)r_a^N}\bar{\mathfrak{A}}_2^{N-1}.\end{aligned}\right\} \qquad (16)$$

From the first equation we know that $\mathfrak{A}_1$ is constant, and maintains its initial value. Since the thermal energy of the emitted electrons is usually very small compared with eU_a, this initial value is small. Solving the second equation we obtain

$$\left.\begin{aligned}\mathfrak{A}_2&=(-u+ic)^{\frac{1}{N}},\\ \int_{u_0}^{u}(u^2+c^2)^{-\frac{N-1}{N}}du&=\frac{N^2e\phi_0}{\pi m(\Omega_1-\Omega_2)r_a^N}(t-t_0),\end{aligned}\right\} \qquad (17)$$

c and u_0 are small real constants proportional to the initial velocity of the electron. According to (17) u increases continually, and consequently all electrons emitted from the cathode reach the anode sooner or later. At the instant when the electron impinges on the anode, $\mathfrak{A}_1\sim0$, $|\mathfrak{A}_2|\sim r_a$, and according to (7) the energy of the electron is

$$E=-\frac{m}{2}(\Omega_1-\Omega_2)\Omega_2r_a^2.$$

Since this E is negative, the electron supplies energy to the oscillation field, and contributes to the generation of the oscillation. The efficiency of the oscillation is found to be

$$\eta = \frac{-E}{eU_a} = \frac{\Omega_1 - \Omega_2}{\Omega_1} = \frac{2\sqrt{\omega_H^2 - \omega_c^2}}{\omega_H + \sqrt{\omega_H^2 - \omega_c^2}}, \quad (18)$$

Hence the efficiency increases with $H (> H_c)$ monotonously and tends to unity in the limit $H \to \infty$.

Further the solution (17) shows that the phase of ζ converges to one of the following N values

$$\Omega_2 t + \frac{\pi}{N}, \quad \Omega_2 t + \frac{3\pi}{N}, \quad \cdots\cdots, \quad \Omega_2 t + \frac{(2N-1)\pi}{N}.$$

Consequently, N rotating clusters of electrons, or "poles", are formed. Examination of the phase relation between these poles and the alternating potentials of the anode segments shows that the electrons are clustered in such a way that they pass the neighborhood of the gaps of the anode segments always from high potential side to low potential side, thus doing work to the oscillating field. This is in harmony with the energy relation discussed above. This automatic selection of phases is the essential point in the oscillation mechanism of the magnetron.

In the special case of two splits magnetron $N = 1$, u increases linearly with t. Hence if we neglect the initial velocities of electrons, the electron pole is represented by a rotating radial sheath of negative charge with uniform surface density. Using this model we can calculate the charge induced electrostatically on each of the anode segments, and identify its time derivative with the induced current on Lecher lines connected to the segments. The phase of this induced current relative to that of the alternating voltage of the anode segments is found to be such that the magnetron viewed from the outer circuit is equivalent to a pure negative resistance. Its magnitude is calculated to be $\frac{\pi\phi_0}{\sigma r_a \omega}$, where σ is the surface charge density of the pole. When the resonance condition (15) is nearly, but not exactly, satisfied, the phase relation changes to some extent, and the equivalent element of a magnetron has some capacitive or inductive part. The convection current due to the capture of electrons by the anode segments gives also the capacitive part, but this convection current is usually small in comparison with the induction current.

The other extreme case $\tau = N$, i. e.

$$\omega = N\Omega_1$$

can be dealt with quite similarly. Electrons leaving the cathode reach ultimately the anode also in this case, but the electrons absorb energy from the oscillating field and the magnetron works in this case as an apparatus to convert the energy of the electric oscillation into heat. Thus, the spontaneous generation of oscillation is of course impossible.

Intermediate cases $1 \leqq \tau \leqq N-1$ can also be investigated. In these cases $|\mathfrak{A}_1|$, $|\mathfrak{A}_2|$ do not increase indefinitely; nevertheless electrons may reach the anode if the anode radius is sufficiently small. Closer examination of energy relation reveals that for $1 \leqq \tau < \frac{N}{2}$ the generation of oscillation is possible with the similar mechanism to that in the case $\tau = 0$.

I express my sincere thanks to Prof. Y. HAGIHARA, to Prof. S. TOMONAGA, and to Asst. Prof. T. MIYAJIMA, for their kind cooperation, without which this study would have been impossible. Our hearty thanks are also due to Mr. S. MIZUMA and to Dr. I. TAKAO for many valuable and stimulating discussions.

Short Notes.

Theory of Elasticity for Finite Displacement.

By Shinsuke SUGAMOTO.

(Read Oct. 7, 1947; Received October 10, 1947)

On the foundation of the Newtonian machanics and of the thermodynamics the equation of motion and its boundary condition of a largely deformable continuous body under no irreversible process except thermal conduction are constructed from both Lagrangean (L) and Eulerian (E) stand-points by using strain energy function $W\,(=\rho_0 u$ or $\rho_0 f)$. Here u and f are internal and free energy per unit mass respectively; ξ, η, ζ and ρ_0 are Cartesian co-ordinates and density of a portion of the body before displacement and $\mathfrak{r}=(x, y, z)$ and ρ after displacement (at time t); $\varepsilon_{\xi\xi}$, $\varepsilon_{\eta\eta}$, $\varepsilon_{\zeta\zeta}$, $\varepsilon_{\eta\zeta}$, $\varepsilon_{\zeta\xi}$, $\varepsilon_{\xi\eta}$ and ε_{xx}, ε_{yy}, ε_{zz}, ε_{yz}, ε_{zx}, ε_{xy} are components of finite strain from the (L) and (E) standpoints respectively defined by

$$\left(\frac{\partial\mathfrak{r}}{\partial\xi}\,\frac{\partial\mathfrak{r}}{\partial\xi}\right)=1+2\varepsilon_{\xi\xi},\qquad \left(\frac{\partial\mathfrak{r}}{\partial\eta}\,\frac{\partial\mathfrak{r}}{\partial\eta}\right)=1+2\varepsilon_{\eta\eta},$$

$$\left(\frac{\partial\mathfrak{r}}{\partial\zeta}\,\frac{\partial\mathfrak{r}}{\partial\zeta}\right)=1+2\varepsilon_{\zeta\zeta},\qquad \left(\frac{\partial\mathfrak{r}}{\partial\eta}\,\frac{\partial\mathfrak{r}}{\partial\zeta}\right)=\varepsilon_{\eta\zeta},$$

$$\left(\frac{\partial\mathfrak{r}}{\partial\zeta}\,\frac{\partial\mathfrak{r}}{\partial\xi}\right)=\varepsilon_{\zeta\xi},\qquad \left(\frac{\partial\mathfrak{r}}{\partial\xi}\,\frac{\partial\mathfrak{r}}{\partial\eta}\right)=\varepsilon_{\xi\eta};$$

$$(\nabla\xi\cdot\nabla\xi)=1-2\varepsilon_{xx},\qquad (\nabla\eta\cdot\nabla\eta)=1-2\varepsilon_{yy},$$

$$(\nabla\zeta\cdot\nabla\zeta)=1-2\varepsilon_{zz},\qquad (\nabla\eta\cdot\nabla\zeta)=-\varepsilon_{yz},$$

$$(\nabla\zeta\cdot\nabla\xi)=-\varepsilon_{zx},\qquad (\nabla\xi\cdot\nabla\eta)=-\varepsilon_{xy}.$$

$\mathfrak{K}$ is body force per unit mass and finally $\mathfrak{T}_{\mathfrak{n}}$ is the tensile stress at the boundary surface whose outer unit normal is $\mathfrak{n}$.

The equation of motion is

$$\text{(L)}\quad \rho_0\frac{d\mathfrak{V}}{dt}=\rho_0\mathfrak{K}+\left(\frac{\partial}{\partial\xi},\frac{\partial}{\partial\eta},\frac{\partial}{\partial\zeta}\right)\left\{\begin{pmatrix}\dfrac{\partial W}{\partial\varepsilon_{\xi\xi}}, & \dfrac{\partial W}{\partial\varepsilon_{\xi\eta}}, & \dfrac{\partial W}{\partial\varepsilon_{\zeta\xi}}\\[2ex] \dfrac{\partial W}{\partial\varepsilon_{\xi\eta}}, & \dfrac{\partial W}{\partial\varepsilon_{\eta\eta}}, & \dfrac{\partial W}{\partial\varepsilon_{\eta\zeta}}\\[2ex] \dfrac{\partial W}{\partial\varepsilon_{\zeta\xi}}, & \dfrac{\partial W}{\partial\varepsilon_{\eta\zeta}}, & \dfrac{\partial W}{\partial\varepsilon_{\zeta\zeta}}\end{pmatrix}\begin{pmatrix}\dfrac{\partial\mathfrak{r}}{\partial\xi}\\[2ex] \dfrac{\partial\mathfrak{r}}{\partial\eta}\\[2ex] \dfrac{\partial\mathfrak{r}}{\partial\zeta}\end{pmatrix}\right\},$$

$$\text{(E)}\quad \rho\frac{d\mathfrak{V}}{dt}=\rho\mathfrak{K}+\left(\frac{\partial}{\partial x},\frac{\partial}{\partial y},\frac{\partial}{\partial z}\right)\left\{\frac{\partial(\xi,\eta,\zeta)}{\partial(x,y,z)}\begin{pmatrix}\dfrac{\partial\xi}{\partial x}, & \dfrac{\partial\eta}{\partial x}, & \dfrac{\partial\zeta}{\partial x}\\[2ex] \dfrac{\partial\xi}{\partial y}, & \dfrac{\partial\eta}{\partial y}, & \dfrac{\partial\zeta}{\partial y}\\[2ex] \dfrac{\partial\xi}{\partial z}, & \dfrac{\partial\eta}{\partial z}, & \dfrac{\partial\zeta}{\partial z}\end{pmatrix}\begin{pmatrix}\dfrac{\partial W}{\partial\varepsilon_{xx}}, & \dfrac{\partial W}{\partial\varepsilon_{xy}}, & \dfrac{\partial W}{\partial\varepsilon_{zx}}\\[2ex] \dfrac{\partial W}{\partial\varepsilon_{xy}}, & \dfrac{\partial W}{\partial\varepsilon_{yy}}, & \dfrac{\partial W}{\partial\varepsilon_{yz}}\\[2ex] \dfrac{\partial W}{\partial\varepsilon_{zx}}, & \dfrac{\partial W}{\partial\varepsilon_{yz}}, & \dfrac{\partial W}{\partial\varepsilon_{zz}}\end{pmatrix}\begin{pmatrix}\nabla\xi\\[2ex] \nabla\eta\\[2ex] \nabla\zeta\end{pmatrix}\right\}.$$

The boundary condition is

$$\text{(L)}\quad \mathfrak{T}_{\mathfrak{n}}=\frac{1}{\dfrac{\partial(x,y,z)}{\partial(\xi,\eta,\zeta)}}\left(\frac{\partial\mathfrak{r}}{\partial\xi},\frac{\partial\mathfrak{r}}{\partial\eta},\frac{\partial\mathfrak{r}}{\partial\zeta}\right)\begin{pmatrix}\dfrac{\partial W}{\partial\varepsilon_{\xi\xi}}, & \dfrac{\partial W}{\partial\varepsilon_{\xi\eta}}, & \dfrac{\partial W}{\partial\varepsilon_{\zeta\xi}}\\[2ex] \dfrac{\partial W}{\partial\varepsilon_{\xi\eta}}, & \dfrac{\partial W}{\partial\varepsilon_{\eta\eta}}, & \dfrac{\partial W}{\partial\varepsilon_{\eta\zeta}}\\[2ex] \dfrac{\partial W}{\partial\varepsilon_{\zeta\xi}}, & \dfrac{\partial W}{\partial\varepsilon_{\eta\zeta}}, & \dfrac{\partial W}{\partial\varepsilon_{\zeta\zeta}}\end{pmatrix}\begin{pmatrix}\left(\mathfrak{n},\dfrac{\partial\mathfrak{r}}{\partial\xi}\right)\\[2ex] \left(\mathfrak{n},\dfrac{\partial\mathfrak{r}}{\partial\eta}\right)\\[2ex] \left(\mathfrak{n},\dfrac{\partial\mathfrak{r}}{\partial\zeta}\right)\end{pmatrix},$$

$$\text{(E)}\quad \mathfrak{T}_{\mathfrak{n}}=\frac{\partial(\xi,\eta,\zeta)}{\partial(x,y,z)}(\nabla\xi,\nabla\eta,\nabla\zeta)\begin{pmatrix}\dfrac{\partial W}{\partial\varepsilon_{xx}}, & \dfrac{\partial W}{\partial\varepsilon_{xy}}, & \dfrac{\partial W}{\partial\varepsilon_{zx}}\\[2ex] \dfrac{\partial W}{\partial\varepsilon_{xy}}, & \dfrac{\partial W}{\partial\varepsilon_{yy}}, & \dfrac{\partial W}{\partial\varepsilon_{yz}}\\[2ex] \dfrac{\partial W}{\partial\varepsilon_{zx}}, & \dfrac{\partial W}{\partial\varepsilon_{yz}}, & \dfrac{\partial W}{\partial\varepsilon_{zz}}\end{pmatrix}\begin{pmatrix}(\mathfrak{n},\nabla\xi)\\[2ex] (\mathfrak{n},\nabla\eta)\\[2ex] (\mathfrak{n},\nabla\zeta)\end{pmatrix}.$$

The equation of continuity is as in the hydrodynamics

$$\text{(L)}\quad \rho\frac{\partial(x,y,z)}{\partial(\xi,\eta,\zeta)}=\rho_0,\qquad \text{(E)}\quad \frac{d\rho}{dt}=-\rho(\nabla\cdot\mathfrak{v}).$$

On the Theory of the Formation of Ferromagnetic Superlattice Alloys.

By Hiroshi SATO.

Research Inst. for Iron, Steel and Other Metals, Tohoku Univ., Sendai.

(Read November 23, 1946; Received November 25, 1947)

Many anomalies in the physical properties have been found experimentally during the formation of superlattice in some ferromagnetic alloys such as Ni_3Mn, Fe_3Al etc.. Such anomalies in these alloys will be considered as the results of the simultaneous occurence of two typical cooperative phenomena—the formation of superlattice and the appearance of spontaneous magnetization. The reason for these conclusions is as follows.

As the magnetic phenomena are determined by the exchange energies due to the transposition of electrons associated with the nearest neighbouring lattice points of Ising's model of ferromagnetism and since the exchange energies may depend upon the kinds of nearest neighbouring atoms, the magnetic properties will change eventually as the configuration of atoms changes. The ferromagnetic state is energetically favourable when each atom is surrounded by atoms having larger exchange energies and the change of spontaneous magnetization will lead to the influence upon the behaviour of superlattice formation and vice versa. In such a way both phenomena are found to be correlated with each other, which correlation will be the very reason for such anomalies to appear.

The statistical theory of this phenomenon is interesting in the point that it treats two cooperative phenomena simultaneously and further the method of treatment will be a instructive pattern of the general problem including two or more cooperative phenomena. A treatment corresponding to Bragg-Williams' approximation will be put into practice as follows:

Let the number of A atoms on I sublattice be denoted by [A/I], and [A/II], [B/I] and [B/II] be defined similarly. (We consider here, for the sake of simplicity, β-brass type of superlattice. This type of superlattice consists of two interpenetrating simple cubic lattices I and II, and all atoms on the one sublattice have all their nearest neighbours on the other sublattice.) As each atom has its magnetic moment parallel or antiparallel to the magnetic field, we can divide each number [A/I] etc. into two classes according to the direction of the magnetic moment. We shall attach a suffix r to the atoms whose magnetic moments are papallel to the direction of field and a suffix l to those which have antiparallel moments. The numbers of these groups [Ar/I] etc. are then determined by *long range order* s as usual and four other variables x, y, u and v specifying the ratio of the spin directions as follows:

$$
\begin{aligned}
[Ar/I] &= \frac{N}{2}\theta(1+s)x,\\
[Ar/II] &= \frac{N}{2}\theta(1-s)y,\\
[Br/I] &= \frac{N}{2}\{1-\theta(1+s\}u,\\
[Br/II] &= \frac{N}{2}\{1-\theta(1-s)\}v,\\
[Al/I] &= \frac{N}{2}\theta(1+s)(1-x),\\
[Al/II] &= \frac{N}{2}\theta(1-s)(1-y),\\
[Bl/I] &= \frac{N}{2}\{1-\theta(1+s)\}(1-u),\\
[Bl/II] &= \frac{N}{2}\{1-\theta(1-s)\}(1-v).
\end{aligned}
\qquad (1)
$$

Herein θ is the concentration of A atoms. Using (1) and expressing the potential energy by V_{AA} etc. for the $A-A$ pairs etc. and further exchange energy by J_{AA} etc. when the magnetic moments of corresponding pairs are parallel, we get free energy for this system as follows:

$$
\begin{aligned}
F(s,x,y,u,v,\theta) = {} & \frac{Nz}{2}\,[V_{BB}-\{1-(u+v)+2uv\}J_{BB}] \\
& +Nz\theta\Big[(V_{AB}-V_{BB})-(J_{AB}-J_{BB})+(u+v)\Big(\frac{1}{2}J_{AB} \\
& -J_{BB}\Big)+\frac{1}{2}(x+y)J_{AB}-(xv+uy)J_{AB}+2uv\,J_{BB} \\
& +\frac{1}{2}(x+v-u-y-2xv+2uy)s\,J_{AB}\Big] \\
& +\frac{Nz}{2}\,\theta^2(1-s^2)[(V_{AA}+V_{BB}-2V_{AB})-(J_{AA}+J_{BB} \\
& -2J_{AB})+(x+y)(J_{AA}-J_{AB})+(u+v)(J_{BB}-J_{AB}) \\
& -2xyJ_{AA}-2uvJ_{BB}+2(xv+uy)J_{AB}] \qquad (2) \\
& +NkT\Big[\frac{1}{2}\,\theta(1+s)x\log\frac{1}{2}\,\theta(1+s)x+\frac{1}{2}\,\theta(1+s) \\
& \times(1-x)\log\frac{1}{2}\,\theta(1+s)(1-x)+\frac{1}{2}\,\theta(1-s)y\log\frac{1}{2}\,\theta \\
& \times(1-s)y+\frac{1}{2}\,\theta(1-s)(1-y)\log\frac{1}{2}\,\theta(1-s)(1-y) \\
& +\frac{1}{2}\{1-\theta(1+s)\}u\log\frac{1}{2}\{1-\theta(1+s)\}u \\
& +\frac{1}{2}\{1-\theta(1+s)\{(1-u)\log\frac{1}{2}\{1-\theta(1+s)\}(1-u) \\
& +\frac{1}{2}\{1-\theta(1-s)\}\,v\log\frac{1}{2}\{1-\theta(1-s)\}v \\
& +\frac{1}{2}\{1-\theta(1-s)\}(1-v)\log\frac{1}{2}\{1-\theta(1-s)\}(1-v)\Big].
\end{aligned}
$$

The equilibrium values of s, x, y, u and v as the function of temperature are determined as usual by solving the simultaneous equations, θ being fixed,

$$\frac{\partial F}{\partial s}=0,\quad \frac{\partial F}{\partial x}=0,\quad \frac{\partial F}{\partial y}=0,\quad \frac{\partial F}{\partial u}=0,\quad \frac{\partial F}{\partial v}=0. \qquad (3)$$

The relative magnetization is then determined assuming each magnetic moment associating with each lattice point to be equal:

$$
\begin{aligned}
M/M_\infty = {} & \theta(1+s)x+\theta(1-s)y+\{1-\theta(1+s)\}u \\
& +\{1-\theta(1-s)\}v-1 \qquad (4)
\end{aligned}
$$

(Even though each magnetic moment is not equal, the essential nature will not be changed.) In this way the bahaviours of superlattice formation and magnetic properties can be determined from these equations.

Even such method of approximation needs five independent variables. It is, however, not only laborious to treat equations with so many variables, but also the phenomena may change sensibly with the relative changes of many adjustable parameters which are introduced into the theory. It is, therefore, too complicated to treat this problem even in Bragg-Williams' approximation in order to get valuable information to advance the experiment, and more simple approximation is desirable.

By equating variables which specify spin directions, $x=y=u=v$, we can separate the free energy (2) into two parts—configurational and magnetic—and then the correlation between two parts enters through exchange enegy J of the magnetic part. This approximation is equivalent to treating the two phenomena separately and assuming the exchange energy J of the magnetic part to be

$$J = Q_{AA}/QJ_{AA}+Q_{BB}/QJ_{BB}+Q_{AA}/QJ_{AB} \qquad (5)$$

where Q is the total number of pairs of atoms and Q_{AA}, Q_{BB} and Q_{AB} are the numbers of $A-A$, $B-B$ and $A-B$ pairs, although this assumption is somewhat more lenient than the assumption $x=y=u=v$.

With this assumption (5) many interesting cases, including the antiferromagnetic one, are worked out, and even in this rough approximation essential points of the anomalous features of various ferromagnetic superlattice alloys such as Ni_3Mn, Ni_3Fe, Fe_3Al, FeCo etc. are found to be thoroughly explained.

The numerical results from sthi simple approximation were published in the Proceeding of the Physical Society of Japan (NIHON BUTSURIGAKU KAISHI) (in Japanese) in four parts* and the full account of the results based upon (2 will be published in this journal n futur.

---

* Now in press.

A General Theory of Ultra-Short-Wave Circuits II.

By Sin-itiro TOMONAGA.

Institute of Physics, Tokyo Bunrika Daigaku.

(Received August 19, 1946).

Introduction.

In the previous paper1) the author developed a general theory for ultrashort-wave circuit systems. There it was pointed out that for such general considerations the quantity called characteristic matix is a very useful mean to characterize the properties of such circuit elemets as wave guides and cavity resonators, to which the impedance concept, the powerful means for general considerations in the ordinary circuit theory, can no longer be applied. It was shown that this characteristic matrix is symmetric and unitary, and owing to these properties one can obtain considerably many informations about the circuit from the general consideration alone without carrying out any detailed calculations. Some simple examples of such general considerations was given in the previous paper.

The aim of the present paper is to give further examples showing how one can obtain the character of various circuit systems using the above mentioned proserties of the characteri tic matrix without detailed calculations. For instance we shall be able to discuss the general properties of cavity resonators.

§ 6. Connection of two circuit systems.

Since the following considerations can be easily generalised, we treat the simplest example of a connection of two circuit systems each having two openings. We suppose a circuit system (a) with two openings 0 and 1, as shown in Fig. 1, is to be connected with another circuit system (b) with the openings 0 and 2. We assume that the wave guides 0 which are to be connected with each other have the cross sections of the same form. It is now required to calculate the characteri tic matrix of the combined system (c) in terms of those of (a) and (b).

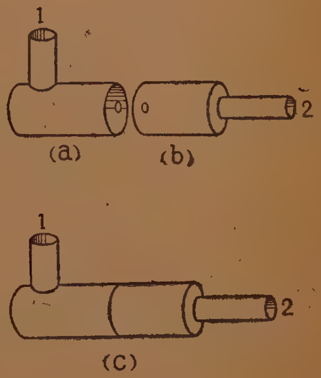

Fig. 1. Connection of two circuits,

To find the characteristic matrix of (c) we need to solve the following problem for all values of l: What waves will go out of the first and the second openings when the l-th wave of unit amplitude enters from the first or the second opening? This problem can be solved in the following way.

Let $a^{N,l}_{N',l'}(N, N'=0, 1; l, l'=1, 2, 3, \cdots\cdot)$ be the matrix elements of the characteristic matrix A of the circuit (a), $b^{N,l}_{N',l'}(N, N'=0, 2; l, l'=1, 2, 3, \cdots\cdot)$ those of the characteristic matrix B of the circuit (b), and $c^{N,l}_{N',l'}(N, N'=1, 2; l, l'=1, 2, 3, \cdots\cdot)$ those of the characteristic matrix C of the combined circuit (c). When the wave of the l-th mode of unit amplitude enters from the first opening, the amplitude of the l'-th wave which is directly reflected back to the first opening is $a^{1,l}_{1,l'}$ according to the definition of the characteristic matrix. Thereby the incident wave is also partly transmitted to the zero-th wave guide. The amplitude of the l''-th wave trahsmitted in this way is $a^{1,l}_{0,l''}$. The transmitted waves enter now into the circuit (b) and they are to be regarded as the incoming waves for the circuit (b). These waves are then partly reflected back toward the circuit (a) and are to be considered as the secondary waves entering into (a) from the zero-th opening. Since, by the definition of the characteristic matrix, the amplitude of the reflected wave of the l'''-th mode is $\sum_{l''} b_{0,l'''}^{0,l''} a_{0,l''}^{1,l}$ at the zero-th opening, the amplitude of the l'-th wave going out of the first opnning contributed by these secondary waves is $\sum_{l'''}\sum_{l''} a_{1,l'}^{0,l'''} b_{0,l'''}^{0,l''} a_{0,l''}^{1,l}$.

If we repeat such consideration further for the tertiary, ... waves and add the contributions from the directly reflected wave and those from the secondary, the tertiary, ... waves we obtain the amplitude of the l-th wave reflected back toward the first opening when the l-th wave of unit amplitude comes into the first opening:

$$c_{1,l'}^{1,l} = a_{1,l'}^{1,l} + \sum_{l'''}\sum_{l''} a_{1,l'}^{0,l'''} b_{0,l'''}^{0,l''} a_{0,l''}^{1,l}$$
$$+ \sum_{l^{\mathrm{V}}}\sum_{l^{\mathrm{IV}}}\sum_{l'''}\sum_{l''} a_{1,l'}^{0,l^{\mathrm{V}}} b_{0,l'}^{0,l^{\mathrm{IV}}} a_{0,l^{\mathrm{IV}}}^{0,l'''} b_{0,l'''}^{0,l''} a_{0,l''}^{1,l}$$
$$+ \cdots \tag{6.1}$$

In the same way we obtain the amplitude of the l'-th wave transmitted to the second opening when the l-th wave of unit amplitude comes into the first epening:

$$c_{2,l'}^{1,l} = \sum_{l''} b_{2,l'}^{0,l''} a_{0,l''}^{1,l}$$
$$+ \sum_{l^{\mathrm{IV}}}\sum_{l'''}\sum_{l''} b_{2,l'}^{0,l^{\mathrm{IV}}} a_{0,l^{\mathrm{IV}}}^{0,l'''} b_{0,l'''}^{0,l''} a_{0,l''}^{1,l} + \cdots \tag{6,2}$$

In the matrix symbolism these can be written as

$$\begin{cases} C_1^1 = A_1^1 + A_1^0B_0^0A_0^1 + A_1^0B_0^0A_0^0B_0^0A_0^1 + \cdots \\ C_2^1 = B_2^0A_0^1 + B_2A_0^0B_0^0A_0^1 + \cdots \end{cases} \tag{6,3}$$

or in closed forms

$$\begin{cases} C_1^1 = A_1^1 + A_1^0B_0^0(1-A_0^0B_0^0)^{-1}A_0^1 \\ C_2^1 = B_2^0(1-A_0^0B_0^0)^{-1}A_0^1, \end{cases} \tag{6,4}$$

which give the partial matrices of the characteristic matrix C. The remaining partial matrices can be found in the same way:

$$\begin{cases} C_2^2 = A_2^2 + B_2^0A_0^0(1-B_0^0A_0^0)^{-1}B_0^2 \\ C_1^2 = A_1^0(1-B_0^0A_0^0)^{-1}B_0^2 \end{cases} \tag{6,5}$$

These partial matrices (6,4) and (6,5) can be obtained also in the following way: we eliminate P_0 and Q_0 from the fundamental relations

$$\begin{cases} P_0 = A_0^0Q_0 + A_0^1Q_1 \\ P_1 = A_1^0Q_0 + A_1^1Q_1 \end{cases} \tag{6,6}$$

and

$$\begin{cases} Q_0 = B_0^0P_0 + B_0^2Q_2 \\ P_2 = B_2^0P_0 + B_2^2Q_2 . \end{cases} \tag{6,7}$$

The latter relations are due to the fact that the outgoing/incoming waves in the zero-th opening of the circuit (a) are to be regarded as the incoming/outgoing waves in the zero-th opening of the circuit (b) when (a) and (b) are connected with each other. By this elimination we obtain immediately the relations existing between Q_1, Q_2 and P_1, P_2:

$$\begin{cases} P_1 = \{A_1^1 + A_1^0B_0^0(1-A_0^0B_0^0)^{-1}A_0^1\}Q_1 \\ \qquad + A_1^0(1-B_0^0A_0^0)^{-1}B_0^2Q_2 \\ P_2 = B_2^0(1-A_0^0B_0^0)^{-1}A_0^1Q_1 \\ \qquad + \{B_2^2 + B_2^0(1-B_0^0A_0^0)^{-1}A_0^0B_0^2\}Q_2 \end{cases} \tag{6,8}$$

which mean in fact that the partial matrices of C are given by (6,4) and (6,5).*

We can now proceed to the question how a system connected with loads is to be treated. We consider, for simplicity, that to the simple two-opening system, as illustrated by Fig, 1 (a), a load is connected. See Fig. 2. The load reflects (and absorbs) the incident waves, and the amplitudes of the reflected waves are, in typical cases, linear functions of the amplitudes of the incoming waves. Thus the load may be regarded as a one-opening

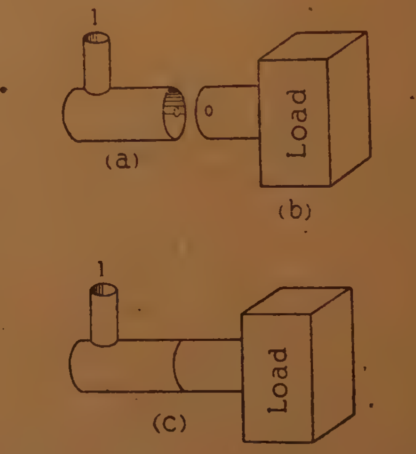

Fig. 2. Connection of circuit and load.

---

* Note that $1+B_0^0(1-A_0^0B_0^0)^{-1}A_0^0 = (1-B_0^0A_0^0)^{-1}$

circuit characterized by the characteristic matrix denoted by L whose rows and columns are the coefficients of this linear relation between amplitudes of the incoming waves and of the outgoing waves. We can then obtain the characteristic matrix C of the one-opening system (c) obtained by connecting the load (b) to the zero-th opening of the circuit (a). This is done in the way similar to the above by eliminating P_0 and Q_0 from

$$\begin{cases} P_0 = A_0{}^0 Q_0 + A_0{}^1 Q_1 \\ P_1 = A_1{}^0 Q_0 + A_1{}^1 Q_1 \end{cases} \qquad (6,9)$$

and

$$Q_0 = LP_0\,, \qquad (6.10)$$

the latter relation being due to the fact that the outgoing/incoming waves in the zero-th opening of (a) are to be regarded as the incoming/outgoing waves for the load. This elimination gives rise to

$$P_1 = A_1{}^0 L(1-A_0{}^0 L)^{-1} A_0{}^1 Q_1\,, \qquad (6.11)$$

which means that the characteristic matrix C of the combined system (c) is given by

$$C = A_1{}^0 L(1-A_0{}^0 L)^{-1} A_0{}^1 \qquad (6.12)$$

§ 7. Application to cylindrical resonators.

As an application of the consideration in the preceding paragraph we shall now treat a two-opening resonator of a cylindrical form.

A two-opening cylindrical resonator as shown in Fig. 3 (c) can be regarded as a connection of two simple two-opening circuits shown in Fig. 3 (a) and (b), so the characteristic matrix of the resonator (c) can be obtained from those of the simpler circuits (a) and (b). The length of the resonator may also be considered as variable, as indicated in the figure.

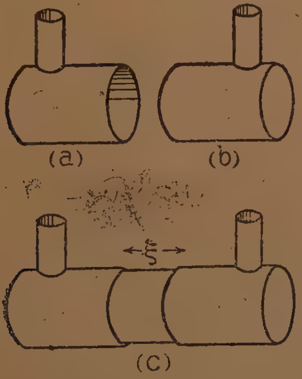

Fig. 3. Cylindrical resonator.

Let the known characteristic matrix of the simple circuits (a) and (b) be respectively A and B. Then, according to the theory of the preceding paragraph, the characteristic matrix C of the resonator can be expressed in terms of A and B:

$$\begin{cases} C_1{}^1 = A_1{}^1 + A_1{}^0 D(\xi) B_0{}^0 D(\xi) \\ \qquad\qquad \{1-A_0{}^0 D(\xi) B_0{}^0 D(\xi)\}^{-1} A_0{}^1 \\ C_2{}^1 = B_2{}^0 D(\xi)\{1-A_0{}^0 D(\xi) B_0{}^0 D(\xi)\}^{-1} A_0{}^1 \\ C_2{}^2 = B_2{}^2 + B_2{}^0 D(\xi) A_0{}^0 D(\xi) \\ \qquad\qquad \{1-B_0{}^0 D(\xi) A_0{}^0 D(\xi)\}^{-1} B_0{}^2 \\ C_1{}^2 = A_1{}^0 D(\xi)\{1\ \ B_0{}^0 D(\xi) A_0{}^0 D(\xi)\}^{-1} B_0{}^2, \end{cases} \qquad (7,1)$$

where $D(\xi)$ denotes the diagonal matrix

$$\begin{bmatrix} e^{ik_1\xi} & & & \\ & e^{ik_2\xi} & & \\ & & e^{ik_3\xi} & \\ & & & \ddots \end{bmatrix} \qquad (7,2)$$

We see that the matrix

$$R = \{1-A_0{}^0 D B_0{}^0 D\}^{-1} \qquad (7,3)$$

or

$$R' = \{1-B_0{}^0 D A_0{}^0 D\}^{-1} = 1 + B_0{}^0 D R A_0{}^0 D \qquad (7,4)$$

plays an impotant role in (7,1). Now, when a matrix M is given, it is in general possible to calculate the matrix (so-called resolvent of M)

$$R = (1-M)^{-1} \qquad (7,5)$$

by expanding it in powers of M (so-called Neuman's series):

$$R = 1 + M + M^2 + \cdots\cdots. \qquad (7,6)$$

In our problem the physical meaning of such an expansion is obvious: the n-th term $\{A_0{}^0 D B_0{}^0 D\}^n$ in the expansion of (7,3) represents, according to the consideration of the preceding paragraph, the contribution from the waves which leak out of the cavity after n-times going and returning in the cavity.

In the essential case where a resonance occurs, however, the convergence of this series is very bad. We apply to this case the following formula :[2]

$$r_\mu{}^\nu = \frac{(-1)^{\mu+\nu}}{\text{Det}(1-M)} \frac{\partial \,\text{Det}(1-M)}{\partial m_\mu{}^\nu} \qquad (7,7)$$

where $r_\mu{}^\nu$ is the matrix element of R referring to the μ-th row and the ν-th column, $m_\mu{}^\nu$ the corresponding matrix element of M, and $\text{Det}(1-M)$ means the following determinant:

$$\text{Det}(1-M) = \begin{vmatrix} 1-m_1{}^1 & -m_1{}^2 & -m_1{}^3 & \cdots \\ -m_2{}^1 & 1-m_2{}^2 & -m_2{}^3 & \cdots \\ -m_3{}^1 & -m_3{}^2 & 1-m_3{}^3 & \cdots \\ \cdots & \cdots & \cdots & \cdots \\ \cdots & \cdots & \cdots & \cdots \end{vmatrix} \qquad (7.8)$$

From (7,7) we see that the matrix elements of R become very large when $\text{Det}(1-M)$ becomes small. We shall see below that this corresponds just to the resonance of the cavity.

To see in what manner this resonance occurs, we introduce so-called secular equation for the unknown λ:

$$\text{Det}(\lambda - M) = 0. \qquad (7,9)$$

Let $\lambda^{(1)}, \lambda^{(2)}, \cdots, \lambda^{(s)}, \cdots$ denote the roots of this equation. Then according to the theory of linear equations we can express $(1-M)^{-1}$ in the form:

$$(1-M)^{-1} = \sum_s \frac{T^{(s)}}{1-\lambda^{(s)}}. \qquad (7,10)$$

By applying this theorem to our case, R and R' can be represented in the forms:

$$\left\{ \begin{aligned} R &= \sum_s \frac{T^{(s)}}{1-\lambda^{(s)}} \\ R' &= \sum_s \frac{T'^{(s)}}{1-\lambda^{(s)}} \end{aligned} \right. \qquad (7,11)$$

where $\lambda^{(s)}$ is the s-th root of the secular equation,

$$\text{Det}\{\lambda - A_0{}^0 D(\xi) B_0{}^0 D(\xi)\} = 0. \qquad (7,12)$$

Suppose now that the frequency ω has a fixed value and the length of the resonator is variable. Then the roots of the secular equation (7,12) vary as functions of ξ. It will then occur that for some values of ξ one of the roots, say the s-th root, approaches unity very closely. In this case $R(\xi)$ and $R'(\xi)$ become very large so that the characteristic matrix considered as a function of ξ shows a peculiar behaviour in the neighbourhood of this point. The same situation occurs also when the length of the resonator is fixed and the frequency ω is considered as variable. For some values of the frequency the characteristic matrix, as a function of ω, shows a peculiar behavior.

To see that this phenomenon really corresponds to the resonance, let us consider the simple caes of sufficiently long and narrow cavity with sufficiently long and narrow openings. They are so long and so narrow that there can exist in the circuit only the waves of the lowest modes.

In this case all partial matrices consist of one row and one column, so that these can be regarded as ordinary numbers. Further, the matrix $D(\xi)$ reduces also into an ordinary function $e^{ik\xi}$. For this reason the calculation of the matrix C is specially simple, because all quantities contained in the formula (7,1) are now ordinary numbers. We obtain thus from (7,1)

$$\left\{ \begin{aligned} c_1{}^1 &= a_1{}^1 + \frac{a_1{}^0 b_0{}^0 a_0{}^1 e^{2ik\xi}}{1-a_0{}^0 b_0{}^0 e^{2ik\xi}} \\ c_2{}^1 &= \frac{b_2{}^0 a_0{}^1 e^{2ik\xi}}{1-a_0{}^0 b_0{}^0 e^{2ik\xi}}, \\ c_2{}^2 &= b_2{}^2 + \frac{b_2{}^0 a_0{}^0 b_0{}^2 e^{2ik\xi}}{1-a_0{}^0 b_0{}^0 e^{2ik\xi}} \\ c_1{}^2 &= \frac{a_1{}^0 b_0{}^2 e^{2ik\xi}}{1-a_0{}^0 b_0{}^0 e^{2ik\xi}}. \end{aligned} \right. \qquad (7,13)$$

Here we have written all partial matrices in small letters, because they are now ordinary numbers.

Since in the practically important case of high Q resonator the coupling between the cavity and the opening is very loose (about the relation between Q of the resonator and the looseness of the coupling will be discussed in the following paragraphs), we may consider that in the partial circuits (a) and (b) the wave coming into one of the openings will be almost perfectly reflected and only small part will be transmitted to the other opening. This means that the absolute values of $a_1{}^1$, $a_0{}^0$, $b_0{}^0$ and $b_2{}^2$ are almost equal to unity and those of $a_0{}^1$, $a_1{}^0$, $b_0{}^2$ and $b_2{}^0$ are very small compared with unity:

$$\left\{ \begin{aligned} & |a_0{}^0|,\ |a_1{}^1|,\ |b_0{}^0| \text{ and } |b_2{}^2| \sim 1 \\ & |a_1{}^0| = |a_0{}^1| < 1, \quad |b_2{}^0| = |b_0{}^2| < 1. \end{aligned} \right. \qquad (7,14)$$

In the further consideration we shall restrict ourselves only to the case of such high Q resonators. Then it is convenient to write down the absolute values and the phases of the various complex numbers distinctly:

$$\left\{\begin{array}{l} a_1^1 = |a_1^1| e^{i\theta_1^1} \\ a_0^0 = |a_0^0| c^{i\theta_0^0}, \quad a_1^0 = a_0^1 = |a_1^0| e^{i\theta_1^0} \\ b_0^0 = |b_0^0| e^{i\varphi_0^0} \\ b_2^2 = |b_2^2| e^{i\varphi_2^2}, \quad b_2^0 = b_2^0 = |b_2^0| e^{i\varphi_2^0}. \end{array}\right. \tag{7,15}$$

Then from the unitary character of the matrix the following relations must hold:

$$\left\{\begin{array}{l} |a_1^1|^2+|a_1^0|^2 = 1 \\ |a_0^0|^2+|a_1^0|^2 = 1 \\ |a_1^1||a_1^0| e^{i(\theta_1^1-\theta_1^0)}+|a_1^0||a_1^0| e^{i(\theta_1^0-\theta_0^0)} = 0 \\ |b_2^2|^2+|b_2^0|^2 = 1 \\ |b_0^0|^2+|b_2^0|^2 = 1 \\ |b_2^2||b_2^0| e^{i(\varphi_2^2-\varphi_2^0)}+|b_2^0|\,|b_0^0| e^{i(\varphi_2^0-\varphi_0^0)} = 0. \end{array}\right. \tag{7,16}$$

For our high Q resonator we obtain then from (7,16) by using (7,14) the following approximate relations:

$$\left\{\begin{array}{l} a_0^0 = \left\{1-\frac{1}{2}\, a_1^0|^2\right\} e^{i\theta_0^0} \\ b_0^0 = \left\{1-\frac{1}{2}|b_2^0|^2\right\} e^{i\varphi_0^0} \\ a_1^1 = -e^{i(2\theta_1^0-\theta_0^0)} \\ b_2^2 = -e^{i(2\varphi_2^0-\varphi_0^0)}. \end{array}\right. \tag{7,17}$$

Now, inserting (7,17) into (7,13), we see that the characteristic matrix of the high Q resonator can be approximately expressed by

$$\left\{\begin{array}{l} c_1^1 = e^{-i(2\theta_1^0-\theta_0^0)} \\ \quad +\dfrac{|a_1^0\ |a_1^0|}{e^{-i(2k\xi+\theta_0^0+\varphi_0^0)}-1+\frac{1}{2}\{|a_1^0|^2+|b_0^2|^2\}} e^{i(2\theta_1^0-\theta_0^0)} \\ c_2^1 = c_1^2 = \dfrac{|b_2^0||a_1^0|}{e^{-i(2k\xi+\theta_0^0+\varphi_0^0)}-1+\frac{1}{2}\{|a_1^0|^2+|b_2^0|^2\}} \\ \qquad \times e^{i(\theta_1^0+\varphi_2^0-\theta_0^0-\varphi_0^0-2k\xi)} \\ c_2^2 = -e^{i(2\varphi_2^0-\varphi_0^0)} \\ \quad +\dfrac{|b_2^0||b_2^0|}{e^{-i(2k\xi+\theta_0^0+\psi_0^0)}-1+\frac{1}{2}\{|a_1^0|^2+|b_2^0|^2\}} e^{i(2\varphi_2^0-\varphi_0^0)}. \end{array}\right. \tag{7,18}$$

We suppose now that we vary the length of the resonator keeping other conditions unaltered. Then we see from (7,18) that $C(\xi)$ shows a peculiar behavior in the vicinity of such values of ξ which make $e^{i(2k\xi+\theta_0^0+\varphi_0^0)}$ unity. We see, for instance, that the transmission coefficient c_2^1 becomes so large as of the order of unity, while it is in general a very small quantitiy of the order of $|a_0^1||b_2^0|$. This means physically that, while in general only very small part of the wave coming into the entrance is transmitted to the exit, considerably large part is transmitted when the length of the resonator is such that the relation

$$2k\xi+\theta_0^0+\varphi_0^0 = 2n\pi \quad (n = 0, 1, 2, \cdots\cdots) \tag{7,19}$$

is satisfied. This is nothing but the resonance of the circuit.

If the wave length of the wave in the cavity is denoted by λ, (7,19) can also be written in the form:

$$\xi = \left(\frac{\theta_0^0+\varphi_0^0}{2\pi}+n\right)\frac{\lambda}{2}, \tag{7,20}$$

which means that the resonance occurs repeatedly every time when the length of the cavity is changed by half a wave-length.

We can see from (7,18) that the absolute value of the transmission coefficient $|c_2^1|$ is always smaller than unity. This can be unity when the resonator is constructed so as

$$|a_1^1| = |b_2^0|, \tag{7,21}$$

and the length of the cavity is just such that the resonance takes place. It is seen from (7,18) that in such a case the transmission is perfect. The reflection coefficients c_1^1 and c_2^2 vanish, in this case, as it should be from the energy law.

Thus, a two-opening resonator constructed in such a way that (7,21) hold permits at resonance the incident wave from the entrance to be perfectly transmitted to the exit. In order that a two-opening resonator should transmit the wave perfectly at resonance without reflection from the entrance to the exit, the coupling between the cavity and the entrance must be equally loose as the coupling between the cavity and the exit. We shall call such a resonator "symmetric". The reflection and tranimisson characteristics of a symmetric resonator are given in Fig. 4.

We can give physical meanings to various terms in (7,18). The first term $e^{-i(2\theta_0^1-\theta_0^0)}$ on the right-hand side for the expression of c_1^1 corresponds to that part of the wave reflected directly at the junction of the wave guide and the cavity, while the second term corresponds to the part due to the wave which is once stored in the cavity and leaks out of it. The fact that for the perfect resonator, constructed so as to satisfy (7,21), the reflected wave vanishes at the resonance is caused by the interference of these two kinds of waves.

To more general cases of resonators of any form with any number of openings such simple treatments can not be applied. It is, however, possible to develop a theory of the general resonators which will be given in the following paragraphs. These paragraphs will also serve to give examples how far-reaching the informations are which can be obtained by general considerations alone without any detailed calculations.

§ 8. Q of resonators and coefficient of leakage.

Before developing the general theory of the resonator we shall give here some remarks of a preparatory nature.

We suppose that an electromagnetic oscillation is excited in a resonator with several openings. If we let it alone, waves will leak out of the openings (it is supposed that the reflection at the outer ends of the wave guides are prevented by some suitable device), and the energy stored in will be lost gradually. We define Q of the resonator as the total energy stored in the resonator divided by the energy lost in one period of the oscillation (we neglect here the energy lost by the Ohmic resistance).

We can obtain Q of a given resonator, if we solve, corresponding to its definition mentioned above, the Maxwell equations under the condition: at the openings there exist only outgoing waves and no incoming waves at all. Such solutions cannot exist for real values of ω, because under such boundary condition the oscillation is necessarily damped. Thus, so as the Maxwell equations (1,1) to allow the solution under such boundary condition, ω must be some special complex numbers. There may exist several such complex frequencies which are characteristics of the given resonator, and they may be called "complex natural frequencies" of the resonator. We call further the oscillations with these complex frequencies "natural oscillations".

We now denote the complex natural frequency by ω_c and the corresponding fields by $\boldsymbol{E}_c$ and $\boldsymbol{H}_c$. If we put

$$\omega_c = \Omega_c - \frac{i}{2}\Gamma_c \tag{8,1}$$

separating the real and the imaginary parts of ω_c, then Ω_c may be regarded as the true frequency and $\Gamma_c/2$ as the damping coefficient of the oscillation. It will be shown in the next paragraph that Ω_c is just the resonance frequency of the resonator and Γ_c is closely related to the sharpness of the resonance.

As in this state of oscillation no incoming waves exist in the wave guides, the electromagnetic fields in the N-th wave guide is given by

$$\begin{cases} \boldsymbol{E}_c(x_N, y_N, z_N) = \sum\limits_l \alpha_{N,l}\boldsymbol{F}^*(x_N, y_N)\, e^{+ik_{Nl}z_N} \\ \boldsymbol{H}_c(x_N, y_N, z_N) = \sum\limits_l \alpha_{N,l}\boldsymbol{G}^*(x_N, y_N)\, e^{+ik_{Nl}z_N} \end{cases} \tag{8,2}$$

where $\boldsymbol{F}$ and $\boldsymbol{G}$ are given by (1,4) and (1,5), but here we must, of course, use as ω the complex frequency ω_c.

We shall now find the relations existing between the damping coefficient $\Gamma_c/2$, Q of the resonator and the amplitudes $\alpha_{N,l}$, ($N = 1, 2, 3, \cdots\cdots$; $l = 1, 2, 3, \cdots\cdots$), of the waves in the wave guides.

For this purpose we use the second theorem in §3. We now use for both dashed and undashed fields the natural fields $\boldsymbol{E}_c$ and $\boldsymbol{H}_c$. Then we obtain

$$\int_\Sigma \{[\boldsymbol{E}\times\boldsymbol{H}^*]_z+[\boldsymbol{E}^*\times\boldsymbol{H}]_z\}d\Sigma$$

$$= i(\omega_c-\omega_c^*)\int_V\{\mu(\boldsymbol{H}^*\cdot\boldsymbol{H})+\varepsilon(\boldsymbol{E}^*\cdot\boldsymbol{E})\}dV. \tag{8,3}$$

According to Poynting's theorem the right- and the left-hand sides of this equation have simple physical meanings:

$$W = \frac{1}{4}\int_V\{\mu(\boldsymbol{H}^*\cdot\boldsymbol{H})+\varepsilon(\boldsymbol{E}^*\cdot\boldsymbol{E})\}dV \tag{8,4}$$

means namely the energy stored in the resonator, and

$$S = \frac{1}{4}\int_\Sigma\{[\boldsymbol{E}\times\boldsymbol{H}^*]_z+[\boldsymbol{E}^*\times\boldsymbol{H}]_z\}d\Sigma \tag{8,5}$$

is the energy which is lost in unit time through the openings.

Now, by the definition we have

$$Q = \frac{\Omega_c W}{S}. \qquad (8.6)$$

If we use here (8,3), (8,4) and (8,5), we have

$$Q = \frac{\Omega_c}{i(\omega_c - \omega^*_c)}, \qquad (8,7)$$

which gives rise to

$$Q = \Omega_c / \Gamma_c \qquad (8,8)$$

or

$$\omega_c = \Omega_c \left(1 - \frac{i}{2Q}\right) \qquad (8,9)$$

Thus in words: If we divide the real part of the complex natural frequency by twice its imaginary part, we obtain Q of the resonator for this natural oscillation.

By using now (8,2) in (8,5) we obtain

$$S = \frac{1}{2} \sum_N \sum_l \left(\frac{\sqrt{k_{Nl}}}{\sqrt{k^*_{Nl}}} \omega_c^* + \frac{\sqrt{k^*_{Nl}}}{\sqrt{k_{Nl}}} \omega_c \right.$$

$$\left. \times |\alpha_{N,l}|^2 e^{i(k_{Nl} - k^*_{Nl}) z_N} \right) \qquad (8,10)$$

If Q of the resonator is large, the imaginary part of ω_c is small. Then, by (8,10) we can put approximately

$$S = \Omega_c \sum_N \sum_l |\alpha_{N,l}|^2, \qquad (8,11)$$

which gives the relation:

$$\text{Energy lost in one period} = \sum_N \sum_l |\alpha_{N,l}|^2, \qquad (8,12)$$

the obvious relation, which expresses that the energy lost is equal to the sum of the energies transported away by various waves through various openings.

It is now convenient to regard the amplitudes of the waves in the wave guides when a natural oscillation is taking place and unit energy is stored in the resonator as giving the degree of leakage of the waves. So we define the coefficient of leakage $\beta_{N,l}$ for the l-th mode through the N-th wave guide by means of

$$\beta_{N,l} = \alpha_{N,l} / \sqrt{W}. \qquad (8,13)$$

We define further the partial Q of the resonator contributed by the l-th mode through the N-th opening by means of

$$\frac{1}{Q_{N,l}} = |\beta_{N,l}|^2 \qquad (8,14)$$

Then we get from (8,6) and (8,11)

$$\frac{1}{Q} = \sum_N \sum_l \frac{1}{Q_{N,l}} = \sum_N \sum_l |\beta_{N,l}|^2. \qquad (8,15)$$

Thus in words: reciprocal of Q of the resonator is obtained by adding the reciprocal of various partial Q's each contributed by a certain mode through a certain opening. The reciprocal of the partial Q is given by the absolute square of the coefficient of leakage.

§ 9. Behavior of resonators in the neighbourhood of the resonance.*

In this and in the following paragraphs we suppose that the resonator has definite size and form, the frequency of the oscillation being considered as variable. Then the study of the behavior in resonance can be carried out by observing the behavior of the characteristic matrix of the resonator as a function of the frequency ω. It is thus required to obtain the behavior of the characteristic matrix when the frequency ω (considered as real) approaches to one of the resonance frequencies Ω_c.

Although our purpose is to find the characteristic matrix for the practically important case of real ω, it is necessary for such consideration to extend the region of ω into the complex plane, noting that the definition of the characteristic matrix in § 2 is equally applicable to complex values of ω.

Now, considering thus the characteristic matrix as a function of ω which can take complex values as well as real values, it is to be noted that it has a singularity at ω_c. This follows from the following fact. When ω becomes ω_c, there must exist such a solution of (1,1) that consists of only outgoing waves at the openings. For $\omega = \omega_c$, thus, the fundamental relation (2,6) must give finite p's notwithstanding that all q's on the right-hand side vanish. But this means that at least one of the matrix elements of the characteristic matrix must become infinite at $\omega = \omega_c$. In this way we obtain the conclusion that, when we regard the characteristic matrix as a function of the complex variable ω, a complex natural frequency ω_c is a singular point (pole) of this function.

---

* The reader will find that the consideration in this paragraph is essentially the same with Breit's. See reference (3).

As the simplest possibility we assume that this singularity is a simple pole. Then we can expand $a^{N,l}_{N',l}$, regarded as a function of ω, in a series of the form:

$$a^{N,l}_{N',l'} = \frac{\Omega_c q^{N,l}_{N',l'}}{\omega-\omega_c} + \xi^{N,l}_{N',l'} + \cdots \tag{9,1}$$

where the coefficients $q^{N,l}_{N',l'}$ and $\xi^{N,l}_{N',l'}$ depend no longer on ω, and at least one of $q^{N,l}_{N',l'}$ does not vanish.

The expansion (9,1) will converge if ω does not much differ from ω_c, and for such ω first two terms will already suffice to give a good approximation. If the resonator has a sufficiently large Q, the imaginary part of ω_c is very small, so the approximation may be also valid for real ω, if ω does not much differ from Ω_c. Thus we obtain an approximate formula for $a^{N,l}_{N',l'}$ which is useful for real ω.

Our next task is to determine the expansion cofficients $q^{N,l}_{N',l'}$ and $\xi^{N,l}_{N',l'}$ as far as the general consideration can attain. To do this we insert (9,1) into (2,2). Then we obtain for the fields in the wave guides

$$\left\{\begin{aligned} & E^{N,l}(x_{N'}, y_{N'}, z_{N'}) \\ & = \sum_{l'}\{\delta^N_{N'}\delta^l_{l'}F^-_{l'}e^{-ik_{N'l'}z_{N'}} + \xi^{N,l}_{N',l'}F^+_{l'}e^{+ik_{N'l'}z_{N'}}\} \\ & \quad + \frac{\Omega_c}{\omega-\omega_c}\sum_{l'} q^{N,l}_{N',l'}F^+_{l'}e^{+ik_{N'l'}z_{N'}} \qquad (9,2) \\ & \text{and the similar equation for} \\ & \qquad\qquad H^{N,l}(x_{N'}, y_{N'}, z_{N'}). \end{aligned}\right.$$

If we multiply this expression by $\omega-\omega_c$ and make $\omega \to \omega_c$, then we obtain

$$\left\{\begin{aligned} E(x_{N'}, y_{N'}, z_{N'}) &= \Omega_c\sum_{l'} q^{N,l}_{N',l'}F^+_{l'}e^{+ik_{N'l'}z_{N'}} \\ H(x_{N'}, y_{N'}, z_{N'}) &= \Omega_c\sum_{l'} q^{N,l}_{N',l'}G^+_{l'}e^{+ik_{N'l'}z_{N'}} \end{aligned}\right. \tag{9,3}$$

as the fields existing in the N'-th wave guide, having the frequency ω_c. We see that these fields consist of only outgoing waves and thus to be identified with the field (8,2):

$$\sum_{l'}\alpha_{N',l'}F^+_{l'}(x_{N'}, y_{N'})e^{ik_{N'l'}z_{N'}}$$

$$= \text{const. } \Omega_c\sum_{l'} q^{N,l}_{N',l'}F^+_{l'}(x_{N'}, y_{N'})e^{ik_{N'l'}z_{N'}}, \tag{9,4}$$

where const. on the right-hand side means the proportionality constant independent of N'.

In order that (9,4) holds, the ratio $q^{N,l}_{N',l'}/\alpha_{N',l'}$ must be constant independent of values of N' and l'. We write this common ratio, which can still depend on N and l, by $\gamma_{N,l}$.

$$q^{N,l}_{N',l'} = \gamma_{N,l}\alpha_{N',l'}. \tag{9,5}$$

Now, as the characteristic matrix is symmatric, we have $q^{N,l}_{N',l'} = q^{N',l'}_{N,l}$ from which it follows that

$$\frac{\gamma_{N,l}}{\alpha_{N,l}} = \frac{\gamma_{N',l'}}{\alpha_{N',l'}} \tag{9,6}$$

for all values of N, l and N', l'. Denoting this common ratio by δ, we obtain

$$q^{N,l}_{N',l'} = q^{N',l'}_{N,l} = \delta\alpha_{N,l}\alpha_{N',l'} \tag{9,7}$$

In this way we find that the expansion coeffients $q^{N,l}_{N',l'}$ are closely related to the coefficients $\alpha_{N,l}$ in (8,2).

If we put

$$\beta_{N,} = \sqrt{\delta}\,\alpha_{N,l} \tag{9,8}$$

(9,1) can be written as

$$a^{N,l}_{N',l'} = \frac{\Omega_c\beta_{N,l}\beta_{N',l'}}{\omega-\omega_c} + \xi^{N,l}_{N',l'}. \tag{9,9}$$

No confusion is caused here by using the same letter β as the coefficient of leakage introduced in the preceding paragraph; because, as a matter of fact, we can show that $\beta_{N,l}$ in (9,8) are just equal to the coefficients of leakage. Our conclusion is thus that the expansion coefficients $q^{N,l''}_{N',l'}$ are obtained from the coefficients of leakage $\beta_{N,l}$ by means of (9,7) and (9,8).

To prove this fact we use the unitary character of the matrix (assuming ω to be real). This gives; by inserting (9,1) into (3,11)

$$\begin{aligned} \delta^N_{N'}\delta^l_{l'} = & \frac{\Omega_c^2\overset{*}{\beta}_{N',l'}\beta_{N,l}}{|\omega-\omega_c|^2}\sum_{l''}\sum_{N''}|\beta_{N'',l''}|^2 \\ & + \frac{\Omega_c\overset{*}{\beta}_{N',l'}}{\omega-\overset{*}{\omega}_c}\sum_{N''}\sum_{l''}\overset{*}{\beta}_{N'',l''}\xi^{N,l}_{N'',l''} \\ & + \frac{\Omega_c\beta_{N,l}}{\omega-\omega_c}\sum_{N''}\sum_{l''}\beta_{N'',l''}\overset{*}{\xi}{}^{N'',l''}_{N',l'} \\ & + \sum_{N''}\sum_{l''}\xi^{N,l}_{N'',l''}\overset{*}{\xi}{}^{N'',l''}_{N',l'} \end{aligned}$$

or

$$= \frac{\Omega_c\beta_{N,l}}{\omega-\omega_c}\Big[\frac{\Omega_c\overset{*}{\beta}_{N',l'}}{\omega_c-\overset{*}{\omega}_c}\sum_{N''}\sum_{l''}|\beta_{N'',l''}|^2$$

$$+\sum_{N''}\sum_{l''}\beta_{N'',l''}\overset{*}{\xi}{}^{N'',l''}_{N',l'}\Big]$$
$$+\frac{\Omega_c\overset{*}{\beta}_{N',l'}}{\omega-\overset{*}{\omega}_c}\Big[\frac{\Omega_c\beta_{N,l}}{\omega_c-\overset{*}{\omega}_c}\sum_{N''}\sum_{l''}|\beta_{N'',l''}|^2$$
$$+\sum_{N''}\sum_{l''}\overset{*}{\beta}_{N'',l''}\xi^{N'',l''}_{N',l'}\Big]$$
$$+\sum_{N''}\sum_{l''}\xi^{N,l}_{N'',l''}\overset{*}{\xi}{}^{N'',l''}_{N',l'}. \qquad (9,10)$$

Since this relation must hold for all real values of ω, the following equalities must be satisfied:

$$\sum_{N''}\sum_{l''}\overset{*}{\xi}{}^{N'',l''}_{N',l'}\,\xi^{N,l}_{N'',l''}=\delta^N_{N'}\,\delta^l_{l'} \qquad (9,11)$$

$$\begin{cases}\dfrac{\Omega_c\beta_{N,l}}{\omega_c-\overset{*}{\omega}_c}\displaystyle\sum_{N''}\sum_{l''}|\beta_{N'',l''}|^2=\sum_{N''}\sum_{l''}\xi^{N'',l''}_{N,l}\overset{*}{\beta}_{N'',l''}\\[2ex] \dfrac{\Omega_c\overset{*}{\beta}_{N,l}}{\omega_c-\overset{*}{\omega}_c}\displaystyle\sum\sum|\beta_{N'',l''}|^2 \\[2ex] \qquad\qquad =-\displaystyle\sum_{N''}\sum_{l''}\overset{*}{\xi}{}^{N'',l''}_{N,l}\beta_{N'',l''}.\end{cases} \qquad (9,12)$$

First, we see from (9,11) that the matrix $\|\xi^{N,l}_{N',l'}\|$ is a unitary one. Next, on multiplying the first equation of (9,12) by $\xi^{N,l}_{N',l'}$ and adding over all values of N and l, we get, by using the unitary property of $\|\xi\|$

$$\frac{\Omega_c}{\omega_c-\overset{*}{\omega}_c}\sum_{N''}\sum_{l''}|\beta_{N'',l''}|^2\sum_N\sum_l\xi^{N,l}_{N',l'}\beta_{N,l}=\overset{*}{\beta}_{N',l'}. \qquad (9,13)$$

Substituting here the second relation of (9,13), we get the important relation:

$$\frac{i(\omega_c-\overset{*}{\omega}_c)}{\Omega_c}=\sum_N\sum_l|\beta_{N,l}|^2 \qquad (9,14)$$

(noting that the imaginary part of ω_c is negative). Since we have

$$\frac{i(\omega_c-\overset{*}{\omega}_c)}{\Omega_c}=\frac{\Gamma_c}{\Omega_c}=\frac{1}{Q},$$

this relation can also be written as

$$\frac{1}{Q}=\sum_N\sum_l|\beta_{N,l}|^2. \qquad (9,15)$$

According to their definition (9,8), $\beta_{N,l}$ is proportional to $\alpha_{N,l}$, and hence proportional to the coefficients of leakage. Now, (9,15) shows that the sum of $|\beta_{N,l}|^2$ is equal to the reciprocal of Q, which was the case for the coefficients of leakage themselves, see (8,14). In this way we can prove that $\beta_{N,l}$ introduced by (9,8) are, in fact, identical which the coefficients of leakage defined in the preceding paragraph.

We can obtain one further relation by substituting (9,14) into (9,12):

$$i\beta_{N,l}=\sum_{N''}\sum_{l''}\xi^{N'',l''}_{N,l}\overset{*}{\beta}_{N'',l''} \qquad (9,16)$$

In this manner we obtain the formula

$$a^{N,l}_{N',l'}=\frac{\beta_{N,l}\beta_{N',l'}}{\left(\dfrac{\omega}{\Omega_c}-1\right)+\dfrac{i}{2}\displaystyle\sum_{N''}\sum_{l''}|\beta_{N'',l''}|^2}+\xi^{N,l}_{N',l'}, \qquad (9,17)$$

which expresses the characteristic matrix in terms of the natural frequency Ω_c and the coefficients of leakage $\beta_{N,l}$, and enables us to discuss the behavior of the resonator in the neighbourhood of the resonance. We obtain from (9,17) the following conclusion: If the resonator has large Q, the coefficients of leakage are very small, so the first term on the right-hand side of (9,17) is in gereral very small. But when ω/Ω_c becomes very close to unity, it is exceptionally so large as of the order of unity. This means that, if we think ω to be increased gradually, the characteristic matrix shows a peculiar behavior when ω passes through Ω_c. In Fig. 4 is indicated the behavior of

$$\left|\frac{\beta_{N,l}\beta_{N',l'}}{\left(\dfrac{\omega}{\Omega_c}-1\right)+\dfrac{i}{2}\sum\sum|\beta_{N'',l''}|^2}\right|^2$$

as a function of ω. The width of the interval of ω in which the first term of (9,17) has an appreciable value is given by

$$|\omega-\Omega_c|<\Omega_c\sum_N\sum_l|\beta_{N,l}|^2=\Omega_c/Q, \qquad (9,18)$$

the sharpness of the resonance is thus given by Ω_c/Q or by Γ_c.

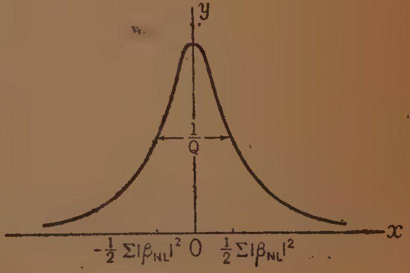

Fig. 4. Graph of
$$y=\frac{|\beta_{Nl}|^2|\beta_{N'l'}|^2}{x^2+\frac{1}{4}(\Sigma|\beta_{Nl}|^2)^2},\quad x=\frac{\omega}{\Omega_c}-1$$

It is of interest to compare the results of this paragraph with that of § 7. There we have considered the length ξ of the resonator to be variable, the frequency ω being fixed. But the result (7,18) can also be regarded as giving the dependence of the characteristic matrix on variable ξ for fixed ω. Denoting the resonance frequency by Ω which satisfies

$$2\sqrt{\Omega^2\mu\varepsilon-\kappa^2}\,\xi+\theta_0^0+\varphi_0^0=0 \tag{9,19}$$

and expanding the right-hand sides of (7,18) in powers of $\omega-\Omega$, considering them as functions of ω, we obtain

$$\left\{\begin{aligned} c_1^1 &= \frac{\dfrac{1}{2\xi\Omega(dk/d\omega)_{\omega=\Omega}}|a_1^0||a_1^0|}{\left(\dfrac{\omega}{\Omega}-1\right)+\dfrac{i}{2}\dfrac{1}{2\xi\Omega(dk/d\omega)_{\omega=\Omega}}\{|a_1^0|^2+|b_2^0|^2\}} \\ &\qquad \times e^{i\left(2\theta_1^0-\theta_0^0+\frac{\pi}{2}\right)} \quad -e^{i(2\theta_1^0-\theta_0^0)} \\ c_2^1 &= c_1^2 \\ &= \frac{\dfrac{1}{2\xi\Omega(dk/d\omega)_{\omega=\Omega}}|a_1^0||b_2^0|}{\left(\dfrac{\omega}{\Omega}-1\right)+\dfrac{i}{2}\dfrac{1}{2\xi\Omega(dk/d\omega)_{\omega=\Omega}}\{|a_1^0|^2+|b_2^0|^2\}} \\ &\qquad \times e^{i\left(\theta_1^0+\varphi_2^0-\frac{\theta_0^0}{2}-\frac{\varphi_0^0}{2}+\frac{\pi}{2}\right)} \\ c_2^2 &= \frac{\dfrac{1}{2\xi\Omega(dk/d\omega)_{\omega=\Omega}}|b_2^0||b_2^0|}{\left(\dfrac{\omega}{\Omega}-1\right)+\dfrac{i}{2}\dfrac{1}{2\xi\Omega(dk/d\omega)_{\omega=\Omega}}\{|a_1^0|^2+|b_2^0|^2\}} \\ &\qquad \times e^{i\left(2\varphi_2^0-\varphi_0^0+\frac{\pi}{2}\right)} \quad -e^{i(2\varphi_2^0-\varphi_0^0)}. \end{aligned}\right.$$

Comparing this with (9,17) we see that in the case of our cylindrical resonatar the coefficients of leakage are given by

$$\left\{\begin{aligned} \beta_1 &= \frac{1}{\sqrt{2\xi\Omega(dk/d\omega)_{\omega=\Omega}}}|a_1^0|e^{i\left(\theta_1^0-\frac{\theta_0^0}{2}+\frac{\pi}{2}\right)} \\ \beta_2 &= \frac{1}{\sqrt{2\xi\Omega(dk/d\omega)_{\omega=\Omega}}}|b_2^0|e^{i\left(\varphi_2^0-\frac{\varphi_0^0}{2}+\frac{\pi}{2}\right)} \end{aligned}\right. \tag{9,21}$$

Thus, in the case of our resonator of the form of Fig. 3 (c), the calculation of the coefficients of leakage is reduced to the calculation of the transmission coefficients for the simpler circuit of the form (a) and (b) of Fig. 3.

Taking the absolute squares of both sides of (9,21) we get the partial Q:

$$\left\{\begin{aligned} \frac{1}{Q_1} &= \frac{1}{2\xi\Omega(dk/d\omega)_{\omega=\Omega}}|a_1^0|^2 \\ \frac{1}{Q_2} &= \frac{1}{2\xi\Omega(dk/d\omega)_{\omega=\Omega}}|b_2^0|^2, \end{aligned}\right. \tag{9,22}$$

which can be interpreted in the following way: Since $\dfrac{dk}{d\omega}$ gives the reciprocal of the group velocity of the wave in the cavity, $1/\{2\xi\Omega(dk/d\omega)\}$ means the number of impacts in which the wave packet hits each one of the end walls of the cavity. As $|a_1^0|^2$ and $|b_2^0|^2$ give the amount of energies transmitted out of the first and the second opening in each such collision, (9,22) will give the energies which leak out in one period of the oscillation.

In (9,20) it is seen that $||\xi||$ has here specially simple form:

$$||\xi|| = \begin{pmatrix} -e^{i(2\theta_1^0-\theta_0^0)} & 0 \\ 0 & -e^{i(2\varphi_2^0-\varphi_0^0)} \end{pmatrix}. \tag{9,23}$$

It is easy to verify that the relation (9,16) holds for this $||\xi||$.

The fact that $||\xi||$ has such a simple form depends on the special construction of our resonator. From the general consideration alone we can only conclude that $||\xi||$ satisfies (9,16), from which (9,23) does not necessarily follow. But if the resonator is so constructed that no direct couplings exist between various openings with one another, and, further, no change of mode of the incoming waves occurs when the waves are reflected at the junction of the cavity and the wave guide (these will be in practice often the case), we can assume without detailed calculations that $||\xi||$ is a diagonal matrix. In such a case (9,16) suffices to determine $||\xi||$. We get in such a case

$$\xi_{N',l'}^{N,l} = \delta_{N'}^{N}\,\delta_{l'}^{l}\,\frac{i\beta_{N,l}}{\overset{*}{\beta}_{N,l}}. \tag{9,24}$$

Then (9,17) becomes

$$a_{N',l'}^{N,l} = \frac{\beta_{N,l}\beta_{N',l'}}{\left(\dfrac{\omega}{\Omega_c}-1\right)+\dfrac{i}{2}\sum\sum|\beta_{N'',l''}|^2} + \delta_{N'}^{N}\,\delta_{l'}^{l}\,\frac{i\beta_{N,l}}{\overset{*}{\beta}_{N,l}} \tag{9,25}$$

or if we put

$$\begin{aligned} \beta_{N,l} &= |\beta_{N,l}|e^{i\theta_{N,l}} \\ &= \frac{1}{\sqrt{Q_{N,l}}}e^{i\theta_{N,l}}, \end{aligned} \tag{9,26}$$

we obtain

$$a_{N',l'}^{N,l} =$$

$$\left\{\frac{\dfrac{1}{\sqrt{Q_{N,l}}}\dfrac{1}{\sqrt{Q_{N',l'}}}}{\left(\dfrac{\omega}{\Omega_c}-1\right)+\dfrac{i}{2}\dfrac{1}{Q}}+i\delta^N_{N'}\delta^l_{l'}\right\}e^{i(\theta_{N,l}+\theta_{N',l'})} \tag{9,27}$$

For the practically important cases where in each wave guide only the wave of one mode exists, we obtain the formula

$$a^N_{N'}=\left\{\frac{\dfrac{1}{\sqrt{Q_N}}\dfrac{1}{\sqrt{Q_{N'}}}}{\left(\dfrac{\omega}{\Omega_c}-1\right)+\dfrac{i}{2}\dfrac{1}{Q}}+id^N_{N'}\right\}e^{i(\theta_N+\theta_{N'})} \tag{9,28}$$

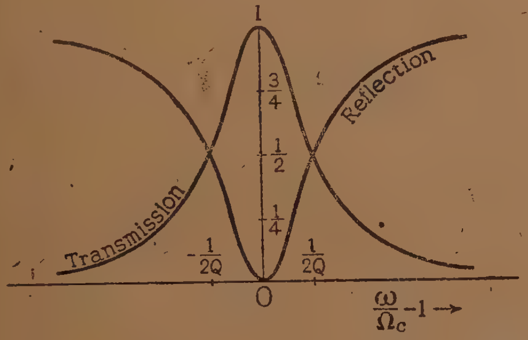

Fig. 5. Reflection and transmission characteristics of a symmetrical resenator

These formulas can be used to discuss the properties of a resonator in the neighbourhood of a resonance. For instance, one can find the behavior of the absolute squares of the reflection coefficients a_1^1, a_2^2 and those of the transmission coefficients a_1^2 and a_1^2 of a symmetric two-opening resonator as functions of ω. They are given by Fig. 5. We shall give some further applications of our formulas in the following two paragraphs.

§ 10. Transmission of energies to various openings.

We suppose a resonator with any number of openings is given. But it is assumed that in each wave guide only the wave of one mode can exist. We shall now discuss how the energies will be transmitted to various openings when the wave enters from the first opening and goes out of the various openings.

In such a resonator the energy transmitted can be calculated by means of the formula (9,28). Thus the energy transmitted to the N-th opening is, per period, given by

$$\left\{\begin{aligned}|a_N{}^1|^2&=\frac{\dfrac{1}{Q_1}\dfrac{1}{Q_N}}{\left(\dfrac{\omega}{\Omega_c}-1\right)^2+\dfrac{1}{4}\left(\dfrac{1}{Q}\right)^2}\qquad (N\neq 1)\\ |a_1{}^1|^2&=\frac{\left(\dfrac{\omega}{\Omega_c}-1\right)^2+\dfrac{1}{4}\left(\dfrac{1}{Q}-\dfrac{2}{Q_1}\right)^2}{\left(\dfrac{\omega}{\Omega_c}-1\right)^2+\dfrac{1}{4}\left(\dfrac{1}{Q}\right)^2}.\end{aligned}\right. \tag{10,1}$$

This shows how the energies are distributed to the exits: As the resonator is of very high Q, only little energies are in general transmitted to the exits, most part of the energy is reflected back to the entrance. The energies are distributed to each exit in proportional to the reciprocal of the partial Q of this opening. When resonance occurs, the transmitted energies become exceptionally large. The energy transmitted to the N-th exit is at resonance amount to

$$|a_N{}^1|^2_{\text{res}}=\frac{4}{Q_1Q_N}\Big/\left(\frac{1}{Q}\right)^2\quad (N\neq 1) \tag{10,2}$$

and the energy reflected back to the entrance is, at resonance

$$|a_1{}^1|^2_{\text{res}}=\left(\frac{1}{Q}-\frac{2}{Q_1}\right)^2\Big/\left(\frac{1}{Q}\right)^2. \tag{10,3}$$

If a resonator is required which at resonance transmits all energy to the exit without reflecting back to the entrance, we need to construct it so that

$$\frac{1}{Q_1}=\frac{1}{Q_2}+\frac{1}{Q_3}+\cdots\cdots \tag{10,4}$$

is satisfied. In words: If it is required that all energy is to be transmitted to the exits at resonance without any reflection, the reciprocal of the partial Q of the entrance must be equal to the sum of the reciprocals of the partial Q's of the exits. This conclusion is the generalisation of the condition (7,21) in the paragraph 7.

§ 11. Energy stored in the resonator.

Our formula (9,27) or (9,28) serves also to determine the energy stored in the resonator. We suppose now that only the wave of the l-th mode is coming in through the N-th opening and no further incoming waves exist in any of the wave guides.

The energy stored in the resonator is given by

$$W=\frac{1}{4}\int_V\{\mu(\overset{*}{H}\cdot H)+\epsilon(\overset{*}{E}\cdot E)\}dV. \qquad (11,1)$$

If we use here the second theorem of § 3, we obtain

$$W=-\frac{i}{4}\lim_{\omega'\to\omega}\frac{1}{\omega-\omega'}\int_\Sigma\{[E\times\overset{*}{H}]_z+[\overset{*}{E'}\times H]_z\}d\Sigma$$

$$=\frac{i}{4}\Big[\frac{\partial}{\partial\omega'}\int_\Sigma\{[E\times\overset{*}{H'}]_z+[\overset{*}{E'}\times H]_z\}d\Sigma\Big]_{\omega'=\omega} \qquad (11,2)$$

We must here use for E and H the field due to the incoming wave of the l-th mode througn the N-th opening, i.e. $E^{N,l}$ and $H^{N,l}$ of (2,2), while for E' and H' also the fields due to the incoming wave of the l-th mode through the N-th opening but with a slightly differnt frequency ω'. Then we have

$$\int_\Sigma\{[E\times\overset{*}{H'}]_z+\overset{*}{E'}\times H]_z\}d\Sigma$$

$$=\int_{\Sigma_N}\{[F_l^-\times\overset{*}{G}{}_l'^-]_{z_N}+[\overset{*}{E}{}_l'^-\times G_l^-]_{z_N}\}d\Sigma$$

$$\times e^{-i(k_{Nl}-\overset{*}{k'}_{Nl})z_N}$$

$$+a_{N,l}^{N,l}\int_{\Sigma_N}\{[F^+\times\overset{*}{G}{}_l'^-]_z+[\overset{*}{F}{}_l'^-\times G_l^+]_z\}d\Sigma$$

$$\times e^{i(k_{Nl}+\overset{*}{k'}_{Nl})z_N}$$

$$+a'^{N,l}_{N,l}\int_{\Sigma_N}\{[F_l^-\times\overset{*}{G}{}_l'^+]_z+[\overset{*}{F}{}_l'^+\times C_l^-]_z\}d\Sigma$$

$$\times e^{-i(k_{Nl}+\overset{*}{k'}_{Nl})z_N}$$

$$+\sum_{N'}\sum_{l'}\overset{*}{a'}{}^{N',l'}_{N,l}a^{N,l}_{N',l'}\int_{\Sigma_{N'}}\{[F_{l'}^+\times\overset{*}{G'}{}_{l'}^+]_{z_{N'}}$$

$$+[\overset{*}{F'}{}_{l'}^+\times G_{l'}^+]_{z_{N'}}\}d\Sigma e^{i(k_{N'l'}-\overset{*}{k'}_{N'l'})z_{N'}} \qquad (11,3)$$

The dashed quantities, such as F', G', k' and $a'^{N,l}_{N',l'}$ are to be considered as belonging to the fields with the frequency ω'.

In differenciating (11,3) with respect to ω', we note that, if the frequency is very colse to the resonance frequency, and the resonator is of very high Q, the matrix elements $a'^{N,l}_{N',l'}$ change very rapidly if one varies ω', while other quantities F', G' and k' are slowly varying functions of ω'. We may thus neglect $\frac{\partial F'}{\partial\omega'}$, $\frac{\partial G'}{\partial\omega'}$ and $\frac{\partial k'}{\partial\omega'}$ as compared with $\partial a'^{N,l}_{N',l'}/\partial\omega'$.

In this way we obtain, after several calculations, using the formula (9,17) for $a'^{N,l}_{N',l'}$,

$$W=-i\omega\sum_{N'}\sum_{l'}\frac{\Omega_c\overset{*}{\beta}_{N,l}\beta_{N',l'}}{(\omega-\overset{*}{\omega}_0)^2}$$

$$\times\left\{\frac{\Omega_c\beta_{N',l'}\beta_{N,l}}{\omega-\omega_c}+\xi^{N,l}_{N',l'}\right\}. \qquad (11.4)$$

Using here (9,12) and (9,14) we obtain finally the simple formula

$$W=\frac{\omega/(\Omega_cQ_{N,l})}{\left(\frac{\omega}{\Omega_c}-1\right)^2+\frac{1}{4}\left(\frac{1}{Q}\right)^2}, \qquad (11,5)$$

which expresses the energy stored in the resonator as a function of ω.

We see from this formula that this energy is in general as small as of the order of $1/Q_{N,l}$, but it increases rapidly when ω approaches to the resonance frequency Ω_c, and at resonance we have

$$W_{\omega=\Omega_c}=\frac{4Q^2}{Q_{N,l}}. \qquad (11,6)$$

This energy is as large as of the order of Q. Thus the energy storage at resonance is proportional to the sharpness of the resonance.

The fields in the cavity become also very large when the resonance takes place. They are nearly of the order of magnitude:

$$\epsilon|E^{N,l}|,\quad \mu|H^{N,l}|\approx\sqrt{\frac{\omega/(\Omega_cQ_{N,l})}{\left(\frac{\omega}{\Omega_c}-1\right)^2+\frac{1}{4}\left(\frac{1}{Q}\right)^2}}, \qquad (11,7)$$

which at resonance amount to

$$\epsilon|E^{N,l}|_{\omega=\Omega_c},\quad \mu|H^{N,l}|_{\omega=\Omega_c}\approx\frac{2Q}{\sqrt{Q_{N,l}}}. \qquad (11,8)$$

The fact that a considerable part of the incident wave is transmitted to the exits notwithstanding the smallness of the coefficients of leakage becomes possible by such large storage of the fields in the cavity.

These results can be verified experimentally by detecting the wave in the cavity. Then, according to our theory, we should obtain a resonace curve of the form of Fig. 4, provided that the detection is of square law (Q of the resonator is, of course, assumed to be very large).

Since the definieion of the characteristic matrix involves explicitly only the amplitudes and the phases of the waves in the wave guides, it seems at first sight to be impossible that it would give any informations about the fields in the cavity. It is, however, not the case. The sharpness of the resonance is closely connected, as we have seen above, with the energy stored in the cavity. This relation corresponds to the so-called uncertainty relation in wave mechanics which is quite familiar to physisists.

This work was carried out in 1944 and reported in the August of the same year before the limited circle of the researchers who were engaged in the studyof ultra-short-wave circuits under the guidance of professor Sonoda. The author expresses his sincere thanks to professor Dr. S. Sonoda for his kind interest taken in this work. The author is also much indepted to Dr. T. Miyazima who has given many valuable helps and suggestions in the course of this work. Dr. Miyazima has also worked out various interesting applications and generalizations of the theory proposed here.

References.

(1) S. Tomonaga: J. Phys. Soc. Japan. **2** (1947).

(2) See, for instance, A. Wintner: Spektraltheorie d. unendlichen Matrizen (Leipzig, 1929) §§ 4, 9 and 10.

(3) G. Breit: Phys. Rev. **58** (1940), 1068.

The Influence of Temperature and Humidity on the Dielectric Constant and Piezo-electric Modulus of Rochelle Salt. I.

By Heiji KAWAI.

Kobayasi Institute of Physical Research, Kokubunji, Tokyo, Japan.

(Received June 11, 1947)

§ 1. Introduction.

Rochelle salt is well known for its conspicuous piezoelectric effect and its anomalous dielectric characters. Results hitherto obtained agree in the general features of variation of ε_a with temperature, but very various values have been measured by different methods. There is a great difference between ε_a's values measured with D. C. and A. C. electric field.1)2)3)4) Measured values with A. C. also differ greatly.5)6) Although it is said that the dielectric properties are not changed for audio-frequencies up to 5000 Hz,7)8) various values of ε_a were reported by many authors for audio-frequencies.3)8)9)10)11) Such a disagreemeut of ε_a's values is attributed to the effect of absorption current, residual current, relaxation time, etc. It is, however, impossible to explain why the values of ε_a for audio-frequencies measured by different observers are so different from each other. Those investigators have been endeavored to get reproducible results. Some causes of the disagreement of ε_a's values are due to unsuitable electrodes, ill sticking of electrodes, internal mechanical strain and impurities. H. Mueller8) says that a slight mechanical strain changes the character of the crystal. Therefore, very soft electrodes must be used. ε_a has different values when crystals have different electrodes.6)13) P. Kobeko and J. Kurtschatov2) used the saturated solution of Rochelle salt for the electrodes. E. Schwartz3) used the mercury electrode. E. Errera14) used tin foil electrodes which were stuck on crystals by Canada balsam. Graphite and metal foil electrodes were found equally suitable. The electrodes must cover the entire surface of the crystal. Otherwise uncovered portion becomes a source of constrianing forces for the inner part of the crystal. Although the above stated attentions are paid and those causes are removed, ε_a's values are not reproducible. This fact becomes a principal difficulty in the practical application of the crystal. With regard to d_{14}, a few measured values were reported.3) 4) 15) 16) 17) The measurements with dynamical method are particularly few and the reliable value of d_{14} is not yet reported.

The author has found that the humidity is essential to this non-reproducible values of ε_a and d_{14} are got at constant temperature and constant humidity. As other constants ε_b, ε_c, d_{25}.... are much smaller than ε_a, d_{14}3)4)8)10) and have no anomaly, the following experiments have been done using the a-cut crystal plate only.

§ 2. Measurement of ε_a.

(1) Samples.

Specimens were cut from a fine large crystal of 300~400 grams in weight by a band sawing machine and were finished by a lathe and other special tools. By such a mechanical finishing, the clean, flat and parallel surfaces could be easily obtained within the accuracy of 0.01 mm. Aluminium, copper or tin foil electrodes were avoided, as they corrode under hot and wet conditions. The electrode of saturated solution of Rochelle salt is not suitable for studying the effects of humidity. The mercury electrode also was not used, since it is hard to handle the surface well. The author used the silver foil electrode, as they do not corrode for many years in the atmosphere. It is very important that the electrodes should stick very closely to the entire surface of the crystal. In this experiment, no paste was used to stick the electrodes as is usually done. The surface of the crystal was first cleaned with benzene and alcohol, and then moistened with alcohol. The silver foil was placed on the surface, and pressed softly in order to stick so closely that it can not be splitted off after alcohol has evaporated. There is no substance between the electrode and the surface of the crystal, and there was nothing undesirable concerning the electrode,

(2) The circuit for measurement.

The capacity of the samples was measured by the bridge method at pure 1000 Hz A.C. from the tuning fork oscillator with a low pass filter.

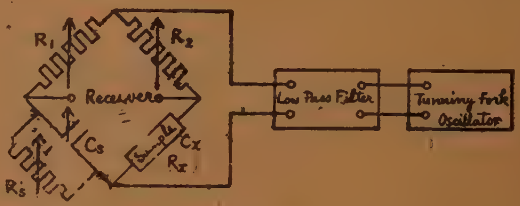

Fig. 1. The circuit for measurement of ε_a.
C_x: Capacity of sample.
R_x: Resistance of sample.

Fig. 1 shows the circuit used for the measurement. C_s is the standard air condenser (maximum about 2000 $\mu\mu$f) and R_1, R_2, C_s,

$$C_x = C_s R_1 / R_2 .$$

ε_a is calculated from

$$C_x = \varepsilon_a S / 4\pi d,$$

where S is the area of the electrodes and d is the thickness of the samples. The end correction is neglected here. As the capacity of the sample is constant at audio-frequencies near 1000 Hz and from some milli-volts to some volts per cm., the source of 1000 Hz and 0.8~1.0 volts per cm. was used in this measurement.

(3) The apparatus for temperature and humidity control.

The sample was put in the desiccator and H_2SO_4 of proper density was used for obtaining constant humidity. The relation between density given by E. M. Collins18) was used. The whole system was brought into a thermostat. The capacity of the lead wire from the thermostat to the bridge was measured previously and the observed values were corrected.

When the temperature and humidity were varied, it seemed to take a long time for the temperature and humidity in the desiccators to become constant, and a much longer time for ε_a to attain the corresponding value to the new condition, Therefore, values of ε_a were measured three times a day at intervals of 6 hours, and when any

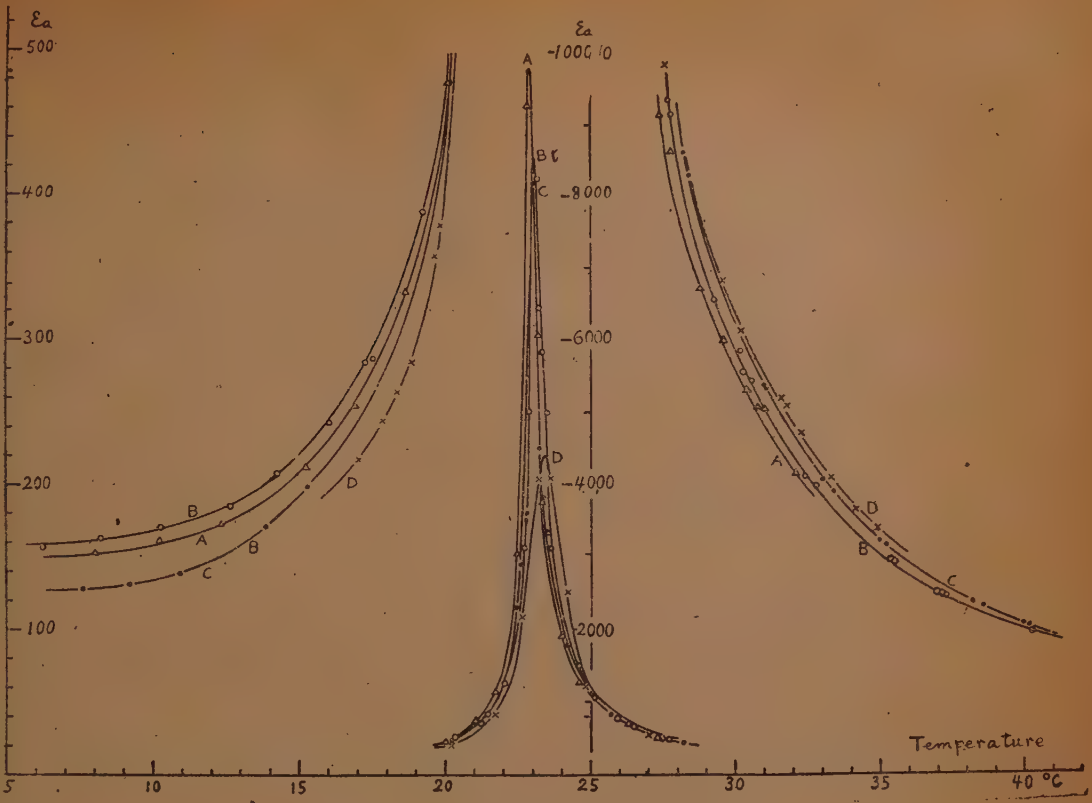

Fig. 2. ε_a, temperature and humidity.
A....Humidity: 80 %. Density of H_2SO_4 at 20°C: 1.188.
B....68 %. 1.232. *C*....53 %. 1.315. *D*....32 %. 1.411.

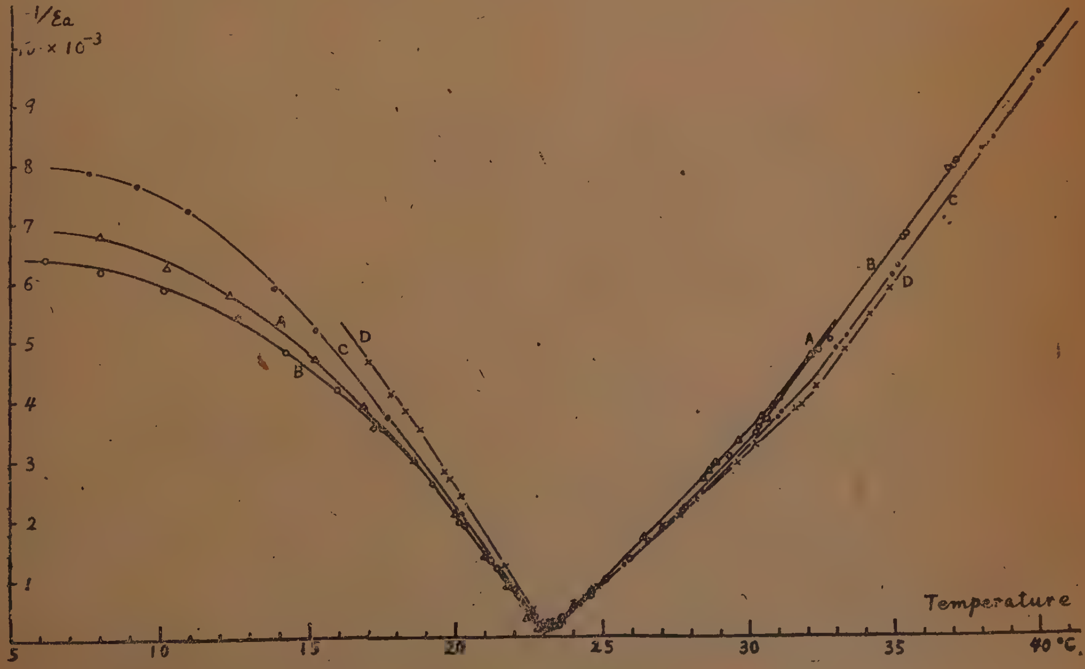

Fig. 3. I/ε_a, temperature and humidity.
A, B, C, D. .... ditto to Fig. 2.

successive three measurements yielded the same results, this value was adapted as ε_a.

(4) Results.

a) The temperature and humidity dependence.

The samples used were 10 pieces and 3~10 mm thick, about 20 mm wide and 40 mm long. Two samples were measured always at the same time. Whenever H_2SO_4 was changed, one of the two samples was interchanged with a new one. When humidity or temperature was changed, at first two samples had often different values, but always took the same value after a sufficiently long time. Namely ε_a becomes constant in a day or so at high humidity, or at low humidity below Curie point, and in several days at low humidity above the Curie point.

In Fig. 2 is shown the dependence of the values of ε_a upon the temperature and humidity. In Fig. 3 is shown the relation between the reciprocal values of ε_a and the temperature and humidity. The measurements at 30~40°C in Fig. 2, 3 were done in summer and that below 30°C in other seasons, and ε_a had the same value when it was measured after a year. This means that ε_a has a constant value in constant temperature and humidity. Above the Curie point the relation between $1/\varepsilon_a$ and temperature is linear and follow the Curie-Weiss' law very well. Namely,

$$1/\varepsilon_a = C(T-T_c).$$

In this equation T is the temperature, C and T_c are constants. These curves consist of two or three straight lines as H. Mueller[8)] has shown. C's are independent of humidity within experimental errors, namely they are

$$C_1 = 0.450\times10^{-3},\quad C_2 = 0.520\times10^{-3},$$

$$C_3 = 0.652\times10^{-3}.$$

The straight lines for C_2 are shorter in lower humidity and they vanish in the humidity lower than 32%. It seems that H. Mueller observed only in low humidity, for he said that straight lines of $1/\varepsilon_a - T$ curves consist of two parts. In Table I T_c, C_1, C_2, C_3 and their ranges for various humidity are shown.

Below the Curie point, the Curie-Weiss' law is not followed but it is noted that the effect of humidity is greater than above the Curie point and ε_a has a maximum value in 70~60% humidity. It seems that this state is characteristic of Rochelle salt and is probably related to the intersecting point of two humidity vs temperature curves,[19)] and that there are two different states i.e. deliquescent or efflorescent states each corresponding to higher or lower humidity than this state. The maximum values of ε_a at the Curie point and the values of the Curie temperature vary with humidity. I suppose that they are chief causes for the inconstancy of the Curie temperature. As ε_a varies very much with a little variation of temperature near the Curie point, determination of the Curie point is very difficult but there is tendency that the lower the humidity, the higher the Curie point and the smaller the maximum values of ε_a. Namely at 70% humidity the Curie point is 22.9°C and ε_a is about 10000, and at 30% humidity they are 23.5°C and about 4000 respectively.

b) Dimensions of samples.

It is probable that there are two kinds of the

Table I. Range of C_1, C_2, and C_3.

	Humidity %		32	53	68	80
C_1	T	°C	23.0	23.0	23.0	22.8
	Range	°C	*C.P.*—32.1	*C.P.*—29.7	*C.P.*—25.7	*C.P.*—25.6
C_2	T	°C		23.9	23.4	23.2
	Range	°C		29.7—31.9	25.7—30.6	25·6—30.8
C_3	T	°C	25.8	25.5	24.9	24.8
	Range	°C	32.1—	31.9—	30.6—	30.8—

effect of humidity, one is only on the surface, the other distributing uniformly within the crystal.

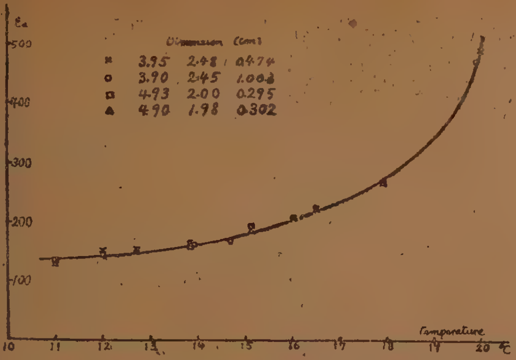

Fig. 4. Dimension of samples and ε_a.

When the effect of humidity is not uniform through the crystal, values of ε_a must be a function of dimensions, especially of thickness. In order to elucidate this point, crystals of various dimensions were measured. In Fig. 4 a part of the measurements is shown. The dimension shown in the third line of the table in Fig. 4 are the thickness in the direction of the a-axis. It is clear from Fig. 4 that values of ε_a are independent of demensions. Therefore, it may be considered that the effect of humidity is uniform through the crystal.

c) The effect of the method of preparation of the crystal.

It is often said that values of ε_a depend upon the methods of preparation. In order to test this view, the measurement was done about the crystals made from saturated solution in various conditions, namely in various temperature, various degrees of temperature lowering, various density, and other various methods of preparation. ε_a of those crystals showed quite the same behavior. In Fig. 5 a part of the results is shown. Consequently it may be concluded that the difference of the method of preparation has no effect on ε_a so long as they are made from saturated solution.

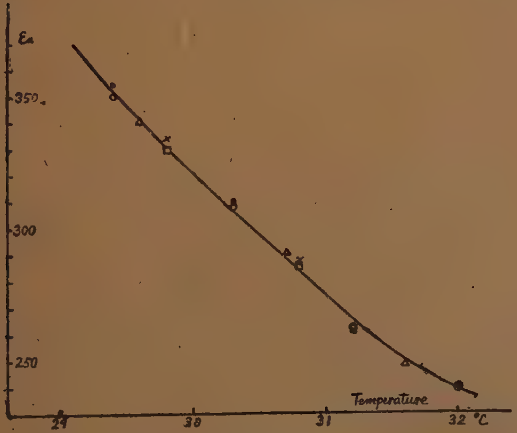

○, ●, ×, □, △.... samples manufactured by different methods.

Fig. 5. Method of manufacture and ε_a.

d) The time effect of the variation of humidity.

When the humidity is altered, ε_a remains the same for some days (about 10 days), and then afterwards quickly takes the value corresponding to the new condition. Such a phenomenon happens both above and below the Curie point. For example in Fig. 6 are shown the values of ε_a (represented by circles) which were measured when humidity was changed from 50% to 70%. Curve *A* in Fig. 6 corresponds to ε_a of 50% humidity and curve *B* to ε_a of 70% humidity. At first, points are on the curve *A* and after a considerably long time (10 days or more) they suddenly move onto the curve *B*. This means that crystals change from the stable state in the previous humidity to the stable state in the present humidity.

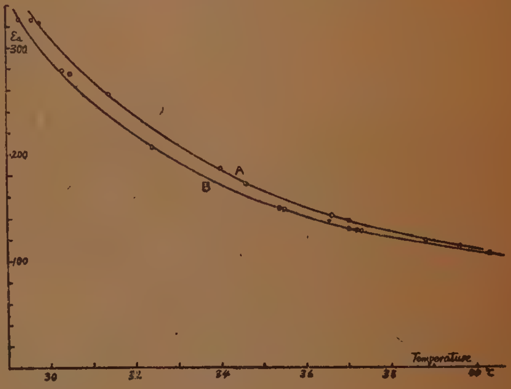

Fig. 6. Variation of humidity from 50% to 30%.

e) The effect of the variation of temperature.

ε_a does not follow imediately the change in temperature. Especially it is remarkable when temperature changes over the Curie point. In this case ε_a is in a quasi-stable state at first and go into another stable state after some days. In Fig. 7 an example is shown. At first ε_a is on the curve *A* (a quasi-stable state), and after a conside-

Table II. Weight change due to humidity variation.

Sample A		Sample B		Temperature	Difference of Weight of A, B. gr.
Weight gr.	Humidity	Weight gr.	Humidity		
9.1447	30 %	9.0828	70 %	13.5°C	0.0619
9.1444	30 %	9.0824	70 %	19.0°C	0.0620
9.1443	30 %	9.0824	70 %	22.2°C	0.0619
9.1445	30 %	9.0824	70 %	24.0°C	0.0621
9.1445	30 %	9.0827	70 %	28.0°C	0.0618
9.1443	30 %	9.0824	70 %	33.0°C	0.0619
9.1446	30 %	9.0825	70 %	19.0°C	0.0623
9.1447	70 %	9.0824	30 %	19.0°C	0.0623
9.1443	70 %	9.0831	30 %	13.5°C	0.0622
9.1444	70 %	9.0833	30 %	15.0°C	0.0621
9.1444	70 %	9.0833	30 %	24.5°C	0.0621
9.1444	70 %	9.0834	30 %	34.0°C	0.0620

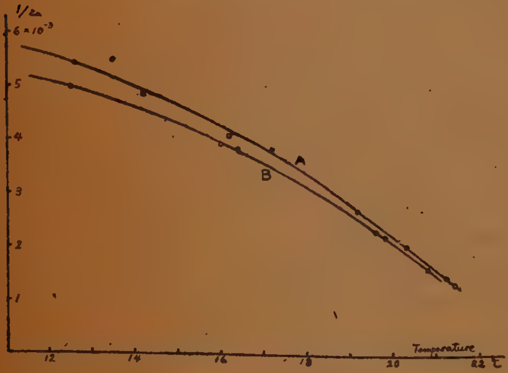

Fig. 7. Variation of temperature over the Curie point.

rable long time suddenly jumps to curve B (a stable state).

f) The water of crystallization.

In order to decide whether the amount of the water of crystallization is affected by the humidity, the weight of Rochelle salt crystal in various humidity was measured by chemical balance. Samples are kept in constant temperature and humidity and now and then they were taken out and balanced. Although the room of the chemical balance is not at constant temperature and humidity, it does not matter because the variation of ε_a does not soon follow the change of temperature and humidity during they are balanced. In Table II an example is shown; samples A and B were taken out and measured by chemical balance after having been kept in 30 % and 70 % humidity at constant temperature during 5~7 days. In the 1st and 2nd columns of the table II weight and humidity of sample A are shown, in the 3rd and 4th columns those of sample B, in the 5th column the temperature of the thermostat, and in the 6th column the difference of weight of A and B. It is known from this table that the difference of weight of A in 30 % and B in 70 % is very neary equal to the difference of weight A in 70 % and B in 30 %. The difference are nearly 0.1 mg. As surface conditions of samples are the same for A and B, the effects of surfaces is independent of the difference of weight between A and B. Therefore, the constancy of this difference shows that the difference between A's and B's weights in 30 % and 70 % is almost 0.1 mg, namely the weight of Rochelle salt crystal varies with humidity within 0.001 %.

(to be continued.)

References.

(1) J. Valasek: Phys. Rev. **24**, (1924), 560.
(2) P. Kobeko and J. Kurtschatov: ZS. f. Phys. **66**, (1930), 196.
(3) E. Schwartz: E. N. T. **9**, (1932), 481.
(4) H. Koerner: ZS. F. Phys. **103**, (1936), 170.
(5) J. G. Frayne: Phys. Rev. **21**, (1924), 348.
(6) A. Zeleny, and J. Valasek: Phys. Rev. **46**, (1934), 450.
(7) G. Busch: Helv. Phys. Acta, **6**, (1933), 315.
(8) H. Mueller: Phys. Rev. **47**, (1935), 175.
(9) W. Mason: Phys. Rev. **55**, (1939), 775.
(10) J. Habluetzel: Helv. Phys. Acta, **12**, (1939). 489.

(11) A. N. Holden and W. Mason: Phys. Rev. **57**, (1940), 54.
(12) R. D. Schulwas-Sorokin and M. V. Posnov: Phys. Rev, **47**, (1935), 166.
(13) H. Koerner: ZS. F. Phys. **94**, (1932), 801.
(14) E. Errera, Phys. ZS. **32**, (1931), 369.
(15) J. Valasek: Phys. Rev. **20**, (1922), 640.
(16) R. D. Schulwas-Sorokin: ZS. f. Phys. **73**, (1932), 700.
(17) O. Norgorden: Phys. Rev. **49**, (1936), 820; **50**, (1936), 782.
(18) E. M. Collins: J. Phys. Chem. **37**, (1933), 1191.
(19) H. Kawai: Nippon Sugaku-Buturigaku Kaisi (in Japanese), **17**, (1943), 270.
(20) H. Mueller: Phys. Rev. **57**, (1940), 829.
(21) H. Kawai: J. Phys. Soc. Jap. **2** (1949), 113.
(22) Y. Kakiuchi: J. Phys. Soc. Jap. **1** (1946), 51.

The Influence of Temperature and Humidity on the Dielectric Constant and Piezo-electric Modulus of Rochelle Salt. II.*

By Heiji KAWAI.

Kobayasi Institute of Physical Research, Kokubunji, Tokyo, Japan.

(Received June 11, 1947)

§ 3. Measurement of d_{14}.

(1) Samples.

The electrodes were stuck upon the surface of the crystal as in the case of the measurement of ε_a. The sample is 45° a-cut crystal, 3.42 cm in length, 0.500 cm in thickness, and 2.00 cm in width.

(2) The measuring apparatus.

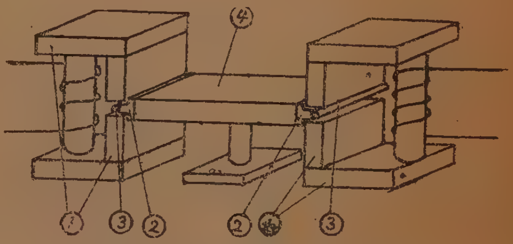

Fig. 8. The measuring apparatus.
(1): Pole pieces of magnets (2): Bases of bakelite. (3): Copper wire. (4): Samples.

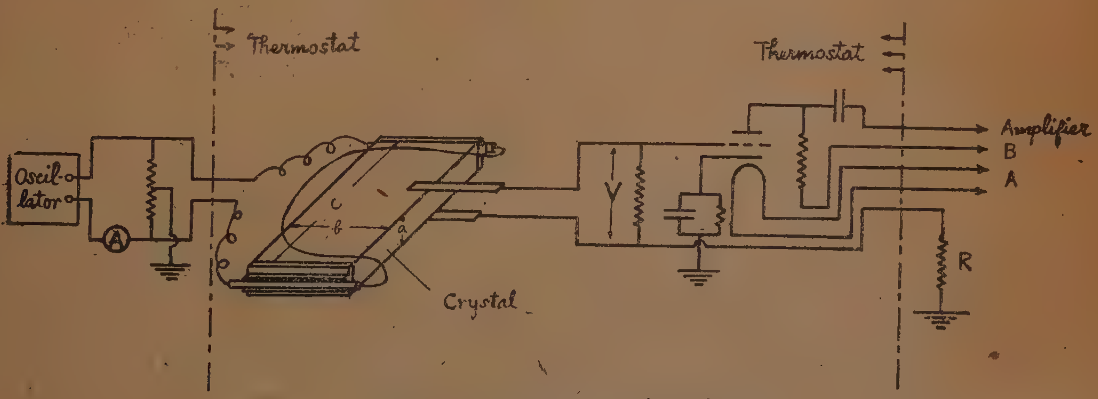

Fig. 9. The circuit diagram.

In Fig. 8 the outline of the apparatus is shown. The bases of bakelite were stuck to two ends of the sample (side of 2.00 cm) by shellac alcohol solution and in center of each base copper wires (diameter 0.5 mm) were stuck which were set in the magnetic field (width 2.00 cm). When 200∼2000 Hz A.C. flows through this copper wires the crystal is subjected to 200∼2000 Hz alternating forces. d_{14} is calculated from the voltage difference appearing between the electrodes as described below. This apparatus and head amplifier were put in a glass box which was kept in constant humidity and put in a thermostat.

---

* This paper is the continuation of the Paper I, Jour. Phys. Soc. Jap. 3, (1948). References should be referred to I.

Fig .9 shows the circuit diagram used for the measurement. The sensitivity of the amplifier was tested by giving proper voltage between both ends of the resistance R (0.490 ohms). The amplifier consists of three UY-6301 and UZ-42, and input voltage was about 0.01∼1 mV throughout this measurement. When the current through exciting coil was 400 mA D.C., the density of magnetic flux was 1.66 and 1.54×10^3. In the following calculation the mean value 1.60×10^3 was used.

(3) Calculation of d_{14}.

The piezoelectric modulus d_{14} was calculated from the electrode voltage of sample as follow.

If we denote the voltage output V, thickness of the sample (in Fig. 9) a, length of sides on which F is not applied b, length of sides on which F is applied c, piezoelectric modulus d_{14}, the circular freqnency ω, the load impedance between Z, electrodes and the total force applied F,

$$V=-\frac{ib}{2a}d_{14}\omega ZF\Big/\left(1+\frac{ibc}{4\pi a}\varepsilon_a\omega Z\right). \qquad (1)^{21,22)}$$

If Z is a pure resistance R,

$$V=\omega\frac{d_{14}b}{2a}FR\Big/\left(1+(R\omega C_f)^2\right)^{\frac{1}{2}} \qquad (2)$$

where $C_f=\varepsilon_a bc/4\pi a$ is the capacity of the crystal which can deform freely. If $(R\omega C_f)^2\ll1$, from (2)

$$V=\omega\frac{d_{14}b}{2a}FR\left\{1-\frac{1}{2}(R\omega C_f)^2\right\}$$

$$d_{14}\fallingdotseq\frac{2aV}{b\omega FR}\left\{1+\frac{1}{2}(R\omega C_f)^2\right\}. \qquad (3)$$

From (3) d_{14} is calculated using the measured value of V. C_f in correction term is calculated from values of ε_a which are known already. In this measurement frequency of 200∼2000 Hz was used. In practical calculation, the straight line representing the linear relation between V and d_{14} was plotted and from its gradient d_{14} was calculated.

(4) Results.

All values of d_{14} were measured after the sample being kept in a constant temperature for 24 hours, and often once more after further 24 hours, to test whether d_{14} varies or not. If the temperature variation is not so large, d_{14} becomes constant enough after 24 hours.

a) The effect of the variation of temperature upon d_{14}.

As this measurement is not so accurate compared with that of ε_a, small variations of d_{14} can not be detected experimentally, but it is concluded that d_{14} has similar characters to ε_a. This measurement was done only in low humidity, otherwise the large surface leakage made the measurement impossible. Variations of d_{14} with humidity were greater below the Curie point than above it. Above the Curie point d_{14} follows the Curie-Weiss' law very well, but no knick point was found; as d_{14} was measured only in low humidity and could not be measured at sufficiently high temperature. In Fig. 10 and 11, curves A show the relations between temperature and d_{14} at about 50 % (density of H_2SO_4 at 20°C: 1.316)

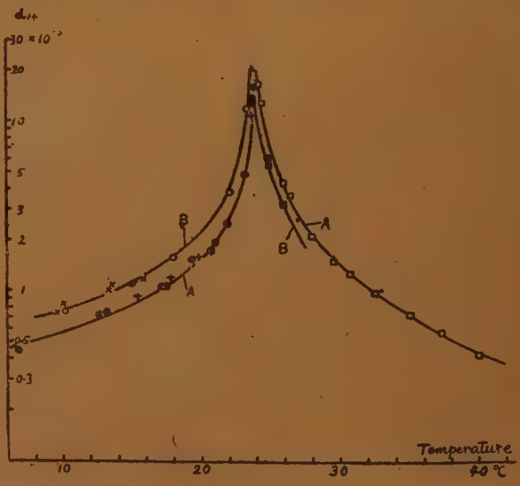

● → ⊙ → ⊡ → □ → × → + ...
sequence of measurements.

Fig. 10. d_{14} in 50 % humidity.

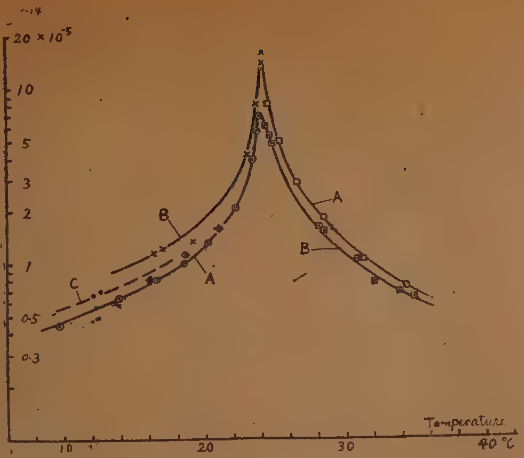

● → ○ → ⊙ → ⊡ → □ → × → + ...

sequence of measurements.

Fig. 11. d_{14} in 30 % humidity.

and about 30 % (density of H_2SO_4 at 20°C: 1.415) humidity. When temperature is changed across the Curie point, at first d_{14} lies on curve *B* in a quasi-stable state for considerable many days, and suddenly jumps to curve *A* in a stable state. This phenomenon is quite reproducible.

b) Variation of humidity.

When the humidity is varied, d_{14} persist the previous value for some days as in the case of ε_a. An example is shown in Fig. 11 which corresponds to the humidity change from 50 % to 30 %. In Fig. 11 a dotted line *C* is a value corresponding to 50 %, namely curve *A* in Fig. 10. When the humidity is changed from 50 % to 30 %, at first d_{14} lies upon the curve *C* and afterwards suddenly moves to the curve *A*. This means that the stable state of d_{14} changes to another stable state corresponding to another humidity suddenly after staying in a previous state for some days like ε_a.

§ 4. Sammaries.

From the results above described the following was concluded:

1) ε_a and d_{14} vary with humidity. When temperature and humidity are defined, ε_a and d_{14} have the definite values.

2) When the humidity is varied, values of ε_a and d_{14} change suddenly to values corresponding to humidity after a considerably long time.

3) When temperature varies across the Curie point, ε_a and d_{14} lie at first in a quasi-stable state for a considerably long time, and then afterward change suddenly to a stable state.

4) Humidity affects not only the surface of the crystal, but also the whole crystal uniformly.

5) Variation of weight of the crystal with humidity is at most within 0.001 %.

6) ε_a is independent of the methods of preparation of the crystal.

From these results it is considered that the change of humidity produces the change of the water of crystallization, but it is not able to be measured, as weight change is within 0.001 %, and ε_a and d_{14} of the crystal of Rochelle salt are so-called structure sensitive, and they change sensible by a little change in the amount of the water of crystallization.

Electron-Diffraction Study on Bahaviors of Metals Deposited on Crystal Surface. Part III. Effect of Centers of Crystallization on Crystal Growth in Metal Films.

By Mieko KUBO and Shizuo MIYAKE.

Kobayashi Institute of Physical Research, Kokubunji-machi, Tokyo.

(Read April 29, 1946; Received August 4, 1947)

§ 1 Introduction.

The crystal growth of the metal, deposited on the smooth crystal surface by the evaporation method in vacuum, is supposed to start in general at the centers of the crystallization, which are located on the surface from the beginning. These "natural centers" may be certain irregular points on the surface in some sense.

Now, in what manner will the crystal growth be influenced by the centers if they are artificially made? The present paper treats this problem. In it, an observation was made on the phenomena occurring when the succesive evaporation of two metals is committed, so that the metal firstly deposited acts as the artificial center of the crystal growth of the secondly deposited metal. Namely, the effect of the first deposited metal of a small quantity on the growth of the secondly deposited metal was studied. The experiment was made on various face-centred cubic metals, deposited on the fresh cloven surface (110) of zincblende.

§ 2 The Knowledge Obtained from Previous Experiments.

The crystal orientations and other characteristic behaviors of several face-centered cubic metals deposited on the zincblende surface were already subjected to experimentation by one of us.[1] Since the former result being necessary for understanding the present experiment, the main facts concerning the previous study will be briefly presented in this section.

A. *The types of the crystal orientation of the each deposited metal.* The results are shown in Table I.

B. *The effect of the polar axes of zincblende on the metallic crystal growth.* The atomic arrangement in the (110) surface of zincblende, which is shown in Fig. 1, is not symmetrical in respect to its [1$\bar{1}$0]-axis. And this asymmetry seems to possess two influences upon the Au-type orientation of the metals. First, the [110] axis of Au-type orientation above mentioned is in-

Table I

	Room temp.	100°C	200°C	300°C	400°C	500°C → Temperature
Au	No orientation	Au-type				
Cu	(310)-type		Au-type	Ni-type		
Ni	No orientation	Ni-type				

Au-type: $(110)_{\mathrm{ZnS}} \perp [110]_{\mathrm{metal}}$, $[110]_{\mathrm{ZnS}} // [110]_{\mathrm{metal}}$

Ni-type: $(110)_{\mathrm{ZnS}} \perp [111]_{\mathrm{metal}}$, $[001]_{\mathrm{ZnS}} // [110]_{\mathrm{metal}}$

(310)-type: $(110)_{\mathrm{ZnS}} \perp [310]_{\mathrm{metal}}$, $[110]_{\mathrm{ZnS}} // [001]_{\mathrm{metal}}$

fact not strictly perpendicular to (110) plane of ZnS. This is illustrated in Fig. 2-a for the case of Au, whereby the atomic arrangement of ZnS surface is assumed as Fig. 1. In the case of other

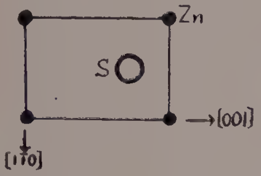

Fig. 1. Atomic arrangement of ZnS surface. [110] axis vertical to the paper and its direction is from the paper to readers.

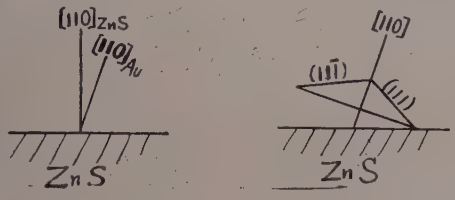

Fig. 2

a. The slant of [110]$_{Au}$ b. Twin plane (11$\bar{1}$)

metals, however, the slant of the axis takes place in the opposit direction. Secondly, the twin formation, which almost always takes place for the Au-type orientation if the film is not too thin, is also asymmetrical for the two possible twin planes, (111) and (11$\bar{1}$). Of these two planes, in general, the one which is lifted upwards as a result of the inclination of [110]-axis as mentioned above ((11$\bar{1}$)-plane in Fig. 2-b) is more effective for the twin formation.

In the following description, these properties will be called "characteristic" properties for each metal on zincblende.

§ 3 Experimental Procedure.

The successive evaporations of two different metals were performed by the device shown in Fig. 3, in which two tungsten filaments for the

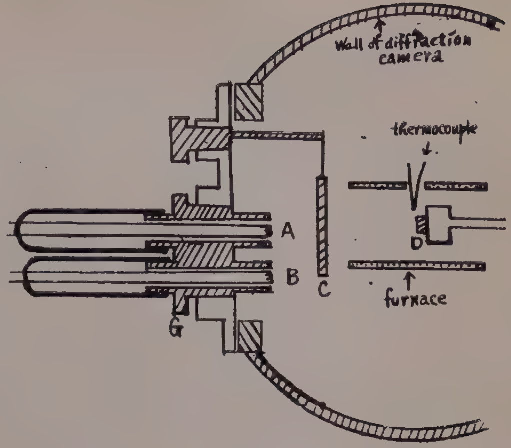

Fig. 3. Experimental Apparatus

The combinations of two metals examined in this experiment are shown in Table II.

Table II

Nuclei	2nd-evaporated metal
Au	Ni, Cu
Cu	Ni
Ni	Au, Cu

Table III-a.

Nuclei : Au	2nd-evaporated metal : Ni		
Orientation	Temperature	Orientation	Direction of orientation
Au-type	120°C	Au-type	+
	150°C	,,	+
	310°C	,,	—
	430°C	,,	—
	440°C	,,	—
	460°C	Au-type	—
	460°C	+Ni-type	—

+ : means that the direction of inclination of [110]-axis is the same as that of gold.
— : means that it is opposite to that of gold.

Table III-b.

Nuclei : Au	2nd-evaporated metal : Ni				
Orientation	Temp.	Mean thickness 10 Å		Mean thickness 100 Å	
		Orientation	Direction of inclination	Orientation	Direction of inclination
Au-type	160°C	Au-type+Ni-type		Au-type+Ni-type	—
	250°C	Au-type	—	Au-type	—
	270°C	Au-type+Ni-type	—	Au-type+Ni-type	—
	300°C	Au-type	—	Au-type	—
	340°C	Au-type+Ni-type			—
	470°C	Au-type		Au-type+Ni-type	—

evaporation of metals (A and B) can be placed alternatively in front of the crystal D, by rotating the ground joint G.

During this procedure, we observed continuously the changes of patterns on the fluolescent screen, and photographs were taken in important stages. The shutter C is to avoid the effect of volatile contamination.

§ 4 Experimental results.

a) The evaporation of Ni on Au-nuclei.

The combination of these two metals is interesting, because their characteristic crystal orientations are quite different from each other in the wide temperature range from 100°C to 500°C, as is shown in Table I.

The experiment was performed for two cases; (A) when the average thickness of Au is thick, and (B) when it is thin.

(A) The mean thickness: Au 30 Å, Ni 100 Å.

The result is shown in Table III-a.

(B) The mean thickness: Au 5 Å, Ni 100 Å.

In this case the evaporation of Ni was carried out in two steps. In the former step the evaporated quantity of metal attains to about 10 Å, whereas in the second step the exaporation of the whole quantity is finished. The photographs were taken in the both stages. The results are shown in Table III-a, and some examples of the patterns are shown in Fig. 4.

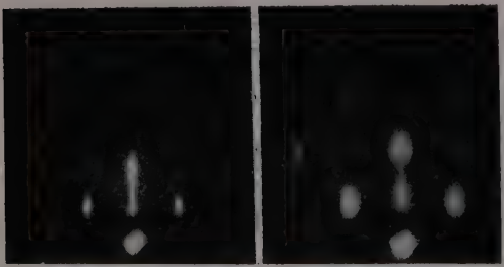

a. *Au-nuclei on ZnS surface made by evaporation.* Pattern is due to Au crystal with Au-type orientation.

b. *Ni crystal evaporated at 270°C on the Au-nuclei shown in Fig. a.* Pattern is due to Ni crystal with Au-type and Ni-type orientations.

Fig. 4 *The evaporatin of Ni on Au-nuclei.* Electron beam being parallel to [100] of ZnS.

We can deduce from these tables that when the surface of zincblende is wholly covered with the first evaporated metal Au, Ni simply succeeds the orientation of Au, but when the surface is only partially covered, that is, when the evaporated quantity of Au is small and the temperature of the base crystal is high, the crystal growth of Ni is apt to reveal its own characteristic properties, such as the appearance of the Ni-type orientation and the inclination of its [110]-axis in the opposite sense.

b) The evaporation of Au on Ni-nuclei.

The mean thickness: Ni~several Å, Au~50 Å

The result is shown in Table IV, and illustrated in Fig. 5.

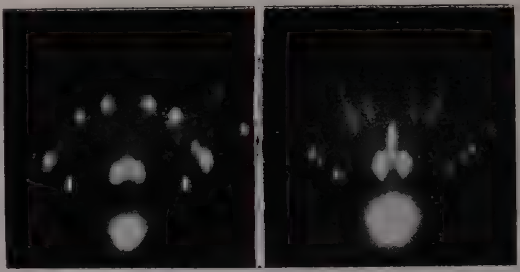

Fig. 5 *The evaporation of Au on Ni-nuclei.*

a. *Ni-nuclei made by evaporation on ZnS surface.* Pattern is due to crystal with Ni-type orientation.

b. *Au crystal evaporated at 420°C on the Ni-nuclei shown in Fig. a.* Pattern is due to Au crystal with Ni-type and Au-type, and Ni crystal with Ni-type orientations.

Electron beam being parallel to [100] of *ZnS*.

Table IV

Nuclei: Ni	2nd-evaporated metal: Au	
Orientation	Temp.	Orientation
Ni-type	220°C	Ni-type
	310°C	Ni-type
	310°C	Ni-type (Ni+Au)*
	410°C	Ni-type+Au-type
	420°C	Ni-type (Ni+Au)* +Au-type
	420°C	Ni-type

* This means that the patterns due to Ni and Au have Ni-type orientation.

In this case the crystal of the first evaporated metal, Ni, is supposed to take a dispersed distribution. Au, evaporated on it generally succeeded the orientation of the Ni-nuclei, but at high temperature the characteristic orientation of Au (Au-type) appeared.

c) The evaporation of Cu on Au-nuclei.

As was illustrated in Tabe I, the characteristic orientation of Cu is the same as that of Au only in the temperature range from 230°C to 330°C, but outside this temperature range they differ from each other. Experiment was made for the following two cases.

(A) The mean thickness: Au 20 Å, Cu 150 Å.

The result is shown in Table V-a.

Table V-a

Nuclei: Au	2nd-evaporated metal: Cu.		
Orientation	Temp.	Orientation	Direction of inclination
Au-type	150°C	Au-type	
	190°C		+
	280°C		+
	300°C		+
	430°C		—
	430°C		—

(B) The mean thickness: Au 5 Å, Cu 150 Å.

In this case, too. the evaporation of Cu was completed in two steps. The result is shown in Table V-b and in Fig. 6.

From Tables V-a and V-b, we can see that the second evaporated Cu succeeds the orientation of the first evaporated Au. But as in the case of Ni, the inclination of the Au-type orientation of Cu is opposite to Au when Au-nuclei are isolated on the surface from each other, i.e. when the temperature of the base is high and the quantity of Au is small.

Table V-b

Nuclei: Au	2nd-evaporated metal: Cu		
	Temp. °C	10 Å thick	150 Å thick
Au-type	150,230	Au-type + $AuCu_3$	Au-type
	230,280	}Au-type	
	320,350		
	420,430	Au-type + $AuCu_3$	
	430,450	Au-type	

d) Evaporation of Cu on Ni-nuclei.

As indicated in Table I, the characteristic orientation of Cu is the same as that of Ni at higher temperature (above 300°C), but below it, they are different. The observation was made for the mean thickness 50 Å and 10 Å for Ni, and 100~200 Å for Cu. In all cases, Cu succeeded the orientation of the Ni-nuclei.

e) Evaporation of Ni on Cu-nuclei. Also in this case, Ni always succeeded the orientation of Cu-nuclei.

§ 5 Discussions.

a) The effect of centers on the orientation of metal crystal. It is believed that the deposited metal layer covers wholly the base surface when

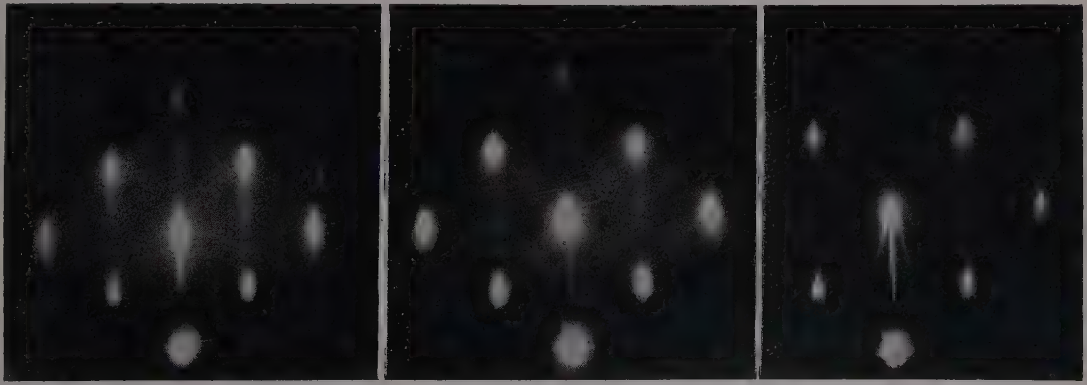

a. *Au-nuclei on ZnS surface made by evaporation.* Pattern is due to Au crystal with Au-type orientation.

b. *After the evaporation of a small quantity (10 Å thick) of Cu at 230°C on Au-nuclei shown in Fig. a.* Pattern is due to $AuCu_3$ having super structure.

c. *After the evaporation of whole quantity of Cu (150 Å thick) was finished.* Pattern is due to Cu crystal with Au-type orientation.

Fig. 6. *The evaporation of Cu on Au-nuclei.*
Electron beam being parallel to [100] of ZnS.

the evaporated quantity of metal is large and the base temperature is low. In such a case the crystal growth of the second evaporated metal may be completely determined by the "artificial centers". In fact, on such a condition, it was observed the second metal succeeds the orientation of the first evaporated metal (§4.1 (A), §4.3 (A) etc.). On the contrary, if the quantity of the first evaporated metal is small and the base temperature is higher, the artificial centers will take dispersive distribution, so that many bare portions may be remained on the base surface. In this case, the crystal growth of the second evaporated metal will be effected by both the artificial centers and the natural centers.

Which of these two sorts of the centers is more effective seems to be related to the combination of metals. Generally speaking, the effect of artificial centers seems to be more predominant than that of the natural ones when the two metals easily form an alloy, and when the second evaporated metal is considered to be mobile on the surface. Otherwise, the second evaporated metal is apt to manifest its own characteristic behavior by the effect of natural centers. The evaporation of Ni on Au-nuclei may be the example of the latter case. On the contrary, in the case of Au evaporated on Ni-nuclei, the influence of artificial centers seems more effective, probably on account of the mobilness of the Au atoms on the surface. Similarly, in the evaporation of Cu on Ni, Ni on Cu and Cu on Au, the effect of the artificial centers seems to be the determining factor.

b) *The starting position of crystal growth.* Next we consider the question from what portion of the nucleus the crystal growth will begin to take place. As shown in Table III-a, Ni evaporated on an Au-type Au nucleus takes the Au-type orientation, and in it, its [110] axis shows an inclination, which increases with its growth. As known from the description in §2, this inclination is due to the direct influence of the zincblende surface. Accordingly, the growth of Ni-crystal takes place under the effects of two origins, the effect of the artificial nuclei and the effect of the zincblende surface. The only place where such condition can be realized is the foot of the crystal nucleus, for example the point A in Fig. 7-a. Therefore, it is supposed that the vaporized metal atoms, after wandering on the surface, finally arrive at the foot of a nucleus, and it is from here the crystal growth commences. Thus, in general the crystal growth of metal is considered to take place by continuing the preexisting bud at its foot.

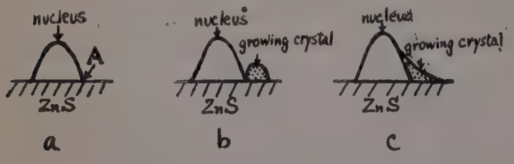

Fig. 7. The manner of crystal growth.

The similar situation is observed also for the twin formation. In the Au-type orientation there occurs twinning on the (III) or (III) plane. As previously mentioned, the habit of twinning is related to the asymmetric arrangement of atoms of zincblende surface, so that it is clear that the twinning in metal crystal occurs under the continuous interaction with the base crystals during its development. Accordingly, the twin formation is always evoked at the foot of the crystal bud which is in growth.

c) *The two manners of the crystal growth.* There are two manners of the crystal growth.

(1) The one is the case of Au evaporated on Ni-nuclei. As is shown in the Table IV, the diffraction patterns from Ni-nuclei and that of Au, both having the Ni-type orientation are coexistent even when the thickness of Au is rather thick (~50Å). In order to reveal such a diffraction pattern, the Au crystal and the Ni-nuclei should not mix or cover each other but being situated independently, touching only at a base point, from where the crystal growth developed. This is illustrated shematically in Fig. 7-b. One of the reasons of such a behavior may be the fact that the relating two metals are difficult to make solid solutions.

(2) In the other cases, only the diffraction spots of the second evaporated metals appear on the pattern, so that the second evaporated metal crystals are supposed to be covering the nuclei as shown in Fig. 7-c. This will happen when the relating two metals are easy to make solid solutions.

d) Solid solution of Au-Cu. When a small quantity of copper (about several Å thick) is evaporated on the nuclei of gold, sometimes there appear patterns which are considered to be due to the solid solution of gold and copper. These patterns are of face-centered cubic lattices, and we observe them at 150°C, 230°C and 420°C (twice), the lattice constants being 3.76Å, 3.73Å, 3.72Å and 3.73Å, respectively. As these lattice constants are very close to that of the super-lattice structure $AuCu_3$ (3.75Å)(2), we can regard the here observed solid solution to have this structure. In fact, sometimes the spots due to the super-lattice reflections could be found. (Fig. 6-b).

§ 6 Summary.

The effect of "artificial centers" upon the crystal growth of metal films was studied, by observing the phenomena which take place when the evaporation of two metals is commited successivly on the zincblende surface in vacuum of the electron diffraction camera. The combinations of various face-centered cubic metals were studied. We can obtain some conclusions about the manner of crystal growth. When Cu was evaporated on Au centers, sometimes the formation of the solid solution of Au-Cu was found.

We are indebted to the Ministry of Education for the research grant.

References.

(1) S. Miyake: (Unpublished yet.)
(2) M. Le Blanc u. G. Wehner: Ann. de phys. **14** (1932) 487.

Statistical Theory of Linear Polymers. IV. Effects of Hinderance for Internal Rotation.

By Ryogo Kubo.
Physical Institute, Faculty of Science, University of Tokyo.

(Received August 5, 1947).

Introduction.

In the preceding papers we gave the theories of intramolecular statistics of linear polymers, rubber elasticity and elastic double refraction,1)2)3) in which the hinderance for the internal rotation of constituent submolecules has been taken into account only in some approximation. Thus a rigorous treatment of the mentioned properties may be of some interest because it will predict the temperature effects of various physical properties which are caused by the existence of the hinderance for internal rotation.

§ 1. Fundamental Equations.

We take a long linear polymer composed of a number of submolecules, the relative orientation of which is determined by some hindering potential. The van der Waals correction due to the finite volume occupied by each submolecule is neglected here as in the paper I. A finite number of skeletal bonds are taken as our unit of the chain which are all of similar form and are sufficient to allow us to take into account only the mutual interaction energy between two neighboring units. For the sake of simplicity, the units are assumed here to be similar with respect to each other, being of a definite form, for example, of a planar figure formed by two neighbouring bonds which makes a definite angle in the case of paraffine-like long chain.

As was explained in I, all the kinetic terms are assumed to be separated off in the partition function, so that we need only to construct it in the configuration space. The configuration of a unit of the chain is specified by a rotation R which is defined as the operation to bring it from a standard position to a rotated position in the space. It may be represented by the transformation between two coordinate systems $S_0(X, Y, Z)$ and $S(x, y, z)$, the former being fixed in the space and the latter to the unit molecule. Thus the configuration of the chain is defined by a set of rotations $R_1, R_2, \cdots R_n$. The configurational energy E is the sum of the hindering potential energy terms each of which is a function of the relative rotation to bring a unit to the orientation assumed by its neighboring unit. Thus we get

$$E(R_1, R_2, \cdots R_n) = \sum_{j=2}^{n} \varepsilon(R_j R_{j-1}^{-1}). \tag{1}$$

The partition function and the free energy of the chain with the specified length r can be obtained by the method described in I. When the number of units n is large, the asymptotic behaviour is determined by the following characteristic equation (cf. Eq. (7), I)

$$\lambda\phi(s, R') = \exp\{sa(R')\} \times \int \exp\{-\varepsilon(R'R''^{-1})/kT\}\phi(s, R'')dR'', \tag{2}$$

where a is the skeletal length vector of the unit whose components are functions of R in the coordinate system S_0 and s is a selecting vector fixed in S_0. The vector s corresponds to the tensile force of the chain.

The free energy $F(r)$ and the orientation-distribution of the constituent unit are given by the largest eigenvalue λ and by the eigenfunction belonging to λ (cf. Eq. (13) I, Eq. (4) III) namely

$$F(r) = kT(sr - n\log\lambda(s)). \tag{3}$$

and

$$\Phi(r, R) = e^{-sa(R)}\{\phi(s, R)\}^2 \Big/ \int e^{-sa}\{\phi(s, R)\}^2 dR, \tag{4}$$

the parameter s being defined as a function of r by the equation

$$n\frac{d\log\lambda}{ds} = r. \tag{5}$$

For the sake of convenience we shall define the operator $\mathfrak{K}$ by

$$\mathfrak{K}\phi = \int K(R'R''^{-1})\phi(R'')dR'', \tag{6}$$

where $K(R'R''^{-1})$ stands for $\exp\{-\varepsilon(R'R''^{-1})/kT\}$. Then Eq. (2) can be written simply in the form

$$\lambda\phi = e^{sa}\mathfrak{K}\phi = \mathfrak{K}_s\phi, \text{ and } e^{sa}\mathfrak{K} = \mathfrak{K}_s, \tag{7}$$

In later discussions we shall normalize the correlation function K as follows

$$\int K(R)dR = 1,$$

$$K(R) = \exp\{-\varepsilon(R)/kT\} \Big/ \int \exp\{-\varepsilon/kT\}dR \tag{8}$$

Then the eigenvalues of Eq. (7) are multiplied by a factor depending only on temperature.

The eigenvalue method is suitable for the discussions of the asymptotic properties. An alternative method shown in the following is useful for obtaining the average values of powers of r.

The generating function $Q_n(s, R)$ or the Laplace-transform of the relative probability $Z_n(\mathbf{r}, R)$ (cf. Eqs. (2) (5) and (6) I) satisfies the recurrence formula

$$Q_n(s, R') = \mathfrak{K}_s Q_{n-1}(s, R''). \tag{9}$$

Now we introduce the generating function for n, i. e.

$$U = \sum_{n=1}^{\infty} Q(s, R)\zeta^{-n}, \tag{10}$$

which can be readily seen to satisfy the inhomogenuous equation

$$U = \zeta^{-1}Q_1 + \zeta^{-1}\mathfrak{K}_s U, \tag{11}$$

$Q_1(R)$ being the Laplace-transform of the initial distribution of the end unit, which becomes equal to $\exp(sa)$ when there is no restriction in the orientation of the end. The generating function $Q_n(s)$ is obtained by the following contour integral

$$Q_n(s) = \frac{1}{2\pi i}\oint\int U\zeta^{n-1}d\zeta dR. \tag{12}$$

Eqs. (2) or (7) and (11) will be solved in section 2 in the forms expanded in powers of s, in which

$$\lambda = \lambda_0 + \lambda_2 s^2 + \lambda_4 s^4 + \cdots, \tag{13}$$

and

$$U(s, R) = U_0 + sU_1 + s^2 U_2 + \cdots. \tag{14}$$

The average values of powers of r are related to the expansion coefficients in (12) and (13) in the following way (cf. Eqs. (18) and (21), I.)

$$<r^2> = 6n\lambda_2/\lambda_0 = \frac{6}{2\pi i}\oint\int U_2(R,\zeta)\zeta^{n-1}d\zeta dR. \quad \text{etc.} \qquad (15)$$

Sometimes we are interested in the averages of certain physical quantity which is a sum of functions depending only on the orientation of each constituent unit. For example, in the case of the theory of double refraction we need the average of polarizability given by the equation

$$<\alpha> = \int\Phi(r,R)\alpha(R)dR. \qquad (16)$$

which formula has been used in III. Here we give another way of its proof as follows.

Let the polarizability tensor and the external electric force be α and f respectively. Then the polarization energy is given by $(f\alpha f)/2$, and the characteristic equation becomes

$$\lambda\psi_\lambda = \exp\left\{-\frac{(f\alpha f)}{2kT}\right\}\mathfrak{R}_s\psi_\lambda \qquad (17)$$

instead of (7). Eq. (3) is valid for the free energy $F(r, f)$. Hence we have for the dipole moment per each unit

$$<\alpha f> = -kT\partial\log\lambda/\partial f.$$

Differentiating Eq. (17) with respect to f_x and assuming f to be small, we get

$$\frac{\partial\lambda}{\partial f_x}+\lambda\frac{\partial\psi_\lambda}{\partial f_x} = -\frac{(\alpha f)_x}{kT}\mathfrak{R}_s\psi_\lambda+\mathfrak{R}_s\frac{\partial\psi_\lambda}{\partial f_x}.$$

By the orthogonality relation

$$\int\exp(-sa)\psi_\lambda\psi_{\lambda'}dR = 0 \quad \text{for} \quad \lambda \neq \lambda',$$

we can easily show that

$$<\alpha f> = \int\Phi(r,R)\alpha(R)fdR,$$

where λ denotes the largest eigenvalue of Eq. (17) (cf. Eq. (4)).

§ 2. Expansion Formulae.

We shall give here solution of Eqs. (7) and (11). Expanding the power series of s, Eq. (7) becomes

$$\lambda\psi = \left\{1+sa+\frac{1}{2}(sa)^2+\cdots\right\}\mathfrak{R}\psi. \qquad (18)$$

We seek for the largest eigenvalue λ and its eigenfunction ψ which become equal to 1 and a constant respectively as s tends to zero, provided that the correlation function K is normalized by Eq. (8). For brevity we shall introduce the projection operators

$$\mathfrak{R}_0\psi(R) = \int\psi(R)dR. \qquad (19)$$

and

$$(1-\mathfrak{R}_0)\psi(R) = \psi(R)-\int\psi(R)dR. \qquad (20)$$

The perturbation method to solve (18) gives us

$$\lambda = 1+\frac{1}{2}\mathfrak{R}_0\left\{(sa)\frac{1+\mathfrak{R}}{1-\mathfrak{R}}(sa)\right\}+\cdots \qquad (21)$$

$$\psi = \psi_0\Big[1+\frac{1}{1-\mathfrak{R}}(sa)$$
$$+\frac{1}{2(1-\mathfrak{R})}(1-\mathfrak{R}_0)(sa)\frac{1+\mathfrak{R}}{1-\mathfrak{R}}(sa)+\cdots\Big], \qquad (22)$$

and the orientation probability

$$\Phi = \exp\{-(sa)\}\{\psi(s,R)\}^2$$
$$= 1+\frac{1+\mathfrak{R}}{1-\mathfrak{R}}(sa)+\frac{1}{2}\frac{1+\mathfrak{R}}{1-\mathfrak{R}}(1-\mathfrak{R}_0)(sa)\frac{1+\mathfrak{R}}{1-\mathfrak{R}}(sa)$$
$$+\frac{\mathfrak{R}(sa)}{1-\mathfrak{R}}\times\frac{sa}{1-\mathfrak{R}}+\cdots \qquad (23)$$

In order to solve Eq. (11) we may proceed in a similar way. Expanding $\exp(sa)$ and U, it will easily be proved that

$$U = \Big[1+\frac{\zeta}{\zeta-\mathfrak{R}}(sa)$$
$$+\frac{1}{2}\frac{\zeta}{\zeta-\mathfrak{R}}(sa)\frac{\zeta+\mathfrak{R}}{\zeta-\mathfrak{R}}(sa)+\cdots\Big]\frac{1}{\zeta-\mathfrak{R}} \qquad (24)$$

§ 3. A Group-theoretical Method.

In the paper I, we have solved the fundamental equation (2) by expanding ψ and K in spherical harmonics. Now we need to take an orthogonal set of functions involving at least three variables defining rotations in three dimensional space, which set is provided by the irreducible representations D_J of the continuous rotational group. The elements of unitary representation is known to satisfy the orthogonality relation

$$\int D_{Jik}(R)D_{I'k'i'}(R^{-1})dR = N_J\delta_{JJ'}\delta_{ii'}\delta_{kk'},$$
$$D_J(R^{-1}) = D_J^{+}(R) \qquad (25)$$

as seen in the representation theory of the rotational group.

We shall expand K and ϕ in series of D_J as

$$K(R) = \sum_J \frac{1}{N_J} \text{trace}\, K_J{}^+ D_J(R) \tag{26}$$

$$\phi(R) = \sum \text{trace}\, A_J D_J(R), \tag{27}$$

where D_J, K_J and A_J are matrices with dimension of $2J+1$, and $K_J{}^+$ is the average of $D_J{}^+(R)$ with respect to the correlation function $K(R)$, i. e.

$$K_J{}^+ = \int K(R) D_J{}^+(R) dR \tag{28}$$

With the use of the orthogonality relation (25) then we get

$$\mathfrak{K}\phi = \sum \text{trace}\, (A^J K_J{}^+ D_J) \tag{29}$$

and

$$f(\mathfrak{K})\phi = \sum_J \text{trace}\, (A_J f(K_J{}^+) D_J) \tag{30}$$

for any function f.

The iteration of $\mathfrak{K}$ or the correlation between the 1st and $(n+1)$—th units is shown to be

$$\mathfrak{K}^n = \sum \frac{1}{N_J} \text{trace}\, (K_J{}^+)^n D_J(R_{n+1}) D_J(R_1{}^{-1}). \tag{31}$$

In such method of treatment we often meet with integrals of the type

$$(\varphi, \mathfrak{M}\phi) = \iint \varphi(R') M(R' R''^{-1}) \phi(R'') dR' dR''$$

$$= \sum_J \text{trace}\, (A_J M_J{}^+ B_J{}^+), \tag{32}$$

where the matrices are given by the expansion coefficients, that is,

$$\begin{aligned} \phi(R) &= \sum \text{trace}\, A_J D_J(R) \\ \varphi(R) &= \sum \text{trace}\, B_J{}^+ D_J(R^{-1}) \\ M(R) &= \sum \text{trace}\, M_J{}^+ D_J(R) \end{aligned} \tag{33}$$

§ 4. Representations D_1 and D_2.

Here we choose real representations. Then D_1 is nothing but the transformation matrix between two coodinate systems S and S_0 which is given in the Table I, where θ, ϕ and ψ are the Eulerian angles.

We denote each of the elements of D_1 simply by the expression of (ik) $(i, k = 1, 2, 3)$. The representation D_1 is generated in the space of three-dimensional vectors. Representations of higher order D_J may of course be constructed from the products of D_1 by the recurrence formula

$$D_J \times D_{J'} = D_{|J+J'|} + D_{|J+J'-1|} + \cdots + D_{|J-J'|}. \tag{34}$$

As the base of the representation D_J we may choose the set of spherical harmonics of J-th order which contains $2J+1$ orthogonal functions.

Thus, the base of the irreducible representation of $D_1 \times D_1$ will be functions

$$\begin{aligned} &\xi_0 = x_1y_1+x_2y_2+x_3y_3, \quad \xi_1 = x_3y_3 - \frac{1}{2}(x_1y_1+x_2y_2) \\ &\xi_2 = \frac{\sqrt{3}}{2}(x_1y_1-x_2y_2), \quad \xi_3 = \frac{\sqrt{3}}{2}(x_2y_3+x_3y_2), \\ &\xi_4 = \frac{\sqrt{3}}{2}(x_3y_1+x_1y_3), \quad \xi_5 = \frac{\sqrt{3}}{2}(x_1y_2+x_2y_1), \\ &\xi_6 = x_2y_3-x_3y_2, \quad \xi_7 = x_3y_1-x_1y_3, \quad \xi_8 = x_1y_2-x_2y_1 \end{aligned} \tag{35}$$

or

$$\xi_\rho = \sum T_{\rho ij} x_i y_j, \tag{36}$$

where the roman and greek indices refer to the bases of the representation $D_1 \times D_1$ and its reduced representation respectively. The representation $D_1 \times D_1$ is reduced by the transformation (36) to

$$T(D_1 \times D_1) T^{-1} = D_0 + D_2 + D_1 = \sum D \tag{37}$$

or for D_2 we have

$$(D_2)_{\rho\sigma} = \sum_{ijkl} T_{\rho ij} (ik)(jl) T^{-1}_{kl\sigma} \quad \rho, \sigma = 1, 2, \cdots 5. \tag{38}$$

Table I.

	X	Y	Z
x	$\cos\phi\cos\theta\cos\psi - \sin\phi\sin\psi$	$\sin\phi\cos\theta\cos\psi + \cos\phi\sin\psi$	$-\sin\theta\cos\psi$
y	$-\cos\phi\cos\theta\sin\psi - \sin\phi\cos\psi$	$-\sin\phi\cos\theta\sin\psi + \cos\phi\cos\psi$	$\sin\theta\sin\psi$
z	$\cos\phi\sin\theta$	$\sin\phi\sin\theta$	$\cos\theta$

Table II.

$T_{\rho,ik}$

(ik) / ρ	(11)	(22)	(33)	(23)	(31)	(12)	(32)	(13)	(21)
0	1	1	1						
1	$-\frac{1}{2}$	$-\frac{1}{2}$	1						
2	$\frac{\sqrt{3}}{2}$	$\frac{\sqrt{3}}{2}$	0						
3				$\frac{\sqrt{3}}{2}$			$\frac{\sqrt{2}}{2}$		
4					$\frac{\sqrt{3}}{2}$			$\frac{\sqrt{3}}{2}$	
5						$\frac{\sqrt{3}}{2}$			$\frac{\sqrt{3}}{2}$
6				1			1		
7					1			1	
8						1			1

$T^{-1}_{ik,\rho}$

ρ / (ik)	0	1	2	3	4	5	6	7	8
(11)	$\frac{1}{3}$	$-\frac{1}{3}$	$\frac{1}{\sqrt{3}}$						
(22)	$\frac{1}{3}$	$-\frac{1}{3}$	$-\frac{1}{\sqrt{3}}$						
(33)	$\frac{1}{3}$	$\frac{2}{3}$							
(23)				$\frac{1}{\sqrt{8}}$			$\frac{1}{2}$		
(31)					$\frac{1}{\sqrt{3}}$			$\frac{1}{2}$	
(12)						$\frac{1}{\sqrt{3}}$			$\frac{1}{2}$
(32)				$\frac{1}{\sqrt{3}}$			$\frac{1}{2}$		
(13)					$\frac{1}{\sqrt{3}}$			$\frac{1}{2}$	
(21)						$\frac{1}{\sqrt{3}}$			$\frac{1}{2}$

The transformation matrices T and T^{-1} are given in the Table II.

The correlation matrices K_1 and K_2 are

$$K_1 = \int K(R)D_1(R)dR \tag{39}$$

and

$$K_2 = T\left(\int K(R)(D_1 \times D_1)dR\right)T^{-1} = T\langle D_1 \times D_1\rangle T^{-1} \tag{40}$$

that is, K_1 is the average of the transformation matrix of two coordinate systems S' and S'' fixed to neighboring units.

In Eq. (2) and other expressions, $\boldsymbol{a}$ is a vector fixed to the system S with definite components (a_1, a_2, a_3) so that its components in S_0 are $\sum_i a_i$ (ik). The function $(\boldsymbol{s}\boldsymbol{a})$, therefore, takes the form

$$(\boldsymbol{s}\boldsymbol{a}) = \sum_{ik} s_k a_i (id) = \operatorname{trace}(\boldsymbol{s}\times\boldsymbol{a})D_1, \tag{41}$$

where $(\boldsymbol{s}\times\boldsymbol{a})$ is the direct product of vectors $\boldsymbol{s}$ and $\boldsymbol{a}$, being the tensor of second rank. When an operator $f(\mathfrak{K})$ is operated on $(\boldsymbol{s}\boldsymbol{a})$ it may be easily seen that

$$\begin{aligned} f(\mathfrak{K})(\boldsymbol{s}\boldsymbol{a}) &= \operatorname{trace}(\boldsymbol{s}\times\boldsymbol{a})f(K_1{}^{+})D_1 \\ &= \operatorname{trace}(\boldsymbol{s}\times f(K_1)\boldsymbol{a})D_1. \end{aligned} \tag{42}$$

We can show also that

$$\mathfrak{K}_0(\boldsymbol{s}\boldsymbol{a})(\boldsymbol{s}\boldsymbol{b}) = \int(\boldsymbol{s}\boldsymbol{a})(\boldsymbol{s}\boldsymbol{b})dR = \frac{1}{3}\boldsymbol{s}^2(\boldsymbol{a}\boldsymbol{b}) \tag{43}$$

Since functions of the type $(1-\mathfrak{K}_0)(\boldsymbol{s}\boldsymbol{a})(\boldsymbol{s}\boldsymbol{b})$ belong to D_2, so the expansion in question may be calculated as follows;

$$\begin{aligned} (\boldsymbol{s}\boldsymbol{a})(\boldsymbol{s}\boldsymbol{b}) &= \sum_{ikjl} s_k a_i (ik) s_l b_j (jl) \\ &= \sum s_k s_l a_i b_j T_{ij\rho}{}^{-1}(\textstyle\sum D)_{\rho\sigma} T_{\sigma kl} \\ &= \sum (\boldsymbol{s}\times\boldsymbol{s})_\sigma C_\rho (\boldsymbol{a}\times\boldsymbol{b})_\rho (\textstyle\sum D)_{\rho\sigma}, \end{aligned} \tag{44}$$

where

$$C_0 = \frac{1}{3}, \quad C_1 = \cdots\cdots = C_5 = \frac{2}{3}, \quad C_6 = \cdots\cdots C_8 = 2, \tag{45}$$

and $(\boldsymbol{s}\times\boldsymbol{s})_\sigma$ and $(\boldsymbol{a}\times\boldsymbol{b})_\rho$ are constructed from its constituent vectors by using the basic functions of (35). Finally we get

$$(1-\mathfrak{K}_0)(\boldsymbol{s}\boldsymbol{a})(\boldsymbol{s}\boldsymbol{b}) = \frac{2}{3}\operatorname{trace}\{(\boldsymbol{s}\times\boldsymbol{s})_{(2)}\times(\boldsymbol{a}\times\boldsymbol{b})_{(2)})D_2\}, \tag{46}$$

where the suffix (2) means the components of the direct products which belong to the base of the irreducible representation D_2 and the meaning of the direct product in the bracket is seen clearly from Eq. (44).

§ 5. General Expression for the Statistical Quantsties.

Now the explicit formulae for various statistical quantities can easily be derived by the use of the results mentioned in the foregoing paragraphs. By Eqs. (15), (21), (43) we get at once

$$<r_n^2> = n\left(\boldsymbol{a}\frac{1+K_1}{1-K_1}\boldsymbol{a}\right) \tag{47}$$

as an asymptotic formula. The exact expression is obtained by Eq. (15) and (24), i. e.

$$<r_n^2> = \frac{1}{2\pi i}\oint\int\frac{\zeta^n}{\zeta-\mathfrak{K}}(s\boldsymbol{a})\,\frac{\zeta+\mathfrak{K}}{\zeta-\mathfrak{K}}(s\boldsymbol{a})$$

$$\times\frac{\mathfrak{K}}{\zeta-\mathfrak{K}}\,Q_1dRd\zeta$$

$$= \frac{1}{2\pi i}\oint\frac{\zeta^n}{(\zeta-1)^2}\left(\boldsymbol{a},\frac{\zeta+K_1}{\zeta-K_1}\boldsymbol{a}\right)d\zeta. \tag{48}$$

The contour integral may be calculated by the sum of residues at poles of the integrand in the usual way. Or introducing the eigenvalues and eigenvectors by

$$K_i\boldsymbol{a}_i = \zeta_i\boldsymbol{a}_i,\quad \boldsymbol{a} = \sum_{i=1}^{3}\boldsymbol{a}_i, \tag{49}$$

Eq. (48) is shown to be

$$<r_n^2> = n\left(\boldsymbol{a}\frac{1+K_1}{1-K_1}\boldsymbol{a}\right)-2\left(\boldsymbol{a}\frac{K_1}{(1-K_1)^2}\boldsymbol{a}\right)$$

$$+2\sum_{i=1}^{3}\frac{\zeta_i^{n+1}}{(1-\zeta_i)^2}(\boldsymbol{a},\boldsymbol{a}_i) \tag{50}$$

$$= \sum_{i=1}^{3}\left\{n\frac{1+\zeta_i}{1-\zeta_i}-2\frac{\zeta_i(1-\zeta_i^n)}{(1-\zeta_i)^2}\right\}(\boldsymbol{a}\boldsymbol{a}_i)$$

$$= \left(\boldsymbol{a},\left\{n\frac{1+K_1}{1-K_1}-2\frac{K_1(1-K_1^n)}{(1-K_1)^2}\right\}\boldsymbol{a}\right)$$

where all the ζ_i's are assumed to be of absolute values smaller than 1.

S. Oka, K. Suzuki and Y. Suzuki have also derived expressions of $<r_n^2>$ for chains with hindered internal rotation. Our results, however, are more generally valid than theirs including all cases they have discussed. Furthermore, calculations of higher moments will be carried more easily and systematically by our method. When n is 1, $<r^2>$ becomes equal to a^2 as is naturally to be expected. As n grows large, $<r_n^2>$ tends to the asymptotic value (47). The deviation $<r_n^2>$ from its asymptotic value is larger when n is small and the correlation is strong.

If the two end-groups are not similar to the main components of the chain, we are forced to take the generating function

$$e^{s\boldsymbol{a}''}\mathfrak{K}''U\mathfrak{K}'e^{s\boldsymbol{a}'} \tag{51}$$

instead of the function (24), in which U has the expression given in (24). The vector $\boldsymbol{a}'$ and the correlation operator $\mathfrak{K}'$ belong to the one end while $\boldsymbol{a}''$ and $\mathfrak{K}''$ to the other end. By using the function (51), Eqs. (51), (42) and (43), it follows

$$<r_n'^2> = <\{\boldsymbol{a}'+\sum\boldsymbol{a}_i+\boldsymbol{a}''\}^2> \tag{52}$$

$$= <(\sum^{n}\boldsymbol{a}_i)^2>+\boldsymbol{a}'^2+\boldsymbol{a}''^2+2\left(\boldsymbol{a}\frac{1-K_1^n}{1-K_1}K_1'\boldsymbol{a}'\right)$$

$$+2\left(n''K_1''\frac{1-K_1^n}{1-K_1}\boldsymbol{a}\right)+2(\boldsymbol{a}''_1K''K_1^{n-1}K_1'\boldsymbol{a}').$$

Although we have worked out the averages of the length of the chain so far, the length vector $\boldsymbol{r}$ will correspond to the total dipole mement of the chain molecule, if the vector $\boldsymbol{a}$ is replaced by the dipole moment of the constituent unit molecule. In all the above equations, therefore, we have only to read $\boldsymbol{a}$'s as the dipole moment $\boldsymbol{m}$'s. In an external electrical field the polymer is found to have the effective dipole moment

$$\boldsymbol{f}<\mu^2>/3kT = \boldsymbol{f}<(\sum\boldsymbol{m})^2>/3kT$$

$$= \frac{\boldsymbol{f}}{3kT}\left(\boldsymbol{m},\left\{n\frac{1+K_1}{1-K_1}-2\frac{K_1(1-K_1^n)}{(1-K_1)^2}\right\}\boldsymbol{m}\right) \tag{53}$$

provided that all the units are similar and have the dipole moment $\boldsymbol{m}$.

If the dipole moments, $\boldsymbol{m}'$ and $\boldsymbol{m}''$ are localized in the end groups and there are no other dipoles, we have from (52)

$$<\mu^2> = \boldsymbol{m}'^2+\boldsymbol{m}''+2(\boldsymbol{m}''K_1''K_1^{n-1}K_1'\boldsymbol{m}'), \tag{54}$$

which may also be proved directly with the use of the correlation function (31).

Next we shall calculate the average of a tensor (16). Let the components of the tensor α be α_{ik} in the coordinate system S. Then we have

$$(f\alpha f) = \sum f_if_j(ik)(jl)\alpha_{kl},$$

where $\boldsymbol{f}$ is a vector fixed in the space. In the same way as in Eq. (44), it may be written as

$$(f\alpha f) = \sum_{\rho\sigma}(\boldsymbol{f}\times\boldsymbol{f})_\sigma c_\rho(\alpha)_\rho(\sum D_{\rho\sigma}$$

$$= \frac{1}{3}\boldsymbol{f}^2\,\mathrm{trace}\,\alpha+\frac{2}{3}\,\mathrm{trace}\,\{(\boldsymbol{f}\times\boldsymbol{f})_{(2)}\times(\alpha)_2)D_2\},$$

the suffix (2) having the same meaning as in Eq. (46). With the use of Eqs. (23), (30), (32) and (44) therefore, we get

$$<(\boldsymbol{f}\alpha\boldsymbol{f})> = \int(\boldsymbol{f}\alpha\boldsymbol{f})\Phi dR$$

$$= \frac{1}{3}\boldsymbol{f}^2\,\mathrm{trace}\,\alpha+\frac{4}{45}\sum_{\sigma=1}^{5}(\boldsymbol{s}\times\boldsymbol{s})_\sigma(\boldsymbol{f}\times\boldsymbol{f})_\sigma$$

$$\sum_{\rho=1}^{5}\left\{\frac{1}{2}\frac{1+K_2}{1-K_2}\left(a\times\frac{1+K_1}{1-K_1}a\right)_{(2)}\right.$$
$$\left.+\left(\frac{K_1}{1-K_1}a\times\frac{1}{1-K_1}a\right)_{(2)}\right\}_{\rho}(\alpha)_{\rho},$$

which is shown to be expressed in a more symmetrical form

$$<(f\alpha f)> = \overline{\overline{\alpha}}f^2+\frac{1}{15}\{3(sf)^2-s^2f^2\}\Delta, \qquad (55)$$

where

$$\overline{\overline{\alpha}} = \frac{1}{3}\,\mathrm{trace}\,\alpha = \frac{1}{3}(\alpha_{11}+\alpha_{22}+\alpha_{33}), \qquad (56)$$

and

$$\Delta = \frac{2}{3}\sum_{\rho=1}^{5}\left\{\frac{1}{2}\frac{1+K_2}{1-K_2}\left(a\times\frac{1+K_1}{1-K_1}a\right)_{(2)}\right.$$
$$\left.+\left(\frac{K_1}{1-K_1}a\times\frac{1}{1-K_1}a\right)_{(2)}\right\}_{\rho}(\alpha)_{\rho}$$
$$=\frac{1}{4}\sum_{ijkl}(\alpha_{ij}-\overline{\overline{\alpha}}\delta_{ij})\left(\frac{1+<D_1\times D_1>}{1-<D_1\times D_1>}\right)_{ijkl}$$
$$\times\left\{\sum_{k'}\left(\frac{1+K_1}{1-K_1}\right)_{kk'}a_{k'}a_l+\left(\frac{1+K_1}{1-K_1}\right)_{ll'}a_ka_{l'}\right\}$$
$$+\sum_{ijkl}(\alpha_{ij}-\overline{\overline{\alpha}}\delta_{ij})\left(\frac{1}{1-K_1}\right)_{ik}\left(\frac{K_1}{1-K_1}\right)_{jl}a_ka_l. \qquad (57)$$

Finally the average components of the tensor will become

$$<\alpha>_{ik} = \overline{\overline{\alpha}}\delta_{ik}+\frac{1}{15}(3s_is_k-s^2\delta_{ik})\Delta. \qquad (58)$$

§ 6. Physical Application.

As we have shown in the paper II, the stress X_0 referred to the initial cross section is given by (cf. Eqs. (40) and (38) I, (20) and (21) II)

$$X_0 = \frac{dRT}{m}\frac{na^2\rho_0^2}{<r_n^2>}\left(A-\frac{1}{A^2}\right) \qquad (59)$$

for amorphous rubber-like solids composed of linear polymers provided that all the junctures of the net work structure of polymers are tight and immobile. Putting the results (47) or (50) in the above formula, we have (for small ρ_0, i. e. the chains are considerably curled in the unstrained state)

$$X_0 = \frac{dRT}{m}\frac{na^2\rho_0^2}{\left(a\left\{n\frac{1+K_1}{1-K_1}-2\frac{K_1(1-K_1^n)}{(1-K_1)^2}\right\}a\right)}, \qquad (60)$$

which allows us to discuss the temperature effects of the elasticity of rubber-like solids due to the hinderance for internal rotation.

Equation (58) leads us immediately to the theoretical discussions of the elastic double refraction of rubber-like solids. Taking average over the possible orientations of axes of chains (or the directions of s or r), we get (cf, Eqs. (17) and (18), II)

$$\overline{s_is_k} = 0 \text{ for } i\neq k.$$
$$\overline{s_1^2} = \frac{A^2s_0^2}{3},\quad \overline{s_2^2} = \frac{B^2s_0^2}{3},\quad \overline{s_3^2} = \frac{C^2s_0^2}{8},$$

where s_0, that is, the measure of the tension of the chains in the unstrained state, is given by

$$s_0 = 3a\rho_0\Big/\left(a\frac{1+K_1}{1-K_1}a\right).$$

By the Lorentz-Lorenz's formula (Eq. (35) III), we have for the double refraction in the uniaxially stressed state

$$\Delta n = n_n-n_L$$
$$=\frac{2\pi}{15}\frac{dN_L}{m}\frac{(n_0^2+2)^2}{n_0}\frac{a^2\rho_0^2\Delta}{\left(a\frac{1+K_1}{1-K_1}a\right)^2}\left(A^2-\frac{1}{A}\right) \qquad (61)$$

and for its ratio to the stress X referred to the actual cross section

$$\frac{\Delta n}{X} = \frac{2\pi}{15}\frac{(n_0^2+2)^2}{n_0kT}\frac{\Delta}{\left(a\frac{1+K_1}{1-K_1}a\right)} \qquad (62)$$

respectively, which are found to give the same result as in Eq. (45) in the paper III for chains without correlation, as shown easily from the substitution of $K_1 = K_2 = 0$ into Eq. (57).

Recently H. A. Kramers[6] and P. Debye[7] have presented theories of the viscosity of highmolecular solutions, which show that the intrinsic viscosity is given by the formula

$$\frac{\Delta\eta}{\eta} = \frac{1}{6}\frac{nf}{\eta}\sum_j<(r_j-rg)^2>. \qquad (63)$$

In the above formula the sum of the mean squares of the distances of the constituent units from the centre of gravity is required to be evaluated, which may be worked out by our method of treatment as follows;

$$\sum_j<(r_j-r_G)^2> = \sum_i\Big<\left(r_i-\frac{1}{n+1}\sum_{j=1}^{n}r_j\right)$$
$$\cdot\left(r_i-\frac{1}{n+1}\sum_{l=1}^{n}r_l\right)\Big>

$$
= \frac{n}{n+1}\left(2\sum_{i=1}^{n} i\langle r_i^2\rangle - n\sum_{i=1}^{n}\langle r_i^2\rangle\right)
$$

$$
-\frac{2}{n+1}\left(a,\sum_{i=1}^{n}\sum_{j=i+1}^{n}\sum_{k=1}^{l}\sum_{l=i+1}^{l} K_1^{l-k}a\right) \qquad (64)
$$

$$
= \left(a,\left\{\frac{n}{6}(n+2)\frac{1+K_1}{1-K_1}-\frac{nK_1}{(1-K_1)^2}\right.\right.
$$

$$
\left.\left.+\frac{2n}{n+1}\frac{K_1^2}{(1-K_1)^3}+\frac{2K_1^2(1-2K_1)(1-K_1^n)}{(n+1)(1-K_1)^4}\right\}a\right).
$$

where r_i is the position vector of i-th unit from one end specified by $i = 0$. Eq. (64) gives us the detailed knowledge of the temperature effect and the changes in the intrinsic viscosity of high-molecular solutions with the length of the chain.

Conclusion.

In the foregoing we have succeeded in giving the general expressions for the statistical quantities of chain molecules which are capable of rotation under the influence of some hindering potentials. Detailed discussions of our results in comparison with the observed properties of actual substances shall be given in later articles.

References.

(1) R. Kubo: J. Phys. Soc. Japan. **2**, 47 (1947) (I).
(2) R. Kubo: ibid. **2**, (1947) 51, (II).
(3) R. Kubo: ibid. **2**, (1947) 84, (III).
(4) S. Oka: Proc. Phys.-Math. Soc. Japan. **24** 657 (1942).
(5) K. Suzuki and Y. Suzuki: This paper read at the symposium on high polymers held in May, 1947.
(6) H. A. Kramers: J. Chem. Phys. **14** (1946) 415.
(7) P. Debye: J. Chem. Phys. **14** (1946) 636.

On the Bombardment of Thorium Tungsten by the Alkali Metal Ions.

By Hazimu KAWAMURA and Jitsuo SHIMAZU.

Mazda Research Laboratory, Tokyo-Shibaura Elec. Co. Kawasaki, Kanagawa, Japan.

(Received August 8, 1947).

When the thorium tungsten is bombarded by ions, the activity is decreased as a result of the spattering of adsorbed thorium atoms.(1) It is said that this effect is decreased when the surface of the tungsten is carbonised. We have investigated this effect with the bombardment of alkali metal ions, and found that this cause lies rather in the form of adsorption potential of the carbonized tungsten than in the adsorption energy itself.

§ 1. Experimental Method.

We employed the caesium, rubidium, and potassium as the bombarding ions, because these atoms may be ionized when they impinge upon a hot tungsten filament. For their ionization potential is smaller than the work function of tungsten, and these elements give no effect on the electron emission of thorium tungsten, so far as the temperature of the filaments are mainteined so high that the alkali atoms are not adsorbed. The bulb emloyed in our experiment was as shown in Fig. 1. A pure tungsten filament F_1 and a carbonized or uncarbonized thoriated tungsten filament F_2 were stretched in cross, whose central portions were set apart by abuot 0.5 mm. The mixture of alkali chromate and alminium powder was used as the getter, from which the alkali metal was flashed by the induction furnace before the bulb was

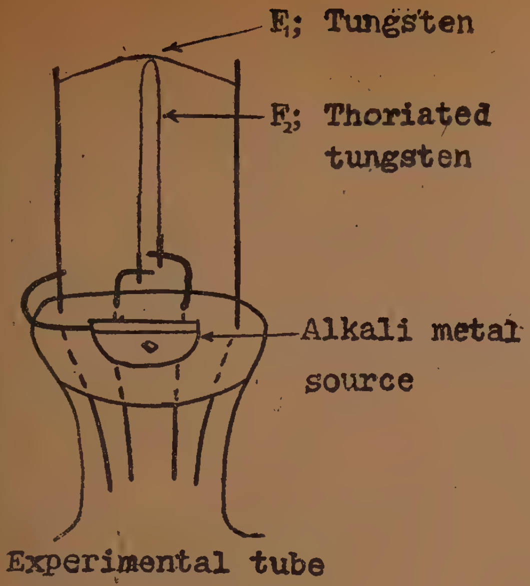

Fig. 1

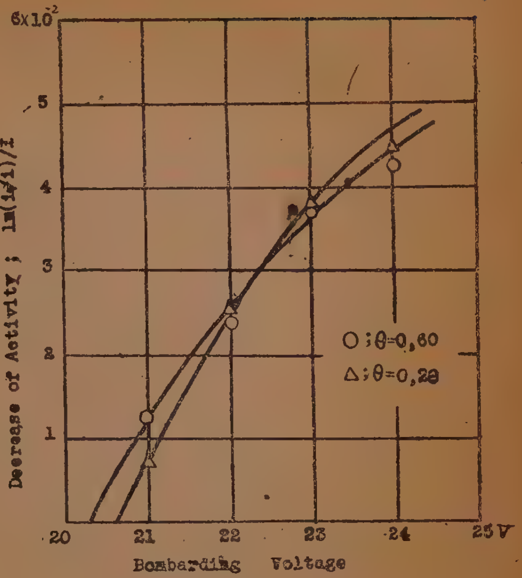

Fig. 2.

tipped off.

The procedure of the experiment was as follows: In order to maintain the vapour pressure of the alkali metal to be constant, the bulb was immersed in a oil bath. The activity of the thoriated tungsten filament F_2 was measured applying 20 volts between F_1 and F_2, after activating at about 2000°K. We chose about 1700°K as the measuring temperature, in order to avoid both the adsorption of alkali atoms and the activation of the thoriated filament. Next, the ion current was measured applying the bombarding voltage between F_1 and F_2, while only F_1 was heated at about 1700°K. F_2 was then bombarded for 10 minutes, heating both F_1 and F_2 at about 1700°K, preventing the adsorption of the alkali atoms on F_2. After the bombardment the activity of F_2 was measured. The same procedure was repeated at different bombarding voltages, after activating F_2 to almost the same degree. The temperature of the oil bath were 60°C for caesium, 80°C for rubidium, and 90°C for potassium. The vapour pressures of alkali atoms are about 10^{-5}mmHg at this temperature, and the ion currents were about .5~50 μA.

§ 2. Result and Discussion.

The results of the uncarbonized filaments with caesium ions were as shown in Fig. 2, where the ordinate is the difference in the logarithm of the activities before and after bombardment divided by the ion current. From this result we can see that there is a threshold voltage at about 20 volts, and that this threshold voltage are almost constant for different inital activities, and therefore for different fraction of surface covered with thorium atoms. To obtain the true threshold values we must consider the correction due to the contact potential difference between F_1 ank F_2, and the potential drops of the heating currents along the filaments. These corrected values for caesium, rubidium, and potassium for carbonized and uncarbonized tungsten filaments are shown in Table I. For carbonized tungsten the decrease of the activities were observed even at the lower voltages than the thrshold in some cases, which seemes to be due to the imperfection of the carbonization.

Table I.

	Cs	Rb	K
W	18.6 V	26 V	53 V
W_2C	46.2 V	68 V	145 V

From this table it is shown that the threshold voltage becomes larger as the mass of the bombarding ion becomes smaller, and also the values for the carbonized filament are larger by about 2.5 times than that for the cabonized one.

If we suppose that an ion of mass m makes head-on collision with a thorium atom of mass M which is adsorbed on tungsten surface, only a part of the initial kinetic energy, with which the ion inpinges upon the surface, may be delivered to the thorium atom. Let E be the initial kinetic energy of the ion and E' the energy delivered to the thorium atom, the law of conservations of energy and momentum tells us $E'/E=4Mm/(M+m)^2$. If E' is larger than the adsorp tion energy U, the struck atom will recoil from the tungsten surface. Therefore, the threshold voltage can be written in the form

$$E=U\frac{(M+m)^2}{4Mm}. \qquad (1)$$

Here we can not take the free mass of thoriun 232 for M, because the thorium atoms are not in free state but are adsorbed on the tungsten surface, and therefore they exhibit far greater resistance against motion due to the adsorption force. Therefore, M which we may call "effective" mass of the adsorbed thorium atom, can be determined by the repulsive forces between an impinging ion and a thorium atom, and a thorium atom and tungsten surface. This effective mass will be equal for Cs, Rb, and K, for these ions have similar electronic configurations. But for carbonized and uncarbonized tungsten, we must assign the different effective masses, because the repulsive force between thorium and tungsten, and thoreum and tungsten carbide are thought to be different. Now the equation (1) may be transformed into,

$$m+M=2\sqrt{N/U}\sqrt{mE}. \qquad (2)$$

Hence there is a linear relation between m and $\sqrt{mE}$. Fig. 3a shows the experimental results for the uncarbonised filaments. Three points for Cs, Rb, and K lie fairly well on a straight line, and from the intersection of this line with abscissa and ordinate, we can determine the effective mass M and the energy of adsorption U. The results for the carbonized filaments are shown in Fig. 3b.

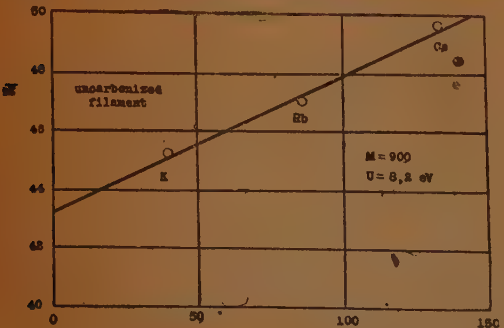

Fig. 3a.

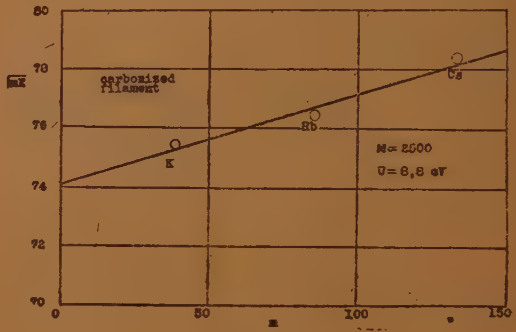

Fig. 3b.

The values of M and U thus obtained are tabulated in Table II.

Table II.

	U (eV)	M (atomic unit)
W	8.2	900
W_2C	8.8	2500

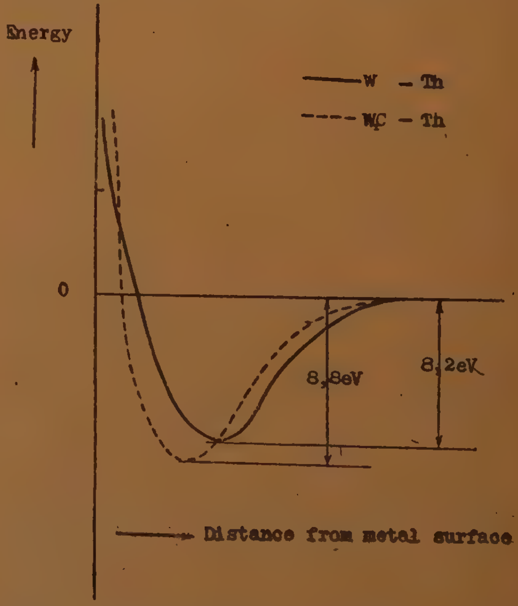

Fig. 4. Potenial curves for the adsorption of thorium atoms at tungsten and carbonized tungsten surface.

The adsorption energy U coinsides fairly well with the Langmuir's[2] value 7.5 eV. and Andrews'[3] value 7.7 eV. for the uncarbonized filament, and Andrews' value 8.8 eV. for the carbonized one. The effective masses are far greater than the free mass of thorium especially for the carbonized tungsten. From these results we can conclude that the strong resistivity of the carbonized tungsten against the ion bombardment is due to the larger effective mass rather than the larger adsorption energy. This also shows us that the repulsive force between W_2C and Th is larger than the force between W and Th as shown in Fig. 4, which probably has some relation to the higher hardness of W_2C.

References.

(1) K. H. Kingdom & I. Langmuir: Phys. Rev., **22** (1923), 148. A. W. Hull: Trans. Amer. Inst. E. E., **49** (1923), 753.

(2) I. Langmuir: Jour. Frank. Inst., **217** (1934), 543.

(3) M. R. Andrews: Phys. Rev., **33** (1929), 454.

On the Ground State of the Hydrogen Molecule.

By Eiiti Isiguro.

Institute of Physics, Faculty of Science, University of Tokyo.

(Received August 16, 1947)

§ 1. Introduction.

The wave function of the hydrogen molecule was already treated by many authors. First of all, Heitler, London1) (*H—L*) and Sugiura2) constructed the wave function from the 1*s* atomic orbitals and calculated the binding energy from this function by perturbation theory. Wang3) improved the *H—L* theory introducing effective nuclear charge and variation principle. Along this line Rosen4), Inui5) and Nordsieck6) made further contributions. James and Coolidge7) (*J—C*) pointed out that the implication of atomic individuality and the omission of an essential coordinate were the theoretical weakness of these functions. On account of this fact they expanded the wave function in power series of the required coordinates and used the Ritz variation principle. In this way they succeeded to obtain the binding energy within the limit of the probable error of the experimental value.

So far as the energy is concerned, their results were completely satisfactory, but when one wants to calculate any other physical quantity with *J—C* function, the actual calculation is often very troublesome or even practically impossible, because *J—C* function contains interelectronic distance ρ explicitly. Hence it is desirable to search fairly good wave function not containing ρ explicitly but contains the full number of required coordinates as ever. From a little different point of view, Nagamiya8) proposed the wave function containing the azimuth angle $(\varphi_1-\varphi_2)$ instead of ρ. According to him *J—C* function has two disadvantages, namely it does not give a good insight of electronic state as other simpler ones and the whole system of functions of *J—C* is not lineary independent, that is, the system with even powers of ρ alone suffices to construct the wave function of the ground state.

Hence we shall use even powers of ρ only in *J—C* method, that becomes the same as using azimuth angle and construct the new wave function for three different internuclear distances. Unfortunately convergency of the series is found to be worse than that of *J—C*. function9).

§ 2. Method of Calculation.

The Hamiltonian of a Hydrogen molecule with fixed nuclei is given by

$$H=-\frac{1}{2}\Delta_1-\frac{1}{2}\Delta_2-\frac{1}{r_{a1}}-\frac{1}{r_{b1}}-\frac{1}{r_{a2}}-\frac{1}{r_{b2}}+\frac{1}{r_{12}}+\frac{1}{R}$$

$$= -\frac{1}{2}\Delta_1 - \frac{1}{2}\Delta_2 + \frac{1}{R}\left\{1 + \frac{2}{\rho} - \frac{4\lambda_1}{\lambda_1^2-\mu_1^2} - \frac{4\lambda_2}{\lambda_2^2-\mu_2^2}\right\} \tag{1}$$

where

$$\begin{cases} \lambda_i = \dfrac{r_{ai}+r_{bi}}{R}, \quad \mu_i = \dfrac{r_{ai}-r_{bi}}{R}, \quad i=1,\ 2 \\ \varphi_i;\ \text{azimuth angle with respect to inter-} \\ \qquad \text{nuclear axis} \end{cases} \tag{2}$$

and atomic units are used throughout.

J—C five terms function, which was recommended by J—C for practical use because of its simplicity and accuracy, is written as

$$\Psi(1.2) = \frac{1}{2\pi} e^{-\delta(\lambda_1+\lambda_2)}[2c_1 + c_2(\mu_1^2+\mu_2^2) + 2c_3\mu_1\mu_2$$

$$+c_4(\lambda_1+\lambda_2)+2c_5\rho] \tag{3}$$

where $\rho = 2r_{12}/R$ (4)

We may put in (3) $2c_5\rho^2$ instead of $2c_5\rho$.

On the other hand

$$\rho^2 = \lambda_1^2+\lambda_2^2+\mu_1^2+\mu_2^2-2-2\lambda_1\lambda_2\mu_1\mu_2$$

$$-2M\cos(\varphi_1-\varphi_2) \tag{5}$$

$$M = \{(\lambda_1^2-1)(\lambda_2^2-1)(1-\mu_1^2)(1-\mu_2^2)\}^{\frac{1}{2}} \tag{6}$$

Then other flexibility will be secured by a little general function,

$$\Psi(1.2) = \frac{1}{2\pi} e^{-\delta(\lambda_1+\lambda_2)}[2c_1 + c_2(\mu_1^2+\mu_2^2) + 2c_3\mu_1\mu_2$$

$$+c_4(\lambda_1+\lambda_2)+c_5(\lambda_1^2+\lambda_2^2)+2c_6\lambda_1\lambda_2\mu_1\mu_2$$

$$+2c_7M\cos(\varphi_1-\varphi_2)] = \sum_{i=1}^{7} c_i\psi_i(1.2) \tag{7}$$

Then we find c's which minimize $\iint \Psi^* H \Psi\, d\tau_1\, d\tau_2$ under the normalization condition $\iint \Psi^* \Psi\, d\tau_1\, d\tau_2 = 1$. For a given value of δ and R, there is one function which satisfies the above condition. Varying R we shall have a potential energy curve of the ground state for each δ. The envelope of this family of curves will then show the lowest energy obtainable for any R with the corresponding most appropriate δ. Change of δ, which is absorbed to some extent in the change of c's, is not so large near equilibrium distance, so we have fixed $\alpha = 2\delta = 1.5$ and calculate the energy for $R = 1.3$, 1.4 and 1.5. The method of calculation is closely analogous to that of J—C. For H_{ij}, where either or both of i and j are 7, a little different method is used. We shall explain it briefly.

The necessary formulas are

$$\Delta_i = \left(\frac{2}{R}\right)^2 \frac{1}{\lambda_i^2-\lambda_i^2}\left[2\lambda_i\frac{\partial}{\partial\lambda_i} + (\lambda_i^2-1)\frac{\partial^2}{\partial\lambda_i^2}\right.$$

$$-2\mu_i\frac{\partial}{\partial\mu_i} + (1-\mu_i^2)\frac{\partial^2}{\partial\mu_i^2}$$

$$\left.+\frac{(\lambda_i^2-\mu_i^2)}{(\lambda_i^2-1)(1-\mu_i^2)}\frac{\partial^2}{\partial\varphi_i^2}\right] \tag{8}$$

$$d\tau_i = \left(\frac{R}{2}\right)^3(\lambda_i^2-\mu_i^2)d\lambda_i d\mu_i d\varphi_i \tag{9}$$

$$\frac{1}{\rho} = \sum_{\tau=0}^{\infty}\sum_{\nu=0}^{\tau} D_{\tau\nu}Q_\tau^\nu(\lambda_+)P_\tau^\nu(\lambda_-)P_\tau^\nu(\mu_1)P_\tau^\nu(\mu_2)$$

$$\cdot\cos\nu(\varphi_1-\varphi_2), \tag{10}$$

where

$$D_{\tau 0} = 2\tau+1, \quad D_{\tau\nu} = (-1)^\nu 2(2\tau+1)$$

$$\cdot\{(\tau-\nu)!/(\tau+\nu)!\}^2, \quad (\nu \geqq 1)$$

and $\lambda_+(\lambda_-)$ is the larger (smaller) of λ_1, λ_2.

From (1) (8) (9) (10) we obtain for $i \neq j$,

$$H_{17} = -\frac{R^5}{150}\left[25W_1^1(2.2) - 10W_1^1(0,2) + W_1^1(0,0)\right.$$

$$\left.+\frac{4}{21}W_3^1(0,0)\right]$$

$$H_{27} = -\frac{R^5}{10}\left[\left\{\frac{1}{3}W_1^1(2,2) - \frac{22}{105}W_1^1(0,2)\right.\right.$$

$$\left.+\frac{1}{35}W_1^1(0,0)\right\} - \frac{4}{45\times7}\left\{W_2^1(0,2)\right.$$

$$\left.\left.-\frac{2}{3}W_3^1(0,0)\right\}\right]$$

$$H_{37} = -\frac{R^5}{90}\left[W_2^1(2,2) - \frac{6}{7}W_2^1(0,2) + \frac{9}{49}W_2^1(0,0)\right.$$

$$\left.+\frac{4}{35\times7}W_4^1(0,0)\right]$$

$$H_{47} = -\frac{R^5}{150}\left[25W_1^1(2,3) - 5W_1^1(0,3) - 5W_1^1(1,2)\right.$$

$$\left.+W_1^1(0,1) + \frac{4}{21}W_3^1(0,1)\right]$$

$$H_{57} = -\frac{R^5}{150}\left[25W_1^1(2,4) - 5W_1^1(0,4) - 5W_1^1(2,2)\right.$$

$$\left.+W_1^1(0,2) + \frac{4}{21}W_3^1(0,2)\right]$$

$$H_{67} = -\frac{R^5}{90}\left[W_2^1(3,3) - \frac{6}{7}W_2^1(1,3) + \frac{9}{49}W_2^1(1,1)\right.$$

$$\left.+\frac{4}{35\times7}W_4^1(1,1)\right].$$

H_{77} is somewhat complicated

$$H_{77}=\frac{R^5}{18}\Big[-8(A_3-A_1)\Big(A_4-\frac{6}{5}A_2+\frac{1}{5}A_0\Big)$$

$$+\Big(A_4-\frac{6}{5}A_2+\frac{1}{5}A_0\Big)^2+2\Big\{\Big(W_0{}^0(4,4)$$

$$-\frac{12}{5}W_0{}^0(2,4)+\frac{2}{5}W_0{}^0(0,4)+\frac{36}{25}W_0{}^0(2,2)$$

$$-\frac{12}{25}W_0{}^0(0,2)+\frac{1}{25}W_0{}^0(0,0)\Big)+\frac{1}{5}\Big(W_2{}^0(4,4)$$

$$-\frac{12}{7}W_2{}^0(2,4)+\frac{36}{49}W_2{}^0(2,2)-\frac{2}{7}W_2{}^0(0,4)$$

$$+\frac{12}{49}W_2{}^0(0,2)+\frac{1}{49}W_2{}^0(0,0)\Big)+\frac{16}{35^2}\Big(W_4{}^0(2,2)$$

$$-2W_4{}^0(0,2)+W_4{}^0(0,0)\Big)+\frac{1}{20}\Big(W_2{}^2(2,2)$$

$$-\frac{2}{7}W_2{}^2(0,2)+\frac{1}{49}W_2{}^2(0,0)+\frac{1}{(105)^2}W_4{}^2(0,0)\Big\}\Big]$$

$$-\frac{R^4}{8}\Big[\Big(A_4-\frac{6}{5}A_2+\frac{1}{5}A_0\Big)\Big(A_4-\frac{16}{3}A_3-2A_2$$

$$+\frac{16}{3}A_1+A_0\Big)\Big],$$

where $W_\tau{}^\nu(m, n)$ and A_n are defined by

$$W_\tau{}^\nu(m,n)=\int_1^\infty\int_1^\infty Q_\tau{}^\nu(\lambda_+)P_\tau{}^\nu(\lambda_-)e^{-\alpha(\lambda_1+\lambda_2)}$$

$$(\lambda_1{}^2-1)^{\frac{\nu}{2}}(\lambda_2{}^2-1)^{\frac{\nu}{2}}d\lambda_1 d\lambda_2$$

$$A_n=\int_1^\infty e^{-\alpha\lambda}\lambda^n d\lambda$$

and are tabulated in Kotani, Amemiya and Simose's paper.10) Matrix elements of unity are given by

$$S_{i7}=0 \text{ for } i\neq 7$$

$$S_{77}=\frac{R^6}{18}\Big(A_4-\frac{6}{5}A_2+\frac{1}{5}A_0\Big)^2$$

Then we get the energy and c's from the roots of the secular equation and the linear homogeneous equations.

§ 3. Results.

Table I. Coefficients in normalized functions.

	$R=1.3$	$R=1.4$	$R=1.5$
Our function: $\delta=0.75$			
C_1	+2.61810	+2.46595	+2.29591
C_2	+0.98603	+0.90325	+0.82526
C_3	−0.70138	−0.67659	−0.64411
C_4	−0.49117	−0.59722	−0.66111
C_5	+0.05030	+0.05031	+0.05333
C_6	+0.00090	+0.01191	+0.01891
C_7	−0.04938	−0.03731	−0 02839
Nagamiya: $\delta=0.75$			
C_1		+2.1942	
C_2		+0.8920	
C_3		−0.6245	
C_4		−0.3175	
C_5		——	
C_6		——	
C_7		−0.03652	
Some related coefficients from $J-C$ 11 terms function*: $\delta=0.75$			
[00000]	+2.47282	+2.29326	+2.10831
[00020]	+1.14862	+1.19526	+1.20876
[00110]	−0.44227	−0.49921	−0 53385
[10000]	−0.82703	−0.86693	−0.87515
[20000]	+0.06100	+0.06621	+0.07168
[00001]	+0.39769	+0.33977	+0.28909
[00002]	−0.02596	−0.02456	−0,02264

* $\Psi=\sum_{(m,n,j,k,p)} C_{mnjkp}[m,n,j,k,p]$

$$[m,n,j,k,p]=\frac{1}{2\pi}e^{-\delta(\lambda_1+\lambda_2)}(\lambda_1{}^m\lambda_2{}^n\mu_1{}^j\mu_2{}^k\rho^p$$

$$+\lambda_1{}^n\lambda_2{}^m\mu_1{}^k\mu_2{}^j\rho^p)$$

We shall summarize the results in Table I. The value of coefficients are compared to that of Nagamiya and $J-C$ 11 terms functions. This comparison seems to serve as a criterion of accuracy of the wave function. Table II shows the values of Ψ in the configuration space of two electrons. Columns (3), (4) and (5), (6) show that electronic repulsion effect is not so large in our function as in $J-C$ function. This is explained as follows. When we construct the energy matrix with the function (7), we can take only the terms with $\nu=0$ or 1 of equation (10) into account. So the rapid convergency of the equation (10) is necessary to obtain a good result. On the other hand, if the above condition holds, we obtain our function from $J-C$ function by expanding ρ terms in Neumann series and so our function coincides with $J-C$ function. Hence if our method gives a good result, $J-C$ method gives also good result, but the opposite is not necessarily true. Table III, IV and Fig. 1 show the binding energy in e. v., most of which are adapted from $J-C$'s paper.

The author have the pleasure to express his sincere thanks for Prof. M. Kotani for his continuous encouragement and helpful guidance throghout the work.

Table II. Values of Ψ in the configuration space of two electrons.

	coordinates					
r_{1a}	0.35	,,	0.35	,,	1.4	1.4
r_{1b}	1.4	,,	1.4	,,	1.4	,,
r_{2a}	0.35	0.7	0.7	,,	1.4	,,
r_{2b}	1.75	0.7	1.4	,,	1.4	,,
r_{12}	0.525	0.7425	0.3556	1.0334	0	2.4249
$\varphi_1-\varphi_2$	—	—	0°	180°	0°	180°
	values of Ψ (normalized)					
H–L	0.0532	0.0849	0.0533	0.0533	0.0219	0.0219
Rosen	0.0702	0.1215	0.0710	0.0710	0.0249	0.0249
J–C 5 terms	0.0798	0.1172	0.0698	0.0777	0.0162	0.0271
11 terms	0.0783	0.1180	0.0667	0.0777	0.0130	0.0271
13 terms	0.0769	0.1162	0.0656	0.0772	0.0142	0.0269
our's	0.0790	0.1094	0.0746	0.0760	0.0215	0.0251

Table III. Binding energy of the hydrogen molecule in e. v.

Function	Binding energy in e. v.	internuclear distance in Bohr radii
J–C 1 terms	−2.56	1.40
5 terms	−4.507	1.40
11 terms	−4.682	1.40
13 terms	−4.697	1.40
Wang	−3.76	1.42
Rosen	−4.02	1.416
Inui-Nordsieck	−4.03	1.40
Nagamiya	−4.21	1.40
Present Paper	−4.262	1.40
Experiment	−4.73±0.04	

Table IV. Energy of H_2 in e. v. for the internuclear distance R in Bohr radii.

R	1.2	1.3	1.4	1.5	1.6	1.7
Inui-Nordsieck		−3.95	−4.03	−4.00		
Present paper		−4.20	−4.26	−4.21		
J–C 11 terms $\delta = 0.875$			−4.67	−4.63	−4.52	−4.35
$\delta = 0.75$	−4.41	−4.62	−4.68	−4.63	−4.49	
Morse curve	−4.49	−4.67	−4.73	−4.68	−4.57	−4.40

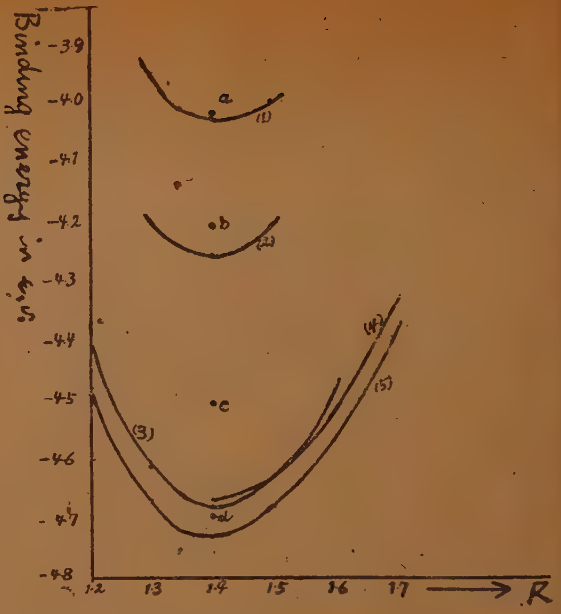

Fig. 1. Energy of H_2 molecule in e. v. against separation of the nuclei in Bohr radii

a: Rosen b: Nagamiya
c: J–C 5 terms function $\delta = 0.75$
d: J–C 13 terms function $\delta = 0.75$
(1) Inui.-Nordsieck
(2) Present function
(3) J–C 11 terms function $\delta = 0.75$
(4) J–C 11 terms function $\delta = 0.875$
(5) Morse curve

References.

(1) W. Heitler u. F. London: ZS. f. Phys, **44** (1927), 455.
(2) Y. Sugiura: ZS. f. Phys. **45** (1927), 88.
(3) S. C. Wang: Phys. Rev. **31** (1928), 579.
(4) N. Rosen: Phys. Rev. **38** (1931), 255, 2099.
(5) T. Inui: Proc. Phys. Math. Soc. Japan, **20** (1938), 770.
(6) A. Nordsieck: Phys. Rev. **58** (1940), 310.
(7) H. M. James and A. S. Coolidge: J. Chem. Phys. **1** (1933), 325.
(8) T. Nagamiya: Proc. Phys, Math, Soc. Japan, **18** (1938), 497.
(9) A. Hylleraas: ZS. f. Phys. **54** (1929), 347.
(10) M. Kotani, A. Amemiya and T, Simose: Proc. Phys. Math. Soc. Japan. **20** (1938), Extra Number 1.

On the Value of the Electric Quadrupole Moment of the Deuteron.

By Eiiti ISIGURO.

Institute of Physics, Faculty of Science, Tokyo University.

(Received August 16, 1947)

§ 1. Introduction.

Since the discovery of the electric quadrupole moment of the deuteron by Kellog, Rabi, Ramsey and Zacharias1), its existence has been interpreted as an evidence for the non-central character of the proton-neutron interaction, which follows from the meson theory of nucleons.

Now from the molecular beam experiment of Kellog and his collaboraters, we know only the product qQ, where Q is the electric quadrupole moment of the deuteron and $2q$ is the gradient of the electric field at one nucleus in the hydrogen molecule*; hence the accuracy of Q obtainable from the experiment depends on the knowledge of the numerical value of q. Now the most accurate evaluation of q hitherto made is that of Nordsieck2). Since, however, the value of Q is an important data for the theoretical physicists, it seems desirable to recalculate it using a more refined wave function of the hydrogen molecule. The calculation reported here has been carried out from these points of view.

According to Nordsieck, q is written as follows

$$q = [q(R)]_{av} \tag{1}$$

where

$$q(R) = +\frac{1}{R^3} - \frac{1}{2}\int d\tau \rho(r, \theta) \frac{3\cos^2\theta - 1}{r^3} \tag{2}$$

where θ is the angle made by the radius vector r with the internuclear line, and $\rho(r, \theta)$ is the electron density. Average is to be taken over the zeroth nuclear vibrational state. To calculate $q(R)$, Nordsieck proposed the electronic wave function

$$\Psi_{\text{Nord.}} = e^{-\frac{1}{2}A(\lambda_1+\lambda_2)}\left[e^{\frac{1}{2}B(\mu_1-\mu_2)} + e^{-\frac{1}{2}B(\mu_1-\mu_2)}\right] \tag{3}$$

where A and B are parameters determined so that the energy has minimum; λ_i, μ_i are the elliptic coordinates of the i-th electron. Although (3) seems to afford a good approximation when the operator depends only on the coordinates of one electron, we calculate q with a more refined function, because only the deviation of wave function from the spherical symmetry contributes to the integral. (2).

§ 2. Caluclation of q.

We used the following function instead of (3)

$$\begin{aligned}\Psi = \frac{1}{2\pi}e^{-\delta(\lambda_1+\lambda_2)}[&2c_1 + c_2(\mu_1^2+\mu_2^2) + 2c_3\mu_1\mu_2 + c_4(\lambda_1 \\ &+\lambda_2) + c_5(\lambda_1^2+\lambda_2^2) + c_6\lambda_1\lambda_2\mu_1\mu_2 + 2c_7M\cos(\varphi_1-\varphi_2)] \\ = \sum_{i=1}^{7}&c_i\psi_2 \end{aligned} \tag{4}$$

$$M = \{(\lambda_1^2-1)(\lambda_2^2-1)(1-\mu_1^2)(1-\mu_2^2)\}^{\frac{1}{2}}$$

c's are tabulated in the foregoing paper; λ_i, μ_i and φ_i are the elliptic coordinates of i-th electron.

Now integration of $q(R)$ is made with elliptic rather than polar coordinates. However, in evaluating the conditionally convergent integral (2), we have to take care to carry out firstly the integration outside the small sphere of radius εR and then tend ε to zero3). Hence we seperate the domain of integration into two parts, namely the region outside the thin ellipsoid $\lambda = 1+2\varepsilon$ and the region between this ellipsoid and the small sphere of radius εR. Then our problem is the calculation of the following integral,

$$\int d\tau\rho(r, \theta)\frac{3\cos^2\theta-1}{r^3}$$

$$= \lim_{\varepsilon\to 0} \underset{\substack{\text{outside the sphere} \\ r=\varepsilon R}}{\iiint} J(\lambda, \mu)\rho(r, \theta)d\lambda d\mu d\varphi. \tag{5}$$

where

$$J(\lambda, \mu) = \frac{\lambda-\mu}{(\lambda+\mu)^2}\left[\frac{3(1+\lambda\mu)^2}{(\lambda+\mu)^2} - 1\right] \tag{6}$$

---

* We write q instead of q' in Nordsieck's paper.

Now putting

$$2P(j,m)=\iint J(\lambda,\mu)e^{-\alpha\lambda}\lambda^j\mu^m d\lambda d\mu$$

$$=\lim_{\varepsilon\to0}\left[\int_{1+2\varepsilon}^{\infty}e^{-\alpha\lambda}\lambda^j d\lambda\int_{-1}^{+1}J(\lambda,\mu)\mu^m d\mu\right.$$

$$\left.+\int_{+1}^{1+2\varepsilon}e^{-\alpha\lambda}\lambda^j d\lambda\int_{2\varepsilon-\lambda}^{+1}J(\lambda,\mu)\mu^m d\mu\right] \quad (7)$$

where

$$\alpha=2\delta,$$

we obtain

$$P(j,m)=M(j,m)+T(j,m) \quad (8)$$

$$\begin{cases} M(j,m)=\dfrac{1}{2}\displaystyle\int_1^{\infty}d\lambda\int_{-1}^{+1}e^{-\alpha\lambda}J(\lambda,\mu)\lambda^j\mu^m d\mu & (9)\\ T(j,m)=\dfrac{1}{2}\displaystyle\lim_{\varepsilon\to0}\int_1^{1+\varepsilon}d\lambda\int_{-\lambda}^{1}e^{-\alpha\lambda}J(\lambda,\mu)\lambda^j\mu^m d\mu & (10)\end{cases}$$

Integration of $M(j,m)$ are carried out as follows;

$$\begin{cases} \displaystyle\int_{-1}^{+1}J(\lambda,\mu)d\mu=6\lambda-(3\lambda^2-1)\log\frac{\lambda+1}{\lambda+1} \\ \displaystyle\int_{-1}^{+1}J(\lambda,\mu)\mu^2 d\mu=2\lambda(42\lambda^2-21) \\ \qquad\qquad -(42\lambda^3-35\lambda^2+3)\log\dfrac{\lambda+1}{\lambda-1} \\ \displaystyle\int_{-1}^{+1}J(\lambda,\mu)\mu^4 d\mu=\lambda(330\lambda^4-268\lambda^2+24) \\ \qquad\qquad -\lambda^2(165\lambda^4-189\lambda^2+42)\log\dfrac{\lambda+1}{\lambda-1}\end{cases} \quad (11)$$

So that

$$\begin{cases} M(j,0)=3A_{j+1}-3f_0(j+2)+f_0(j) \\ M(j,2)=42A_{j+3}-21A_{j+1}-42f_0(j+4) \\ \qquad\qquad +35f_0(j+2)-3f_0(j) \\ M(j,4)=165A_{j+5}-134A_{j+3}+12A_{j+1} \\ \qquad\qquad -165f_0(j+6)+189f_0(j+4)-42f_0(j+2)\end{cases} \quad (12)$$

where

$$\begin{cases} A_n=\displaystyle\int_1^{\infty}e^{-\alpha\lambda}\lambda^n d\lambda \\ f_0(j)=\dfrac{1}{2}\displaystyle\int_1^{\infty}\log\frac{\lambda+1}{\lambda-1}e^{-\alpha\lambda}\cdot\lambda^j d\lambda\end{cases} \quad (13)$$

are given by the table of M, Kotani, A. Amemiya and T. Simose[4]. Further we put

$$\int_1^{1+\varepsilon}e^{-\alpha\lambda}\cdot\lambda^j d\lambda=F(j). \quad (14)$$

Then

$$2T(j,0)=\lim_{\varepsilon\to0}\left[\frac{1}{\varepsilon}\{12F(j+3)-8F(j+1)\}\right.$$

$$-\frac{3}{2\varepsilon^2}\{5F(j+4)-6F(j+2)+F(j)\}$$

$$\left.+\frac{2}{\varepsilon^3}\{F(j+5)-2F(j+3)+F(j+1)\}\right]$$

$$=\frac{2}{3}e^{-\alpha}$$

Or generally we obtain

$$T(j,m)=(-1)^m\frac{1}{3}e^{-\alpha} \quad (15)$$

Thus $T(j,m)$ does not depend on j, and takes plus or minus sign according as m is even or odd. This means that only the value close to the origin contributes the integral. From (8) (12) (15) we obtain $P(j,m)$. Further we define $L(k,n)$ and $N(j,k,m,n)$ as follows

$$L(k,n)=\frac{1}{2}\int_1^{\infty}\int_{-1}^{+1}e^{-\alpha\lambda}(\lambda^2-\mu^2)\lambda^k\mu^n d\lambda d\mu$$

$$=\frac{1}{n+1}A_{k+2}-\frac{1}{n+3}A_k, \quad (16)$$

$$N(j,k,m,n)=P(j,m)L(k,n) \quad (17)$$

Then we obtain the integral,

$$q_{ij}=\lim_{\epsilon\to0}\underset{\substack{\text{outside the sphere}\\ r=\varepsilon R}}{\iint}\frac{3\cos^2\theta-1}{r^3}\phi_i\phi_j d\tau_1 d\tau_2 \quad (18)$$

in terms of $N(j,k,m,n)$, for example,

$$q_{11}=2R^3N(0,0,0,0)$$

$$q_{77}=R^3[N(2,2,2,2)+N(2,2,0,0)+N(0,0,2,2)$$
$$+N(0,0,0,0)+N(2,0,2,0)+N(2,0,0,2)$$
$$+N(0,2,2,0)+N(0,2,0,2)-N(2,2,2,0)$$
$$-N(2,2,0,2)-N(2,0,2,2)-N(2,0,0,0)$$
$$-N(0,2,2,2)-N(0,2,0,0)-N(0,0,2,0)$$
$$-N(0,0,0,2)]$$

Then from (2), (4) and (18) we obtain

$$\varepsilon(R)=\frac{1}{R^3}-\sum_{i,j}c_ic_jq_{ij} \quad (19)$$

The values of $q(R)$ are tabulated in Tab. I. Our value is smaller than that of Nordsieck by about 0.006 atomic units for each R.

Table I. Values of $q(R)$ in atomic units.

R	Nordsieck	Present calculation
1.3	+0.2462	+0.24063
1.4	+0.1755	+0.16942
1.5	+0.1257	+0.11971

Now we must average $q(R)$ over the zero point vibration of the molecule. Adapting a formula $a/R+b/R^2+c/R^3$ to the values in Tab. I. we obtain

$$q(R) = 0.14542/R-1.03039/R^2+1.62241/R^3. \quad (20)$$

To average $q(R)$, Morse potential function⁵⁾ and Jeppeson's experimental data⁶⁾ are used. The values of q are given in Tab. II.

Table II. Values of q in atomic units, values of q in cm⁻³ are also given in brackets.

q	Nordsieck	Present calculation
HD	$+0.1768(1.193\times10^{24})$	$+0.1729(1.169\times10^{24})$
D_2	$+0.1763(1.190\times10^{24})$	$+0.1723(1.165\times10^{24})$

§ 3. Numerical Value of the quadrupole moment Q.

From q together with the experiment of Kellog etc. we find the quadrupole moment of the deuteron, Q;

$$Q = -\frac{2\mu_d H'''}{e^2 q} \quad (21)$$

where q is the electronic charge; μ_d is the magnetic dipole moment of the deuteron, H''' is the magnetic field in gauss obtained from the analysis of the radiofrequency spectra and is related to the hyperfine structure due to quadrupole moment. Introducing these values into (21) we obtain

$$Q = +2.79\times10^{-27}\ \text{cm}^2, \quad (22)$$

whereas Nordsieck's value is $+2.73\times10^{-27}$ cm².

Nordsieck considered that the error of his calculation is within 2%, on the other hand (2.79—2.73)/2.79 equals 2%. At any rate, from Nordsieck's and the present calculation, convergency of the electric quadrupole moment of the deuteron with the successive electronic wave function seems to be fainly good, and we may assume the safe estimate of error of (22) is also 2%.

The author wishes to express his gratitude to Prof. M. Kotani for suggesting this problem and for his generous assistance.

References.

(1) J. M. Kellog, I. I. Rabi, N. F. Ramsey and J. R. Zacharias: Phys. Rev. **57** (1940), 677.
(2) A. Nordsieck: Phys. Rev. **58** (1940), 310.
(3) H. B. Casimir: On the interaction between atomic nuclei and electrons (1936).
(4) M. Kotani: A. Amemiya and T. Simose, Proc. Phys. Math. Soc. Japan, **20** (1938) Extra Number I.
(5) P. M. Morse: Phys. Rev. **34** (1929), 57.
(6) C. R. Jeppson: Phys. Rev. **45** (1934), 480. Phys. Rev. **49** (1936), 797.

Analytical Expression of Self-consistent Wave Functions for Lithium, Boron, Carbon and Oxygen.

By Simpei TUTIHASI.

Department of Industrial Chemistry, Kyoto University.

(Received August 18, 1947)

For dealing with atomic and molecular problems which include any detailed calculations, good approximations of the atomic wave functions are needed first of all. Well-known methods for this purpose are the Ritz method of series, the variational method with variable parameters, and the Hartree and Fock method of self-consistent field. The former two are applicable only to a few lighter atoms, whereas the last is applicable to any complex atom. Many results of elaborate computations of self-consistent atomic wave functions were published. These functions, however, are expressed in tabular forms, and they are not convenient for dealing general properties of atomic or molecular systems.

J. C. Slater[1] showed a method to obtain simple and available analytical expressions of tabular self-consistant one-electron functions. I have calculated such analytical expressions for a few atoms as reference materials for later works. So far as the principal quantum numbers are small, the computations are simple. For large principal quantum numbers, however, nodes of the radial functions with smaller azimuthal quantum numbers become numerous, and the computation becomes laborious and inaccurate. Thus, as an example, I have established an analytical expression up to $3p$ radial function of Lithium I. The results are reported in the following table.

One-electron functions are written in the usual form $R_{nl}(r)Y_{lm_l}(\theta, \varphi)$. In the table rR_{nl}'s (Hartree's P_{nl}) are given where r is measured in atomic units. The one-electro radial functions of the same azimuthal quantum number in this table are not exactly orthogonal. Thus, if one will make use of this analytical expressions for constructing any symmetric wave functions in the form of determinants, one should make them orthogonal and normalized. The method is explained in Slater's paper[1].

In conclusion, I wish to express my sincere thanks to Prefessor G. Araki for the interest he has had in this work.

Table.[2]

Lithium.

	Li I. $1s^2 2s$	Li I. $1s^2 2p$	Li I. $1s^2 3p$
$1s$	$8.96re^{-2.76r}$	$8.96re^{-2.76r}$	$8.96re^{-2.76r}$
$2s$	$0.82re^{-1.92r}$ $-0.31r^2e^{-0.58r}$		
$2p$		$r^2(0.21e^{-0.50r}$ $+0.09e^{-2.68r})$	
$3p$			$0.18r^2e^{-0.49r}$ $+r^3(0.05e^{-1.04r}$ $+0.01e^{-0.31r})$

Boron.

	B I. $1s^2 2s^2 2p$
$1s$	$20.26re^{-4.73r}$
$2s$	$5.11re^{-5.94r}-2.08r^2e^{-1.25r}$
$2p$	$r^2(1.54e^{-1.82r}+0.47e^{-0.78r})$

Carbon.

	C I. $1s^2 2s^2 2p^2$	C I. $1s^2 2s 2p^3$
$1s$	$25.14re^{-5.48r}$	$26.42re^{-5.61r}$
$2s$	$5.92re^{-4.89r}$ $-3.94r^2e^{-1.62r}$	$5.95re^{-4.91r}$ $-3.98r^2e^{-1.62r}$
$2p$	$r^2(3.55e^{-2.58r}$ $+1.26e^{-1.25r})$	$r^2(3.47e^{-2.35r}$ $+1.05e^{-1.15r})$

Oxygen.

	O I. $1s^2 2s^2 2p^4$	O II. $1s^2 2s^2 2p^3$
$1s$	$42.44re^{-7.70r}$	$42.44re^{-7.70r}$
$2s$	$9.69re^{-6.73r}$ $-9.46r^2e^{-2.31r}$	$10.11re^{-6.66r}$ $-10.32r^2e^{-2.37r}$
$2p$	$r^2(9.62e^{-3.16r}$ $+1.47e^{-1.32r})$	$r^2(9.89e^{-3.14r}$ $+2.63e^{-1.66r})$

	O III. $1s^2 2s^2 2p^2$	O IV. $1s^2 2s^2 2p$
$1s$	$42.44re^{-7.70r}$	$42.44re^{-7.70r}$
$2s$	$10.64re^{-6.51r}$ $-11.73r^2e^{-2.47r}$	$11.34re^{-6.38r}$ $-13.66r^2e^{-2.60r}$
$2p$	$r^2(9.35e^{-3.62r}$ $+5.16e^{-2.05r})$	$r^2(10.50e^{-3.93r}$ $+7.10e^{-2.37r})$

References.

(1) J. C. Slater: Phys. Rev., **42** (1932), 33.

(2) Sources of tabular functions are as follows: Lithium; S. Weintroub: Proc. Phys. Soc., **48** (1936), 535. Boron; F. W. Brown, J. H. Bartlett and C. G. Dunn: Phys. Rev., **44** (1933), 296. Carbon; C. C. Torrance: Phys. Rev., **46** (1934), 388. Oxygen; D. R. Hartree and M. M. Black: Proc. Roy. Soc. London (A), **139** (1933), 311.

Doublet-intervals of Lithium I, Boron I and Oxygen IV.

By Simpei TUTIHASI.

Department of Industrial Chemistry, Kyoto University.

(Received September 2, 1947)

The quantum mechanical fine structure formula of the energy levels of hydrogen-like atoms was first derived by Pauli1). Its complete expression was later given by Dirac2) on the basis of his relativistic equation of the electron. Further the Pauli formula was found to be semi-relativistic approximation of Dirac's. These formulae have been recognized to be in exact agreement with experiments3).

Alkali-doublets have often been believed to be represented by the above mentioned hydrogenic formulae4) with the effective atomic number of alkalis. However, these formulae never explain inversions of alkali-doublets.

In order to get a correct formula, alkali-like atoms must be considered as many-electron atoms. Such a calculation was first carried out by David5) for Li $1s^2\ 2p$, but he did not arrive at a general formula. The general doublet formula for alkali atoms was later derived by Araki6), taking into account the electromagnetic interactions between all atomic electrons. The result of his numerical calculation for an inverted doublet of copper was in good agreement with an observation. His radial functions were of hydrogen-like atoms with suitable screening constants.

According to Araki the interval of the alkali-doublet is given by

$$ {}^2L_{l-\frac{1}{2}} - {}^2L_{l+\frac{1}{2}} = (2l+1)(z-\sigma)\mu^2\bar{r}^{-3}, $$

where Z is the atomic number of the atom, μ is the Bohr magneton, and σ is a screening constant due to the spin-orbit interactions between the valence electron and the core electrons. σ and $\bar{r}^{-3}$ are given as follows:

$$ \sigma = \sum_{n'l'} 2(2l'+1)(\zeta_{n'l',nl} + 3\tilde{\zeta}_{n'l',nl}), $$

$$ \bar{r}^{-3} = \int_0^\infty \frac{1}{r^3}[R_{nl}(r)r]^2 dr, $$

$$ \zeta_{n'l',nl} = -\frac{1}{\bar{r}^{-3}} \int_0^\infty \int_0^\infty \frac{1}{r_2} \frac{\partial a_0}{\partial r_2} $$

$$ \times [R_{n'l'}(1)R_{nl}(2)r_1 r_2]^2 dr_1 dr_2, $$

$$ \tilde{\zeta}_{n'0,nl} = -\frac{1}{(2l+1)\bar{r}^{-3}} \int_0^\infty \int_0^\infty \frac{a_l}{r_2} R_{n'0}(1) \frac{dR_{n'0}(2)}{dr_2} $$

$$ \times R_{nl}(1)R_{nl}(2) r_1^2 r_2^2 dr_1 dr_2, $$

$$ a_\nu = \frac{r_1^\nu}{r_2^{\nu+1}} \quad (r_1 \leqq r_2) $$

$$ = \frac{r_2^\nu}{r_1^{\nu+1}} \quad (r_2 < r_1), $$

and R's are normalized radial functions.

In the present paper, intervals of ${}^2P$ of several atoms are calculated according to the above mentioned general formula, for configurations which consist of one p-electron and closed shells, namely Boron I $1s^2\ 2s^2\ 2p$, Lithium I $1s^2\ 2p$, Lithium I $1s^2\ 3p$ and Oxygen IV $1s^2\ 2s^2\ 2p$. For the computation of parameters, analytical expressions of self-consistent radial functions, which were published in the previous paper7), are used. The value of the physical constant. which is adopted in the present calculations, is $\alpha^2 R$ cm^{-1} = 5.822 cm^{-1}. $\bar{r}^{-3}$ is given by $\dfrac{Z^3}{n^3(l+1)\left(l+\frac{1}{2}\right)l}$ atomic units for hydrogen-like atoms. The screening constant s is defined by

$$ \bar{r}^{-3} = \frac{(Z-s)^3}{n^3(l+1)\left(l+\frac{1}{2}\right)l} \quad \text{(in atomic units).} $$

The results are shown in Tables I, II, III, IV and V. It is to be noted that the contribution from 1s to σ is greater than 1 per electron. Parameters ζ and $\tilde{\zeta}$ give the measure of the strength of the spin-orbit interactions between electrons in the atoms. Values of these parameters are slightly larger than Araki's result8) for B $\zeta_{10,21}$ and $\zeta_{20,21}$, smaller for O $\zeta_{10,21}$, $\zeta_{20,21}$ and B $\tilde{\zeta}_{10,21}$, and nearly equal to for O $\tilde{\zeta}_{10,21}$. Our $\tilde{\zeta}_{20,21}$ of B is positive, whereas Araki's is negative. For O $\tilde{\zeta}_{20,21}$ the both have the same sign.

In conclusion the author wishes to express his hearty thanks to Professor G. Araki for the kind interest he taken in the present work.

Table I. Intervals of doublets (in cm^{-1})

Atoms	Symbols	Calc.	Obs.
Li I. $1s^2\,2p$	$^2P_{\frac{1}{2}}-{}^2P_{1\frac{1}{2}}$	0.21	0.34
Li I. $1s^2\,3p$	$^2P_{\frac{1}{2}}-{}^2P_{1\frac{1}{2}}$	0.05	
B I. $1s^2\,2s^2\,2p$	$^2P_{\frac{1}{2}}-{}^2P_{1\frac{1}{2}}$	9.549	15
O IV. $1s^2\,2s^2\,2p$	$^2P_{\frac{1}{2}}-{}^2P_{1\frac{1}{2}}$	380.177	387

Table II. Calculated values of σ.

	$2p$	$3p$
Li	2.4790	2.5522
B	2.9110	
O	2.6664	

Table III. Calculated values of $\overline{r^{-3}}$
(in atomic unit)

	$2p$	$3p$
Li	0.0455	0.0134
B	0.5234	
O	8.1621	

Table IV. Calculated values of s.

	$2p$	$3p$
Li	1.9702	1.9723
B	2.6754	
O	2.1923	

Table V. Calculated values of ζ and $\tilde{\zeta}$.

	Li I.	B I	O IV
$\zeta_{10,21}$	0.8527	0.7740	0.6763
$\zeta_{20,21}$		0.0986	0.0752
$\zeta_{10,31}$	0.8060		
$\tilde{\zeta}_{10,21}$	0.1289	0.1774	0.2087
$\tilde{\zeta}_{20,21}$		0.0169	−0.0148
$\tilde{\zeta}_{10,31}$	0.1567		

References.

(1) W. Pauli: ZS. f. Phys., **43** (1927), 601.

(2) P. A. M. Dirac: Proc. Roy. Soc. London (A), **117** (1928), 610.

(3) R. F. Bacher and S. Goudsmit: *Atomic energy states*, (1932).

(4) R. A. Millikan and I. S. Bowen: Phys. Rev. **23** (1924), 764; **24** (1924), 209, 223.

(5) E. David: ZS. f. Phys., **91** (1934), 289.

(6) G. Araki: Proc. Phys. Math. Soc. Japan, **21** (1939), 508.

(7) S. Tutihasi: J. Phys. Soc. Japan, **3** (1947), in press.

(8) G. Araki: Proc. Phys. Math. Soc. Japan, **19** (1937), 592.

Theory of Electromagnetic Oscillation on Plate Conductor.

By Tokio SAKURAI.

Electrotechnical Laboratory, Ministry of Communications.

(Read October 6, 1947, Received August 20, 1947.)

Since the progress of short-wave technics necessiates the investigation of electromagnetic oscillation on a plate conductor, the fundamental theoretical treatments of the subject are considered in this paper. In order to save the pages of this treatment the notation in J. A. Stratton's "Electromagnetic Theory" is used except when special explanation is added.

§ 1. Wave Function of Plate.

A plate conductor is located on the xy-plane of the rectangular xyz-coordinates. Rectangular curvilinear coordinates u_1, u_2, u_3-lines are oriented symmetrically with respect to xy-plane excludingthe sign of direction, u_3-lines starting perpendicularly from the surface of the plate and at the starting point $u_3 = 0$, and u_1-lines running from upper side to the lower side of xy-plane and intersecting with xy-plane at $u_1 = 0$. Therefore, u_1-lines on the plate surface cross perpendicularly the edge of the plate at $u_1 = 0$. u_2-lines are distributed in like manner in the same direction on both surfaces of the plate, while u_1-lines in opposite direction on upper and lower surfaces of the plate.

ψ expresses a general wave function satisfying

$$\nabla^2\psi_{mn}+K^2\psi_{mn} = 0 \qquad (k = \omega\sqrt{\varepsilon\mu}) \tag{1.1}$$

where

$$\nabla^2\psi = \frac{1}{h_1h_2h_3}\left[\frac{\partial}{\partial u_1}\left(\frac{h_2h_3}{h_1}\frac{\partial\psi}{\partial u_1}\right)+\frac{\partial}{\partial u_2}\left(\frac{h_3h_1}{h_2}\frac{\partial\psi}{\partial u_2}\right)+\frac{\partial}{\partial u_3}\left(\frac{h_1h_2}{h_3}\frac{\partial\psi}{\partial u_3}\right)\right], \tag{1.2}$$

$$(dx)^2+(dy)^2+(dz)^2 = h_1^2(du_1)^2+h_2^2(du_2)^2+h_3^2(du_3)^2. \tag{1.3}$$

If the edge of the plate is assumed to be curved slowly, u_2-lines running parallel to the edge may be regarded as straight lines in the neighbourhood of any selected point P on the edge of the plate. Therefore, we can choose u_1, u_3 such that the surfaces, u_1-constant and u_3-constant, intersect with parabolic cylinders whose elements are parallel to u_2-lines in the neighbourhood of P. Hence if we remove the origin of the rectangular coordinate ξ, η, ζ to P, make η axis coincide with the tangential line of the edge on P and keep ζ axis parallel to z-axis. then the relations between ξ, η, ζ and u_1, u_2, u_3 are as follows:

$$u_1^2 = \sqrt{\xi^2+\zeta^2}-\zeta, \quad u_2 = \eta, \quad u_3^2 = \sqrt{\xi^2+\zeta^2}+\zeta, \tag{1.4}$$ [1)]

$$h_1 = h_3 = \sqrt{u_1^2+u_3^2}, \quad h_2 = 1. \tag{1.5}$$

Hence on the plate surface

$$u_1 = \sqrt{-2\xi}, \qquad u_3 = \zeta/\sqrt{-2\xi}. \tag{1.6}$$

Consequently *on the plate surface* (1.1) becomes acceding to (1.5), (1.6)

$$\frac{\partial^2\psi_{mn}}{\partial\xi^2}+\frac{1}{2\xi}\frac{\partial\psi_{mn}}{\partial\xi}+\frac{\partial^2\psi_{mn}}{\partial\eta^2}+\frac{\partial^2\psi_{mn}}{\partial\zeta^2}+K^2\psi_{mn} = 0. \tag{1.7}$$

If we suppose that the variation of ψ_{mn} is approximately sinusoidal* in ξ-direction and denote by $\lambda^{(1)}$ the wave length of ψ_{mn} in ξ-direction,

$$\psi_{mn} \simeq e^{\pm 2j\pi|\xi|/\lambda^{(1)}}U(\eta, \zeta). \tag{1.8*}$$

The second term is negligible as compared with the first one in the left-hand side of (1.7), when

$$|\xi| \gg \lambda^{(1)}/4\pi. \tag{1.9}$$

In this case (1.5) becomes approximately

$$\frac{\partial^2\psi_{mn}}{\partial\xi^2}+\frac{\partial^2\psi_{mn}}{\partial\eta^2}+\frac{\partial^2\psi_{mn}}{\partial\zeta^2}+K^2\psi_{mn} = 0. \tag{1.10}$$

The domain in which the coefficients of wave equation (expressed by rectangular coordinates) are constant as in (1.10) shall be called *central domain*, while the domain in which those coefficients are variable as in (1.7) shall be called *boundary*

---

* This fact is shown in (1.21.)

domain. If

$$|\xi_0| = \lambda^{(1)}/4, \qquad (1.11)$$

the condition (1.9) is nearly satisfied. Therefore, it is convenient to select the closed curve whose distance $|\xi_0|$ from the edge of the plate is given by (1.11) as *separating line* of both domains and to define the domain outside this line as *boundary domain* and inside this line as *central domain*.

If we substitute into (1.1)

$$\psi_{mn} = V_{mn}(u_1, u_3)\exp(\pm jk_m^{(2)}), \quad (k_m^{(2)*}: \text{const.}) \qquad (1.12)^*$$

and use (1.5), we have

$$\frac{\partial^2 V_{mn}}{\partial u_1^2}+\frac{\partial^2 V_{mn}}{\partial u_3^2}+\{k^2-(k_m{}^{(3)})^2\}(u_1{}^2+u_3{}^2)V_{mn} = 0. \qquad (1.13)$$

If we put

$$V_{mn}(u_1, u_3) = \varphi_{mn}(u_1)g_{mn}(u_3), \qquad (1.14)$$

(1.13) breaks up into following two equations

$$\frac{d^2\varphi_{mn}}{du_1^2}+a_n{}^2\varphi_{mn}+\}k^2-(k_{mn}{}^{(2)})^2\}u_1{}^2\varphi_{mn} = 0, \qquad (1.15)$$

$$\frac{d^2 g_{mn}}{du_3^2}-a_n{}^2 g_{mn}+\{k^2-(k_m{}^{(2)})^2\}u_3{}^2 g_{mn} = 0. \qquad (1.16)$$

If we solve (1.16) and use (1.6)

$$g_{mn} \simeq e^{-\alpha_n\zeta}, \quad \text{(on the plate surface)} \qquad (1.17)$$

where

$$\alpha_n = a_n/\sqrt{-2\xi}. \qquad (1.18)$$

If we substitute (1.17) into (1.15) and use (1.1), we get

$$\frac{d^2\varphi_{mn}}{d\xi^2}+\frac{1}{2\xi}\frac{d\varphi_{mn}}{d\xi}+\{k^2-(k_m{}^{(2)})^2+\alpha_n{}^2\}\varphi_{mn} = 0. \qquad (1.19)$$

If there exists the relation (1.9), we can put

$$\lambda_{mn}{}^{(1)} = 2\pi/\sqrt{k^2-\{k_m{}^{(2)}\}^2+\alpha_n{}^2}, \qquad (1.20)$$

and the fundamental solution of (1.19) is approximately of the form

$$\varphi_{mn} = e^{\pm 2j\pi|\xi|/\lambda_{mn}{}^{(1)}}. \qquad (1.21)$$

Hence the variation of ψ_{mn} is approximately sinusoidal in ξ-direction and is of the form (1.12). If we substitute (1.18) and (1.20) into (1.11), and solve the equation thus obtained, we get the distance $|\xi_0|$ of the separating line from the plate edge as follows:

$$|\xi_0| = \frac{\pi}{2}\frac{1}{\sqrt{k^2-(k_m^{(2)})^2}}\{\sqrt{1+p^2{}_{mn}}-p_{mn}\}, \qquad (1.22)$$

where

$$p_{mn} = a_n^2/\{2\pi\sqrt{k^2-(k_m^{(2)})^2}\}. \qquad (1.23)$$

There are two fundamental solutions of (1.19), which we express by $\overset{e}{\varphi}_{mn}$, and $\overset{o}{\varphi}_{mn}$, the former being even and the latter being odd function of u_1. Since $u_1 = 0$ on the edge of the plate, the behavior of these functions near the edge is known by (1.19) and (1.6) as follows:

$$\overset{e}{\varphi}_{mn} \simeq \cos(a_n\sqrt{-2\xi}), \quad \overset{o}{\varphi}_{mn} \simeq \sin(a_n\sqrt{-2\xi}). \qquad (1.24)$$

If we solve* (1.19) so as to behave like (1.24) near the plate edge, the forms of $\overset{e}{\varphi}_{mn}$, $\overset{o}{\varphi}_{mn}$ in the boundary domain are completely determined. Hence by (1.17), (1.14) and (1.12) the form of ψ_{mn} in the boundary domain is completely decided.**

In the central domain the wave equation becomes (1.10), which can be solved by familiar method. If we solve this equation so as to make electromagnetic field expressed by wave functions in both central and boundary domains continuously connected with each other, the wave function in entire plate surface is completely determined.

§ 2. Properties of Field on Plate Surface.

Let Π_n and $\Pi_n{}^*$ be electric and magnetic Hertz vectors and i_1, i_2, i_3 be unit vectors along u_1, u_2, u_3 lines respectively. The field on plate surface due to both Hertz vectors is

$$\begin{aligned} E &= \nabla\nabla\Pi+k^2\Pi, & E^* &= -j\omega\mu\nabla\times\Pi^*, \\ H &= j\omega\varepsilon\nabla\times\Pi, & H^* &= \nabla\nabla\cdot\Pi^*+k^2\Pi^*. \end{aligned} \qquad (2.1)$$

---

* Precisely speaking, the factor $\exp(\pm jk^{(2)}\eta)$ must be $a\exp(\pm jk^{(2)}\eta)$, where a and $k_m{}^{(2)}$ may be slowly variable functions of η. But since this variation is small compared with the sinusoidal variation of $\exp(\pm jk_m{}^{(2)}\eta)$ and V_{mn}, we have neglect this fact.

** Concerning the practical solutions we shall see in my next paper with the tittle "*Approximate Evaluation of Electromagnetic Oscillating Modes on Plate Conductor with slowly curved Edge.*"

Hence

$$\Pi = \psi i_3, \qquad \Pi^* = \psi^* i_3, \qquad \text{(on central domain)} \tag{2.2}$$

$$\Pi = \bar{\psi} i_2, \qquad \Pi^* = \bar{\psi}^* i_2, \qquad \text{(on boundary domain)} \tag{2.3}$$

Since ψ_{mn} and ψ^*_{mn} satisfy (1.10) on the separating line, these functions must be approximately of the form

$$\left.\begin{aligned} \psi_{mn} &= (c_{mn} \cos k^{(1)}_{mn}\xi \mp c'_{mn} \sin k^{(1)}_{mn}\xi) \exp j(\pm k^{(2)}_m \eta \pm k^{(3)}_n \zeta) \\ \psi^*_{mn} &= (c^*_{mn} \cos k^{(1)}_{mn}\xi + c^{*\prime}_{mn} \sin k^{(1)}_{mn}\xi) \exp j(\pm k^{(2)}_m \eta \pm k^{(3)}_n \zeta), \end{aligned}\right\} \tag{2.4}$$

where

$$k^2 = (k^{(1)}_{mn})^2 + (k^{(2)}_m)^2 + (k^{(3)}_n)^2 = (k^{*(1)}_{mn}) + (k^{*(2)}_m)^2 + (k^{*(3)}_n)^2. \tag{2.5}$$

The two wave functions on boundary domain whose superposed field is continuously connected with the field of $\bar{\psi}$ are on the separating line

$$\left.\begin{aligned} \bar{\psi}_{mn} &= (A_{mn} \cos k^{(1)}_{mn}\xi + A'_{mn} \sin k^{(1)}_{mn}\xi) \exp j(\pm k^{(2)}_m \eta \pm k^{(3)}_n \zeta), \\ \bar{\psi}^*_{mn} &= (B_{mn} \cos k^{(1)}_{mn}\xi + B'_{mn} \sin k^{(1)}_{mn}\xi) \exp j(\pm k^{(2)}_m \eta \pm k^{(3)}_n \zeta). \end{aligned}\right\} \tag{2.6}$$

The fields are calculated by substituting (2.4) in (2.2) or (2.5) in (2.3) and using the relation (2.1). The field deduced from ψ in central domain and the field obtained by superposing the fields deduced from $\bar{\psi}$ and $\bar{\psi}^*$ in boundary domain are continuously connected on the separating line, if

$$\left.\begin{aligned} A_{mn} &= \frac{-(\pm k^{(2)}_m)(\pm k^{(3)}_n)}{k^2-(k^{(2)}_m)^2} C_{mn}, & B'_{mn} &= \frac{j\omega\varepsilon k^{(1)}_{mn}}{k^2-(k^{(2)}_m)^2} C_{mn}, \\ A_{mn} &= \frac{-(\pm k^{(2)}_m)(\pm k^{(3)}_u)}{k^2-(k^{(2)}_m)^2} C'_{mn}, & B_{mn} &= \frac{-j\omega\varepsilon k^{(1)}_{mn}}{k^2-(k^{(2)}_m)^2} C'_{mn}. \end{aligned}\right\} \tag{2.7}$$

The two wave functions in boundary domain whose superposed field is continuously connected with the field of ψ^*_{mn} are on separating line

$$\left.\begin{aligned} \bar{\psi}_{mn} &= (B^*_{mn} \cos k^{*(1)}_{mn}\xi + B^{*\prime}_{mn} \sin k^{*(1)}_{mn}\xi) \exp j(\pm k^{*(2)}_m \eta \pm k^{*(3)}_n \zeta), \\ \bar{\psi}^*_{mn} &= (A^*_{mn} \cos k^{*(1)}_{mn}\xi + A^{*\prime}_{mn} \sin k^{*(1)}_{mn}\xi) \exp j(\pm k^{*(2)}_m \eta \pm k^{*(3)}_n \zeta). \end{aligned}\right\} \tag{2.8}$$

The field of ψ^* in central domain and the superposition field of $\bar{\psi}$ and $\bar{\psi}^*$ given by (2.8) are continuosly connected on the separating line, if

$$\left.\begin{aligned} A^*_{mn} &= \frac{-(\pm k^{*(2)}_m)(\pm k^{(3)}_n)}{k^2-(k^{*(2)}_m)^2} C^*_{mn}, & B^{*\prime}_{mn} &= \frac{-j\omega\mu k^{*(1)}_{mn}}{k^2-(k^{(2)}_m)^2} C_{mn}, \\ A^{*\prime}_{mn} &= \frac{-(\pm k^{*(2)}_m)(\pm k^{*(3)}_n)}{k^2-(k^{*(2)}_m)^2} C^{*\prime}_{mn}, & B^*_{mn} &= \frac{j\omega\mu k^{*(1)}_{mn}}{k^2-(k^{*(2)}_m)^2} C^{*\prime}_{mn}. \end{aligned}\right\} \tag{2.9}$$

The functional forms of $\bar{\psi}_{mn}$ and $\bar{\psi}^*_{mn}$ in (2.6) and (2.8) in entire boundary domain are evaluated from (1.12) to (1·14). If we use φ^e_{mn} explained after (1.14) in place of φ_{mn} implied in $\bar{\psi}_{mn}$ and $\bar{\psi}^*_{mn}$, we denote them $\bar{\psi}^e_{mn}$ and $\bar{\psi}^{*e}_{mn}$. If φ^o_{mn} is used, they are $\bar{\psi}^o_{mn}$ and $\bar{\psi}^{*o}_{mn}$. The functional forms of ψ_{mn} and ψ^*_{mn} in (2.4) on entire central domain are determined, if we solve (1.1) so as to satisfy (2.7) or (2.9) on separating line assuming that the propagation constant perpendicular to plate surface is equal to $k^{(3)}_n$ or $k^{*(3)}_n$. If the values of ψ_{mn} are equal to each other on the corresponding points of both plate surfaces, the notation ψ^e_{mn} is used. But the signs of ψ_{mp} are reversed on the corresponding points of both plate surfaces, the notation ψ^{o}_{mp} is used.** If we remember that the differentation with respect only to u_1 is antisymetrical on both corresponding points, the following fact is easily provable.

---

* Concerning the practical evaluation of ψ and ψ using these conditions, I shall discuss in my next paper.

** As we shall see in my next paper $k^{(3)}$ of ψ_e and ψ_o do not coinside with each other. In order to show this discretely suffix p is used for ψ_o, while suffix n is used for ψ_e.

(i) The field of ψ^{e}_{mn} is continuously connected on the separating line with the superposition field of $\bar{\psi}^{e}_{mn}$ and $\bar{\psi}^{*o}_{mn}$.

(ii) The field of ψ^{o}_{mp} is continuously connected on the separating line with the superposition field of $\bar{\psi}^{o}_{mp}$ and $\bar{\psi}^{*e}_{mp}$.

(iii) The field of ψ^{*e}_{mn} is continuaously connected on the separating line with the superposition field of $\bar{\psi}^{*e}_{mn}$ and $\bar{\psi}^{o}_{mp}$.

(iv) The field of ψ^{*o}_{mp} is continuously connected on the separating line with the superposition field of $\bar{\psi}^{*o}_{mp}$ and $\bar{\psi}^{e}_{mp}$.

Though we can not express by ψ the oscillating modes on plate conductor as explained above, we shall use the notation ψ to express the mode on entire plate whose field coinsides with the field of ψ on central domain. If we remember (2.1), (2.2) and (2.3), we can easily prove that the fields of ψ^{e}_{mn} and ψ^{*o}_{mp} modes satisfy

$$\left.\begin{aligned} &E_z^{(+)} = -E_z^{(-)}, \quad E_x^{(+)} = E_x^{(-)}, \quad E_y^{(+)} = E_y^{(-)}, \\ &H_z^{(+)} = H_z^{(-)}, \quad H_x^{(+)} = -H_x^{(-)}, \quad H_y^{(+)} = -H_y^{(-)}, \end{aligned}\right\} \tag{2.10}$$

and that the fields of ψ^{o}_{mp} and ψ^{*e}_{mn} modes satisfy

$$\left.\begin{aligned} &E_z^{(+)} = E_z^{(-)}, \quad E_x^{(+)} = -E_x^{(-)}, \quad E_y^{(+)} = -E_y^{(-)}, \\ &H_z^{(+)} = -H_z^{(+)}, \quad H_x^{(+)} = H_x^{(-)}, \quad H_y^{(+)} = H_y^{(-)}, \end{aligned}\right\} \tag{2.11}$$

on the plate, where (+) and (—) in equations mean the field on the upper and lower plate surfaces respectively.

§ 3. Excitation of Oscillating Modes by External Field.

Let $\bar{E}, \bar{H}$ be the external field when the plate were not placed. When the plate are introduced in the field $\bar{E}, \bar{H}$, the field becomes the sum of $\bar{E}, \bar{H}$ and E, H where E, H are the field due to current and charge induced on the plate by $\bar{E}, \bar{H}$. Since the tangential electric and normal magnetic components must vanish on conductor, this field is subject to the following conditions.

$$\left.\begin{aligned} &\bar{E}_x+E_x = \bar{E}_y+E_y = \bar{H}_z+H_z = 0, \\ &\text{(on both surfaces of the plate)} \end{aligned}\right\}. \tag{3.1}$$

Since $\bar{E}, \bar{H}$ are continuous throughout the plate, E, H must satisfy (2.10) and not (2.11). Therefore, ψ^{o}_{mp} and ψ^{*e}_{mn} modes are not excited on the plate, and the field on the plate conductor is the linear combination of the fields of ψ^{e}_{mn} and ψ^{*o}_{mp} modes. The surface electric current density $\boldsymbol{K}$ and the charge density Q of these modes are given by

$$\boldsymbol{K} = -2(H_y^{(+)}i - H_x^{(-)}j), \quad Q = 2\varepsilon E_z^{(+)}, \tag{3.2}$$[2]

where i, j are unit vectors directed in x, y-directions, the field intensities on any observing point due to the source $\boldsymbol{K}$, Q are expressed as follows:

$$\left.\begin{aligned} \boldsymbol{E} &= \frac{1}{4\pi}\int_S \left\{-j\omega \boldsymbol{K}\frac{e^{-jkr}}{r} + \frac{1}{\varepsilon} Q \nabla\left(\frac{e^{-jkr}}{r}\right)\right\} dS, \\ \boldsymbol{H} &= \frac{1}{4\pi}\int_S \left\{\boldsymbol{K} \times \nabla\left(\frac{e^{-jkr}}{r}\right)\right\} dS, \end{aligned}\right\}, \tag{3.3}$$[3]

where r is the distance between observing point and the surface element dS of the plate and ∇ is the gradient operator acting on the plate surface.

Since $H_x^{(+)}$, $H_y^{(+)}$, $E_z^{(+)}$ and ψ^{e}_{mn} and ψ^{*o}_{mp} modes can be calculated by (2.1), (2.2) and (2.3), we can evaluate by (3.2) $\boldsymbol{K}$ and Q of these modes. Hence the field $\boldsymbol{E}$, $\boldsymbol{H}$ on any point are determined by (3.3).

Now we shall discuss the dispersing field due to the hole made on plate conductor of infinite breadth placed on xy-plane. If the hole were not made, the external field $\bar{E}', \bar{H}'$ propagated from $z>0$ side of plate is completely reflected by xy-plane. Hence

$$\bar{E}'_x = \bar{E}'_y = \bar{H}'_z = 0 \quad \text{(on all } xy \text{ plane).} \tag{3.4}$$

But $\bar{E}'_z$, $\bar{H}'_x$, $\bar{H}'_y$ may not be equal to zero on $z>0$ side of xy-plane. If we use $\bar{E}', \bar{H}'$ even when the hole is made, $\bar{E}'_z$, $\bar{H}'_x$, $\bar{H}'_y$ are zero on $z<0$ side of xy-plane, while these are not zero on $z>0$ side. Hence such a discontinuity of the field must be cancelled by superposing the field E', H' due to current and charge induced on the hole surface by $\bar{E}', \bar{H}'$. Since the sum of $\bar{E}', \bar{H}'$ and E', H' must be continuous through the hole surface, we have by (3.4)

$$\left.\begin{aligned} &E_x'^{(+)} = E_x'^{(-)}, \quad E_y'^{(+)} = E_y'^{(-)}, \quad H_z'^{(+)} = H_z'^{(-)}, \\ &\bar{H}_x'^{(+)} + H_x'^{(+)} = H_x'^{(-)}, \quad \bar{H}_y'^{(+)} + H_y'^{(+)} = H_y'^{(-)}, \\ &\bar{E}_z'^{(+)} + E_z'^{(+)} = E_z'^{(-)}, \quad \text{(on hole surface).} \end{aligned}\right\} \tag{3.6}$$

We now introduce the field $\boldsymbol{E}^{(+)}$, $\boldsymbol{H}^{(+)}$ which are combined with $\boldsymbol{E}'$, $\boldsymbol{H}'$ as follows:

$$\left.\begin{aligned} &\boldsymbol{E}^{(+)} = \boldsymbol{E}', \quad \boldsymbol{H}^{(+)} = \boldsymbol{H}', \quad \text{(on } z>0 \text{ side} \\ &\boldsymbol{E}^{(-)} = -\boldsymbol{E}', \quad \boldsymbol{H}^{(-)} = -\boldsymbol{H}', \quad \text{(on } z<0 \text{ side} \end{aligned}\right\}. \tag{3.7}$$

By (3.5) these field satisfy on plate surface

$$E_x^{(+)} = -E_x^{(-)}, \quad E_y^{(+)} = -E_y^{(-)}, \quad H_z^{(+)} = -H_z^{(-)}. \tag{3.8}$$

Since by (2.10) the fields of ψ_{mn}^{e} and ψ_{mn}^{*o} modes does not satisfy (3.8), these modes do not excited on the hole surface. Hence on the hole surface they must be linear combinations of the fields of ψ_{mn}^{o} and ψ_{mn}^{*e} modes. Since the fields of these modes satisfy (2.11), we have by (3.6) and (3.7)

$$\left.\begin{aligned} \bar{H}_x'^{(+)} + 2H_x^{(+)} &= \bar{H}_y'^{(+)} + 2H_y^{(+)} \\ &= \bar{E}_z'^{(+)} + 2E_z^{(+)} = 0, \\ &\text{(on the hole surface.)} \end{aligned}\right\}. \tag{3.9}$$

Since (2.11) is satisfied, there are no electric current and charge on the hole surface of ψ_{mp}^{o} and ψ_{mn}^{*e} modes. But the [illegible] are magnetic current K^* and charge Q^* of these modes given by the following formulae

$$\boldsymbol{K}^* = 2(E_y^{(+)}\boldsymbol{i} - E_x^{(+)}\boldsymbol{j}), \quad Q^* = 2\mu H_z^{(+)}. \tag{3.10}$$

The field $\boldsymbol{E}^{(+)}$, $\boldsymbol{H}^{(+)}$ on any point due to K^*, Q^* are given by

$$\left.\begin{aligned} \boldsymbol{E}^{(\pm)} &= -\frac{1}{4\pi}\int_S \left\{ \boldsymbol{K}^* \times \nabla\left(\frac{e^{-jkr}}{r}\right)\right\} dS, \\ \boldsymbol{H}^{(\pm)} &= \frac{1}{4\pi}\int_S \left\{ -j\omega\varepsilon \boldsymbol{K}^* \frac{e^{-jkr}}{r} \right. \\ &\qquad \left. + \frac{Q^*}{\mu}\nabla\left(\frac{e^{-jkr}}{r}\right)\right\} dS. \end{aligned}\right\}. \tag{3.11}$$

It is easily shown that the field $\boldsymbol{E}^{(\pm)}$, $\boldsymbol{H}^{(\pm)}$ given by (3.11) satisfy the condition on the plate, *i. e.*, the vanishment of tangential electric and normal magnetic field. The fields $\boldsymbol{E}'$, $\boldsymbol{H}'$ are calculated by combining (3.7) and express the field due to electric current and charge induced by external field $\bar{\boldsymbol{E}}'$, $\bar{\boldsymbol{H}}'$. The sum of $\bar{\boldsymbol{E}}'$, $\bar{\boldsymbol{H}}'$ and $\boldsymbol{E}'$, $\boldsymbol{H}'$ expresses the dispersing field due to the hole made on plate conductor of infinite breadth.

References.

(1) Stratton, Electromagnetic Theory, p. 54.
(2) Stratton, *loc. cit.* pp. 483-484, (1), (10).
(3) These are obtaied by replacing i by $-j$ in Stratton, *loc. cit.*, p. 466, (21).

On the Apparent Temperature Coefficient of Work Function.

By Tetsuya ARIZUMI.

Kawanishi Machine Works, Co. Ltd. Kobe.

(Read at Apr. 28, 1947; Received August 22, 1947)

§ 1. Introduction.

There are many methods to determine the thermionic constants experimentally. When the cathode surface is covered with an uniform work function, the value of thermionic constants, experimentally obtained by one method, coincides with the value by the other, but when there coexist many different work functions on the cathode surface, experimental value of thermionic constants depend upon the method to be used for their determination, as pointed out in foregoing several papers.(1) In these papers the author has shown that the work function obtained by the Richardson line method, φ_t^*, and the one by the initial velocity method, φ_k^*, are given by

$$\varphi_t^* = \frac{\sum\limits_n p_n\left(\varphi_n - T\frac{\partial\varphi_n}{\partial T}\right)\varepsilon^{-\frac{e\varphi_n}{kT}}}{\sum\limits_n p_n\varepsilon^{-\frac{e\varphi_n}{kT}}}, \tag{1}$$

$$\varphi_k^* = \frac{e}{kT}\log\left(\sum_n p_n\varepsilon^{-\frac{e\varphi_n}{kT}}\right) \tag{2}$$

respectively, where φ_n is the n-th work function and p_n the ratio of the area with the work function φ_n to the total surface area of the cathode. These formulae show that φ_t^* and φ_k^* are functions of temperature and thus the value of the temperature coefficient of work function depends upon the experimental method used for its determination. One will encounter practical difficulties in experimental determination of the temperature coefficient by means of the above-mentioned methodes, and especially it is almost impossible to make use of the Richardson line method, unless the variation of work function is very predominant. The methods mainly used for measurement of temperature coefficient are based on difference in contact potentials and the photoelectric phenomena, which in this paper are not touched. The third method is a calorimetric one which will be discussed with the Richardson line method and and the initial velocity method in this paper.

The experimental value of work function determined by the calorimetric method is, of course, equal to the value by other methods, so long as the work function is uniform over the cathode surface. When there co-exist many work functions on the cathode surface, what relationship does hold between the "average" work function measured by this method and the true one and between their temperature coefficients? What relationship does hold between two of experimental temperature coefficients measured by different methodes? In this paper these question will be answered and experimental results hitherto obtained will be discussed.

§ 2. Measurement of temperature coefficient by means of the initial velocity method.

The average work function experimentally determined by the initial velocity method is given by (2). When p_n is independent of temperature, φ_k^* is a function of T or $1/T$ and thus its temperature coefficient can be obtained by differentiating (2) with T. So.

$$\frac{\partial\varphi_k^*}{\partial T} = \frac{k}{e}\left(\log\sum_n p_n\varepsilon^{-\frac{e\varphi_n}{kT}}\right) + \frac{1}{T}\frac{\sum\limits_n p_n\left(\varphi_n - T\frac{\partial\varphi_n}{\partial T}\right)\varepsilon^{-\frac{e\varphi_n}{kT}}}{\sum\limits_n p_n\varepsilon^{-\frac{e\varphi_n}{kT}}} \tag{4}$$

Substituting (1) and (2) into (4),

$$\frac{\partial\varphi_k^*}{\partial T} = \frac{1}{T}(\varphi_k^* - \varphi_t^*) \tag{5}$$

As shown in the foregoing paper,

$$\varphi_k^* - \varphi_t^* = \frac{kT}{e}\log\frac{A}{A^*}. \tag{6}$$

Thus (5) is written in the simple form,

$$\frac{\partial\varphi_k^*}{\partial T} = \frac{k}{e}\log\frac{A}{A^*}. \tag{5'}$$

Apparently, it seems to be independent of the true temperature coefficients, but as seen from (4), there must be some relation between the "average" temperature coefficient and the true one, although more or less complicated. For simplicity, the case when n is equal to 2 will be considered. If

$$i_1 = p_1AT^2\varepsilon^{-\frac{e\varphi_1}{kT}} \gg p_2AT^2\varepsilon^{-\frac{e\varphi_2}{kT}} = i_2,$$

the following relation hold as shown in the foregoing paper,

$$\varphi_t^* = \varphi_1, \quad \varphi_k^* = \varphi_1 + \frac{kT}{e}\log\frac{1}{p_1}. \tag{7}$$

Thus (5) becomes

$$\frac{\partial\varphi_k^*}{\partial T} = \frac{\partial\varphi_1}{\partial T} + \frac{k}{e}\log\frac{1}{p}. \tag{8}$$

If $i_1 \ll i_2$, $\varphi_t^* = \varphi_2 = \varphi_k^*$

so that

$$\frac{\partial\varphi_k^*}{\partial T} = \frac{\partial\varphi_2}{\partial T}, \tag{8'}$$

is obtained. (8) and (8') show that the apparent temperature coefficiet coinsides with the true one only when almost all emission current comes from the portion with the higher work function, while the former is always larger than the latter when it is mainly contributed from the lower work function, because p_1 is always smaller than unity.

Now, assuming

$$\frac{\partial\varphi_1}{\partial T}=\frac{\partial\varphi_2}{\partial T}=\cdots\cdots=\frac{\partial\varphi_n}{\partial T}\equiv\frac{\partial\varphi}{\partial T}, \tag{9}$$

(4) reduces to

$$\frac{\partial\varphi_k^*}{\partial T}=\frac{\partial\varphi}{\partial T}+\frac{1}{T}(\varphi_k^*-\varphi_{ta}^*), \tag{5$''$}$$

where

$$\varphi_{ta}^*=\frac{\sum_n p_n\varphi_n\varepsilon^{-\frac{e\varphi_n}{kT}}}{\sum_n p_n\varepsilon^{-\frac{e\varphi_n}{kT}}} \tag{10}$$

and the following relation holds between φ_t^* and φ_{ta}^*.

$$\varphi_t^*=\varphi_{ta}^*-T\frac{\partial\varphi}{\partial T}. \tag{11}$$

φ_{ta}^* is the apparent work function purely due to the co-existance of many work functions. In the following it will be discussed whether the condition (9) does hold for general cases. For simplicity, the case when there co-exist only two different work function is considered. Putting

$$\frac{\partial\varphi_1}{\partial T}=\frac{\partial\varphi}{\partial T}+\Delta_1,\qquad \frac{\partial\varphi_2}{\partial T}=\frac{\partial\varphi}{\partial T}+\Delta_2 \tag{12}$$

the second term of (4) or (1) is written as follows:

$$\varphi_t^*=\frac{p_1\varphi_1\varepsilon^{-\frac{e\varphi_1}{kT}}+p_2\varphi_2\varepsilon^{-\frac{e\varphi_2}{kT}}}{p_1\varepsilon^{-\frac{e\varphi_1}{kT}}\;p_2\varepsilon^{-\frac{e\varphi_2}{kT}}}$$

$$-T\frac{\partial\varphi}{\partial T}-T\frac{p_1\Delta_1\varepsilon^{-\frac{e\varphi_1}{kT}}+p_2\Delta_2\varepsilon^{-\frac{e\varphi_2}{kT}}}{p_1\varepsilon^{-\frac{e\varphi_1}{kT}}+p_2\varepsilon^{-\frac{e\varphi_2}{kT}}} \tag{13}$$

In this case we have

$$\varphi_{ta}^*=\frac{p_1\varphi_1\varepsilon^{-\frac{e\varphi_1}{kT}}+p_2\varphi_2\varepsilon^{-\frac{e\varphi_2}{kT}}}{p_1\varepsilon^{-\frac{e\varphi_1}{kT}}+p_2\varepsilon^{-\frac{e\varphi_2}{kT}}}$$

So that the third term may be neglected as compared with the second term, the following condi. tions must be satisfied:

$$\text{if}\quad 1>\frac{p_2}{p_1}\varepsilon^{-\frac{e}{kT}(\varphi_2-\varphi_1)},\qquad \frac{\partial\varphi}{\partial T}>\Delta_1$$

$$\text{and}\quad\text{if}\quad 1<\frac{p_2}{p_1}\varepsilon^{-\frac{e}{kT}(\varphi_2-\varphi_1)},\qquad \frac{\partial\varphi}{\partial T}>\Delta_2. \tag{14}$$

When the difference of work functions is small, for example, when the work function depends only upon the cristallographinc orientation, the relation $\partial\varphi_n/\partial T>\Delta_n$, will hold for any n, and thus the relation (9) must hold for pure polycristalline cathodes.

To evaluate the true temperature coefficient $\partial\varphi/\partial T$, from the relation (5$''$), $\partial\varphi_k^*/\partial T$, φ_k^* and φ_{ta}^* are necessary to be known. Of these three quantities, the former two can be determined experimentally, but the last one cannot be obtained experimentally. It is, however, calculated theoretically when the work function of each cristal face and the ratio of areas with their own work functions to the total cathode surface area are known. Accordingly, the direct application of this method to a polycristalline cathode to determine the true temperature coefficient, is very difficult.

§ 3. Calorimetric method.

Another method to determine the work function experimentally is the calorimetric method[2]. The principle of this method is based upon the following fact; when an electron evaporates from the cathode, it takes from the cathode just as much as the heat of evaporation $e\left(\varphi+\frac{2kT}{e}\right)$. This cooling effect is measured by the variation of heating input to the cathode. When the work function is uniform all over the cathode surface, the experimental work function determined by this method is, of course, equal to the true one or experimental value obtained by other methods. However, when there co-exist many work functions on the same cathode surface, the experimental value is nothing but an "average" value in a sense. If φ_c^* is the "average" value and i_s is the total emission current, the heat taken from the cathode is given by

$$i_s\left(\varphi_c^*+\frac{2kT}{e}\right) \tag{15}$$

On the other hand, the true cooling effect is not uniform all over the cathode surface, but differs from place to place, so that it is given by

$$\sum_n i_n\left(\varphi_n+\frac{2kT}{e}\right) \tag{16}$$

Equating (15) to (16), the following relation is obtained.

$$\left(\varphi_c^*+\frac{2kT}{e}\right)\sum_n AT^2\varepsilon^{-\frac{e\varphi_n}{kT}}$$

$$=\sum_n\left(\varphi_n+\frac{2kT}{e}\right)AT^2\varepsilon^{-\frac{e\varphi_n}{kT}} \tag{17}$$

Thus, φ_c^* is given by

$$\varphi_c^*=\frac{\sum\limits_n p_n\varphi_n\varepsilon^{-\frac{e\varphi_n}{kT}}}{\sum\limits_n p_n\varepsilon^{-\frac{e\varphi_n}{kT}}} \tag{18}$$

Comparing with (1), the relation

$$\varphi_c^*=\varphi_t^*+T\frac{\sum\limits_n p_n\frac{\partial\varphi_n}{\partial T}\varepsilon^{-\frac{e\varphi_n}{kT}}}{\sum\limits_n p_n\varepsilon^{-\frac{e\varphi_n}{kT}}} \tag{19}$$

is easily deduced. If $\partial\varphi_n/\partial T$ vanishes for any n, φ_c^* coincides with φ_t^*. Davisson and Lester's result on pure tungsten is shown in table (1), showing that the coincidence between values obtained by both methods is satisfactory within experimental error. Even in the case of the oxide coated cathode several results(6) have been published without sufficient coincidence between φ_t^* and φ_c^*. In this case there is a predominant change in electron emission with time as pointed out by Blewett[7] and Kawamura[8]. So that exact value of work function must not be expected from this method in which it takes long time for measurement.

Table I

Thermionic constant of pure tungsten.

Observer	R, l, method	Cal, method
S. Dushmann & others (3)	4.53	
S. Davisson & L. H. Germer (4)	4.55	4.52
H. Lester (5)		4.43

§ 4. Measurement of temperature coefficient of work function by means os the calorimetric method.

As seen from (18), the experimental work function determined by the calorimetric method is is a function of temperature and thus it is easily differentiated with T;

$$\frac{\partial\varphi_c^*}{\partial T}=\left(\sum_n p_n\varepsilon^{-\frac{e\varphi_n}{kT}}\right)^{-2}\left[\frac{\partial}{\partial\left(\frac{1}{T}\right)}\left(\sum_n p_n\varphi_n\varepsilon^{-\frac{e\varphi_n}{kT}}\right)\cdot\left(\sum_n p_n\varepsilon^{-\frac{e\varphi_n}{kT}}\right)-\left(\sum_n p_n\varphi_n\varepsilon^{-\frac{e\varphi_n}{kT}}\right)\cdot\frac{\partial}{\partial\left(\frac{1}{T}\right)}\left(\sum_n p_n\varepsilon^{-\frac{e\varphi_n}{kT}}\right)\right] \tag{20}$$

Making use of (4) and the formulae

$$\frac{\partial}{\partial\left(\frac{1}{T}\right)}\left(p_n\varphi_n\varepsilon^{-\frac{e\varphi_n}{kT}}\right)=p_n\left\{\frac{e}{k}\left(T\frac{\partial\varphi_n}{\partial T}-\varphi_n\right)\varphi_n-T^2\frac{\partial\varphi_n}{\partial T}\right\}\varepsilon^{-\frac{e\varphi_n}{kT}}$$

$$\frac{\partial}{\partial\left(\frac{1}{T}\right)}\left(p_n\varepsilon^{-\frac{e\varphi_n}{kT}}\right)=p_n\left(T\frac{\partial\varphi_n}{\partial T}-\varphi_n\right)\varepsilon^{-\frac{e\varphi_n}{kT}}$$

(20) is written in the form,

$$\frac{\partial\varphi_c^*}{\partial T}=\frac{\sum\limits_n p_n\frac{\partial\varphi_n}{\partial T}\varepsilon^{-\frac{e\varphi_n}{kT}}}{\sum\limits_n p_n\varepsilon^{-\frac{e\varphi_n}{kT}}}+\frac{e}{kT^2}\left(\sum_n p_n\varepsilon^{-\frac{e\varphi_n}{kT}}\right)^{-2}\left\{\sum_n p_n\varphi_n\left(\varphi_n-T\frac{\partial\varphi_n}{\partial T}\right)\varepsilon^{-\frac{e\varphi_n}{kT}}\cdot\sum_n p_n\varepsilon^{-\frac{e\varphi_n}{kT}}-\sum_n p\varphi_n\varepsilon^{-\frac{e\varphi_n}{kT}}\cdot\sum_n p_n\left(\varphi_n-T\frac{\partial\varphi_n}{\partial T}\right)\varepsilon^{-\frac{e\varphi_n}{kT}}\right\} \tag{21}$$

The co-relation between $\partial\varphi_c^*/dT$ and $\partial\varphi_n/dT$ is too complicated to be predicted, but if (9) holds it becomes very simple as follows:

$$\frac{\partial\varphi_e^*}{\partial T}=\frac{\partial\varphi}{\partial T}+\frac{e}{kT^2}\left\{\frac{\sum\limits_n p_n\varphi_n^2\varepsilon^{-\frac{e\varphi_n}{kT}}}{\sum\limits_n p_n\varepsilon^{-\frac{e\varphi_n}{kT}}}-\left(\frac{\sum\limits_n p_n\varphi_n\varepsilon^{-\frac{e\varphi_n}{kT}}}{\sum\limits_n p_n\varepsilon^{-\frac{e\varphi_n}{kT}}}\right)^2\right\} \tag{22}$$

The first term of the right hand side is equal to the true temperature coefficient and the second term is the apparent one due to the co-existence of many work functions on the cathode surface.

Multiplying by AT^2 the numerator and denominator of the right hand side of (21), $\partial\varphi_c^*/\partial T$ is written by

$$\frac{\partial\varphi_c^*}{\partial T}=\sum_n\left(\frac{i_n}{i_s}\right)\frac{\partial\varphi_n}{\partial T}+\frac{e}{kT^2}\left\{\sum_n\left(\frac{i_n}{i_s}\right)\varphi_n\left(\varphi_n-T\frac{\partial\varphi_n}{\partial T}\right)\right.$$

$$\cdot\sum\left(\frac{i_n}{i_s}\right)-\sum_n\left(\frac{i_y}{i_s}\right)\varphi_n\cdot\sum_n\left(\frac{i_n}{i_s}\right)\left(\varphi_n\ \ T\frac{\partial\varphi_n}{\partial T}\right)\Bigg\} \qquad (21')$$

where

$$i_s=\sum_n i_n$$

which shows the total emission current from the cathode. In the special case when $n=2$, $\partial\varphi_c{}^*/\partial T$ is given by

$$\frac{\partial\varphi_c{}^*}{\partial T}=\left(\frac{i_1}{i_s}\right)\frac{\partial\varphi_1}{\partial T}+\left(\frac{i_2}{i_s}\right)\frac{\partial\varphi_2}{\partial T}$$

$$+\frac{e}{kT^2}\left(\frac{i_1}{i_s}\right)\left(\frac{i_2}{i_s}\right)(\varphi_1-\varphi_2)\left\{(\varphi_1-\varphi_2)-T\left(\frac{\partial\varphi_1}{\partial T}-\frac{\partial\varphi_2}{\partial T}\right)\right\} \qquad (21'')$$

where $\qquad i_s=i_1+i_2$

Neglecting the difference between $\partial\varphi_1/\partial T$ and $\partial\varphi_2/\partial T$, (21″) becomes

$$\frac{\partial\varphi_c{}^*}{\partial T}=\left(\frac{i_1}{i_s}\right)\frac{\partial\varphi_1}{\partial T}+\left(\frac{i_2}{i_s}\right)\frac{\partial\varphi_2}{\partial T}+\frac{e}{kT^2}\left(\frac{i_1}{i_s}\right)\left(\frac{i_2}{i_s}\right)(\varphi_2-\varphi_1)^2 \qquad (21''')$$

The first and second terms are true temperature coefficients of work function and the third term is the apparent temperature coefficient. If $i_1>i_2$, $\partial\varphi_c{}^*/\partial T$ is equal to the coefficient $\partial\varphi_1/\partial T$, and if $i_1<i_2$ it is equal to $\partial\varphi_2/\partial T$. The third term is symmetric with regard to i_1/i_s or i_2/i_s when the temperature is fixed and thus

if $i_1/i_s=0$ or $i_2/i_s=0$, $\quad\partial\varphi_c{}^*/\partial T=0$

and if $i_1/i_s=i_2/i_s$ or $i_1=i_2$, $\partial\varphi_c{}^*/\partial T$ becomes maximum,

§ 5. Measurement of the temperature coefficient of work function by means of the Richardson line method.

In the case of cathode in which there co-exist many work functions, the "average" work function determined by means of the Richardson line method is given by (1). Its temperature coefficient is easily obtained by differentiating (1) with T.

$$\frac{\partial\varphi_c{}^*}{\partial\left(\frac{1}{T}\right)}=\frac{1}{\left(\sum\limits_n p_n\varepsilon^{-\frac{e\varphi_n}{kT}}\right)^2}$$

$$\left[\frac{\partial}{\partial\left(\frac{1}{T}\right)}\left\{\sum_n p_n\left(\varphi_n-T\frac{\partial\varphi_n}{\partial T}\right)\varepsilon^{-\frac{e\varphi_n}{kT}}\right\}\cdot\sum_n p_n\varepsilon^{-\frac{e\varphi_n}{kT}}\right.$$

$$\left.-\sum_n p_n\left(\varphi_n-T\frac{\partial\varphi_n}{\partial T}\right)\varepsilon^{-\frac{e\varphi_n}{kT}}\cdot\frac{\partial}{\partial\left(\frac{1}{T}\right)}\left(\sum_n p_n\varepsilon^{-\frac{e\varphi_n}{nT}}\right)\right] \qquad (23)$$

making use of (4) and the following relation

$$\frac{\partial}{\partial\left(\frac{1}{T}\right)}\left\{p_n\left(\varphi_n-T\frac{\partial\varphi_n}{\partial T}\right)\varepsilon^{-\frac{e\varphi_n}{kT}}\right\}$$

$$=p_n\left\{T^3\frac{\partial^2\varphi_n}{\partial T^3}-\frac{e}{k}\left(\varphi_n-T\frac{\partial\varphi_n}{\partial T}\right)^2\right\}\varepsilon^{-\frac{e\varphi_n}{kT}}$$

(23) becomes

$$\frac{\partial\varphi_c{}^*}{\partial T}=\frac{e}{kT^2}\frac{1}{\left(\sum\limits_n p_n\varepsilon^{-\frac{e\varphi_n}{kT}}\right)^2}\times$$

$$\left[\sum_n p_n\left(\varphi_n\ -T\frac{\partial\varphi_n}{\partial T}\right)^2\varepsilon^{-\frac{e\varphi_n}{kT}}\cdot\sum_n p_n\varepsilon^{-\frac{e\varphi_n}{kT}}\right.$$

$$\left.-\left\{\sum_n p_n\left(\varphi_n\ \ T\frac{\partial\varphi_n}{\partial T}\right)\varepsilon^{-\frac{e\varphi_n}{kT}}\right\}^2\right]-T\frac{\sum\limits_n p_n\frac{\partial^2\varphi_n}{\partial T^2}\varepsilon^{-\frac{e\varphi_n}{kT}}}{\sum\limits_n p_n\varepsilon^{-\frac{e\varphi_n}{kT}}} \qquad (24)$$

As seen in (24), the second derivative is contained in the formula, differing from other methodes. The co-relationship between the apparent temperature coefficient $\partial\varphi_t{}^*/\partial T$ and the true one are very complicated in the above expression, but, if the above mentioned conditions (9) and $\partial^2\varphi_n/\partial T^2=0$ are satisfied, (24) becomes a very simple expression:

$$\frac{\partial\varphi_t{}^*}{\partial T}=\frac{e}{kT^2}\left\{\frac{\sum\limits_n p_n\varphi_n{}^2\varepsilon^{-\frac{e\varphi_n}{kT}}}{\sum\limits_n p_n\varepsilon^{-\frac{e\varphi_n}{kT}}}-\left(\frac{\sum\limits_n p_n\varphi_n\varepsilon^{-\frac{e\varphi_n}{kT}}}{\sum\limits_n p_n\varepsilon^{-\frac{i\phi_n}{kT}}}\right)^2\right\} \qquad (25)$$

Multiplying by AT^2 the numerator and denominator of the right hand side of the above fomula, (25) is written as a function of the emission current, i_n;

$$\frac{\partial\varphi_t{}^*}{\partial T}=\frac{e}{kT^2}\left\{\sum_n\left(\frac{i_n}{i_s}\right)\varphi_n{}^2-\left(\sum_n\frac{i_n}{i_s}\varphi_n\right)^2\right\} \qquad (26)$$

Similarly, the more general expression can be deduced from (24),

$$\frac{\partial\varphi_t{}^*}{\partial T}=\frac{e}{kT^2}\left[\sum_n\left(\frac{i_n}{i_s}\right)\left(\varphi_n-T\frac{\partial\varphi_n}{\partial T}\right)^2\right.$$

$$\left.-\left\{\sum_n\left(\frac{i_n}{i_s}\right)\left(\varphi_n-T\frac{\partial\varphi_n}{\partial T}\right)\right\}^2\right]-T\sum_n\left(\frac{i_n}{i_s}\right)\frac{\partial^2\varphi_n}{\partial T^2} \qquad (24')$$

Comparing (22) with (25), the important relation

$$\frac{\partial\varphi_c^*}{\partial T} - \frac{\partial\varphi_t^*}{\partial T} = \frac{\partial\varphi}{\partial T} \qquad (26)$$

can be obtained. This shows that when there is no difference between work functions of cristal faces or their difference are negligibly small, the difference between the temperature coefficient obtained by means of calorimetric and Richardson line methodes gives the true temperature coefficient. To determine in practice the temperature coefficient from the Richardson line method, however, is a very diffcult task, and thus, to obtain the true temperature coefficient from the relation (26) will be difficult. But when values of work functions of cristal faces are already known, $\partial\varphi_t^*/\partial T$ is calculated from (25) or (25′) and from these values and $\partial\varphi_c^*/\partial T$, the true coefficient $\partial\varphi/\partial T$ will be evaluated. As seen in (26), $\partial\varphi_c^*/\partial T$ coincides with $\partial\varphi_t^*/\partial T$ only when the true coefficient vanishes.

§ 6. An example.

As an example, the case when there co-exist only two different work functions $\varphi_1 = 3.0$ e. v. and $\varphi_2 = 4.0$ e. v. will be discussed at first. In this case, the variation of φ_t^* and φ_k^* are shown in the foregoing papers[9] and thus only the temperature coefficient will be treated. For simplicity φ_1 and φ_2 are assumed to have the same true temperature coefficient, that is,

$$\frac{\partial\varphi_1}{\partial T} = \frac{\partial\varphi_2}{\partial T} = \frac{\partial\varphi}{\partial T}.$$

$\partial\varphi_k^*/\partial T$ is easily calculated from these values of φ_k^* and φ_t^* obtained in foregoing papers. In Fig. 1 the temperature variation of $\partial\varphi_k^*/\partial T$ is shown with p as a paremeter. The temperature range is from 1,200°K to 2,200°K. When p is equal to 10^{-1}, $\partial\phi_k^*/\partial T$ is almost constant, $2\cdot10^{-4}$ e. v./deg., over all temperature range. When p becomes smaller, the variation of $\partial\varphi_k^*/\partial T$ becomes more predominant and when p is nearly equal to 10^{-4}, the temperature variation is maximum. If p decreases beyond this value, $\partial\varphi_k^*/\partial T$ begins to decrease and at $p = 10^{-6}$ its variation is only between 10^{-4} e. v./deg. and zero. In Fig. 2 the variation of $\partial\varphi_k^*/\partial T$ is shown verus p and T as a parameter, where instead of p, log. p is used. The variations of $\partial\varphi_k^*/\partial T$ v. s. T are very complicated while its variations v. s. log. p are much simpler. When the temperature is lower the maximum value of $\partial\varphi_k^*/\partial T$ is larger and these maximum points shifts to the smaller p value, In all cases the initial increases of these curves are almost linear.

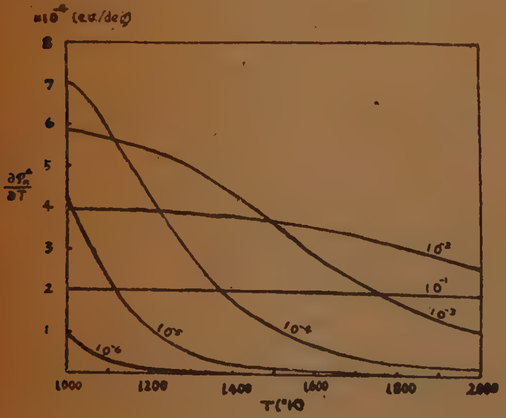

Fig. 1.

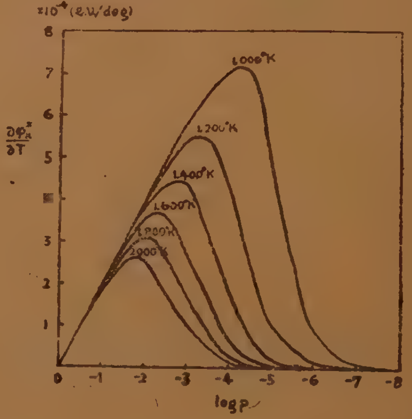

Fig. 2

Under the condition (27), $\partial\varphi_t^*/\partial T$ is quite equal to $\partial\varphi_c^*/\partial T$, which is calculated from the relation (21′′). Wheh i_2/i_s is used instead of log. p, the curves are parabola quite symmetrical with regard to $i_2/i_s = 0.5$. Such relations are shown in

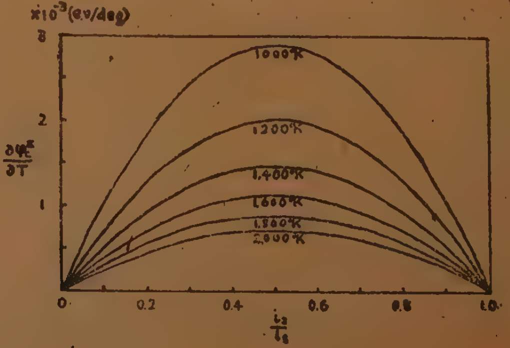

Fig. 3

Fig. 3. When the temperature is lower, the maximum value of $\partial\varphi_c^*/\partial T$ becomes larger. In Fig. 4 $\partial\varphi_c^*/\partial T$ is shown against T with i_2/i_s as a parameter. All curves decrease uniformly with the increase of temperature, but their variation is larger when i_2/i_s is larger. If the above two Figs. are transformed into the Figs. in which p is ordinate, curves become very complicated as shown in Figs. 5 and 6. From Fig. 5 in which the ordinate is log. p and the parameter T, it is seen that the maximum values of $\partial\varphi_c^*/\partial T$ are larger and their maximum points situate at smaller p, when the temperature is lower. The remarkable difference to $\partial\varphi_k^*/\partial T$ is that (1) the former is always larger than the latter, and (2) the former is not zero over rather a wide range of p, while the latter is limited in much nallower range. Fig. 6 shows the temperature variation of $\partial\varphi_c/\partial T$ with p parameter. As seen in this Fig., curves are very complicated. At $p = 10^{-2}$, $\partial\varphi_c^*/\partial T$ increases monotonously with the increase of temperature, while they decrease monotonously with the increase of temperature, when p become s smaller than 10−

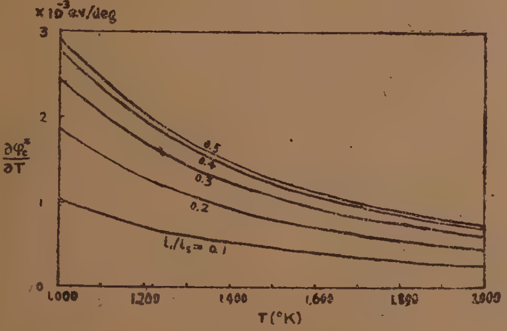

Fig. 4

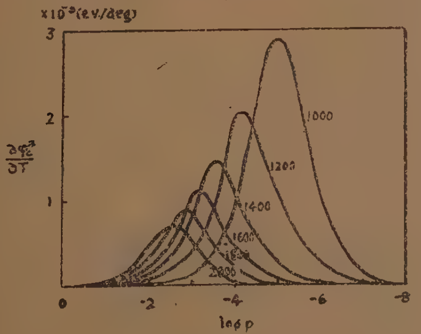

Fig. 5

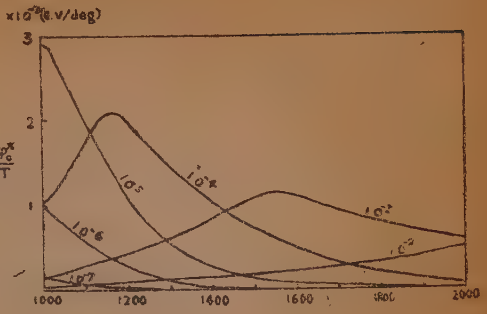

Fig. 6

In the intermediate region, the curves have a maximum as seen in the curves $p = 10^{-4}$. This is a remarkable difference between $\partial\varphi_k^*/\partial T$ and $\partial\varphi_c^*/\partial T$.

In the above mentioned special case when there co-exist only two different work functions and their difference is more or less large, these curves are of very special forms as seen in the Figs. from 1 to 6, but in such general cases as when there co-exist many work functions and their difference is very small, for example, in cases of pure polycristalline metals, such special phenomena as described in the above paragraph will not be experienced.

§ 7. In the case of oxide-coated cathode.

The temperature coefficient of work function of the oxide-coated cathode was determined by means of the initial velocity method and its value is found to be $3.60 \cdot 10^{-4}$ e. v./deg. This experiment was carried out by Sano.[10] Unfortunately the activation degree of the cathode used in his mesurement is quite unknown so that the direct comparison of the present theory with his experiments is impossible. As shown in the previous paper, however, in the best activated state of the oxide-coated cathode its work function at 800°K is as followed:

$$\varphi_t^* = 1.00 \text{ e. v. and } \varphi_k^* = 1.46 \text{ e. v.}$$

Thus, $\partial\varphi_k^*/\partial T$ is given by 5.8×10^{-4} e. v./deg., in good accordance with Sano's result within experimental error.

In the case of the oxide-coated cathode it remains questioned still to be whether the assumption (9) holds, because the work function φ_1 and φ_2 are written by

$$\varphi_1 = \frac{1}{2}E+V \quad \text{and} \quad \varphi_2 = E+V \qquad (29)$$

respectively, according to the present semi-conductor theory[11], where E is the energy difference between conduction band and impurity level and V that between conduction band and vacuum level. Thus, the temperature coefficient depends upon whether E or V is a fuction of T. If V is a constant and E a function of T, $\partial\varphi_1/\partial T$ must differ from $\partial\varphi_2/\partial T$, while if E is a constant and V a function of T, $\partial\varphi_1/\partial T$ must be equal to $\partial\varphi_2/\partial T$.

As pointed out in § 2, $\partial\varphi_k{}^*/\partial T$ is given by (8) at the best activated state, while at the non-activated state it is given by (8′), If p_1 is well known $\partial\varphi_1/\partial T$ is calculated from (8). In the case when E is a constant and V is a function of temperature, $\partial\varphi_1/\partial T$, calculated from (8) is equal to the experimental result obtained at the non-activated state, while in the case when V is constant and E is a function of temperature, the former must differ from the latter. That is, the important question whether E or V is a function of temperature will be answered by measuring the temperature coefficient both at the best activated state and at the non-activated state. Up to the present, however, experiments are still too insufficient to answer the above question.

§ 8. Temperature coefficient of work function of pure polycristalline tungsten.

In the case of pure tungsten, the thermionic work function of comparatively many cristal faces have been known. In Table II, data obtained by Nichols (12) are shown where he measured the thermionic constant of five cristal faces.

Table II

Thermionic constants of pure tungsten

Cristal face	(111)	(112)	(116)	(001)	(110)
A	35	125	53	117	15
φ	4.35	4.66	4.36	4.53	4.65

On the surface of polycristalline wire, many other faces than the above mentioned faces will appear. It is still to be questioned what kinds of faces frequently appear on the polycristalline wires. In the following calculation it is assumed that only the above five faces appear with the same chance. The calculated temperature coefficient are shown in Table III.

Table III

Temperature coefficient of work function of pure tungsten

	temperature 1,500°K	2,200°K	experimental value	$\partial\varphi/\partial T$
$\partial\varphi_k{}^*/dT$	3.255	1.832	8.0	ca. 4.7
$\partial\varphi_c{}^*/dT$	4.345	2.595	6.0	ca. 3.5

As seen in the above table $\partial\varphi_k{}^*/\partial T$ is smaller than $\partial\varphi_c/\partial T$ and the experimental values[13] are always larger than theoretical ones. This shows the existence of the true temperature coefficient. Probably it is about 4.0 e.v./deg. Measured values of the temperature coefficient are almost constant probably because the true one is comparatively large. This is a cause to the result that the temperature coefficient experimentally obtained by several methods is independent of temperature.

§ 9. Conclusion.

On the cathodes where there co-exist many work functions such as the polycristalline wire, the temperature coefficient of work function experimentally determined by several methods were calculated by the theory developed in foregoing several papers. The temperature coefficient determined by the initial velocity method seems to be independent of the true temperature coefficient and it is given by a simple relation as shown in (5′) or (6). On the other hand, the temperature coefficient of work function determined by means of the Richardson line method or the calorimetric method are complex functions of true temperature coefficients. In the special case when true temperature coefficients of all cristal faces are the same, the "avarage" temperature coefficient becomes very simple forms. It is divided into two parts: one is the true coefficient and the other is the apparent coefficient caused by the co-existence of many work functions. They are given by (22) and (25) respectively. The true temperature coefficient is equal to the difference of both "average" temperature coefficients. At the present state, it is more or less difficult to determine the true temperature coefficient of work function by the above procedure. Moreover, it is more difficult to determine the true value by comparing the theoretical and experimental results. In this paper such comparison was carried out on the oxide coated cathode and the tungsten, the exact value could not be obtained probably because of more or less large experimental errors are accompanied by experiments hitherto obtained. According to the calculated results, however, it will be concluded that the true temperature coefficient is smaller than the results experimentally determined up to the present time and it is independent of temperature.

Reference.

(1) T. Arizumi, Proc. Phys. Soc. Japan.
(2) Schottky: Handbuck d, Experimental Physik (Leipzig 1928) 111-2.
(3) S. Dushmann & others: Gen. El. Rev., **26**, (1923) 139; Phys. Rev., **25** (1425) 338.
(4) C. Davisson & L. H. Germer: Phys. Rev., **20** (1922) 300: ebenda, **30** (1927) 634.
(5) H. Lester: Phil. Mag., **31** (1916) 197.
(6) See, for example, T. Arizumi: Proc. Phys. Soc. Japan.
(7) Blewett: Phys, Rev., **55** (1939) 714.
(8) H. Kawamura & A. Shinohara: Matsuda Kenkyu Jiho, **17** (1942) 453.
(9) T, Arizumi: loc. cit.
(10) S. Sano: J. Elec. Comm. Japan (in Japanese) **27** (1944) 166.
(11) H. Kawamura: J. Phys-Math Soc. Japan (in Japanese) **17**, (1944) 159.
(12) M. H. Nichols: Phys, Rev., **59**, (1941) 944.
(13) F. Krüger & G. Stabenow: Ann. d Phys., **22**, (1935), 713; S. Sano & K. Koga: J. Elec. Comm. Japan. (In Japanese) **27** (1944) 483.

Idea and Design of Wire-and-Plate Type Counter.

By Kazuji HASIMOTO.

The Hitati Central Research Laboratory.

(Received August 22, 1947)

The parallel wire-and plate type counter which is convenient to the measurement of cosmic ray shower has been recently constructed. Fig. 1 and Fig. 2 show the general and preliminary designs of the counter. Three or five central tungsten wires are put between two parallel plates.

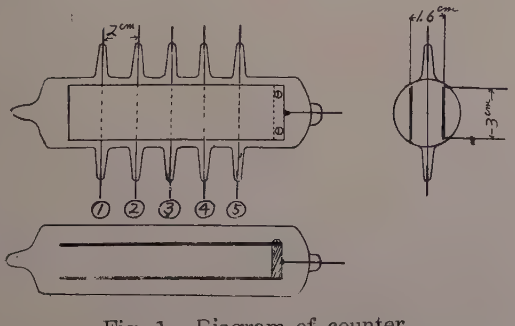

Fig 1. Diagram of counter.
(five central wires)

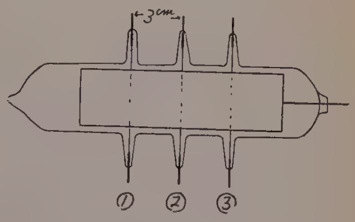

Fig. 2. Diagram of counter.
(three central wires)

The central wires are arranged 2 or 3 cm apart from each other and the parallel brass plates which sandwich the central wires are both 15 cm long.

and 3 cm wide as shown in Fig. 1 and Fig. 2.

Fig. 3. Photograph of a counter. (five central wires)

Fig. 3 is the photograph of the test counter which countains five central wires.

The central wires may be denoted No. 1. No. 2. and so on. It is desirable to seal the argon and alcohol into the counter, but in this preliminary investigation, dried air and alcohol have been sealed up at 50 mmHg and 10_{mm}Hg respectively which are substituted for argon. The characteristic curves of thesecounters are shown in Fig. 4 and Fig. 5.

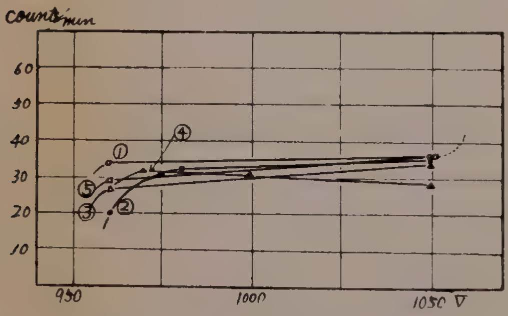

Fig. 4. Characteristic curves. (5 central wires

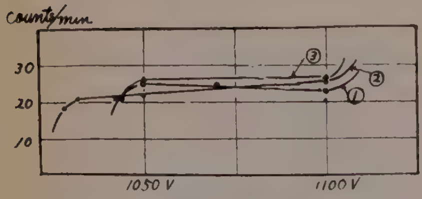

Fig. 5. Characteristic curves. (3 central wires)

In this case the counter pulse and plateau are not so excellent as those of counter containing argon and alcohol.

It is important to examine whether or not the discharge of one special central wire is induced by the neighbouring discharge. These experiments have been carried out as follows. Let C be the counting rate obtained from one special central wire when neighbouring wires are in action, and C' be its rate when others are not in action. If there occurs no induced discharge on the special central wire from neighbouring ones, C may be equal to C': otherwise C may be larger than C' by the induced phenomena. Therefore, C/C' may denote the mutual induction effect of the neighbouring wires. Table I shows these experimental data. In table I, the notation 1_{2345} etc, mean the counting rate obtained from the central wire No. 1 when neighbouring wires No. 2 etc, are in action, and the notation 1 etc, without suffix means the counting rates of No. 1 alone. Moreover, if two or three central wires are connected together counting rate may be two or three times larger than that of individual wire. Table II shows the results of counting rate obtaind from the test counter which has three central wires. In Table II, 2+3 etc, show the counting value in the case when No. 2 and No. 3 central wires are connected. These measurements of counting have been carried out by the natural counts. As shown in Table I there are some chances of mutual induced discharge by neighbouring cental wires.

Table I. The quantity of the induced counting rates

C : The counting rates obtained from one special central wire when neighbouring wires are in action

C' : Counting rates when others are not in action.

Connection	1_{2345}	2_{1345}	3_{1245}	4_{2235}	5_{1234}
$\frac{C}{C'}$	1.1	1.2	1.5	1.3	1.3
Connection	1_2	1_3	1_4	1_5	
$\frac{C}{C'}$	1.2	1.1	1.1	1.1	
Connection	3_2	3_4	3_1	3_5	
$\frac{C}{C'}$	1.2	1.2	1,1	1.0	

Table II. Counting rates obtained from three central wires.

connections of central wires	1	2	3	1+2	1+3	1+2+3
counts/min	23.6	24.8	24.4	48.8	49.6	69.0

These chances, however, may be decreased or eliminated by the further improvement of the counter.

The counter pulse of the connected central wires is observed in part to be multiplied in its height in comparison with that of special one according to coincident discharge. For example, in the case of five central wires where they are connected together the height of pulse may be five times greater when the discharge has occured at the same time. Table III shows an example of the percentage of double-height pulses in the total pulsations when two of the central wires are connected.

Table III. The percentage of the double height pulses in the total pulsations when two central wires are connected,

distance between two central wires	% of double height pulse
2 cm	45
3 cm	27
4 cm	12
6 cm	4.3
8 cm	a little

The author has described here on the construction and character of the parallel-plate-type counter.

If the excellent counter of this type is constructed under the idea and design mentioned above, accurate measurement of the cosmic ray shower may carried out more conveniently because it requires many small counters to be arranged.

The author is especially indebted to Dr, Y. Toriyama for his generous and stimulating discussions on the various points in the course of this study.

Notes on the Production of Geiger-Mueller Counters and the Discharge Mechanism.

Kazuji Hashimoto.

The Hitachi Central Research Laboratory.

(Received August 22, 1947)

§ 1. Introduction.

As is well known the Geiger-Mueller counters contain argon and alcohol vapour at the rate of the optimum condition. However, if the production has been carried out with careless arrangement of the evacuating system, the counter with the same character can not always be obtained, for it is difficult to fill all the counters with the gas and vapour at the same proportion. The most skilful method about the distribution of gas has been examined from the standpoint of discharge mechanism of the counters.

This method will serve as a reference in sealing two or more kinds of vapour in the vacuum tube.

§ 2. Gas Mixture and Characteristic Curve.

It is necessary to seal argon gas and alcohol vapour in the exact proportion to give the counters the same character. In the present experiment the gas consists of alcohol (10 mmHg) and argon (50 mmHg), for the most excellent voltage plateau of the counter will be obtained as shown in Fig. 1 (curve D) in this optimum pressure.

When the total pressure is constant at 60 mm Hg. we obtain curve D having the most sufficient character.

If the pressure of alcohol vapour is too high or too low the starting potential, at which the counter begins to work, and voltage plateau are

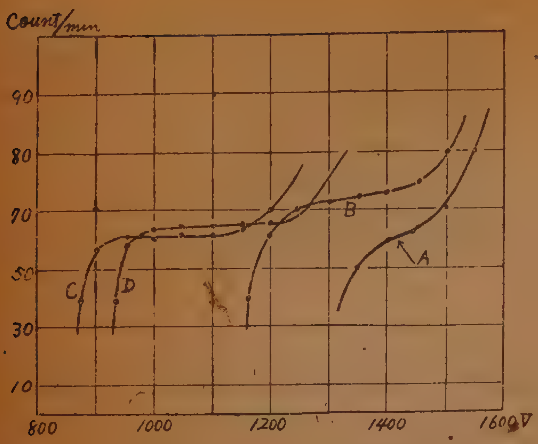

Fig. 1 The characteristic curves of the counter contains various gas compositions.

A: Alcohol: 30 mm Hg, Argon: 30 mm Hg
B: Alc: 20 mm Hg, Ar: 40 mm Hg
C: Alc: 5 mm Hg, Ar: 55 mm Hg
D: Alc: 10 mm Hg, Ar: 50 mm Hg

changed as shown in Fig. 1. The anode of the counter used in this experiment is 0.1 mm tungsten wire, and the cylindrical cathode is of brass approximately 10 cm long and 2.3 cm in diameter.

§ 3. New Technique about Gas Sealing

To fill up gases in the counters the author adopted formerly the method as shown in Fig. 2. At alcohol vapour was admitted into the counter at first, 10mmHg, and subsequently argon at 50mmHg.

In this method the alcohol vapour which remains in the glass piping was pushed by the argon subsequently admitted so that, remote counters A, A′, B, B′, etc. in order contain more excess alcohol vapour than the counters D, E, D′.

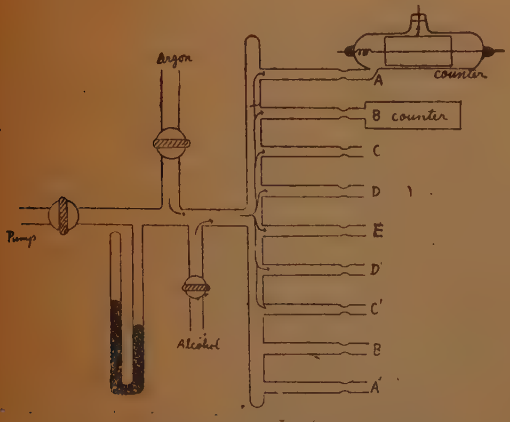

Fig. 2. Diagram of gas distribution. (formerly adopted)

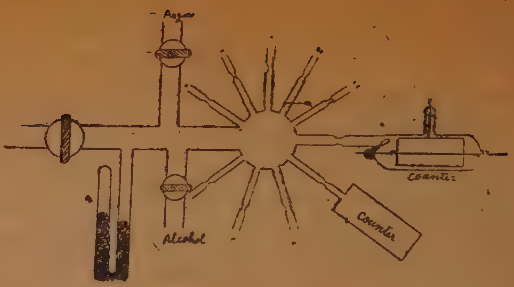

Fig. 3. Diagram of gas distribution. (new method)

The characteristic curves of these counters A, A′ etc. resemble the curve A or B as shown in Fig. 1. respectively, for they contain excess alcohol vapour.

But counters D, E, D′ show that excellent character which is shown by the curve D in Fig. 1. Now the author adopted a new method as shown in Fig. 3.

By this method alcohol vapour is not pushed especially into the special counter by argon and naturally every counter can contain argon and alcohol vapour at desirable proportion and their characters remain always the same.

There is more skilful method that argon and alcohol are mixed previously in order to seal the vapour into the counter at desirable proportion.

§ 4. On the Discharge Mechanism.

The fact that the counters AA′ etc which were produced by the method as shown in Fig. 2. do not contain argon and alcohol vapour at desirable ratio have been proved by the identification of every characteristic curves of the counter with the curves shown in Fig. 1. However, the experimental fact that the starting potential and the voltage plateau are changed with the variation of the vapour pressure and the composition of the sealed gas may also be proved from the standpoint of the electric discharge mechanism of the counter. Especially the starting potential of a Geiger-Mueller counter may be calculated approximately in advance, if desired, for the ideal case of a perfectly smooth cylinder and central wire. In practice it sometimes happens that the potential to be applied to the counter with a mixted gas at known pressure, must be caluculated.

In such a case it may be secured by using the following consideration of the electric discharge mechanism with the corresponding equation. Let E_x be the field intensity at x apart from the central wire, then,

$$E_x = \frac{V}{x \log \dfrac{R}{r}},$$

where V is the potential difference between the cylinder and the central wire, R the radius of the cathode cylinder, and r the radius of the central wire. Let W be the energy of an electron accelerated between the cylinder and the central wire, then,

$$W = Ve = \int_r^R E_x e\, dx.$$

If E_r is the field intensity at the surface of the wire, then,

$$\frac{E_r}{E_x} = \frac{x}{r}.$$

Therefore, the potential difference necessary to produce a field intensity E_r at r is given by

$$V = \int_r^R E_r\, r \cdot \frac{1}{x}\, dx = E_r r \log \frac{R}{r} \quad \text{.............(1)}$$

An electron produced in the Geiger-Mueller counter moves to the central wire by the electric field and ionizes alcohol molecules or excites argon atoms in the field with rapidly changing intensity which appears near the central wire. The excited argon radiates photons which ionize alcohol molecules so that the cumulative ionization of alcohol molecules occurs along the central wire by the catalytic action of argon. When the positive ion sheath of alcohol is produced along the central wire according to its immobility, the steep central field and therefore the electric discharge in the counter may disappear.

If the cumulative ionization of alcohol vapour in the field on the central wire, E_r multiplied by the mean free path λ_{12} of an electron must be equal to the ionization potential V_i of alcohol at the pressure and temperature used, then,

$$V_i = E_r \lambda_{12} \quad \text{.....................(2)}$$

From equation (1) and (2) the following equation may be obtained.

$$V = \frac{V_i}{\lambda_{12}} r \log \frac{R}{r} \quad \text{.................(3)}$$

(3) gives the starting potential difference. The mean free path λ_{12} of an electron in the mixed gas, alcohol and argon, is given by

$$\lambda_{12} = \frac{\lambda_1 \lambda_2}{(n_1 \sqrt{\lambda_2} + n_2 \sqrt{\lambda_1})^2} \quad \text{.............(4)}$$

Where n_1, n_2, is the mixing ratio of gases, and λ_1, λ_2 are the mean free paths of an electron in argon and alcohol respectively. When these equations are applied to the counters of various gas composition the starting potential may be computed by the substitution of the following concrete values, namely

$r = 0.005$ cm $\quad R = 1.15$ cm

$V_i = 10.8 \sim 11.0$ eV (ionization potential of alcohol)

λ_1 (alcohol) $= 0.009$ cm (at 1 mm Hg)

λ_2 (argon) $= 0.027$ cm (at 1 mm Hg)

Table I shows, with respect to various gas composition, the starting potential of the counters computed from the equation (3) and (4) and the concrete values compared with the experimental data. Here the theoretical starting potential are somewhat different from the actual experimental data.

This difference may be due to the fact that the pressure of the mixed gas and the size of the wire and cylinder are not known accurately enough to give closer results, or due to the slight irregularities in the structure of counters, wire and cylinder. More plausible explanation, however, is that the amplification is not great enough to record the impulses until the voltage reaches the experimental value.

Aknowledgment.

The author wishes to thank Dr. Y. Toriyama and Dr. H. Hamada for their interest and suggestions throughout the progress of this research.

Table I The starting potential of the counter for various gas composition.

gas ratio.	Mean free path of an electron λ_{12} (60 mm Hg)	Starting potential (V) (theoretical value)	Starting potential (V) (experimental value)
Alcohol : 10 mm Hg Argon : 50 mm Hg	0.00035 cm	860	950
Alc. : 20 mm Hg Ar. : 40 mm Hg	0.000285	1050	1150
Alc. : 30 mm Hg Ar. : 30 mm Hg	0.00024	1250	1350

Three Point Spark Discharge Tube.

Kazuji HASHIMOTO.

The Hitachi Central Research Laboratory.

(Received August 22, 1947)

§ 1. Introduction.

Resently the three point spark discharge tube which was used for the modulation of the magnetron has been in demand for the relay and the substitution of thyratron. The tube possesses two electrodes, anode and cathode: the latter has a needle point which plays the auxiliary electrode for the spark discharge. Generally this discharge tube contains hydrogen at 300 mm Hg. Here it is investigated how the time lag and disorder of main spark discharge are affected by the pressure of hydrogen and by the size and form of the electrodes.

§ 2. Description of the Tube and Electric Circuits.

Fig. 1 is a vertical section of the tube. The main semi-spherical electrodes, anode A and cathode B, which are situated 10 mm apart from each other, are sealed up in the glass tube. The cathode has a hole of 0.5 mm in diameter at the top and two auxiliary needle electrodes C and E are situated closely to this hole.

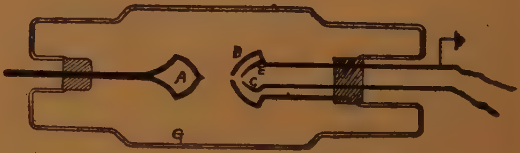

Fig. 1. Diagram of vertical section through the tube.

A: anode. B: cathode. C: needle point. E: needle point connected to B. G: glass tube.

When the constant voltage about 4 kv is applied between main electrode A and B and sufficient voltage of 500 cycle for sparking is applied to the auxiliary needle electrode the spark discharge occurs in the main gaps A and B with the same frequency. Some optimum conditions satisfied by this spark discharge tube must be as follows:

1) The main spark discharge must occur by the needle spark discharge at one to one correspondence.
2) The durations of both main and auxiliary discharge must be as short as possible.
3) The time lag between the main discharge and auxiliary one is constant and its disorder must

be within 0.1 μs at most.

4) The life of the tube is desirable to be long.

Above all, tungsten needle and molybdenum cathode cap have to be prevented from being consumed.

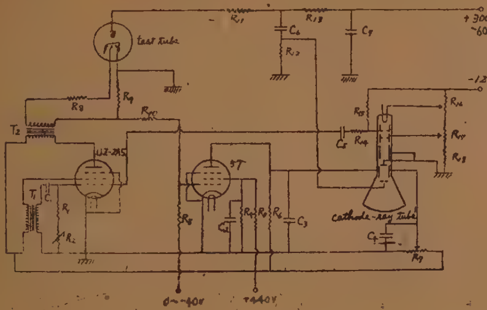

C_1: 0.01 μF
C_2: 1 μF
C_3: 0.0001 μF
C_4: 2 μF
C_5: 0.0001 μF
C_6: 0.001 μF
C_7: 2 μF

R_1: 100 KΩ
R_2: 500 KΩ
R_3: 500 KΩ
R_4: 100 KΩ
R_5: 150 KΩ
R_6: 500 KΩ
R_7: 500 KΩ
R_8: 10 KΩ
R_9: 10 KΩ

R_{10}: 1 MΩ
R_{11}: 330 Ω
R_{12}: 30 Ω
R_{13}: 500 KΩ
R_{14}: 100 KΩ
R_{15}: 2 MΩ
R_{16}: 100 KΩ
R_{17}: 500 KΩ
R_{18}: 500 KΩ

T_1: 1000 : 1000 (turn ratio)
T_2: 200 : 1200 (turn ratio)

Fig. 2. Diagram of circuit.

Fig. 2 shows the diagram of circuit for testing the character of the tube. The 500 cycle blocking oscillation caused by the tube *UZ*–2 A 5 affects on the auxiliary needle gap of the test tube, at the same time the cathode-ray tube is modulated in its brightness on the sweeping time axis, the longitudinal axis being oscillated by the main discharge current of the test tube.

Fig. 3 is the sketch of the general blocking pulsation used to the auxiliary spark discharge. Fig. 4 shows the figure observed on the screen of the cathode-ray tube from which the constancy of the time lag or disorder between the main and auxiliary discharge of the test tube has been estimated.

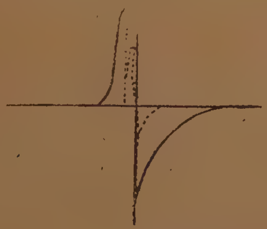

Fig. 3. The fig. of blocking oscillation.
Full line..............voltage
Dotted line..........current

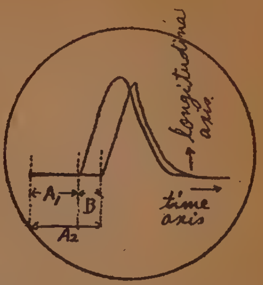

Fig. 4. Schematic view of the time lag A_1A_2 and disorder *B* on the cathode-ray tube.
Time axis is oscillated by auxiliary spark discharge, longitudinal axis oscillated by main spark discharge.

§ 3. Results and Discussions.

Many spark discharge tubes which have various forms of electrodes have been constructed.

Table I shows the forms of electrodes and the character of these test tubes.

In these experiments the character of the tube is affected by the polartty of auxiliary spark needle point *C* and the form of main electrodes.

In the case of No. 1–7 of table 1 the anode is a rod 5 mm in diameter, the cathode is a plate or a semi-concaved cap and the needle has negative polarity. These test tube have indicated the most excellent character.

These experimental facts will be understood from the following consideration.

The streamer extending from each electrode in the test tube is shown in Fig. 5 or Fig. 6 according to the form of electrode. In Fig. 5 positive

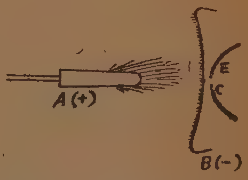

Fig. 5. Streamers in the irregular electric field.

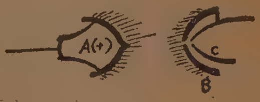

Fig. 6. Streamers in the substantially uniform electric field.

Table I.

combination of various type of electrodes	NO	main spark voltage V_0 (needle point in no action)	main spark vol-age V (needle point in action)	polarity of needle point C	disorder μs
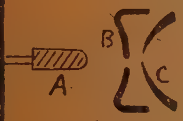	1	8700	3500	⊕ ⊖	0.5 0.1
	2	8880	3830	⊕ ⊖	0.8 0.1
	3	8890	3950	⊕ ⊖	0.6 0.2
	4	8770	3700	⊕ ⊖	0.6 0.3
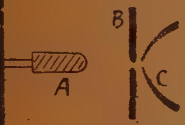	5	8650	3900	⊕ ⊖	0.4 0.1
	6	8450	3600	⊖	0.2
	7	7900	3770	⊖	0.1
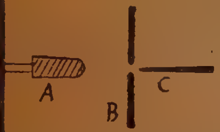	8	8340	4050	⊖	0.3
	9	8700	4000	⊖	0.4
	10	8500	4100	⊖	0.3
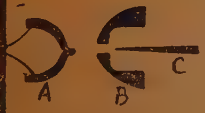	11	7200	4800	⊖	2
	12	7120	4720	⊖	1.1
	13	7200	4700	⊖	0.7
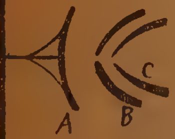	14	7850	4000	⊖	2
	15	8000	4200	⊖	2
	16	8900	4200	⊖	1.5
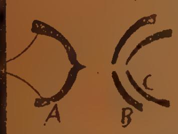	17	7250	3200	⊕ ⊖	2 1
	18	7120	3300	⊖	1.5
	19	7330	3400	⊖	1.0

streamers easily extend by the concentrated field intensity, but on the contrary negative ones have not so much tendency to extend, that the main spark discharge is extremely affected by the existence of auxiliary needle spark discharge. In Fig. 6 anode and cathode forms are substantially the same. Therefore, negative and positive streamers extend more uniformly from each electrode in comparison with the case of Fig. 5.

Therefore, in this case the main spark discharge is not so much affected by the auxiliary one, because the space where the auxiliary spark occurs is included in the extending streamer. Actually, in the case of Fig. 5 the difference of sparking voltage of main gap according to whether auxiliary spark exists or not, is larger than that of Fig. 6.

Many experiments have been carried out with respect to the various electrode types and the consideration above mentioned are made clear, i. e. it is important to design these spark discharge tubes so that the main electrode form may be confronted with each other since the field intensity is weakend on the surface of the electrode which has an auxiliary needle point.

Fig. 7 shows the design of the most excellent spark discharge tube which is constructed under these ideas and experiments.

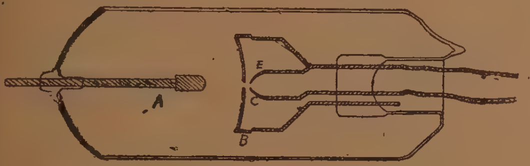

Fig. 7. Diagram of excellent spark discharge tube.

Fig. 8 shows the value of the main sparking voltage of this tube plotted against the hydrogen pressure according to the polarity of main electrode and to the condition of needle spark discharge. Of course the time lag and the disorder of the main spark discharge are also affected by the peak voltage of the blocking pulsation at the needle point, but in this connection this test tube keeps excellent stability.

Now the investigation on the character of the test tube has been chiefly carried out on the tube as shown in Fig. 7.

Fig. 9 shows the time lag of the main discharge due to the polarity of electrode and auxiliary blocking pulsation. There are large difference among time lag owing to the condition of electrode polarity. The pulsation figure denoted under the curves shows the wave form of auxiliary discharge current of the needle point.

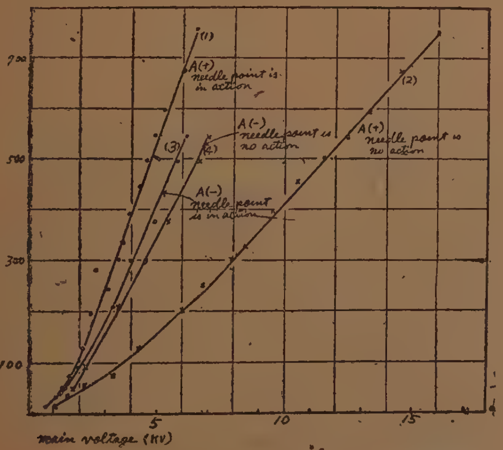

Fig. 8. Main voltage against H_2 pressure according to the polarity of the electrode A in Fig. 7.

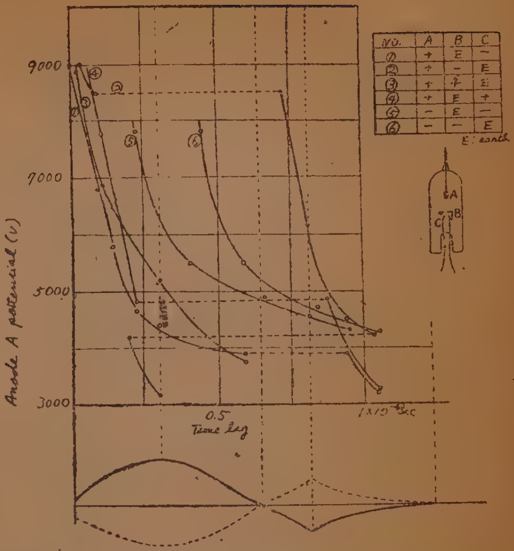

NO.	A	B	C
①	+	E	−
②	+	−	E
③	+	+	E
④	+	E	+
⑤	−	E	−
⑥	−	−	E

Fig. 9. Time lag of main discharge concerning to the polarity of electrode *A*, *B*, *C*, and auxiliary blocking pulsation.

In Fig. 9 the time lag of the main spark discharge in connection with the auxiliary spark discharge is shown. The value of the time lag is not always so acculate but the relative connection between each curves is easily understood as shown in Fig. 9.

From these experimental data, it is clear that the time lags and disorders in the condition of *A* being positive, are smaller than these for *A* being negative.

The disorder is not denoted in the Fig. 9.

When the electrode *A* is negative the main spark discharge voltage is higher than that of opposite polarity.

This fact is also understood from Fig. 8.

When negative blocking pulsations act on the needle point, the time lags and disorders take the smallest value as compared with other conditions.

It is valuable to notice in Fig. 9 that the time lag curves 2 and 4 have the discontinuous point concerning the main sparking voltage in which anode *A* is positive and needle point has higher potential than that of concave cathode *B*.

The reason for the existence of these discontinuous points may be understood from the following considerations.

When the potential *A* is not too high and the concave cathode *B* has lower potential than the needle point *C*, electrons cannot escape from the small hole.

But the negative blocking pulsation of the oscillatory current is an alternating current, so that in the later part of a cycle the point *B* has higher voltage than *C* and electrons can escape from the small hole. If anode *A* has very high potential the electrons produced between the space of *B* and *C* can reach the anode *A* regardless of the polarity of *B* and *C*.

Therefore if the tube is constructed conveniently to keep the concave cathode *B* negative against the needle point *C*, further intersting experiments may be expected.

The character of the test tube concerning to hydrogen pressure has also been determined. Fig. 10 shows the disorder of the test tube concerning to the hydrogen pressure and main sparking voltage. Fig. 11 is plotted from the same data of Fig. 10. to see the relations among disorder, hydrogen pressure and main sparking voltage.

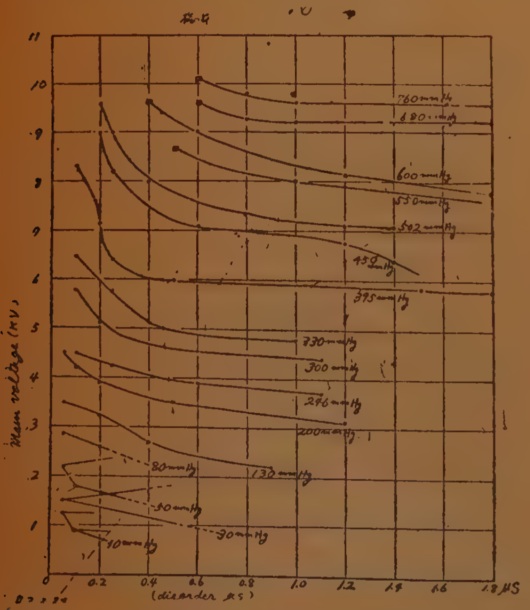

Fig. 10. The main voltage and disorder of the test tube concerning H_2 pressure.

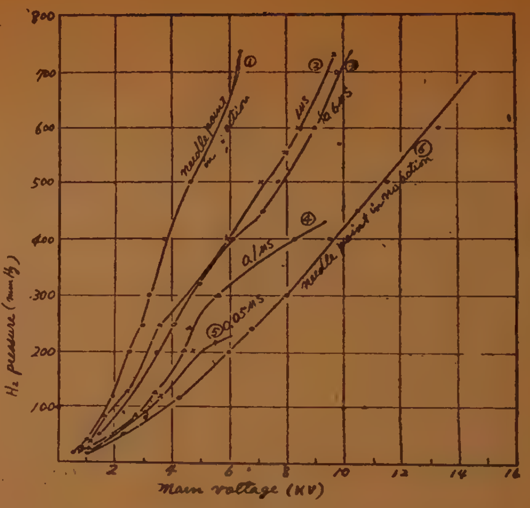

Fig. 11. The characteristic curves of the test tube according to H_2 pressure and main voltage.

①: Main spark voltage (needle point is in action)
②: Voltage and pressure curve at 1 μS disorder
③: ,, ,, ,, ,, at 0.6 μS ,,
④: ,, ,, ,, ,, 0.1 μS ,,
⑤: ,, ,, ,, ,, 0.05 μS ,,
⑥: Main spark voltage (needle point is not in action)

§ 4. Summary.

1. As hydrogen pressure is constant and auxiliary spark discharge is in action, the main spark discharge begins from a critical low voltage. In this condition the time lag and disorder are very large. They decrease as main voltage increases. But this connection is limited at the constant value according to hydrogen pressure. If the main voltage takes its value over the spark voltage V_0 in which the needle point is in no action, the main spark discharge does not correspond to the auxiliary spark discharge.
2. The main voltage with constant disorder increases according to the hydrogen pressure.
3. If it is desired to maintain the value of the disorder less than 0.1 μs in the test tube, hydrogen must be contained at the pressure 10∼400 mm Hg.
4. In the test tube an excellent characteristics may be obtained at the hydrogen pressure 10∼200 mm Hg and in this condition the disorder is 0.05 μS.
5. At the pressure less than 50 mm Hg the dis-

order may decrease but the range of main spark voltage may become narrow.

6. The disorder increases with the hydrogen pressure in the range of 400～760 mm Hg.
7. The time lag decreases as main voltage increases, but at 550 mm Hg or more the time lag increases suddenly at the certain definite main voltage.
8. In this test tube the peak value of current carrying capacity is 7 A, or 15 A at hydrogen pressure 200 mm Hg or 500 mm Hg respectively.
9. The voltage drop of the test tube is about 1200 V at 200 mm Hg.
10. The peak value of the blocking pulsation is 1200 V and 80 mA.

Acknowledgement.

The author wishes to express his appreciation and thanks Dr. Y. Toriyama for the suggestion of the problem and for his discussion and guidance during the course of this investigation.

On the Theory of Antiferromagnetism.*

By Noboru Tsuya.

Research Institute for Iron, Steel and Other Metals, Tohoku University.

(Received September 2, 1947)

§ 1. Introduction.

Recently magnetic properties of the so-called antiferromagnetic substances have been studied experimentally by Bizette-Squire-Tsai,1) Föex-Graff,2) Squire,3) Haraldsen4)5) and others. The susceptibility of these substances takes a Λ-form with the rise of temperature; during the cooling from a high temperature, it increases gradually according to the law

$$\chi = \frac{C}{\theta + T} \tag{1}$$

and after reaching a maximum value at a certain temperature it decreases gradually with the fall of temperature. At the absolute zero it retains a certain value χ_0 or entirely vanishes as shown in Fig. 1. These substances are composed of transition metals as Fe, Mn, Co, ... etc. and of non-metallic elements such as O, S, Te, Se .... etc.; probably these substances are the semiconductors of ionic binding.

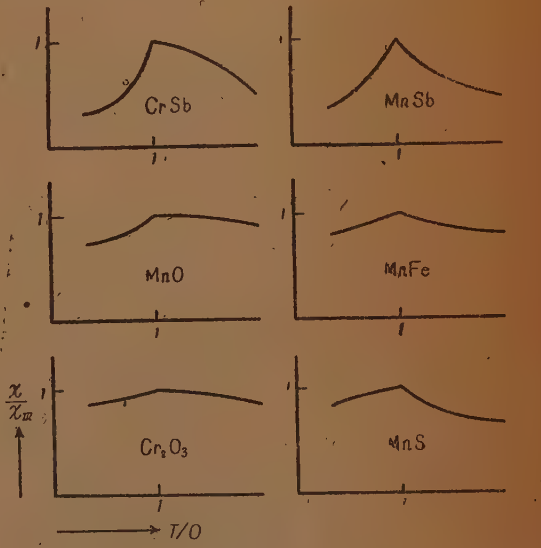

Fig. 1.

The antiferromagnetism of these substances has been worked out theoretically by Bitter,6) Van Vleck,7) Firgau8) and Y. Takagi9) on the spin lattice statistics assuming that the Heisenberg's exchange integral J takes a negative value. Recently Miyahara10) developed a theory based on Slater's theory of ferromagnetism with the aid of the Wilson model of semi-conductors. According to the experimental data, however, there are various types of antiferromagnetism ; in some cases the susceptibility curve is concave upwards in the lower temperature side and convex in the higher and other cases to reverse types occur and further there are different cases of Λ-type variation, in which the susceptibility curves on both sides are concave upwards. Certain substances possess more than one peak in susceptibility-temperature curve, although there appears only one peak in most substances. Those varieties of the type of antiferromagnetism, however, are not yet been explained successfully by the above mentioned theories. We have here discussed this problem on the basis of Miyahara's band theory,[10] assuming that the many types of antiferromagnetism are caused by the various types of state density distribution. and thus we are able to explain the existence of various types of antiferromagnetism. Moreover, it is expected from our theory that the susceptibility does not always vanish at the absolute zero of temperature.

---

* Due to the fund for the research of Natural Science of the Dept. of Edcation. (Name of project: Ferromagnetism of Semiconductors. Persons in charge: Tokutaro Hirone and Noboru Tsuya.)

§ 2. Calculation of the magnetism.

According to the electronic model of antiferromagnetic substances proposed by Miyahara, the free energy F of whole crystal of semiconductor is expressed by the state density $D_i(E)$ of occupied electronic energy bands as follows[11] (cf. Appendix)

$$F = U - T\Phi = \sum_i J_{ii}S_i^2/L + N\zeta + \Omega \tag{2}$$

$$\begin{aligned}\Omega = &-kT\sum_i\int \log\{1+\exp[(\zeta - E + \mu H - [J_{ii}S_i + \frac{1}{2}\sum_j J_{ij}S_j]/L/kT]\}\cdot D_i(E)dE\\ &-kT\sum_i\int \log\{1+\exp[(\zeta - E - \mu H + [J_{ii}S_i + \frac{1}{2}\sum J_{ij}S_j]/L)/kT]\}\cdot D_i(E)dE,\\ &\qquad (i, j = 1, 2, 3, \cdots\cdot)\end{aligned} \tag{3}$$

where S_i is the total spin quantum number corresponding to the i-th energy band, N the total number of electrons in the energy bands now in consideration, L the number of nuit cells contained in the crystal. ζ is the Fermi energy and J_{ij} the Slater's exchange integral caused by transposition of a pair of electrons, one of which is in the i-th band and the other in the j-th. Here the Summation extends over all energy bands in question. μ is the Bohr magneton and k the Boltzmann constant. From the thermodynamical relations

$$N = -\frac{\partial\Omega}{\partial\zeta}, \tag{4}$$

$$\frac{\partial F}{\partial S_i} = 0, \qquad (i = 1, 2, 3, \cdots\cdot) \tag{5}$$

and

$$M = -2\mu\sum_i S_i. \tag{6}$$

We are then able to obtain M as a function of Temperature. Now the relation (5) and (4) are transformed into

$$\begin{aligned}-2S_i = &\int\Big\{1+\exp[(\zeta - E + \mu H - J_iS_i/L - \frac{1}{2}\sum_{j\neq i} J_{ij}S_j/L)/kT]\Big\}^{-1}\cdot D_i(E)dE\\ &-\int\Big\{1+\exp[(\zeta - E - \mu H + J_iS_i/L + \frac{1}{2}\sum_{j\neq i} J_{ij}S_i/L)/kT]\Big\}^{-1}\cdot D_i(E)dE,\\ &\qquad (i, j = 1, 2, 3, \cdots\cdot)\end{aligned} \tag{7}$$

and

$$\begin{aligned}N = &\sum_i\int\Big\{1+\exp[(\zeta - E + \mu H - J_iS_i/L - \frac{1}{2}\sum_{j\neq i} J_{ij}S_j/L)/kT]\Big\}^{-1}\cdot D_i(E)dE\\ &+\sum_i\int\Big\{1+\exp[(\zeta - E - \mu H + J_iS_i/L + \frac{1}{2}\sum_{j\neq i} J_{ij}S_j/L)/kT]\Big\}^{-1}\cdot D_i(E)dE.\\ &\qquad (i, j = 1, 2, 3, \cdots\cdot)\end{aligned} \tag{8}$$

When we assume that the value $M/(\mu N/2)$ is considerably small compared with 1, the susceptibility χ is given by

$$\chi = \frac{\partial M}{\partial H} = 2\mu^2\sum_i \left[\int \exp[(E-\zeta)/kT]\{1+\exp[(E-\zeta)kT]\}^{-2}\cdot D_i(E)dE\right]\cdot$$
$$\cdot\left[kT-(J_{ii}/L)\int \exp[(E-\zeta)/kT]\{1+\exp[(E-\zeta)/kT]\}^{-2}eD_i(E)dE\right]^{-1},$$
$$(i=1,\ 2,\ \cdots) \tag{9}$$

where ζ is determined from the following relation

$$N = 2\sum_i\int\{1+\exp[(E-\zeta)/kT]\}^{-1}D_i(E)dE, \tag{10}$$

and we have assumed that J_{ij} is very small compared with J_{ii}, so that we may put $J_{ij}=0$ approximately.

In order to calculate the specific heat, we must compute the internal energy U as a function of T and differentiate with respect to T at constant volume, namely,

$$U = 2\sum_i\int\{1+\exp[(E-\zeta)/kT]\}^{-1}D_i(E)EdE \tag{11}$$

and

$$C = (\partial U/\partial UT)_{H,\zeta,V}. \tag{12}$$

§ 3. Interpetation of Typical Types of Antiferromagnetism.

Firstly we consider a semiconductor, whose state density $D_i(E)$ is shown in Fig. 2 and further we shall assume for simplicity that the width of the hand in very narrow so that $D_i(E)$ is approximately represented by Dirac's δ function, i.e.,

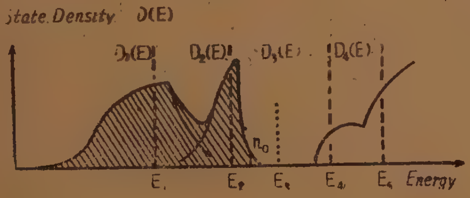

Fig. 2.

$$D_i(E) = Lb_i\delta(E_i-E). \tag{13}$$

When we denote by n_0 the number of electronic hole per unit cell in E_1 band at absolute zero temperature, n_0 is given by the following equation

$$N/Lb_1 = 1-n_0/2, \tag{14}$$

and for χ and ζ we obtain the following relations

$$\chi = 2L\mu^2\sum_i b_i\xi_i(1+\xi_i)^{-2}$$
$$\times[kT-J_{ii}b_i\xi_i(1+\xi_i)^{-2}]^{-1} \tag{15}$$

and

$$(1-n_0/2)N/L = \sum_i b_i(1+\xi_i)^{-1},$$

where

$$\xi_i = \exp[(E_i-\zeta)/kT], \tag{16}$$

At the absolute zero of temperature therefore, χ is given by

$$\chi_{T=0} = n_0\mu L, \tag{17}$$

which leads to the result that the susceptibility χ is not always zero but retains a certain value χ_0 at absolute zero of temperature. Most of the antiferromagnetic substances have been observed experimentally to have certain values of χ_0 at the absolute zero of temperature. Since the susceptibilities χ_0 will not always be attributed to the free ferromagnetic impurities contained in the substance, but they may sometimes be due to electronic hole in E_1-band, it is highly desirable to carry out the measurement of χ_0 in the chemically pure substances. Now we shall consider the case of $n_0=0$, i. e., the E_1-band is completely full of electrons. Assuming for the parameters J_{ii}, b_i, (E_i-E_1) and $(i=1,\ 2,\ \cdots)$ the various possible values (c. f. Table I), after numerical calculations, we may obtain manifold types of $\chi-T$ relation as shown in Fig. 3.

The various types of Λ-transition are shown to occur owing to energy band structures of electrons in the substances, including the case of more than one peak of susceptibility. In those models of electronic structure, in which the band breadth of $D_i(E)$ is zero, temperature at the maximum of anomalous heat capacity appears at lower side of θ, namely the temperature corresponding to maximum χ. Assuming for the density distribution $D_i(E)$ an appropriate breadth, however, we shall-

Table I.

Curve	b_2/b_1	b_3/b_1	$\frac{E_2-E_1}{k\Theta}$	$\frac{E_2-E_1}{k\Theta}$	$\frac{Jb_1}{2k\Theta}$	Type
(1.1)	0.1	0.5	2.0	4.0	2.0	—
(1.2)	,,	,,	,,	,,	3.2	CrSb, MnO, CrO
(1.3)	,,	,,	,,	,,	4.0	—
(2.1)	2.0	—	3.3	—	2.0	—
(2.2)	,,	—	,,	—	2.5	MnS
(2.3)	,,	—	,,	—	2.8	—
(3.1)	1.5	—	3.3	—	1.2	—
(3.2)	,,	—	,,	—	1.5	MnS
(4.1)	0.1	0.1	2.5	7.5	4.8	—
(4.2)	,,	,,	,,	,,	5.5	—
(4.3)	,,	,,	,,	,,	6.0	MnO, MnSe, CrO
(5.1)	0.2	—	3.3	—	2.4	—
(5.2)	,,	—	,,	—	5.5	—
(6.1)	0.1	1.0	1.3	3.8	1.9	—
(6.2)	,,	,,	,,	,,	2.5	—
(6.3)	,,	,,	,,	,,	3.1	FeS

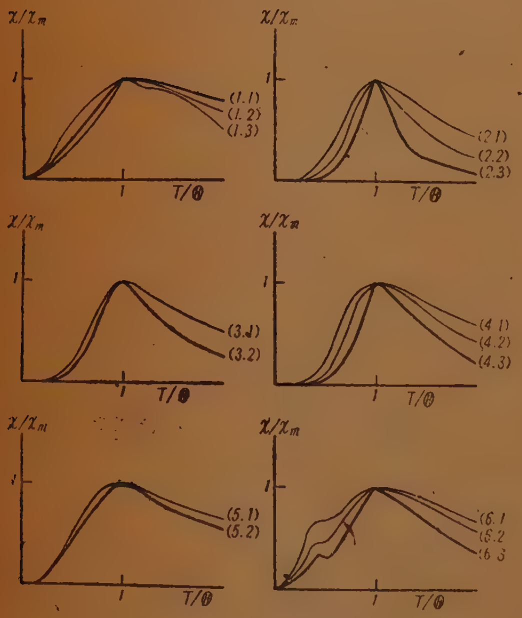

Fig. 3.

be able to make the former temperature coincide with Θ or appear somewhat higher than Θ. The mentioned temperature of anormalous haet capasity, therefore, will be expected to coincide with the observed one if we use the correct state density distribution. Although we have assumed here that the state density is expressed by δ-function and further $J_{ii} = J_{jj} = \cdots$, the obtained behaviours of χ with respect to T may be considered to still hold quantitatively for the more general cases, in which $J_{ii} \neq J_{jj} \neq \cdots$ and $D_i(E)$ have some breadth.

§ 4. The Magnetic and Thermal Characteristic of Maganous Selenide.

Now we shall show that a quantitative explanation for the magnetic and thermal data of MnSe may be given from our above mentioned model. Taking $E_2-E_1 = 0.0313$ eV, $E_3-E_1 = 0.0982$ eV, $J_{11} = J_{22} = 0.0491$ eV, $J_{33} = 0$, $b_1 = 1.00$, $b_2 = 0.28$, $b_3 = 1.39$ and $n_0 = 0.01$ for the various quantities

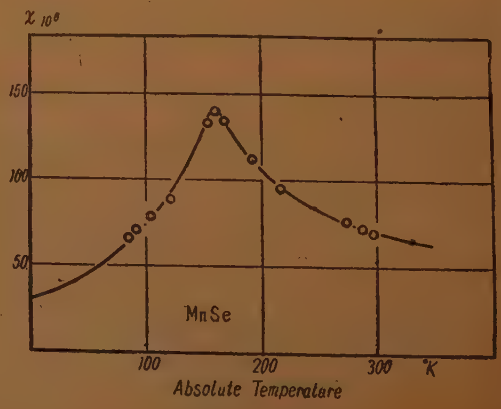

Fig. 4.

involved in the electronic band structure, we can compute numerically the relation between the susceptibility and temperature as shown in Fig. 4.

The experimental data on MnSe due to Squire[13)] are expressed by (small circles in the figure) showing that theoretical curve coincide satisfactorily the figure with that of the experimental observation. We are able to get the heat capacity C from the following relation

$$C = \frac{\partial U}{\partial T}, \tag{18}$$

where

$$U = U_0 = \sum_i 2Lb_i(E_i - E_1)(1+\xi_i)^{-1} - \sum_i J_{ii}S_i^2/L, \tag{19}$$

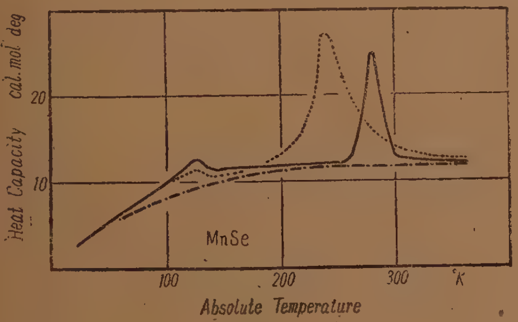

Fig. 5.

In Fig. 5, the full line is the experimental data on MnSe given by K. K. Kelley[14)], the broken line the heat capacity due to lattice vibration and the dotted line represents the sum of vibrational and calculated heat capacities from (18). One of the two maxima of our calculated anormalous heat capacity is due to the electrons in the energy band E_2 and the other due to those in the band E_3. As seen from the figure, the temperature at maximum heat capacity does not always coincide with the temperature corresponding to maximum χf, which result is a remarkable one elucidated from the present theory.

The susceptibility at the absolute zero temperature is understood from n_0.

Taking into consideration the agreement of theoretical results with experimental data both in magnetic and thermal characters of MnSe, it may be quite reasonable to conclude that the electronic structures of MnSe are correctly specified by the assumed values of parameters mentioned above.

In conclusion, the writer is indebted to valuable suggestions and discussions given by Dr. Miyahara as well as by Dr. Hirone throughout this investigation.

Appendix.

(Reduction of the formula of Free Energy.)

Here we shall consider the expression of the free energy for the substances in question. In the following discussion the notations have the same meaning as defined before.

If we devide the energy range of each energy band into small ranges E_{ik}, $E_{ik}+\delta E_{ik} = E_{i,\,k+1}$ and of we put N_{ik} for the number of electrons occupying the eigenstates in δE_{ik}, then the total energy U and the total number of electrons N are given by

$$U = \sum_i \Big(\sum_k N_{ik}E_{ik}\Big) + f(\cdots, N_{ik}, \cdots) \tag{1}$$

and

$$N = \sum_i \sum_k N_{ik}.$$

Now if we denote the number of eigenstates in the energy range δE_{ik} by Z_{ik}, we are able to distribute N electrons into these ranges in

$$W = \prod^{i} \prod^{k} Z_{ik}!/N_{ik}!(Z_{ik}-N_{ik})! \tag{3}$$

different ways. Fixing the values of U, N and H, the entropy Φ with respect to this distribution is given by

$$\Phi = k\log W = k\sum_{ik} Z_{ik}\{\log Z_{ik} - (N_{ik}/Z_{ik})\log N_{ik} - (1-N_{ik}/Z_{ik})\log(Z_{ik}-N_{ik})\}. \tag{4}$$

The most probable value of N_{ik} becomes

$$N_{ik}/Z_{ik} = [1+\exp(\alpha+\beta E_{ik}+\beta(\partial f/\partial N_{ik}))]^{-2} \tag{5}$$

and the corresponding value of entropy is

$$\Phi = \sum_{i,k} \log\left\{1+\exp\left(-\alpha-\beta E_{ik}-\beta\frac{\partial f}{\partial N_{ik}}\right)\right\}+\alpha N+\beta U+\beta\sum_{i,k}(N_{ik}/Z_{ik})(\partial f/\partial N_{ik}), \tag{6}$$

α and β being Lagrange's parameters.

Next, we should have to consider the form of $f(\cdots\cdot, N_{ik}\cdots\cdot)$ in (1). The exchange integral J_{ij}, concerning two electrons with parallel spin, one of which is lying in the i-th band and the other in the j-th, may be expressed in the form

$$\begin{aligned} J_{jj} = \sum_p\sum_q \Bigg\{ & \sum_{\lambda=1,}^{l}\sum_{\mu=1}^{m} \exp[i(k_i-k_j\,,\ R_{p\lambda}-R_{q\mu})]\int_q\int_p u_{i\lambda}{}^*(1)u_{j\mu}{}^*(2)\frac{e^2}{r_{12}}\,u_{i\lambda}(2)u_{j\mu}(1)d\tau_{12} \\ & +\sum_{\mu=1,}^{m}\sum_{\nu=1}^{n}\exp[i(k_i-k_j\,,\ R_{p\mu}-R_{q\nu})]\int_q\int_p u_{i\mu}{}^*(1)u_{j\nu}{}^*(2)\frac{e^2}{r_{12}}\,u_{i\mu}(2)u_{j\nu}(1)d\tau_{12} \\ & +\sum_{\nu=1,}^{m}\sum_{\lambda=1}^{l}\exp[i(k_i-k_j\,,\ R_{p\nu}-R_{q\lambda})]\int\int u_{i\nu}{}^*(1)u_{j\lambda}(2)\frac{e^2}{r_{12}}\,u_{i\nu}(2)u_{i\lambda}(1)d\tau_{12} \\ & + \ ,, \qquad ,, \quad \Bigg\}, \end{aligned} \tag{7}$$

where p and q run over the total number of unit cells L, m, n, and l etc. are the number of different kinds of atoms in one unite cell of the said compound, and $\lambda = 1,2 \cdots\cdot m$, $\mu = 1.2 \cdots\cdot n$, $\nu = 1.2 \cdots\cdot l$, etc. The main part of this integral arises from the atomic integral, in which a pair of electrons are found in the same atom. This part is then given by

$$L\left\{m\underset{\text{(type of atom } m)}{\iint u_i{}^*(1)u_j{}^*(2)(e^2/r_{12})u_i(2)u_j(1)d\tau_{12}}+n\underset{(\ ,,\ n)}{\iint}\ ,,\ \ ,,\ d\tau_{12}+\cdots\cdot\right\}. \tag{8}$$

For example, if the substance is composed of two sorts of atoms, m and n, then (8) is reduced to

$$L\left\{m\underset{(m)}{\iint}\ ,,\ ,,\ d\tau+n\underset{(n)}{\iint}\ ,,\ ,,\ d\tau\right\}. \tag{9}$$

Since the wave functions $u_i(1)$ etc. are normalized with the factor $(L.m)^{-\frac{1}{2}}$, then (8) turns out to be

$$L\left\{m[(mL)^{-\frac{1}{2}}]^4J_{ij}^m+n[(nL)^{-\frac{1}{2}}]^4J_{ij}^n+\cdots\cdot\right\} = (J_{ij}^m/m+J_{ij}^n/n+\cdots\cdot)/L. \tag{10}$$

using the expression J_{ij}^m for

$$\underset{\text{(type of atom } m)}{\iint u_i{}^*(1)u_j{}^*(2)(e^2/r_{12})u_i{}^*(2)u_j(1)d\tau_{12}},$$

which is almost equal to atomic exchange integral. The remaining part of (7), due to the nearest neighbours, is considerably small, so that we may neglect this part; then (7) becomes

$$J_{ij} = \bar{J}_{ij}/L, \quad \bar{J}_{ij} \equiv (J_{ij}^m/m+J_{ij}^n/n+\cdots\cdot). \tag{11}$$

For example, in the case of body-centered iron, $\bar{J}_{ij}$ in (11) is equal to

$$\bar{J}_{ij} = \bar{J}_{ij}^m|2 \qquad (i, j = 1,\ 2,\ \cdots\cdot)$$

Taking into account the distribution of the spins of electrons in each energy bands, f becomes

$$f = -\sum_i(J_{ii}S_i^2/L)-\sum_{i\neq j}\sum(J_{ij}S_iS_j/L), \tag{12}$$

and by using the relation $s_i = \frac{1}{2}\sum_k N_{ik}\delta_{ik}$ the expression (12) changes into

$$f = -\frac{1}{4}\left\{\sum_i(J_{ii}/L)(\sum_k N_{ik}\delta_{ik})^2+\sum_{i\neq j}(J_{ij}/L)(\sum_k N_{ik}\delta_{ik})(\sum_h N_{jh}S_{jh})\right. \tag{13}$$

where δ_{ik} is equal to $+1$ when the spin magnetic moment is parallel to the magnetic field, and otherwise to -1. $(N_{ik}/Z_{ik})\partial f/\partial N_{ik}$ is also easily found from the above equation (13).

Using these formulas the free energy F is obtained as follows.

$$F = U-T\Phi = \sum J_{ii}S_i^2/L+N\zeta+\Omega$$

$$\Omega = -kT\sum_i \log\left\{1+\exp[(\zeta-E_i-\delta_i(J_{ii}S_i+\frac{1}{2}\sum_j J_{ij}S_j)/L)/kT]\right\}, \tag{14}$$

where

$$N = -\frac{\partial\Omega}{\partial\zeta}, \quad \frac{\partial F}{\partial S_i}=0, \quad (i=1,\ 2,\ \cdots\cdot) \tag{15}$$

and
$$M = -2\mu\sum_i S_i,$$

The mentioned expression of free energy differs from the Hirone-Miyahara's in the following respect. The exchange interaction energy depends not only upon the total spin number S but also upon the group of S_i ($i=1, 2 \cdots\cdot$). Therefore, in regard to the expression of magnetization we get essentially different form.

Reference.

(1) Bizette-Squire-Tsai, Compt. Rend., **207** (1938), 449.
(2) Föex-Graff, „ „ **209** (1933), 160.
(3) Squire, Phys. Rev., **56** (1939), 922.
(4) Haraldsen, Z. anorg. allg. Chem., **231** (1937), 78.
(5) Haraldsen-Neuber, Z. anorg. allg. Chem., **234** (1937), 337.
(6) Bitter, Phys. Rev., **54** (1938), 97.
(7) Van Vleck, J. Chem. Phys., **9** (1941), 85.
(8) Firgau, Ann. d. Phys.,
(9) Y. Takagi, Proc. Phys.-Math. Soc. Japan, **24** (1942), 133.
(10) Miyahara, Proc. Phys.-Math. Soc. Japan, **22** (1940), 528.
(11) Hirone-Miyahara, Niypon Subutsu-gakkai-shi, **17** (1943), 92.
(12) Sqire, loc. cit,
(13) K, K. Kelley, J. Am. Chem. Soc , **61** (1931), 2 3.

The Radial Distribution Function in Liquid Argon.*

By Syû Ono

Institute of Applied Science, Faculty of Engineering Kyusyu University, Hukuoka.

(Received September 2, 1947)

The radial distribution function in liquid argon which is obtainable as a solution of Kirkwood's integral equation is calculated numerically, making use of the approximation as to the coupling parameter. The result obtained is compared with experimental radial distribution functions.

§ 1. Introduction.

In monatomic liquids, the radial distribution function or Menke's probability function $g(r)$ is used to express the probability that two molecules i and k are in the specified volume elements $d\omega_i$ and $d\omega_k$ separated by a distance r, in the form

$$g(r)\frac{d\omega_i}{v}\frac{d\omega_k}{v}, \tag{1}$$

where v is the volume of the container. Owing to the absence of long range order in liquid, we obtain from (1)

---

* Translated from the paper, BUSSEIRON KENKYU, 2 (1943), 15, appeared originally in Japanese; the content of this paper was reported at the regular meeting of the Osaka branch of the Physico-Mathematical Society of Japan on April 1, 1943.

$$\lim_{r\to 0} g(r) = 1 . \qquad (2)$$

This $g(r)$ is obtainable from X-ray diffraction patterns given by liquid. Attempts to calculate $g(r)$ theoretically from the interatomic potential have been made by Wall, Coulson, Rushbrooke, Lennard-Jones and Corner[1)], based on the cage model of liquid. In their theories, undetermined parameters, such as the number of atoms on each coordination shell, which are adjusted so as to make the agreement between theory and experiment as good as possible, are introduced. And liquids have no evidence of long range order characterized by the regular successive coordination shells assumed in the cage model, but only of rapid damped local order in the density distribution arround each molecule.

For these reasons, the author will discuss from a different point of view, and will carry out the numerical calculation of the distribution function from the interatomic potential, by using Kirkwood's integral equation, to which the brief description will be given in the next section.

§ 2. The Derivation of the Integral Equation due to Kirkwood.[2)]

Let us consider the case where the potential energy of the assembly of N atoms can be written as a sum of terms, each depending only on the distance r_{ik} of two molecules i and k:

$$V_N = \sum_{k>l}^{N} V(r_{kl}) , \qquad (3)$$

where $V(r_{ik})$ is the potential energy of the pair of molecules i and k as a function of their distance r_{ik}. This condition would be almost exactly satisfied in gaseous and liquid argon.

As shown in Fowler's book[3)] the radial distribution function $g(r)$ in such an assembly is expressed by

$$\left.\begin{aligned} & g(r_{ik}) = \exp(-\beta W_i^k) , && \text{(a)} \\ & \exp(-\beta W_i^k) \\ & \quad = \frac{v^2 \int\int\cdots\int \exp(-\beta V_N) d\omega_1 d\omega_2 \cdots d\omega_{N-2}}{\int\int\cdots\int \exp(-\beta V_N) d\omega_1 d\omega_2 \cdots d\omega_N} , && \text{(b)} \\ & \beta = \frac{1}{kT} , && \text{(c)} \end{aligned}\right\} (4)$$

where k is Boltzmann's constant, T is the absolute temperature and $d\omega_i$ is the volume element of atom i. Here the integration in the numerator of (4b) is to be performed with regard to the coordinates of all atoms except i and k, and the integration in the subspace of each atom is extended over a region bounded the volume of the container. It is, however, a tedious task to carry out the integrations in (4b) exactly, but Kirkwood has shown that W_i^k is approximately obtainable as a solution of an integral equation.

In order to prove this, we will consider a hypothetical assembly whose potential energy is

$$\left.\begin{aligned} V_N(\lambda_i) &= \sum_{k>l\neq i} V_{kl} + \lambda_i V_i \\ V_i &= \sum_k V_{ik} , \end{aligned}\right\} \qquad (5)$$

where λ_i, called coupling parameter, varies between zero and unity. When a value unity is assigned to λ, we have a real assembly of N atoms. If, on the other hand, a value zero is assigned to λ, we have an assembly of N-1 atoms. And we define $W_i^k(\lambda_i)$ and $W^s{}_{ik}(\lambda_i)$ by

$$\exp(-\beta W_i^k(\lambda_i)) = \frac{v^2 \int\int\cdots\int \exp\{-\beta V_N(\lambda_i)\} d\omega_1 d\omega_2 \cdots d\omega_{N-2}}{\int\int\cdots\int \exp\{-\beta V_N(\lambda_i)\} d\omega_1 d\omega_2 \cdots d\omega_N} , \qquad (6)$$

$$\exp(-\beta W_{ik}^s(\lambda_i)) = \frac{v \int\int\cdots\int \exp\{-\beta V_N(\lambda_i)\} d\omega_1 d\omega_2 \cdots d\omega_{N-3}}{\int\int\cdots\int \exp\{-\beta V_N(\lambda_i)\} d\omega_1 d\omega_2 \cdots d\omega_{N-2}} , \qquad (7)$$

where the integrations in the numerator of (6) and the denominator of (7) are with regard to the coordinates of all atoms except i and k, and in denominator of (7) over all but those of i, k and s, and $W_i^k(\lambda_i)$ depends only on the relative coordinates of the atom pair k and i in the absence of long range force. We will use the alternative notation

$$W_i^k(\lambda_i) \equiv W(\lambda_i , r_{ik}) \qquad (8)$$

to clearly designate its dependence on r_{ik} and λ_i. And we have at once

$$\left.\begin{aligned} W_i^k(1) &= W_i^k , \\ W_i^k(0) &= 0 , \end{aligned}\right\} \qquad (9)$$

using (5) and (6), where W_i^k is defined in (4b). Neglecting the small term of the order of $1/N$, we obtain

$$W_i^k(\lambda_i) = \lambda_i V(r_{ik})$$
$$+\frac{N}{v}\int_0^{\lambda_i}\int V(r_{ik})\left[\exp\{-\beta W^s{}_{ik}(\lambda_i)\}\right.$$
$$\left.-\exp\{-\beta W_i^s(\lambda_i)\}\right]d\omega_s d\lambda_i\,. \qquad (10)$$

If there be one more relation between $W_i^k(\lambda_i)$ and $W_{ik}^s(\lambda_i)$, we obtain an equation which $W_i^k(\lambda_i)$ has to satisfy, eliminating $W_{ik}^s(\lambda_i)$ from (10).

The force acting at the center of gravity of atom k for a fixed configuration of the other atoms is

$$F_k(\lambda_i) = -\nabla_k V_N(\lambda_i),$$

where ∇_k is the gradient operator associated with

$$_{ik}\langle F_k\rangle$$
$$= \frac{\iint\cdots\int \nabla_k V_N(\lambda_i)\exp\{-\beta V_N(\lambda_I)\{d\omega_1 d\omega_2\cdots d\omega_{N-2}}{\iint\cdots\int \exp\{-\beta V_N(\lambda_i)\}d\omega_1 d\omega_2\cdots d\omega_{N-2}}.$$

Hence differentiation of both side of (6) yields

$$_{ik}\langle F_k\rangle = -\nabla_k W_i^k(\lambda_i).$$

The function $W_i^k(\lambda_i)$ is therefore the potential of the mean force acting at the center of gravity of atom k when i is held fixed at some point in its vicinity. Similarly $W_{ik}^s(\lambda_i)$ is the potential of the mean force acting on atom s, averaged over the configuration of all atoms except i, k and s.

Then we will assume superposition in the potentials of mean force

$$W_{ik}^s(\lambda_i) = W_i^s(\lambda_i) + W_k^s(1). \qquad (11)$$

Though the additivity expressed in (11) holds for the direct action of i and k on s through the terms $V_{ks}+\lambda_i V_{is}$, it cannot hold exactly for their indirect action on s through their effect on the distribution of the remaining $N-3$ atoms. If we substitute the approximation (11) into (10), we obtain the integral equation

$$W_i^k(\lambda_i) = \lambda_i V(r_{ik})$$
$$+\frac{N}{v}\int_0^{\lambda_i}\int V(r_{is})\exp\{-\beta W_i^s(\lambda_i)\}$$
$$\times\left[\exp\{-\beta W_k^s(1_i)\}-1\right]d\omega d\lambda_i\,. \qquad (12)$$

If we use the new symbols r, r_1, r_2 and λ instead of r_{ik}, r_{is}, r_{ks} and λ_i, we can rewrite the integral equation in the form

$$W(\lambda,r) = \lambda V(r)$$
$$+\frac{N}{v}\int_0^{\lambda}\int V(r_1)\exp\{-\beta W(\lambda,r_1)\}$$
$$\times\left[\exp\{-\beta W(1,r_2)\}-1\right]d\omega d\lambda\,, \qquad (13)$$

where the notation shown in (8) is used.

§ 3. Numerical Calculation of the Solution of the Integral Equation by means of the New Assumption as to the Coupling Parameter.

Since it is difficult to solve the non-linear integral equation (13), or to find the general behavior of its solution, we will introduce a physically reasonable assumption as to the relation between $W(\lambda, r)$ and λ to solve it approximately. In dilute gases, the potential of the mean force between atoms i and k reduces to

$$W(\lambda, r) = \lambda V(r), \qquad (14)$$

for the encounters in which more than two atoms participate occur so rarely. It is evident that (14) satisfies (11). This implies that the relation (11) holds in the limit of increasing volume. Substitution of (14) into (13) leads to

$$W(1,r) = V(r)$$
$$-\frac{NkT}{v}\int\left[1-\exp\{-\beta V(r_1)\}\right]$$
$$\times\left[1-\exp\{-\beta V(r_2)\}\right]d\omega\,. \qquad (15)$$

Kirkwood[2] calculated the distribution function from (15), assuming a certain type of $V(r)$; de Boer and Michels[4] performed the similar calculation for compressed argon gas at higher temperature. The author tried to compute the distribution function of liquid argon from Lennard-Jones' interatomic potential[5] according to (15), but the result obtained was very much different from the experimental value. Thus, it has been concluded that the assumption (14) is very poor approximation for liquid.

Here we introduce the assumption of the linear dependence on λ

$$W(\lambda, r) \doteq \lambda W(1, r) \qquad (16)$$

instead of (14). (16) can be justified in the limit of increasing volume from (14), because $W(\lambda, r)$ tends to $\lambda V(r)$ as the volume increases. Making use of (16), we can considerably simplify (13).

In order to make further progress, it is necessary to assume a definite form for $V(r)$. We will assume the form

$$V(r) = \phi_0\left\{\left(\frac{r_0}{r}\right)^{12} - 2\left(\frac{r_0}{r}\right)^{6}\right\},$$

where r_0 is the value of r for the minimum potential and ϕ_0 is the absolute value of the minimum potential. Setting $r/r_0 = x$, $r_1/r_0 = x_1$, and $r_2/r_0 = x_2$, we can rewrite (13) in the form

$$W(\lambda,x) = \lambda V(x) + \frac{\beta\tau}{x}\int_0^{\lambda} d\lambda \int_0^{\infty} dx_1 \cdot x_1 V(x_1) \exp\{-\beta W(\lambda, x_1)\} \times \int_{|x-x_1|}^{x+x_1} x_2[\exp\{-\beta W(1, x_2)\} - 1]dx_2\,, \tag{17}$$

where

$$\tau = \frac{2\pi N r_0{}^3}{V}.$$

If (16) be utilized, we have at once

$$W(1, x) = \lambda V(x) - \frac{\tau}{x}\int_0^{\infty} dx_1 \frac{x_1 V(x_1)}{W(1, x_1)} [\exp\{-\beta W(1, x_1)\} - 1] \times \int_{|x-x_1|}^{x+x_1} x_2[\exp\{-\beta W(1, x_2)\} - 1]dx_2\,. \tag{18}$$

We have only to calculate $W(1, x)$ for the purpose of computing the distribution function. It should be possible to determine by numerical calculation the self-consistent functions which satisfy (18). When the liquid is one mole in mass, V is the molar volume and N is Loschmidt's number.

§ 4. Comparison with Experiment.

The numerical calculation was carried out for a mole of liquid argon at 90°K. The values of r_0 and ϕ_0 for argon are

$$\phi_0 = 16.5 \times 10^{-15}\ \text{erg}, \qquad r_0 = 3.825\ \text{Å},$$

which have been calculated by Lennard-Jones⁵⁾ from the temperature dependence of the second virial coefficient.

The self-consistent solution of (18) has been calculated by the trial and error method, the integration in each step being carried out numerically. The calculated curve is shown in Fig. 1 together with the experimental ones due to Eisenstein and Gingrich⁶⁾, and due to Lark-Horovitz and Miller⁷⁾ which are obtained at 90°K. The agreement between theory and experiment is sufficient, although there may be small discrepancies between them. Especially, it is remarkable that the distance and the magnitude of the first maximum are in quantitative agreement with the experimental ones, And it must be emphasized that the adjustable parameters as used in the theories based on the cage model of liquid is not utilized in our theory. The small second maxima of the experimental curves are not obtained from the present theory. But more precise interatomic potential is necessary for us to discuss these small discrepancies.

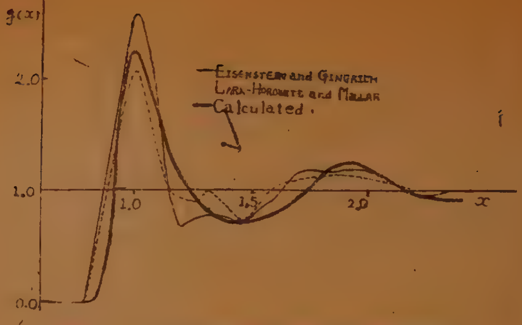

Fig. 1. Comparison with experiment.

On the other hand, if the radial distribution function and hence $W(1, r)$, be known, $V(r)$ is obtainable as a solution of (18), which can be regarded as a Fredholm's integral equation of the second kind.

The good agreement between theory and experiment implies that the assumption of linearity (16) presented by the author as well as the assumption of superposition (11) by Kirkwood would be physically valid.

The author's best thanks are due to Prof. Oomori for his helpful discussion.

Note Added in Translation.

Recently, Kirkwood and Elizabeth Monroe Boggs have carried out the similar calculation. In their theory, the coupling parameter λ is related to certain observed physical properties of the liquid and to the diameter of closest approach.

References.

1) J. Corner and J, E. Lennard-Jones : Proc. Roy. Soc. **178** (1941), 401.

(2) J. G. Kirkwood: J. Chem. Phys. 3 (1935), 300.
(3) R. H. Fowler: Statistical Mechanics, 2nd. ed. (1936) p. 254.
(4) J. de Boer and A. Michels: Physica 6 (1939), 97.
(5) J. E. Lennard-Jones: Proc. Roy. Soc. **106** (1924), 463.
(6) A. Eisenstein and N. S. Gingrich: Phys. Rev. **58** (1940), 307.
(7) K. Lark-Horovitz and E. P. Miller: Nature **146** (1940), 459.
(8) J. G. Kirkwood and Elizabeth Monroe Boggs: J. Chem. Phys. **10** (1942), 344.

On the Statistical Theory of Rubber-like Elasticity.

By Takuzo SAKAI and Akira ISIHARA.

Faculty of Science, Tokyo University.

(Read May 12, 1947, Received Sept. 5, 1947)

§ 1. Introduction.

According to the theories, initiated by Kuhn and elaborated by others¹⁾, the modulus of elasticity of rubber-like substances at the beginning of elongation is given by

$$\varepsilon_0 = 3\rho RT/M, \qquad (1)$$

where ρ is the density of the substance, R the gas constant, T the absolute temperature and M the molecular weight of one of the elementary chains which constitute the network of the substance. From the theoretical point of view, especially considered from the principles of statistical mechanics, the above theory is not all satisfactory. One of the present authors put forward a theory some years ago²⁾, according to which the modulus is given by

$$\varepsilon_0 = 3\rho RT\lambda_0^2/m, \qquad (2)$$

where λ_0 is the original distance between the two ends of a chain divided by the length of the chain, and m the molecular weight of a kinematical unit (sometimes called kinetic unit or effective constitutional unit) of the chain. λ_0 is effectively equal to the natural length divided by the greatest streched length of the sample.

If we take $\rho = 1$, $\varepsilon_0 = 10\,\mathrm{kg/cm^2}$, $T = 300°\mathrm{K}$, then $M = 7700$ according to (1), and $m = 120$ according to (2). In the latter case we take $\lambda_0 = 1/8$. The above figure of m means that the kinematical unit consists of about two isoprenes in the case of rubber, and is a reasonable result. It seems to be natural that the molecular weight of the constitutional unit of a chain enters the so-called equation of state of rubber-like substances as in the case of ideal gases where the constitutional unit is an atom or molecule. Because the kinematical unit of a chain is defined as the unit which behaves itself like a free atom when the chain makes thermal motions.

Of course the distance between the junctures of the network will be distributed according to the law of random flight by dint of the micro-Brownian motion of the constitutional units. The appearance of the molecular weight M of the chain as a whole in the equation of elasticity like (1) is due to this variation of the distances. But the degrees of junctures are small compared to those of the constitutional units. Thus we can expect that the thermal motion of junctures contributes a negligibly small effect to the elasticity compared to that of constitutional units, and that the correction to our formulae (2) will be of the order of m/M. The object of the present paper is to show these considerations in a mathematical form.

§ 2. Mathematical Treatment.

We take an idealized case which represents the essential features of the above consideration, in order to get a simple mathematical formulation. A very long chain is divided into N parts, each of which is assumed to contain the same number of kinematical units for the sake of simplicity. This number of kinematical units is denoted by n. Each of these parts corresponds to a chain in the network. In reality, however, there are some branches of chains at each of the junctures, but we omit the effect of these branches for the sake of simplicity too.

Let the i-th chain be represented by the vector x_i, which is drawn from the terminal point of the vector representing the preceding chain to the initial point of the vector representing the next chain. These vectors take various orientations and lengths, the distribution of which in space is determined by the principles of statistical mechanics. The orintation of x_i is specified by the polar angle θ_i and the azimuthal angle Φ_i, the polar axis of which is the straight line connecting the two ends A and B of the very long chain mentioned at the beginning of this article (see Fig. 1). Let N_i be the number of those vectors whose terminal points lie in the elementary region $\Delta V_i = x_i^2 \sin \theta_i \, d\theta_i d\Phi_i$. If the numbers $N_1, N_2, \cdots, N_i, \cdots$ of chains corresponding to various orientations and lengths be given, the number of configulations of this state is proportional to

$$N! \prod_i [(\Delta V_i)^{N_i}/N_i!]. \tag{3}$$

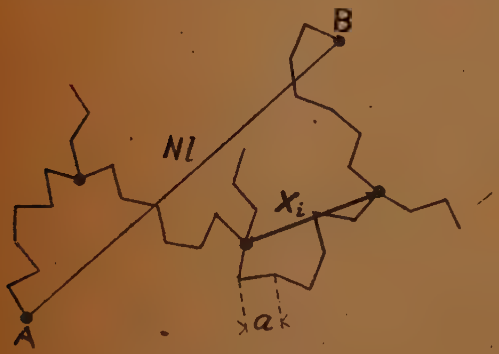

Fig. 1.

Now each of the chains themselves consists of a number of kinematical units. This number is denoted above by n. The kinematical unit has also its own orientation. Let the number of those units which belong to the i-th chain and have the orientation in the solid angle $\Delta\omega_j = \sin\theta_j \, d\theta_j d\varphi_j$ be denoted by n_{ij}. The polar axis of the polar angle θ_j and the azimuthal angle φ_j is the vector x_i. Then the number of configuration of the i-th chain itself is given by

$$n! \prod_j [(\Delta\omega_j)^{n_{ij}}/n_{ij}!]. \tag{4}$$

Thus the number of configurations of the very long chain is given by

$$G = N! n! \prod_i \frac{1}{N_i!} [\Delta V_i \prod_j (\Delta\omega_j)^{n_{ij}}/n_{ij}!]^{N_i} \tag{5}$$

when N_i's and n_{ij}'s are specified. According to the original idea of Meyer and Ferri³⁾, we have only to consider the configurational entropy, as long as we are concerned with the stress of rubber-like substances. This entropy is given by $k \log G$. In the case of thermal equiliblium, the numbers N_i's and n_{ij}'s are determined by making $\log G$ have the maximum value under the following conditions:

$$\sum_i N_i = N, \tag{6}$$

$$\sum_i N_i x_i \cos\theta_i = Nl, \tag{7}$$

$$\sum_j n_{ij} = n, \tag{8}$$

$$\sum_j a n_{ij} \cos\theta_j = x_i, \tag{9}$$

where N, Nl, n, x_i must be kept constant for the variations of N_i's and n_{ij}'s. Here Nl is the distance between A and B (Fig. 1), and a is the length of a kinematical unit.

Making use of the Stirling's formulae for factorials, we get

$$N_i = w_i \exp(\Lambda x_i \cos\theta_i + \mu) \cdot \Delta V_i, \tag{10}$$

$$n_{ij} = \exp(\lambda_i \cos\theta_j + \alpha_i) \cdot \Delta\omega_j, \tag{11}$$

where

$$w_i = n^n \exp(-\lambda_i x_i/a - \alpha_i n), \tag{12}$$

and Λ, μ, λ_i, α_i are constants. From (8) and (9), we get

$$x_i/(na) = \coth\lambda_i - 1/\lambda_i,$$

$$\exp\alpha_i = n\lambda_i/\sinh\lambda_i. \tag{13}$$

Thus (10) can be written in the form

$$N_i = n^n \exp(-\lambda_i x_i/a - \alpha_i n + \Lambda x_i \cos\theta_i + \mu) \cdot \Delta V_i. \tag{14}$$

Let $n(x)dx$ be the number of chains whose representative vectors have their lengths between x and $x+dx$, then

$$n(x) = \iint N_i \sin\Theta_i d\Theta_i d\Phi_i \cdot x^2$$

$$= 4\pi e^{\mu-nf(x)} x^2 \sinh \Lambda x/(\Lambda x), \qquad (15)$$

where

$$f(x) = \lambda x/(an) - \log(\sinh\lambda/\lambda). \qquad (16)$$

The above expression for $n(x)$ gives the law of distribution of the lengths of the vectors representing the chains. The total number N of chains can then be written down in the form

$$N = 4\pi e^{\mu}\int_0^{an} e^{-nf(x)} x^2 \sinh \Lambda x/(\Lambda x)\cdot dx. \qquad (17)$$

From (6), (7) and (14), we get also the relation

$$Nl = \frac{\partial N}{\partial \Lambda}. \qquad (18)$$

If $1 > l/(an)$, i. e. the average length l of the vectors is small compared to the length an of the chain, we can expand $\sinh \Lambda x/(\Lambda x)$ in the integrand of (17) in a series of powers of Λx. This will be ascertained from the result which will be obtained on this assumption. In this case we come to evaluate the integral

$$a_{2k} = \int_0^{an} e^{-nf(x)} x^{2k} dx, \quad (k = 0,\ 1,\ 2,\ \cdots\cdot).$$

Now the above condition for the possibility of expansion means also that $1 > x/(an)$, and hence λ is also small as can be seen from (13). In fact we get

$$\lambda = 3x/(an) + O[(x/an)^3],$$

where $O[a]$ means that this quantity is of the order of a. Thus we can write

$$e^{-nf(x)} = \exp\Big[-\frac{3n}{2}\Big(\frac{x}{an}\Big)^2\Big]\cdot\Big[1-\frac{9n}{20}\Big(\frac{x}{an}\Big)^4+\cdots\cdot\Big], \qquad (19)$$

and we get

$$a_{2k} = \frac{1.3\cdots\cdot(2k-1)}{2^{k+1}}\Big(\frac{2na}{3}\Big)^{k+1/2}\sqrt{\pi}$$

$$\Big[1-\frac{1}{5n}\,\frac{(2k+1)(2k+3)}{4}\Big].$$

Then from (27) and (18), we get

$$a\Lambda = \frac{3l}{na}\Big[1+\frac{1}{n}+\frac{3}{5}\Big(\frac{l}{na}\Big)^2\Big(1+\frac{3}{n}\Big)\Big], \qquad (20)$$

which shows that $a\Lambda$ is really of the order of $l/(na)$ as above mentioned. The law of the distribution of the lengths of chains takes the from

$$n(x) = C\exp\Big[-\frac{3n}{2}\Big(\frac{x}{an}\Big)^2\Big]\cdot x^2. \qquad (21)$$

This function for the distribution has frequently been used by Kuhn and others[1]. They derived it from the consideration of random flight. We have derived it from the ordinary principle of statistical mechanics.

§ 3. Calculation of Stress.

If we denote the entropy per chain by s, then $Ns = k\log G$. From (5), (10), (11) and (6), (7), (8), (9), we get

$$s/k = \log N - l\Lambda - \mu. \qquad (22)$$

Let l_0 be the average original length of the vector representing the chain, and its orientation be specified by the polar coordinates Θ_0 and Φ_0, whose polar axis is in the direction of stretching. In the stretched state the above length becomes l.

Now we assume that the volume of the substance does not change when stretched. This is substantially explained from the act that the vacant regions produced by stretching the chains will be filled up by molecules belonging to those chains which are in less strained conditions, because the chains have always the tendency to contract owing to the micro-Brownian motions, so that the molecules are always in the state of closest packing. If we denote the coordinates of the terminal point of the chain in the original state by x_0, y_0, z_0, whose origin is the initial point of the chain, z_0 being the coordinates in the direction of stretching, then z_0 will be multiplied by r, whereas x_0 and y_0 by $1/\sqrt{r}$ when stretched. Therefore we get

$$l^2 = l_0^2(r^2\cos^2\Theta_0 + \sin^2\Theta_0/r). \qquad (23)$$

Thus in the stretched state the average entropy $\bar{s}$ per chain is given by

$$\bar{s} = \int_0^{2\pi} d\Phi_0 \int_0^{\pi/2} s\cdot \sin\Theta_0 d\Theta_0 d\Phi_0/(2\pi).$$

where s is defined by (22) and in the expression of s by (23). Let the number of chains per unit volume be denoted by ν, then the free energy per unit volume becomes

$$\Psi = -T\nu\bar{s} = -T\nu\int_0^{\pi/2} s\cdot\sin\theta_0 d\theta_0,$$

where the internal energy has been omitted. Thus the tension σ is given by

$$\sigma = \frac{\partial\Psi}{\partial r} = \nu kT\int_0^{\pi/2}\left(\Lambda + l\frac{\partial\Lambda}{\partial l} + \frac{\partial\mu}{\partial l}\right)\frac{\partial l}{\partial r}\sin\theta_0 d\theta_0. \tag{24}$$

From (6), (7) and (10), we get the identity

$$l\frac{\partial\Lambda}{\partial l} + \frac{\partial\mu}{\partial l} = 0 \tag{25}$$

when N is kept constant. Thus if we use the approximate expression (20) for Λ, we get

$$\sigma = \frac{\rho RT\lambda_0^2}{m}\left\{\left(r - \frac{1}{r^2}\right)\left[1 + O\left(\frac{m}{M}\right)\right]\right.$$
$$\left.+ \frac{9\lambda_0^2}{25}\left(r^3 + \frac{1}{3} - \frac{4}{3}\frac{1}{r^3}\right)\left[1 + O\left(\frac{m}{M}\right)\right]\right\}. \tag{26}$$

§ 4. Discussions.

(i) Although we have taken into account the law of distribution of the lengths of vectors representing the chains, the dependence of the tension upon M is negligibly small, contrary to the formulae (1). This is due to the fact that the number of junctures is much smaller than the number of the kinematical units as remarked in the introduction. The above law of distribution has mainly be utilized in obtaining the average length l of the vectors as can be seen from the equation (6). Therefore, we can well imagine that the junctures are fixed in space and that the chains have the same average distance between their two ends. Also we see that the branching of chains at the junctures will have no effect.

(ii) We have purposely given no explicit expression for the terms of the order m/M in the equation (26). The reason is that these terms come from those of the order $1/n$ in the equation (20), while we have already neglected the terms of this order when we applied the Stirling's formulae for factorials.

(iii) The terms containing the factor $9\lambda_0^2/25$ in (26) is small, so that we can write (26) in the form

$$\sigma = \frac{\rho RT\lambda_0^2}{m}\left(r - \frac{1}{r^2}\right), \tag{27}$$

where the factor $r - 1/r^2$ comes from the fact that the volume does not change when stretched. This can be seen from the process by which we have obtained the equation (23) for l.

References.

(1) W. Kuhn, Koll. Zeitschr. **76** (1936) 258. H. Mark, Chem. Rev. **25** (1939) 121. F. T. Wall, J. Chem. Phys. **10** (1842) 132, 485, **11** (1943) 527. R. Kubo, Nippon Sugaku-Buturigakukai Kaisi, **17** (1943) 273.

(2) T. Sakai, Nippon Sugaku-Buturigakukai Kaisi, **17** (1943) 226. Also other papers by T. Sakai and by Y. Oti presented to Nippon Buturigakukai, but not yet printed when this manuscript was prepared.

(3) K. H. Meyer & C. Ferri, Helvet. Chim. Acta, **18** (1935) 570.

Short Notes

An Electron Diffraction Study of Anodic Films Formed on Aluminium.1)

By Susumu YOSHIDA.

The Mechanical Laboratory, Ministry of Commerce and Industry.

(Received October 23, 1947)

The crystal structure of anodic films formed on aluminium is not well known in spite of several investigations hitherto made by *X*-ray and electron diffraction. This is perhaps because the diffraction patterns are sometimes confused by impurities or unstable intermediate products, or they are very faint owing to the small thickness and minute grain size of the film. To make these clear, the author carried out the present investigation by electron diffraction using transmission and reflection methods.

(a) Diffuse haloes.

Films anodized in 3 % oxalic acid solution gave three diffuse haloes in both transmission and reflection experiments. The specimens for transmission were prepared in the form of thin transparent films, free from the anodized aluminium foils by dissolving away the base aluminium in dilute hydrochloric acid. Those for reflection were thickly anodized aluminium plates of 1 mm thickness the surface of which were etched with 40 % hydrofluoric acid; those only cleaned up and not etched, gave no clear diffraction patterns. The temperature of anodizing bath was 20~30°C, voltage applied ranges from 5 V to 50 V D.C., and the process was finished in 2~10 seconds for transmission specimens and in 1~4 hours for reflection specimens. As these haloes do not seem to be due to the surface character or charging-up effect and they show no changes by further etching in the case of reflection specimens, it is considered that the films consist of substance showing these haloes. The averaged positions of the haloes are given in the table. They agree neither with the rings of pure aluminium nor with those of γ'-Al$_2$O$_3$, which was assumed to be an imperfect and modified form of γ-Al$_2$O$_3$ by Verwey2) in the explanation of Burgers' result on anodic film. These haloes change into the patterns of γ-Al$_2$O$_3$ when heated, and agree with (220) and (440) rings of γ.Al$_2$O$_3$, in accordance with Belwe's3) results, and moreover the third halo with (660) or γ-Al$_2$O$_3$. Accordingly, it may be considered that the atoms in those films are arrayed already in the lattice of γ-Al$_2$O$_3$, forming small crystal grains which show broad haloes. Only the reflection from (hh0) being observed, it is supposed that they are conglomerates of minute crystals bounded by {110} surfaces.

Table. *d*(Å) of the haloes.

	Obs. values	Beliwe	γ-Al$_2$O$_3$ (a = 7.90 Å)	
			d (Å)	(*hkl*)
I	2.9	2.8	2.76	220
II	1.3	1.4	1.38	440
III	0.93		0.92	660

(b) Böhmite.

Contrary to the above results, films anodized in 3 % sulphuric acid solution and those steam-treated after anodic treatment in sulphuric and oxalic acid solution showed comparatively sharp ring patterns, which changed to the patterns of γ-Al$_2$O$_3$ when heated. Patterns due to various specimens coincided with each other on the whole except small details. Those diffraction rings agreed well with those of böhmite which was obtained from hot water treated anodic films prepared by Harrington.5) Patterns from some of various aluminium hydroxides, which Biltz and others6) studied by X-rays, agree also with these. (Fig. 1) As suggested by Verwey in the case of γ-Al$_2$O$_3$, it may also be supposed that many hydrates of Al_2O_3 of various degree of atomic arrangement exist in the process of formation. This is admitted also by Biltz's investigation. It is perhaps due to the fact that the results of the author and Harrington and Biltz agree in general but differ in some details.

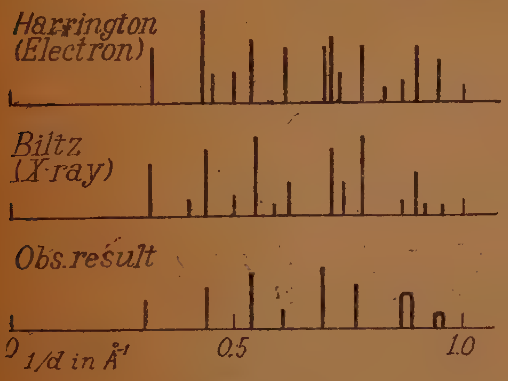

Fig. 1.
Diffraction from "Böhmite"

References.

(1) A more detailed paper will be published in Ôyô-Buturi (in Japanese).

(2) E. J. W. Verwey: Z. f. Krist. **91** (1935) 317.

(3) F. Belwe: Z. f. Phys. **100** (1936) 162.

(4) The crystal structure of böhmite is not yet known. A molecular formula, γ-Al_2O_3-H_2O is given to it, for it becomes γ-Al_2O_3 when dehydrated.

(5) R. A. Harrington: H. R. Nelson; Trans. Amer. Inst. Min. Met. Eng. **137** (1940) 62.

(6) W. Biltz; G. A. Lehrer and K. Meisel: Z. f. anorg. Chem. **172** (1925) 292.

On the Structure of "90°-Magnetic Wall" in the Ferromagnetic Crystal.

By Noboru TSUYA.

Research Institute for Iron, Steel and Other Metals, Tohoku University, Sendai, Japan.

(Received January 13, 1948)

It is usually assumed1) that a ferromagnetic material consists of domains of microscopic size, in each of which the electronic spins are lined up to give a spontaneous magnetization. It is also found experimentally that there are two types of boundaries (magnetic wall) in magnetic domains, namely 180°-wall and 90°-wall; in the case of the former, the directions of spontaneous magnetization of both sides of the boundary are oriented oppositely with respect to each other, and in the case of the latter, those directions differ by 90°. The structure and the behaviour of the former have already been investigated quantum-mechanically by Bloch2), while the discussions concerning the latter are, so far as we know, not yet worked out quantum mechanically. The present short note gives the results of an investigation for the purpose of making clear the above mentioned structure of the 90°-wall.

Now for simplicity, we shall confine ourselves only to the case in which there are two groups of electrons whose directions of spin are exactly perpendicular to each other. Using the usual spin functions α and β3) with z axis as spin axis, the state of the spin, the direction of which orients itself to the direction of the x-axis (which we denote by x-spin), is represented by $2^{-1/2}[\alpha(\sigma)+\beta(\sigma)]\equiv\Omega(\sigma)$4), where σ is a spin variable. Then the wave function of the whole crystal, having l x-spins on the lattice points $n_1, n_2, n_3, \cdots, n_l$, and z-spins on the remaining points, can be written by the following determinantal form:

$$\Phi(n_1, n_2, \cdot\cdot, n_l) = (N!)^{-\frac{1}{2}}\sum_P \delta_P P\phi_1(1)\alpha(1)\phi_2(2)\alpha(2)\cdot\cdot$$

$$\phi_{n_i}(n_i)\Omega(n_i)\cdot\cdot\phi_n(n)\alpha(n), \qquad (1)$$

where P is the usual permutation operator of the coordinate of the electrons and δ_P is 1 when P is even permutation and otherwise -1. Then the general wave function of the system is given by a linear form,

$$\Psi = \sum_{n_1,\ldots n_l} b(n_1, n_2, \cdots\cdot, n_l)\Phi(n_1, n_2, \cdots\cdot, n_l) \qquad (2)$$

whose coefficients shall be determined by diagonalizing the matrix of the Hamiltonian H. which consists of the electronic kinetic energies, electron-electron Coulomb energies and the electron-atom core interactions. In this way the above mentioned process is reduced to the eigenvalue problem of the following type.

$$H'b(n_1, n_2, \cdots\cdot, n_e) = \varepsilon JH_0 b(b_1, n_2, \cdots\cdot, n_c) \qquad (3)$$

where J is the usual exchange integral and ε the energy parameter. Operating the inverse matrix $\mathrm{H}_0{}^{-1}$ on both sides from the left and writing $\mathrm{H}_0{}^{-1}\cdot\mathrm{H}' \equiv \mathrm{H}$, then (3) becomes:

$$Hb(n_1, n_2, \cdots\cdot, n_e) = \varepsilon Jb(n_1, n_2, \cdots\cdot, n_e), \qquad (4)$$

It can be shown that the new Hamiltonian operator **H** containing the operators, which decrease or increase the number of z- and x- spins by unity, has exactly the same form as in the case of Bloch's[5)]. So that this eigenvalue problem may be treated exactly in a similar way to Bloch's case. Then it is concluded that the 90°-wall can really exist and that the breadth δ of the wall is given by $\delta = a(J/C)^{1/2} \fallingdotseq (100 \sim 1000)a$, where a is the lattice constant and c is a energy of the spinspin or spin-orbit interactions which give rise to the internal stress (magnetostriction), crystal energy or demagnetizing force etc. Of course in that case the energy for its occurence must be lower than that for the 180°-wall or for the case where there is no magnetic wall.

In addition, for the above mentioned reason, it is clear that the spin state due to 90°-wall is constructed by the superposition of those due to 180°-wall, so that there is no essential difference between these magnetic walls. For example, the velocity of the 90°-wall displacement is given by the Katayama's[6)] formula derived for 180°-wall by substituting l with δ and $\sqrt{\varphi^*\varphi\,\psi^*\psi}$ with

$$\sqrt{\frac{1}{2}(\varphi^*\varphi+1)\psi^*\psi},$$

then this velocity being of the same order as for the 180°-walls. i.e.

$$v_{180°}/v_{90°} = (\delta/l)\left[\int\sqrt{\varphi^*\varphi\psi\psi}\,dz\right]^2$$

$$\left[\int\sqrt{\frac{1}{2}(\varphi^*\varphi+1)\psi^*\psi}\,dz\right]^{-1} \sim 0.8\,l/\delta.$$

References.

(1) R. Becker & W. Döring: Ferromagnetismus, Springer (1939).
(2) F. Bloch: ZS. f. Phys., **74** (1932), 295.
(3) R. Becker & W. Döring: loc. cit. P. 84.
(4) $\sigma_x\Omega(\sigma) = \Omega(\sigma)$; $\sum_\sigma \Omega^*\sigma_2\Omega = \sum_\sigma \Omega^*\sigma_y\Omega = 0$
(5) F. Bloch: loc. cit.
(6) T. Katayama: Shortly to be published in this Journal.

On Transitional Region in Phase Change of Barium Titanate.

By Shizuo MIYAKE and Ryuzo UEDA.

Kobayashi Institute of Physical Research, Kobubunji Tokyo, Japan.

(Received January 19, 1948)

In the previous papers[1)2)] we reported the experimental observation on the phase change of barium titanate ($BaTiO_3$), in which we confirmed the existence of a transformation from the tetragonal lattice into the cubic one at the Curie point about 110°C. We also found the fact that there exists a transitional region of the temperature interval of about 10°C below the Curie point. For the purpose to examine this region more closely, we performed the following dilatometer and X-ray measurements on the same sample as the one we used before.

(1) *Dilatometer measurements.*

The dilatometer used here consisted of a glass capillary stem and a glass bulb. A powder sample of ca. 1.8 gr was inserted into the bulb, and the dilatometer was filled with paraffin oil whose meniscus in the capillary was read by using a cathetometer.

Fig. 1 shows the volume vs. temperature curve in the neighborhood of the Curie point, which could be obtained by comparing the dilatometer measuements and the changes of lattice volume observed in X-ray study as formerly reported. The ordinate corresponds to the volume of the sample plus a constant. The volume of the sample increases linearly until 99°C. From this temperature the curve almost stops to increase for an interval of about 10°C, but again it begins to ascend steeply at 110°C. Von Hippel and his co-workers3) have found a similar anomalous region in thermal expansion of barium titanate over the range of 95°∼120°C.

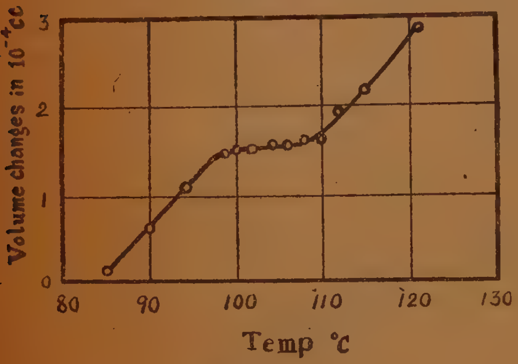

Fig. 1.

Von Hippel and others also reported the existence of another anomaly in dielectric constant and thermal expansion at about 10°C, but we could not observe any corresponding singularity at this temperature in our dilatometer measurements.

(2) *X-ray measurements.*

We next made the study on the change of the fine structure of the Debye line of (510)(431)-reflection in the transitional temperature range, using CuK_α radiation. The intensity distribution of the lines was measured by using a microphotometer.

At 110°C, we can see two main peaks which are clearly corresponding to the K_{α_1} and K_{α_2} lines of (510)(431)-reflection of the cubic lattice. As the temperature is lowered, the lines begin to broaden slightly and the broadening reaches its maximum at 102°C. At 98°C they begin to recover the sharpness again, but a small hump appears outside the main peak lines. Lowering the temperature about 12°C, namely at about 86°C, the main lines become sharper and the small hump splits into three peaks, which correspond to the reflections from the tetragonal lattice. The variation in the intensity distribution of the lines as here observed may be explained in the following manner: Each crystallite of the powder sample is considered as being a small single crystal of a perfect cubic lattice of the perovskite type above the Curie point. Passing the temperature down the Curie point, each crystallite will begin to split out into many domains, each of which is considered to be of a tetragonal lattice, having a spontaneous electric polarization along *c*-axis. Such a domain structure may alternatively described as a twinned structure, whose existence has recently been confirmed by Kay and Rhodes4) on the barium titanate single crystal in their beautiful work. The small size of these domains and the lattice distortion will make the Debye lines diffuse as actually observed. Below the transitional temperature range, each domain gradually grows up into a larger tetragonal crystallite and, as the result, Debye lines in the multiplet will become sharper again.

Lattice constant *a* which is calculated on the

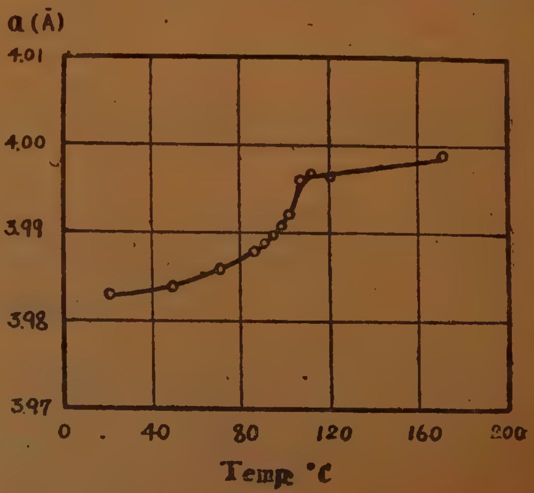

Fig. 2.

main lines is shown in Fig. 2. In a recent paper[5], it has been reported that the cubic and tetragonal lattices coexist in some temperature range near the Curie point, and that axial ratio c/a has a discontinuity in the transition. This result seems to differ from ours. For, according to our observation, the change of the lattice constant at the Curie point accompanies no discontinuity, though its variation in the transitional region is rather rapid. Also, we have no evidence for the coexistence of the two phases in any temperature range near the Curie point so far as our powder sample is concerned.

The more detailed results will be reported shortly in this Journal.

In conclusion we wish to express our sincere thanks to Mr. T. Ogawa, who gave us the sample according to our proposal. This study was helped by the research grant given from the Ministry of Education.

References.

(1) S. Miyake and R. Ueda: Jour. Phys. Soc. Japan., **1**, (1946), 32.

(2) S. Miyake and R. Ueda: ibid., **2** (1947) 93.

(3) A. von Hippel, R. G. Breckenridge, F. G. Chesley and Laszlo Tisz: Ind. Eng. Chem., **38**, (1946), 1097.

(4) H. F. Kay and R. G. Rhodes: Nature **160** (1947), 126.

(5) M. G. Harwood, P. Popper and D. F. Rushman: ibid., **160** (1947), 58.

On Melting of Polymer Crystals.

By Akira ISIHARA

Physical Institute, University of Tokyo

(Received July 19, 1947)

§ 1. Introduction.

It seems that there exist two features in the melting of paraffin homologues such as normal paraffin and those whose terminal groups are substituted by carboxyl groups, ester groups or keton groups etc. Firstly, their melting points as a function of their degree of polymerization is raised at first linearly with the number of their carbon atoms, then tend to saturation gradually, and finally converge to about 400°K as in Fig. I.(1) Secondly, these polymers show so called "premelting"(2), and thereby their specific heats(3,4) or thermal expansion coefficients(5) show a sharp λ-typ peak. To a certain degree this is affected (especially in the case of crystal state) by impurities(3,5), as has been considered by some authors(6). But, according to the systematic measurements of Ubbelohde(2), Van Hook and L. Silber(4) and others(6,7) this is also the feature of pure substances. Accordingly we must explain these two facts if we wish to treat the melting of these homologues. Two authors already tried to treat the former feature theoretically, but it seems not complete as yet. In this paper we treat these problems by using statistical mechanics.

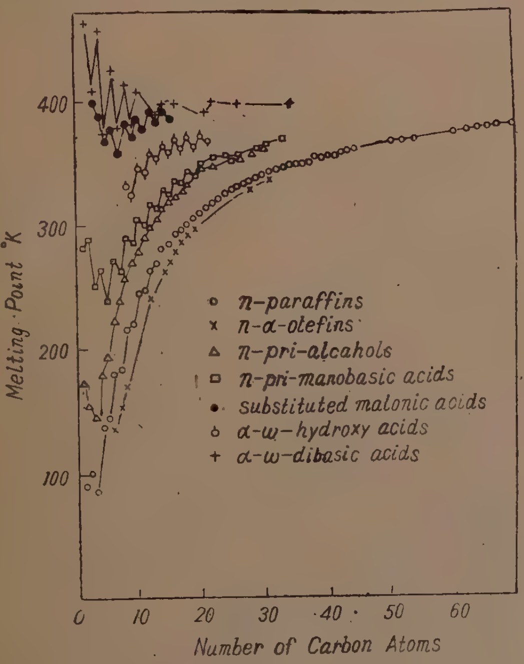

Fig. 1. Melting points of paraffin homologue series.

§ 2. Theory.

It can be conceived that there exist two kinds of molecules in such melting range, one in the crystalline state and the other in the liquid state. Let the number of the former be Nx and that of the latter $N(1-x)$ (N is the total number of molecules), f_c and f_l the partition function of each molecule, and φ_c and φ_l the potential energy (measured from the gas state) of the molecules in the crystalline and liquid state respectively. Then the free energy ϕ of the system is given by:

$$\exp(-\phi/kT) = f_c^{Nx} \exp\left(\frac{Nx\varphi_c}{kT}\right) \times f_l^{N(1-x)} \exp\left(\frac{N(1-x)\varphi_l}{kT}\right) \frac{N!}{(Nx)!\,N(1-x)!}. \qquad (1)$$

We assume here that the potential energies are proportional to the degree of order x:

$$\varphi_c = \frac{\alpha x}{2}, \quad \varphi_l = \frac{\beta(1-x)}{2}. \qquad (2)$$

These assumption resembles that in the order-disorder theory of alloys, and represents that the melting is a cooperative phenomena.

From equation (1) we get:

$$\phi = NkT\left\{x\log x + (1-x)\log(1-x) - \frac{\alpha x^2}{2kT} - \frac{\beta(1-x)^2}{2kT} + xF - \log f_l\right\}, \qquad (3)$$

where

$$F = \log\frac{f_l}{f_c}. \qquad (4)$$

The equilibrium value of x at any temperature, and the melting point itself can be determined from the conditions that:

$$x = \frac{1}{2}: \qquad \frac{\partial \psi}{\partial x} = 0\,, \quad \frac{\partial^2 \psi}{\partial x^2} = 0\,.$$

Thus

$$x = \frac{f_c e^{\frac{\alpha x}{kT}}}{f_c e^{\alpha x/kT} + f_l e^{\beta(1-x)/kT}}\,, \tag{5}$$

$$\alpha + \beta = 4kT_0\,, \tag{6}$$

$$\alpha - \beta = 2kT_0 F_0\,, \tag{7}$$

where T_0 means the melting point, F_0 the value of F at $T = T_0$. The meaning of these equations are obvious. It is to be noted that in this case not only the difference of potential energies of two states but also the vibrational energies participate in the transition.

Relation to the case of Bragg-Williams can be obtained as follows. Designating

$$y = 2x - 1\,, \tag{8}$$

and rewriting equation (5) we get

$$y = \tanh\left(\frac{T_0}{T} y + \frac{1}{2}\left(\frac{T_0 F_0}{T} - F\right)\right). \tag{9}$$

When the vibrational energies are zero, this reduces to the case of Bragg-Williams:

$$y = \tanh \frac{T_0}{T} y\,. \tag{10}$$

From equation (9) we can see that the vibrational energy of molecules participates in the transition as above stated. This fact will be more clear if we calculate the specific heat of the system.

From equation (3) the internal energy is given by:

$$U = NkT^2\left\{x \frac{f_c'}{f_c} + (1-x)\frac{f_l'}{f_l} - \frac{1}{kT^2}\left(\frac{\alpha}{2}x^2 + \frac{\beta}{2}(1-x)^2\right)\right\}, \tag{11}$$

where $'$ means the derivative with respect to the temperature. From this equation the specific heat is calculated as follows:

$$C = Nk\left\{x\left(T^2\frac{f_c'}{f_c}\right)' + (1-x)\left(T^2\frac{f_l'}{f_l}\right)' - \left(\frac{\alpha x - \beta(1-x)}{kT}\right)\frac{dx}{dT} - T^2 F' \frac{dx}{dT}\right\}. \tag{12}$$

The meaning of the first and the second terms is obvious. The third and the fourth terms represent the energy necessary to raise crystalline molecules to the liquid state. These abnormal part of specific heat can be written as follows:

$$C_{ab} = N\{(\alpha x - u_c) - (\beta(1-x) - u_l)\}\left(-\frac{dx}{dT}\right), \tag{13}$$

where u_c and u_l are the internal energy of the molecule of each state. The meaning of this equation is also clear.

If we expand F in a series of powers of $(T - T_0)$, assuming it varies continuously with temperature, we can obtain:

$$C_{ab} = \frac{Nk}{9}\left\{Z^{-\frac{2}{3}} - Z^{-\frac{1}{3}} + \ldots\ldots\right\}, \tag{14}$$

where

$$Z = \left\{\frac{3}{2}(F_0 + T_0 F_0')\right\}^{-2}\left(\frac{T - T_0}{T_0}\right). \tag{15}$$

The first term of equation (14) is an even function, whereas the second term is an odd function; there must be a sharpe peak of λ-type. These asymmetry terms come from the second term on the right side of equation (9). The melting range $(T - T_0)/T_0$ at some constant value of C_{ab} or Z is proportional to $(F_0 + T_0 F_0')^2$, and the latter represents the change of entropy at the melting point. The increase in entropy at melting is the order of 2 E.U. in the case of ordinary simple substances, but in the polymers it is considered to be larger since in this case there is a change in internal configurations. Accordingly, these polymers reveal comparatively wide melting range.

Now let us consider the molecules composed of n carbon atoms. These molecules have 3 $(3n+2)$ degrees of freedom. 6 of these represent the motion of a molecule as a whole and we take for convenience Einstein model for these degrees of freedom and designate their characteristic temperature by Θ. Among the remaining freedoms, the most important are those corresponding to $3n-6$ skeletal vibrations. For these freedoms, we also take Einstein model, and designate their characteristic temperature by θ. On the other hand, the liquid molecule must be composed of a "segment" as is mentioned in many investigations.

For example, the experiments of Ramaneffect performed by Simanouti and Mizushima(8) show that the elongated molecules in the form of saw-teeth which contain more than 12 carbon atoms do not seem to exist in the liquid state. Accordingly, we consider that each liquid molecule is separated into γ-segments. Let us take Einstein model for the liquid state and designate the charatceristic temperature of the segment as a whole by Θ', and that of the internal degrees of freedom of a segment by θ'. Then

$$f_c = \frac{1}{(1-e^{-\Theta/T})^6} \cdot \frac{1}{(1-e^{-\theta/T})^{3(n-2)}}, \qquad (16)$$

$$f_l = \left\{ \frac{1}{(1-e^{-\Theta'/T})^6} \cdot \frac{1}{(1-e^{-\theta'/T})^{3(n-2)}} \right\}^{n/\gamma}. \qquad (17)$$

When the temperature is high enough,

$$F = \log\frac{f_l}{f_c} \doteqdot 6\log\frac{\Theta}{\theta} + 3\left(\log\frac{\theta}{\theta'} + \frac{2}{\gamma}\log\frac{\theta'}{\Theta'}\right)n. \qquad (18)$$

On the other hand the binding energy of these polymers is van der Waals' interaction energy and it has an additive character.

Accordingly, we can put

$$\alpha = a + bn, \qquad (19)$$

where b represents the potential energy difference per CH_2 group between crystalline and liquid state, and a represents the contribution to this from the end groups. Then from equation (6) and (7),

$$\alpha = kT_0(2+F_0). \qquad (20)$$

If we put

$$\left.\begin{aligned} c &= k\left(2+6\log\frac{\Theta}{\theta}\right), \\ d &= 3k\left(\log\frac{\theta}{\theta'} + \frac{2}{\gamma}\log\frac{\theta'}{\Theta'}\right), \end{aligned}\right. \qquad (21)$$

then the melting point is expressed as follows:

$$T_0 = \frac{a+bn}{c+dn}. \qquad (22)$$

This is precisely the equation deduced experimentally by Garner and others(9). It can be easily shown that this expression is also valid when we take the second approximation in (18). When n becomes large enough,

$$T \to T_{\infty} = \frac{b}{d} = \frac{b}{3k\left(\log\frac{\theta}{\theta'} + \frac{2}{\gamma}\log\frac{\theta'}{\Theta'}\right)}. \qquad (23)$$

The terms on the right side depend upon internal vibrational freedom of molecules in the state of solid, the potential energy per CH_2 group and the state of a segment, and does not include the terms characterizing the molecule as a whole. Therefore, T_{∞} represents the asymptotic melting temperature characteristic of homologues when their degree of polymerization becomes large.

From equation (22), if we put

$$\alpha = \frac{a}{b}, \quad \beta = \frac{c}{d}, \qquad (24)$$

we obtain:

$$\frac{1}{\left(\frac{T_0}{T_{\infty}} - 1\right)} = \frac{1}{\alpha - \beta}(n+\beta). \qquad (25)$$

This relation is shown in Fig. 2, taking T_{∞} as 415°K.

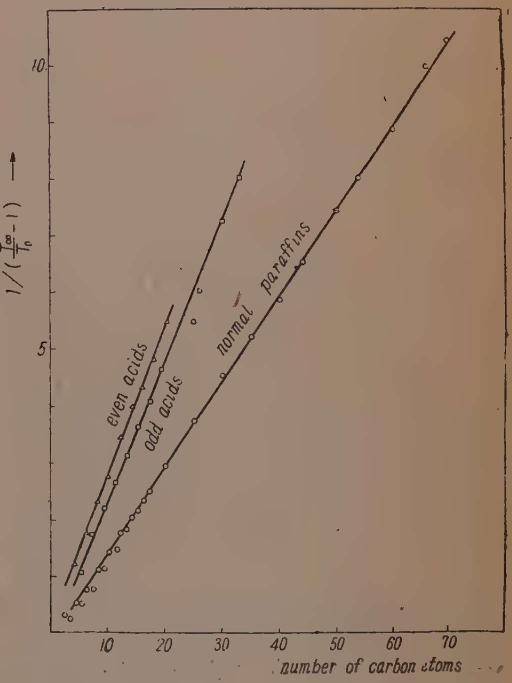

Fig. 2. Relation between the melting points T_0 and the number of carbon atoms.

From equation (23)

$$b = 3kT_{\infty}\left(\log\frac{\theta}{\theta'} + \frac{2}{\gamma}\log\frac{\theta'}{\Theta'}\right)$$

$$\doteqdot 1.0 \times 10^{-13}\ \text{erg}.$$

This value is of the same order as the lattice energy per CH_2 of normal paraffin calculated by Müller (1.3×10^{-13} erg) and the same value was deduced from sublimation heat by Ubbelohde(8). As we cansee from equation (25), the greater the slope of the straight line of Fig. 2 and the higher its intersect on the ordinate axis, the smaller the effect of end groups. From the figure we can obtain the ratio a/b:

normal paraffin	$a = 6.66\,b$,
even acid	$= 4.54\,b$,
odd acid	$= 4.14\,b$.

That is, the end effect is largest in the case of normal paraffin. The interaction energy of CH_3 groups seems smaller than that of COOH groups and therefore the above result seems queer. But as is shown in Fig. 3(11) the spacing of C axis of these crystals is in the above order, and therefore the order seems to be legitimate (The a and b-spacings are nearly constant.).

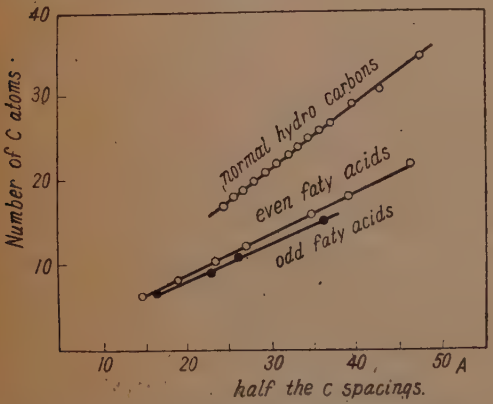

Fig. 3. The C spacings of a number of related long chain hydrocarbon compounds.

The entropy-change of melting is derived from equation (18) and is approximately:

$$\Delta S = R\left\{6\log\frac{\Theta}{\theta} + 3\left(\log\frac{\theta}{\theta'} + \frac{2}{\gamma}\log\frac{\theta'}{\Theta'}\right)n\right\}.$$

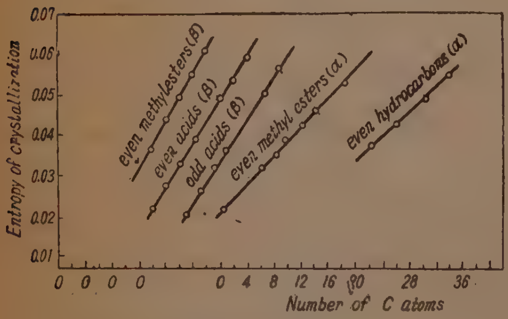

Fig. 4. Entropies of fusion vs. number of carbon atoms
α......vertical crystal form.
β......tilted crystal form.

Therefore, ΔS plotted against the number of carbon atoms must be a straight line and be parallel for each homolougues. This is shown in Fig. 4(9).

The specific heats of crystalline and liquid state can be obtained from equation (16) and (17),

$$C_{\text{crys}} = 3R\left\{2f_E\left(\frac{\Theta}{T}\right) + (n-2)f_E\left(\frac{\theta}{T}\right)\right\},$$

$$C_{\text{liq}} = 3R\frac{n}{\gamma}\left\{3f_E\left(\frac{\Theta'}{T}\right) + (\gamma-2)f_E\left(\frac{\theta'}{T}\right)\right\},$$

where f_E represents Einstein function. Approximately $f_E\left(\frac{\Theta}{T}\right) \simeq 1$, $f_E\left(\frac{\theta}{T}\right) \simeq 0.5$, and therefore the curve of the specific heat of crystalline state vs. carbon atoms must be a straight line passing about 6 cal. at $n = 0$. This is shown in Fig. 5(12).

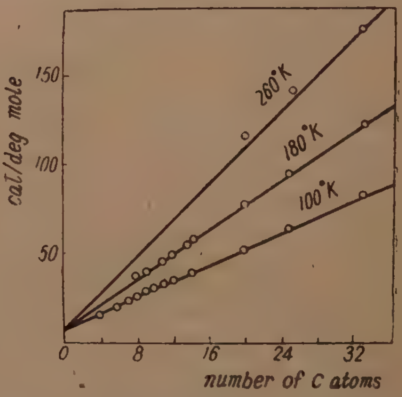

Fig. 5. Relation between the specific heats of solid normal paraffins and their carbon atoms.

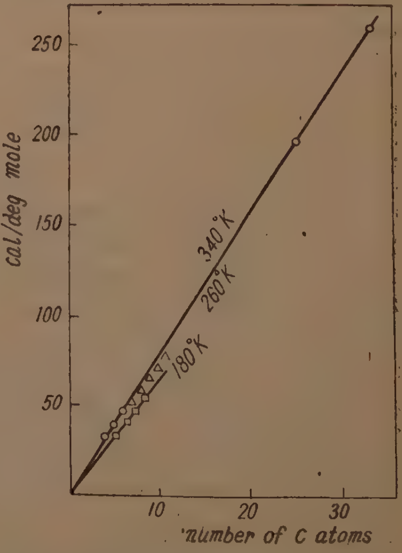

Fig. 6. Relations between the specific heats of liquid normal paraffins and their carbon atoms.

And the curve of the specific heat of liquid state must be a straight line passing through the origin. This is shown in Fig. 6(12).

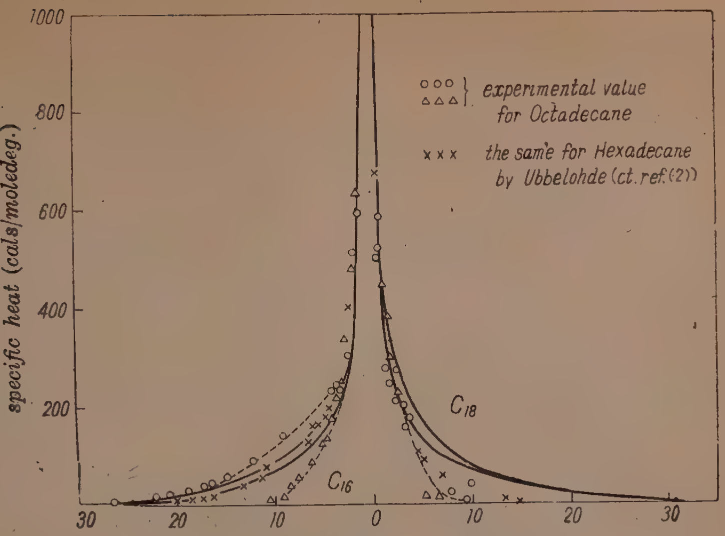

Eig. 7. Abnormal specific heat of Octadecane and Hexadecane at their melting points—: calculated.

From these graphs, we find approximately that $\Theta = 100$, $\theta = 250$, $\Theta' = 126$, $\theta' = 240$ and $\gamma = 5$. Using these figures we calculated the specific heat near the melting point of hexadecane and octadecane, and is illustrated in Fig. 7. As these values are somewhat arbitrary and we did not fit the theretical curve to the experimental curve so rigorously, coincidence is not so good particularly in the range of liquid state. But it may be noted that the specific heat increases considerably steeper than in the theory of Bragg-Williams (in this case the peak is only the order of several calories per mole), and secondly the melting range of hexadecane is somewhat smaller than that of octadecane in the theoretical curve.

In the above considerations we have confined ourselves to the melting of paraffin homologues only, but the saturation phenomena as in Fig. 1 has been observed in the boiling points of paraffin homologues, too, and in the second order transition of polystyrene(13), and in the freezing points of polyisobutyrene and rubber(14), and these treatments and concepts seem to be adaptable to these cases.

In conclusion, I wish to express my hearty thanks to Professor T. Sakai for his kind guidance and also T. Simanouti for his valuable informations on the present subject.

References.

(1) A. M. King and W. E. Garner: J. Chem. Soc., (1931), 578. R. E, Powell, C. R, Clark and H. Eyring: J. Chem. Phys. **9** (1941), 268.

(2) A. Müller: Proc. Roy. Soc. **127** (1932), 514.

(3) A. R. Ubbelohde: Trans. Farad. Soc. **34** (1938), 282.

(4) N. Bekkedahl and L. A. Wood J. Res. Nat. Bur. Stand. **19** (1937), 551.

(5) A. Van Hook and L. Silber: J. Chem. Phys. **11** (1942), 686.

(6) Overstreet and Giauque: J. Am. Chem. Soc. **59** (1937), 25: Witt and Kemp: ibid. **59** (1937) 273.

(7) Egan and Kemp: ibid. **59** (1937), 1264; Strelkow and Harshkovsky: Phys. Zeits. der Sowjet. **12** (1937), 45; Strelkow: Sow. Phys. **12** (1937), 23, 73; J. W. Oldham and A. R. Ubbelohde: Proc. Roy. Soc. **176** (1940), 50.

(8) T. Simanouti and S. Mizushima: J. Chem. Soc. of Japan, **64** (1943), 1064; etc.

(9) W. E. Garner, K. van Bibber and A. M. King: J. Chem. Soc. (1931), 1533; etc. K. H. Meyer, and A. Van der Wyk: Helv. Chim. Acta, **20** (1937), 1913.

(10) A. Müller: Proc, Roy. Soc. **154** (1936), 624; **158** (1937), 403; **178** (1941), 227; etc.

(11) A. Müller: Proc. Roy. Soc. **114** (1927), 542, **120** (1928), 437; **127** (1930), 417. Wykoff: The structure of crystals pp. 378.

(12) A. R. Ubbelohde: Trans. Farad. Soc. **35** (1939), 843; M. L. Huggins: J. Phys. Soc. **43** (1939), 1095.

(13) K. Ueberriter: Koll. Zeits, **102** (1943), 272; R. F. Boyer and R. S. Spencer: J. App. Phys. **16** (1945), 594.

(14) K. Ueberriter: Zeits. Phys. Chem. **B45** (1940), 361.

On the Thermionic Constants of the Polycrystalline Metal (II).

By Tetsuya ARIZUMI

Kawanishi Kikai Seisakusho Co. Ltd., Kobe.

(Read July 17, 1942, Received March 17, 1947)

§ 1. Introduction.

To measure the difference of contact potentials is one of the important methods of determining work function. When V_{12} is the difference of contact potentials and φ_1 and φ_2 are the work functions of two metals, the following relation holds;

$$V_{12} = -(\varphi_1 - \varphi_2) \qquad (1)$$

When either of φ_1 or φ_2 has been known, the unknown one is calculated from the equation (1). The one method of determining the difference of contact potentials is to measure directly by an electrometer. This is the most important method, by means of which several accurate data have been already obtained, but in the present paper it will not be considered. The second method is to make use of the thermionic emission current from the cathode. Thermo-electrons emitted from the cathode have the initial velocity corresponding to the cathode temperature whose distribution obeys the Fermi-Dirac's law. Thus the small amount of electron current flows into the anode even when the anode potential is slightly negative and it is represented in the form

$$i = i_s \exp\left(-\frac{eV}{kT}\right) \quad V < 0, \qquad (2)$$

where i_s is the saturation current and V the negative potential of the anode. For $V > 0$, all the electrons emitted from the cathode should flow into the anode, and from the theoretical viewpoint, gives the definite saturation current corresponding to the cathode temperature. Accordingly, if there is no difference of contact potentials between the cathode and the anode, the "Anlaufstrom" approaches the saturation current at null anode potential, but, if there is the difference of contact potentials, the kink points on the current-voltage curves are expected to move to negative or positive side according to whether the difference of contact potentials is positive or negative.

Thus from the sign and the amount of the displacement of the kink point we are able to determine the sign and value of the difference of contact potentials. Such method to measure the difference of contact petentials may well be called "initial velocity method" in the following.

When all surfaces of both the cathode and the anode have uniform work functions, the difference of contact potentials determined from the above mentioned method and thus the value of the work function should coincide with the real value, but when there co-exist the regions of different work functions both surfaces of the cathode and the anode, as in a polycrystalline metal, the experimental value will be an average one in a sence. Is there any correlation between the work function determined by the initial velocily method φ_K^* and the one obtained from the Richardson line method φ_t^*? To make clear such questions is the main object of the present paper.

§ 2. Correlation between φ_t^* and φ_K^*.

In almost all experiments, polycrystalline metals have been used for the cathode and the anode, on both surfaces of which the work functions are not uniform. In such a case the saturation current cannot be represented simply by

$$i_s = AT^2 \exp\left(-\frac{e\varphi}{kT}\right) \qquad (3)$$

as pointed out in the previous paper(1), while the "Anlaufstrom" will be expressed by (2), although anode potential V differs from the value obtained in a system with uniform work function. To avoid such ambiguity, it is assumed that the anode has a single work function in the following calculation.

In the case of the plane electrodes, the Anlaufstrom is given by (2), where V is of course the effective potential. If V is the potential supplied to the anode, and φ_c and φ_a are work functions of the cathode and the anode respectively, we have

$$V = -V_a+\varphi_a-\varphi_c. \qquad (4)$$

Now dividing the cathode surface into the domains of small area with uniform work functions, the emission current from such a divided area is given by

$$\varDelta i_n = \varDelta i_{sn} \exp\left\{-\frac{e}{kT}(-V_a+\varphi_a-\varphi_c)\right\}. \qquad (5)$$

When σ_n is the area of one of such divided portions and φ_n its work function, $\varDelta i_{sn}$ is represented by

$$\varDelta i_{sn} = \sigma_n A T^2 \exp\left(-\frac{e\varphi_n}{kT}\right). \qquad (6)$$

Substituting (6) into (5), and summing up all over the cathode surface, the total Anlaufstrom is represented by

$$\begin{aligned} i &= \sum_n \varDelta i_n \\ &= AT^2 \exp\left\{-\frac{e}{kT}(-V_a+\varphi_a)\right\}\cdot\sum \sigma_n, \qquad (7) \end{aligned}$$

while the total emission current from the cathode is given by

$$i_s = \sum_n \varDelta i_{sn} = AT^2 \sum_n \sigma_n \exp\left(-\frac{e\varphi_n}{kT}\right). \qquad (8)$$

As the relation $i = i_s$ is satisfied for the case of the difference of contact potentials being zero, we obtain

$$V_a-\varphi_a = -\frac{kT}{e}\log\frac{\sum\limits_n \sigma_n}{\sum\limits_n \sigma_n \exp\left(-\frac{e\varphi_n}{kT}\right)}. \qquad (9)$$

As shown in the previous paper, the following relation holds:

$$\varphi_i^* = \frac{kT}{e}\log\frac{A^*}{A}\cdot\frac{\sum\limits_n \sigma_n}{\sum\limits_n \sigma_n \exp\left(-\frac{e\varphi_n}{kT}\right)}. \qquad (10$$

Substituing (10) into (9), we obtain

$$V_a-\varphi_a = -\varphi_i^*.$$

Since $\varphi_c = \varphi_a - V_a$ at $V=0$, *i. e.*, $i = i_s$ refers to the average value determined from the initial velocity method, φ_c will be denoted by φ_k^* and then the following relation is obtained.

$$\varphi_k^*-\varphi_i^* = \frac{kT}{e}\log\frac{A}{A^*}. \qquad (11)$$

As pointed out in the previous paper(1), A^* is in general smaller than A for the cathode with many work functions, φ_k^* is always larger than φ_i^*.

Since φ_i^* and A^* in (11) is given as functions of φ_n:

$$\varphi_i^* = \frac{\sum\limits_n p_n\left(\varphi_n+T\frac{\partial\varphi_n}{\partial T}\right)\exp\left(-\frac{e\varphi_n}{kT}\right)}{\sum\limits_n p_n \exp\left(-\frac{e\varphi_n}{kT}\right)}, \qquad (12)$$

and

$$\begin{aligned} \log\frac{A^*}{A} &= \log\left\{\sum_n p_n \exp\left(-\frac{e\varphi_n}{kT}\right)\right\} \\ &\quad + \frac{e}{kT}\frac{\sum\limits_n p_n\left(\varphi_n+T\frac{\partial\varphi_n}{\partial T}\right)\exp\left(-\frac{e\varphi_n}{kT}\right)}{\sum p_n \exp\left(-\frac{e\varphi_n}{kT}\right)} \qquad (13) \end{aligned}$$

as shown in the previous paper, φ_k^* in (11) is represented in the simple form

$$\varphi_k^* = -\frac{kT}{e}\log\left\{\sum_n p_n \exp\left(-\frac{e\varphi_n}{kT}\right)\right\}, \qquad (14)$$

showing that φ_k^* is a function of the cathode-teperature as well as φ_n.

Especially when $n=2$, and further,

$$i_1 = p\exp\left(-\frac{e\varphi_1}{kT}\right) \gg (1-p)\exp\left(-\frac{e\varphi_2}{kT}\right) = i_2,$$

φ_k^* becomes

$$\varphi_k^* = \varphi_1 + \frac{kT}{e}\log\frac{1}{p}. \qquad (15)$$

Since φ_i^* is equal to φ_1 under the same condition, φ_k^* differs from φ_i^*. On the contrary, if $i_1 \ll i_2$, we have $\varphi_k^* = \varphi_2$, φ_k^* coinciding with φ_i^*. This shows that, when almost all emission current comes from the portions with lower work function, the value determined by the Richardson line method differs from the one determined from the initial velocity method, while both values coincide with each other when emission current is mainly contributed from the portions with higher work function.

§ 3. Numerical Data.

As an illustration, the case where there are only two different work functions $\varphi_1 = 3.0$ *e. v.* and $\varphi_2 = 4.0$ *e. v.*, will be treated in this paragraph. The calulation of φ_k^* is easy to be carried out using the formula (15). In Fig. 1 the relation between φ_k^* and T is shown with p parameter. In general the variation of φ_k^* is comparatively small when p is large and it is almost constant when p is expremely small. Only when p is of medium value, the variation becomes appreciable. Fig. 2 shows the variation of φ_k^* against p. The slope of curve is rather smooth for the lower cathode, temperature, but, the higher the temperature, the steeper the slope of the curves. In other words, φ_k^* varies from φ_1 to φ_2 in the slight change of p. According to the initial velocity method, therefore, the more accurate value of the difference of contact potentials will be obtained when the measurement will be carried out at the lower temperature.

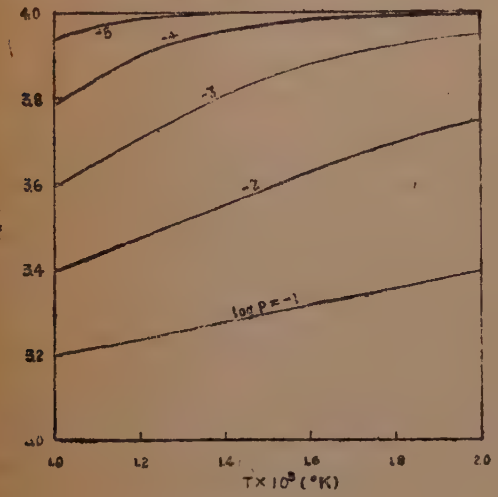

Fig. 1.

The formula (15) will be written as

$$\varphi_k^* = \frac{kT}{e}\left(\log A - \log\frac{i_s}{T^2}\right), \quad (15')$$

which is actually the same as the one to determine the work function by means of the Richardson line method. In the latter, φ_t^* and A^* are determined from the inclination of the experimental curve, while in the former φ^*_k is calculated under the assumption that A is constant.

§ 4. Comparison with Experiments.

In the cases of pure metals, especially tungsten, many results on the thermionic constants have been obtained by the Richardson line method, but few by the initial velocity method, and thus it is rather difficult to compare in detail the theory with experiments. In Table I, there are shown work functions of tungsten and tantalum, experimentally determined by the Richardson line method and

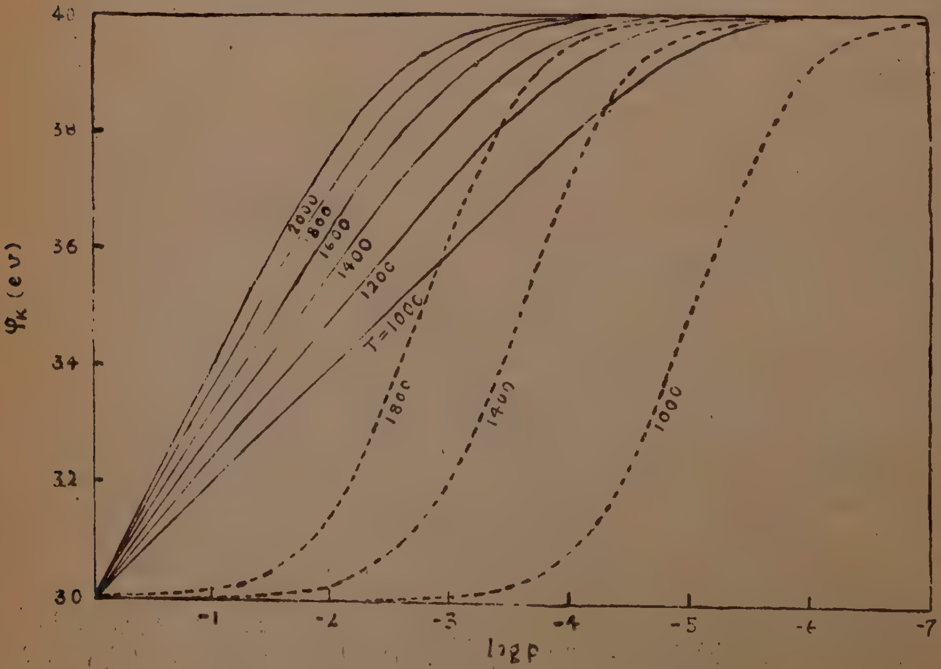

Fig. 2. Full lines show φ_k^* and dotted lines φ_t^*.

only one result by the method, deviced by Sano(4), which is, in principle, similar to the initial velocity method, modified to some extent.

The work functions of these two metals, obtained by the initial velocity method, are larger than those by the Richardson line method as expected from the present theory.

Table I.

Tungsten		Tantalum	
Observer	Work function (e.v.)	Observer	Work functions.
L. Langmuir(2)	4.5	A. B. Cardwell(8)	4.10
L. Langmuir(2)	4.27	H. C. Rentschler & others(6)	4.12
K. K, Smith(2)	4.48	A. B. Cardwell(9)	4.15
C. Davisson & L. H. Germer(2)	4.55		
S. Dushmann & others(2)	4.53		
H. J. Spanner(2)	4.3		
C. Zwikker(2)	4.50		
C. Zwikker(2)	4.58		
A. H. Warner(2)	4.25		
M. C. Johnson & F. A. Vick(3)	4.55		
H. B. Waldin & L. V. Whitney(4)	4.63		
W. B. Nottingham(5)	4.73		
H. C. Rentschler & others(6)	4.60		
A. W. Warner(7)	4.54		
Average	4.51	Average	4.12
S. Sano & K. Koga(10)	4.67	S. Sano & K. Koga(10)	4.24

If the thermionic constants of all crystal surfaces and moreover the ratio of each of these surfaces to the total cathode surface area are known, the average themionic constants will be calculated by (12), (13) and (14). Up to the present, however, the accurate knowledge on these quantities is very poor for all metals. Only in the case of tungsten, the thermionic constants of some of the crystal surfaces have been measured accurately, but the frequency of appearace of these crystal surface on the polycrstalline wire is quite unknown, so that under the assumption that the crystal surfaces, whose thermionic constants have been known, have the equal probability to appear on the polycrystalline surface, the work function φ_t^* and φ_k^* was calulated, in which Nichols'(11) data were used for the thermionic constants of each crystal surface, except for the Richardson constant. As discussed in detail in the previous paper, the theoretical value, 120A/cm^2·deg^2 was assumed for that of each crystal surface, instead of the experimental one. Under such assumption, $\varphi_t^* = 4.44$ e. v. and $\varphi_k^* = 4.48$ e. v. at 1700° K is obtained, which are smaller than the corresponding values in Table 1. The discrepancy will be caused for various reasons, one of which is presumably the inaccuracy of the thermionic constants of each crystal surface of the single crystal. But the relation $\varphi_k^* > \varphi_t^*$ holds, as expected from the theory.

Finally the calculation of φ_k^* of pure tungsten from (15′) by making use of experimental values of temperature T and total emission current i_s was carried out. In Table II, experimental values of emissions, φ_k^* calculated from (15′) and φ_t^* are shown. As seen in the table, the work function, calculated from the initial velocity method, is always larger than that from the Richardson line method. The average value of φ_t^* is 4.51 e. v.

Table II.

Tem. (°K)	Emission (A)	φ_k^* (e.v.)	φ_l^* (e.v.)
1470	1.85×10^{-8}	4.708	4.52
1539	9.97×10^{-8}	4.713	
1613	5.63×10^{-7}	4.722	
1695	2.87×10^{-6}	4.731	
1786	1.60×10^{-5}	4.737	
1887	8.83×10^{-5}	4.745	

while the present experimental value is 4.52 e. v. and the experimental value of φ_k^* is 4.67 e. v., while the calculated one is 4.73 e.v. This good agreement seems to support the present theory.

§ 5 Conclusion.

In the present paper the initial velocity method of determining the work function of the thermionic cathode was considered in details. If the cathode surface is covered with the sub-surfaces of uniform work function, the experimentally determined value of the work function is, of course, independent of the used methods. When there co-exist regions of different work functions on the cathode surface, the experimental value of the work function determined by the initial velocity method is different from that determined by the Richardson line method, and both values are connected by the the comparatively simple relation (11). Making use of the results obtained in the preceding paper, φ_k^*, the work function determined by the initial velocity method, is represented by a function of φ_l, p_l, and T. In general, the analysis of φ_k^* is a difficult task when there co-exist many regions having differeent work functions on the cathode surface, but it is rather easy in the simplest case when there co-exist only two different work functions. In this paper, φ_k^* was estimated in the case of two different work functions, $\varphi_1 = 3.0$ e. v. and $\varphi_2 = 4.0$ e. v. and it has been compared with the work function calculated from the Richardson line method. Generally speaking, φ_k^* is always larger than φ_l^* and the former becomes to be equal to the latter only when almost all emission is contributed from the region with the higher work function. On the other hand, when almost all emission current comes from the region with the lower work function, φ_k^* is larger than φ_l^* by the quantity related to p. Such difference between φ_k^* and φ_l^* shows a possibility of analyzing the thermionic constants of the composite cathode when accurate values of the work function can be measured by both methods.

In conclusion, the author wishes to acknowldge late Dr. Kusunose for his encouragement.

References.

(1) T. Arizumi: Proc. Phys. Soc. Japan **3**, (1948) 186.

(2) A. L. Reiman: Thermionic Emission, London. (1934) Chap. 2.

(3) M. C. Johnson & F. A. Vick: Proc. Roy. Soc., London (A) **158** (1934), 35.

(4) H.B. Waldin & L. V. Whitney: Phys. Rev., **50** (1936), 735.

(5) W.B. Nottingham: Phys. Rev., **49** (1936), 78.

(6) H.C. Rentschler & Others: Rev. Sci. Instr., **3** (1932), 794.

(7) A.W. Warner: Phys. Rev., **38** (1931), 1971.

(8) A.B. Cardwell: ebenda, **47** (1936), 628.

(9) A.B. Cardwell: ebenda, **38** (1931) 2041.

(10) S. Sano & K. Koga: J. Elec. Comm. (in Japanese) No. 236, (1942) 764.

(11) Nichols: Phys. Rev. **57** (1940), 297.

Thermionic Constants of the Oxide-coated Cathode.

By Tetsuya ARIZUMI.

Kawanishi Kikai Seisakusho, Co. Ltd., Kobe.

(Read at July, 1942: Received July 1, 1947)

§ 1. Introduction.

Although many works have been done to determine the thermionic constants of the oxide coated cathods, their results have distributed over wide range. Such wide distribution has been considered to be due to the complexity of the cathode, i.e. difference of the activated state, method of treatment and high sensitivity to residual gas. In spite of the high accuracy with which recent experiments have been carried out, the experimental values of work function do not always coincide with each other, suggesting the fact that the obtained values depend upon the method of measurement. On the other hand, the values of Richardson constant of the oxide-coated cathode obtained by means of the Richardson line method, are much smaller than the theoretical value or those of pure metals, being no more than thousandth of the theoretical value. No hypothesis has been proposed with success to explain such anomalous Richardson constant.

The wide distribution of the work function and the abnormal Richardson constant seems to be easily explained by the coexistence of many work functions, as already pointed out. In the present paper the analysis of the thermionic constants of the oxide-coated cathods will be carried out, making use of the theory obtained in the previous papers.(1)

Table I.

Thermionic constants of the oxide-coated cathode.

Name	date	method	φ e.v.	A a/cm², deg²
A. Wehnelt(2)	1904	R	3.85	
Jentzsch(3)	1908	,,	3.58	
Spanner(4)	1924	,,	1.85	
C. Davisson & L. H. Germer(5)	1924	,,	1.79	
,, ,,	,,	C	1.79	
Michel & Spanner(6)	1925	,,	1.65	
L. R. Koller(7)	,,	R	1.04	1.07×10^{-3}
Rothe(8)	1926	,,	0.95	
W. Espe(9)	1927	,,	0.99	3×10^{-4}
F. Detels(10)	,,	,,	1.36	9.3×10^{-4}
C. Davisson(11)	1928	,,	1.00	1×10^{-2}
W. Espe(12)	1929	,,	1.10	
W. S. Huxford(13)	1931	P	1.32	
W. Heinze(14)	1933	C	1.87	
Found(15)	1934	special	1.96	
E. Patai & S. Tomeschek(16)	1936	R	1.04	1.8×10^{-2}
W. Heinze & S. Wagener(17)	1938	K	1.50	
N. Morgulis & A. Nagowsky(18)	,,	R	1.72	
E. Nishibori, H. Kawamura & K. Hirano(19)	1941	P	1.63	
S. Sano(20)	1942	K	1.77	

§ 2. Experimental Results.

The thermionic constants of the oxide coated cathode have been measured very often since Wehnelt. The results are shown in Table I. In the table, R expresses the thermionic constants measured by the Richardson line method, K by the initial velocity method, C by the calorimeteric method and P by the photoelectric method. Wehnelt's and Jentzsch's results are much larger than the others', probably due to the insufficient degree of vaccuum. Except for these two results the work function ranges from about 2.0 e.v. to 0.95 e.v., and the measured values by the Richardson line method have a distribution from 0.95 e.v. to 1.85 e.v., while the data determined from calorimetric or initial velocity method have not values of about 1.0 e.v..

When there co-exist two different work functions on the same cathode surface, the average work function and the average Richardson constant, determined from the Richardson line method, are given by the following expressions respectively:

$$\varphi_t^* = \frac{\sum_{n=1}^{2} p_n\left(\varphi_n + T\frac{\partial\varphi_n}{\partial T}\right)\exp\left(-\frac{e\varphi_n}{kT}\right)}{\sum_{n=1}^{2} p_n\exp\left(-\frac{e\varphi_n}{kT}\right)} \tag{1}$$

$$\log\frac{A^*}{A} = \log\left\{\sum_{n=1}^{2} p_n\exp\left(-\frac{e\varphi_n}{kT}\right)\right\} + \frac{e}{kT}\,\frac{\sum_{n=1}^{2} p_n\left(\varphi_n + T\frac{\partial\varphi_n}{\partial T}\right)\exp\left(-\frac{e\varphi_n}{kT}\right)}{\sum_{n=1}^{2} p_n\exp\left(-\frac{e\varphi_n}{kT}\right)}. \tag{2}$$

On the other hand, the average work function, determined from the initial velocity method is given by

$$\varphi_k^* = -\frac{kT}{e}\log\left\{\sum_{n=1}^{2} p_n\exp\left(-\frac{e\varphi_n}{kT}\right)\right\}, \tag{3}$$

and the following relationship holds between φ_t^* and φ_k^*,

$$\varphi_k^* - \varphi_t^* = \frac{kT}{e}\log\frac{A}{A^*}. \tag{4}$$

In the above expressions, φ_t^* and φ_k^* are the average work functions, determined by the Richardson line method and the initial velocity method respectively, A the true Richardson constant, A^* the average Richarnson constant experimentally determined, and φ_n specifies the n-th work function and p_n is the ratio of the area with the n-th work function to the total cathode area (1 cm²). If almost all emission current comes from the parts of lower work function, i.e., the relation

$$i_1 = p_1AT^2\exp\left(-\frac{e\varphi_1}{kT}\right) \gg p_2AT^2\exp\left(-\frac{e\varphi_2}{kT}\right) = i_2,$$

$$p_1 + p_2 = 1, \qquad \varphi_1 < \varphi_2$$

holds between i_1 and i_2, the following expressions are obtained.

$$\left.\begin{aligned} \varphi_t^* &= \varphi_1 \qquad & A^* &= p_1A \\ \varphi_k^* &= \varphi_1 + \frac{kT}{e}\log\frac{1}{p_1} \end{aligned}\right\} \tag{5}$$

On the contrary, if almost all emission current comes from the parts of higher work function, i.e., i_1 is negligibly smaller than i_2, the following relations are obtained:

$$\left.\begin{aligned} \varphi_t^* &= \varphi_k^* = \varphi_2 \\ A^* &= A \end{aligned}\right\} \tag{6}$$

The expression (5) shows that φ_k^* is always larger than φ_t^*, unless p_1 is equal to unity. Thus, it will be expected theoretically that experimental values of φ_t^* distribute in the range from φ_1 to φ_2, while φ_k^* has a narrower range from $\varphi_1 + (kT/e)\cdot\log(1/p)$ to φ_2.

Experimental results are in good agreement with the expectation from the theory. As seen in Table I. the lowest value of the order of 1.0 e.v. is obtained only in the case of the Richardson line method, while in the other method such lower values have never been found. The higher values of the order of about 1.80 e.v. have been observed in all methods. The Richardson constant of this cathode is of very small order of 10^{-2} to 10^{-4} A/cm² deg². Such extremely small value of the Richardson constant is easily understood from the author's theory. When almost all emission current comes from the parts of lower work function, the average Richardson constant is equal to p_1A, as shown in (5). Thus, if p_1 is very small, the experimental Richardson constant should be very small. Both the work function and the Richardson constant suggest that there co-exist two or more different work functions on the surface of the oxide-coated cathode and its maximum value is of about 1.8 e.v. and its minimum one is of about 1.0 e.v.

§ 3. Numerical Calculation of Thermionic Constants of the Oxide-coated Cathode.

In this paragraph the apparent thermionic constants of the oxide-coated cathode will be calculated numerically. As mentioned in the foregoing paragraphs, on the surface of oxide-coated cathode, there coexist the lower work function of about 1.0 e.v. and the higher work function of about 1.8 e.v. The Richardson constants A_1 and A_2 for φ_1 and φ_2, are still unknown, but, in the following, $A_1 = A_2 = A$ is assumed for simplicity. In this case A^*/A is determined and thus it is unnecessary to assume the special value for A.

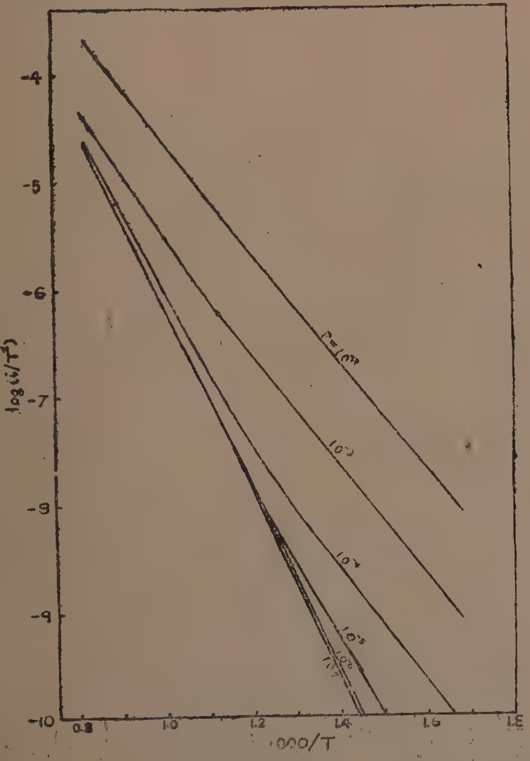

Fig. 1 The Richardson diagram.

In Fig. 1 the Richardson lines calculated under the assumption that $A_1 = A_2 = 120\ A/\mathrm{cm}^2 \cdot \mathrm{deg}^2$ are shown with p parameter. As seen in the figure, the curves are concave upwards, the work function increasing with temperature. Such phenomena have never been found experimentally. The inclinations of experimental curves are observed usually to become lower as the temperature increases. The discrepancy between the theory and experiments will be ascribed to the following several effects:

(1) The available temperature range in experiments being narrow,

(2) The existence of the remarkable time change of the emission current,

(3) The effect of the space charge limitation at higher temperature,

(4) The increase of the dissociated free barium in the oxide at higher temperature.

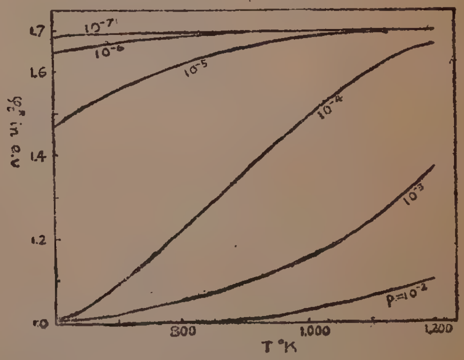

Fig. 2. Temperature change of the work function.

Fig. 2 shows the temperature change of the work function with p parameter, calculated for $\varphi_1 = 1.0$ e.v. and $\varphi_2 = 1.7$ e.v. When p is large or very small, the variation of the work function is very small, while, when p ranges from 10^{-2} to 10^{-6}, its change is predominant. Corresponding to the change of φ_t^*, A^* changes most predominantly in the same p region, as shown in Fig. 3, where

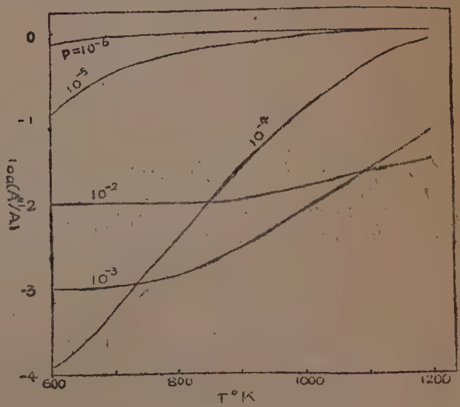

Fig. 3. Temperature change of the Richardson constant,

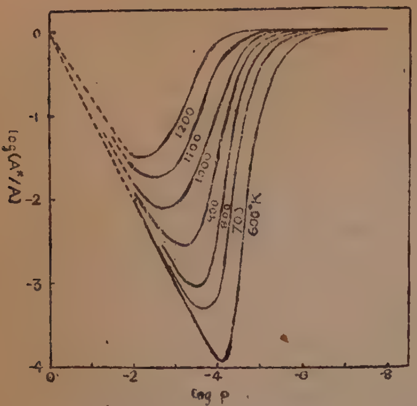

Fig. 4. The relationship between the Richardson constant and p.

$\log(A^*/A)$ is used instead of A^* as the ordinate and T the abscissa. In general, $\log(A^*/A)$ increases with temperature, but for large or very small values of p, its increment is very small. Fig. 4 shows the co-relationship between $\log(A^*/A)$ and $\log p$ with T parameter in which $\log(A^*/A)$ decreases linearly at first and then begins to increase rather sharply. When the temperature is lower, the minimum value of the curve decreases. Only in the case of the homogeneous cathode with a uniform work function of 1.0 or 1.7 e.v. equal to the true original value, independent of the cathode-temperature. In the case of $0<p<1$, A^* value is always smaller than the true one.

The relation between φ_t^* and $\log p$ is shown in Fig. 5 with the parameter T. φ_t^* increases always as p decreases. As T becomes larger, the curve shifts to the left.

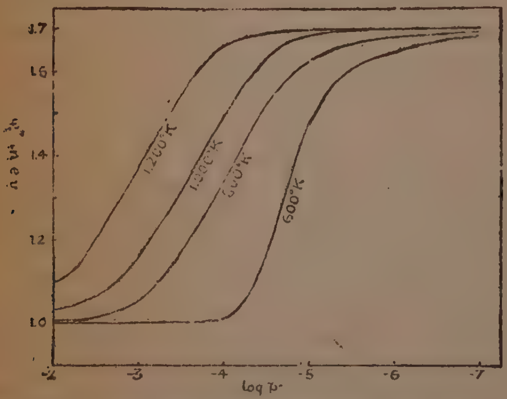

Fig. 5. The relationship between the work function and p.

In Fig. 6 φ_k^* calculated from (3) is shown against $\log p$ with T parameter. Comparing this figure with Fig. 2, the variation of φ_k^* is found to be not so wide as φ_t^* and the relation $\varphi_k^*>\varphi_t^*$ to hold always. Fig. 7 shows the relation between φ_k^* and $\log p$.

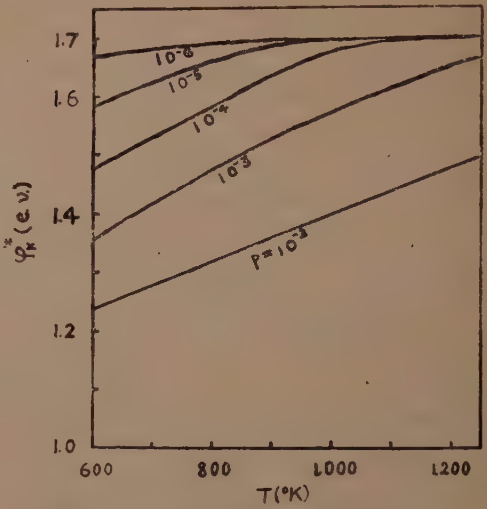

Fig. 6. Temperature change of φ_k^*.

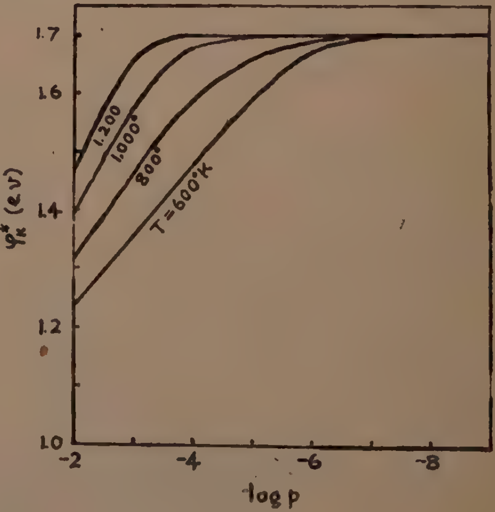

Fig. 7. The relationship between φ_k^* and p.

φ_k^* increases almost linearly with the decrease of $\log p$ at first and then gradually approaches φ_2, showing the different behaviour from φ_t^*. Moreover, the inclination of curves becomes steeper, as the cathode temperature becomes the higher, in sharp contrast to φ_t^*.

If one of the four quantities, φ_t^*, φ_k^*, A^* and p is given, all the other quantities are to be determined by making use of Fig. 2 to Fig. 7. As an example, the relations of these four quantities

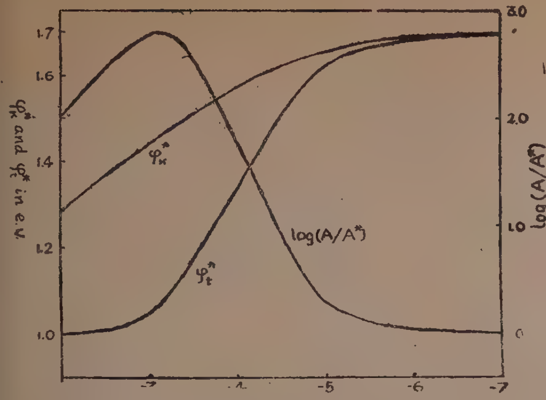

Fig. 8. The co-relationship among A^*, φ_t^* and φ_k^*.

at 800°K are shown in Fig. 8, in which the variation-range of φ_k^* is smaller than that of φ_t^*, that is to say, the experimental values of work function determined by the initial velocity method have a narrower range than that by the Richardson line method. In the range of $\log p > -3$, φ_t^* is almost constant and $\log(A^*/A)$ and φ_k^* show large variations, while in the range of $-3 > \log p > -5$, all three quantities make great changes, although the variation of φ_k^* is larger than that of φ_t^*. At last in the range of $\log p < -5$, all quantities tend to their own definite values: φ_k^* and φ_t^* approximate to 1.70 e.v. and $\log (A^*/A)$ to zero.

The next question is to determine A_1, A_2, φ_1, φ_2 and p which satisfy the following conditions; $\varphi_t^* = 1.0$ e.v., $\varphi_k^* = 1.5$ e.v and $A^* = 10^{-2}$ A/cm^2. deg.^{2} in the best activated state. The procedure for the above case will be extended to determine A_n and φ_n in order to choose the best agreement with those calculated results.

The value of φ_1, however, is equal to 1.0 e.v. according to many measurements. As it requires great labour to change A_1 and A_2 independently, a parameter q is introduced, which connects A_1 and A_2 by the relation $A_1 = qA_2$. In Fig. 9 log (A^*/A_1) and φ_t^* are shown against $\log p$ with parameter q and in Fig. 10 they are shown with φ_2 parameter.

From these results the best agreement with the experimental results will be obtained by taking $\varphi_2 = 1.75$ e.v. and $A_2 = 10^{-1} A_1$ and with the progress of activation of the cathode, p is found to change from 10^{-7} to 10^{-3}. Moreover, the results show that the Richardson constant remains almost unchanged during the activation process.

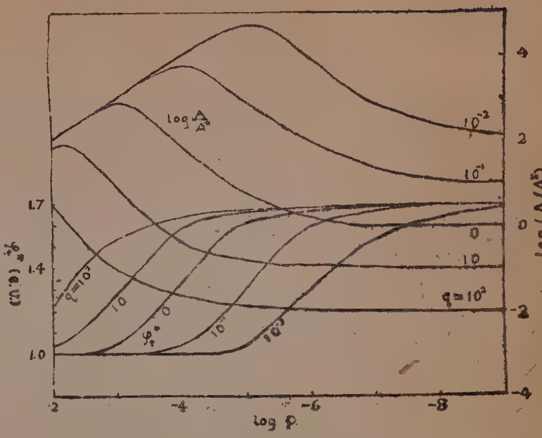

Fig. 9. The correlationship between φ_t^*, A^* and p with parameter q.

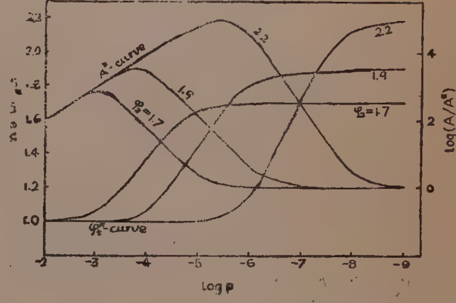

Fig. 10. The correlation between φ_t^*, A^* and p with parameter φ_2.

§ 4. Comparison of the Theory with Experiments.

Recently Sano(20) published new results in which the thermionic constants of the oxide-coated cathode were measured at the same time by means of both the Richardson line method and the initial velocity method.

Since the cylindrical electrode was used in his experiment, the preceeding theoretical expressions are unavailable in their original forms. If the radius of the anode is R and that of the cathode $r (R < 2r)$, the "Anlaufstrome" is represented by

$$i = i_s \cdot \frac{R}{r} \cdot \exp\left\{-\frac{e}{kT}(-V_a + \varphi_a - \varphi_c)\right\}, \tag{7}$$

and the relation between φ_t^* and φ_k^* becomes

$$\varphi_k^* - \varphi_t^* = \frac{kT}{e}\left(\log\frac{R}{r} + \log\frac{A}{A^*}\right) \tag{8}$$

instead of (4). It is written in the following form,

$$\varphi_k{}^* = \frac{kT}{e}\left\{\log\frac{R}{r} - \log\left(\sum_n p_n \exp\left(-\frac{e\varphi_n}{kT}\right)\right)\right\}. \qquad (9)$$

According to Sano's results Richardson line of the oxide-coated cathode is composed of two parts, from the one part of which the results as shown in the Table II are obtained. From his $\varphi_l{}^*$, A^* and Fig. 8, other quantities are estimated. The results are also shown in the Table 2. The agreement of the experimental value with the calculated one is rather satisfactory.

Sano measured the Richardson constant and work function for the cathode of various composition by means of his method and obtained the results as shown in the Table III. On the other hand, the recent data by the Richardson line method due to Patai and Tomaschek[16] are also shown in the table. Making use of (10), $\varphi_k{}^*$ is calculated from Sano's A_i and Patai and Tomaschek's A^* and $\varphi_l{}^*$, the results of which are shown in the right column of the Table 3, being in satisfactory agreement with the experiments. Patai and Tomaschek obtained the following results as shown in the second and the third columns in the Table IV at six different activation states. On the Fig. 8 $\log(A^*/A)$ is determined corresponding to each $\varphi_l{}^*$, B is calculated from the experimental A^* and $\log(A^*/A)$ thus evaluated. The results are shown in the third and fourth columns in the table.

The calculated results coincide not only with each other, but with A value determined from the initial velocity method, shown in Table 4, being in accordance with the theoretical prediction in the preceding paragraph.

§ 5. Emission Formula of the Oxide-coated Cathod.

From the above analysis, it has been concluded

Table II. comparison with the experiments.

	R. l. method		i.v. method		
	A^*	$\varphi_l{}^*$	A_i	$\varphi_k{}^*$	A^*/A
experimental	6.8×10^{-2}	1.13	42	1.55	−2.8
calculated	—	—	—	1.53	−2.77

Table III. Comparism with experimental results.

Composition	i.v. method		R. l. method		Calculated
	A_i	$\varphi_k{}^*$	A^*	$\varphi_l{}^*$	$\varphi_k{}^*$
100 % $BaCO_3$	246	1.77	1.8×10^{-2}	1.04	1.74
75 % $BaCO_3$	16	1.59			1.56
50 % $BaCO_3$	54	1.57			1.63
25 % $BaCO_3$	34	1.36			1.61

In the table 75 % $BaCO_3$ shows that the remaining 25 % of the material is $SrCO_3$.

Table IV. Comparism with experimental data.

Activation state	experimental		calculated	
	A^*	$\varphi_l{}^*$	$\log(A/A^*)$	A
before	0.1181	1.231	2.32	25
activation 1	0.1595	1.18	2.55	56.8
,, 2	0.1150	1.24	2.26	20.9
,, 3	0.0359	1.062	2.78	21.7
,, 4	0.0182	1.039	2.75	10
deactivection	0.5890	1.410	1.48	17.9

that there co exist mainly two different work functions on the surface of the oxide-coated cathode, and the Richardson constants corresponding to two different work functions are almost equal to each other. Thus, the thermionic emission current from the oxide-coated cathode should be written in the form,

$$i = AT^2\left[p\exp\left(-\frac{e\varphi_1}{kT}\right) + 1-p)\exp\left(-\frac{e\varphi_2}{kT}\right)\right] \quad (10)$$

per unit surface area, where

$A \doteqdot 10 \sim 50$ A/cm², deg², $\varphi_1 \doteqdot 1.0$ e.v. $\varphi_2 \doteqdot 1.75$, e.v.

On the other hand, tha theoretical expression of the thermionic emission current from the oxide-coated cathode is gived by

$$i_s = DA'n_0^{\frac{1}{2}}T^{\frac{5}{4}}\exp\left\{-\frac{e}{kT}\left(\frac{E}{2}+V\right)\right\} \quad (11)$$

in well-activated state, while when the activation of the cathode is insufficient, the emission formula is given by

$$i_s = DA''n_0T\exp\left\{-\frac{e}{kT}(E+V)\right\}, \quad (12)$$

which is deduced using Nijboer's⁽²¹⁾ theory of semiconductor. These expressions show that the work function changes from $E+V$ to $E/2+V$ with the progress of the activation.

The theoretical and the analytical formulae can be connected by the assumption that φ_1 and φ_2 correspond to $E/2+V$ and $E+V$ respectively. Thus the obtained results show that there coexist two parts of different work functions. Perhaps the oxide-coated cathode is composed of the mixed state of two crystals whose work functions are $E/2+V$ and $E+V$ respectively. From the above menticned results, E and V are found to be 1.5 e.v. and 0.25 e.v. in good agreement with Kawamura's results.(22)

Formulae (11) and (12) show that the Richardson constant should vary with the progress of the activation and some experiment supports the theory qualitatively. However, all experimental values, hitherto obtained, are the average value estimated under the assumption that there exists only one work function all over the cathode surface, and accordingly it seems to be unable to conclude from the experimental results that the Richardson constant does vary with the activation of the cathode.

The above analysis shows that the apparent Richardson constant is changeable, but the true one remains almost unchanged with the progress of the activation, in contrary to the theoretical prediction. Strictly sperking, however, there are some ambiguities in the above analytical works, and thus it is rather difficult at present to discuss the discrepancy between the theory and the analytical works. The more detailed discussion will be published together with the data of our experiments in the near future.

From the above analysis, it becomes clear that the activation of the oxide-coated cathode is no other than to form the crystals with the work function $E/2+V$ (activation centres) on the cathode surface and further that the ratio of the area of these activation centres to the total cathode surface area is approximately 10^{-7} in insufficient activated state, while it becomes to be $10^{-3} \sim 10^{-4}$ in the best activated state.

§ 6. Conclusion.

The main object of this paper was to analyse the thermionic constants of the oxide-coated cathode making use of the theory that has been developed in the foregoing papers. Thermionic work functions experimentally obtained are different from each other due to the methods of observation used in the experiments. Making use of such difference the possibilities of analysing the thermionic constants of the oxide-coated cathode have been pointed out. The values of the measured work functions in the Richardson line method range from 1.0 e.v. to 1.8 e.v., while in the initial velocity method from 1.5 e.v. to 1.8 e.v. The analysis of the experimental results shows that there coexist mainly two different work functions on the cathode surface of 1.0 and 1.75 e.v. respectively, and moreover, the value of the Richardson constant carrespanding to each work function is of almost equal order of magnitude from 10 to 60 A/cm². deg². Accordingly the thermionic emission current from the oxide-coated cathode may be concluded to be represented in the form,

$$i \doteqdot AT^2\left\{p\exp\left(-\frac{e\varphi_1}{kT}\right)+(1-p)\exp\left(-\frac{e\varphi_2}{kT}\right)\right\}$$

per unit surface area. And as predicted from the semi-conductor theory, φ_1 and φ_2 are written as follows.

$$\varphi_1=\frac{E}{2}+V, \qquad \varphi_2=E+V$$

Perhaps each term of the above emission formula holds only for a single crystal having different content of free barium atoms respectively. However, the fact that the Richardson constant is independent of the activated state, seems to require the further investigations in future.

References.

(1) T. Arizumi: J. Phys. Soc. Japan **3**, (1948) 186;
(2) A. Wehnelt: Ann. d. Phys. **14**, (1904) 425.
(3) Jentzsch: ebenda, **27**, (1909). 129.
(4) Spanner: ebenda, **75**, (1924). 609.
(5) C. Davisson & L. H. Germer: Phys. Rev., **24**, (1924), 666.
(6) Michel & Spanner: Zeits. f. Phys., **35**, (1925), 395.
(7) L. R. Koller: Phys. Rev., **25**, (1925), 671.
(8) Rothe: Zeits. f. Phys., **36**, (1926), 737.
(9) W. Espe: Wiss. Veroff. a. d. Siemens Werke, **5**, (1927) 29 & 46.
(10) F. Detels: Jahrb. d. drahtl. Teleg., **30**, (1927) 10 & 52.
(11) C. Davisson: Rev. Mod. Phys., **2**, (1928) 381.
(12) W. Espe: Zeits. f. Phys., **10**, (1929) 489.
(13) W. S. Huxford: Phys. Rev., **38**, (1931) 379.
(14) W. Heinze: Ann. d. Phys., **16**, (1933) 41.
(15) Found: ebenda, **45**, (1934) 519.
(16) E. Patai & Z. Tomaschek: Kolloid Zeits., **74**, (1936) 253.
(17) W. Heinze & S. Wagener: Zeits. I. Phys. **110**, (1937) 164.
(18) N. Morgulis & A. Nagorsky: Toch. Phys. U. S. S. R. **5**, (1938) 848.
(19) E. Nishibori, H. Kawamura & K. Hirano: Proc. Phys.-Math. Soc. Japan, **23**, (1941) 37.
(20) S, Sano: J. Elec. Comm. Japan, (in Japanese) **27**, (1943) 116.
(21) Nijboer: Proc. Phys. Soc., **51**, (1934) 575.
(22) H. Kawamura: Matsuda Kenkyu Jiho (in Japanese) **16**, 1941, No. 4.

Order-Disoder Transformation in the Alloy Ni_3Mn.

By Takao Satô.

Faculty of Engineering. Kyushu University.

(Read May 9, 1947, Received July 1, 1947).

§ 1. Introduction.

Several investigations on Nickel-Manganese system have shown that a superlattice is formed when the components of the system is such as to form Ni_3Mn(1). The evidence for the existence of this superlattice is mainly due to the studies of the electrical resistance, magnetic porperties and the specific heat. It is very difficult to detect directly the ordered structure by X-ray methods because the atomic numbers of the component atoms differ slightly, and any such attempt has not yet succeeded.

Recently the thermoelectric properties of this alloy have been studied experimentally by Jaffee(2) but further measurements seem to be desirable to get the knowledge concerning the essential nature of the phenomena. The author has repeated the experiments on the thermo-electromotive force during heat treatments by the method which are frequently used for the study of ferromagnetic substances(3).

§ 2. Experimental Details and Results.

The materials used were electrolytic nickel and Merk's manganese. They are melted together, casted into a cylindrical form of 5 mm. in length and annealed enough in an evacuated furnace. The electrical resistance was measured by the usual current and potential method, although we made no effort to get the absolute values. As the rate of order-disorder transformation of this alloy is very low, it requires a great deal of trouble to get the resistance-temperature curve in the equilibrium state. Therefore, it was measured at the rate of about 20°/hour in both heating and cooling. The results are shown in Fig. 1.

Above 540°C the resistance is proportional to the absolute temperature since it is mainly due to thermal agitations of atoms, while below 460°C it decreases rapidly with decreasing temperature. The resistance-temperature curve of Ni_3Mn has no sharp knick, as shown in Fig. 1, similar to the case of Cu_3Pd superlattice alloy(4).

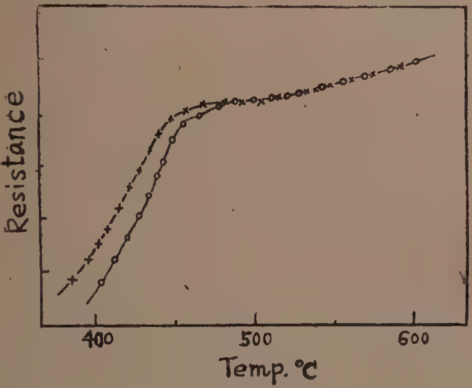

Fig. 1. Electric resistance-temperature curve
○ heating, × cooling, rate 20°C/hour

Kaya and Kussmann(5) has already reported that the superlattice transformation point is 510°C and the magnetic Curie point is 460°C. We made a careful measurent of the resistance, but could not find any anomaly near 510°C in agreement with Thompson's experiments(6).

For the measurement of the thermoelectric power, the writer has adopted the method used for the measurement of anomalous behaviour of the thermoelectric properties of ferromagnetic substances. The thermoelectric power was obtained by measuring directly the thermo-electromotive force of the sample coupled with platinum wire during a homogeneous heat treatment keeping small temperature difference between two ends of the sample. This temperature difference was about 1°—3° which occurred in the electric furnace. We used Alumel-Chromel differential couple for the measurement of these temperature differences. The thermo-electromotive force and the temperature differennce were measured by a short period galvanometer which has a high voltage sensitivity to measure the interesting variation which we might miss by usual potentiometer methods. The thermo-electric power was obtained by dividing the thermo-electromotive force by the temperature difference at each temperature. Though there is reproducibility in the relative variation with temperature, we cannot obtain reproducible result in the measurement of the absolute value. And since our main interest lies in the relative variation of the thermoelectromotive force near the transformation points, we made no effort to get absolute values of the electromotive force. The results are shown in Fig. 2. to Fig. 4.

§ 3. Discussion of the Results.

Jaffee has measured the thermo-electromotive force of a quenched Ni_3Mn wire in disordered atomic arrangement coupled with platinum wire, one side of which was kept at 0°C and the other side at varying temperature, heating rapidly until 530°C and then cooling very slowly. The cold junction is kept always in disordered atomic arrangement while at the hot junction the atomic arrangement will change from the disorderd to the ordered one and intermediate states will exist elsewhere in the sample. Jaffee obtained the thermoelectric power by a graphical differentiation from the thermo-electromotive force versus temperature curve and he has reported that two nearly equal peaks were obtained near 460°C. But it might be very difficult to get two peaks by graphical differentiation of his thermoelectromotive force versus temperature curve.

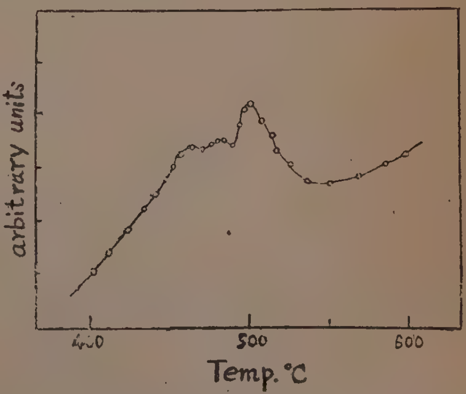

Fig. 2. Thermoelectric-temperature curve
Heating rate 20°C/hour

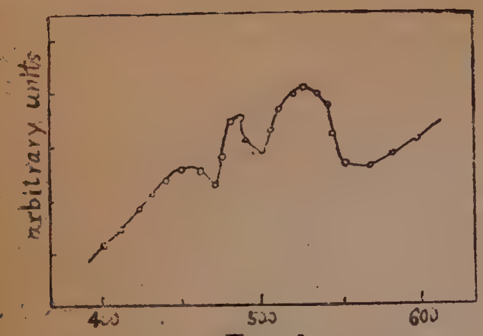

Fig. 3. Thermoelectric-temperature curve
Heating rate 1°C/min

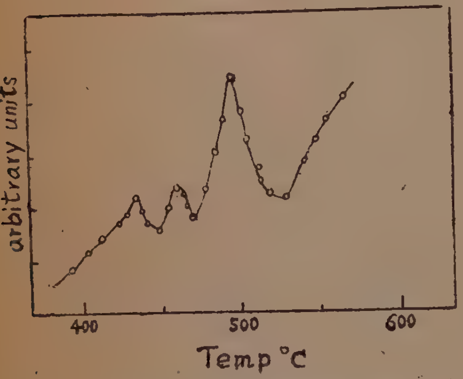

Fig. 4. Thermoelectric-temperature curve
Cooling rate 1°C/min

By the method adopted by the writer three peaks were found in the thermoelectric power-temperature curve and their positions and heights depend on the heating and cooling processes. Three peaks appear clearly separated in rapid heating and cooling (Fig. 3 and Fig. 4), but two peaks at the side of low temperature are not clearly separated enough in the heating rate of 20°/hour (Fig. 2).

Thompson has found two critical points at 460°C and 510°C from magnetic properties and at 490°C and 540°C by the measurement of the specific heat and Kaya and Kussmann found 460°C and 510°C from magnetic measurement as well as Thompson, whilst Kaya and Nakayama(6) did not find two peaks in the measurement of the specific heat. A large peak near 505°C and anomalies near 460°C and 480°C are found in the measurement of the thermoelectric power (Fig. 3). Three temperatures 450°C, 480°C and 530°C specify the positions of maximum in the case of rapid heating. The writer has considered it reasonable to compare the curve in Fig. 3. with the specific heat measurement, since the specific heat measurements are carried out with heating rate of about 1°—2° per minute. The anomalies at 480°C and 530°C seem to correspond to those found by Thompson at 490°C and 540°C and also correspond to those at 460°C and 540°C observed by Thompson, and Kaya and Kussmann. As Ni_3Mn alloy is a ferromagnetic superlattice alloy, it may be reasonable to assume the relation between the magnetic transformation and the order-disorder transformation. According to the investigations of the thermoelectric power of ferromagnetic substances, the thermoelectric power changes its value at Curie point, a qualitative explanation of which was given by Mott(8) from the standpoint of the modern theory of solids. The writer has investigated the thermoelectric power near the transformation point of a non-ferromagnetic super lattice alloys of Mg-Cd system and β-brass(9), and an interesting change at the transformation point has been found.

As repeatedly pointed out by Sykes and his collaborators(10) in the kinetic considerations of order-disorder transformation process in the superlattice alloy, the transformation due to temperature change takes place in two steps, that is, the growth of relatively highly ordered nuclei on the one hand, and the change of the degree of order inside the exitsing nuclei, on the other. For a typical non-ferromagnetic superlattice alloys such as Cu_3Au in which long distance order can be easily established, such simple considerations would be actually effective. But, judging from the form of the anomalous electrical resistance temperature curve, the writer is of the opinion that the transformation mechanism of the Ni_3Mn alloy would be more complicated.

According to the electron theory of metals(11), the absolute thermoelectric power S of metals or alloys may be written, in the first order of kT/ζ_0, by the equation

$$S = \frac{\pi^2}{3}\,\frac{kT}{e}\left\{\frac{\partial \log \sigma(E)}{\partial E}\right\}_{E=\zeta}$$

where

$$\sigma(E) = \frac{2e^2}{\ }\int\left(\frac{\partial E}{\partial k}\right)^2 \tau(k)\frac{ds}{|\mathrm{grad}\,E|},$$

the integration being taken over the surface of the Fermi distribution. The quantity $\sigma(E)$ represents the electrical conductivity of metal when the maximum energy ς of the Fermi distribution is equal to E. $\sigma(\varsigma)$, therefore, is the actual conductivity of the metal. The thermoelectric power depends, therefore, on the way in which the mean free path and the effective mass of electrons, which determines $\sigma(E)$, vary with energy. Therefore, though we cannot observe any anomaly by measuring the change of the electrical resistance with temperature, we might be able to find it by the measurement of the thermoelectric power.

It is certain that very small ordered nuclei (whose dimensions are, according to Sykes and his collaborators, less then about 50–100Å), which do not contribute to the electrical resistance, play an important part in the phenomena of order-disorder transformation. It can be expected that changes of these ordered nuclei will result in some changes in the electronic structure of the alloy and hence some anomaly in thermoelectric power will appear.

As there is an intimate correlation between ferromagnetic and order-disorder transformation in the ferromagnetic superlattice alloy, it is difficult to investigate each of them separately. But, as the Ni_3Mn alloy has a very long time of relaxation, the writer has expected to obtain interesting results for the magnetic properties by quenching the atomic rearrangement and thus avoiding the effects of order-disorder transformation.

Since thermoelectric power often shows changes which cannot be obtained in the electrical resistance-tempratue curve, it will serve as a valuable indicator in the experimental investigations relating to the phenomena of transformation. The method will be recommended also for the studies of higher order effects, but it should be remarked that some care must be taken for any sample having long relaxation time especially.

The writer is indebted to Prof. A. Harasima and Prof. K. Oomori for their valuable advices and criticisms and to Ass. Prof. T. Okada for his friendly discussions. The expense of this research has been defrayed from the Scientific Rerearch Expenditure of the Educational Ministry.

References.

(1) S. Kaya and A. Kussmann: Z. f. Phys. **72** (1931), 292. S. Kaya and M. Nakayama: Proc. Phys-Math. Soc. Jap. **22** (1940), 126. N. Thompson: Proc. Phys. Soc., **52** (1940), 217.

(2) R. I. Jaffee: Phys. Rev., **66** (1944), 288.

(3) J. Dorfmann and R. Jaanus: Z. f. Phys., **54** (1927), 277. K. E. Grew: Phys. Rev., **41** (1932), 356. A. Hammer: Ann. d. Phys., **30** (1937), 728.

(4) F. W. Jones and C. Sykes: J. Inst. Metals, **65** (1939), 419.

(5) (6) (7) Loc. cit.

(8) N. F. Mott: Proc. Roy. Soc., **156** (1936), 368.

(9) Unpublished.

(10) C. Sykes and H. Evans: J. Inst. Metals, **58** (1936), 255. C. Sykes and F. W. Jones: Proc. Roy. Soc. **157** (1936), 213. C. Sykes and F. W. Jones: Proc. Roy. Soc. **166** (1938), 376.

(11) Cf. N. F. Mott and H. Jones: Theory of the properties of metals and alloys (1936).

On the Displacement Velocity of the Domain Boundary of Ferromagnetic Substance.*

By Tatsuya KATAYAMA.

Research Institute for Iron, Steel and Other Metals, Tôhoku University, Sendai.

(Read November 23, 1946; Received October 1, 1947)

§ 1. Introduction.

It has been known that the magnetic characteristics of the ferromagnetic substance under high-frequency alternating magnetic field are widely different from its statical characteristics. The origins for such differences are partly attributed to the existence of macroscopic eddy current, magnetic hysteresis, etc., but it has been pointed out that fundamental aspects of the elementary process of magnetization must be taken into consideration in investigating the causes of this difference. Experiments on the Barkhausen Effect(1), therefore, are especially interesting in this respect, as they make it possible to observe some dynamical aspects of the elementary process of magnetization. Various experimental results of this effect are well explained by assuming that the inside of the ferromagnetic solid is divided into domains, which are spontaneously magnetized up to saturation corresponding to temperature, and that under proper external conditions the boundaries of the domains propagate with finite velocities. Such supposition is supported by Bloch's theoretical consideration and the experimental observation on the Large Barkhausen Effect(2). Thus, the displacement of the domain boundary, i.e., the magnetic wall displacement, plays an importnnt rôle in the dynamical magnetization-process of the ferromagnetics, and the theoretical and experimental investigations thereof are of great interest.

Now the wall displacement eventually means that some electron spins near the boundary between two domains successively reverse their directions, one domain gaining in its size consuming the other. The displacement velocity should be finite, as the spin inversion, i.e., the elementary process of the wall displacement, is carried out under the influence of mutual interaction between the spin system, the system of thermal vibrations of the crystal lattice, and of the external magnetic field. Very few attempts, however, have been made from this atomistic standpoint(3). The reason for this meager theoretical investigation may perhaps be due to the difficulties to obtain the wave functions which describe the magnetic wall within the ferromagnetic crystal. Now, we have attempted to solve the problem along this line, constructing the eigenfunction, which approximately corresponds to the Bloch solution(4) for a magnetic wall, by the use of the Heitler-London-Heisenberg model, and, further, treating the wall displacement as the transition phenomenon between the spin states designated by these eigenstates. In the following shall be reported the method and the results obtained.

§ 2. Hamiltonian of the Ferromagnetic Crystal and the Perturbation Term.

The Hamiltonian of ferromagnetic crystal, when the thermal vibrations of the crystal are taken into consideration, is

$$
\begin{aligned}
H_t = \sum -\frac{\hbar^2}{2m}\Delta_i + \sum_{i,f} V_f(\mathbf{r}_i-\mathbf{R}_f) \\
+\frac{1}{2}\sum_{i,k}\frac{e^2}{r_{ik}}+\frac{1}{2}\sum_{f,g}V_{fg}(\mathbf{R}_f-\mathbf{R}_g) \\
-\frac{e}{mc}\sum_i(\mathbf{s}_i\cdot\mathbf{H})+\sum_{f,i}\frac{e^2Z}{2m^2c^2}\cdot\frac{([\mathbf{r}_{fi}\cdot\mathbf{p}_i]\cdot\mathbf{s}_i)}{r^3{}_{fi}} \\
+\sum_{i,i'}\frac{e^2}{2m^2c^2}\cdot\frac{([\mathbf{r}_{ii'}\cdot(2\mathbf{p}_{i'}-\mathbf{p}_i)]\cdot\mathbf{s}_i)}{r^3} \qquad (1)\\
+\frac{1}{2}\sum_{i,i'}\frac{e^2}{m^2c^2}\cdot\frac{-3(\mathbf{s}_i\cdot\mathbf{r}_{ii'})(\mathbf{s}_{i'}\cdot\mathbf{r}_{ii'})+r^2{}_{ii'}(\mathbf{s}_i\cdot\mathbf{s}_{i'})}{r^5{}_{ii'}} \\
+\sum_{q,j}\hbar\omega_{q,j}\left(N_{q,j}+\frac{1}{2}\right).
\end{aligned}
$$

---

*) This is a part of the investigations of the Special Committee of the Theoretical Physics in the National Research Council (1946). Item: Fundamental Study of Ferromagnetism; Ferson in charge: Tokutarô Hirone.

in which the various notations mean as follows: i, i', k = numbers of electrons. f, g = numbers of lattice points. r_i = coordinate vector of i-th electron. R_f = coordinate vector of f-th atom core. s_i = spin vector of i-th electron. H = external magnetic field. m = mass of an electron. Z = effective charge number of atom core. c = light velocity. p_i = momentum vector of i-th electron. $2\pi\hbar$ = Planck's constant. $\hbar\omega_{q,j}$ = energy quantum of lattice vibration having propagation vector $\boldsymbol{q}$ and polarization j. $N_{q,j}$ = number of energy quantum $(\boldsymbol{q}, j)$.

$$\Delta_i = \frac{\partial^2}{\partial x_i^2} + \frac{\partial^2}{\partial y_i^2} + \frac{\partial^2}{\partial z_i^2},$$

$$r_{ik} = |\mathbf{r}_{ik}| = |\mathbf{r}_i - \mathbf{r}_k|, \quad r_{fi} = |\mathbf{r}_{fi}| = |\mathbf{r}_i - \mathbf{R}_f|.$$

Further, the meanings of each term in (1) are as follows: 1st term = kinetic energy of crystal electrons. 2nd term = mutual interaction energy between the atom cores and electrons. 3rd term = mutual interaction energy between electrons themselves. 4th term = mutual interaction energy between the atom cores themselves. 5th term = additive energy due to the external field. 6th, 7th, and 8th terms = magnetic interaction energies of the types of (spin × orbit) and (spin × spin). 9th term = vibrational energy of crystal lattice.

The atom core, which belongs to the f-th lattice point, displaces around its mean position $\boldsymbol{R}_{fo}$ as a result of lattice vibration. Let the displacement be $\boldsymbol{u}_f$, then we have

$$\mathbf{R}_f = \mathbf{R}_{fo} + \mathbf{u}_f. \tag{2}$$

As is well known(5), the displacement may be expanded into Fourier series,

$$\mathbf{u}_f = \frac{1}{\sqrt{N}} \sum_{q,j} \mathbf{e}_{q,j}(a_{q,j} \exp(i_q \mathbf{R}_{fo}) + a^*_{q,j} \exp(-i_q \mathbf{R}_{fo})), \tag{3}$$

and the matrix elements of the normal coordinates are as follows:

$$\left.\begin{aligned} (N_{q,} -1|a_{q,j}|N_{q,j}) &= \sqrt{\frac{\hbar N_{q,j}}{2M\omega_{q,j}}} \exp(-i\omega_{q,j}t), \\ (N_{q,} +1|a^*_{q,j}|N_{q,j}) &= \sqrt{\frac{\hbar(N_{q,j}+1)}{2M\omega_{q,j}}} \exp(i\omega_{q,j}t), \end{aligned}\right\} \tag{4}$$

where, $\boldsymbol{e}_{q,j}$ represents the polarization vector, N and M are the total number of lattice points and the mass of an atom core respectively. In order to carry out the calculation further, it is necessary to expand H_t in series with respect to $\boldsymbol{u}_f$ and separate it into a part, which is not related with the thermal vibration, and another one representing the additive terms due to thermal vibration. Waller(6) assumed that the electrons, which are responsible to paramagnetism, follow exactly the thermal motions of lattice points, when he calculated the probability of spin inversion in paramagnetic substance. Here, we shall assume that only the atom cores follow the thermal motion at if they were rigid bodies, while the ferromagnetic electrons entirely do not. Correctly speaking, we must reasonably take into account the change of electron distribution due to thermal motion(7), which procedure makes our calculation unnecessarily complicated for our present rough estimation. Thus, as in Muto's case,(3) $\boldsymbol{r}_{ii'} = \boldsymbol{r}_{ii'o}$ (Hereafter, index (o) will always express the quantities, in which the thermal motion is neglected). while, refering to (2), it becomes $\boldsymbol{r}_{fi} = \boldsymbol{r}_{fio} - \boldsymbol{u}_f$. As the relation $|\boldsymbol{u}_f| \ll |\boldsymbol{r}_{fio}|$ is always satisfied except for extemely high temperatures, we may expand H_t in series with respect to $\boldsymbol{u}_f$. Retaining up to the linear terms in $\boldsymbol{u}_f$, H_t becomes the following form;

$$H_t = H_0 + H_1 + \sum_{q,j} h\omega_{q,j}\left(N_{q,j} + \frac{1}{2}\right), \tag{5}$$

where H_1 includes $\boldsymbol{u}_f$ while H_0 does not.

$$\begin{aligned} H_1 = &-\sum_{i,} \boldsymbol{u}_f \cdot \mathrm{grad}\, V_f(\boldsymbol{r}_i - \boldsymbol{R}_{fo}) \\ &+ \sum_{f,g} (\boldsymbol{u}_f - \boldsymbol{u}_g) \cdot \mathrm{grad}\, V_{fg}(\boldsymbol{R}_{fo} - \boldsymbol{R}_{go}) \\ &+ \sum_{i,f} \frac{e^2 Z}{2m^2c^2} \left\{ 3\frac{(\mathbf{r}_{fio}\ \mathbf{u}_f)}{r^5_{fio}} ([\mathbf{r}_{fio} \cdot \mathbf{p}_i] \cdot \mathbf{s}_i) - \frac{([\mathbf{u}_f \cdot \mathbf{p}_i] \cdot \mathbf{s}_i)}{r^3_{fio}} \right\}. \end{aligned} \tag{6}$$

The first and second terms in H_1 are the perturbation terms necessary for estimating the above stated change of electron distribution due to thermal vibration, which are now out of question. We shall also leave out of consideration the second term in the curved bracket expression, because its matrix element turns out to be zero under space integration. Thus, there will remain only the first term in the mentioned brackat expression. Considering the mentioned term as a perturbation, we may investigate the transition between the eigenstates, which shall be worked out in the next section. In addition, we note here that we shall drop off hereafter the index (o) as no confusion will occur.

§ 3. Eigenfunctions.

Bloch(4) found that the magnetic wall can exist as the solution of the non-perturbed system H_0, but actually its eigenfunction has not been obtained yet. As it may be difficult to obtain the eigenfunction by a frontal attack, we shall construct it rather artificially in a manner which does not contradict with Bloch's solution regarding the spin distribution.

For simplicity, we shall assume that the crystal is a simple cubic lattice, the Z-axis coinciding with one of the crystallographic axes, and that the magnetic wall lies perpendicular to it. Let G be the number of lattice points along a cube edge, then $N = G^3$ and the number of lattice points on each lattice plane perpendicular to Z-axis is G^2. Now, according to Bloch, the direction of magnetization, or in other words, the direction of the electron spin does not change abruptly at the wall, but continuously in what we may call a transition layer.

In Fig. 1 the situation is schematically represented in two dimensions. If the small terms up to electrostatic interaction e^2/r_{ik} are neglected, the solutions of the non-perturbed system are given by the well known determinantal wave function. To construct the determinantal wave function we must give the distribution of both spins directed along $+Z$ or $-Z$ direction on the lattice points. Thus, in our case, we must not only give the numbers of $-Z$ spins $n_1, n_2, n_3, \cdots, n_l$ on each lattice plane (l = the total number of lattice planes in the transition layer), but also specify the distribution of spins on each lattice plane. We shall designate the spin distribution with $p_s^{(k)}$ (s is the number of the lattice plane, i.e., $s = 1, 2, 3, \cdots, l$). Each of the notations p_1'', p_1'', $\cdots$, $p_1^{(k)}$, $\cdots$, etc. (Note that all have the suffix (1).), for example, corresponds respectively to any one of the distributions of n_1 right spins and $G^2 - n_1$ left spins on the G^2 lattice points. Then, any one of spin distributions on the whole crystal may be expressed by a set of notations

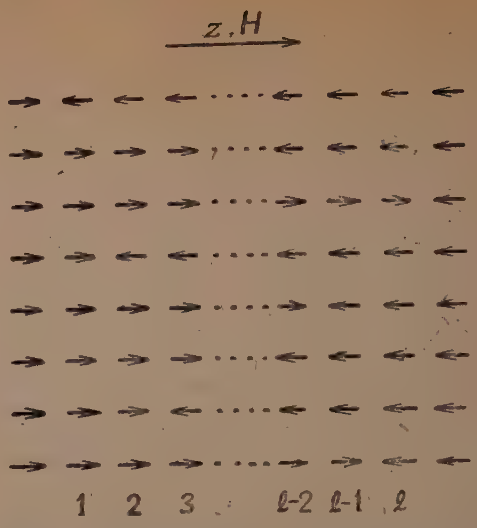

Fig. 1. The transition layer between two neighbouring domains. The spins of left hand domain are all $+Z$ spins and those of right hand domain $-Z$ spins. The ratio of numbers of both spins on one lattice plane changes continuously in the layer. We note here that the field H is applied in the $+Z$ direction.

$$n_1,\ n_2,\ \cdots,\ n_l;\ p_1^{(i)},\ p_2^{(j)},\ \cdots,\ p_l^{(k)}$$

or $$(n_1,\ p_1^{(i)})(n_2,\ p_2^{(j)})\cdots(n_l,\ p_l^{(k)}).$$

Thus, the determinantal wave function in our case may be written down as follows.

$$\Psi\big((n_1,\ p_1^{(\ )})(n_2,\ p_2^{(j)})\cdots(n_l,\ p_l^{(k)})\big)$$

$$= \frac{1}{N!}\sum_P \varepsilon(P)\cdot S(n_1,\ p_1^{(i)})(n_2,\ p_2^{(j)})\big)\prod_{i=1}^{N}\varphi_i(r_i) \quad (7)$$

where, $\sum_P$ means the summation over all permutations of the electron coordinates (including spin coordinates), and $\varepsilon(P)$ is $+1$ when the permutation is even and -1 when it is odd. φ_i is the atomic wave function centered about the i-th lattice point. $S((n_1,\ p_1^{(i)})(n_2 .\ p_2^{(j)})\cdots(n_l \cdot p_l^{(k)}))$ is the spin eigenfunction of the whole crystal corresponding to the distribution $(n_1,\ p_1^{(i)})(n_2,\ p_2^{(j)})\cdots(n_l,\ p_l^{(k)})$. We shall assume that the eigenfunction corresponding to a state having a magnetic wall may be expressed in terms of (7) as follows.

$$\Psi_0 = \frac{1}{\sqrt{F_0}}\sum_{i,j,\cdots,k}\Psi(n_1,\ p_1^{(i)})(n_2,\ p_2^{(j)})\cdots(n_l,\ p_l^{(k)})). \quad (8)$$

Here, the summations with respect to $i, j, \cdots, k$ extend over all spin distributions on each lattice plane. Moreover, the normalizing factor F_0 is given by

$$F_0=\frac{G^2!}{(G^2-n_1)!\,n_1!}\cdot\frac{G^2!}{(G^2-n_2)!\,n_2!}\cdots\frac{G^2!}{(G^2-n_l)!\,n_l!}\tag{9}$$

The states adjoining to (8) may be considered to be the states in which the magnetic moment of the crystal as a whole is larger or smaller by 2β than the state Ψ_0 (β = Bohr magneton). At first, we shall confine our consideration to the former case, i.e., the state having larger magnetic moment. The amount of displacement of the magnetic wall caused by the transition into this new state may be considered to be a/G^2 (a = lattice constant), for the magnetic moment increases by an amount $2G^2\beta$ when the magnetic wall advances by a. The eigenfunction of such state can not be constructed like Ψ_0. Thereupon, we shall replace it by a state in which the magnetic wall, while lying in the same position as in Ψ_0 will yet have magnetic monent which is larger by 2β. If we denote such a state by Ψ_1, then it takes a form

$$\begin{aligned}\Psi^1=&\frac{1}{\sqrt{l\cdot F_{11}\cdot(N!)}}\sum_{i,j,\cdots,k}\Psi((n_1-1,\,p_1^{(\ )})(n_2,\,p_2^{(j)})\\&\qquad\cdots(n_l,\,p_l^{(k)}))\\&+\frac{1}{\sqrt{l\cdot F_{12}\cdot(N!)}}\sum_{i,j,\cdots,k}\Psi((n_1,\,p_1^{(i)})(n_2-1,\,p_2^{(j)})\\&\qquad\cdots(n_l,\,p_l^{(k)}))\\&+\cdots\cdots\\&+\frac{1}{\sqrt{l\cdot F_{1l}\cdot(N!)}}\sum_{i,j,\cdots,k}\Psi((n_1,\,p_1^{(i)})(n_2,\,p_2^{(j)})\\&\qquad\cdots(n_l-1,\,p_l^{(k)})),\end{aligned}\tag{10}$$

weere

$$\begin{aligned}F_{1i}=&\frac{G^2!}{(G^2-n_1)!\,n_1!}\cdots\frac{G^2!}{(G^2-n_i+1)!\,(n_i-1)!}\\&\cdots\frac{G^2!}{(G^2-n_l)!\,n_l!}=F_0\cdot\frac{n_i}{G^2-n_i+1}.\end{aligned}\tag{11}$$

§ 4. Transition Probability.

Based on the above preliminary consideration, we can obtain the matrix element necessary for finding the transition probability of a process in which the magnetic moment of the crystal in the $+Z$ direction increases by 2β, the relaxed energy $2\beta H$ being converted into thermal energy; i.e., a lattice wave satisfying the relation $2\beta H=\hbar\omega_{q,i}$ being emitted. Now, to find the said probability it will be sufficient to calculate the matrix element of the above mentioned perturbation between the eigenstates Ψ_0 and Ψ_1, which respectively include thermal vibrational eigenstates in each case. Considering (3) and (4), we find that the matrx element will be

$$\frac{1}{\sqrt{N}}\frac{3Ze^2\hbar}{2im^2c^2}\sqrt{\frac{\hbar(N_{q,j}+1)}{2M\omega_{q,j}}}\exp(i\omega_{q,j}t)\cdot$$

$$\left(\Psi_1\left|\sum_{f,i}\frac{(\mathbf{r}_{fi}\mathbf{e}_{q,j})}{r_{fi}^{s}}([\mathbf{r}_{fi}\cdot\nabla_i]\cdot\mathbf{s}_i)\exp(-i\mathbf{q}\mathbf{R}_f)\right|\Psi_0\right).\tag{12}$$

For simplicity, we shall assume that the electrons, which are responsible to ferromagnetism are s-electrons and that the neighbouring atomic wave functions are mutually orthogonal. Then, using (8) and (10), we find that the matrix element (12) vanishes except for the case, in which the wave number vector q lies in the $\pm Z$ direction, i. e., perpendicular to the magnetic wall. If q lies perpendicular to the magnetic wall, we find that (12) becomes as follows:

$$-\frac{1}{\sqrt{lN}}\frac{2\pi Ze^2\hbar}{im^2c^2}\sqrt{\frac{\hbar(N_{q,}\ +1)}{2M\omega_{q,}}}\exp(i\omega_{q,j}t)$$

$$\cdot G^2\left[\sqrt{\frac{n_1}{G^2}\cdot\frac{(G^2-n_1+1)}{G^2}}+\cdots+\sqrt{\frac{n_l}{G^2}\cdot\frac{(G^2-n_l+1)}{G^2}}\right]$$

$$\cdot E\cdot F.\tag{13}$$

Here, the factors E and F are given by the following equations (q being of course, in the Z direction)

$$\left.\begin{aligned}E&=\int_0^\infty\varphi(r)\,\frac{d\varphi(r)}{dr}\,dr,\\F&=\sum\exp(-i_q\mathbf{R}_f)\cdot\frac{(\mathbf{e}_{q,j}[\gamma\cdot\mathbf{R}_f])}{R^{s5}},\end{aligned}\right\}\tag{14}$$

in which γ is a vector with components $\left(\frac{\hbar}{2},\ \frac{i\hbar}{2},\ 0\right)$. Moreover, if we neglect the quantities of the order of magnitude $1/G^2$ the expression between the braces of equation (13) may be transformed into an integral form in terms of Bloch's spin density functions φ, $\psi^{(4)}$, namely

$$\frac{1}{a}\int_{|\psi|^2=0}^{|\psi|^2=1}\sqrt{|\phi|^2\cdot|\varphi|^2}\,dz\tag{15}$$

Quite similarly, we can obtain the matrix element, which is necessary for finding the probability of a process, in which the magnetic moment of the crystal in the field direction decreases by 2β and in which at the same time a lattice wave satisfying the relation $2\beta H=\hbar\omega_{q,j}$ is absorbed. It becomes

$$-\frac{1}{\sqrt{lN}}\frac{2\pi Ze^2\hbar}{im^2c^2}\sqrt{\frac{\hbar N_{q,j}}{2M\omega_{q,j}}}\exp(-i\omega_{q,j}t)$$

$$\cdot G^2\left[\sqrt{\frac{(n_1+1)}{G^2}\cdot\frac{(G^2-n_1)_1}{G^2}}+\cdots\cdots+\sqrt{\frac{(n_l+1)}{G^2}\cdot\frac{(G^2-n_l)}{G^2}}\right]\cdot E\cdot F^*, \qquad (16)$$

in which q is confined in Z-direction just as in the case of (13), and

$$F^* = \sum \exp(i_q \mathbf{R}_l)\cdot\frac{(\mathbf{e}_{q,j}\cdot[\gamma^*\cdot R_f])}{R_l{}^5}, \qquad (17)$$

where $\gamma^* = \frac{\hbar}{2}(1, -1, 0)$. Further, the expression between the braces of equation (16) may also be given by (15).

Let us denote with $P_{0,1}$ the transition probability of a process, in which the magnetic wall proceeds by a distance a/G^2, or in other words, the magnetic moment increases by 2β, and the energy relaxed from the crystal converts into a quantum of thermal vibration between $\hbar\omega_q$ and $\hbar\omega_q+d(\hbar\omega_q)$.

Then, according to the usual procedure(8), it may be given by

$$P_{0,1} = \sum_j \frac{Ga}{2\pi}\cdot\int |B_{0,1}|^2\,\frac{2\left\{1-\cos\frac{1}{\hbar}(2\beta H-\hbar\omega_{q,j})t\right\}}{(2\beta H-\hbar\omega_{q,j})^2}\,dq,$$

where $B_{0,1}$ is the matrix element given by (13). The integrand in the right side of this equation has a sharp maximum at $2\beta H = \hbar\omega_{q,j}$. If we denote the phase velocity of a lattice wave (q, j) with u_j, then $\omega_{q,j} = u_j|q|$. So that there are two q's, which fulfil the relation $2\beta H = \hbar\omega_{q,j}$ on q_z-axis. Thus, we must double the above expression when we transform it into integral form with respect to $\omega_{q,j}$, namely

$$P_{0,1} = \sum_j \frac{Ga}{\pi}\int |B_{0,1}|^2\,\frac{2\left\{1-\cos\frac{1}{\hbar}(2\beta H-\hbar\omega_{q,}\ )t\right\}}{(2\beta H-\hbar\omega_{q,j})^2}\,\frac{1}{\hbar u_j}\,d(\hbar\omega_{q,j})$$

$$= \sum_j \frac{2Gat}{\hbar^2 u_j}\,|B_{0,1}|^2\hbar\omega_{q,j} = 2\beta H.$$

Putting $B_{0,1}$, given by (13), into this expression, we have

$$P_{0,1} = \sum_j \frac{(2\pi)^2}{Nl}\,\frac{Z^2e^4\hbar^2}{m^4c^4}\,\frac{\hbar(N_{q,j}+1)}{2M\omega_{q,j}}\cdot\frac{G^4}{a^2}\cdot\frac{2Gat}{\hbar^2u_j}\left[\int\sqrt{|\psi|^2\cdot|\varphi|^2}\,dz\right]^2\cdot E^2\cdot|F|^2. \qquad (18)$$

Quite similarly, the transition probability of a process, in which the magnetic moment of the crystal decreases by 2β, may be given by

$$P_{0,1} = \sum_j \frac{(2\pi)^2}{Nl}\,\frac{Z^2e^4\hbar^2}{m^4c^4}\,\frac{\hbar N_{q,j}}{2M\omega_{q,j}}\cdot\frac{G^4}{a^2}\cdot\frac{2Gat}{\hbar^2u_j}\left[\int\sqrt{|\psi|^2\cdot|\varphi|^2}\,dz\right]^2\cdot|E|^2\cdot|F^*|^2, \qquad (19)$$

It is clear from the definition that $|F|^2 = |F^*|^2$. Now, if we remember that q is on the q_z-axis, it is easy to see that

$$\left.\begin{array}{l}|F|^2 = |F^*|^2 = 0, \text{ in the case of longitudinal} \\ \quad\text{wave, and that} \\ |F|^2 = |F^*|^2 = \frac{\hbar}{2}\left|\sum_f \frac{(R_f)_z}{R_f^5}\cdot\sin q(R_f)_z\right|^2, \text{ in the} \\ \quad\text{case of transversal wave.}\end{array}\right\} \qquad (20)$$

From the above two transition probabilities, we can obtain the velocity of the magnetic wall displacement by a simple consideration. It becomes

$$v = (P_{0,1}-P_{0,-1})\frac{a}{G^2}\,\frac{1}{t}$$

$$= \frac{4(2\pi)^2Z^2e^4\hbar^2}{m^4c^4l}\cdot\frac{1}{2M\omega_q u}\cdot\left[\int\sqrt{|\psi|^2\cdot|\varphi|^2}\,dz\right]^2\cdot|E|^2\cdot|F|^2. \qquad (21)$$

$|F|^2$ is almost determined by the terms in which the R_f's have small values, so that it may be thought to be proportional to q^2. Thus, $|F|^2\sim\hbar^3q^2C/a^6$ where C is a proper constant. Inserting this relation into (21) we shall have

$$v\sim 2(2\pi)^2\,\frac{Z^2e^4\hbar^2\beta H}{m^4c^4lMu^3a^6}\cdot\left[\int\sqrt{|\psi|^2\cdot|\varphi|^2}\,dz\right]^2\cdot|E|^2\cdot C. \qquad (22)$$

§ 5. Summary.

Summarizing the considerations mentioned above, we obtain the following results:

(1) Only the transversal lattice waves having wave number vectors perpendicular to the boundary surface take part in the magnetic wall displacement:

(2) The propagation velocity is proportional to the field H and does not contain temperature T explicitly in its expression.

If ϕ simply takes sine form as in Bloch's case*, it may easily be shown that the expression (15) is proportional to l. Therefore, the velocity (22) is proportional to l, or in other words, proportional to the thickness of the magnetic wall. If we remember the model, simplifying assumptions and eigenfunctions we have adopted, it could not be expected that (22) would bear quantitative comparison with the results of experiments. To answer the question as to what extent the above obtained predictions have grasped the essential features, we must wait for, for example, detailed experimental studies on the ferromagnetic semiconductors.

---

*) Reference (4), p 325.

Further it should be remarked that we have neglected in the above calculation the higher order transition process in which two or more lattice quanta are emitted or absorbed by the spin inversion process. Even in the case of such higher order process, as Muto suggested(8), we might have transition probability, which is not so small. Moreover, the velocity may show another temperature dependency.

Now, if a wall displacement occurs in the ferromagnetic solid, a microscopic eddy current is generally induced inside, so that the magnetic field caused by it may tend to prevent the wall displacement. From this point of view various attempts(9) have been made to calculate electrodynamically the velocity of the wall displacement. Exact calculations, however, are difficult, as the distribution of the eddy current is very complicated. Now, there are some experimental facts, which contradict with what is expected from such electrodynamical consideration. In the first place, the velocities of the wall displacements observed in the metallic ferromagnetics at extremely low temperatures show no striking difference from that at ordinary temperatures, though the former is somewhat smaller than the latter*. In the second place, there are also no essential differences between the velocities of ferromagnetic semi-conductors and of metallic ferromagnetics(10). Because of these facts, the dynamical problem of the wall displacement does not seem to be solved thoroughly, even if the electrodynamical calculations were carried out completely. Therefore, it seems to us to be necessary to approach to the problem from the atomistic standpoint. It should here be noted that our calculation must be regarded only as a preliminary attempt from such standpoint to deduce a qualitative explanation of the discrepancy between the experimental results and the electrodynamical consideration, and to furnish a reference to the explanation of the characteristics of ferromagnetic substance under high-frequency alternating magnetic field.

Finally, we note here that an atomistic investigation on the influence of stress on the wall displacement may also be of interest, which we are desiring to attempt on another occasion.

In conclusion we should like to express our sincere thanks to Dr. Tokutarô Hirone for suggesting the problem and for many helpful discussions and suggestions during the course of the present investigation.

References.

(1) Becker und Döring: Ferromagnetismus, Julius Springer, (1939), 176.

(2) T. Hirone: Butsurigaku Kôen-Shû, **1** (1941), 129.

(3) A study on the spin-Umklappung of electrons in the ferromagnetic crystals magnetized up to saturation has been carried out. T. Mutô and M. Nogami: Scientific Papers of I.C.P.R. **39** (1942), 319.

(4) F. Bloch: Zeits. f. Phys., **74** (1932), 295.

(5) A. Sommerfeld und H. Bethe: Handb. der Phys., 24/II, 503.

(6) I. Waller: Zeits. f. Phys., **79** (1932), 370.

(7) A. Sommerfeld und H. Bethe: loc. cit., 505.

(8) S. Kikuchi: Ryôshirikigaku, Iwanami Shôten, (1933) 111.

(9) Becker und Döring: loc. cit. 237. R. Kimura: Nippon Sûgakubutsurigaku-kaishi, **17** (1943), 458. Sixtus and Tonks: Phys. Rev., **37** (1931), 930.

(10) T. Okamura, T. Hirone and S. Miyahara: Proc. Phys.-Math. Soc. Japan, **23** (1941), 132.

---

*) Experiments carried out by T. Hujimura not yet published).

Cooperative Phenomena in Pd-H System I.

By Akira HARASIMA, Tomoyasu TANAKA and Kiitiro SAKAOKU.

Facutly of Science, Kyusyu University.

(Read March 15, 1947; Received October 1, 1947).

Abstract.

Some modifictions are made in Lacher's theory of the solubility of hydrogen in palladium by considering the change in energy of protons with the volume of the metal. Existence of two phases with different lattice constants and unsymmetrical form of the absorption isotherm are explained.

§ 1. Introduction.

The solubility of hydrogen in palladium has been studied experimentally by Sieverts(1), Lined and Borelius(2), Krüger and Gehm(3), and Gillespie and his co-workers(4). It is shown that at very high temperatures or at very low pressures the amount of hydorogen dissolved in palladium is proportional to the square root of the hydrogen pressure p. But below a certain difinite temperature, if the pressure of hydrogen is raised, a kind of cooperative phenomena can be observed.

The existence of two solid phases at temperatures below the critical temperture has been comfirmed by X-ray investigations(2, 3). The absorption of hydrogen does not alter the lattice structure, but causes a considerable expansion depending on the quantity of hydrogen absorbed. For the two phases two distinct lattice constants have been detected by X-rays.

Theoretical formulae of solubility of hydrogen in palladium were originally derived by R. Lacher(5), and compactly reviewed by R. H. Fowler and E. A. Guggenheim(6).

In Lacher's theory, it is assumed that the absorbed H atoms are completely ionized into protons and electrons, and these protons become tightly bound to certain sites in palladium lattice without affecting their lattice structure while electrons join the main body of metallic electrons, and, besides, there should be a weak interaction between absorbed protons, so that the assembly of hydrogen in palladium can be treated as a cooperative one. Isotherms, obtained theoretically, provided the existence of two solid phases, and the critical temperature was given in terms of interaction potential between protons in palladium.

The observation of Gillespie and Galstaun indicates that the isotherms of equilibrium of hydrogen and palladium are not completely symmetrical with respect to the critical point, while in Lacher's theory they become symmetric. In this paper we take into account the dependence of potentials between protons and the sites and of mutal interaction between neighboring protons upon the lattice constant of palladium. And the theoretical isotherms are re-calculated. It gives the theoretical interpretations of the volume change of palladium lattice on absorption of hydorogen, and the non-symmetrical nature of the equilibrium isotherms.

§ 2. The Hydogen-Palladium System.

Gillespie and Galstaun have shown that there is a critical temperature below which the absorption isotherms show that two solid phases are present. It is convenient to express the composition of the solution by the ratio r of the number of hydrogen atoms to the number of palladium atoms. When $r \leqq r_\alpha$ or $r \geqq r_\beta$, only one phase is present. In the intermediate range there are two phases. An inspection of Fig. 1 shows that the isotherms consist of three distinct parts. When r is less than r_α or greater than r_β, the pressure increases with increasing concentration. When $r_\alpha < r < r_\beta$, the pressure remains constant and it is in this region that X-ray experiments shows the presence of two distinct palladium lattices.

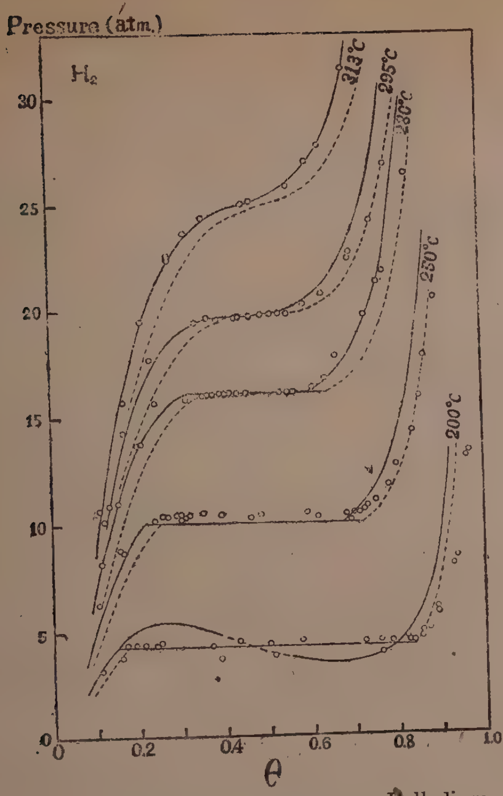

Fig 1. Isotherms of Hydrogen-Palladium Equilibrium.

———— Theoretical curves (This paper)

- - - - - - - - Theoretical curves (Lacher)

○○○○○○○ Experimental (Gillespie and Galstaun)

At critical temperature r is 0.270. The value of r_α, at which the second phase appears, decreases while the value of r_β, at which the first phase disappears, increases as the temperature decreases.

Palladium is a transition metal and has two bands of allowed electron states, namely the s and d bands, both of which overlap with each other. The s band can accommodate two electrons per atom and the d band ten. Palladium furnishes only ten, with the result that the two bands are not completely filled. When Pd is alloyed with Au, which has one more electron than palladium, measurements of the susceptibility and electrical resisatnce can be explained by assuming that the extra electron goes into the d band, which is filled up when electrons per atom have been added between 0.55 and 0.60*. Similarly, when palladium is alloyed with hydrogen, its paramagnetic susceptibilty decreases and becomes zero when hydrogen atoms per palladium atom have been added(7), between 0.53 and 0.66. This suggests that the dissolved hydrogen is almost completely ionized and that the detached electrons go into the d shell. It suggests that the process of hydrogen absorption will reach completion when $r=0.6$ approximately.

§ 3. The Partition Function.

The partition function for the dissolved hydrogen will be constructed by assuming that there are potential energy holes in palladium for the protons to go into. All these holes are assumed to be equivalent and we denote the number of holes by N_s. We denote by $a(T)$ the partition function for the vibrations of the absorbed H atom relative to the lattice when it is removed far from other protons, and by ϕ the energy in its lowest quantum state, the zero of energy being taken as that of a free atom in its lowest quantum state. And ϕ is assumed to be a function of the volume of palladium, so that it can be written:

$$\phi=\phi_0+\left(\frac{\partial\phi}{\partial V}\right)_{V=V_0}(V-V_0) \tag{3.1}$$

where V_0 is the volume of pure metal.

In order to explain the occurrence of critical phenomena, we must assume further that the energy of absorption depends on the number of holes filled, increasing as the number of holes filled increases. The protons with their compensating atmosphere of negative electrons must attract each other according to some unspecified law of force. We put this interaction potential of each pair of absorbed protons, which are nearest neighbors, equal to $-2w/z$, where the factor $2/z$ is included for convenience and z is the possible maximum number of protons around one proton, or the total interaction energy at saturation being equal to $-w$ per one proton. And w is also assumed to be a function of volume of the system, as

$$w=w_0+\left(\frac{\partial w}{\partial V}\right)_{V=V_0}(V-V_0) \tag{3.2}$$

We consider a solid phase as composed of N palladium atoms and N_A protons, then the partition function can be given by the equation.

---

* Mott and Jones, "*Properties of Metals and Alloys*", p. 189 (Oxford, 1936).

$$e^{-F/kT}=\sum_{N_{AA}}\omega(N_A,\,N_{AA})\exp\left[\frac{2w}{z}\frac{N_{AA}}{kT}\right]$$
$$\times\left[e^{\phi/kT}a(T)\rho\right]^{N_A}\left[e^{u/kT}b(T)\right]^{N}, \tag{3.3}$$

where

F = Helmholtz's free energy of the solid phase,

N_{AA} = Number of neighboring pairs of protons,

$\omega(N_A,\,N_{AA})$ = number of possible arrangements of N_A protons in N_S holes to give N_{AA} pairs.

$e^{u/kT}b(T)$ = the partition function of palladium,

ρ = the statistical spin weight of proton,

and summation is taken over all possible number of N_{AA} compatible with fixed N_S and N_A.

It is obvious that

$$\sum_{N_{AA}}\omega(N_A,\,N_{AA})=\frac{N_s!}{N_A!\,(N_s-N_A)!}, \tag{3.4}$$

because it represents the number of possible arrangement of N_A protons over identical N_s positions. Then we define a kind of mean value $\overline{\overline{N}}_{AA}$ of N_{AA} for the sake of mathematical convenience by the equation

$$\sum_{N_{AA}}\omega(N_A\,,\,N_{AA})e^{\left(\frac{2w}{z}N_{AA}\right)/kT}$$
$$=\frac{N_s!}{N_A!\,(N_s-N_A)!}e^{\frac{2w}{z}\overline{\overline{N}}_{AA}/kT} \tag{3.5}$$

Now we shall further assume that $\overline{\overline{N}}_{AA}$ is given in Bragg-Williams approximation by

$$\overline{\overline{N}}_{AA}=\frac{1}{2}z\frac{N_A}{N_s}N_A\,. \tag{3.6}$$

Then we obtain an expression for the Helmholtz free energy of the system,

$$-\frac{F}{kT}=N_s\log N_s-N_A\log N_A$$
$$-(N_s-N_A)\log(N_s-N_A)+N_A\log a\,(T,\,V)\rho$$
$$+\frac{1}{kT}\left[\phi\,N_A+w\frac{N_A{}^2}{N_s}\right]$$
$$+\frac{1}{kT}[Nu+NkT\log b(T,\,V)] \tag{3.7}$$

or

$$-\frac{F}{kT}=-N_s(\theta\log\theta+(1-\theta)\log(1-\theta))$$
$$+\frac{1}{kT}[\phi\,N_s\,\theta+wN_s\,\theta^2]+N_s\,\theta\log a\,(T,\,V)\rho-\frac{F_{Pd}}{kT} \tag{3.8}$$

where we put for brevity $N_A=N_s(N_A/N_s)=N_s\,\theta$, θ being the fraction of occupation of the holes with protons (F_{Pd} is the free energy of the solid phase when there are no protons in it).

§ 4. Equilibrium Conditions.

The free energy which is given by Eq. (3.8) is a function of volume, temperature and the number of protons $N_s\theta$. If F is plotted as a function of volume, curves something like those in Fig. 2 can be obtained, regarding θ as a parameter. In thermal equilibrium at constant temperature, since potential energies u, ϕ, w and the partition functions $a(T,\,V)$, $b(T,\,V)$ are all functions of volume of soild phase, the volume of the solid actually realized, should be the one which will make the free energy F minimum. Let F_{Pd} and F become minimum at V_0 and V respectively. V_0, V is given by

$$\left(\frac{\partial F_{Pd}}{\partial V}\right)_T=0,\ at\ V=V_0, \tag{4.1}$$

$$\left(\frac{\partial F}{\partial V}\right)_{T,\,\theta}=0,\ at\ V=V. \tag{4.2}$$

From Eq. (3.7)

$$-\frac{1}{kT}\left(\frac{\partial F}{\partial V}\right)_{V=V}=\frac{1}{kT}\left[N_s\theta\frac{\partial\phi}{\partial V}+N_s\theta^2\frac{\partial w}{\partial V}\right]$$
$$+N_s\theta\frac{\partial\log a}{\partial V}-\frac{1}{kT}\left(\frac{\partial F_{Pd}}{\partial V}\right)_{V=V}=0\,. \tag{4 3}$$

And the last term of (4.3) is expanded in Taylor series as

$$\left(\frac{\partial F_{Pd}}{\partial V}\right)_{V=V}=\left(\frac{\partial F_{Pd}}{\partial V}\right)_{V=V_0}$$
$$+\left(\frac{\partial^2F_{Pd}}{\partial V^2}\right)_{V=V_0}(V-V_0)+\cdots \tag{4.4}$$

The first term of this equation vanishes according to (4.1). Since

$$-\left(\frac{\partial F_{Pd}}{\partial V}\right)=p,$$

the second term can be written in the form

$$\left(\frac{\partial^2F_{Pd}}{\partial V^2}\right)_{V=V_0}=-\left(\frac{\partial p}{\partial V}\right)_{V_0}=\frac{1}{\kappa V_0} \tag{4.5}$$

where $\kappa=-\frac{1}{V_0}\left(\frac{\partial V}{\partial p}\right)_{V=V_0}$ is the compressibility of metallic Pd.

Then from (4.3) we obtain the volume change of palladium due to the absorption of hydrogen as a function of θ,

$$\frac{\Delta V}{\kappa V_0}=N_s\left[\theta\left(\frac{\partial\phi}{\partial V}\right)+\theta^2\left(\frac{\partial w}{\partial V}\right)\right], \qquad (4.6)$$

where we neglect the derivative of $\log a\ (T,V)$ as a slowly varying function of volume.

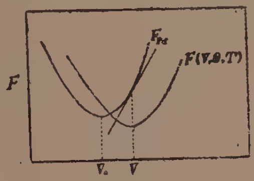

Fig. 2

We assume the quantity w to be a decreasing function of V so that the sign of $\left(\frac{\partial w}{\partial V}\right)$ shall be negative. We further asssume that the absolute value of $\left(\frac{\partial\phi}{\partial V}\right)$ is large compared with that of $\left(\frac{\partial w}{\partial V}\right)$, that is, the volume change of palladium due to the absorption of hydrogen is accounted for mainly by the behavior of potential ϕ between Pd and hydrogen as a function of volume. From the data shown by J. O. Linde and G. Borelius in their X-ray investigations, the amount of relative volume change of palladium when saturation is reached in equilibrium with gaseous hydrogen, can be estimated to be about eight percent. From these considerations we assume the sign of $\left(\frac{\partial\phi}{\partial V}\right)$ to be positive, and using the Linde and Borelius' data we can find from Eq. (4.6) its numerical value $6.22\cdot10^3$ *cal.* per *g-atom*, per *c. c.*

Substituting Eq. (4.6) into Eqs. (3.1) and (3.2), we can find ϕ and w as a function of θ, by the equations

$$\phi=\phi_0+\kappa V_0N_s\theta\left(\frac{\partial\phi}{\partial V}\right)^2+\kappa V_0N_s\theta^2\left(\frac{\partial\phi}{\partial V}\right)\left(\frac{\partial w}{\partial V}\right) \qquad (4.7)$$

$$w=w_0+\kappa V_0N_s\theta\left(\frac{\partial\phi}{\partial V}\right)\left(\frac{\partial w}{\partial V}\right); \qquad (4.8)$$

where the term including $\left(\frac{\partial w}{\partial V}\right)^2$ is neglected as is a small quantity of higher order.

There is another equilibrium condition. The dissolved hydrogen is in equilibrium with gaseous hydrogen. According to the fundamental equation of thermodynamics*, the absolute activity λ, or the chemical potential μ of hydrogen should have the same value in the dissolved state as in the gaseous state. This condition is expressed by,

$$\log\lambda=\frac{\mu}{kT}=\frac{1}{kT}\left(\frac{\partial F}{\partial N_A}\right)_{T,V}$$
$$=\log\lambda_H=\log\lambda_{H_2}^{\frac{1}{2}}=\frac{1}{2}\frac{1}{kT}\left(\frac{\partial F_{\text{gas}}}{\partial N_{\text{gas}}}\right) \qquad (4.9)$$

where λ_{H_2} and λ_H are the absolute activities of molecular and atomic hydrogens in gaseous phase. λ_{H_2} is easily obtained from the partition function of molecular hydrogen in gaseous phase. The partition function of molecular hydrogen in gaseous phase is given by

$$f(T)=\frac{(2\pi\cdot2m_HkT)^{3/2}V_g}{h^3}\cdot\frac{8\pi^2AkT}{h^2}\cdot\frac{\rho^2}{2}\cdot e^{\chi_d/kT}, \qquad (4.10)$$

where $2m_H$ is the mass of hydrogen molecule, A is its moment of inertia, and χ_d its dissociation energy of its lowest quantum state, V_g is the volume of gaseous phase, and ρ the statistical spin weight of proton. Then for the free energy of gas, F_g, we have

$$F_g=N_gkT\left\{\log\frac{N_g}{V_g}-1\right\}-\frac{5}{2}N_gkT\log T$$
$$-N_gkT\log\left\{\frac{(2\pi\cdot2m_Hk)^{3/2}}{h^3}\cdot\frac{8\pi^2Ak}{h^2}\frac{\rho^2}{2}\right\} \qquad (4.11)$$

and

$$\frac{1}{2}\left(\frac{\partial F_g}{\partial N_g}\right)=\frac{1}{2}kT\log p-\frac{7}{4}kT\log T$$
$$-\frac{1}{2}kT\log\left\{\frac{(2\pi\cdot2m_Hk)^{3/2}}{h^3}\cdot\frac{8\pi^2Ak}{h^2}\cdot\frac{\rho^2}{2}\right\}-\frac{1}{2}\chi_d \qquad (4.12)$$

where we assume the gas to be ideal. On the other hand, from Eq. (3.8)

$$\left(\frac{\partial F}{\partial N_A}\right)_{T,V}=\frac{1}{N_s}\left(\frac{\partial F}{\partial\theta}\right)_{T,V}$$
$$=kT\log\frac{\theta}{1-\theta}-[\phi+2w\theta]-kT\log a(T)\rho. \qquad (4.13)$$

§ 5. Equation of Isotherm.

From the second condition of equilibrium we obtain,

---

* See for example, E. A. Guggenheim, "*Modern Thermodynamics*".

$$\log p^{\frac{1}{2}} = \log\frac{\theta}{1-\theta} - \frac{1}{kT}\left[\phi - \frac{1}{2}\chi_d + 2w\theta\right] - \log a(T) + \frac{7}{4}\log T + \log\left[\frac{(2\pi\cdot 2m_H k)^3}{h^3}\cdot\frac{8\pi^2 Ak}{h^2}\cdot\frac{1}{2}\right]^{\frac{1}{2}}. \tag{5.1}$$

Substituting (4.7) and (4.8) in this equation, we obtain

$$\log p^{\frac{1}{2}} = \log\frac{\theta}{1-\theta} - \frac{1}{kT}\left[\left(\phi_0 - \frac{1}{2}\chi_d\right) + \left(2w_0 + N_s\kappa V_0\left(\frac{\partial\phi}{\partial V}\right)^2\right)\theta + 3N_s\kappa V_0\left(\frac{\partial\phi}{\partial V}\right)\left(\frac{\partial w}{\partial V}\right)\theta^2\right] + \log f(T), \tag{5.2}$$

where we have put for brevity

$$f(T) = \left[\frac{(2\pi\cdot 2m_H k)^{3/2}}{h^3}\cdot\frac{8\pi^2 Ak}{h^2}\cdot\frac{1}{2}\right]^{\frac{1}{2}} T^{\frac{7}{4}}/a(T). \tag{5.3}$$

Or, putting

$$\chi_0 = \phi_0 - \frac{1}{2}\chi_d$$

$$\chi = 2w_0 + N_s\kappa V_0\left(\frac{\partial\phi}{\partial V}\right)^2$$

$$-\frac{1}{2}\chi' = 3N_s\kappa V_0\left(\frac{\partial\phi}{\partial V}\right)\left(\frac{\partial w}{\partial V}\right) \tag{5.4}$$

where, χ_0, χ and χ' are all positive constants, then we obtain,

$$\log p^{\frac{1}{2}} = \log\frac{\theta}{1-\theta} - \frac{1}{kT}\left[\chi_0 + \chi\theta - \frac{1}{2}\chi'\theta^2\right] + \log f(T). \tag{5.5}$$

This equation gives the relation between the hydrogen pressure and the number of hydrogen atoms in the palladium in equilibrium with the gas. If we neglect the volume dependence of potentials ϕ and w, then χ' becomes zero, and this equation reduces to

$$\log p^{\frac{1}{2}} = \log\frac{\theta}{1-\theta} - \frac{1}{kT}\left[\phi_0 - \frac{1}{2}\chi_d + \kappa\theta\right] + \log f(T), \tag{5.6}$$

which is completely identical with the one which was obtained by Lacher.

§ 6. Critical Conditions, and Nonsymmetric Isotherms.

The equation (5.5), like that of Lacher's (5.6), has one maximum and one minimum below a certain temperature. The critical point is obtained from

$$\frac{dp}{d\theta} = 0, \qquad \frac{d^2p}{d\theta^2} = 0. \tag{6.1}$$

T is considered fixed in the process of differentiations.

From Eq. (5.5), the first equation of (6.1) can be written as

$$\frac{\kappa}{kT} = \frac{1}{\theta(1-\theta)} + \frac{\chi'}{kT}\theta, \quad at\ \theta = \theta_c, \tag{6.2}$$

and the second as

$$\frac{\chi'}{kT} = \frac{1-2\theta}{\theta^2(1-\theta)^2}.$$

Gillespie and Galstaun have shown that at critical point $p = 20.0$ atm., $T_c = 295$°C, $r = 0.270$, so that if we assign the value $N_s/N = 0.6$ as stated in § 2, the value of θ is found to be 0.450.

Using these values, χ and χ' can be determined from (6.2) and (6.3). From Eq. (6.3) we can justify the positive sign of χ' assumed in the previous section, because the observed θ_c is less than $\frac{1}{2}$.

Thus we can interpret the nonsymmetric properties of equilibrium isotherms, and at the same time the expansion of palladium lattice, in terms of the potential of protons in palladium. can easily be seen that the larger the expansion of palladium the more remarkable the deviation of isotherms from symmetry becomes. If we neglect χ', Eq. (6.3) requires to be $\frac{1}{2}$ for θ_c and the isotherm becomes symmetric with respect to $\theta = \frac{1}{2}$ as indicated by Lacher.

Values of constants obtained are listed in Table I.

Table I.

χ	$5.4\cdot10^3$	$4.5\cdot10^3$	(Lacher)
χ'	$1.84\cdot10^3$	0	(Lacher)
$\frac{\partial(N\phi)}{\partial V}$	$= 6.22\times10^3$ cal./g-atom, cm		
$\frac{\partial(Nw)}{\partial V}$	$= -0.41\times10^3$,,		

Below the critical temperature, the equilibrium stable isotherm can be obtained by means of the law of equal area in $\log p \sim \theta$ diagram, on account of which we may determine three values of θ, namely θ_α, θ_0, and θ_β. And if we substitute this θ_0 in Eq. (5.5), the pressure corresponding to the horizontal part is determined. In this procedure,

Table II.

	θ_α			θ_β		
	theor.	obs.	Lacher	theor.	obs.	Lacher
200°C	0.145	0.205	0.170	0.790	0.853	0.830
250°C	0.225	0.250	0.265	0.690	0.709	0.735
280°C	0.325	0.417	0.360	0.590	0.550	0.640

we can also determine the value of $\log f(T)$ which was left untouched as an unknown factor, at every temperature. θ_α, θ_β are compared with observations, in Table II.

Calculated isotherms are given in Fig. 1. The nonsymmetrical shape of isotherms may be seen, and they reprsent the observed isotherms more adequately at high temperatures and small concentrations, but the agreement is not yet so satisfactory at low temperatures and large concentrations.

References.

(1) A. Sieverts and H. Hagen: Zeits. f. Phys. Chem. **174**, (1935) 247.

(2) J. O. Linde and G. Bolelius: Ann. d. Physik [IV], **84**, (1927) 747.

(3) F. Krüger and G. Gehm: Ann. d. Physik [V], **16**, (1933) 174.

(4) L. J. Gillespie and F. P. Hall: J. Amer. Chem. Soc. **48**, (1926) 1207.

L. J. Gillespie and L. S. Galstaun: *ibid.* **58**, (1936) 2565.

(5) R. Lacher: Proc. Roy. Soc. **A161**, (1937). 525

(6) R. H. Fowler and E. A. Guggenheim: "*Statistical Thermodynamics*" p. 558 (Cambridge, 1939).

(7) B. Svensson: Ann. d. Physik [V], **18**, (1933) 299.

Cooperative Phenomena in Pd-H System II.

By Tomoyasu TANAKA, Kiitiro SAKAOKU and Akira HARASIMA.

Faculty of Science, Kyusyu University.

(Read May 11, 1947; Received October 1, 1947).

Abstract.

In the first paper we discussed the cooperative phenomena which are observed when hydrogen is absorbed in palladium by considering the change of energy of the protons with the volume of the metal, and explained the volume changes and unsymmetrical form of the absorption isotherm which are observed when hydrogen is absorbed in palladium. In the present paper we further consider the oscillation of the protons and apply the theory to the case of absorption of deuterium in palladium.

§ 1. Introduction.

In our first paper with the above title, which henceforth will be denoted as Paper I, we took into account the effect of volume change of metal upon the energies of absorbed hydrogen in palladium for the interpretation of unsymmetrical form of absorption isotherm.

Observations on the absorption of deuterium in palladium are reported in a series of papers by Gillespie and his co-workers(1). In this case the deviation of the form of isotherms from symmetry is more remarkable. We have applied the formula obtained in paper I to this Pd-D system. But the agreement was rather poor, especially at lower temperatures. In this paper we further take into account the variation of the frequency of the thermal agitation of proton in its stable site in the palladium lattice. The method was suggested by G. S. Rushbrooke in his paper(2) on the theory of cooperative phenomena, and afterward by T. Nagamiya and S. Yomosa in their theory of superlattices(3).

§ 2. Partition function.

Rushbrooke suggested that if, in the case of adsorption, the effect of the variation of the frequency of vibration with the amount of adsorption was taken into accent in the partition function, the critical conditions would have to be modified. In his theory he has assumed that for each adsorbed molecule there is one harmonic vibration whose frequency varies linearly with the number of adsorbed molecules, *i. e.* with θ, as

$$\nu = \nu_0 + \nu_1 \theta, \tag{1}$$

In this paper we shall consider the frequency ν of absorbed proton as a function of θ, but from some physical considerations a slightly different form from Eq. (1) has been used.

In paper I we have obtained the partition function of hydrogen and palladium system, which is given by (Eqs. (3.3), (3.5) and (3.6) of paper I)

$$e^{-F/kT} = \frac{N_s!}{N_A!(N_s-N_A)!} \cdot \exp\left[\frac{wN_A^2}{N_s}\frac{1}{kT}\right]\left[e^{\phi/kT}a(T)\right]^{N_A}\left[e^{u/kT}b(T)\right]^{N}, \tag{2}$$

where N_s is the number of possible sites of protons to go into, N_A the number of absorbed protons, $-w$ the interaction energy of protons, ϕ the energy required to carry one proton out of its stable site in palladium to the point at infinity, $a(T)$ the partition function for the excited states of vibration of a proton, and $[e^{u/kT}b(T)]^N$ is the partition function of N palladium atoms.

Since an approximate method of Bragg and Williams is used in our theory, it is assumed that, as the total number N_A of absorbed protons increases, the number of protons surrounding one specified proton also increases in proportion to N_A, and the energy of each absorbed proton in its lowest state is represented as a linear function of $\theta = N_A/N_s$, where θ denotes the fraction of sites occupied by absorbed protons.

As for the partition function $a(T)$, we assume a three dimensional isotropic harmonic oscillator, so $a(T)$ may be written:

$$a(T) = \exp\left[-\frac{1}{2}\frac{h\nu}{kT}\right] \Big/ \left(1-\exp\left[-\frac{h\nu}{kT}\right]\right), \tag{3}$$

where ν is the frequency of vibration. This vibrational frequency depends on the type of potential hole in which proton executes a harmonic oscillation. In the case of proton, the absorption energy increases as the number of absorbed protons increases, and is simply represented as a linear function of θ. Then if this energy function is expanded in a power series of the displacement of proton from its position of minimum energy, all the coefficients should be linear in θ, and especially the coefficient of the quadratic term, which represents the constant of the restoring force, is also linear in θ. Hence the frequency of harmonic oscillator must be proportional to the square root of the force constant, and inversely proportional to the square root of its mass. For this reason it would be more natural to consider ν^2, instead of ν, as a linear function of θ, so that we have

$$\nu^2 = \nu_0^2 + \nu_1^2 \theta. \tag{4}$$

Similar considerations were made by T. Nagamiya and S. Yomosa(3). They considered the effect of thermal agitation of atoms on the behavior of order-disorder transition in binary alloys. They put the frequency of any atom proportional to the square root of a linear function of the Bragg-Williams' long range order parameter s. In our theory the parameter θ plays the same rolé as the parameter s in binary alloys. Now we have a complete partition function from Eqs. (2), (3) and (4).

The equilibrium conditions may be written down by the same procedure as in paper I, that is, by differentiating the free energy F by V and θ.

From the first condition, the volume change of palladium due to the absorption of hydrogen can be given in the form,

$$\frac{\Delta V}{\kappa V_0} = N_s\theta\left(\frac{\partial\phi}{\partial V}\right)+N_s\theta^2\left(\frac{\partial w}{\partial V}\right)+N_s\theta kT\frac{\partial\log a}{\partial V}. \tag{5}$$

This equation is similar to that of the expression in paper I, except that the last term is added. κ is again the compressibility of palladium, and V_0 is the volume of palladium when there are no protons in it. From the second condition, the equation of isotherm can be obtained.

$$\log p^{\frac{1}{2}} = \log\frac{\theta}{1-\theta}-\frac{1}{kT}\left[\phi-\frac{1}{2}\chi_d+2w\theta\right]$$
$$+\log f(T)-\theta\frac{\partial\log a(T)}{\partial\theta}-\log a(T), \tag{6}$$

where χ_d is the dissociation energy of hydrogen molecule, and $a(T)$ is given by Eq. (3) as a function of $\nu(\theta)$ and temperature.

Substituting Eqs. (3) and (4) in this equation, we have the final expression for the equation of isotherm,

$$\log p^{\frac{1}{2}} = \left[\log\frac{\theta}{1-\theta}+\log f(T)+3\log(1-e^{-\frac{h\nu}{kT}})\right]$$
$$-\frac{1}{kT}\left[\chi_0+\chi_1\theta-\frac{1}{2}\chi_2\theta^2-\frac{3}{2}h\nu-3\left(\frac{1}{2}+\varepsilon\right)h\nu\eta\theta\right], \tag{7}$$

in which we have introduced many notations, indicated as follows:

For the case of light hydrogen,

$$f(T) = \left[\frac{(2\pi\cdot 2m_H k)^{3/2}}{h^3}\cdot\frac{8\pi^2 A_H k}{h^2}\cdot\frac{1}{2}\right]^{\frac{1}{2}} T^{\frac{7}{4}}, \tag{8}$$

$$\chi_0 = \phi_0-\frac{1}{2}\chi_d{}^{H_2}, \tag{9}$$

$\chi_d{}^{H_2} = 109.0$ kilo-calories per mole: the dissociation energy of light hydrogen molecule(4),

$$\varepsilon = \exp\left[-\frac{h\nu}{kT}\right]\Big/\left(1-\exp\left[1-\frac{h\nu}{kT}\right]\right), \tag{10}$$

$$\eta = \frac{1}{\nu}\frac{d\nu}{d\theta} = \xi/2(1+\xi\theta), \tag{11}$$

$$\xi = \nu_1{}^2/\nu_0{}^2, \tag{12}$$

$$\nu^2 = \nu_0{}^2+\nu_1{}^2\theta = \nu_0{}^2(1+\xi\theta), \tag{13}$$

$$\chi_1 = 2w_0+N_s\kappa V_0\left(\frac{\partial\phi}{\partial V}\right)^2, \tag{14}$$

$$\chi_2 = -6N_s\kappa V_0\left(\frac{\partial\phi}{\partial V}\right)\left(\frac{\partial w}{\partial V}\right). \tag{15}$$

For the heavy hydrogen,

$$f(T) = \left[\frac{(2\pi\cdot 2m_D k)^{3/2}}{h^3}\cdot\frac{8\pi^2 A_D k}{h^2}\cdot\frac{1}{2}\right]^{\frac{1}{2}} T^{\frac{7}{4}}, \tag{16}$$

$$= 2^{\frac{5}{4}}[f(T) \text{ for light hydrogen}], \tag{17}$$

because $m_D = 2m_H,\ A_D = 2A_H,$

$$\chi_0 = \phi_0-\frac{1}{2}\chi_d{}^D, \tag{18}$$

$\chi_d{}^D = 110.8$ kilo-calories per mole: the dissociation energy of heavy hydrogen molecule(4).

Other quantities for heavy hydrogen are given by the same equation as that for light hydrogen. For the detailed reduction to get these formulas, we refer to our paper I.

The critical condition is given by

$$\frac{dp}{d\theta} = 0, \qquad \frac{d^2p}{d\theta^2} = 0. \tag{19}$$

From the first condition we obtain

$$\frac{\chi_1}{kT} = \frac{\chi_2}{kT}\theta+\frac{1}{\theta(1-\theta)}+3(1+2\varepsilon)x\eta$$
$$-3\left[(\varepsilon+\varepsilon^2)x^2+\left(\frac{1}{2}+\varepsilon\right)x\right]\eta^2\theta, \tag{20}$$

at $T = T_c$, $\theta = \theta_c$.

And the second condition can be written as,

$$\frac{\chi^2}{kT} = \frac{1-2\theta}{\theta^2(1-\theta)^2}+9\left[(\varepsilon+\varepsilon^2)x^2+\left(\frac{1}{2}+\varepsilon\right)x\right]\eta^2$$
$$-3\left[(\varepsilon+3\varepsilon^2+2\varepsilon^3)x^3+3(\varepsilon+\varepsilon^2)x^2+3\left(\frac{1}{2}+\varepsilon\right)x\right]\eta^3\theta, \tag{21}$$

at $T = T_c$, $\theta = \theta_c$, where

$$x = \frac{h\nu}{kT},\quad \eta = \frac{1}{\nu}\frac{d\nu}{d\theta},$$
$$\varepsilon = \exp\left[-\frac{h\nu}{kT}\right]\ \left(1-\exp\left[-\frac{h\nu}{kT}\right]\right). \tag{22}$$

These equations are rather complicated, no term being neglected in them. Rushbrooke assumed for the sake of simplicity as

$$h\nu_0 \ll kT,\quad h\nu_1 \ll kT,$$

and expanded the vibrational partition function in powers of $h(\nu_0+\nu_1\theta)/kT$. For the case of proton and deuteron, however, the vibrational energy is much larger and almost comparable with kT, so that we cannot make such simplifications.

If we know the values of ν_0 and ξ, then all the values of parameters x, η, ε at the critical point can be determined from the Eqs. (10), (11) and (13). Substituting these values in Eqs. (20) and (21) we obtain the numerical values of χ_1 and χ_2. Quantities χ_1 ann χ_2, as seen from their definig equations (14) and (15), are both determined from the types of energies of mutal interactions between protons (or deuterons), and proton (or deuteron) and palladium.

As is well known(4), there is a difference between the dissociation energies of light and heavy hydrogen molecules, and this is considered as the result of the difference in their zero point energies of molecular vibrations. The amount of this difference is adequately interpreted from the difference of their inertial masses, and other contributions to their dissociation energies are considered to be the same for both cases.

In our case of proton or deuteron in palladium the types of potentials can be considered to be the same. Thus, we must have the same numerical values for constants χ_1 and χ_2. And further, since the mass of deuteron is twice that of proton, we must have

$$\text{(the frequency of proton)} = \sqrt{2}\cdot\text{(the frequency of deuteron)}.$$

Consequently there are only 4 unknown quantities ν_0, ξ (or ν_1), χ_1 and χ_2 for either proton or deuteron. Writing down the Eqs. (20) and (21) for both cases of proton and deuteron, we shall obtain four equations from which we are able to determine χ_1, χ_2, ν_0 and ξ simultaneously.

§ 3. Comparison of the theory with the experiment.

We do not carry out the numerical calulation in a manner stated above from the following reasons:

a. At the critical point the isotherm has a horizonal tangent. So the critical temperature T_c is determined fairly accurately from the experimental data, but the fraction θ_c of absorption at this point, cannot be determined with sufficient accuracy from the observed isotherm, while it has a great effect on determining the values of χ_1 and χ_2 from Eqs. (20) and (21). The observed critical constants are given in Table II.

b. The osillating frequency ν is considered as a function of θ only in our calculation. But it may also depend on the volume of the metal, so that the vibrational partition $a(T)$ becomes also a function of volume. We have neglected the corresponding terms in the equation (5) as a small quantity. On the other hand, as far as we know, any available X-ray data on *Pd-D* system are now lacking, from which the information of volume change of palladium can be obtained. It is easily seen from Eq. (5) that if there is a difference between hydrogen and deuterium in the manner of change of ΔV, the dependence of $a(T)$ on volume will be different for *H* from that for *D*. This point is not considered in our theory.

We shall only test the effect of the thermal agitation on the isotherm After some numerical calculations we have confirmed that if the frequency of proton increased with the number of absorbed protons, then the width of horizonal part of isotherms would increase.

In Lacher's theory, the forms of isotherms could be completely determined by giving the value χ_1. The isotherms are shown to become symmetric with respect to the critical point, and the length of the horizontal part of each isotherm—the region of two coexistent solid phases—is determined definitely. In paper I where the dependence of potentials between protons and the sites and that of mutual interaction between neighboring proton upon the lattice constant of palladium have been shown to lead to the non-symmetric form of observed isotherms, the length of the horizontal part was automatically determined. If the effect of thermal agitation of absorbed proton is also taken into account as done in this paper, the following behavior of isotberms may be found: If the frequuecy increases as the number of dissolved protons increases, then the length of the horizontal part of isotherm becomes longer, while if the frequency decreases as the number of dissolved protons increases, then that part of isotherm becomes narrower. Now we shall assume the amount of the increase of frequencies, when saturation is reached, to be 10 *per cent* of the value for $\theta = 0$ for proton and 40 *per cent* for deuteron.

The observed hydrogen pressures corresponding to the horizontal part of isotherms are well represented in the following empirical equations

$$\log_{10} p_{atm.} = 4.6018-1877.82/T \quad \text{for } H \qquad (23)$$

and

$$\log_{10} p_{atm.} = 4.6330-1696.11/T \quad \text{for } D, \qquad (24)$$

and these equations are referred to as "*vapor pressure equations*" by Gillespie and others(1).

On the other hand, our formula (7) is composed of two parts; one is slowly varying with temperature T, and the other is inversely proportional to T. Comparing with this temperature-insensible term and the observed constant term of (23) and (24) at critical temperature T_c, we obtain the following values of frequencies

$$h\nu_c = 0.9409\cdot 10^3 \ cal./g\text{-}atom., \quad \nu_c = 9.872\cdot 10^{12} \ sec^{-1}. \qquad (25)$$

$$h\nu_c = 0.6669\cdot 10^3 \ cal./g\text{-}atom., \quad \nu_c = 6.997\cdot 10^{12} \ sec^{-1}. \qquad (26)$$

and their ratio happens to be

$$\nu_c^H/\nu_c^D = 1.414 \simeq \sqrt{2}. \qquad (27)$$

as anticipated before. This result comfirms us to assume that the forms of potential holes are identical for H and D. Assuming the values of frequency-increase to be,

$$\xi = \nu_1^2/\nu_0^2 = 0.210, \ 10 \ per \ cent \text{ increase for } H, \qquad (28)$$

and

$$\xi = \nu_1^2/\nu_0^2 = 0.960, \ 40 \ per \ cent \text{ increase for } D, \qquad (29)$$

and using (25) and (26), the values of parameters are all determined from the critical conditions (20) and (21), and they are listed in Table I, and other constants are also given in Table II and III.

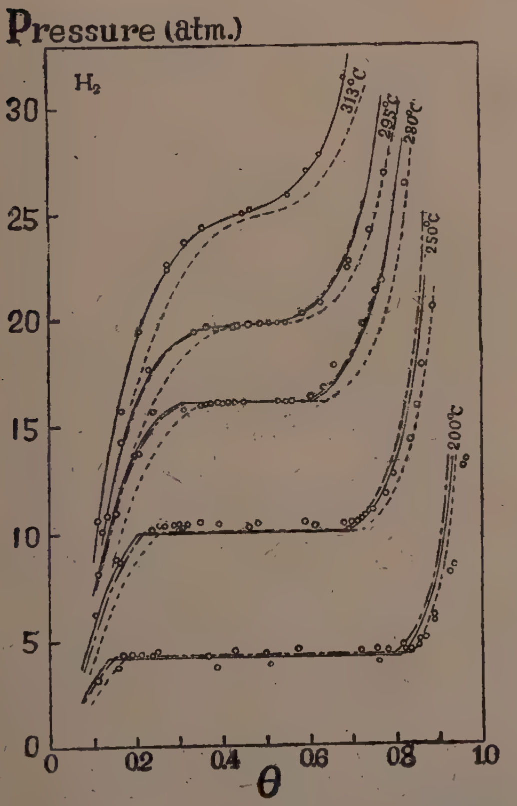

Fig. 1. Isotherms of Hydrogen-Palladium Equilibrium.

———— Theoretical (Paper II)
— — — — Theoretical (Paper I)
—·—·— Theoretical (Lacher)
○○○○○○ Experimental (Gillespie and Galstaun)

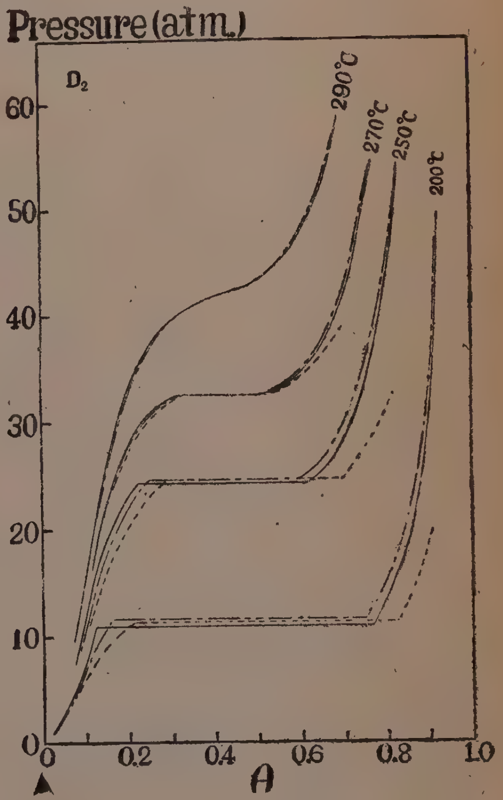

Fig. 2. Isotherms of Deuterium-Palladium Equilibrium.

———— Theoretical (Paper II)
— — — — Theoretical (Paper I)
- - - - - - Experimental (Gillespie and Dawn)

Table I.

	χ_0	χ_1	χ_2	w_e	ϕ_0
H	3.31 (1.60)	6.13 (5.39)	2.02 (1.84)	0.75 (0.38)	57.8 (56.1)
D	2.97 (1.73)	8.53 (5.76)	4.93 (3.06)	1.90 (0.57)	58.4 (57.1)

The unit of energies is *kilo-calories* per *g-atom*. Values in parentheses are those obtained in paper I.

Table II.

Critical constants.

	T_c	p_c	θ_c
H	568°*K*	19.79 *atm*	0.450
D	549°*K*	35.0 *atm*	0.417

Table III.

	ε	x	η	ξ
H	0.76778	0.83397	0.095934	0.210
D	1.18574	0.61157	0.34278	0.960

The value of χ_0 is determined so as to give the observed value of pressure precisely at T_c and θ_c, when all the other parameters except χ_0 are substituted in the equation of isotherm. After all the parameters are thus determined, we are able to obtain the isotherm for any temperature. The pressures corresponding to the horizontal part of isotherms are determined by the law of equal areas. In this manner the vapor pressures are automatically determined. Calculated isotherms are given in Figs. (1) and (2).

References.

(1) L. J. Gillespie and F. P. Hall: J. Amer. Chem. Soc. **48**, (1926) 1207.
L. J. Gillespie and L. S. Galstaun: J. Amer. Chem. Soc. **58**, (1936) 2565.
L. J. Gillespie and W. R. Downs: J. Amer. Chem Soc. **61**, (1939) 2496.

(2) G. S. Rushbrooke: Proc. Camb. Phil. Soc. **34**, (1938) 424.

(3) T. Nagamiya and S. Yomosa: *Nippon Sugaku-Buturigaku Kaisi*, Vol. 16, (1942). 375 (Published by the Phys. -Math. Soc. Japan, in Japanese).

(4) A. Farkas: "*Orthohydrogen, Parahydrogen and Heavy Hydrogen*" P. 155. (Camb. 1935)

Grayhical Solution of Wave Equations.

By Isao OSIDA.

Department of Dynamics, Faculty of Engineering, University of Nagoya.

(Read, on May 6, 1944; Received, October 11, 1947)

§ 1. Introduction.

Wave equations can be solved graphically(1) as well as numerically(2). For the one-dimonsional wave equation

$$\frac{\partial^2 u}{\partial t^2} = V^2 \frac{\partial^2 u}{\partial x^2} \tag{1}$$

where u is displacement, t the time, x the coordinate and V the velocity, we introduce a small time interval τ and a small length S, and change it to a difference form by approximate relation

$$\frac{\partial^2 u}{\partial t^2} \doteqdot \frac{1}{\tau^2}\{u(x,\ t-\tau)-2u(x,\ t)+u(x,\ t+\tau)\},$$

$$\frac{\partial^2 u}{\partial x^2} \doteqdot \frac{1}{S^2}\{u(x-s,\ t)-2u(x,\ t)+u(x+s,\ t,\}. \tag{2}$$

Introducing (2) into (1), and putting

$$S = V\tau, \tag{3}$$

we have a simple relation(3)

$$u(x,\ t+\tau) = u(x-V\tau,\ t)+u(x+V\tau,\ t)-u(x,\ t-\tau) \tag{4}$$

which enables us to compute graphically or numerically the 'future' displadement $u(x,\ t+\tau)$ from the 'present' displacement $u(x\pm V\tau,\ t)$ and the 'past' displacement $u(x,\ t-\tau)$.

§ 2. Construction.

Fig. 1. shows the graph of the displacement, taking x as the abscissa, u as the ordinate and t as the parameter. Then the relation (4) tells us that the four points E, G, I and K expressing these four displacements $u(x,\ t-\tau)$, $u(x-V\tau,\ t)$, $u(x,\ t+V\tau)$ and $u(x,\ t+\tau)$ respectively from a parallelogram on the graph, so that we are able to find K from the first three; E, G and I. Let the middle point of GI, J, produce ET through J, so that EJ = KJ, the point K is thus found. Applying the procedure for various x we can draw a curve expressing the 'future' displacement $u(x,\ t+\tau)$. Accordingly, if we know the first two curves, say $u(x, 0)$ and $u(x,\ \tau)$, we can find the displacement $u(x,\ n\tau)$ at any time thereafter by repeating the above process.

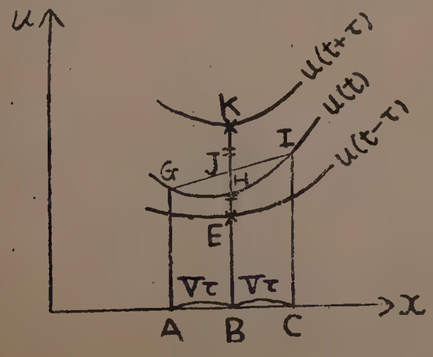

Fig. 1.

§ 3. Initial and Boundary Conditions.

If there is given as the initial condition the initial displacement $u(x,\ 0)$ and the initial velocity $\left(\frac{\partial u}{\partial t}\right)_{t=0}$, we can find $u(x,\ \tau)$ by an approximate relation

$$u = (x,\ \tau) \doteqdot u(x,\ 0)+\tau\left(\frac{\partial u}{\partial t}\right)_{t=0},$$

which can also be constructed in the graph (Fig. 2).

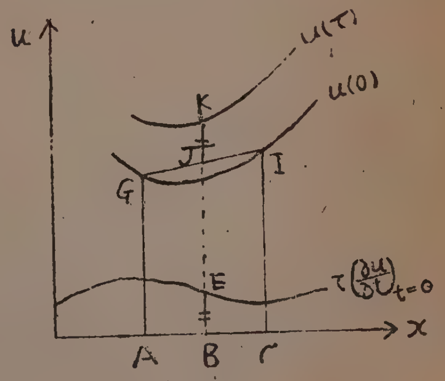

Fig. 2

Boundary conditions must be taken into account, too. If the boundary is so fixed that for instance $u(0,\ t)\equiv 0$ at the boundary $x = 0$ or the displacement at the boundary is given by a function of time, no difficulty occurs. If $\left(\frac{\partial u}{\partial x}\right)_{x=0} = 0$, as it is at a free end, the displacement at the boundary can be obtained by the same construction as stated above, imagining that the displacement curve countinues to the opposite side of $x = 0$, being symmetric with respect to the straight line $x = 0$ (Fig. 3).

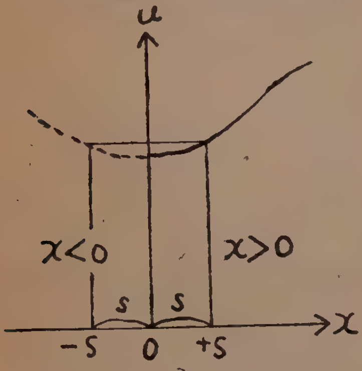

Fig. 3

§ 4. An Example.

For example, we solve (1) under the conditions

$$u(0, t) = 0 \quad \text{if} \quad t < 0$$

$$u(0, t) = \sin\left(\frac{2\pi V}{L} t\right) \quad \text{if} \quad t > 0,$$

$$u\left(\frac{L}{4}, t\right) = 0$$

$$u(x, 0 = 0 \quad \text{and} \quad \left(\frac{\partial u}{\partial t}\right)_{t=0} = 0, \quad \text{if} \quad t = 0 .$$

Putting $\tau = \frac{L}{36V}$, $S = V\tau = \frac{L}{36}$, and the result obtained after 15 processes, that is the solution for $t = 15\tau$, is compared with the exact analytical solution which is expressed by small circles in Fig. 4. The agreement is satisfactory.

5. Telegraphic Equation.

The vibration under dissipating force is expressed by the so-called telegraphic equation:

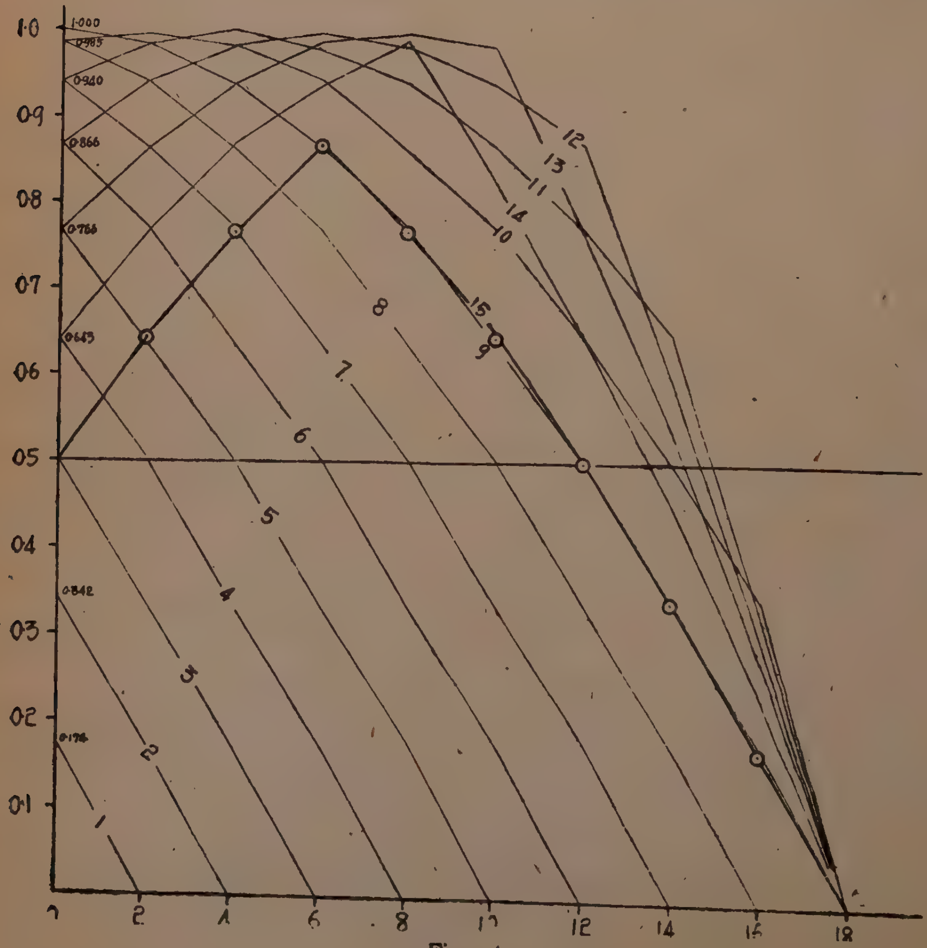

Fig 4

$$\frac{\partial^2 u}{\partial t^2}+A\frac{\partial u}{\partial t}+Bu-C\frac{\partial^2 u}{\partial x^2}=0\,,$$

where A, B and C are constants. This is transformed into the simpler form if we change the dependent variable u to $ue^{-At/2}$, that is,

$$\frac{\partial^2 u}{\partial t^2}-\beta u-\gamma\frac{\partial^2 u}{\partial x^2}=0$$

Using the differences (2) instead of the differentials, and putting

$$S^2=\frac{\gamma\tau^2}{1-\dfrac{\beta\tau^2}{2}}\,,$$

we have

$$u(x,\,t+\tau)\doteqdot\left(1-\frac{\beta\tau^2}{2}\right)\{u(x-s,\,t)+u(x+s,\,t)\}$$
$$-u(x,\,t-\tau) \qquad (5)$$

In Fig. 5. let

$$\overline{AB}=\overline{BC}=S$$
$$\overline{AD}=u(x-s,\,t),\quad \overline{CF}=u(x+s,\,t)$$
$$\overline{BG}=u(x,\,t-\tau),\quad \overline{BH}=u(x,\,t+\tau)$$
$$\overline{DL}=\overline{LF},\quad L\times BL=\theta,\quad \sin^2\theta=\frac{\beta\tau^2}{2}\,,$$
$$LN\perp BX,\ NM\perp BL$$
$$\overline{BL}=\frac{1}{2}(\overline{AD}+\overline{CF})\,,$$

then

$$\overline{BM}=\overline{BN}\cos\theta=\overline{BL}\cos^2\theta=\overline{BL}(1-\sin^2\theta)$$
$$=\overline{BL}\left(1-\frac{\beta\tau^2}{2}\right)$$

and (5) becomes

$$\overline{BH}=\left(1-\frac{\beta\tau^2}{2}\right)(2\overline{BL})-\overline{BG}=\overline{BM}+\overline{MG}.$$

This leads to $\overline{MG}=\overline{MH}$, or to that M is the middle point of $\overline{HG}$. Accordingly we can find the unknown point H, which represents $u(x,\,t+\tau)$, from the known three D, F and G.

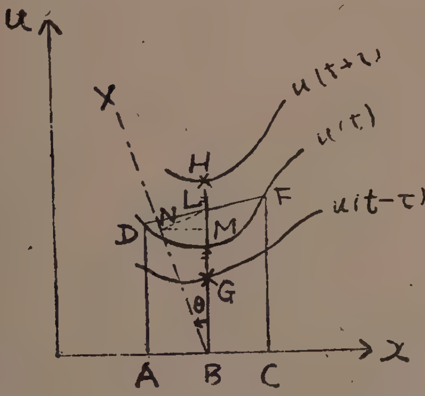

Fig. 5

§ 6. Two-Dimensional Equation.

Two-dimensional wave equation

$$\frac{\partial^2 u}{\partial t^2}=V_x^2\frac{\partial^2 u}{\partial x^2}+V_y^2\frac{\partial^2 u}{\partial y^2} \qquad (6)$$

can also be solved graphically. Using diffrences instead of the differential quotient, it holds

$$u(x,\,y,\,t+\tau)=\frac{1}{2}\{u(x+V_x\tau,\,y+V_y\tau,\,t)$$
$$+u(x-V_x\tau,\,y+V_y\tau,\,t)+u(x+V_x\tau,\,y-V_y\tau,\,t)$$
$$+u(x-V_x\tau,\,y-V_y\tau,\,t)\}-u(x,\,y,\,t-\tau)+R,$$

where R is small residual term,

$$R\doteq-\frac{1}{3}V_x^2V_y^2\tau^4\frac{\partial^4 u}{\partial x^2\partial y^2}+\cdots$$

This is verified by expansion referring to the original equation (6). Neglecting R and denoting the mean displacement of the four adjacent points $(x\pm V_x\tau,\ y\pm V_y\tau)$ by $\bar{u}$, we have

$$u(x,\,y,\,t+\tau)\doteqdot\bar{u}(x,\,y,\,t)+\{\bar{u}(x,\,y,\,t)$$
$$-u(x,\,y,\,t-\tau)\} \qquad (7)$$

We prepare the diagrams such as Fig. 1 for each value differing by $V_y\tau$, that is, for $\cdots y-2V_y\tau$, $y-V_y\tau$, y, $y+V_y\tau$, $y+2V_y\tau$, and arrange them side by side with equal spacing as shown in Fig. 6. In this figure, denote the middle point of the two points expressing $u(x-V_x\tau,\,y-V_y\tau,\,t)$ and $u(x+$

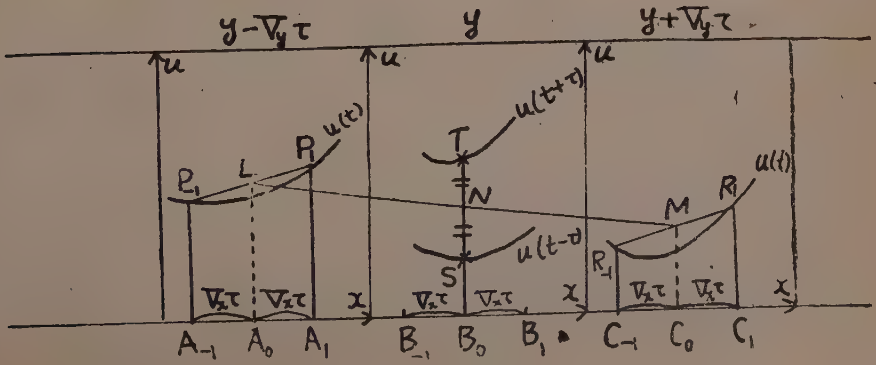

Fig. 6

$V_x\tau, y-V_y\tau, t)$ by L, and the middle point of the two expressing $u(x-V_x\tau, y+V_y\tau, t)$ and $u(x+V_x\tau, y+V_y\tau, t)$ by M. Then the middle point N of LM expresses the avarage value $\bar{u}(x, y, t)$ of the four. If the point representing $u(x, y, t-\tau)$ is S, the relation (7) teaches us that the point T expressing $u(x, y, t+\tau)$, which we are intend to find, is obtainable as the point of symmetry of S with respect to N. Repeating the precedure we are able to find from given initial conditions the displacement after any time interval.

§ 7. Three Dimensional Equation.

This idea of solution can be applied to the three-dimensional equation,

$$\frac{\partial^2 u}{\partial t^2} = V_x^2\frac{\partial^2 u}{\partial x^2}+V_y^2\frac{\partial^2 u}{\partial y^2}+V_z^2\frac{\partial^2 u}{\partial z^2}$$

This transforms into

$$u(x, y, z, t+\tau) \doteqdot \bar{u}+\{\bar{u}-u(x, y, z, t-\tau)\}$$

approximately, where $\bar{u}$ means the mean displacement of the eight adjacent ones $u(x\pm V_x\tau, y\pm V_y\tau, z\pm V_z\tau, t)$. This is of the same form with (7), and the procedure is shown in Fig. 7.

A slight modification will solve the equation when the propagation velocity V is not constant but a function of time or the coordinate.

In conclusion the author expresses his sincere thanks to Dr. Prof. Yasundo Takahashi, Dr. Yoshihiko Takahashi, Assoc. Prof. T. Koga for their helpful advices and encouragements, to Miss Fukazu for her help to prepare the diagrams and to the Hattori Hōkō Kai for their financial support.

Reference.

(1) I. Osida, Jour. Met. Soc. **21** (1943) 198~216, **22** (1944) 98~104 (in Japanese).

(2) For numerical solutions, see S. Homma, Jour. Met. Soc. **19** (1941), 358, Y. Simose, ibid. **21** (1941) 285~261.

(3) This holds not approximately but exactly, as it is proved by expansion referring to (1).

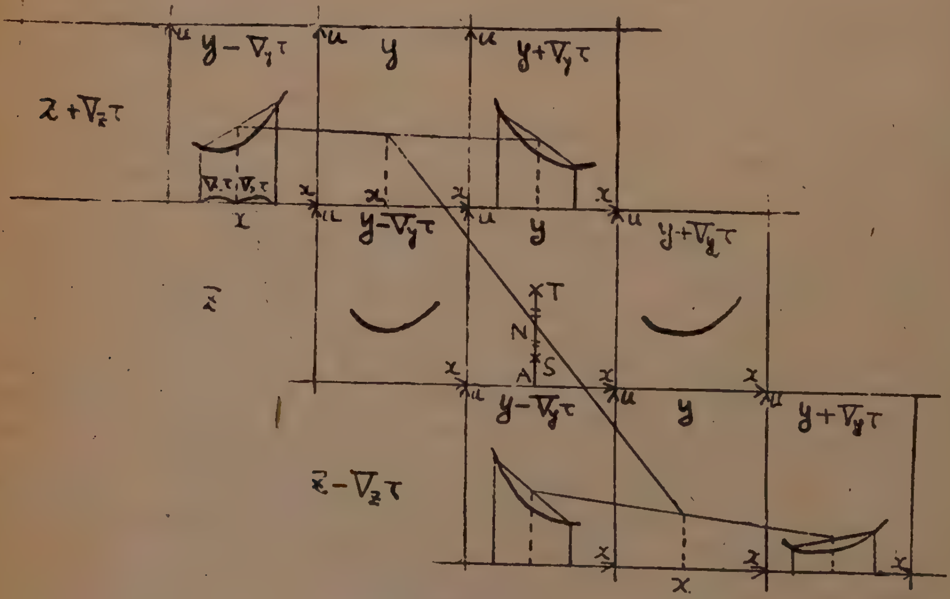

Fig. 7

On the Application of Graphical Methods to the Problems of Heat Conduction.

(A Study on the Graphical Integration of the Partial Differential Equations of Diffusson Type.)

By Isao OSIDA.

Department of Dynamics, Faculty of Engineering, University of Nagoya.

(Read October 16, 1942, October 23, 1943, May 6, September 16 and November 18, 1944, Received October 11, 1947)

1. Introduction and Summary.

The application of the analytical method to the problems of heat conduction(1) is confined to some ideal cases which scarcely occur in practice. Even if the exact solution is obtained the numerical calculations are semetimes awkwardly laborious.

In 1924, E. Schmidt(2) has deviced an elegant graphical method which can solve easily the one-dimensional problems and, having been made no essential progress in this field, his method is widely used even now by engineers almost in its original form(3).

Since 1942 the present author(4) has studied Schmidt's method and has succeeded to extend his method to the inhomogeneous cases in which the coefficient of heat conduction, the density and the specific heat vary with the coordinate, to the non-linear cases in which these quantities vary with temperature and also to the two or three dimensional problems. The processes are so simple that even a person who is not familiar with mathematics can obtain the result in a short time(5).

To the author's regret, space forbids the full description of the work, so we shall give in the following only a brief sketch of it. The detailed paper in Japanese with much more examples will be published in future.

§ 2. Schmidt's Method.

The one-dimensional form of the equation of heat conduction is

$$\frac{\partial u}{\partial t}=\kappa\frac{\partial^2 u}{\partial x^2}, \qquad (2.1)$$

where u is temperature, t time, x the coordinate and the thermal diffusivity, that is

$$\kappa=\frac{K}{c\rho}, \qquad (2.2)$$

where K is the coefficient of heat conduction, ρ the density and c the specific heat.

Using a small time interval τ and a small length s along the coordinate axis, we have

$$\left.\begin{aligned}\frac{1}{\tau}\{u(x,t+\tau)-u(x,t)\}&=\frac{\partial u}{\partial t}+R_1,\\ \frac{1}{s^2}\{u(x-s,t)-2u(x,t)+u(x+s,t)\}&=\frac{\partial^2 u}{\partial x^2}+R_2\end{aligned}\right\} \qquad (2.3)$$

where R_1 and R_2 represent small residual terms being given by Taylor's expansion, these are

$$\left.\begin{aligned}R_1&=\frac{\tau}{2}\frac{\partial^2 u}{\partial t^2}+\frac{\tau^2}{6}\frac{\partial^3 u}{\partial t^3}+\cdots\cdot,\\ R_2&=\frac{s^2}{12}\frac{\partial^4 u}{\partial x^4}+\frac{s^4}{360}\frac{\partial^6 u}{\partial x^6}+\cdots\cdot.\end{aligned}\right\} \qquad (2.4)$$

Introducing (2.3) into (2.1), we have

$$u(x,t+\tau)=\left(1-\frac{2\kappa\tau}{s^2}\right)u(x,t)+\frac{\kappa\tau}{s^2}\{u(x-s,t)+u(x+s,t)\}+R, \qquad (2.5)$$

where R is given by

$$R=\tau(R_1-\kappa R_2)=\frac{\kappa^2\tau^2}{2}\left(1-\frac{s^2}{6\kappa\tau}\right)\frac{\partial^4 u}{\partial x^4}+\cdots\cdot \qquad (2.6)$$

because of $\frac{\partial}{\partial t}=\kappa\frac{\partial^2}{\partial x^2}$ by (2.1). If τ is very small, we can neglect R and have from (2.5)

$$u(x,t+\tau)\fallingdotseq\frac{\left(1-\frac{2\kappa\tau}{s^2}\right)u(x,t)+\frac{2\kappa\tau}{s^2}\bar{u}(x,t)}{\left(1-\frac{2\kappa\tau}{s^2}\right)+\frac{2\kappa\tau}{s^2}}, \qquad (2.7)$$

where $\bar{u}$ denotes the mean temperature of the two adjacent points on both sides, that is,

$$\bar{u}(x,t) = \frac{1}{2}\{u(x-s,\,t)+u(x+s,\,t)\}.$$

(2.7) means that on the graph of u plotted against x the point Q′ representing $u(x,\,t+\tau)$ divides the element QT, which joins the two points, Q and T, expressing $u(x,t)$ and $\bar{u}(x,t)$ respectively, in the ratio $\frac{2\kappa\tau}{s^2} : \left(\frac{2\kappa\tau}{s^2}\right)$: or, that is the same thing, Q′ is obtained as the point distant $\frac{2\kappa\tau}{s^2}$ of the total length $\overline{TQ}$ from Q towards T.

In order to have the smallest error, (2.6) teaches us that we may take $s = \sqrt{6\kappa\tau}$, and in order to have the simplest construction, let

$$s = \sqrt{2\kappa\tau}, \tag{2.8}$$

then (2.7) becomes

$$u(x,\,t+\tau) \doteqdot \bar{u}(x,t) = \frac{1}{2}\{u(x-s,\,t)+u(x+s,\,t)\}. \tag{2.9}$$

This states that if the two points P and R, representing $u(x-s,\,t)$ and $u(x+s,\,t)$ respectively, are given on the graph, the middle point Q′ of PR represents $u(x,\,t+\tau)$. This simple construction found by E. Schmidt enables us to find from given initial temperature distribution that of after any time interval on application step by step (Fig. 1).* The error in this case is found by insertion of (2.8) in (2.6) to be

$$R = \frac{\kappa^2\tau^2}{3}\frac{\partial^4 u}{\partial x^4}+\cdots\cdots \tag{2.10}$$

The smaller error is obtained if we put

$$s = \sqrt{4\kappa\tau}. \tag{2.11}$$

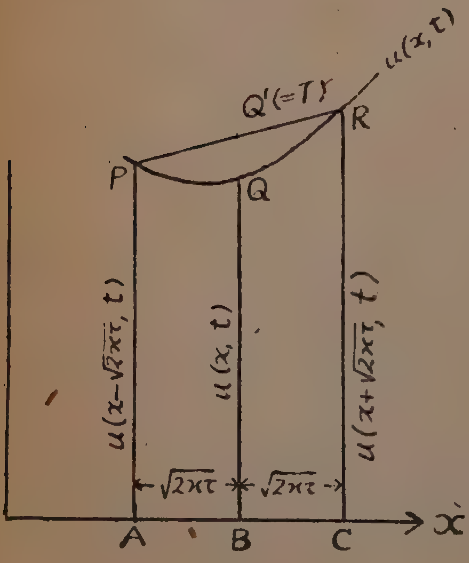

Fig. 1

In this case (2.7) becomes

$$u(x,\,t+\tau) \doteqdot \frac{1}{2}\{u(x,t)+\bar{u}(x,t)\}$$

$$= \frac{1}{4}\{u(x-s,\,t)+2u(x,\,t)+u(x+s,\,t)\} \tag{2.12}$$

and Q′ comes to the middle of QT. The construction is achieved by repeating twice the former construction with halved s (Fig. 2). The error is given by

$$R = \frac{1}{6}\kappa^2\tau^2\frac{\partial^4 u}{\partial x^4}+\cdots\cdots \tag{2.13}$$

which is a half of (2.10).

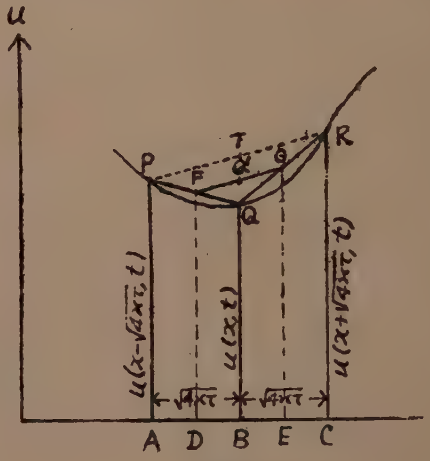

Fig. 2

§ 3. The Errors.

We have derived the expression of the error accompanied by a single process. We shall prove in the following that when we repeat the process many times there is no tendency to the accumulation of errors, but our approximate solution approaches to the exact one asymptotically. This is the main reason why Schimidt's method leads us to the satisfactory result in practice.

For instance, if we repeat the procedure given by (1.12), we have

$$u(x,\,t+2\tau) = \sum_{j=-2}^{2} A_j u(x+js,\,t),$$

where A_j equals to the coefficient of X^j in the expansion of $\frac{1}{2^2}\left(\frac{1}{X}+X\right)^2$. In general, if we repeat the process n times, we have

---

* For the points on the boundaries the boundary condition must be taken into account. This is easily introduced by the aid of the 'images'. See the reference (3).

$$u(x,\ t+n\tau) = \sum_{j=-n}^{n} A_j u(x+js,\ t), \tag{3.1}$$

where A_j equals to the coefficient of X^j in the expansion of $\frac{1}{2^n}\left(\frac{1}{X}+X\right)^n$. By Cauchy's residue theorem on the integration of complex functions we have

$$A_j = \frac{1}{2\pi i\times 2^n}\oint\frac{1}{X^{j+1}}\left(\frac{1}{X}+X\right)^n dX \tag{3.2}$$

Calculating the asymptotic expansion for large n by the method of steepest descent, as common in mathematical statistics, we arrive at the result

$$A_j \to \sqrt{\frac{1}{2\pi n}}\exp\left(-\frac{1}{2n}j^2\right) \text{ if } n\to\infty. \tag{3.3}$$

On the other hand, the exact solution when there is no boundary and the medium extends infinitely is

$$u(x,\ t+n\tau) = \frac{1}{\sqrt{4\pi\kappa n\tau}}\int_{-\infty}^{\infty} u(x+\xi,\ t) \cdot\exp\left(-\frac{\xi^2}{4\kappa n\tau}\right)d\xi. \tag{3.4}$$

One can recognize that when n becomes very large, our solution (3.1) approaches asymptotically to (3.4) if we take (3.3) and that $\xi = js$ into consideration.

If there are boundaries on which the temperature are given or there passes no heat flow, we can reduce the problem to that of infinite region by the aid of the principle of images and the above proof stands as it was.

It goes without saying that there is another error unavoidable on construction which is at least 0.2 mm in length on the graph.

If $u(x,\ t)$, $u(x-s,\ t)$ and $u(x+s,\ t)$ on the right hand side of (2.5) have the same amount of such error being independent of each other, we take the mean square error equally σ. Then the mean square error ρ of $u(x,\ t+\tau)$ is given by

$$\rho^2 = \left(1-\frac{2\kappa\tau}{s^2}\right)^2\sigma^2 + \left(\frac{\kappa\tau}{s^2}\right)^2(\sigma^2+\sigma^2)$$
$$= \left(1-\frac{4\kappa\tau}{s^2}+\frac{6\kappa^2\tau^2}{s^4}\right)\sigma^2,$$

if we lay aside R for a moment. ρ becomes minimum if we put $s=\sqrt{3\kappa\tau}$, and taking R into consideration we can have the knowledge about the optimum value of s from the discussion above.

§ 4. The Variable Coefficients.

If the specific heat C, the density ρ and the coefficient of heat conduction K are functions of the coordinate x, the fundamental equation is

$$c\rho\frac{\partial u}{\partial t} = \frac{\partial}{\partial x}\left(K\frac{\partial u}{\partial x}\right). \tag{4.1}$$

We introduce a new variable ξ such as

$$\int\frac{dx}{K(x)} = \xi \tag{4.2}$$

in (4.1) and putting

$$\frac{1}{C\rho K} = \mu \tag{4.3}$$

we have

$$\frac{\partial u}{\partial t} = \mu(\xi)\frac{\partial^2 u}{\partial\xi^2},$$

which is of the same form with (2.1) except that the coefficient μ is a function of ξ. Accordingly we can deal with such a problem using varying intervals $s=\sqrt{2\mu\tau}$ or $s=\sqrt{4\mu\tau}$ and applying the construction of Fig. 1 or Fig. 2 respectively.

For the cases of cylindrical and of spherical symmetry with constant coefficients (2.1) becomes

$$\frac{\partial u}{\partial t} = \frac{\kappa}{r}\frac{\partial}{\partial r}\left(r\frac{\partial u}{\partial r}\right)$$

and

$$\frac{\partial u}{\partial t} = \frac{\kappa}{r^2}\frac{\partial}{\partial r}\left(r^2\frac{\partial u}{\partial r}\right)$$

respectively. They can be solved by this method by imagining as if they are one-dimensional problems such that

$$x = r,\quad c\rho = r,\quad K = \kappa r$$

and

$$x = r,\quad c\rho = r^2,\quad K = \kappa r^2$$

respectively(6).

If K, c and ρ are functions of temperature, the case is more complicecated. We introduce a new dependent variable Φ such as

$$\frac{d\Phi}{du} = K$$

instead of the temperature u itself and the fundamental equation (4.1) becomes

$$\frac{\partial\Phi}{\partial t} = F(\Phi)\frac{\partial^2\Phi}{\partial x^2},$$

where

$$F(\Phi) = \left[\frac{K(u)}{c(u)\rho(u)}\right]_{u\to\Phi}.$$

If one takes x as abscissa and Φ as the ordinate and force to perform the construction of Fig. 2 with given s, the ratio $QQ' : QT = \frac{2F\tau}{s^2}$ is not equal to $\frac{1}{2}$, but varies with the ordinate Φ. In order to apply the similar construction in this case, let $QF : QP = QG : QR = QQ' : QT = \frac{2F\tau}{s^2}$, which varies with Φ. This can be approximately realized by taking curved DF and FG, the distance s, of which from BQ is given by $\frac{2F\tau}{s^2} \times s = \frac{2F(\Phi)\tau}{s}$ (Fig. 3).

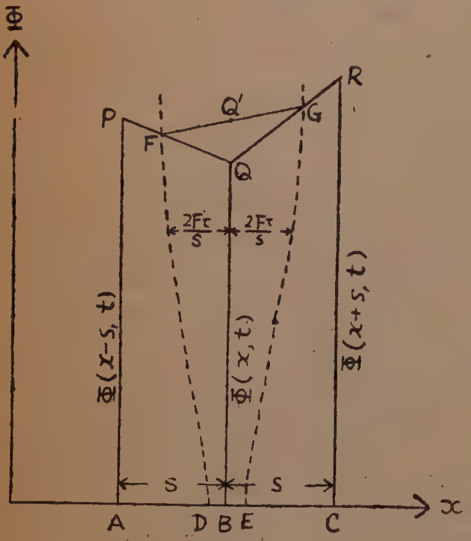

Fig. 3

It is favourable that s is larger than the largest $\frac{2F(\Phi)\tau}{s}$ appearing in the figure, and that the ratio $\frac{2F(\Phi)\tau}{s^2}$ lies near $\frac{1}{2}$, if possible.

We shall give a practical example. An industrial furnace surrounded by a fire brick wall of 25 cm thick, the temperature being initially zero, was raised suddenly to the temperature of 1,000° C. How the temperature in the wall is raised if $K = 1.0 + 0.001\,u$ kcal/m. h. °C,

$$\rho = 1700 \text{ kg/m}^3$$

and $$c = 0.3 \text{ kcal/kg. °C. ?}$$

For simplicity we assume that the outward radiation is so small that we may consider as as adiabatic condition $\frac{\partial u}{\partial x} = 0$ holds just outside of the wall, where $x = 25$ cm. We have

$$\Phi = u(1 + 0.005\,u)$$

and

$$F(\Phi) = \frac{1}{500}\sqrt{1 + 0.002\,\Phi}$$

Fig. 4 shows the construction made by taking $s = 0.05$ m $= 5$ cm, and $\tau = 0.3125$ h $= 18.75$ min. and repeating the process 32 times. The rise of the temperature with time just outside of the wall is shown by the curve I in Fig. 5. The curve II shows that under the same condition assuming that K is constantly equal to 1.5 kcal/m h.°C, the mean value at 0°C and 1,000°C. This gives too high temperatures at first and too low ones later on.

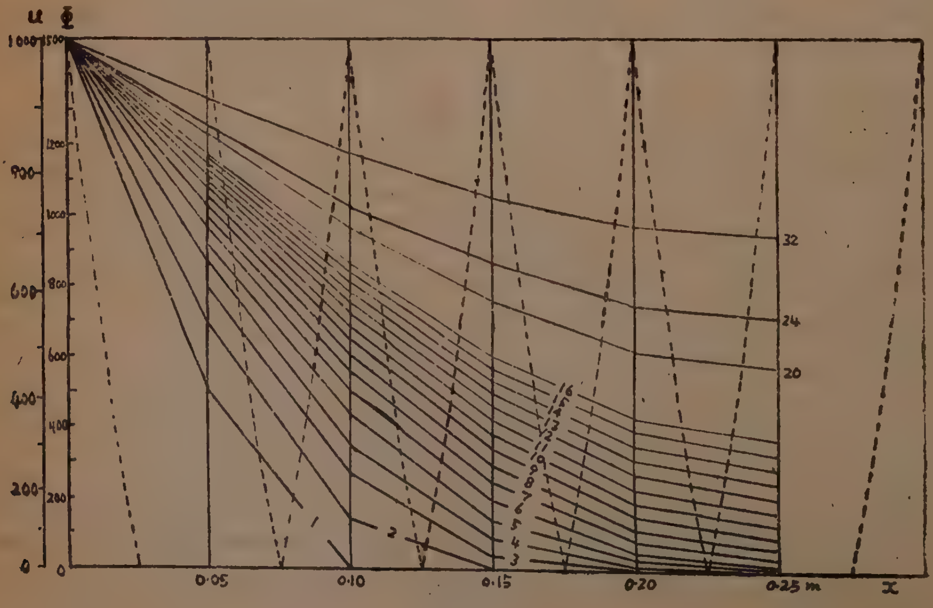

Fig. 4

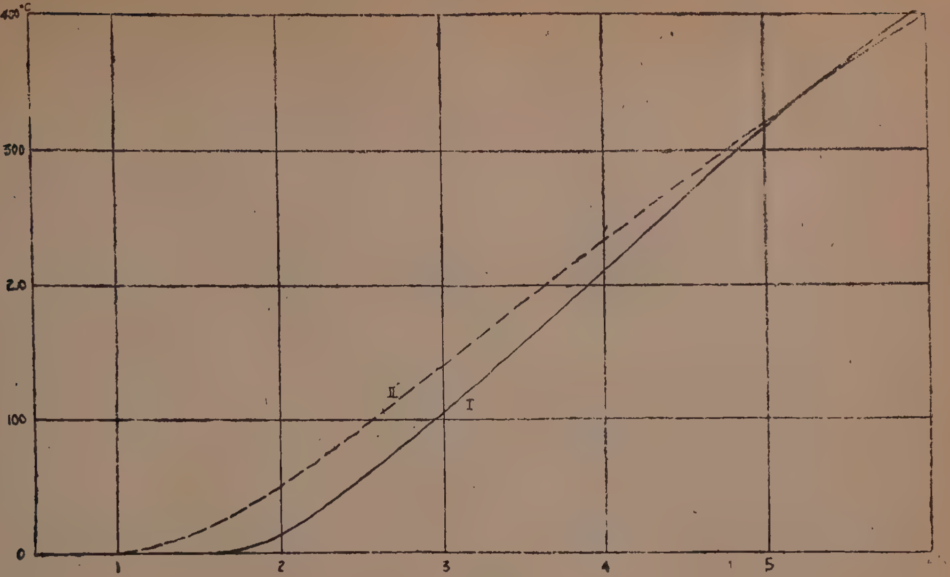

Fig. 5

§ 5. The Two-Dimensional Problems.

The two-dimensional equation is

$$\frac{\partial u}{\partial t}=\kappa_x\frac{\partial^2 u}{\partial x^2}+\kappa_y\frac{\partial^2 u}{\partial y^2}, \qquad (5.1)$$

where the thermal diffusivity κ_x for x-direction and κ_y-direction are not necessarily equal. There are many ways to express (5.1) in difference forms. We shall show in the next the two of them: the one is

$$u(x, y, t+\tau)=\frac{1}{4}\{u(x-s_x, y-s_y, t)+u(x+s_x, y-s_y, t)$$
$$+u(x-s_x, y+s_y, t)+u(x+s_x, y+s_y, t)\}+R, \qquad (5.2)$$

where

$$\left.\begin{aligned} s_x&=\sqrt{2\kappa_x\tau}, \quad s_y=\sqrt{2\kappa_y\tau}, \\ R&=-\frac{1}{12}\left(s_x^4\frac{\partial^4 u}{\partial x^4}+s_y^4\frac{\partial^4 u}{\partial y^4}\right)+\cdots, \end{aligned}\right\} \qquad (5.3)$$

and another is

$$u(x, y, t+\tau)=\frac{1}{16}\{u(x-s_x, y-s_y, t)+u(x+s_x, y-s_y, t)$$
$$+u(x-s_x, y+s_y, t)+u(x+s_x, y+s_y, t)\}$$
$$+\frac{1}{8}\{u(x-s_x, y, t)+u(x+s_x, y, t)$$
$$+u(x, y-s_y, t)+u(x, y+s_y, t)\}$$
$$+\frac{1}{4}u(x, y, t)+R, \qquad (5.4)$$

where

$$\left.\begin{aligned} s_x&=\sqrt{4\kappa_x\tau}, \quad s_y=\sqrt{4\kappa_y\tau}, \\ R&=-\frac{1}{96}\left(s_x^4\frac{\partial^4 u}{\partial x^4}+s_y^4\frac{\partial^4 u}{\partial x^4}\right)+\cdots \end{aligned}\right\} \qquad (5.5)$$

These expressions are easily verified by expansion considering the relation (5.1).

Neglecting R, (5.2) states that the temperature of the point (x, y) after a short time period τ is given by the mean of the four adjacent points $(x\pm s_x,\ y\pm s_y)$. In other words, we can find the temperature $u(x, y, t+\tau)$ in question by making the average in x-direction at first and next in y-direction according to the construction shown in Fig. 1. This process is carried out with ease if we arrange the diagrams of $u(x, y, t)$ plotted vs. x side by side, the adjacent two of which correspond to the values of y differing by s_y from each other. Then we find the average of $u(x-s_x, \cdots)$ and $u(x+s_x, \cdots)$ by the procedure of Fig. I, imagining that the heat streams occur only in x-direction, and then apply the same process combining the mean temperatures thus found, imagining that the flow of heat occurs only in y-direction in turn, as shown in Fig. 6. It is obvious from (5.2) that the average of the average temperatures thus found equals to $u(x, y, t+\tau)$ if we neglect the small term R.

Similarly we can find the same $u(x, y, t+\tau)$ by the repeated applications of the process of Fig. 2, at first in x-direction and next in y-direction. This is justified by (5.4) if we neglect R. The procedure is shown in Fig. 7

A semi-infinite solid limited by a plane $y=0$

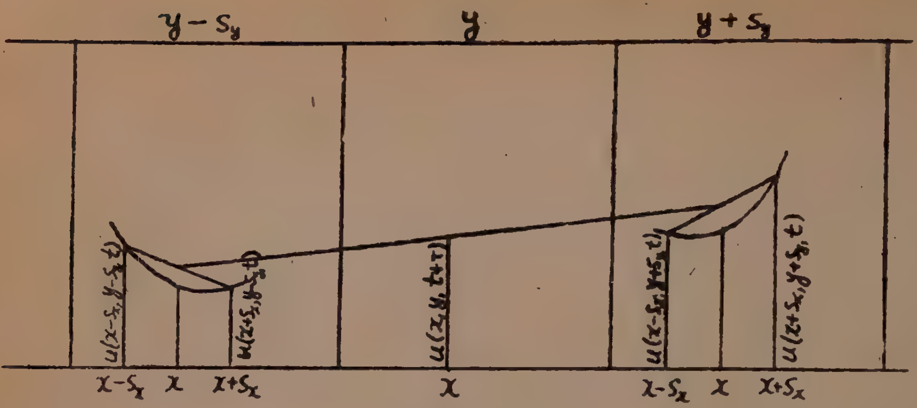

Fig. 6

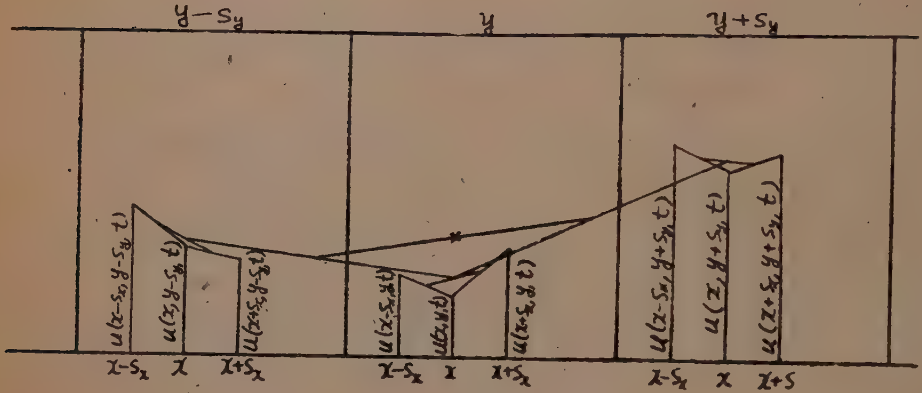

Fig. 7

and extending to the negative side of y has a triangular projection confined by the two planes such as $x+y=4$ cm. and $x-y=4$ cm. The temperature of the solid bulk is initially 100°C and all the surfaces are kept constantly at zero. The process of cooling is studied by the method of Fig. 6, putting $s=1$ cm. Then $\tau=\frac{1}{2\kappa}$; and on repeating 8 times we have the temperature distribution after $\frac{4}{\kappa}$ seconds. Fig. 8 shows the process and Fig. 9 shows the final result by the aid of isothermals.

§ 6. The Stationry States.

Since $\frac{\partial u}{\partial t}=0$ for the stationary states, we can find them on repeating the above processes until no change of the temperature takes place. Thus we can find the solution of Laplace's equation

$$\frac{\partial^2 u}{\partial x^2}+\frac{\partial^2 u}{\partial y^2}=0 \tag{6.1}$$

as a problem of heat conduction, by finding the stationary state under given boundary conditions. Since the initial condition may be taken arbitrarily and since the construction may be done roughly until we come near the final state, we can arrive at the result rather soon if these are appropriately chosen.

Fig. 10 shows the stationary temperature distribution in a rectangular pole of infinite length, the cross-section being 4×5 cm² and one of the four sides being kept 100°C and the other three, zero. The figures in the brackets are the temperature calculated from the exact solution of (6.1), which are in good agreement with the graphical results.

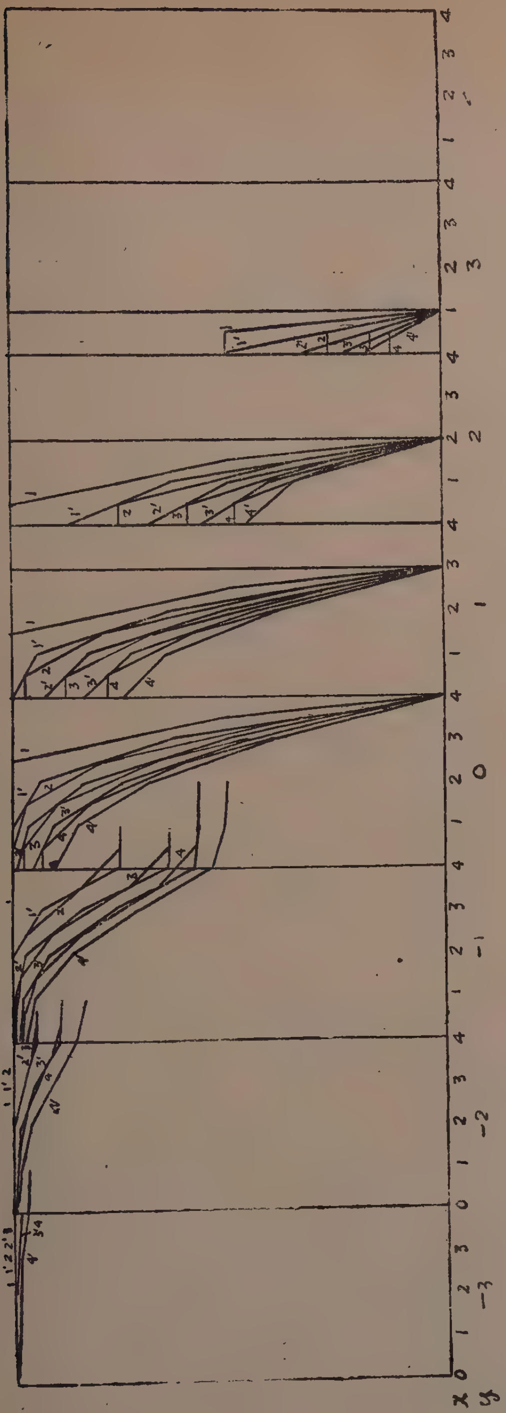

Fig. 8

§ 7. Thin Plates and Three Dimensional Solids.

The temperature u of a thin plate of thickness z radiating from the both surfaces is given by the solution of

$$\frac{\partial u}{\partial t}=\kappa\left(\frac{\partial^2 u}{\partial x^2}+\frac{\partial^2 u}{\partial y^2}\right)-\frac{2\alpha}{zc\rho}u \tag{7.1}$$

where α is the heat transmission coefficient of the surface and the temperature of the surrounding space is taken $u=0$. (7.1) is written approximately as

$$u(x,\ y,\ t+\tau)=\frac{1}{1+\dfrac{\alpha s^2}{\kappa zc\rho}}\bar{u} \tag{7.2}$$

where $\bar{u}$ and s are given by

$$\bar{u}=\frac{1}{4}\{u(x-s,\ y-s,\ t)+u(x+s,\ y-s,\ t)$$

$$+u(x-s,\ y+s,\ t)+u(x+s,\ y+s,\ t)\}$$

and

$$\frac{2\kappa\tau}{s^2}=1-\frac{2\alpha\tau}{zc\rho}$$

respectively. $\bar{u}$ is found by the construction of Fig. 6, we may shorten it merely by the multiplication of the constant factor $\dfrac{1}{1+\dfrac{\alpha s^2}{\kappa zc\rho}}$, which is easily done on the graph.

Lastly we shall deal with the three-dimansional problems. The fundamental equation

$$\frac{\partial u}{\partial t}=\kappa_x\frac{\partial^2 u}{\partial x^2}+\kappa_y\frac{\partial^2 u}{\partial y^2}+\kappa_z\frac{\partial^2 u}{\partial z^2} \tag{7.3}$$

can be written approximately in difference form in many ways. One of them is

$$u(x,\ y,\ z,\ t+\tau)\fallingdotseq\frac{1}{8}\sum u(x\pm s_x,\ y\pm s_y,\ z\pm s_z,\ t), \tag{7.4}$$

where $\sum$ means to add the eight member being generated by the all possible combination of the plus and the minus signes and s_x, s_y and s_z mean $\sqrt{2\kappa_x,\tau}$, $\sqrt{2\kappa_y\tau}$ and $\sqrt{2\kappa_z\tau}$ respectively. (7.4) tells us that the temperature $u(x,\ y,\ z.\ t+\tau)$ in question is obtained by making the average of those of the eight adjacent points. We make many diagrams of the tpye of Fig. 6 for each value of z, the succeeding two differ by s_z, and arrange them in shifted position as shown in Fig. 11. Then we make the mean of u of the two adjacent points with different x and same y and z at first, secon-

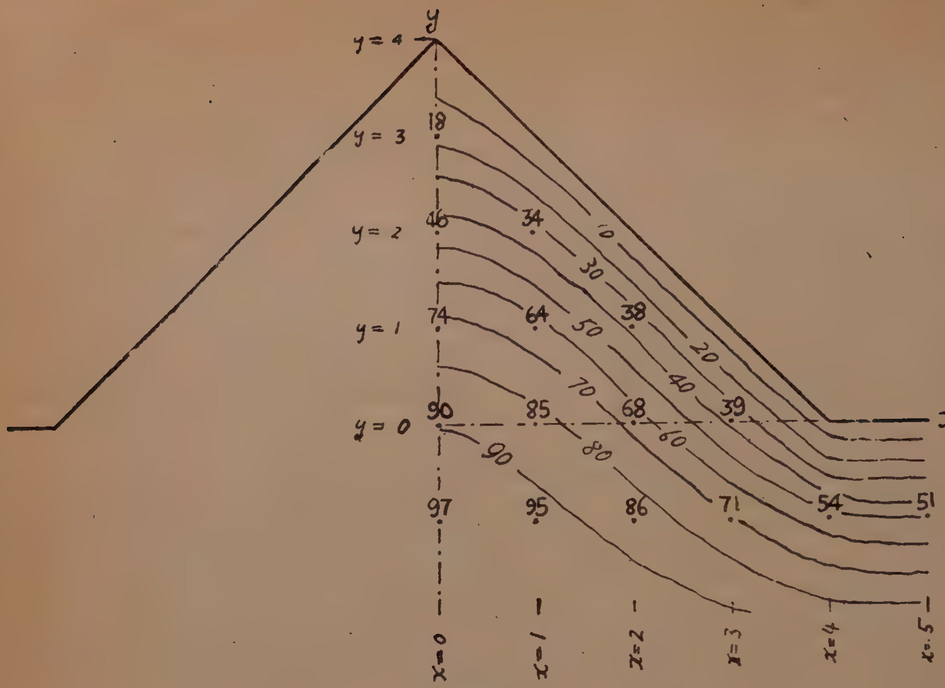

Fig. 9

dly average them with respect to y keeping x and z constant, and lastly average them again with respect to z keeping x and y constant, then we have the resulting $u(x, y, z, t+\tau)$.

A semi-infinite solid limited by the plane $z=0$ and extended to the negative side of the z-axis has a cubic projection of 3 cm × 3 cm × 3 cm, confined by the planes $x=0,3$ cm; $y=0,3$ cm and $z=3$ cm. The initial temperature is 100°C overall and the surface are kept at zero constantly. Putting $s_x=s_y=s_z=1$ cm and applying the process four times at every point, we have the temperature distribution for $t=\frac{1}{2\kappa}\times 4=\frac{2}{\kappa}$ sec. Fig. 12 shows the isothermals for the cross sections $y=1.5$ cm and $z=0$. A few hours' work suffices to solve such a problem which is too laborious to handle by other methods.

§ 8. Conclusion.

We have ommited much details especially concerning the practical techniques. As the error increases with s and with the higher differential quotiant of u, we can accelerate the process by taking larger s as the temperature curve becomes smoother. There are too many remarks of such a sort to be mentioned here.

The combinations of the above methods will solve other sorts of problems such as heat conduction in a finite cylinder, in an inhomogeneous plates, etc.

It goes withont saying that the above methods are valid to the problems such as diffusion, which obey the same differential equation.

In conclusion the author expresses sincere thanks to Dr. Prof. Yamanouchi and Dr. Prof. Kotani for their interest and encouragement throughout the work. He takes his opportunity to thank Dr. Yosihiko Takahasi, Dr. Prof. Yasundo Takahasi, and Dr. Prof. Koga for their helpful discussions and enconragements. He is indebted also to Miss Fukazu for her help to prepare the diagrams, and to the Hattori Hōkō Kai and the Nippon Gakujutsu Shinkō Kai for the financial support.

References.

(1) J. Fourier: La théorie analytique de la chaleur (1832), G. Kirchhoff: Vorlesungen über der Theorie der Wärme (1894), Ph. Frank and R. v. Mises: Die Differential- und Integralgleichungen der Mechanik und Physik, II.

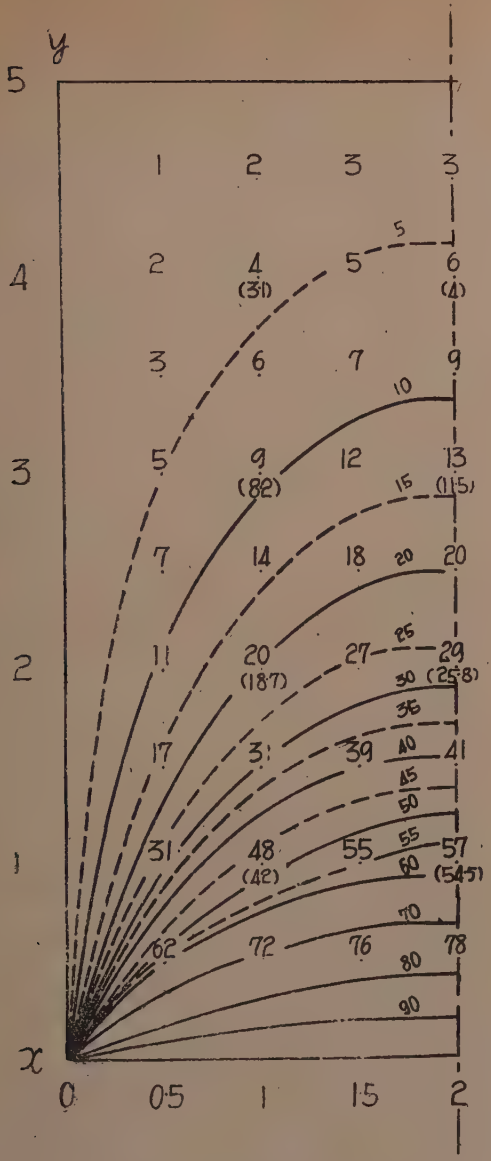

Fig. 10

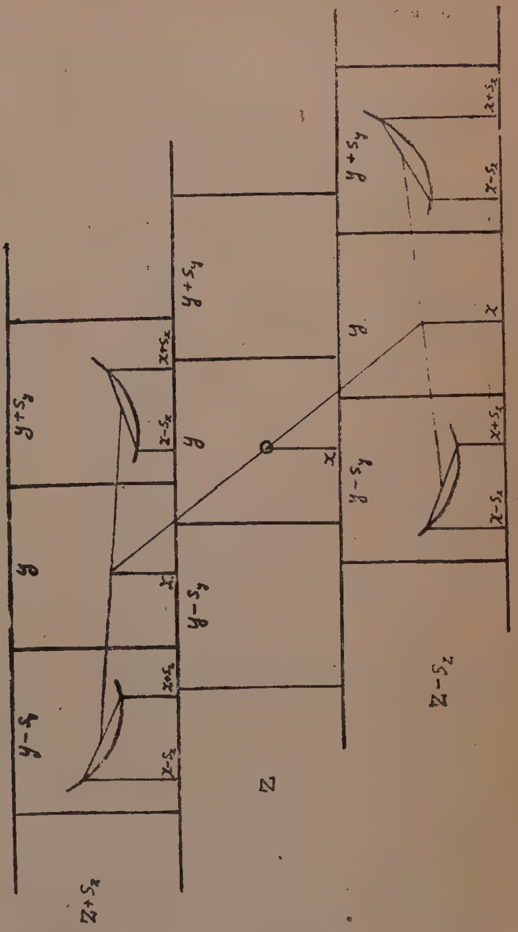

Fig. 11

(1935), etc.

(2) E. Schmidt; Festschrift für siebzigsten Geburtstag August Föppls (Berlin 1924), 179, W. Nusselt: Z. VDI. **71** (1927), 85, A. Nessi and L. Nissole: Methode graphiques pour l'étude des installations chauffage (Paris 1929).

(3) H. Grober and S. Erk: Die Grundgesetzen der Wärmeübertragung, 2. Aufl. (Berlin 1933), 92, M. ten Bosch: Die Wärmeübergang (Berlin 1927), 280, T. K. Sherwood and C. E. Reed: Applied Mathematics in Chemical Engineering, (New York and London, 1939), 241, etc.

4) I. Osida: Journal of the Meteorological Society of Japan **20** (1942), 207, **21** (1943), 198, **22** (1944), 98 (in Japanese).

(5) Since 1942, Dr. Yosihiko Takahasi has worked out another system of graphical method which needs a planimeter. See the Journal of the Meteorological Society of Japan **19** (1941), 321, 418, **20** (1942) 188, 402, **21** (1943), 130, **22** (1944), 81, 88, 98, Kikai to Zairyo **78** (1942), 524 (in Japanese).

(6) E. Schmidt: Z. VDI. **75** (1931), 969; Trinks: Industrial Furnaces, Appendix; Yasundo Takahasi; Journal of the Japan Society of Mechanical Engineers **9** (1943), 35 (in Japanese).

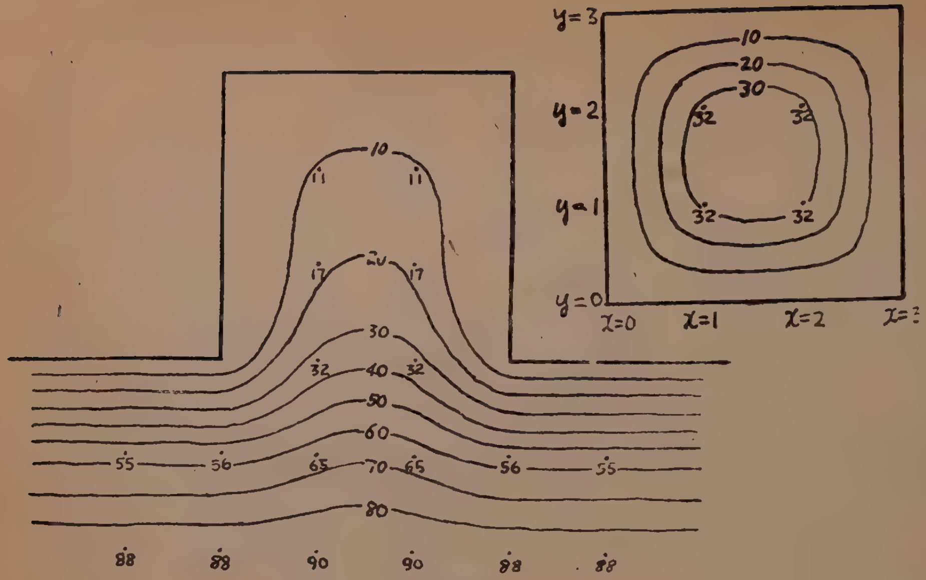

Fig. 12

Graphical Treatment of Mechanical and Electrical Vibrations.

By Isao OSIDA.

Department of Dynamics, Faculty of Engineering, University of Nagoya.

(Read December 14, 1946. Received October 20, 1947).

The equation of the one-dimensional mechanical vibration is

$$\frac{d^2x}{dt^2}+2k\frac{dx}{dt}+\nu^2x=\frac{F(t)}{m} \quad\text{................}(1)$$

where t is time, x the displacement, m the mass, $F(t)$ the external force, and k and ν constants. If $F(t)$ is given, we can write down the analytical solution of the equation (1) in the integral form which is shown in ordinary text books. However, it is rather laborious in practice to find the behaviour of the system corresponding to any given $F(t)$ by calculating the integrals. The graphical method in the following will furnish a convenient tool for this purpose.⁽¹⁾

Using a small time interval τ, we can express approximately the time derivatives in (1) in difference forms, namely

$$\frac{dx}{dt}\doteqdot\frac{1}{2\tau}\{x(t+\tau)-x(t-\tau)\}$$

$$\frac{d^2x}{dt^2}\doteqdot\frac{1}{\tau^2}\{x(t-\tau)-2x(t)+x(t+\tau)\}$$

By substitution, we have

$$x(t+\tau)\doteqdot\frac{2-\nu^2\tau^2}{1+k\tau}x(t)$$
$$-\frac{1-k\tau}{1+k\tau}x(t-\tau)+\frac{1}{1+k\tau}\,\frac{F\tau^2}{m}\quad\text{.........}(2)$$

This will serve as the fundamental equation instead of (1) if τ is small.

Fig. 1 shows x plotted vs. t on ordinary rectan-

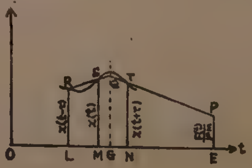

Fig. 1

gular coordinate paper. L and M represent time $t-\tau$ and t on the abscissa respectively, and LR and MS the corresponding displacements $x(t-\tau)$ and $x(t)$, which we suppose to be given on the graph. What is the procedure to find the next displacement $x(t+\tau)$? We take another three points N, G and E on the time axis having the abscissae such as

$$\overline{\mathrm{MN}} = \overline{\mathrm{LM}} = \tau,\ \overline{\mathrm{MG}} = \mathrm{C} = \frac{1-k\tau}{1+k\tau-\nu^2\tau^2}\tau$$

$$\text{and} \qquad \overline{\mathrm{ME}} = l = \frac{2k}{\nu^2}$$

respectively, and for E we take a point P such that the ordinate PE equals to $\frac{F(t)}{\nu^2 m}$. Let Q be the point where the straight line RS intersect with the perpendicular GQ. Combine P and Q; the straight line PQ will intersect the ordinate NT at T. Then NT gives the displacement $x(t+\tau)$ in question. Repeating the procedure, we can find the displacements $x(0)$, $x(\tau)$, $x(2\tau)$, $x(3\tau)$, $\cdots\cdot$ for every time points succeeding with the interval τ, if we know the first two, say $x(0)$ and $x(\tau)$. Smoothing out by a curve we find the final result.

In most cases, as the initial conditions besides the initial displacement $x_{t=0} = x(0)$, the initial velocity $\left(\frac{dx}{dt}\right)_{t=0} = \dot{x}(0)$ is given instead of $x(\tau)$. We preceed as follows.

If we put $t=0$ in (1) we have

$$\left(\frac{d^2x}{dt^2}\right)_{t=0} = -2kx(0)-\nu^2\dot{x}(0)+\frac{F(0)}{m}$$

Using this, we have from the approximation,

$$x(\tau) \doteqdot \dot{x}(0)+\dot{x}(0)\tau+\frac{\tau^2}{2}\left(\frac{d^2x}{\dot{x}t^2}\right)_{t=0},$$

the relation between $x(\tau)$ and $x(0)$:

$$x(\tau) \doteqdot \left(1-\frac{\nu^2\tau^2}{2}\right)x(0)+(1-k\tau)\tau\dot{x}(0)+\frac{F(0)\tau^2}{2m}, \ldots\ldots(3)$$

which can also be expressed graphically.

Fig. 2 shows the procedure to find $x(\tau)$ from $x(0)$ and $\dot{x}(0)$. We take the point P on the axis such as $\overline{\mathrm{OP}} = x(0)$, where 0 is the origin, draw the straight line PQ having the slope $\frac{dx}{dt} = \dot{x}(0)$ and let the point of intersection S with the ordinate $t = a \doteqdot \frac{1-k\tau}{1-\frac{\nu^2\tau^2}{2}}\tau$. Let R the point such as

$$t = l = \frac{2k}{\nu^2},\ x = \frac{1}{\nu^2}\frac{F(0}{m}.$$

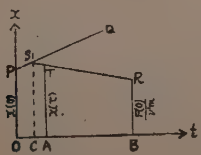

Fig. 2

Taking a point A on the time axis such as $\overline{\mathrm{OA}} = \tau$, draw the perpendicular AT to the time axis at A and let it intersect with SR at T, then AT gives $x(\tau)$. The proof is also simple. Once $x(\tau)$ is found in this way, the construction stated above can be applied one after another.

For example, we search for the solution of

$$\frac{d^2x}{dt^2}+6\frac{dx}{dt}+25x = f(t),$$

when

$$f(t) = \begin{cases} 0, \text{ if } t<0 \text{ or } t>0.5, \\ 5, \text{ if } 0<t<0.5, \end{cases}$$

under the initial condition

$$x = 0 \text{ and } \frac{dx}{dt} = 0 \text{ if } t = 0.$$

Taking $\tau \doteqdot 0.1$, we have

$$m = 1,\ k = 3,\ \nu = 5,\ l = 0.24,\ c = 0.0667,\ a = 0.08.$$

It is advantageous to draw the curve of $\frac{F(t)}{\nu^2 m}$, being shifted by l from its original position as shown by the dotted line in Fig. 3, before the above procedure is applied. Taking into consideration that at the point $t=0$ and $t=0.5$ of discontinuity the value of $f(t)$ becomes $\frac{0+0.5}{2} = 0.25$, our method is applied, and the result is shown by the full line. This takes only twenty minutes or so. The cross marks express the displacement calculated by the exact solution

$$x = \frac{1}{20}[4-4e^{-3t}\cos 4t-3e^{-3t}\sin 4t],\ (0 \leqq t \leqq 0.5)$$

$$x = \frac{1}{20}[e^{1.5}(3\cos 2+4\sin 2)-3]e^{-3t}\sin 4t$$

$$-\frac{1}{20}[e^{1.5}(3\sin 2-4\cos 2)+4]e^{-3t}\cos 4t,\ (t \geqq 0.5).$$

The agreement is satisfactory for the purpose of finding the wave form.

The equation of the transient phenomena of an electric circuit is of the same form as (1), and

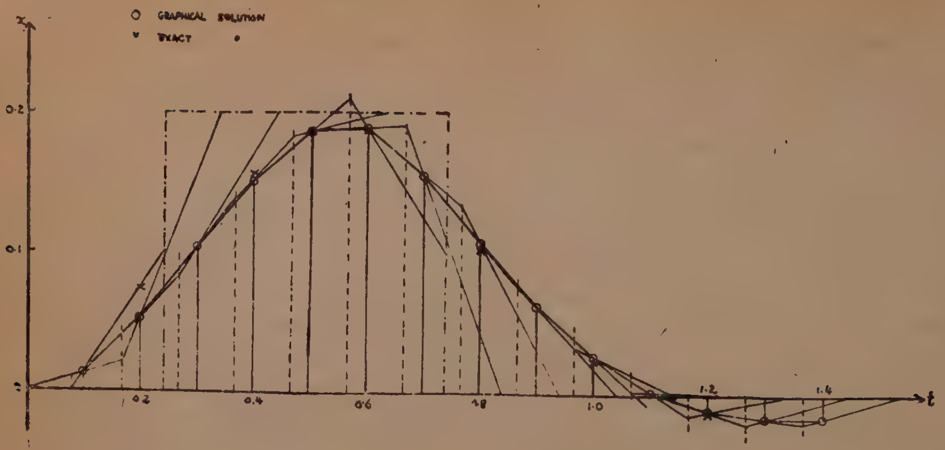

Fig. 3

can be solved in the similar way. For L—C—R circuit,

$$L\frac{d^2i}{dt^2}+R\frac{di}{dt}+\frac{i}{C}=\frac{dE}{dt},$$

where L is the inductance, R the resistance, C the capacity, i the current and E the voltage applied. If the curve of $E(t)$ is given by a graph, we can find $\frac{dE}{dt}$ by graphical differentiation, then the above treatment can be applied without any alteration.

The use of the graphical method saves much trouble accompanied by dealing with functions and integrations. A little alteration will enable us to deal with the case that k and ν^2 are functions of time, for which the analytical method is invalid.

As a matter of course the mechanization of the above process by the use of rods, pins, etc. will give much more benefit for the practical engineers who have to treat many of the similar problems.

In conclusion, the author expresses his thanks to Prof. K. Shogenji, Prof. T. Yamanouchi, D. Prof. Yasundo Takahashi, Dr. Yoshihiko Takahashi and Associate Proffessors Y. Furuya, Y. Kasuga T. Koga and K. Yamamoto for their invaluable advices and encouragements, and also to the Hattori Hoko Kai and to the Nippon Gakujutsu Shinko Kai for their financial supports.

References.

(1) I have deviced another graphical method in 1944, but it is applicable only to the case $k=0$ while ν is any function of time or displacement. Dr. Yasundo Takahashi has also reported a graphical method which is published in the Journal of the Japan Society of Mechanical Engineering, Vol. 49, pp. 114–116, 1946. Granting that the present method is more refined, I own much to his idea.

Mathematical Treatment on the Decay of a Vibrating System due to the Emission of Sound Wave into the Surrounding Medium.

By Zyuro SAKADI and Eiiti TAKIZAWA.

Department of Dynamics, Faculty of Engineering, University of Nagoya.

(Received October 13, 1947)

§ 1. Preliminaries and Notations.

The phenomena of decay of a vibrating system seem mainly due to the emission of sound wave into the surrounding medium and not to the friction in the vibrating system. The following 7 cases were examined, the first 6 cases by Sakadi and the last by Takizawa.

1. Radial vibration of an elastic sphere in the atmosphere,
2. Infinitely extended membrane, the 2 media in both sides may be different,
3. Torsional vibration of an infinite circular cylinder in viscous fluid,
4. Transverse vibration of an infinite, stretched string,
5. Infinitely extended plate,
6. Extensional vibration of an infinite thin rod in viscous fluid,
7. Radial vibration of a circular cylinder in the atmosphere.

Let

x_j: orthogonal coordinates,

ξ_j: displacement components in the elastic body (measured from the static state),

ξ: normal displacement in the case of membrane, plate and string,

u_j: velocity components in the medium,

A_{ij}: stress components in the elastic body,

n_j: outward normal to the body surface,

Φ: velocity potential in the case of air,

a: sound velocity in the air,

p_0: pressure in the static state.

All values at the boundary surface in the static state will be denoted by ξ_j^0, n_j^0.

§ 2. Elastic Sphere in the Air.

Let $r^2 = x_j^2 = x_1^2 + x_2^2 + x_3^3$, and the body occupy the region $r < c$.

In the body we have:

$$A_{ij} = -p_0\delta_{ij} + \lambda\frac{\partial\xi_k}{\partial x_k}\delta_{ij} + \mu\left(\frac{\partial\xi_j}{\partial x_i} + \frac{\partial\xi_i}{\partial x_j}\right)$$
$$= -p_0\delta_{ij} + B_{ij},$$

$$\sigma\frac{\partial^2\xi_i}{\partial t^2} = \frac{\partial A_{ij}}{\partial x_j} = (\lambda+\mu)\frac{\partial}{\partial x_i}\left(\frac{\partial\xi_k}{\partial x_k}\right) + \mu\Delta\xi_i. \tag{1}$$

In the air:

$$\rho\frac{\partial u_i}{\partial t} = -\frac{\partial p}{\partial x_i}, \tag{2}$$

$$u_j = -\frac{\partial\Phi}{\partial x_j}, \quad p = p_0 + \bar{p} = p_0 + \rho\frac{\partial\Phi}{\partial t}, \tag{3}$$

ρ: density in the static state,

$$\frac{\partial^2\Phi}{\partial t^2} = a^2\Delta\Phi. \tag{4}$$

The boundary conditions are:

$$(-p_0 - \bar{p})n_j = -pn_j = A_{jk}n_k = -p_0 n_j + B_{jk}n_k,$$

that is,

$$-\bar{p}^0 n_j^0 = B_{jk}^0 n_k^0, \tag{5}$$

and

$$\left(\frac{\partial\Phi}{\partial r}\right)^0 = -n_k^0\frac{\partial\xi^0{}_k}{\partial t}. \tag{6}$$

For the case of radial vibration we put:

$$\xi_j = \frac{\partial\varphi}{\delta x_j},$$

φ, Φ: functions of t and r.

The equations (1) become:

$$\frac{\partial^2\varphi}{\partial t^2} = \frac{\lambda+2\mu}{\sigma}\Delta\varphi = b^2\Delta\varphi. \tag{7}$$

The 2 conditions (5) and (6) are:

$$-\rho\left(\frac{\partial\Phi}{\partial t}\right)^0 = \lambda(\Delta\varphi)^0 + 2\mu\left(\frac{\partial^2\varphi}{\partial r^2}\right)^0, \tag{8}$$

$$\left(\frac{\partial \Phi}{\partial r}\right)^0 = -\left(\frac{\partial^2 \varphi}{\partial t \partial r}\right)^0. \tag{9}$$

(7) and (4) can be solved:

$$\varphi = \frac{f(bt-r)-f(bt+r)}{r},$$

$$\Phi = \frac{F(at-r)}{r},$$

where the conditions that φ is continuous at $r=0$ and Φ represents divergent wave are taken into account. From the boundary conditions (8) and (9) we get:

$$F(at-c) = c(\alpha-b)f''(bt-c)-c(\alpha+b)f''(bt+c)$$
$$+(\beta-b)f'(bt-c)+(\beta+b)f'(bt+c)$$
$$+\frac{\beta}{c}f'(bt-c)-\frac{\beta}{c}f(bt+c),$$

and

$$\frac{bc}{a}(\alpha-b)f'''(bt-c)\quad\frac{bc}{a}(\alpha+b)f'''(bt+c)$$
$$+\frac{b\beta+a\alpha\ b^2}{a}f''(bt-c)+\frac{b\beta-a\alpha+b^2}{a}f''(bt+c)$$
$$+\frac{a+b}{ac}\beta f'(bt-c)+\frac{a-b}{ac}\beta f'(bt+c)$$
$$+\frac{\beta}{c^2}f(bt-c)-\frac{\beta}{c^2}f(bt+c)=0, \tag{10}$$

with

$$\frac{\lambda+2\mu}{\rho a}=\alpha, \quad \frac{4\mu}{\rho a}=\beta.$$

Taking

$$f(z) = \Re P e^{i\frac{\omega}{b}t},$$

and hence

$$\varphi = -2\Re iP\frac{e^{i\omega t}}{r}\sin\frac{\omega}{b}r, \quad \Phi = \Re Q\frac{e^{i\omega\left(t-\frac{r}{a}\right)}}{r}, \tag{11}$$

we obtain from (10) after some calculation:

$$1-e\eta^2\left(1+\varepsilon\frac{\eta^2}{1+in\eta}\right)^{-} = \frac{\eta}{\operatorname{tg}\eta}, \tag{12}$$

where

$$\eta=\frac{c}{b}\omega, \quad e=\frac{\alpha}{\beta}=\frac{\lambda+2\mu}{4\mu}, \quad \varepsilon=\frac{b^2}{\beta a}=\frac{\lambda+2\mu}{4\mu\sigma}\rho,$$

$$n=\frac{b}{a}=\sqrt{\frac{\lambda+2\mu}{\sigma}}\cdot\frac{1}{a}.$$

The equation (12) for η coincides with the formula:

$$1-e\eta^2=\frac{\eta}{\operatorname{tg}\eta}. \tag{13}$$

c.f. Love's "The Mathematical Theory of Elasticity", 4th edition, p. 285 for the limitting case $\varepsilon\to 0$, that is, $\rho\to 0$. (13) has infinite number of positive roots which, for $e=\frac{1}{2}+\frac{\lambda}{4\mu}>\frac{1}{2}$, are all greater than $\frac{\pi}{2}\left(>\frac{3}{2}\right)$. Hence we assume that ρ is small of the first order and putting

$$1-e\eta_0^2=\eta_0/\operatorname{tg}\eta_0, \ (\eta_0>0), \ \omega_0=\frac{b}{c}\eta_0,$$

$$\eta=\eta_0(1+\delta),$$

into (12) we get the result:

$$\delta=-\varepsilon\frac{e\dfrac{\eta_0^2}{1+in\eta_0}}{e^2\eta_0^2-3e+1},$$

the denominator of which

$$e^2\eta_0^2-3e+1=\left(e\eta_0-\frac{3}{2\eta_0}\right)^2+1-\left(\frac{3}{2\eta_0}\right)^2>0.$$

Hence we can put

$$\delta=-\varepsilon(q-iq'), \quad q>0, \quad q'>0,$$

and the time factor in φ and Φ becomes:

$$e^{i\omega t}=e^{i\omega_0(1+\delta)t}=e^{i\omega_0(1-\varepsilon q)t}e^{-\varepsilon\omega_0 q' t},$$

showing the damping of vibration. But the expression (11) for Φ takes the form

$$\Phi=\Re Q\frac{e^{i\omega_0(1+\delta)t}}{r}e^{-i\omega_0(1-\varepsilon q)\frac{r}{a}}e^{+\varepsilon\omega_0 q'\frac{r}{a}}$$

which becomes ∞ for $r\to\infty$. This unfavourableness can not be avoided if we do not take viscosity in air into account. Hence we assume viscosity in air and add to the right sides of (2) the frictional terms

$$\rho a^2 s \Delta u_i \qquad [\text{or simply } -\rho\kappa u_i].$$

Then (3) and (4) are to be replaced by

$$p=\rho\left(\frac{\partial\Phi}{\partial t}-a^2 s\,\Delta\Phi\right), \ \left[=\rho\left(\frac{\partial\Phi}{\partial t}+\kappa\Phi\right)\right],$$

and

$$\frac{\partial^2\Phi}{\partial t^2}=a^2\Delta\Phi+a^2 s\frac{\partial}{\partial t}\Delta\Phi, \ \left[=a^2\Delta\Phi-\kappa\frac{\partial\Phi}{\partial t}\right],$$

respectively.

Taking again

$$\Phi=\Re e^{i\omega t}\psi=\Re\Psi,$$

we get:

$$p=\Re\frac{\rho}{1+i\omega s}\frac{\partial\Psi}{\partial t}, \ \left[=\Re\rho\left(1-i\frac{\kappa}{\omega}\right)\frac{\partial\Psi}{\partial t}\right].$$

and

$$\frac{\partial^2 \Psi}{\partial t^2} = a^2(1+i\omega s)\Delta\Psi, \quad \left[= \frac{a^2}{1-i\frac{\kappa}{\omega}}\Delta\Psi\right].$$

These show that we have to replace a^2 by $a^2(1+i\omega s)$ $\left[a^2 \Big/ \left(1-i\frac{\kappa}{\omega}\right)\right]$ and ρ by

$$\rho/(1+i\omega s), \quad \left[\rho\left(1-\frac{\kappa}{\omega}\right)\right].$$

Then we have for $\rho \to 0 (\eta \to \eta_0,\ \omega \to \omega_0)$

$$\Phi = \Re Q \frac{1}{r} e^{i\omega_0 t} e^{-i\omega_0 r/a\sqrt{1+i\omega_0 s}}$$

$$\left[= \Re \frac{1}{r} e^{i\omega_0 t} e^{-i\omega_0\sqrt{1-2i\kappa/\omega_0}\cdot r/a}\right]$$

$$= \Re Q \frac{1}{r} e^{i\omega_0 t} e^{-iqr} e^{-q'r} (q>0,\ q'>0)$$

and the same circumstances hold also for small positive ρ.

§ 3. Infinite Membrane.

Let the plane of the membrane be $x_3 = 0$, and for the gas in the region $x_3 > 0$ the same notations as in II will be adopted, while for that in $x_3 < 0$ all corresponding quantities will be denoted by $(')$ sign.

The equation for membrane is:

$$\sigma \frac{\partial^2 \xi}{\partial t^2} = p'^0 - p^0 + T\Delta_1 \xi \quad \left(\Delta_1 = \frac{\partial^2}{\partial x_1^2} + \frac{\partial^2}{\partial x_2^2}\right) \tag{14}$$

while those for gases are:

$$\left.\begin{aligned} &u_j = -\frac{\partial \Phi}{\partial x_j}, \quad u'_j = -\frac{\partial \Phi'}{\partial x_j}, \\ &p = p_0 + p = p_0 + \rho\frac{\partial \Phi}{\partial t}, \quad \frac{\partial^2 \Phi}{\partial t^2} = a^2 \Delta\Phi, \\ &p' = p_0 + p' = p_0 + \rho'\frac{\partial \Phi'}{\partial t}, \quad \frac{\partial^2 \Phi'}{\partial t^2} = a'^2 \Delta\Phi', \end{aligned}\right\} \tag{15}$$

The boundary conditions are:

$$\left(\frac{\partial \Phi}{\partial x_3}\right)^0 = \left(\frac{\partial \Phi'}{\partial x_3}\right)^0 = -\frac{\partial \xi}{\partial t}.$$

Inserting (15) into (14) we get:

$$\sigma \frac{\partial^2 \xi}{\partial t^2} = \rho'\left(\frac{\partial \Phi'}{\partial t}\right)^0 = \rho\left(\frac{\partial \Phi}{\partial t}\right)^0 + T\Delta_1 \xi. \tag{16}$$

Putting

$$\xi = \Re e^{i\omega t} \xi(x_1, x_2),$$

$$\Phi = \Re e^{i\omega t} e^{\gamma x_3} \Phi(x_1, x_2),$$

$$\Phi' = \Re e^{i\omega t} e^{\gamma' x_3} \Phi'(x_1, x_2)$$

in (15) and (16) we have:

$$\left.\begin{aligned} &\Delta_1 \xi + k^2 \xi = 0, \\ &k^2 = \frac{\sigma}{T}\omega^2 \left\{1 + \frac{1}{\sigma}\left(\frac{\rho'}{\gamma'} - \frac{\rho}{\gamma}\right)\right\}, \\ &\gamma^2 + \frac{\omega^2}{a^2} = \gamma'^2 + \frac{\omega^2}{a'^2} = k^2. \end{aligned}\right\} \tag{18}$$

The equation (17) has for real positive k the continuous and finite solutions:

$$\xi = C_m J_m(kr) \begin{matrix}\cos \\ \sin\end{matrix}\ m\theta \quad \begin{pmatrix} x_1 = r\cos\theta, \\ x_2 = r\sin\theta \end{pmatrix},$$

and from (18)

$$\left.\begin{aligned} &\omega^2 = \frac{T}{\sigma} k^2 \left\{1 + \frac{1}{\sigma}\left(\frac{\rho'}{\gamma} - \frac{\rho}{\gamma}\right)\right\}^{-1}, \\ &\gamma^2 = k^2 - \frac{\omega^2}{a^2}, \\ &\gamma'^2 = k^2 - \frac{\omega^2}{a'^2}. \end{aligned}\right\} \tag{19}$$

When, as in II we assume viscosity terms $a^2 s \Delta u_i$, $a'^2 s' \Delta u_i'$ in (2) and in the corresponding equations for $x_3 < 0$, and as boundary conditions we take that the particles of the gases, do not adhere to the membrane but slide along its surface, while the velocity potentials exist, and we have, instead of (19), the following equations (20):

$$\left.\begin{aligned} &\omega^2 = \frac{T}{\sigma} k^2 \left\{1 + \frac{1}{\sigma}\left(\frac{\rho'}{\gamma'(1+i\omega s')} - \frac{\rho}{\gamma(1+i\omega s)}\right)\right\}^{-1}, \\ &\gamma^2 = k^2 - \frac{\omega^2}{a^2(1+i\omega s)}, \\ &\gamma'^2 = k^2 - \frac{\omega^2}{a'^2(1+i\omega s')}. \end{aligned}\right\} \tag{20}$$

Again we put $\rho \to 0$, $\rho' \to 0$ and when γ and γ' are finite we have:

$$\left.\begin{aligned} &\omega \approx \omega_0 = \sqrt{\frac{T}{\sigma}}\, k, \\ &\gamma^2 \approx \gamma_0^2 = k^2\left(1 - \frac{T}{a^2\sigma(1+i\omega_0 s)}\right), \\ &\gamma'^2 \approx \gamma_0'^2 = k^3\left(1 - \frac{T}{a'^2\sigma(1+i\omega_0 s')}\right), \end{aligned}\right\}, \tag{21}$$

and for ω, when the first order terms of ρ and ρ' are considered,

$$\omega^2 = \omega_0^2 \left\{1 - \frac{1}{\sigma}\left(\frac{\rho'}{\gamma_0'(1+i\omega_0 s')} - \frac{\rho}{\gamma_0(1+i\omega_0 s)}\right)\right\}. \tag{22}$$

From (21) we see that:

$$\gamma_0 = -(q+iq'),\quad \gamma_0' = q''+iq''', \tag{23}$$

and from (22),

$$\omega = q^{(4)}+iq^{(5)}, \tag{24}$$

with positive q's.

(24) shows the damping due to ρ and ρ' and (23) show that $e^{\gamma x_3}(e^{\gamma' x_3})$ has negative real exponent for $x_3 > 0 (x_3 < 0)$ in the limitting case $\rho \to 0$, $\rho' \to 0$ and this holds also for small positive ρ and ρ'. The solutions of (19) or (20), in which γ is of the same order as ρ or γ' as ρ', represent, so to speak, free vibration in the gas and the membrane vibrates forcibly so that we neglect the discussion of these cases.

§ 4. Torsional Vibration of a Circular Cylinder.

Let $x_1 = r\cos\theta$, $x_2 = r\sin\theta$, and the cylinder occupy the region $r < c$.

$$A_{ij} = -\bar{p}_0 \frac{\lambda\delta_{ij}+\mu e_{ij}}{\lambda+\mu} + \lambda\frac{\partial\xi_k}{\partial x_k}\delta_{ij} + \mu\left(\frac{\partial\xi_j}{\partial x_i}+\frac{\partial\xi_i}{\partial x_j}\right).$$

where

$$e_{ij} = \begin{cases} 1, & \text{when } i=j=1 \text{ or } i=j=2. \\ 0, & \text{otherwise.} \end{cases}$$

The equations for the viscous fluid are:

$$\rho\frac{\partial u_i}{\partial t} = -\frac{\partial p}{\partial x_i} + \nu\Delta u_i,$$

$$\frac{\partial u_j}{\partial x_j} = 0.$$

Putting $p = p_0 + \bar{p}$,

the boundary conditions become:

$$-\bar{p}^0 n_j^0 + \nu\left(\frac{\partial u_j}{\partial x_k}+\frac{\partial u_k}{\partial x_j}\right)^0 n_k^0 = \lambda\left(\frac{\partial\xi_k}{\partial x_k}\right)^0 n_j^0$$

$$+\mu\left(\frac{\partial\xi_j}{\partial x_k}+\frac{\partial\xi_k}{\partial x_j}\right)^0 n_k^0,$$

$$-\left(\frac{\partial\xi_1}{\partial t}\right)^0 n_2^0 + \left(\frac{\partial\xi_2}{\partial t}\right)^0 n_1^0 = -u_1^0 n_2^0 + u_2^0 n_1^0.$$

Putting

$$\xi_1 = -\sin\theta\,\Re\,\frac{\cos}{\sin}\,\gamma x_3\cdot e^{i\omega t}\cdot V,$$

$$\xi_2 = \cos\theta\,\Re\,\frac{\cos}{\sin}\,\gamma x_3\cdot e^{i\omega t}\cdot V,$$

$$u_1 = -\sin\theta\,\Re\,\frac{\cos}{\sin}\,\gamma x_3\cdot e^{i\omega t}\cdot U,$$

$$u_2 = \cos\theta\,\Re\,\frac{\cos}{\sin}\,\gamma x_3\cdot e^{i\omega t}U,\quad (\gamma > 0),$$

$$\xi_3 = 0,\quad u_3 = 0,$$

we gain:

$$\frac{d^2V}{dr^2}+\frac{1}{r}\frac{dV}{dr}+\left(\kappa^2-\frac{1}{r^2}\right)V = 0,\quad \kappa^2 = \frac{\sigma\omega^2}{\mu}-\gamma^2, \tag{25}$$

$$\frac{d^2U}{dr^2}+\frac{1}{r}\frac{dU}{dr}+\left(\kappa'^2-\frac{1}{r^2}\right)U = 0,\quad \kappa'^2 = -i\frac{\rho\omega}{\nu}-\gamma^2, \tag{26}$$

$$\bar{p}' = 0$$

$$U^0 = i\omega V^0,\quad \left(\frac{d}{dr}\left(\frac{V}{r}\right)\right)^0 = \frac{\nu}{\mu}\left(\frac{d}{dr}\left(\frac{U}{r}\right)\right)^0. \tag{27}$$

(25) and (26) are solved by:

$$V = C\cdot J_1(\kappa r),$$

$$U = D\cdot H_1^{(1)}(\kappa' r).$$

From (27):

$$\frac{\kappa J_2(\kappa c)}{J_1(\kappa c)} = i\frac{\nu}{\mu}\omega\kappa'\frac{H_2^{(1)}(\kappa' c)}{H_1^{(1)}(\kappa' c)} \tag{28}$$

For $\nu \to 0$ we obtain:

$$J_2(\kappa_0 c) = 0,\quad \omega_0^2 = \frac{\mu}{\sigma}(\kappa_0^2+\gamma^2),$$

with κ_0 zero or real positive.

For small positive ν:

$$\kappa' = \sqrt{-i}\sqrt{\frac{\rho\omega}{\nu}},\quad (\Re(\sqrt{-i}) < 0),$$

and the right side of (28) becomes:

$$\sqrt{-i}\frac{\omega}{\mu}\sqrt{\rho\omega\nu}.$$

When $\kappa_0 > 0$ we put:

$$\kappa = \kappa_0 + \varepsilon,\quad \omega = \omega_0 + \frac{\mu\kappa_0}{\sigma\omega_0}\varepsilon,$$

and from (28):

$$\varepsilon c\kappa_0\frac{J_2'(\kappa_0 c)}{J_1(\kappa_0 c)} = \varepsilon c\kappa_0 = \sqrt{-i}\frac{\omega_0}{\mu}\sqrt{\rho\omega_0\nu},$$

$$\omega = \omega_0 + \sqrt{-i}\frac{\sqrt{\rho\omega_0\nu}}{\sigma c}.$$

When $\kappa_0 = 0$, $\kappa = \varepsilon$ we have:

$$\varepsilon^2 = 4\sqrt{-i}\frac{\omega_0}{\mu c}\sqrt{\rho\omega_0\nu},$$

$$\omega = \omega_0 + 2\sqrt{-i}\frac{\sqrt{\rho\omega_0\nu}}{\sigma c},$$

Hence in all cases we have:

$$\omega = \omega_0 + (-1+i)q, \quad (q > 0).$$

The time factor therefore damps according to e^{-qt} and in the fluid $U \to 0$ for $r \to \infty$, because of the relation:

$$H_1^{(1)}(\kappa' r) \sim \frac{1}{\sqrt{r}} e^{i(-q'+iq'')r}.$$

§ 5. Transverse Vibration of a Stretched String.

Let a string of circular section of radius c be stretched from $x_3 = -\infty$ to $x_3 = +\infty$ and vibrate in the x_1-direction and put $x_1 = r\cos\theta$, $x_2 = r\sin\theta$. We must assume that the displacement ξ is small compared with c. Then the equations of motion, when we neglect terms of order $c_2\xi$ due to the deformation of the cross section, will be shown easily as follows:

$$\sigma \frac{\partial^2 \xi}{\partial t^2} = -c\int_{-\pi}^{\pi} \bar{p} \cos\theta d\theta + T\frac{\partial^2 \xi}{\partial x_3^2}, \tag{29}$$

and the boundary condition is:

$$-\left(\frac{\partial \Phi}{\partial r}\right)^0 = \cos\theta \frac{\partial \xi}{\partial t}. \tag{30}$$

We put:

$$\Phi = \Re e^{i\omega t} \cdot \begin{matrix}\cos\\ \sin\end{matrix}\, \gamma x_3 \cdot \cos\theta \cdot \Phi,$$

$$\xi = \Re e^{i\omega t} \cdot \begin{matrix}\cos\\ \sin\end{matrix}\, \gamma x_3 \cdot C,$$

and from (3), (4), (29) and (30) we obtain:

$$\left.\begin{aligned} &\Phi = D \cdot H_1^{(1)}(\kappa r), \\ &\kappa^2 = \frac{\omega^2}{a^2} - \gamma^2, \quad \Re(\kappa) < 0, \\ &\sigma\omega^2 - T\gamma^2 = \rho S\omega^2 \frac{H_1^{(1)}(\kappa c)}{\kappa c H_1^{(1)}(\kappa c)} \end{aligned}\right\} \tag{31}$$

where $S = \pi c^2$.

When we assume viscosity term $s\rho a^2 s \Delta u_i$ in (2), we have following relations instead of (31):

$$\left.\begin{aligned} &\kappa^2 = \frac{\omega^2}{a^2(1+i\omega s)} - \gamma^2, \\ &\sigma\omega^2 - T\gamma^2 = \rho S \frac{\omega}{+i\omega S} \frac{H_1^{(1)}(\kappa c)}{\kappa c H_1^{(1)\prime}(\kappa c)}. \end{aligned}\right\} \tag{32}$$

For $\rho \to 0$ we have

$$\omega_0^2 = \frac{T}{\sigma}\gamma^2, \quad k_0^2 = \frac{\omega_0^2}{a^2(1+i\omega_0 s)} - \gamma^2,$$

and for small ρ, by putting

$$\omega = \omega_0(1+\delta),$$

$$\delta = \frac{\rho S \omega_0^2}{2\sigma(1+i\omega_0 s)} \frac{H_1^{(1)}(\kappa_0 c)}{\kappa_0 c H_1^{(1)\prime}(\kappa_0 c)}. \tag{33}$$

I can not in general determine in which quadrant of the complex plane the factor with H in (33) lies for $\kappa_0 c = -q + iq'$, but for $|\kappa_0 c| \to \infty$, by using asymptotic expansions for H's we easily verify that δ has positive imaginary part, showing the damping of vibration.

§ 6. Infinitely Extended Plate.

We can treat this case quite similarly to the case of membrane. The plane of plate is $x_3 = 0$.

The equation for plate is:

$$\sigma \frac{\partial^2 \xi}{\partial t^2} = -h\Delta_1\Delta_1\xi + (p'^0 - p^0),$$

and the boundary conditions are of the same form as in III.

Putting also

$$\xi = \Re e^{i\omega t}\xi,$$

$$\Phi = \Re e^{i\omega t} e^{\gamma x_3} \cdot \Phi,$$

$$\Phi' = \Re e^{i\omega t} e^{\gamma' x_3} \cdot \Phi',$$

we have:

$$\Delta_1 \xi + k^2 \xi = 0 \tag{34}$$

$$\left.\begin{aligned} &\omega^2 = \frac{hk^4}{\sigma}\left\{1 + \frac{1}{\sigma}\left(\frac{\rho'}{\gamma'} - \frac{\rho}{\gamma}\right)\right\}^{-1}, \\ &\gamma^2 = k^2 - \frac{\omega^2}{a^2}, \\ &\gamma'^2 = k^2 - \frac{\omega^2}{a'^2}. \end{aligned}\right\} \tag{35}$$

When we consider viscosity in the gases of both sides, (35) are replaced by:

$$\left.\begin{aligned} &\omega^2 = \frac{hk^4}{\sigma}\left\{1 + \frac{1}{\sigma}\left(\frac{\rho'}{\gamma'(1+i\omega s')} - \frac{\rho}{\gamma(1+i\omega s)}\right)\right\}^{-1}, \\ &\gamma^2 = k^2 - \frac{\omega^2}{a^2(1+i\omega s)}, \\ &\gamma'^2 = k^2 - \frac{\omega^2}{a'^2(1+i\omega s')}. \end{aligned}\right\} \tag{36}$$

The equation (34) shows that k must be real positive and (36) is then quite the same form as (20).

§ 7. Extensional Vibration of a Thin Rod with Circular Section in Viscous Fluid.

Let $x_1^2+x_2^2=r^2$, and the region of the cylinder be $r\leqq c$.

Further

η: displacement of rod particle in x_3-direction,

E: Young's modulus,

$u_1^2+u_2^2=u_r^2$.

Then the equations for the rod and the fluid are:

$$\sigma\frac{\partial^2\eta}{\partial t^2}=E\frac{\partial^2\eta}{\partial x_3^2}+2\pi c\nu\left(\frac{\partial u_3}{\partial r}\right)^0, \tag{37}$$

$$\left.\begin{aligned}\rho\frac{\partial u_r}{\partial t}&=-\frac{\partial F}{\partial r}+\nu\left(\frac{\partial^2}{\partial r^2}+\frac{1}{r}\frac{\partial}{\partial r}+\frac{\partial^2}{\partial x_3^2}-\frac{1}{r^2}\right)u_r,\\ \rho\frac{\partial u_3}{\partial t}&=-\frac{\partial F}{\partial x_3}+\nu\left(\frac{\partial^2}{\partial r^2}+\frac{1}{r}\frac{\partial}{\partial r}+\frac{\partial^2}{\partial x_3^2}\right)u_3,\\ \frac{\partial u_r}{\partial r}&+\frac{u_r}{r}+\frac{\partial u_3}{\partial x_3}=0,\end{aligned}\right\} \tag{38}$$

In (37) we neglected terms of order $c^2\eta$.

The boundary conditions are seen to become:

$$u_3^0=\frac{\partial\eta}{\partial t}, \tag{39}$$

$$u_r^0=-c\tau\frac{\partial^2\eta}{\partial t\partial x_3}, \tag{40}$$

where τ: Poisson's ratio.

Owing to the smallness of c we can, without considerable error, replace (40) by:

$$u_r^0=0, \tag{41}$$

Putting

$$\begin{aligned}\eta&=\Re e^{i\omega t}\begin{matrix}\cos\\ \sin\end{matrix}\gamma x_3\cdot\eta,\\ u_3&=\Re\ ,,\quad ,,\quad\cdot u_3(r),\\ u_r&=\Re e^{i\omega t}\begin{matrix}\sin\\ -\cos\end{matrix}\gamma x_3\cdot u_r(r),\\ \bar p&=\Re\ ,,\quad ,,\quad\cdot\bar p(r),\end{aligned}$$

into (38) and (39) we get:

$$\eta=\frac{1}{i\omega}u_3^0,\quad \gamma u_3=u_r'+\frac{u_r}{r},$$

$$\begin{aligned}&\left(\frac{d^2}{dr^2}+\frac{1}{r}\frac{d}{dr}-\frac{1}{r^2}-\kappa^2\right)\left(\frac{d^2}{dr^2}+\frac{1}{r}\frac{d}{dr}-\frac{1}{r^2}-\gamma^2\right)\cdot u_r\\ &=\left(\frac{d^2}{dr^2}+\frac{1}{r}\frac{d}{dr}-\frac{1}{r^2}-\gamma^2\right)\left(\frac{d^2}{dr^2}+\frac{1}{r}\frac{d}{dr}-\frac{1}{r^2}-\kappa^2\right)\cdot u_r\\ &=0,\end{aligned} \tag{42}$$

where

$$\kappa^2=\gamma^2+i\frac{\omega\rho}{\nu},\quad \Re(\kappa)>0.$$

(42) has the solution:

$$u_r=\gamma AH_1^{(1)}(i\kappa r)+\gamma BH_1^{(1)}(i\gamma r),$$

which, by (41), becomes to:

$$u_r=\frac{\gamma c}{i}\left(\frac{H_1^{(1)}(i\kappa r)}{H_1^{(1)}(i\kappa c)}-\frac{H_1^{(1)}(i\gamma r)}{H_1^{(1)}(i\gamma c)}\right).$$

From this we obtain:

$$u_3=c\left\{\frac{\kappa}{H_1^{(1)}(i\kappa c)}H_0^{(1)}(i\kappa r)-\frac{\gamma}{H_1^{(1)}(i\gamma c)}H_0^{(1)}(i\gamma r)\right\},$$

$$\left(\frac{\partial u_3}{\partial r}\right)^0=-ic(\kappa^2-\gamma^2)=c\frac{\omega\rho}{\nu}.$$

Hence we get from (37) the following equation to determine ω.

$$\gamma^2E-\omega^2\sigma=2\pi ic\rho\omega^2\left\{\kappa\frac{H_0^{(1)}(i\kappa c)}{H_1^{(1)}(i\kappa c)}-\gamma\frac{H_0^{(1)}(i\gamma c)}{H_1^{(1)}(i\gamma c)}\right\}^{-1}.$$

When $\nu\to 0$, we have:

$$\omega\to\omega_0=\gamma\sqrt{\frac{E}{\sigma}},$$

$$\kappa\to\frac{1+i}{\sqrt{2}}\sqrt{\frac{\omega_0\rho}{\nu}},\quad \frac{H_0^{(1)}(i\kappa c)}{H_1^{(1)}(i\kappa c)}\to i,$$

and putting

$$\omega=\omega_0+\delta$$

we have:

$$\delta=\frac{\pi c}{\sigma}\sqrt{\frac{\rho\omega_0\nu}{2}}(i-1)=q(i-1),$$

and:

$$e^{i\omega t}=e^{i(\omega_0-q)t}e^{-qt}.$$

§ 8. Radial Vibration of a Circular Cylinder in the Atmosphere.

Let $x_1=r\cos\theta$, $x_2=r\sin\theta$, and the cylinder occupy the region $-\infty<x^5\leqslant+\infty$, $r\leqq c$.

The equation of motion for the body is:

$$\sigma\frac{\delta^2\xi_r}{\partial t}=(\lambda+2\mu)\frac{\partial}{\partial r}\left(\frac{1}{r}\frac{\delta(r\xi_r)}{\partial r}\right), \tag{43}$$

where ξ_r represents the radial displacement.

The equations for gas are:

$$\left.\begin{aligned}u_r&=-\frac{\partial\Phi}{\partial r},\\ p&=p_0+p=p_0+\rho\frac{\partial\Phi}{\partial t},\\ \frac{\partial^2\Phi}{\partial t^2}&=a^2\Delta\Phi.\end{aligned}\right\} \tag{44}$$

The boundary conditions become:

$$\left.\begin{aligned} -\rho\left(\frac{\partial \Phi}{\partial t}\right)^0 &= \lambda\left(\frac{1}{r}\frac{\partial(r\xi_r)}{\partial r}\right)^0+2\mu\left(\frac{\partial \xi_r}{\partial r}\right)^0, \\ -\left(\frac{\partial \Phi}{\partial r}\right)^0 &= \frac{\partial \xi_r{}^0}{\partial t}. \end{aligned}\right\} \tag{45}$$

Putting

$$\xi_r = \Re e^{i\omega t}U(r),$$

$$\Phi = \Re e^{i\omega t}\Phi(r),$$

into (43) and (44) we have:

$$\frac{d^2U}{dr^2}+\frac{1}{r}\frac{dU}{dr}+\left(\kappa^2-\frac{1}{r^2}\right)U=0 \tag{46}$$

$$\frac{d^2\Phi}{dr^2}+\frac{1}{r}\frac{d\Phi}{dr}+\kappa'^2\Phi=0, \tag{47}$$

with

$$\kappa^2=\frac{\sigma}{\lambda+2\mu}\cdot\omega^2,$$

$$\kappa'^2=\frac{\omega^2}{a^2},\quad \Re(\kappa')<0.$$

The solutions of (46) and (47) are given by:

$$U=A\cdot J_1(\kappa r),$$

$$\Phi=B\cdot H_0{}^{(1)}(\kappa' r).$$

From (45) we obtain

$$\frac{i\omega\rho H_0{}^{(1)}(\kappa' c)}{\kappa' H_0{}^{(1)\prime}(\kappa' c)}=\frac{(\lambda+2\mu)\kappa c J_1{}'(\kappa c)+\lambda J_1(\kappa c)}{i\omega c J_1(\kappa c)}. \tag{48}$$

If we take into account of the frictional terms, the equation (48) is to be replaced by:

$$\frac{i\omega\dfrac{\rho}{1+i\omega s}H_0{}^{(1)}\left(\dfrac{\kappa' c}{\sqrt{1+i\omega s}}\right)}{\dfrac{\kappa'}{\sqrt{1+i\omega s}}H_0{}^{(1)\prime}\left(\dfrac{\kappa' c}{\sqrt{1+i\omega s}}\right)}=\frac{(\lambda+2\mu)\kappa c J_1{}'(\kappa c)+\lambda J_1(\kappa c)}{i\omega c J_1(\kappa c)}.$$

For $\rho\to 0$ we have:

$$(\lambda+2\mu)\kappa_0 c J_1{}'(\kappa_0 c)+\lambda J_1(\kappa_0 c)=0, \tag{49}$$

$$\omega_0=\sqrt{\frac{\lambda+2\mu}{\sigma}}\cdot\kappa_0,$$

with κ_0 real positive.

When ρ is small, we put

$$\omega=\omega_0(1+\delta),$$

and we obtain:

$$\delta=\frac{\omega_0 a c\rho(\lambda+2\mu)}{\{\sigma\omega_0{}^2c(\lambda+2\mu)-2\mu(\lambda+\mu)\}\sqrt{1+i\omega_0 s}}\times\frac{H_0{}^{(1)}\left(\dfrac{\kappa_0' c}{\sqrt{i+i\omega_0 s}}\right)}{H_1{}^{(1)}\left(\dfrac{\kappa_0' c}{\sqrt{1+i\omega_0 s}}\right)},$$

with $\kappa_0'=-\omega_0/a$ real negative.

Considering the case $|\kappa_0' c|\to+\infty$, which corresponds to large roots of (49), we can easily verify that δ has positive imaginary part. Accordingly, the time factor shows the damping of vibration.

Approximate Evaluation of Electromagnetic Oscillating Modes on Plate Conductor with Slowly Curved Edge.

By Tokio SAKURAI.

Electrotechnical Laboratory, Ministry of Communications.

(Read November 3. 1947, Received October 22, 1947)

The method of approximate evaluation of the electromagnetic oscillating modes is related in this paper. In order to save the pages of this treatment the notations in the first paper(1) and in "J.A. Stratton: Electromagnetic Theory" are used except when special explanations are mentioned.

§1. General Considerations of Non-resonant Case.

As we have already explained in the first section of my preceding paper(1) $\bar{\varphi}_{nm}$ has following expression in boundary domain

$$\bar{\varphi}_{mn} = \bar{f}_{mn}(u_1, u_2)e^{-a_n Z/\sqrt{-2\xi}}e^{j\omega t}, \qquad (1.1)^{(2)}$$

where

$$f_{mn} = \phi_{mn}(u_1)e^{\pm jk_m^{(2)} u_2}, \qquad (1.2)^{(2)}$$

$\psi_{mn}, f_{mn}, \varphi_{mn}$ stand for $\bar{\psi}^e_{mn}, \bar{\psi}^e_{mn}$; $\bar{f}^e_{mn}, \bar{f}^o_{mn}$; $\bar{\psi}^e_{mn}, \varphi^o_{mn}$ respectively. Since $k_n^{(3)}$ of ψ can be regarded approximately constant throughout the central domain, substituting

$$\psi_{mn} = f_{mn}(x, y)e^{-jk_n^{(3)} z}e^{j\omega t} \qquad (1.3)$$

in (1.10) in my previous paper, we get in the central domain

$$\frac{\partial^2 f_{mn}}{\partial x^2} + \frac{\partial^2 f_{mn}}{\partial y^2} + (\lambda_{mn})^2 f_{mn} = 0, \qquad (1.4)$$

where

$$(\lambda_{mn})^2 = k^2 - k_n^{(2)}, \qquad (1.5)$$

$\psi_{mn}, f_{mn}, \lambda_{mn}$ stand for ψ^e_{mn}, ψ^o_{mn}; f^e_{mn}, f^o_{mn}; $\lambda^e_{mn}, \lambda^o_{mn}$ respectively.

From (2.7) in my preceding paper we deduce

$$C_{mn} = \Gamma_{mn}A_{mn} \qquad C'_{mn} = \Gamma_{mn}A_{mn}, \qquad (1.6)$$

where

$$\Gamma_{mn} = \{k^2-(k_m^{(2)})^2\}/k_n^{(3)}(\pm k_m^{(2)}) \qquad (17)$$

If we compare the forms of ψ_{mn} and ψ_{mn} introduced by (2.4)′, (2.6)′ in my first paper*, we recognize that (1.6) is equal to the following conditions on the separting line

$$f_{mn} = \Gamma_{mn}\bar{f}_{mn}, \quad \frac{\partial \bar{f}_{mn}}{\partial \nu} = \Gamma_{mn}\frac{\partial f_{mn}}{\partial \nu} \qquad (1.8)$$

where ν is the outward normal on the separating line lying on the plate surface. Hence if we solve (1.4) so as ${}_m\Gamma_n\bar{f}_{mn}$ and its derivatives are continuously connected with those of $\bar{f}_{mn}$ through the separating line, the form of f_{mn} and values of $k_m^{(2)}$ λ^2_{mn} are completely determined. Since the functional form of φ^o_{mn} differs from that of φ^e_{mn}, f^o_{mn} and λ^o_{mn}, etc., it differs from f^e_{mn} and λ^e_{mn}, etc. To show this difference definitely we use suffix p instead of n for f^o_{mn} and λ^o_{mn}, etc. and write them like f^o_{mp} and λ^o_{mp}, etc. hereafter. By (1.1), (1.3) and (1.8) we have

$$a_n = jk_n^{(3)}\sqrt{2|\xi_0|}, \qquad a_p = jk_p^{(3)}\sqrt{2|\xi_0|} \qquad (1.9)$$

where $|\xi_0|$ is the distance of the separating line from the plate edge and its value is given by (1.22)′. Since by (1.9) the values of a_n, a_p are decided and by (1.8) the ratio of $\bar{\psi}$ and ψ on the separting line is determined, the form of $\bar{\psi}^e_{mn}, \bar{\psi}^o_{mp}$ given by (1.1) are completely determined, if we proceed as explained after (1.12)′.

By (2.5)′ and (2.7)′

$$j\omega\varepsilon\, C^{(1)}_{mn} = K^{(1)}_{mn}\Gamma^*_{mn}B'_{mn}, \qquad (1.10)$$

where

$$\Gamma^*_{mn} = \{k^2-(k_m^{(2)})^2\}/\{k^2-(k_n^{(3)})^2-(k_m^{(2)})^2\}. \qquad (1.11)$$

If we remember (2.4), (2.6) and (i), (ii) in the second section in the first paper, we find that (1.10) is equivalent to any of two following relations

$$\left.\begin{aligned} j\omega\varepsilon f^e_{mn} &= \Gamma^*_{mn}\partial\bar{f}^{*o}_{mn}/\partial\nu, \\ j\omega\varepsilon f^o_{mp} &= \Gamma^*_{mp}\partial\bar{f}^{*e}_{mp}/\partial\nu. \end{aligned}\right\} \qquad (1.12)$$

Since $k_m^{(2)}$ and $k_n^{(3)}$ are already determined, the value of Γ^* given by (1.11) is known. Hence by (1.12) the relation of $\bar{f}^*$ to f which is already determined is known. Therefore, proceeding as explained after (1.12)′ we can completely determine $\bar{f}^{*o}_{mn}$ or $\bar{f}^{*e}_{mp}$.

If we put

$$\left.\begin{aligned} C_{mn} &= j\sqrt{\frac{\mu}{\varepsilon}}\,C^*_{mn}, & A_{mn} &= j\sqrt{\frac{\mu}{\varepsilon}}\,A^*_{mn}, \\ C'_{mn} &= j\sqrt{\frac{\mu}{\varepsilon}}\,C^{*\prime}_{mn} & A'_{mn} &= j\sqrt{\frac{\mu}{\varepsilon}}\,A^{*\prime}_{mn}, \\ j\sqrt{\frac{\mu}{\varepsilon}}B_{mn} &= B^*_{mn} & j\sqrt{\frac{\mu}{\varepsilon}}\,B'_{mn} &= B^{*\prime}_{mn}, \end{aligned}\right\} \qquad (1.13)$$

and substitute (1.13) for (2.7)′ we obtain immediately (2.9)′. This fact is equivalent to the following relations

$$\psi = j\sqrt{\frac{\mu}{\varepsilon}}\,\psi^*, \qquad \bar{\psi} = j\sqrt{\frac{\mu}{\varepsilon}}\,\bar{\psi}^* \qquad (1.14)$$

by (2.4)′, (2.6)′ and (2.8)′ where ψ represents ψ^e_{mn} or ψ^o_{mn}, ψ^* represents ψ^{*e}_{mn} or ψ^*_{mp}, $\bar{\psi}$ represents $\bar{\psi}^e_{mn}$, $\bar{\psi}^o_{mn}$, $\bar{\psi}^e_{mp}$ or $\bar{\psi}^o_{mp}$, $\bar{\psi}^*$ represents $\bar{\psi}^{*e}_{mn}$, $\bar{\psi}^{*o}_{mn}$, $\bar{\psi}^{*e}_{mp}$ or $\bar{\psi}^{*o}_{nm}$ respectively. From (1.14) it is evident that

$$\left.\begin{aligned} &k^{*(1)}_{mn} = k^{(1)}_{mn}, \quad k^{*(1)}_{mp} = k^{(1)}_{mp}, \\ &k^{*(2)}_{m} = k^{(2)}_{m}, \quad k^{*(3)}_{n} = k^{(3)}_{n}, \quad k^{*(3)}_{p} = k^{(3)}_{p}. \end{aligned}\right\} \qquad (1.15)$$

$$\lambda^*_{mn} = \lambda_{mn}, \quad \lambda^*_{mp} = \lambda_{mp}. \qquad (1.16)$$

---

(1) T. Sakurai, *Theory of Electromagnetic Oscillation on Plate Conductor*, This Journal.

(2) These are obtained by combining (1.12), (1.14), (1.17), (1.18) in my previous paper.

* In the following the formulae in the preceding paper are indicated by ′.

§ 2. General Considerations of Resonant Case.

Resonant phenomenon takes place[(3)] when

$$a_n = k_n^{(3)} = 0. \tag{2.1}$$

In this case by (2.5)′ and (1.15), (2.1)

$$k^2-(k_m^{(2)})^2 = k^2-(k_m^{*(2)})^2 = (k_{mn}^{(1)})^2 = (k_{mn}^{*(1)})^2. \tag{2.2}$$

Since Γ_{mn} becomes infinite according to (1,7) when (2.1) holds, the method related in foregoing section is invalid in this case. Combining (2.2) above related with (2.7)′ and (2.9)′ we get

$$k_{mn}^{(1)} B'_{mn} = j\omega\varepsilon C_{mn}, \quad k_{mn}^{(1)} B_{mn} = -j\omega\varepsilon C'_{mn}, \tag{2.3}$$

$$k_{mn}^{(1)} B^{*\prime}_{mn} = -j\omega\mu C^*_{mn}, \quad k_{mn}^{(1)} B^*_{mn} = j\omega\mu C^{*\prime}_{mn}. \tag{2.4}$$

If we compare (2.4)′, (2.6)′, (2.8)′ with (1.1), (1.3) and remember (2.1), (2.2), we find that (2.3), (2.4) are equivalent to the following conditions respectively:

$$\left.\begin{aligned} j\omega\varepsilon f_{mp}^{o} &= \frac{\partial f_{mp}^{*e}}{\partial\nu}, \quad j\omega\varepsilon\frac{\partial f_{mp}^{o}}{\partial\nu} = -\{k^2-(k_p^{(2)})^2\}\bar{f}_{mp}^{*e}, \\ j\omega\varepsilon f_{mn}^{e} &= \frac{\partial \bar{f}_{mn}^{*o}}{\partial\nu}, \quad j\omega\varepsilon\frac{\partial f_{mn}^{e}}{\partial\nu} = -\{k^2-(k_n^{(2)})^2\}\bar{f}_{mn}^{o}. \end{aligned}\right\} \tag{2.5}$$

$$\left.\begin{aligned} -j\omega\mu f_{mp}^{*o} &= \frac{\partial \bar{f}_{mp}^{e}}{\partial\nu}, \quad j\omega\mu\frac{\partial f_{mp}^{*o}}{\partial\nu} = \{k^2-(k_p^{(2)})^2\}\bar{f}_{mp}^{e}, \\ -j\omega\mu f_{mn}^{*e} &= \frac{\partial \bar{f}_{mn}^{o}}{\partial\nu}, \quad j\omega\mu\frac{\partial f_{mn}^{e*}}{\partial\nu} = \{k^2-(k_n^{(2)})^2\}\bar{f}_{mn}^{o}. \end{aligned}\right\} \tag{2.6}$$

Substituting (2.1) into (1.4), (1.5) we have

$$\frac{\partial^2 f}{\partial x^2}+\frac{\partial^2 f}{\partial y^2}+k^2 f = 0, \tag{2 7}$$

where f stands for f_{mn}^{e}, f_{mp}^{o}, f_{mn}^{*e} or f_{mp}^{*o}. If we solve (2 7) so as to satisfy (2.5) or (2.6) and substitute the solution thus obtained in (1.3) we get the wave function in central domain. In order that the solution of (2.7) satisfying (2 5) or (2.6) may exist, the magnitude of the central domain must be of appropriate value, which determines the resonant magnitude of the plate.

It is notable that by (1.6) A, A', A^*, $A^{*\prime}$ become zero by (2.1), which shows with (2.6)′ (2.8)′, (2.5) and (2.6) the following facts:

(i) The field of ψ_{mn}^{e} is contionously connected through separating line with the field of $\bar{\psi}_{mn}^{*o}$ and the field of ψ_{mn}^{e} vanishes in boundary domain.

(ii) The field of ψ_{mp}^{o} is continuously connected through separating line with the field of ψ_{mp}^{*e} and the field of ψ_{mp}^{o} vanishes in boundary domain.

(iii) The field of ψ_{mn}^{*o} is continuously connected through separating line with the field of $\bar{\psi}_{mn}^{o}$ and the field of $\bar{\psi}_{mn}^{*e}$ vanishes in boundary domain.

(iv) The field of ψ_{mp}^{*o} is cout'nuously connected through separating line with the field of $\bar{\psi}_{mp}^{e}$, and the field of $\bar{\psi}_{mp}^{*o}$ vanishes in boundary domain.

§ 3. Calculation in Non-resonant Case.

When oscillating mode is far from resonant state and a_n or a_p becomes so large that

$$a_n^2,\ a_p^2 \gg 2\pi k \tag{3.1}$$

holds, (1.15) in my previous paper[(1)] becomes approximately

$$d^2\varphi_{mn}/du_1^2+a_n^2\varphi_{mn} = 0. \tag{3.2}$$

The fundamental solutions of (3.2) are

$$\varphi_{mn}^{e} = \cos a_n u_1, \quad \varphi_{mn}^{o} = \sin a_n u_1. \tag{3.3}$$

Hence by (1.2)

$$\left.\begin{aligned} \bar{f}_{mn}^{e} &= \cos a_n u_1 e^{\pm jk_m^{(2)}u_2}, \\ \bar{f}_{mn}^{o} &= \sin a_n u_1 e^{\pm jk_m^{(2)}u_2}, \end{aligned}\right\} \tag{3.4}$$

The distance $|\xi_0|$ of the separating line from the plate edge becomes by (1.22)′

$$|\xi_0| \simeq \pi^2/2a_n^2, \quad \pi^2/2a_p^2. \tag{3.5}$$

Hence by (1.9)

$$jk_n^{(3)} \simeq a_n^2/\pi, \quad jk_p^{(3)} \simeq a^2{}_p/\pi. \tag{3.6}$$

Using (1.6) in my previous paper and remembering that $u_1 = \pi/a$ by (3.5) on the separating line, we get from (3.4)

$$\left.\begin{aligned} \bar{f}_{mn}^{e} &= -e^{\pm jk_m^{(2)}u_2}, \quad \frac{\partial \bar{f}_{mn}^{e}}{\partial\nu} = 0, \\ \bar{f}_{mp}^{e} &= 0, \quad \frac{\partial \bar{f}_{mp}^{o}}{\partial\nu} = \left(\frac{a_p}{\pi}\right)e^{\pm jk_m^{(2)}u_2} \end{aligned}\right\} \tag{3.7}$$

Hence by (1.8) the boundary conditions of f_{mn}^{e} and f_{mp}^{o} on the separating line become

---

(3) We find that there is no loss of the oscillating mode when (2.1) holds, evaluting Poynting vector on plate surface, which means no other than that the mode is in resonance.

$$\frac{\partial f^e_{mn}}{\partial \nu} = 0, \quad (3.8) \qquad f^o_{mp} = 0. \quad (3.9)$$

The equation satisfied by these function in the central domain becomes by (1.4), (1.5) and (3 6)

$$\frac{\partial^2 f}{\partial x^2}+\frac{\partial^2 f}{\partial y^2}+\left\{k^2+\left(\frac{a^2}{\pi}\right)^2\right\}f = 0, \qquad (3.10)$$

where f stands for f^e_{mn} or f^o_{mp} and a stands for a_n or a_p. If we solve (3.10) so as to satisfy (3.8) or (3.9), we obtain f^e_{mn} or f^o_{mp}. Hence by (1.3) we get the wave functions in the central domain, The values of a_n or a_p are also determined in solving this boundary problem. Hence by (3.5) they determines the thickness of the boundary domain.

Take, for example, a circular plate conductor with the radius length c. In this case by (3.5) the separating line becomes the circle with radius length $c-(\pi^2/2a^2)$. The solutions of (3.10) are expressed by circular coordinates r, θ as follows:

$$f = \frac{\sin}{\cos} m\theta J_m(r\sqrt{k^2+(a^2/\pi)^2}), \qquad (3.11)$$

Substituting (3.11) into (3.3) and (3 9), we get

$$\left.\begin{aligned}\{k^2+(a^2_{mn}/\pi)^2\}\{c-\pi/2a^2_{mn}\}^2 &= (u'_{mn})^2,\\ \{k^2+(a^2_{mp}/\pi)^2\}\{c-\pi/2a^2_{mp}\}^2 &= (u_{mp})^2,\end{aligned}\right\} \qquad (3.12)$$

where u'_{mn} is the m-th root of $dJ_m(u)/du = 0$ and u_{mp} is the p-th root of $J_m(u) = 0$. Remembering (3.1) we get from (3.12)

$$a_{mn} \simeq \pi u'_{mn}/c, \qquad a_{mp} \simeq \pi u_{mp}/c. \qquad (3.13)$$

Combining (3.13) with (3.5), we obtain the values of the thikness of boundary domain as follows:

$$|\xi_0| \simeq \pi c/2u'_{mn} \qquad |\xi_0| \simeq \pi c/2u_{mp}. \qquad (3.14)$$

§ 4. Calculation in Resonant Case.

Since (2.1) and (2.2) hold in resonant case, (1.15) in my previous paper becomes

$$d^2\varphi/du_1^2+(k^{(1)})^2u_1^2\varphi = 0. \qquad (4.1)$$

The fundamental solutions of (4.1) are

$$\left.\begin{aligned}\varphi^e &= c^e u^{1/2} J_{-1/4}(k^{(1)}u_1^2/2),\\ \varphi^o &= c^o u^{1/2} J_{1/4}(k^{(1)}u_1^2/2),\end{aligned}\right\} \qquad (4.2)^{(4)}$$

where c^e and c^o are integral constants. Using the relation

$$k^{(1)}u_1^2/2 = k^{(1)}|\xi| = s, \qquad (4.3)$$

(4.2) can be written as follows:

$$\varphi^e = s^{1/4}J_{-1/4}(s), \quad \varphi^o = s^{1/4}J_{1/4}(s). \qquad (4.4)$$

Since (2.1) holds, by (1.22)′

$$k^{(1)}|\xi_0| = s_0 = \pi/2. \qquad (4.5)$$

on separating line. Hence by (4.4) and (4.5)

$$\left.\begin{aligned}[\varphi^e]_{s=s_0} = 0{,}29,\ [d\varphi^e/ds]_{s=s_0} &= -s_0^{1/4}J_{3/4}(s_0)\\ &= -0{,}70,\\ [\varphi^o]_{s=s_0} = 6{,}6,\ [d\varphi^o/ds]_{s=s_0} &= s_0^{1/4}J_{-3/4}(s_0)\\ &= -0{,}34.\end{aligned}\right\} \qquad (4.6)^{(5)}$$

$$\left.\begin{aligned}j\omega\varepsilon f^o_{mp} &= 0.70\sqrt{k^2-(k^{(2)}_m)^2}\, e^{\pm jk^{(2)}_m u_1},\\ j\omega\varepsilon f^o_{mp}/\partial\nu &= -0{,}29\{k^2-(k^{(2)}_m)^2\}e^{\pm jk^{(2)}_m u_2},\end{aligned}\right\} \qquad (4.7)$$

$$\left.\begin{aligned}j\omega\varepsilon f^e_{mn} &= 0.34\sqrt{k^2-(k^{(2)}_m)^2}\, e^{\pm jk^{(2)}_m u_2}\\ j\omega\varepsilon\partial f^e_{mn}/\partial\nu &= -6{,}6\{k^2-(k^{(2)}_m)^2\}e^{\pm jk^{(2)}_m u_2}\end{aligned}\right\} \qquad (4.8)$$

$$\left.\begin{aligned}j\omega\mu f^{*o}_{mp} &= -0.70\sqrt{k^2-(k^{(2)}_m)^2}\, e^{\pm jk^{(2)}_m u_2},\\ j\omega\mu\partial f^{*o}_{mp}/\partial\nu &= 0.29\{k^2-(k^{(2)}_m)^2\}e^{\pm jk^{(2)}_m u_2},\end{aligned}\right\} \qquad (4.9)$$

$$\left.\begin{aligned}j\omega\mu f^{*e}_{mn} &= -0.34\sqrt{k^2-(k^{(2)}_m)^2}\, e^{\pm jk^{(2)}_m u_2},\\ j\omega\mu\, \partial f^{*e}_{mn}/\partial\nu &= 6.6\sqrt{k^2-(k^{(2)}_m)^2}\, e^{\pm jk^{(2)}_m u_2}\end{aligned}\right\} \qquad (4.10)$$

In the case of circular plate conductor with radius length c the solutions of (2.7) become

$$f = \frac{\sin}{\cos} m\theta J_m(kr). \qquad (4.11)$$

If we substitute (4.11) in relations from (4.7) to (4.10) and remember that

$$k^{(2)}_m = m/r_n, \quad m/r_p \qquad (4.12)$$

on the separating line, we have

$$\left.\begin{aligned}J'_m(kr_n)+1.9\sqrt{1-(m/kr_n)^2}J_m(kr_n) &= 0,\\ J'_m(kr_p)+0.41\sqrt{1-(m/kr_p)^2}J_m(kr_p) &= 0,\end{aligned}\right\} (4.13)$$

where r_n and r_p is the radius length of the separating line in the cases of f^e_{mn}, f^{*e}_{mn} and f^o_{mp}, f^{*o}_{mp} respectively. Let v_{mn} and v_{mp} be the nth and pth roots of

---

(4) Forsyth, Treatise on Differential Equation, p. 196.

(5) These values are calculated using tables in Jahnke and Emde, Tables of Functions, p. 223. (2.5) and (2 6) become in this case

$$\left.\begin{aligned} J'_m(v_{mn})+1.9\sqrt{1-(m/v_{mn})^2}\,J_m(v_{mn}) &= 0, \\ J'_m(v_{mp})+0.41\sqrt{1-(m/v_{mp})^2}\,J_m(v_{mp}) &= 0. \end{aligned}\right\} \quad (4.14)$$

If we calculate by (2.2) and (4.5) the thickness of boundary domain and add them to r_n and r_p respectively, we have

$$c_m = \frac{\lambda v_m}{4}\left\{\frac{2}{\pi}+\frac{1}{\sqrt{v_m^2-m^2}}\right\}, \qquad (4.15)$$

where c_m stands for c_{mn}, c_{mn} and v_m stands for v_m, v_{mp} respectively, and λ is the wave length in free space. These c_{mn} and c_{mp} are resonant radii of the circular plate conductor of f^e_{mn} and f^o_{mp} modes respectively.

Particularly when $m=0$, (4.14) becomes

$$J_1(v_{on}) = 1.9J_o(v_{on}), \quad J_1(v_{op}) = 0.41J_o(v_{op}). \quad (4.16)$$

The roots of these equations are

$$\left.\begin{aligned} v_{on} &= 1.9,\ 5.0,\ 8.1,\ 11.8,\ 14.4,\ \cdots\cdots, \\ v_{op} &= 0.80,\ 4.8,\ 7.4,\ 10.6,\ 13.7,\ \cdots\cdots. \end{aligned}\right\} \quad (4.17)$$

(4.15) becomes in this case

$$\left.\begin{aligned} c_{on} &= 0.55\,\lambda,\ 1.05\,\lambda,\ 1.55\,\lambda,\ 2.14\,\lambda,\ 2{,}6\,\lambda \\ c_{op} &= 0.38\,\lambda,\ 1.02\,\lambda,\ 1.43\,\lambda,\ 1.95\,\lambda,\ 2{,}5\,\lambda \end{aligned}\right\} \quad (4.18)$$

When $m=1$, we have by (4.14) and (4.15)

$$\left.\begin{aligned} v_{1n} &= 3.3,\ 6{,}5,\ 9.7,\ 12.8,\ \cdots\cdots, \\ v_{1p} &= 2.4,\ 5.7,\ 8.9,\ 12.1,\ \cdots\cdots. \end{aligned}\right\} \quad (4.19)$$

$$\left.\begin{aligned} c_{1n} &= 0.79\,\lambda,\ 1.29\,\lambda,\ 1.80\,\lambda,\ 2.3\,\lambda.\ \cdots\cdots, \\ c_{1p} &= 0.65\,\lambda,\ 1.16\,\lambda,\ 1.66\,\lambda,\ 2.2\,\lambda,\ \cdots\cdots. \end{aligned}\right\} \quad (4.20)$$ (6)

---

(6) There are the smallest values of c_{1n} and c_{1p} smaller than any of (4.20). But the method in this paper is too rough to evaluate them.

Tables Useful for Construction of Irreducible Representation Matrices of Symmetric Group.

By Takahiko YAMANOUCHI.

Institute of Applied Mathematics, Second Faculty of Engineering, University of Tokyo.

(Received October 25, 1947)

§ 1. Introduction.

In the group-theoretical treatment of many-electron problems in quantum mechanics, it is often necessary to have the i.r.m. (irreducible representation matrices) of the symmetric group S_n. The following tables have been prepared to provide a simple means for their construction up to the degree $n=6$. The method is in principle based upon the double decomposition:

$$S_n = G+GP_1G+\cdots\cdots+GP_mG \qquad (1)$$

by a subgroup G, which is capable of simple representation. Each element of S_n can then be expressed in the form:

$$P = G_jP_iG_k, \qquad (2)$$

where G_j and G_k are the elements of G. Thus the i.r.m. of any element P can be obtained from that of P_i, the representant of each class in (1), by pre- and post- multiplication of simple i.r.m. of G. By taking the subgroup G as wide as the simplicity of its representation allows, the number of the representants P_i can be reduced to 2 or 3 in our case.

We take G as the subgroup $\{H, K\}$ of order 48, where $H=\{(12), (34), (56)\}$ and $K=\{(13)(24), (15)(26)\}$. H is an abelian group of order 8, whose elements are all cyclic of order 2, so that they can be represented by diagonal matrices in every irreducible representation, with ± 1 as the diagonal elements. Also H is an invariant subgroup of G, and K is isomorph to the factor group G/H. By a suitable choice of base vectors, the i. r. m. of K can be made to have the from that each row or column has only one non-vanishing element (monomial representation).

The elements of G have the form

$$G_j = H_\alpha K_\beta, \tag{3}$$

where H_α and K_β belong to H and K respectively. Since the i.r.m. of H_α is diagonal, all the elements of G are monomially represented. The pre- or post- multiplication of such matrices merely permutes the rows and columns of the matrix besides multipiying them by numerical factors.

The irreducible representations in this table are limited to physically significant ones, which are characterised by the multiplicity μ of n-electron system. The notation $R_n{}^\mu$ will be employed for such representation.

§2. Explanations.

Table 1 gives the expressions (2) for all elements of S_6 in classified order, by the numbers i, j of the elements of G and the representants of the classes in (1), $X = (13)$. $Z = (135)$. This table includes, of cource, all the elements of S_n for $n \leqq 6$. For $R_5{}^4$, however, we can use only those elements of G that do not permute the numeral 6. For this reason, another representant $Y = (15)$ has to be introduced, and certain elements have different forms from those of S_6. These 32 elements are marked with asterisk in the table, and their expressions in terms of Y are given at the end of the table.

Table 2 lists the 48 elements of G in the form (3), in which the elements of H and K are expressed by special symbols $A, B, \cdots\cdots; I, J, \cdots\cdots$.

Table 3 contains the i.r.m. of the elements of G and H as well as the representants X, Y, Z for each $R_n{}^\mu \cdot R_n{}^{n+1}$, for which the i.r.m. is ± 1 according to the parity of the elements, is omitted from the table. For diagonal matrices, the elements are written in a row to save the space.

Example. Find the i.r.m. of $P = (1\,2\,4\,6\,3\,5)$ for $R_6{}^5$.

We find $P = 31\,X\,13$ from Table 1,

and $31 = QI,\ 13 = RK$ from Table 2.

Thus $P = QIXRK$. From Table 3. $R_6{}^5$, we can easily find

$$QI: \begin{pmatrix} 0 & 1 & 0 & 0 & 0 \\ 1 & 0 & 0 & 0 & 0 \\ 0 & 0 & 0 & -1 & 0 \\ 0 & 0 & 1 & 0 & 0 \\ 0 & 0 & 0 & 0 & -1 \end{pmatrix}, \quad RK: \begin{pmatrix} 0 & \omega^2 & 0 & 0 & 0 \\ \omega & 0 & 0 & 0 & 0 \\ 0 & 0 & 1 & 0 & 0 \\ 0 & 0 & 0 & 0 & -1 \\ 0 & 0 & 0 & -1 & 0 \end{pmatrix}$$

$$QIX: \frac{1}{2}\begin{pmatrix} -1 & -1 & i & -i & 0 \\ -1 & -1 & -i & i & 0 \\ i & -i & 1 & 1 & 0 \\ i & -i & -1 & -1 & 0 \\ 0 & 0 & 0 & 0 & 2 \end{pmatrix}.$$

So we obtain :

$$P: \frac{1}{2}\begin{pmatrix} -\omega & \omega^2 & i & 0 & i \\ -\omega & -\omega^2 & -i & 0 & -i \\ -i\omega & i\omega^3 & 1 & 0 & -1 \\ -i\omega & i\omega^2 & -1 & 0 & 1 \\ 0 & 0 & 0 & -2 & 0 \end{pmatrix}.$$

TABLE I.

(1)	1		

(12)	2		
(13)		*X*	
(14)	14	*X*	2
(15)*	12	*X*	12
(16)	13	*X*	13
(23)	2	*X*	2
(24)	7	*X*	
(25)*	39	*X*	13
(26)	37	*X*	12
(34)	3		
(35)*	9	*X*	9
(36)	10	*X*	10
(45)*	34	*X*	10
(46)	33	*X*	9
(56)	4		

(123)		*X*	2
(124)	14	*X*	
(125)*	47	*X*	13
(126)	45	*X*	12
(132)	2	*X*	
(134)	8	*X*	2
(135)		*Z*	
(136)	4	*Z*	4
(142)	7	*X*	2
(143)	3	*X*	
(145)	3	*Z*	3
(146)	12	*Z*	11
(152)*	21	*X*	12
(153)	9	*Z*	9
(154)	40	*Z*	6
(156)	18	*X*	13
(162)	22	*X*	13
(163)	38	*Z*	5
(164)	45	*Z*	2
(165)	19	*X*	12
(234)	15	*X*	
(235)	2	*Z*	2
(236)	6	*Z*	6
(243)	5	*X*	2
(245)	5	*Z*	5
(246)	12	*Z*	9
(253)	39	*Z*	11
(254)	48	*Z*	4
(256)	48	*X*	12
(263)	46	*Z*	3
(264)	37	*Z*	
(265)	46	*X*	13
(345)*	43	*X*	10
(346)	44	*X*	9
(354)*	25	*X*	9
(356)	16	*X*	10
(364)	26	*X*	10
(365)	17	*X*	9
(456)	42	*X*	9
(465)	41	*X*	10

(12)(34)	5		
(12)(35)*	16	*X*	9
(12)(36)	17	*X*	10
(12)(45)*	42	*X*	10
(12)(46)	41	*X*	9
(12)(56)	6		
(13)(24)	7		
(13)(25)	17	*Z*	4
(13)(26)	9	*Z*	
(13)(45)	8	*Z*	5
(13)(46)	33	*Z*	9
(13)(56)	4	*X*	
(14)(23)	8		
(14)(25)	30	*Z*	11
(14)(26)	25	*Z*	3
(14)(35)	14	*Z*	2
(14)(36)	31	*Z*	6
(14)(56)	31	*X*	2
(15 (23)	10	*Z*	6
(15 (24)	37	*Z*	9
(15)(26)	9		
(15)(34)*	18	*X*	12
(15)(36)	18	*Z*	3
(15)(46)	12	*Z*	
(16)(23)	16	*Z*	2
(16)(24)	29	*Z*	5
(16)(25)	10		
(16)(34)	19	*X*	13
(16)(35)	13	*Z*	11
(16)(45)	19	*Z*	4
(23)(45)	15	*Z*	3
(23)(46)	32	*Z*	11
(23)(56)	6	*X*	2
(24) 35)	7	*Z*	
(24)(36)	23	*Z*	4
(24)(56)	23	*X*	
(25)(34)*	48	*X*	13
(25)(36)	27	*Z*	5
(25)(46)	21	*Z*	2
(26)(34)	46	*X*	12
(26)(35)		*Z*	9
(26)(45)	28	*Z*	6
(34)(56)	11		
(35)(46)	12		
(36)(45)	13		

(1234)	8	*X*	
(1235)		*Z*	2
(1236)	4	*Z*	6
(1243)	3	*X*	2
(1245)	3	*Z*	5
(1246)	21	*Z*	9
(1253)	47	*Z*	11
(1254)	40	*Z*	4
(1256)	40	*X*	12
(1263)	38	*Z*	3
(1264)	45	*Z*	
(1265)	38	*X*	13
(1324)	14		
(1325)	10	*Z*	4
(1326)	16	*Z*	
(1342)	15	*X*	2
(1345)		*Z*	3
(1346)	4	*Z*	11
(1352)	2	*Z*	
(1354)	8	*Z*	2
(1356)		*Z*	4
(1362)	6	*Z*	4
(1364)	24	*Z*	6
(1365)	4	*Z*	
(1423)	15		
(1425)	26	*Z*	11
(1426)	29	*Z*	3
(1432)	5	*X*	
(1435)	3	*Z*	
(1436)	11	*Z*	4
(1452)	5	*Z*	3
(1453)	14	*Z*	5
(1456)	3	*Z*	11
(1462)	20	*Z*	11
(1463)	44	*Z*	9
(1465)	11	*Z*	3
(1523)	17	*Z*	6
(1524)	45	*Z*	9
(1526)	16		
(1532)	16	*Z*	9
(1534)	47	*Z*	6
(1536)	18	*Z*	11
(1542)	48	*Z*	6
(1543)	25	*Z*	9
(1546)	12	*Z*	4
(1562)	27	*X*	13
(1563)	47	*Z*	5
(1564)	40	*Z*	2
(1623)	9	*Z*	2
(1624)	25	*Z*	5
(1625)	17		
(1632)	46	*Z*	5
(1634)	38	*Z*	2
(1635)	13	*Z*	3
(1642)	37	*Z*	2
(1643)	45	*Z*	5
(1645)	19	*Z*	
(1652)	28	*X*	12
(1653)	17	*Z*	9
(1654)	45	*Z*	6
(2345)	2	*Z*	5
(2346)	18	*Z*	9
(2354)	15	*Z*	
(2356)	2	*Z*	6
(2364)	32	*Z*	4
(2365)	6	*Z*	2
(2435)	5	*Z*	2
(2436)	20	*Z*	6
(2453)	7	*Z*	3
(2456)	19	*Z*	9
(2463)	23	*Z*	11
(2465)	20	*Z*	5
(2534)	39	*Z*	4
(2536)	4	*Z*	9
(2543)	48	*Z*	11
(2546)	21	*Z*	6
(2563)	39	*Z*	3
(2564)	48	*Z*	
(2634)	46	*Z*	
(2635)	22	*Z*	5
(2643)	37	*Z*	3
(2645)	28	*Z*	2
(2653)	46	*Z*	11
(2654)	37	*Z*	4
(3456)	35	*X*	9
(3465)	36	*X*	10
(3546)	18		
(3564)	29	*X*	10
(3645)	19		
(3645)	30	*X*	9

(12345)		*Z*	5
(12346)	27	*Z*	9
(12354)	8	*Z*	
(12356)		*Z*	6
(12364)	24	*Z*	4
(12365)	4	*Z*	2
(12435)	3	*Z*	2
(12436)	11	*Z*	6
(12453)	14	*Z*	3
(12456)	28	*Z*	9
(12463)	31	*Z*	11
(12465)	11	*Z*	5
(12534)	47	*Z*	4
(12536)	6	*Z*	9
(12543)	40	*Z*	11
(12546)	12	*Z*	6
(12563)	47	*Z*	3
(12564)	40	*Z*	
(12634)	38	*Z*	
(12635)	13	*Z*	5
(12643)	45	*Z*	3
(12645)	19	*Z*	2
(12653)	38	*Z*	11
(12654)	45	*Z*	4
(13245)*	22	*X*	10
(13246)	21	*X*	9
(13254)*	17	*X*	13
(13256)	10	*Z*	
(13264)	16	*X*	12

Table 1 (Countinued)

(13265)	16	*Z*	4
(13425)	10	*Z*	11
(13426)	16	*Z*	3
(13452)	2	*Z*	3
(13456)		*Z*	11
(13462)	6	*Z*	11
(13465)	4	*Z*	3
(13524)*	45	*X*	9
(13526)	16	*X*	
(13542)	15	*Z*	2
(13546)	4	*X*	13
(13562)	2	*Z*	4
(13564)	8	*Z*	6
(13624)	47	*X*	10
(13625)	17	*X*	
(13642)	32	*Z*	6
(13645)	4	*X*	12
(13652)	6	*Z*	
(13654)	24	*Z*	2
(14235)*	46	*X*	9
(14236)	48	*X*	10
(14253)*	26	*X*	13
(14256)	26	*Z*	3
(14263)	25	*X*	12
(14265)	29	*Z*	11
(14325)	26	*Z*	4
(14326)	29	*Z*	
(14352)	5	*Z*	
(14356)	3	*Z*	4
(14362)	20	*Z*	4
(14365)	11	*Z*	
(14523)*	19	*X*	10
(14526)	34	*X*	2
(14532)	7	*Z*	5
(14536)	3	*X*	13
(14562)	5	*Z*	11
(14563)	35	*Z*	9
(14623)	18	*X*	9
(14625)	33	*X*	2
(14632)	36	*Z*	9
(14635)	3	*X*	12
(14652)	20	*Z*	3
(14653)	31	*Z*	5
(15234)	38	*Z*	9
(15236)	10	*X*	2
(15243)	30	*Z*	6
(15246)	41	*X*	
(15263)	4	*X*	10
(15264)	14	*X*	9
(15324)*	41	*X*	12
(15326)	2	*X*	9
(15342)	39	*Z*	6
(15346)	18	*Z*	4
(15362)	27	*Z*	11
(15364)	40	*X*	2
(15423)*	44	*X*	12
(15426)	23	*X*	10
(15432)	29	*Z*	9
(15436)	12	*Z*	11
(15462)	21	*Z*	4
(15463)	18	*X*	
(15623)	17	*Z*	2
(15624)	30	*Z*	5
(15632)	39	*Z*	5
(15634)	47	*Z*	2
(15642)	48	*Z*	2
(15643)	40	*Z*	5
(16234)	9	*Z*	5
(16235)	9	*X*	2
(16243)	25	*Z*	2
(16245)	42	*X*	
(16253)	4	*X*	9
(16254)	14	*X*	10
(16324)	42	*X*	13
(16325)	2	*X*	10
(16342)	46	*Z*	2
(16345)	13	*Z*	
(16352)	22	*Z*	3
(16354)	38	*X*	2
(16423)	43	*X*	13
(16425)	23	*X*	9
(16432)	37	*Z*	5
(16435)	19	*Z*	3
(16452)	28	*Z*	
(16453)	19	*X*	
(16523)	9	*Z*	6
(16524)	40	*Z*	9
(16532)	10	*Z*	9
(16534)	38	*Z*	6
(16542)	37	*Z*	6
(16543)	30	*Z*	9
(23456)	13	*Z*	9
(23465)	6	*Z*	5
(23546)	15	*X*	12
(23564)	15	*Z*	4
(23645)	15	*X*	13
(23654)	32	*Z*	
(24356)	5	*Z*	6
(24365)	20	*Z*	2
(24536)	23	*X*	12
(24563)	7	*Z*	11
(24635)	23	*X*	13
(24653)	23	*Z*	3
(25346)	27	*Z*	6
(25364)	48	*X*	
(25436)	12	*Z*	9
(25463)	27	*X*	2
(25634)	39	*Z*	
(25643)	48	*Z*	3
(26345)	22	*Z*	2
(26354)	46	*X*	
(26435)	28	*Z*	5
(26453)	28	*X*	2
(26534)	46	*Z*	4
(26543)	37	*Z*	11
(12)(345)*	35	*X*	10
(12)(346)	36	*X*	9
(12)(354)*	29	*X*	9
(12)(356)	9	*X*	10
(12)(364)	30	*X*	10
(12)(365)	10	*X*	9
(12)(456)	34	*X*	9
(12)(465)	33	*X*	10
(13)(245)*	13	*X*	10
(13)(246)	12	*X*	9
(13)(254)*	10	*X*	13
(13)(256)	17	*Z*	
(13)(264)	9	*X*	12
(13)(265)	9	*Z*	4
(13)(456)	42	*Z*	9
(13)(465)	24	*Z*	5
(14)(235)*	38	*X*	9
(14)(236)	40	*X*	10
(14)(253)*	30	*X*	13
(14)(256)	30	*Z*	3
(14)(263)	29	*X*	12
(14)(265)	25	*Z*	11
(14)(356)	14	*Z*	6
(14)(365)	31	*Z*	2
(15)(234)	46	*Z*	9
(15)(236)	17	*X*	2
(15)(243)	26	*Z*	6
(15)(246)	33	*X*	
(15)(263)	6	*X*	10
(15)(264)	7	*X*	9
(15)(346)	18	*Z*	
(15)(364)	12	*Z*	3
(16)(234)	16	*Z*	5
(16)(235)	16	*X*	2
(16)(243)	29	*Z*	2
(16)(245)	34	*X*	
(16)(253)	6	*X*	9
(16)(254)	7	*X*	10
(16)(345)	13	*Z*	4
(16)(354)	19	*Z*	11
(23)(145)*	28	*X*	10
(23)(146)	27	*X*	9
(23)(154)*	36	*X*	12
(23)(156)	10	*Z*	2
(23)(164)	35	*X*	13
(23)(165)	16	*Z*	6
(23)(456)	15	*Z*	11
(23)(465)	32	*Z*	3
(24)(135)*	37	*X*	9
(24)(136)	39	*X*	10
(24)(153)*	33	*X*	12
(24)(156)	26	*Z*	5
(24)(163)	34	*X*	13
(24)(165)	48	*Z*	9
(24)(356)	7	*Z*	4
(24)(365)	23	*Z*	
(25)(134)	17	*Z*	11
(25)(136)	10	*X*	
(25)(143)	30	*Z*	4
(25)(146)	41	*X*	2
(25)(163)		*X*	10
(25)(164)	31	*X*	9
(25)(346)	27	*Z*	2
(25)(364)	21	*Z*	5
(26)(134)	9	*Z*	3
(26)(135)	9	*X*	
(26)(143)	25	*Z*	
(26)(145)	42	*X*	2
(26)(153)		*X*	9
(26)(154)	31	*X*	10
(26)(345)	22	*Z*	6
(26)(354)	3	*Z*	9
(34)(125)*	40	*X*	13
(34)(126)	38	*X*	12
(34)(152)*	27	*X*	12
(34)(156)	12	*X*	13
(34)(162)	28	*X*	13
(34)(165)	13	*X*	12
(34)(256)	39	*X*	12
(34)(265)	37	*X*	13
(35)(124)	14	*Z*	
(35)(126)	2	*Z*	9
(35)(142)	7	*Z*	2
(35)(146)	11	*X*	13
(35)(162)	22	*Z*	11
(35)(164)	45	*X*	2
(35)(246)	7	*X*	12
(35)(264)	37	*X*	
(36)(124)	31	*Z*	4
(36)(125)	18	*Z*	5
(36)(142)	23	*Z*	6
(36)(145)	11	*X*	12
(36)(152)	27	*Z*	3
(36)(154)	47	*X*	2
(36)(245)	7	*X*	13
(36)(254)	39	*X*	
(45)(123)	8	*Z*	3
(45)(126)	19	*Z*	6
(45)(132)	15	*Z*	5
(45)(136)		*X*	13
(45)(162)	28	*Z*	4
(45)(163)	13	*X*	
(45)(236)	32	*X*	12
(45)(263)	22	*X*	2
(46)(123)	24	*Z*	11
(46)(125)	12	*Z*	2
(46)(132)	41	*Z*	9
(46)(135)		*X*	12
(46)(152)	21	*Z*	

Table 1 (Continued)

(46)(153)	12	*X*	
(46)(235)	32	*X*	13
(46)(253)	21	*X*	2
(56)(123)	4	*X*	2
(56)(124)	31	*X*	
(56)(132)	6	*X*	
(56)(134)	24	*X*	2
(56)(142)	23	*X*	2
(56)(143)	11	*X*	
(56)(234)	32	*X*	
(56)(243)	20	*X*	2

(12)(34)(56)	20		
(12)(35)(46)	21		
(12)(36)(45)	22		
(13)(24)(56)	23		
(13)(25)(46)	44	*Z*	6
(13)(26)(45)	35	*Z*	2
(14)(23)(56)	24		
(14)(25)(36)	24	*Z*	9
(14)(26)(35)	42	*Z*	5
(15)(23)(46)	36	*Z*	4
(15)(24)(36)	41	*Z*	11
(15)(26)(34)	25		
(16)(25) 34)	26		
(16)(23)(45)	43	*Z*	
(16)(24)(35)	34	*Z*	3
(16)(25)(34)	26		

(12)(3456)	43	*X*	9
(12)(3465)	44	*X*	10
(12)(3546)	27		
(12)(3564)	25	*X*	10
(12)(3654)	28		
(12)(3654)	26	*X*	9
(13) 2456)	19	*X*	9
(13)(2465)	18	*X*	10
(13)(2546)	44	*Z*	2
(13)(2564)	17	*X*	12
(13)(2645)	35	*Z*	6
(13)(2654)	16	*X*	13
(14)(2356)	45	*X*	10
(14)(2365)	47	*X*	9
(14)(2536)	33	*Z*	5
(14)(2563)	26	*X*	12
(14)(2635)	8	*Z*	9
(14)(2653)	25	*X*	13
(15)(2346)	44	*X*	
(15)(2364)	36	*Z*	11
(15)(2436)	30	*X*	2
(15)(2463)	41	*Z*	4
(15)(2634)	15	*X*	9
(15)(2643)	20	*X*	10
(16)(2345)	43	*X*	
(16)(2354)	43	*Z*	3
(16)(2435)	29	*X*	2
(16)(2453)	34	*Z*	
(16)(2534)	15	*X*	10
(16)(2543)	20	*X*	9
(23)(1456)	22	*X*	9
(23)(1465)	21	*X*	10
(23)(1546)	36	*Z*	
(23)(1564)	44	*X*	13
(23)(1645)	43	*Z*	4
(23)(1654)	43	*X*	12
(24)(1356)	46	*X*	10
(24)(1365)	48	*X*	9
(24)(1536)	41	*Z*	3
(24)(1563)	41	*X*	13
(24)(1635)	34	*Z*	
(24)(1653)	42	*X*	12
(25)(1346)	36	*X*	2
(25)(1364)	31	*Z*	9
(25)(1436)	26	*X*	
(25)(1463)	33	*Z*	6
(25)(1634)	24	*X*	9
(25)(1643)	3	*X*	10
(26)(1345)	35	*X*	2
(26)(1354)	36	*Z*	5
(26)(1435)	25	*X*	
(26)(1453)	42	*Z*	2
(26)(1534)	24	*X*	10
(26)(1543)	3	*X*	9
(34)(1256)	47	*X*	12
(34)(1265)	45	*X*	13
(34)(1526)	29		
(34)(1562)	21	*X*	13
(34)(1625)	30		
(34)(1652)	22	*X*	12
(35)(1246)	14	*X*	12
(35)(1264)	45	*X*	
(35)(1426)	34	*Z*	5
(35)(1462)	20	*X*	13
(35)(1624)	42	*Z*	3
(35)(1642)	37	*X*	2
(36)(1245)	14	*X*	13
(36)(1254)	47	*X*	
(36)(1425)	32	*Z*	9
(36)(1452)	20	*X*	12
(36)(1524)	33	*Z*	11
(36)(1542)	39	*X*	2
(45)(1236)	24	*X*	12
(45)(1263)	13	*X*	2
(45)(1326)	43	*Z*	2
(45)(1362)	2	*X*	13
(45)(1623)	35	*Z*	
(45)(1632)	22	*X*	
(46)(1235)	24	*X*	13
(46)(1253)	12	*X*	2
(46)(1325)	36	*Z*	6
(46)(1352)	2	*X*	12
(44)(1523)	44	*Z*	4
(46)(1532)	21	*X*	
(56)(1234)	24	*X*	
(56)(1243)	11	*X*	2
(56)(1324)	31		
(56)(1342)	32	*X*	2
(56)(1423)	32		
(59)(1432)	20	*X*	

(123)(456)	8	*Z*	11
(123)(465)	24	*Z*	3
(124)(356)	14	*Z*	4
(124)(365)	31	*Z*	
(125)(346)	18	*Z*	2
(125))364)	12	*Z*	5
(126)(345)	13	*Z*	6
(126)(354)	5	*Z*	9
(132)(456)	34	*Z*	9
(132)(465)	32	*Z*	5
(135)(246)	33		
(135)(264)	7	*Z*	9
(134)(256)	17	*Z*	3
(134)(265)	9	*Z*	11
(136)(245)	34		
(136)(254)	36	*Z*	5
(142)(356)	7	*Z*	6
(142)(365)	23	*Z*	2
(143)(256)	30	*Z*	
(143)(265)	25	*Z*	4
(145)(236)	35		
(145)(263)	34	*Z*	6
(146)(235)	36		
(146)(253)	41	*Z*	2
(152)(346)	27	*Z*	
(152)(364)	21	*Z*	3
(153)(246)	33	*Z*	
(153)(264)	37		
(154)(236)	44	*Z*	3
(154)(263)	38		
(156)(234)	10	*Z*	5
(156)(243)	26	*Z*	5
(162)(345)	22	*Z*	4
(162)(354)	28	*Z*	11
(163)(245)	42	*Z*	4
(163)(254)	39		
(164)(235)	35	*Z*	11
(164)(253)	40		
(165)(234)	39	*Z*	9
(165)(243)	29	*Z*	6

(123456)	22	*Z*	9
(123465)	4	*Z*	5
(123546)	8	*X*	12
(123564)	8	*Z*	4
(123645)	8	*X*	13
(123654)	24	*Z*	
(124356)	3	*Z*	6
(124365)	11	*Z*	2
(124536)	31	*X*	12
(124563)	14	*Z*	11
(124635)	31	*X*	13
(124653)	31	*Z*	3
(125346)	18	*Z*	6
(125364)	40	*X*	
(125436)	20	*Z*	9
(125463)	18	*X*	2
(125634)	47	*Z*	
(125643)	40	*Z*	3
(126345)	13	*Z*	2
(126354)	38	*X*	
(126435)	19	*Z*	5
(126453)	19	*X*	2
(126534)	38	*Z*	4
(126543)	45	*Z*	11
(132456)	28	*X*	9
(132465)	27	*Z*	10
(132546)	36	*Z*	2
(132564)	10	*X*	12
(132645)	43	*Z*	6
(132654)	9	*X*	13
(134256)	10	*X*	3
(134265)	16	*Z*	11
(134526)	43	*X*	2
(134562)	2	*Z*	11
(134625)	44	*X*	2
(134652)	6	*Z*	3
(135246)	41		
(135264)	14	*Z*	9
(135426)	43	*Z*	5
(135462)	6	*X*	13
(135624)	38	*X*	10
(135642)	15	*Z*	6
(136245)	42		
(136254)	44	*Z*	5
(136425)	23	*Z*	9
(136452)	6	*X*	12
(136524)	40	*X*	9
(136542)	32	*Z*	2
(142356)	37	*X*	10
(142365)	39	*X*	9
(142536)	41	*Z*	5
(142563)	30	*X*	12
(142635)	15	*Z*	9
(142653)	29	*X*	13
(143256)	26	*Z*	
(143265)	29	*Z*	4
(143526)	29	*X*	
(143562)	5	*Z*	4
(143625)	30	*X*	
(143652)	20	*Z*	
(145236)	43		
(145263)	42	*Z*	6
(145326)	34	*Z*	2
(145362)	5	*X*	13

Table 1 (Continued)

(145623)	13	*X*	9
(145632)	43	*Z*	9
(146235)	44		
(146253)	33	*Z*	2
(146325)	41	*Z*	6
(146352)	5	*X*	12
(146523)	12	*X*	10
(146532)	23	*Z*	5
(152346)	36	*X*	
(152364)	44	*Z*	11
(152436)	26	*X*	2
(152463)	33	*Z*	4
(152634)	8	*X*	9
(152643)	11	*X*	10
(153246)	41	*Z*	
(153264)	45		
(153426)	32	*X*	10
(153462)	27	*Z*	4
(153624)	33	*Z*	3
(153642)	48	*X*	3
(154236)	36	*Z*	3
(154263)	46		
(154326)	5	*X*	9
(154362)	21	*Z*	11
(154623)	44	*Z*	
(154632)	27	*X*	
(156234)	17	*Z*	5
(156243)	30	*Z*	2
(156324)	33	*X*	13
(156342)	39	*Z*	2
(156423)	36	*X*	13
(156432)	48	*Z*	5
(162345)	35	*X*	
(162354)	35	*Z*	3
(162435)	25	*X*	2
(162453)	42	*Z*	
(162534)	8	*X*	10
(162543)	11	*X*	9
(163245)	34	*Z*	4
(163254)	47		
(163425)	32	*X*	9
(163452)	22	*Z*	
(163524)	42	*Z*	11
(163542)	46	*X*	2
(164235)	43	*Z*	11
(164253)	48		
(164325)	5	*X*	10
(164352)	28	*Z*	3
(164523)	35	*Z*	4
(164532)	28	*X*	
(165234)	47	*Z*	9
(165243)	25	*Z*	6
(165324)	34	*X*	12
(165342)	46	*Z*	6
(165423)	35	*X*	12
(165432)	26	*Z*	9

Elements marked with asterisk

(to be used for $R_5{}^4$.)

(15)		*Y*	
(25)	2	*Y*	2
(35)	7	*Y*	7
(45)	8	*Y*	8

(125)		*Y*	2
(152)	2	*Y*	
(345)	14	*Y*	8
(354)	15	*Y*	7
(12)(35)	14	*Y*	7
(12)(45)	15	*Y*	8
(15)(34)	3	*Y*	
(25)(34)	5	*Y*	2
(12)(345)	7	*Y*	8
(12)(354)	8	*Y*	7
(13)(245)	5	*Y*	8
(13)(254)	15	*Y*	2
(14)(235)	5	*Y*	7
(14)(253)	14	*Y*	2
(23)(145)		*Y*	8
(23)(154)	8	*Y*	
(24)(135)		*Y*	7
(24)(153)	7	*Y*	
(34)(125)	3	*Y*	2
(34)(152)	5	*Y*	
(13245)	3	*Y*	8
(13254)	8	*Y*	2
(13524)	2	*Y*	7
(14235)	3	*Y*	7
(14253)	7	*Y*	2
(14523)	2	*Y*	8
(15324)	14	*Y*	
(15423)	15	*Y*	

TABLE II.

1	*E*	(1)	17	*CJ*	(1625)	33	*L*	(135)(246)
2	*A*	(12)	18	*BK*	(3546)	34	*QL*	(136)(245)
3	*B*	(34)	19	*CK*	(3645)	35	*RL*	(145)(236)
4	*C*	(56)	20	*S*	(12)(34)(56)	36	*PL*	(146)(235)
5	*P*	(12)(34)	21	*AK*	(12)(35)(46)	37	*M*	(153)(264)
6	*Q*	(12)(56)	22	*SK*	(12)(36)(45)	38	*PM*	(154)(263)
7	*I*	(13)(24)	23	*CI*	(13)(24)(56)	39	*RM*	(163)(254)
8	*PI*	(14)(23)	24	*SI*	(14)(23)(56)	40	*QM*	(164)(253)
9	*J*	(15)(26)	25	*BJ*	(15)(26)(34)	41	*AL*	(135246)
10	*QJ*	(16)(25)	26	*SJ*	(16)(25)(34)	42	*CL*	(136245)
11	*R*	(34)(56)	27	*PK*	(12)(3546)	43	*SL*	(145236)
12	*K*	(35)(46)	28	*QK*	(12)(3645)	44	*BL*	(146235)
13	*RK*	(36)(45)	29	*PJ*	(34)(1526)	45	*AM*	(153264)
14	*AI*	(1324)	30	*RJ*	(34)(1625)	46	*BM*	(154263)
15	*BI*	(1423)	31	*QI*	(56)(1324)	47	*SM*	(163254)
16	*AJ*	(1526)	32	*RI*	(56)(1423)	48	*CM*	(164253)

TABLE III.

R_3^2 the same as for R_4^1.

R_4^3

$A:\ (-1\ \ -1\ \ 1)$ $B:\ (-1\ \ 1\ \ -1)$ $P:\ (1\ \ -1\ \ -1)$

$$I:\ \begin{pmatrix} -1 & 0 & 0 \\ 0 & 0 & 1 \\ 0 & 1 & 0 \end{pmatrix} \qquad X:\ \frac{1}{2}\begin{pmatrix} 0 & -\sqrt{2} & \sqrt{2} \\ -\sqrt{2} & -1 & -1 \\ \sqrt{2} & -1 & -1 \end{pmatrix}$$

R_4^1

$A:\ (-1\ \ 1)$ $B:\ (-1\ \ 1)$ $P:\ (1\ \ 1)$ $I:\ (1\ \ 1)$

$$X:\ \frac{1}{2}\begin{pmatrix} 1 & -\sqrt{3} \\ -\sqrt{3} & -1 \end{pmatrix}$$

R_5^4

$A:\ (-1\ \ -1\ \ -1\ \ 1)$ $B:\ (-1\ \ -1\ \ 1\ \ -1)$ $P:\ (1\ \ 1\ \ -1\ \ -1)$

$$I:\ \begin{pmatrix} 1 & 0 & 0 & 0 \\ 0 & -1 & 0 & 0 \\ 0 & 0 & 0 & 1 \\ 0 & 0 & 1 & 0 \end{pmatrix}$$

$$X:\ \frac{1}{2}\begin{pmatrix} -2 & 0 & 0 & 0 \\ 0 & 0 & -\sqrt{2} & \sqrt{2} \\ 0 & -\sqrt{2} & -1 & -1 \\ 0 & -\sqrt{2} & -1 & -1 \end{pmatrix} \quad Y:\ \frac{1}{4}\begin{pmatrix} 1 & -\sqrt{5} & 0 & -\sqrt{10} \\ -\sqrt{5} & -3 & 0 & \sqrt{2} \\ 0 & 0 & -4 & 0 \\ -\sqrt{10} & \sqrt{2} & 0 & -2 \end{pmatrix} \quad Z:\ \frac{1}{4}\begin{pmatrix} -1 & -\sqrt{5} & \sqrt{10} & 0 \\ \sqrt{5} & 1 & \sqrt{2} & -2\sqrt{2} \\ 0 & 2\sqrt{2} & 2 & 2 \\ \sqrt{10} & -\sqrt{2} & 0 & 2 \end{pmatrix}$$

R_5^2 (the same as for R_6^1.)

R_6^5

$A:\ (-1\ -1\ \ 1\ -1\ -1)$ $B:\ (-1\ -1\ -1\ \ 1\ -1)$ $C:\ (-1\ -1\ -1\ -1\ \ 1)$
$P:\ (\ 1\ \ 1\ -1\ -1\ \ 1)$ $Q:\ (\ 1\ \ 1\ -1\ \ 1\ -1)$ $R:\ (\ 1\ \ 1\ \ 1\ -1\ -1)$
$S:\ (-1\ -1\ \ 1\ \ 1\ \ 1)$

$$I:\ \begin{pmatrix} 0 & 1 & 0 & 0 & 0 \\ 1 & 0 & 0 & 0 & 0 \\ 0 & 0 & 0 & 1 & 0 \\ 0 & 0 & 1 & 0 & 0 \\ 0 & 0 & 0 & 0 & 1 \end{pmatrix} \quad J:\ \begin{pmatrix} 0 & \omega & 0 & 0 & 0 \\ \omega^2 & 0 & 0 & 0 & 0 \\ 0 & 0 & 0 & 0 & 1 \\ 0 & 0 & 0 & 1 & 0 \\ 0 & 0 & 1 & 0 & 0 \end{pmatrix} \quad K:\ \begin{pmatrix} 0 & \omega^2 & 0 & 0 & 0 \\ \omega & 0 & 0 & 0 & 0 \\ 0 & 0 & 1 & 0 & 0 \\ 0 & 0 & 0 & 0 & 1 \\ 0 & 0 & 0 & 1 & 0 \end{pmatrix}$$

$$L:\ \begin{pmatrix} \omega & 0 & 0 & 0 & 0 \\ 0 & \omega^2 & 0 & 0 & 0 \\ 0 & 0 & 0 & 0 & 1 \\ 0 & 0 & 1 & 0 & 0 \\ 0 & 0 & 0 & 1 & 0 \end{pmatrix} \quad M:\ \begin{pmatrix} \omega^2 & 0 & 0 & 0 & 0 \\ 0 & \omega & 0 & 0 & 0 \\ 0 & 0 & 0 & 1 & 0 \\ 0 & 0 & 0 & 0 & 1 \\ 0 & 0 & 1 & 0 & 0 \end{pmatrix}$$

$$X:\ \frac{1}{2}\begin{pmatrix} -1 & -1 & -i & i & 0 \\ -1 & -1 & i & -i & 0 \\ i & -i & -1 & -1 & 0 \\ -i & i & -1 & -1 & 0 \\ 0 & 0 & 0 & 0 & -2 \end{pmatrix} \quad Z:\ \frac{1}{2}\begin{pmatrix} -\omega^2 & 0 & i & i\omega & i\omega^2 \\ 0 & -\omega & -i & -i\omega^2 & -i\omega \\ i\omega & -i\omega^2 & 1 & 0 & 1 \\ i & -i & 1 & 1 & 0 \\ i\omega^2 & -i\omega & 0 & 1 & 1 \end{pmatrix}$$

$$\mathbf{R}_6^3$$

$A:\ (-1\ -1\ -1\ \ 1\ -1\ -1\ -1\ \ 1\ \ 1)$

$B:\ (-1\ -1\ -1\ -1\ \ 1\ -1\ \ 1\ -1\ \ 1)$

$C:\ (-1\ -1\ -1\ -1\ -1\ \ 1\ \ 1\ \ 1\ -1)$

$P:\ (\ 1\ \ 1\ \ 1\ -1\ -1\ \ 1\ -1\ -1\ \ 1)$

$Q:\ (\ 1\ \ 1\ \ 1\ -1\ \ 1\ -1\ -1\ \ 1\ -1)$

$R:\ (\ 1\ \ 1\ \ 1\ \ 1\ -1\ -1\ \ 1\ -1\ -1)$

$S:\ (-1\ -1\ -1\ \ 1\ \ 1\ \ 1\ -1\ -1\ -1)$

$$I:\ \begin{pmatrix}
1 & \cdot & \cdot & \cdot & \cdot & \cdot & \cdot & \cdot & \cdot \\
\cdot & \cdot & 1 & \cdot & \cdot & \cdot & \cdot & \cdot & \cdot \\
\cdot & 1 & \cdot & \cdot & \cdot & \cdot & \cdot & \cdot & \cdot \\
\cdot & \cdot & \cdot & \cdot & 1 & \cdot & \cdot & \cdot & \cdot \\
\cdot & \cdot & \cdot & 1 & \cdot & \cdot & \cdot & \cdot & \cdot \\
\cdot & \cdot & \cdot & \cdot & \cdot & -1 & \cdot & \cdot & \cdot \\
\cdot & \cdot & \cdot & \cdot & \cdot & \cdot & \cdot & 1 & \cdot \\
\cdot & \cdot & \cdot & \cdot & \cdot & \cdot & 1 & \cdot & \cdot \\
\cdot & \cdot & \cdot & \cdot & \cdot & \cdot & \cdot & \cdot & 1
\end{pmatrix}
\qquad
J:\ \begin{pmatrix}
1 & \cdot & \cdot & \cdot & \cdot & \cdot & \cdot & \cdot & \cdot \\
\cdot & \cdot & \omega & \cdot & \cdot & \cdot & \cdot & \cdot & \cdot \\
\cdot & \omega^2 & \cdot & \cdot & \cdot & \cdot & \cdot & \cdot & \cdot \\
\cdot & \cdot & \cdot & \cdot & \cdot & -1 & \cdot & \cdot & \cdot \\
\cdot & \cdot & \cdot & \cdot & -1 & \cdot & \cdot & \cdot & \cdot \\
\cdot & \cdot & \cdot & -1 & \cdot & \cdot & \cdot & \cdot & \cdot \\
\cdot & \cdot & \cdot & \cdot & \cdot & \cdot & \cdot & \cdot & 1 \\
\cdot & \cdot & \cdot & \cdot & \cdot & \cdot & \cdot & 1 & \cdot \\
\cdot & \cdot & \cdot & \cdot & \cdot & \cdot & 1 & \cdot & \cdot
\end{pmatrix}$$

$$:\ \begin{pmatrix}
1 & \cdot & \cdot & \cdot & \cdot & \cdot & \cdot & \cdot & \cdot \\
\cdot & \cdot & \omega^2 & \cdot & \cdot & \cdot & \cdot & \cdot & \cdot \\
\cdot & \omega & \cdot & \cdot & \cdot & \cdot & \cdot & \cdot & \cdot \\
\cdot & \cdot & \cdot & -1 & \cdot & \cdot & \cdot & \cdot & \cdot \\
\cdot & \cdot & \cdot & \cdot & \cdot & 1 & \cdot & \cdot & \cdot \\
\cdot & \cdot & \cdot & \cdot & 1 & \cdot & \cdot & \cdot & \cdot \\
\cdot & \cdot & \cdot & \cdot & \cdot & \cdot & 1 & \cdot & \cdot \\
\cdot & \cdot & \cdot & \cdot & \cdot & \cdot & \cdot & \cdot & 1 \\
\cdot & \cdot & \cdot & \cdot & \cdot & \cdot & \cdot & 1 & \cdot
\end{pmatrix}$$

$$L:\ \begin{pmatrix}
1 & \cdot & \cdot & \cdot & \cdot & \cdot & \cdot & \cdot & \cdot \\
\cdot & \omega & \cdot & \cdot & \cdot & \cdot & \cdot & \cdot & \cdot \\
\cdot & \cdot & \omega^2 & \cdot & \cdot & \cdot & \cdot & \cdot & \cdot \\
\cdot & \cdot & \cdot & \cdot & \cdot & 1 & \cdot & \cdot & \cdot \\
\cdot & \cdot & \cdot & -1 & \cdot & \cdot & \cdot & \cdot & \cdot \\
\cdot & \cdot & \cdot & \cdot & -1 & \cdot & \cdot & \cdot & \cdot \\
\cdot & \cdot & \cdot & \cdot & \cdot & \cdot & \cdot & \cdot & 1 \\
\cdot & \cdot & \cdot & \cdot & \cdot & \cdot & 1 & \cdot & \cdot \\
\cdot & \cdot & \cdot & \cdot & \cdot & \cdot & \cdot & 1 & \cdot
\end{pmatrix}
\qquad
M:\ \begin{pmatrix}
1 & \cdot & \cdot & \cdot & \cdot & \cdot & \cdot & \cdot & \cdot \\
\cdot & \omega^2 & \cdot & \cdot & \cdot & \cdot & \cdot & \cdot & \cdot \\
\cdot & \cdot & \omega & \cdot & \cdot & \cdot & \cdot & \cdot & \cdot \\
\cdot & \cdot & \cdot & \cdot & -1 & \cdot & \cdot & \cdot & \cdot \\
\cdot & \cdot & \cdot & \cdot & \cdot & -1 & \cdot & \cdot & \cdot \\
\cdot & \cdot & \cdot & 1 & \cdot & \cdot & \cdot & \cdot & \cdot \\
\cdot & \cdot & \cdot & \cdot & \cdot & \cdot & \cdot & 1 & \cdot \\
\cdot & \cdot & \cdot & \cdot & \cdot & \cdot & \cdot & \cdot & 1 \\
\cdot & \cdot & \cdot & \cdot & \cdot & \cdot & 1 & \cdot & \cdot
\end{pmatrix}$$

$$X:\ \begin{pmatrix}
-1 & \sqrt{10} & \sqrt{10} & \cdot & \cdot & \cdot & \cdot & \cdot & -\sqrt{15} \\
\sqrt{10} & -1 & -1 & 3i & -3i & \cdot & \cdot & \cdot & -\sqrt{6} \\
\sqrt{10} & -1 & -1 & -3i & 3i & \cdot & \cdot & \cdot & -\sqrt{6} \\
\cdot & -3i & 3i & -3 & -3 & \cdot & \cdot & \cdot & \cdot \\
\cdot & 3i & -3i & -3 & -3 & \cdot & \cdot & \cdot & \cdot \\
\cdot & \cdot & \cdot & \cdot & \cdot & \cdot & -3\sqrt{2} & 3\sqrt{2} & \cdot \\
\cdot & \cdot & \cdot & \cdot & \cdot & -3\sqrt{2} & -3 & -3 & \cdot \\
\cdot & \cdot & \cdot & \cdot & \cdot & 3\sqrt{2} & -3 & -3 & \cdot \\
-\sqrt{15} & -\sqrt{6} & -\sqrt{6} & \cdot & \cdot & \cdot & \cdot & \cdot & -3
\end{pmatrix}$$

$$Z:\ \frac{1}{4}\begin{pmatrix} -1 & 0 & 0 & -\sqrt{\frac{10}{3}} & \sqrt{\frac{10}{3}} & -\sqrt{\frac{10}{3}} & \sqrt{\frac{5}{3}} & \sqrt{\frac{5}{3}} & \sqrt{\frac{5}{3}} \\ 0 & 2\omega^2 & 0 & -\frac{2}{\sqrt{3}} & \frac{2\omega}{\sqrt{3}} & -\frac{2\omega^2}{\sqrt{3}} & -2\sqrt{\frac{2}{3}} & -2\sqrt{\frac{2}{3}}\omega & -2\sqrt{\frac{2}{3}}\omega^2 \\ 0 & 0 & 2\omega & -\frac{2}{\sqrt{3}} & \frac{2\omega^2}{\sqrt{3}} & -\frac{2\omega}{\sqrt{3}} & -2\sqrt{\frac{2}{3}} & -2\sqrt{\frac{2}{3}}\omega^2 & -2\sqrt{\frac{2}{3}}\omega \\ \sqrt{\frac{10}{3}} & \frac{2}{\sqrt{3}}\omega & \frac{2}{\sqrt{3}}\omega^2 & 0 & 2 & 0 & -\sqrt{2} & \sqrt{2} & -\sqrt{2} \\ -\sqrt{\frac{10}{3}} & -\frac{2}{\sqrt{3}} & -\frac{2}{\sqrt{3}} & 0 & 0 & 2 & \sqrt{2} & \sqrt{2} & -\sqrt{2} \\ \sqrt{\frac{10}{3}} & \frac{2}{\sqrt{3}}\omega^2 & \frac{2}{\sqrt{3}}\omega & -2 & 0 & 0 & \sqrt{2} & -\sqrt{2} & -\sqrt{2} \\ \sqrt{\frac{5}{3}} & -2\sqrt{\frac{2}{3}}\omega & -2\sqrt{\frac{2}{3}}\omega^2 & \sqrt{2} & \sqrt{2} & \sqrt{2} & 1 & 1 & 1 \\ \sqrt{\frac{5}{3}} & -2\sqrt{\frac{2}{3}} & -2\sqrt{\frac{2}{3}} & \sqrt{2} & -\sqrt{2} & -\sqrt{2} & 1 & 1 & 1 \\ \sqrt{\frac{5}{3}} & -2\sqrt{\frac{2}{3}}\omega^2 & -2\sqrt{\frac{2}{3}}\omega & -\sqrt{2} & -\sqrt{2} & \sqrt{2} & 1 & 1 & 1 \end{pmatrix}$$

$\mathbf{R}_6^1$

$A:\ (-1\ \ 1\ \ -1\ \ -1\ \ 1)$ $B:\ (-1\ \ -1\ \ 1\ \ -1\ \ 1)$ $C:\ (-1\ \ -1\ \ -1\ \ 1\ \ 1)$

$P:\ (1\ \ -1\ \ -1\ \ 1\ \ 1)$ $Q:\ (1\ \ -1\ \ 1\ \ -1\ \ 1)$ $R:\ (1\ \ 1\ \ -1\ \ -1\ \ 1)$

$S:\ (-1\ \ 1\ \ 1\ \ 1\ \ 1)$

$$I:\ \begin{pmatrix} -1 & \cdot & \cdot & \cdot & \cdot \\ \cdot & \cdot & 1 & \cdot & \cdot \\ \cdot & 1 & \cdot & \cdot & \cdot \\ \cdot & \cdot & \cdot & 1 & \cdot \\ \cdot & \cdot & \cdot & \cdot & 1 \end{pmatrix} \qquad J:\ \begin{pmatrix} -1 & \cdot & \cdot & \cdot & \cdot \\ \cdot & \cdot & \cdot & 1 & \cdot \\ \cdot & \cdot & 1 & \cdot & \cdot \\ \cdot & 1 & \cdot & \cdot & \cdot \\ \cdot & \cdot & \cdot & \cdot & 1 \end{pmatrix} \qquad K:\ \begin{pmatrix} -1 & \cdot & \cdot & \cdot & \cdot \\ \cdot & 1 & \cdot & \cdot & \cdot \\ \cdot & \cdot & \cdot & 1 & \cdot \\ \cdot & \cdot & 1 & \cdot & \cdot \\ \cdot & \cdot & \cdot & \cdot & 1 \end{pmatrix}$$

$$L:\ \begin{pmatrix} 1 & \cdot & \cdot & \cdot & \cdot \\ \cdot & \cdot & \cdot & 1 & \cdot \\ \cdot & 1 & \cdot & \cdot & \cdot \\ \cdot & \cdot & 1 & \cdot & \cdot \\ \cdot & \cdot & \cdot & \cdot & 1 \end{pmatrix} \qquad M:\ \begin{pmatrix} 1 & \cdot & \cdot & \cdot & \cdot \\ \cdot & \cdot & 1 & \cdot & \cdot \\ \cdot & \cdot & \cdot & 1 & \cdot \\ \cdot & 1 & \cdot & \cdot & \cdot \\ \cdot & \cdot & \cdot & \cdot & 1 \end{pmatrix}$$

$$X:\ \frac{1}{2}\begin{pmatrix} 0 & \sqrt{2} & -\sqrt{2} & 0 & 0 \\ \sqrt{2} & -1 & -1 & 0 & 0 \\ -\sqrt{2} & -1 & -1 & 0 & 0 \\ 0 & 0 & 0 & 1 & -\sqrt{3} \\ 0 & 0 & 0 & -\sqrt{3} & -1 \end{pmatrix} \qquad Z:\ \frac{1}{4}\begin{pmatrix} -2 & \sqrt{2} & \sqrt{2} & \sqrt{2} & -\sqrt{6} \\ -\sqrt{2} & -1 & 3 & -1 & \sqrt{3} \\ -\sqrt{2} & -1 & -1 & 3 & \sqrt{3} \\ -\sqrt{2} & 3 & -1 & -1 & \sqrt{3} \\ \sqrt{6} & \sqrt{3} & \sqrt{3} & \sqrt{3} & 1 \end{pmatrix}$$

Interaction between Electrons and Ions in Semiconductors. I.

By Ryogo KUBO.

Physical Departement. Faculty of Science, University of Tokyo.

(Read Oct. 1944, and Oct. 1946; Received Octover 29, 1947).

Introduction.

In ionic crystals the interaction between electrons and charged ions in the lattices is so strong that the electronic motion and the vibrations of lattice ions are too closely coupled with each other to be separated. For example, when an electron is trapped in a defect of the lattice, its charge distribution causes a certain local polarization of the lattice and the wave function of the electron itself must be affected by this polarization. This situation was already pointed out by Mott and Gurney⑴. Theoretical computation, however, has not been carried out.

This strong coupling makes it also possible that an electron may dig its own hole in an ionic crystal and be trapped in it as suggested by Landau⑵. Though this possibility has not yet been realized by experiments, it has a rather sound theoretical basis, and its detailed discussion may throw light on various properties of semiconductors.

In this article the coupling between electrons and the ionic lattice will be discussed to the approximation in which the lattice is replaced roughly by a continuous dielectric medium with static and optical dielectric constants, κ and κ_0. More rigorous treatment considering the atomic structure of the lattice will be given in another occasion.

In the section 1, it will generally be shown that the normal electronic state of a localized electron is determined by the minimum condition of the energy of the whole system including the electron and the lattice. According to this theorem the electronic wave function and the polarization of the lattice can be calculated by the variation method. For simplicity, the computation has been made for the model that the lattice defect is represented by an extra charge embedded in the continuum.

§ 1. A Fundamental Theorem.

Suppose that an electron is trapped at a lattice defect which can be approximately represented by an extra positive charge Q locarized in an ideal ionic lattice. The energy of the total system consisting of the electron and the lattice is then composed of interaction energy terms U_1 between Q and the lattice, U_2 between the electron and the lattice, and U_3 between Q and the electron, the internal energy U_4 of the lattice polarized by the charge of the electron, and finally the kinetic energy K of the electron (*cf.* Fig. 1).

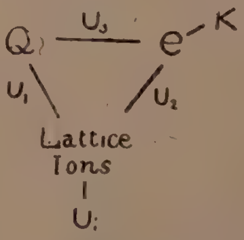

Fig. 1.

The polarization of the lattice cannot closely follow the rapid motion of the electron. Regarding the space charges due to the polarization as true charges, we can suppose that the charges due to the polarization, lattice defect and the electron are mutually interacting through the medium with dielectric constant κ_0, which is due to the polarization of ionic cores of the lattice and represents the shielding effect of the electric interaction between the true charges. When the energy state of the whole system is stable, the ionic lattice must be polarized by the average distribution of the electron. Thus the energy terms mentioned above are functionals of the wave function ψ and the polarization $\boldsymbol{P}_4(\boldsymbol{r})$. The total energy must be minimized by suitable choice of ψ and $\boldsymbol{P}_4(\boldsymbol{r})$. Any deviation of the electronic distribution from its final stable one causes displacements in the lattice and then change in the wave function. Thus repeating the process, the whole system approaches to the stable state, the excess energy being emitted into the medium as heat waves during the relaxation process.

The energies U_1, U_2 and U_i are the functionals of $\boldsymbol{P}_i$; U_2 involves also the wave function ψ of the electron, while U_3 and K are the functionals depending only on ψ. The energy of the electron takes the form

$$H(\psi, \boldsymbol{P}_i) = K(\psi)+U_2(\psi, \boldsymbol{P}_i)+U_3(\psi). \tag{1}$$

The electrostatic energy U of the lattice is given by

$$U = U_1(\boldsymbol{P}_i)+U_2(\psi, \boldsymbol{P}_i)+U_i(\boldsymbol{P}_i). \tag{2}$$

It must be noted that U does not include the term U_3. The total energy E of the system is of course

$$\begin{aligned} E &= U_1+U_2+U_3+U_i+K \\ &= H+U_P, \end{aligned} \tag{3}$$

where

$$U_P = U_1+U_i \tag{4}$$

is independent of ψ.

The electronic energy H, determined by the Schrödinger's equation for the electron which involves $\boldsymbol{P}_i$ as a parameter, is the adiabatic potential for the vibration of the lattice. The stable state of the system, the electron plus the lattice, must be described by the polarization $\boldsymbol{P}_i$ which corresponds to the minimum of E. Thus we proceed in the following manner.

By the Schrödinger's equation

$$\left(\frac{\delta H}{\delta\psi}\right)_{\boldsymbol{P}_i} = 0, \tag{5}$$

ψ can be found as a functional of $\boldsymbol{P}_i$. (The notation in Eq. (5) means that we take the variation of H as the functional of ψ with given $\boldsymbol{P}_i$). Then the stable state is to be determined by the condition

$$\delta E = 0 \tag{6}$$

or

$$\begin{aligned} \frac{\delta E(\psi(\boldsymbol{P}_i), \boldsymbol{P}_i)}{\delta \boldsymbol{P}_i} &= \frac{\delta H}{\delta \boldsymbol{P}_i}+\frac{\delta U_P}{\delta \boldsymbol{P}_i} \\ &= \left(\frac{\delta H}{\delta\psi}\right)_{\boldsymbol{P}_i}\left(\frac{\delta\psi}{\delta \boldsymbol{P}_i}\right)+\left(\frac{\delta H}{\delta \boldsymbol{P}_i}\right)_{\psi} \\ &\quad +\frac{\delta U_P}{\delta \boldsymbol{P}_i} = 0. \end{aligned} \tag{6'}$$

According to the condition (5), Eq. (6)′ reduces to

$$\left(\frac{\delta U}{\delta \boldsymbol{P}_i}\right)_{\psi} = 0. \tag{7}$$

By the use of Eqs. (1), (2) and (4) Eq. (7) tells us that the polarization $\boldsymbol{P}_i$ is determined by the minimum condition of U for given ψ. It is nothing but the field equation of the electrostatics in which the defect charge and the charge distribution of the trapped electron are given as the sources.

If the functional form of $\boldsymbol{P}_i(\psi)$ is known by Eq. (7), the condition (6) becomes

$$\begin{aligned} 0 = \frac{\delta E(\psi, \boldsymbol{P}_i(\psi))}{\delta\psi} &= \left(\frac{\delta H}{\delta\psi}\right)_{\boldsymbol{P}_i}+\left(\frac{\delta H}{\delta \boldsymbol{P}_i}\right)_{\psi}\frac{\delta \boldsymbol{P}_i}{\delta\psi} \\ &\quad +\left(\frac{\delta U_P}{\delta \boldsymbol{P}_i}\right)_{\psi}\frac{\delta \boldsymbol{P}_i}{\delta\psi} \\ &= \left(\frac{\delta H}{\delta\psi}\right)_{\boldsymbol{P}_i}+\left(\frac{\delta(U_2+U_P)}{\delta \boldsymbol{P}_i}\right)_{\psi}\frac{\delta \boldsymbol{P}_i}{\delta\psi} = \left(\frac{\delta H}{\delta\psi}\right)_{\boldsymbol{P}_i} \end{aligned}$$

Thus we arrive at the theorem:

The condition of

$$\left(\frac{\delta H}{\delta\psi}\right)_{\boldsymbol{P}_i} = 0 \tag{Ia}$$

and

$$\frac{\delta E(\psi(\boldsymbol{P}_i), \boldsymbol{P}_i)}{\delta \boldsymbol{P}_i} = 0 \tag{Ib}$$

is equivalent to that of

$$\left(\frac{\delta U}{\delta \boldsymbol{P}_i}\right)_{\psi} = 0 \tag{IIa}$$

and

$$\frac{\delta E(\psi, \boldsymbol{P}_i(\psi))}{\delta\psi} = 0. \tag{IIb}$$

Usually we apply the method (I). The functional $\psi(\boldsymbol{P}_i)$, however, cannot easily be known in its completely analytical form, while $\boldsymbol{P}_i(\psi)$ can easily be obtained by the electrostatics.

It might be worth while to note that the process of determining the stable state through the equations

$$\left(\frac{\delta U}{\delta \boldsymbol{P}_i}\right)_{\psi} = 0$$

and

$$\frac{\delta H(\psi, \boldsymbol{P}_i(\psi))}{\delta\psi} = 0$$

cannot be justified. This means that we try to get the stable state by the Schrödinger's equation in which the potential itself involves the wave function, its functional form being obtained by the solution of the electrostatic equation (IIa).

This procedure has been suggested by Mott and Gurney(3) as a self-consistent equation. However, it is erroneous as shown above and, instead, we must take (IIb).

§ 2. Explicit Forms of the Energy.

As a first approximation, we take here the hole model. Suppose that a spherical hole with the radius a is made in the continuous dielectric and the charge Q is localized in the centre or distributed on the wall of the hole, in which an electron is trapped.

Let $\boldsymbol{P}_i$ and ρ_i denote the dipole moment and the space charge density caused by the displacement of the lattice ions. According to the electrostatics they are related by

$$\rho_i = -div\, \boldsymbol{P}_i\,. \tag{8}$$

The total polarization, that is, the sum of the ionic and the electronic polarzation is expressed by $\boldsymbol{P}$, which is given by

$$\boldsymbol{P} = (\chi_i + \chi_e)\boldsymbol{E}, \tag{9}$$

where $\boldsymbol{E}$ is the strength of the electric field, and χ_i and χ_e are the ionic and electronic susceptibilities respectively, which are related to the dielectric constants by the formulae

$$\begin{aligned} \kappa &= 1+4\pi(\chi_i+\chi_e) \\ \kappa_0 &= 1+4\pi\chi_e\,. \end{aligned} \tag{10}$$

Eq. (7) takes the form

$$\operatorname{div} \boldsymbol{D} = 4\pi(\rho_+ - \rho_-), \tag{11}$$

where $\boldsymbol{D}$ is the electric displacement, ρ_+ and ρ_- the charge densities of the extra defect charge and of the trapped electron. By Eqs. (8), (9), (10) and (11) we get

$$\boldsymbol{P}_i = \frac{1}{4\pi}\left(1-\frac{\kappa_0}{\kappa}\right)\boldsymbol{D} \tag{12}$$

$$\rho_i = -\left(1-\frac{\kappa_0}{\kappa}\right)(\rho_+ - \rho_-). \tag{13}$$

Eqs. (11), (12) and (13) give us $\boldsymbol{P}_i$ and ρ_i in terms of the wave function ψ.

In particular, if ρ_+ and ρ_- are spherically symmetric, the solution of (11) is given by

$$D(r) = \frac{e}{r^2}(p_+ - p_-), \tag{14}$$

where we put

$$ep_\pm = \int_0^r \rho_\pm 4\pi r^2 dr. \tag{15}$$

Similarly we define

$$ep_i = \int_0^r \rho_i 4\pi r^2 dr, \tag{16}$$

for which we get

$$p_i = -\left(1-\frac{\kappa_0}{\kappa}\right)(p_+ - p_-) = -cf(r), \tag{17}$$

where

$$c = 1-\frac{\kappa_0}{\kappa}, \quad f(r) = p_+(r) - p_-(r), \tag{18}$$

Eq. (17) describes the stable polarization of the lattice for the case where the defect and the electronic charge distribution is specified.

When polarized, the lattice is strained and in a somewhat higher energy state. Its internal energy U_i is

$$U_i = \frac{1}{2}\iiint \rho_i \varphi_i dv + \frac{1}{2\chi_i}\iiint \boldsymbol{P}_i^2 dv, \tag{19}$$

where φ_i is the electrostatic potential due to the polarization itself, namely,

$$\varphi_i = -\int_\infty^r \frac{ep_i}{\kappa_0 r^2}dr. \tag{20}$$

The second term of (19) is of the mechanical nature.

Integrating the first term of (19) by part and making use of Eqs. (10), (12), (14), (12) and (18), we get

$$\begin{aligned} U_i &= \frac{e^2}{2\kappa_0}\frac{\kappa}{\kappa-\kappa_0}\int_r^\infty \frac{p_i^2}{r^2}dr \\ &= \frac{e^2 c}{2\kappa_0}\int_r^\infty (f^2/r^2)dr. \end{aligned} \tag{21}$$

Next we bring the defect charge Q into the polarized lattice. Naturally the ions are then fixed in the displaced positions. The work to be done in this process consists of two parts; the first one W_1 must be done against the electric force due to the space charge caused by the polarization, and the second W_2 against the reaction field in the medium with the dielectric constant κ_0. W_1 is given by

$$W_1 = -\int_0^\infty 4\pi\rho_+ r^2 dr\int_\infty^r \frac{ep_i}{\kappa_0 r^2}dr = \int_0^\infty \frac{e^2 p_+ p_i}{\kappa_0 r^2}dr.$$

Thus we get

$$U_1' = \int_0^\infty \frac{e^2 p_+ p_i}{\kappa_0 r^2} dr + W_2 = \frac{e^2 c}{\kappa_0}\int_0^\infty \frac{p_+ f}{r^2} dr + W_2 . \tag{22}$$

Hence we have

$$U_P = \frac{e^2 c}{\kappa_0}\int_0^\infty \frac{(f+p_+)^2 - p_+^{\,2}}{r^2} dr + W_2$$

$$= \frac{e^2 c}{2\kappa_0}\int_0^\infty \frac{p_-^{\,2}}{r^2} dr + \text{constant}, \tag{23}$$

where the additive constant is independent of the distribution of the electron.

As the third step we bring the electron into the lattice. The force $F(r)$ acting on it is divided into two parts; one is the force due to the charges ρ_+ and ρ_i, and the other is the image force F_i which depends on the shape of the hole. We have, therefore,

$$F(r) = \frac{e^2}{\kappa_0 r^2}(p_+ + p_i) + F_i(r), \text{ for } r > a. \tag{24}$$

The work required to construct the electron cloud in the lattice is thus given by

$$U_e = U_0 + U_2$$

$$= \int_0^\infty 4\pi r^2 \frac{\rho_-}{e} dr \int_\infty^r F(r) dr = -\int_0^\infty F(r) p_-(r) dr \tag{25}$$

In absence of the hole (i. e. $a = 0$) Eq. (25) takes the simpler form.

$$U_e = -\frac{e^2}{\kappa_0}\int_0^\infty \frac{(p_+ + p_i)p_-}{r^2} dr \tag{26}$$

If the hole exists, the effect of the image force is to be taken into account though it is rather complicated. Moreover, the continuum model fails to be valid near the hole and its relation to the actual atomic structure is not easily seen. If we assume F to be identically equal to zero in the sphere with radius R and neglect the image force approximately, Eq. (25) becomes

$$U_e = -\int_R^\infty \frac{e^2}{\kappa_0 r^2}(p_+ + p_i) p_- dr. \tag{27}$$

If the potential is assumed to drop by the amount ΔV abruptly at $r = R$, (27) is replaced by

$$U_e = -\int_R^\infty \frac{e^2}{\kappa_0 r^2}(p_+ + p_i) p_- dr - \Delta V p_-(R). \tag{28}$$

These models are similar to those of Tibbs(4), the difference being the inclusion of the effects due to the displacement of ions.

The kinetic energy K is expressed in terms of ψ in the usual manner. Thus we have expressions for all the energy terms mentioned at the beginning of the section 1.

§ 3. Electron Trapped by the Positive Defect in a Dielectric Continuum.

As the simplest case, we shall suppose that a positive point charge of valence 1, is embedded in a continuous dielectric medium. At first no hole is assumed to exist. As the trial wave function of a trapped electron we take

$$\psi = \left(\frac{\alpha^3}{8\pi}\right)^{1/2} \exp(-\alpha r/2), \tag{29}$$

the space density being given by

$$\rho_- = \frac{e\alpha^3}{8\pi} e^{-\alpha r}. \tag{30}$$

Thus we have

$$1 - p_- = (1 + \alpha r + \frac{1}{2}\alpha^2 r^2) e^{-\alpha r}. \tag{31}$$

In the stable configuration of the lattice, we have, from Eq. (17),

$$p_i = -c(1 - p_-) \tag{32}$$

Hence

$$U_e = -\int_0^\infty \frac{e^2}{\kappa_0 r^2}\{1 - c(1 - p_-)\} p_- dr. \tag{33}$$

Integrating by parts, we get

$$U_e = -\frac{e^2}{\kappa_0}\{(1+c)q - 2cs\},$$

where q and s are the integrals

$$q = \frac{\alpha^3}{2}\int_0^\infty e^{-\alpha r} r dr = \alpha/2$$

$$s = \frac{\alpha^3}{2}\int_0^\infty 1 + \alpha r + \frac{1}{2}\alpha^2 r^2) e^{-2\alpha r} r dr = \frac{11}{2}\alpha.$$

Thus, the integral (33) becomes

$$U_e = -\frac{e^2 \alpha}{2\kappa_0}(1 - \frac{3}{8}c). \tag{34}$$

Taking the ionized state as our zero point of the energy, we get

$$U_p = \frac{e^2 c}{2\kappa_0}\int_0^\infty \frac{p_-^{\,2}}{r^2} dr = \frac{e^3 c}{2\kappa_0} 2(q - s)$$

$$= \frac{e^2 c}{2\kappa_0} \cdot \frac{5}{16}\alpha \tag{35}$$

by Eq. (23). The kinetic energy of the electron is

$$K=\frac{\hbar^2}{2m}\frac{\alpha^2}{4} \tag{36}$$

The energy H of the electron and the total energy E of the whole system are given by

$$H=\frac{\hbar^2}{2m}\frac{\alpha^2}{4}-\frac{e^2\alpha}{2\kappa_0}\left(1-\frac{3}{8}c\right) \tag{37}$$

and

$$E=H+U_p=\frac{h^2}{2m}\frac{\alpha^2}{4}-\frac{e^2\alpha}{2\kappa_0}\left(1-\frac{11}{16}c\right), \tag{38}$$

which is transformed into

$$E=\frac{W_H}{\kappa_0{}^2}\left\{x^2-2x\left(1-\frac{11}{16}c\right)\right\}, \tag{39}$$

where

$$x=\frac{1}{2}\alpha a_0\kappa_0,\quad a_0=\hbar^2/me^2, \tag{40}$$

W_H is the Rydberg's constant and a_0 the radius of the hydrogen atom.

The stable state is determined by the condition

$$dE/dx=0, \tag{41}$$

which gives the lowest $1s$ state of the trapped electron as follows.

$$E_{1s}=-\frac{W_H}{\kappa_0{}^2}\left(1-\frac{11}{16}c\right)^2, \tag{42}$$

The radius of the electron cloud is given by

$$\frac{1}{\alpha}=\frac{\kappa_0 a_0}{2\left(1-\frac{11}{16}c\right)}. \tag{43}$$

The polarization energy is written as

$$U_p=\frac{W_H}{\kappa_0{}^2}\frac{5}{8}c\left(1-\frac{11}{16}c\right) \tag{44}$$

and

$$H_{1s}=E_{1s}-U_p=-\frac{W_H}{\kappa_0{}^2}\left(1-\frac{11}{16}c\right)\left(1-\frac{1}{16}c\right). \tag{45}$$

The thermal work function φ_{th}, that is, the work required to ionize the trapped electron by thermal agitation, is equal to $-E$, while the optical work function ϕ_{ph} is equal to $-H$. The ratio of the two quantities is

$$\phi_{\text{th}}/\phi_{\text{ph}}=\frac{1-\frac{11}{16}c}{1-\frac{1}{16}c}=\frac{5\kappa+11\kappa_0}{15\kappa+\kappa_0}, \tag{46}$$

which is naturally smaller than 1 in accordance with the Frank-Condon's principle. Only in the case $\kappa=\kappa_0$, or in the absence of ionic displacement, the two work functions are equal to each other. In Fig. 2 E, H, and $\phi_{\text{th}}/\phi_{\text{ph}}$ are given as functions of κ_0/κ.

The F-band in alkali-halide crystals is generally supposed to be caused by the electrons trapped at vacant negative lattice points or the defect extra positive charge. It is the absorption due to the transtion from 1_s state to 2_p of the trapped electron. The 2_p state will be discussed in the next paper.

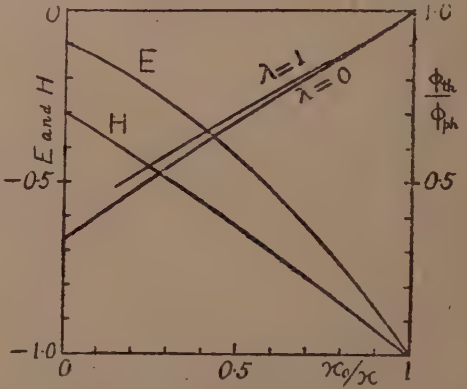

Fig. 2. E, H and $\phi_{th}/\phi_{ph}(=|E|/|H|)$ as functions of κ_0/κ. The unit of the ordinate for E and H is $W_H/\kappa_0{}^2$. The curve $\lambda=1$ represents ϕ_{th}/ϕ_{ph} for the modified hole model (cf. §4) where E is assumed equal to zero.

The result obtained above shows that the expected absorption lies in far infrared regions in contradiction to the experience. This discrepancy, of course, comes from the inappropriateness of our model. However, better agreements cannot be expected by any model of such hole type in which we cut off the potential at a radius R and put the inner potential equal to its heigt at R. In such a model the 1_s state will still be of higher energy. As was shown by Tibbs(4), the absorption frequency expected from the mentioned model is smaller than the experimental values, even when the polarization effect is not taken into account.

§ 4. A modified Hole Model.

Now, we shall take a hole model which is shown in Fig 3; the potential is assumed to jump by the amount ΔV at the wall $r=R$. We apply to this model the method described above.

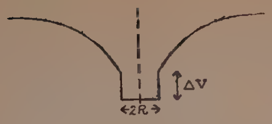

Fig. 3.

As the simplest trial wave function we choose

$$\psi = \varphi\left(\frac{\alpha^3}{56\pi}\right)^{1/2}\left(1+\frac{\alpha r}{2}\right)e^{-\alpha r/2}, \tag{47}$$

for the derivative must vanish at $r = 0$. With this wave function ψ we obtain from the equation (15)

$$p_-(r) = 1-\left\{1+\alpha r+\frac{1}{2}(\alpha r)^2+\frac{1}{7}(\alpha r)^3+\frac{1}{56}(\alpha r)^4\right\}e^{-\alpha r}. \tag{48}$$

When we calculate the integrals of the types (23) and (33) by integration by part, attention must be paid to the contribution from the point $r = R$. After some elementary calculations, we get

$$E = \frac{W_H}{\kappa_0{}^2}\Big[\frac{3}{28}\lambda^2\xi^2+\lambda\{2(f_1(\xi)e^{-\xi}-cf_2(\xi)^{-2\xi})-(2-c)\} \\ -\epsilon p_-(R)\Big], \tag{49}$$

where

$$f_1(\xi) = 1+0.67856\xi+0.17856\xi^2+0.017857\xi^3$$
$$f_2(\xi) = 0.5+0.78566\xi+0.57130\xi^2+0.24988\xi^3 \\ +0.07135\xi^4+0.013354\xi^5+0.001515\xi^6 \\ +0.0000798\xi^7 \tag{50}$$

and

$$\xi = \alpha R, \quad \lambda = \kappa_0 a_0/R, \quad \epsilon = \kappa_0{}^2 \varDelta V/W_H, \tag{51}$$

The stable 1*s* state can be obtained by the condition (IIb) for various values of λ, ϵ and c. For $\epsilon = 0$, $|E|$ decreases with increasing λ as is naturally expected. In Fig. 2, $|E|/|H|$ is shown as the function of c for $\lambda = 1$ and $\epsilon = 0$. It runs closely to the curve for $\lambda = 0$ given by Eq. (46). Fig. 4 shows E, H and $|E|/|H|$ as functions of ϵ for the case where $c = 0.6$ and $\lambda = 1$. The ratio $|E|/|H|$ varies rather slowly with ϵ, whole $|E|$ and $|H|$ themselves increase with ϵ.

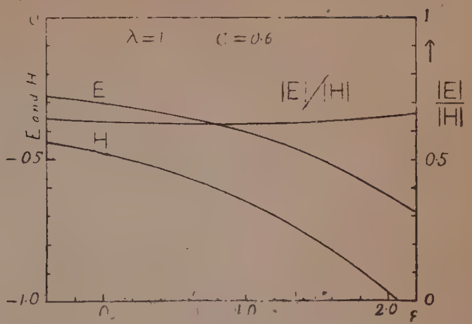

Fig. 4. E, H and |E|/|H| as functions of the depth of the potential hole in the modified hole model.

A suitable choice of ϵ and λ allows us to bring the calculated 1*s* level low enough to get the agreement between theoretical and experimental values of F-absorption of alkali-halides. Tibbs' attempt for KCl corresponds to this case[(4)]. Such ambiguity of the model, however, be unfavourable from the quantitative standpoint.

§ 5. Conclusion.

Our theory developed here is rather qualitative or semiquantitative at the present stage. The results obtained above suggest to us that the model used in § 3 may give a useful keys to the relative magnitudes of E, H and other energies, though it is insufficient for the computation of energies for real crystals.

Applications of the method to other cases and detailed discussion will be given in the next paper.

In conclusion, the author wishes to express his deep appreciation to Prof. K. Ochiai for his valuable discussions and interest given to this work.

References.

(1) N. F. Mott and R. W. Gurney: Electric Process in Ionic Crystals, (1940).
(2) L. Landau: Phys. Zeits. Sowjet. **3**, (1933) 664.
(3) Reference (1),
(4) S. R. Tibbs: Trans. Faraday Soc. **35**, (1939) 1471.

On the Theory of Scattering of Hydrogen Atomic Ray by the Ferromagnetic Substance.*

By Tokutarô HIRONE and Noboru TSUYA.

Research Institute of Iron, Steel and other Metals, Tohoku University.

(Received November 1, 1947)

§1. Introduction.

It has been usually assumed that the ferromagnetic substance is divided into a number of elementary domains, which are spontaneously magnetized to technical saturation. Although this assumption is very plausible for the explanation of various characteristics of ferromagnetic substances, yet there are no direct experimental evidences for the existence of such a domain structure of ferromagnetic substances. If we assume the existence of such domains, various experimental facts concerning the Barkhausen effect during the magnetization of the ferromagnetic substance are well explained.

It should be noted, however, that those facts do not prove directly the existence of such domains.(1) Now the magnetic moment of the spontaneously magnetized domain is usually supposed to be attributed to the spin moments of electrons occupying the $3d$ electronic energy band of the transition metals, so that a simple and direct method for the detection of the domain structure and spontaneous magnetization may be to measure the scattering cross section of the particles which interact with those $3d$ electrons in the metal without giving them any considerable disturbances. By the magnetic scattering of the neutrons,(2) however, the difference of the cross section for the magnetized and unmagnetized states of the ferromagnetic substance is not so large, so that it is difficult to recognize or detect the domain structure by observing this effect.** In the case of the scattering of the fast electron beam,(3) it may be considered that the process is too complicated because of the ionization, the excitation and the temperature rise of the scatterer during the process of scattering: while in the case of the slow electron beam, the theoretical treatment of the process can not be carried out under simple approximation, which renders a complete treatment of this problem very laborious. Moreover, we may expect that the intensity of the deflected beam is so weak that (by its observation) we may not be able to expect any information on the domain structure and the spontaneous magnetization.

On the other hand, by the scattering of hydrogen atomic ray, of which the energy is of the order of kT, we may expect to be able to distinguish the above mentioned difference, owing to the exchange effect between a pair of electrons which belong to the hydrogen atom and the ferromagnetic substance. As seen in the following, it is found from our theoretical consideration that:

i) In the hydrogen atomic ray the magnetic scattering is completely screened out by the electronic scattering.

ii) The scattering cross section due to electric interaction is of the order of $10^{-12}\,\mathrm{cm}^2$ per atom.

iii) The cross section of scattering under a paramagnetic state is about 10 per cent greater than that under an unmagnetized state of the ferromagnetic substance. This leads us to expect to obtain by experiments along the above mentioned lines, some direct informations on the domain structure in the ferromagnetic substance.

---

* This report is a portion of the investigation of the special committee for theoretical physics in National Research Council of Japan. (Subject: Theory of Ferromagnetism, Committee Member: Tokutarô Hirone).

** Recently F. Bloch, M. Hamermesh and H. Staub have shown that the cross section measurement gives certain information about the domain size of the ferromagnetic crystals: Phys. Rev. **64** (1943) 47.

§2. The Hamiltonian of the System and the Wave Functions.

We consider now a system composed of a hydrogen atom and a ferromagnetic scatterer. The total Hamiltonian H of the system may be devided into two parts, H_0 for the unperturbed system and H', which is again a sum of the magnetic and electric interaction terms, H_m and H_e:

$$H = H_0 + H' \tag{2.1}$$

$$H' = H_m + H_e. \tag{2.2}$$

Here H_0 is the sum of the Hamiltonian of the hydrogen atom and that of the ferromagnetic substance when they lie far apart from each other, having a form

$$H_0 = H_{\text{hydrogen}} + H_{\text{solid}}, \tag{2.3}$$

where

$$H_{\text{hydrogen}} = -\frac{\hbar^2}{2m}\Delta_r - \frac{\hbar^2}{2M}\Delta_R - \frac{e^2}{|R-r|} \tag{2.4}$$

and

$$\begin{aligned} H_{\text{solid}} = & -\frac{\hbar^2}{2m}\sum_{\nu}^{N}\Delta_\nu \\ & + e^2\Big[\sum_{m>n}^{N}\frac{1}{r_{mn}} + \sum_{\mu>\nu}^{N}\frac{1}{r_{\mu\nu}} - \sum_{m\neq\mu}\frac{1}{r_{m\mu}}\Big] \\ & + \sum_q\sum_{j=1}^{3}\Big(N_{qj}+\frac{1}{2}\Big)\hbar\omega_{qj} \\ & + \sum_m^N\Big(u_m, \operatorname{grad} e^2\Big[\sum_n^N\frac{1}{r_{mn}} - \sum_\nu^N\frac{1}{r_{m\nu}}\Big]\Big), \end{aligned} \tag{2.5}$$

where

$$u_m = N^{-\frac{1}{2}}\sum_q\sum_{j=1}^{3} e_{qj}\,(a^*\exp[-i(q, r_m)] + a\exp i(q, r_m)]).$$

In these expressions m, n (1, 2, $\cdots N$) specifies the number of atomic cores composing the scatterer and μ, ν (1, 2, $\cdots N$) that of electrons in the solids. Δ_ν is the Laplacian operator concerning the ν-th electron coordinates, r_{mn} etc stand for $|r_m - r_n|$ etc.; m and M are the mass of the electron and the proton, respectively. The third and fourth terms in the above expression (2.5) are the lattice vibration terms, where N_{Qj} means the number of lattice quanta, which have the j-th ($j = 1, 2, 3$) polarization, the wave number vector q and the frequency ω_{qj}. The lattice vibrations do not have any considerable effect on the present problem, so that we may neglect this term in the following calculations.

The interaction term H' is composed of electric and magnetic terms. The electric interaction term H_e is expressed by

$$H_e = \sum_{m=1}^{N}\sum_{\nu=1}^{N} e^2\Big[\frac{1}{r_{\xi\nu}} + \frac{1}{r_{mR}} - \frac{1}{r_{R\nu}} - \frac{1}{r_{n\nu}}\Big], \tag{2.6}$$

while the magnetic interaction term H_m is made up of two terms, one for the spin-spin interaction and the other for the spin-orbit interaction, namely:

$$\begin{aligned} H_M = & \mu^2\sum_\nu^N\Big(\sigma^{(\xi)}\Big[\operatorname{grad}_{(\xi)}, \frac{[\sigma^{(\nu)}, r_{\xi\nu}]}{|r_{\xi\nu}|^3}\Big]\Big) \\ & + i\mu\frac{e\hbar}{mc}\sum_\nu^N\Big(\sigma^{(\xi)}, \frac{[r_{\xi\nu}, \operatorname{grad}_{(\nu)}]}{|r_{\xi\nu}|^3}\Big), \end{aligned} \tag{2.7}$$

where $\mu = eh/2mc$ = Bohr magneton.

Now if we designate with R the coordinate of the proton of the hydrogen atom, then the solution of (2.4) takes a form,

$$\exp[i(\mathfrak{K}, \mathfrak{R})]\phi(\mathfrak{R}-r), \tag{2.8}$$

where $\phi(r)$ is the wave function of the lowest state of the hydrogen atom with the spin function $\Omega(\sigma)$, thus

$$\phi(r) = (\pi a)^{-\frac{3}{2}}\exp(-r/a)\Omega(\sigma), \tag{2.9}$$

where $a = \hbar^2/me^2$ = Bohr radius.

If we denote with $\varphi_n(r_\nu)$ the atomic wave function of the ν-th electron on the n-th atom in the solid including the spin function, then the antisymmetric wave function of the total system, corresponding to the Hamiltonian H_0, is written in a determinantal form;

$$\begin{aligned} & \exp[i(\mathfrak{K}, \mathfrak{R})]\chi(r_\xi, r_1, \cdots\cdots r_N) \\ & = \exp[i(\mathfrak{K}, \mathfrak{R})][(N+1)!]^{-1/2} \\ & \sum_P(-)^P P\phi(\mathfrak{R}-r_\xi)\cdots\cdots\varphi_m(r_\mu)\cdots\cdots\varphi_N(r_N), \end{aligned} \tag{2.10}$$

where P means the permutation of the electrons. Here the normalization factor for the proton wave is omitted, which we shall later take into account in calculating the cross section.

§3. Differential Cross Section.

Now it can be supposed that the interaction energy H′ between the hydrogen atom and the ferromagnetic substance is small compared with the total energy H of this system, so that Born's method for the calculation of the scattering process may be applicable. Neglecting the multiple scatterings and adsorption of the hydrogen atom on the scatterer, and normalizing the number of the incident beam passing a unit area per unit time to unity, we obtain the seattered wave:

$$\Psi_{\text{scatt}} = -\frac{M}{2\pi\hbar^3}\sum_{\tau}\frac{|\mathfrak{K}_\tau|}{|\mathfrak{K}_0|}\cdot\frac{1}{R}$$

$$\cdot\exp(i|\mathfrak{K}_\tau|R)\chi_\tau(r_i, r_1, \cdots r_\nu, \cdots)W_\tau. \qquad (3.1)$$

Consequently the differential cross section dQ of the scattering in the solid angle between (θ, Φ) and $(\theta+d\theta, \Phi+d\Phi)$ is given by

$$dQ = \left(\frac{M}{2\pi\hbar^2}\right)^2\sum_{\tau}\frac{|\mathfrak{K}_\tau|^2}{|\mathfrak{K}_0|^2}|W_\tau|^2\sin\theta d\theta d\Phi. \qquad (3.2)$$

As it shows, the cross section is completely determined if we are able to get the transition matrix element W_τ between the initial and final states which takes the following form

$$W_\tau = \int\exp[i(\mathfrak{K}_0-\mathfrak{K}_\tau, \mathfrak{R})]\chi_\tau^*(r_i, \cdots r_\nu, \cdots)$$

$$H'\chi(r_i, \cdots r_\nu, \cdots)d\tau. \qquad (3.3)$$

Here H' is the interaction term given by (2.2). Now we introduce the two symbols $\mathfrak{C}_n$ and $\mathfrak{A}_n$ for the Coulomb and the exchange integrals between a s-electron of the hydrogen atom and a 3-d electron in the metal, i.e.,

$$\mathfrak{A}_n = \exp[i(\mathfrak{K}_0-\mathfrak{K}, \mathfrak{r}_n)]\int\exp[i(\mathfrak{K}_0-\mathfrak{K}, \mathfrak{R})]$$

$$|\phi(\mathfrak{R}-\mathfrak{r}_i)|^2H'|\varphi_n(\mathfrak{r}_\nu)|^2d\tau_R d\tau_i d\tau_\nu, \qquad (3.4)$$

$$\mathfrak{A}_n = \exp i(\mathfrak{K}_0-\mathfrak{K}, \mathfrak{r}_n)]\int\exp[i(\mathfrak{K}_0-\mathfrak{K}, \mathfrak{R})]$$

$$\phi^*(\mathfrak{R}-\mathfrak{r}_\nu)\varphi_n^*(r_i)H'(\bar{\varphi}_n(\mathfrak{r}_\nu)\phi(\mathfrak{R}-\mathfrak{r}_i)d\tau_R d\tau_i d\tau_\nu \qquad (3.5)$$

In these integrals the summations with respect to the spin variables are not taken into account. Neglecting the small terms, W_τ takes a form:

$$W_\tau = \sum_n(\mathfrak{C}_n S-\mathfrak{A}_n S^P), \qquad (3.6)$$

where S means the result of the summation, with respect to the spin variables, of the product of the spin eigenfunctions belonging to the initial and final states, while S^P has the same meaning as above, except for the exchange in the final product of the spin variables, one of which belongs to the hydrogen and the other to the p-th atom in the solid.

i) Electric interaction.

The electric interaction term H_e is expressed by

$$H_e = \sum_n^N H_{e,n}, \quad H_{e,n} = e^2\left[\frac{1}{R}+\frac{1}{r_{in}}-\frac{1}{r_{Rn}}-\frac{1}{r_i}\right] \qquad (3.7)$$

which by using the formula (2–6) and denoting the value $\mathfrak{K}_0-\mathfrak{K}$ by $\mathfrak{k}$ gives rise to the Coulomb integral $\mathfrak{C}_n^e$

$$\mathfrak{C}_n^e = \exp[i(\mathfrak{k}, r_n)]\pi a^2e^2[1-F_{dd}(\mathfrak{k})[f_c^e(\mathfrak{k}), \qquad (3.8.1)$$

$$f_c^e = [1+(a|\mathfrak{k}|/2)^2]^{-1}+[1+(a|\mathfrak{k}|/2)^2]^{-2}, \qquad 3.8.2)$$

$$F_{dd}(\mathfrak{k}) = \int\exp[i(\mathfrak{k}, \mathfrak{r})]|\varphi(r)]^2d\tau_r.^{(4)} \qquad (3.8.3)$$

In a similar manner, the exchange integral $\mathfrak{A}_n^e$ due to electronic interaction may be expressed by

$$\mathfrak{A}_n^e = \exp[i(\mathfrak{k}, \mathfrak{r}_n)]\pi a^2e^2[1-F_{sd}(\mathfrak{k})]f_a^e(\mathfrak{k}). \qquad (3.9)$$

ii) Magnetic interaction.

Here, we shall assume for simplicity that the 3d valency electrons of each atom involved in the scatterer have central symmetric orbits, then there remains only the spin-spin interaction term of H_m. By a short calculation, it may be proved that $\mathfrak{C}_{nm}$ takes a form

$$\mathfrak{C}_{nm} = \exp[i(\mathfrak{k}, \mathfrak{r}_n)]4\pi\mu^2$$

$$\left(\left[(i'|\sigma^{(i)}|i), \frac{\mathfrak{k}}{|\mathfrak{k}|}\right], \left[\frac{\mathfrak{k}}{|\mathfrak{k}|}, (\nu'|\sigma^{(\nu)}|\nu)\right]\right)f_c^m(\mathfrak{k}),$$

$$(3\ 10\ 1)$$

$$f_c^m(\mathfrak{k}) = [1+(a|\mathfrak{k}|/2)^2]^{-2}. \qquad (3.10.2)$$

On the other hand, $\mathfrak{A}_n^m$ is approximately expressed by

$$\mathfrak{A}_n^m = \exp[i(\mathfrak{k}, \mathfrak{r}_n)]4\pi\mu^2$$

$$\left(\left[(\nu'|\sigma^{(i)}|i), \frac{\mathfrak{k}}{|\mathfrak{k}|}\right], \left[\frac{\mathfrak{k}}{|\mathfrak{k}|}, (i'|\sigma^{(\nu)}|\nu)\right]\right)f_a^m(\mathfrak{k})$$

$$(3.11)$$

These four integrals (3.11), (3.8), (3.9) and (3.10) have the common factor $\exp[i(\mathfrak{K}_0-\mathfrak{K}, \mathfrak{r}_n)]$, so that we may represent the quantities $\mathfrak{C}_n^e$ etc. with $\exp[i(\mathfrak{K}_0-\mathfrak{K}, \mathfrak{r}_n)]\mathfrak{C}^e$ etc..

§ 4. Scattering by a Ferromagnetic Solid.

To treat the calculation as simply as possible, the following case is at first considered. In each domain let the spins of only a few electrons be antiparallel to the spontaneous magnetization, and the direction of the remaining electronic spins be parallel to the spontaneous magnetization. The direction of spontaneous magnetization in different domains will take independent directions of each other. In addition, we assnme that the beam of the hydrogen atom interacts with each domain independently. If the polar and azimuthal angles of the direction of the resultant spin moment in a demain with respect to the direction of polarization of the incident beam are $(-\vartheta, -\omega)$ and if we take the direction $(-\vartheta, -\omega)$ as the z-axis of our rectangular coordinate, then we have for the wave function of incident beam $\phi = \begin{pmatrix}\phi_+\\ \phi_-\end{pmatrix}$;

$$\begin{pmatrix}\phi_+\\ \phi_-\end{pmatrix} = \exp[i(\mathfrak{K}, \mathfrak{R})]\phi(\mathfrak{R}-\mathfrak{r}_i)\begin{pmatrix}\cos\dfrac{\vartheta}{2}\\ \sin\dfrac{\vartheta}{2}\exp(i\omega)\end{pmatrix} \tag{4.1}$$

Hence our $(N+1)$ body problem has a solution $\chi = \begin{pmatrix}\chi_+\\ \chi_-\end{pmatrix}$, including the spin function, as follows:

$$\chi_+\Omega_+ = \sum_{n_1\cdot\,n_l} C_+(n_1, \cdot\cdot n_\nu, \cdot\cdot n_l)$$

$$\cdot\frac{\cos\dfrac{\vartheta}{2}}{\sqrt{(N+1)!}}\sum_P(-)^P P\phi(\mathfrak{R}-\mathfrak{r}_i)\alpha(i)\cdot\cdot\varphi_{n_\nu}(r_{n_\nu})\times\beta(n_\nu) \tag{4.2.1}$$

$$\chi_-\Omega_- = \sum_{n_1\cdot\cdot n_l} C_-(n_1, \cdot\cdot n_\nu, \cdot\cdot n_l)$$

$$\cdot\frac{\sin\dfrac{1}{2}\vartheta e^{i\omega}}{\sqrt{(N+1)!}}\sum_P(-)^P P\phi(\mathfrak{R}-\mathfrak{r}_i)\beta(i)\cdot\cdot\phi_{n\nu}(r_{n_\nu})\times\beta(n_\nu) \tag{4.2.2}$$

where $C(n_1\cdot\cdot n_\nu\cdot\cdot n_l)$ is the coefficient of the wave function which has the antiparallel spins at the lattice points $n_1, \cdot\cdot n_\nu\cdot\cdot n_l$. These coefficients may be approximately given by Bloch's function of spin wave. Putting $n \equiv G^3$, they take a form of

$$C_+ = C_- = c(n_1, \cdot\cdot n_\nu, n_\nu\cdot\cdot\cdot n_l)[G^{3l}l\,!]^{\ l/2}$$

$$\sum_{P'}^{l!}\exp\left[i\sum_{\nu=1}^{l}(\mathfrak{K}_\nu, \mathfrak{r}_{n_{P'\nu}})\right], \tag{4.3}$$

where $\mathfrak{K}_\nu$ is the spin wave number vector.

In the first place we shall consider an electric scattering, in which l does not change before and after collision. Now the spontaneous magnetization J of the domain stands in linear relation with the number of antiparallel spins l contained in it. If we denote by J_0 the saturation magnetization, i.e., the value of magnetization when all the spins are parallel to the spontaneous magnetization, we have

$$J/J_0 = 1-2lG^{-3}, \tag{4.4}$$

We introduce the matrix elements $W_{l\to l}^{+\to+}$, in which the spin of incident and scattered beams are parallel to each other and in which l remains unchanged. If we define similarly $W_{l\to l}^{-\to-}$, then the matrix elements $W_{l\to l}^{+\to+}$ and $W_{l\to l}^{-\to-}$ are given by

$$W_{l\to l}^{+\to+} = \cos^2\frac{\vartheta}{2}L(\mathfrak{K}_0-\mathfrak{K}$$

$$\cdot\delta\begin{pmatrix}\mathfrak{K}_1', & \cdot\cdot\mathfrak{K}_\nu', & \cdot\cdot\mathfrak{K}_l'\\ \mathfrak{K}_1, & \cdot\cdot\mathfrak{K}_\nu, & \cdot\cdot\mathfrak{K}_l\end{pmatrix}\left[\mathfrak{C}^e-\frac{1}{2}(1+J/J_0)\mathfrak{R}_e\right] \tag{4.51}$$

$$W_{l\to l}^{-\to-} = \sin^2\frac{\vartheta}{2}L(\mathfrak{K}_0-\mathfrak{K})$$

$$\cdot\delta\begin{pmatrix}\mathfrak{K}_1', & \cdot\cdot\mathfrak{K}_\nu', & \cdot\cdot\mathfrak{K}_l'\\ \mathfrak{K}_1, & \cdot\cdot\mathfrak{K}_\nu, & \cdot\cdot\mathfrak{K}_l\end{pmatrix}\left[\mathfrak{C}^e-\frac{1}{2}(1-J/J_0)\mathfrak{A}^e\right], \tag{4.52}$$

where

$$\cdot\delta\begin{pmatrix}\mathfrak{K}_1', & \cdot\cdot\mathfrak{K}_\nu', & \cdot\cdot\mathfrak{K}_l'\\ \mathfrak{K}_1, & \cdot\cdot\mathfrak{K}_\nu, & \cdot\cdot\mathfrak{K}_l\end{pmatrix}$$

$$\equiv\sum_{P''}^{l!}P'\delta(\mathfrak{K}_1-\mathfrak{K}_1')\cdot\cdot\delta(\mathfrak{K}_\nu-\mathfrak{K}_\nu')\cdot\cdot\delta(\mathfrak{K}_l-\mathfrak{K}_e') \tag{4.6}$$

and

$$L(\mathfrak{K}) = \sum_n^N\exp[i(\mathfrak{K}, \mathfrak{r}_n)]. \tag{4.7}$$

the last expression $L(\mathfrak{K})$ being Laue's factor. In a similar manner we obtain the other matrix elements different from zero as follows.

$$W_{l\to l+1}^{+\to-} = -\sin^2\frac{\vartheta}{2}\mathfrak{A}^e\sqrt{\frac{1}{2}(1-J/J_0)}$$

$$\cdot\sum_{\nu'=1}^{l+1}(l+1)^{-1}L(\mathfrak{K}_0-\mathfrak{K}-\mathfrak{K}_\nu')\delta\begin{pmatrix}\mathfrak{K}_1', \cdot\cdot\mathfrak{K}'_{\nu-1}, \mathfrak{K}'_{\nu+1}\cdot\cdot\mathfrak{K}'_{l+1}\\ \mathfrak{K}_1, \cdot\cdot\mathfrak{K}_{\nu-1}, \mathfrak{K}_{\nu+1}\cdot\cdot\mathfrak{K}_{l+1}\end{pmatrix}, \tag{4.8}$$

$$W_{l\to l-1}^{-\to+} = -\cos^2\frac{\vartheta}{2}\mathfrak{A}^e\sqrt{\frac{1}{2}(1-J/J_0)}$$

$$\cdot\sum_{\nu=1}^{l}l^{-1}L(\mathfrak{K}_0-\mathfrak{K}+\mathfrak{K}_\nu)\delta\begin{pmatrix}\mathfrak{K}_1', \cdot\cdot\mathfrak{K}'_{\nu-1}, \mathfrak{K}'_{\nu+1}\cdot\cdot\mathfrak{K}_l'\\ \mathfrak{K}_1, \cdot\cdot\mathfrak{K}_{\nu-1}, \mathfrak{K}_{\nu+1}'\cdot\cdot\mathfrak{K}_l\end{pmatrix}. \tag{4.9}$$

Now we shall consider the Laue's factor $L(\mathfrak{K})$. Since $|\mathfrak{K}_\nu|$ etc. are small compared with $|\mathfrak{K}_0|$ near the saturation of the ferromagnetic state, $\mathfrak{K}_0-\mathfrak{K}-\mathfrak{K}_\nu'$ etc. are nearly equal to $\mathfrak{K}_0-\mathfrak{K}$. The Laue's factor $L(\mathfrak{K})$ is zero except for the case $\mathfrak{K} = 2\pi g_{n_1, m_2, m_3}(m_i = 0, 1, 2, \cdot\cdot)$, in which g_{m_1, m_2, m_3} etc. designate each of the vectors of the reciprocal lattice. When $\mathfrak{K}$ satisfies above relations, $|L(\mathfrak{K})|$

becomes G^3. Therefore, we are able to expect that the diffraction pattern of scattered beam is quite similar to Laue's pattern which is obtained by the X-ray.

The cross section due to magnetic interaction is also obtained in the similar way in which case the scattering patterns are exactly of the same as that in the electric scattering.

Now we have to compare the intensities of both the electric and magnetic scattering. We take, for example, the ratio of $\mathfrak{E}^m/\mathfrak{E}^e$ to be

$$\mathfrak{E}^m/\mathfrak{E}^e \sim (2\mu/ae)^2 \sim 10^{-6}. \qquad (4.10)$$

From this figure, it is easily found that the magnetic scattering is completely masked out by the electric one.

In order to apply these results to the unmagnetized state of the ferromagnetic substance, we have to average the matrix elements for every direction of ϑ and ω; thus we have the differential cross section dQ;

$$dQ = \left(\frac{M}{2\pi\hbar^2}\right)^2 \left[\frac{1}{4\pi}\int \sin\vartheta d\vartheta d\omega \left(|W_{l\to l}^{+\to+}|^2 + |W_{l\to l}^{-\to-}|^2 + |W_{l\to l+1}^{+\to-}|^2 + |W_{l\to l+1}^{-\to+}|^2\right)\right] \sin\Theta d\Theta d\Phi$$

$$\backsim \left\{\left[\mathfrak{E}^e - \frac{1}{2}(1-J/J_0)\mathfrak{A}^e\right]^2 + \left[\mathfrak{E}^e - \frac{1}{2}(1+J/J_0)\mathfrak{A}^e\right]^2 + (1-J/J_0)\mathfrak{A}^{e2}\right\} \sin\Theta d\Theta d\Phi. \qquad (4.11)$$

If the energy of the hydrogen beam are 0.01 ev (∼100°k, $1/\mathfrak{K}_0$ $1 \sim 8.10^3$ cm^{-1}) or 0.1 ev (∼1000°k, $1/\mathfrak{K}_0$ $1 \sim 2.10^9$ cm^{-1}), then the cross sections per atom are 10^{-12}cm^2 and 10^{-13}cm^2 respectively.

§ 5. Scattering under a Paramagnetic State of the Ferromagnetic Solid.

If the temperature of the ferromagnetic substance is raised above its Curie point, then the spontaneous magnetization disappears and J/J_0 takes the value zero, so that the number of antiparallel spins is equal to that of the parallel spins. In this case the formula (4.11) does not give a good approximation and hence it is not perfectly correct to put $J=0$ directly in (4.11). However, we may expect that an exact treatment would lead to a result which is not far from that obtained by putting $J=0$ in (4.11); then the ratio of the scattering cross sections above and below the Curie temperature $Q_{J=J_0}/Q_{J=0}$ is given by

$$\frac{Q_{J=J_0}}{Q_{J=0}} = \frac{2\mathfrak{E}^{e2} - 2\mathfrak{E}^e\mathfrak{A}^e + \mathfrak{A}^{e2}}{2\mathfrak{E}^{e2} - 2\mathfrak{E}^e\mathfrak{A}^e + 3\mathfrak{A}^{e2}/2} = \begin{cases} 0.8, & \text{for } \mathfrak{E}^e = 1.5\mathfrak{A}^e, \\ 0.9, & \phantom{\text{for }} \mathfrak{E}^e = 2\mathfrak{A}^e, \end{cases} \qquad (5.1)$$

If the result of the experiments along these lines are favourable for the present theory, that is, if the caltulated difference of the cross section between ferromagnetic and paramagnetic states of the mentioned substance can be experimentally confirmed, it leads us to deduce the existence of the domain structure even in the unmagnetized state of the ferromagnetic solid.

References.

(1) The experimental facts concerning the domain structures are fully criticized by W. F. Brown, Rev. Mod. Phys., **17** (1945), 15.

(2) F. Bloch: Phys. Rev., **50** (1936), 259; J. Schwinger, Phys. Rev., **51** (1937), 544; F. Bloch, Phys. Rev., **51** (1937), 992; O. Halpern and M. H. Johnson, Phys. Rev., **52** (1937), and **55**, (1939), 898; O. Halpern and T. Holstein, Phys. Rev., **59** (1941), 960; O. Halpern, M. Hamermesh and M. H. Johnson, Phys. Rev., **59**, (1941), 981; T. Mutô, Sci. Rep. I. P. C. R., **40** (1943), 333.

(3) T. Mutô; Oral statement at the anual meeting of Phys. Soc. Japan, (1947), May.

(4) O. Halpern and M. H. Johnson obtained this integral approximately in Phys. Rev., **55** (1939), 898.

Determination of Intermolecular Forces from the Equation of State of Gases.

By Taro KIHARA.

Physical Institute, Faculty of Science, University of Tokyo.

(Received December 7, 1947)

§1. Introduction.

The equation of state of gases may be expressed in the form

$$pv = kT\left(1+\frac{B}{v}+\frac{C}{v^2}+\cdots\right)$$

(p = pressure, v = volume per molecule, k = Boltzmann constant, T = absolute temperature), where the coefficients B, C, ... are functions of the temperature, usually called second, third, ... virial coefficients.

For any gas composed of spherically symmetric identical molecules, theoretical expressions for the virial coefficients were given by Born and Mayer(1), on the assumption that classical statistics can be used, and that the potential energy of the whole system can be expressed as the total sum of terms, $U(r_{ij})$, each depending only on the distance r_{ij} between two molecules i and j. By means of the function

$$f(r) = \exp\left[-\frac{U(r)}{kT}\right]-1,$$

the expressions are

$$B = -\frac{1}{2}\int f(r_{12})\,d\tau_1 = -2\pi\int_0^\infty f(r)r^2dr,$$

$$C = -\frac{1}{3}\iint f(r_{12})f(r_{13})f(r_{23})\,d\tau_1 d\tau_2, \qquad (1)$$

with

$$d\tau_i = dx_i\,dy_i\,dz_i\,.$$

Lennard-Jones(2) evaluated the second virial coefficient for molecules with an interaction energy

$$U(r) = \frac{\lambda}{r^n}-\frac{\mu}{r^m}$$

$$= U_0\left\{\frac{m}{n-m}\left(\frac{r_0}{r}\right)^n-\frac{n}{n-m}\left(\frac{r_0}{r}\right)^m\right\}, \qquad (2)$$

finding that

$$B = \frac{2\pi}{3}\left(\frac{\lambda}{kT}\right)^{\frac{3}{n}}\left\{\Gamma\left(\frac{n-3}{n}\right)-\frac{3}{n}\sum_{\tau=1}^{\infty}\Gamma\left(\frac{\tau m-3}{n}\right)\frac{y^\tau}{\tau!}\right\},$$

$$y = \frac{\mu}{kT}\left(\frac{kT}{\lambda}\right)^{\frac{m}{n}}$$

or

$$B = \frac{2\pi}{3}r_0{}^3\left(\frac{m}{n-m}z\right)^{\frac{3}{n}}\left\{\Gamma\left(\frac{n-3}{n}\right)\right.$$

$$\left.-\frac{3}{n}\sum_{\tau=1}^{\infty}\Gamma\left(\frac{\tau m-3}{n}\right)\frac{1}{\tau!}\left(\frac{n}{m}\right)^\tau\left(\frac{m}{n-m}z\right)^{\frac{n-m}{n}\tau}\right\},$$

$$z = U_0/kT$$

It was found also by Lennard-Jones that the temperature variations of the second virial coefficient, predicted by this model with $m = 6$, $10 \leq n \leq 14$, coincide with observed values, and thus the parameters r_0 and U_0 for some gases were determined.

Unfortunately, however, the second virial coefficient is not sensitive to the shape of $U(r)$. The third virial coefficient, on the other hand, is sensitive as I have pointed out in the preceding paper(3). It is therefore desirable to investigate also the third virial coefficient, which is performed in this paper by the use of a special model $m = 6$, $n = 12$.

§2. Reduction of the Integral.

Assuming the model (2), the third virial coefficient (1) can be expanded into an infinite series as shown in this section. The integration variables of (1) are transformed as follows:

$$\iint d\tau_1 d\tau_2 = 3\iint_{r_{12}\geqq r_{13},\,r_{12}\geqq r_{23}} d\tau_1 d\tau_2$$

$$= 3\times 4\pi\int_0^\infty R^5dR\int_0^{\frac{\sqrt{3}}{2}}2\pi y\,dy\int_{1-\sqrt{1-y^2}}^{\sqrt{1-y^2}}dx,$$

where (Fig. 1)

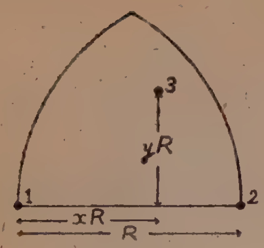

Fig. 1

$R = r_{12}$, $(x^2+y^2)R^2 = r_{13}^2$, $\{(1-x)^2+y^2\}R^2 = r_{23}^2$.
Namely

$$\frac{1}{3}\iint d\tau_1\, d\tau_2 = 4\pi^2\int_0^\infty R^5 dR\int_0^{\frac{3}{4}} d(y^2)\int_{1-\sqrt{1-y^2}}^{\sqrt{1-y^2}} dx.$$

First we consider the integration with regard to R. By integrating by parts we have

$$-\int_0^\infty f(r_{12})f(r_{13})f(r_{23})R^5 dR$$

$$= \frac{1}{6}\int_0^\infty \frac{\partial f(r_{12})f(r_{13})f(r_{23})}{\partial R} R^6 dR. \qquad (3)$$

Now the product of 3 f's is transformed into a sum :

$$f(r_{12})f(r_{13})f(r_{23})$$

$$= f^{(0)}-\{f^{(1)}+f^{(2)}+f^{(3)}\}+\{f(r_{12})+f(r_{13})+f(r_{23})\},$$

$$f^{(0)} = \exp\left[-\frac{U(r_{12})+U(r_{13})+U(r_{23})}{kT}\right]-1,$$

$$f^{(1)} = \exp\left[-\frac{U(r_{12})+U(r_{13})}{kT}\right]-1,$$

$$f^{(2)} = \exp\left[-\frac{U(r_{12})+U(r_{23})}{kT}\right]-1,$$

$$f^{(3)} = \exp\left[-\frac{U(r_{13})+U(r_{23})}{kT}\right]-1.$$

If we assume $m > 6$ for the present (later we consider the limit $m \to 6$), we can integrate term by term, then, in the same method as adopted by Lennard-Jones, (3) is expanded into

$$\frac{1}{6}\left(\frac{\lambda}{kT}\right)^{\frac{6}{n}}\left\{A_0\Gamma\left(\frac{n-6}{n}\right)-\frac{6}{n}\sum_{\tau=1}A_\tau\Gamma\left(\frac{\tau m-6}{n}\right)\frac{y^\tau}{\tau!}\right\}$$

$$y = \frac{\mu}{kT}\left(\frac{kT}{\lambda}\right)^{\frac{m}{n}},$$

where

$$A_\tau = (1+\xi^n+\eta^n)^{\frac{6}{n}}\left\{\frac{1+\xi^m+\eta^m}{(1+\xi^n+\eta^n)^{m/n}}\right\}^\tau$$

$$-(1+\xi^n)^{\frac{6}{n}}\left\{\frac{1+\xi^m}{(1+\xi^n)^{m/n}}\right\}^\tau-(1+\eta)^{\frac{6}{n}}\left\{\frac{1+\eta^m}{(1+\eta^n)^{m/n}}\right\}^\tau$$

$$-(\xi^n+\eta^n)^{\frac{6}{n}}\left\{\frac{\xi^m+\eta^n}{(\xi^n+\eta^n)^{m/n}}\right\}^\tau+(1+\xi^6+\eta^6),$$

$$\xi = R/r_{13}, \quad \eta = R/r_{23}, \quad \tau = 0, 1, 2, \cdots\cdots.$$

Expressing in r_0 and U_0, we have finally

$$C = \frac{\pi^2}{3} r_0^6 \sum_{\tau=0}^{\infty} k_\tau\left(\frac{m}{n-m}z\right)^{\frac{n-m}{n}\tau+\frac{6}{n}}, \quad z = \frac{U_0}{kT}$$

$$k_\tau = -\frac{12}{n}\frac{1}{\tau!}\left(\frac{n}{m}\right)^\tau\Gamma\left(\frac{\tau m-6}{n}\right)$$

$$\cdot\int_0^{\frac{3}{4}}\int_{1-\sqrt{1-y^2}}^{\sqrt{1-y^2}} A_\tau dx d(y^2).$$

We must carry out numerical calculation to investigate the behaviour of K_τ. For $\tau \gg 1$, however, the method of steepest descent can be applied to the integrand

$$A_\tau \sim 3^{\frac{6}{n}}\left\{\frac{1+\xi^m+\eta^m}{(1+\xi^n+\eta^n)^{m/n}}\right\}^\tau$$

and it is found that

$$\int_0^{\frac{3}{4}}\int_{1-\sqrt{1-y^2}}^{\sqrt{1-y^2}} A_\tau dx d(y^2)$$

$$\sim \frac{36}{m(n-m)}\frac{\pi}{2\tau}3^{\frac{n-m}{n}\tau+\frac{6}{n}-\frac{1}{2}}$$

For the special case of $m = 6$, when K_1 becomes indefinite form, we may directly take the limit $m \to 6$, since in the original form this value is not any singular point :

$$\lim_{m\to 6}\Gamma\left(\frac{m-6}{n}\right)A_1 = \ln\frac{(1+\xi^n)(1+\eta^n)}{1+\xi^n+\eta^n}$$

$$+\xi^6\ln\frac{(1+\xi^n)(\xi^n+\eta^n)}{\xi^n(1+\xi^n+\eta^n)}+\eta^6\ln\frac{(1+\eta^n)(\xi^n+\eta^n)}{\eta^n(1+\xi^n+\eta^n)}.$$

§ 3. Numerical calculation of K_τ.

Choosing the exponents of r as $m = 6$, $n = 12$, i. e. adopting the potential

$$U(r) = U_0\left\{\left(\frac{r_0}{r}\right)^{12}-2\left(\frac{r_0}{r}\right)^6\right\}, \qquad (4)$$

we have

$$C = \frac{\pi^2}{3}r_0^6\sum_{\tau=0}^{\infty}K_\tau Z^{\frac{\tau}{2}+\frac{1}{2}}, \quad Z = \frac{U_0}{kT}, \qquad (5)$$

$$K_\tau \sim -\frac{2^\tau}{\tau!}\Gamma\left(\frac{\tau-1}{2}\right)\frac{\pi}{2\tau}3^{\frac{\tau}{2}} \qquad (6)$$

with K_τ given in Table 1. This values of K_τ were obtained for $\tau < 12$ by numerical integration according to Gauss-Lobatto's scheme (taking 9 points with respect to x, 7 points with respect to y^2), and were taken from the asymptotic form (6) for $\tau \geq 12$. In Table 2, the calculated value of c/r_0^6 and B/r_0^2 are given as function of $-\log_{10}z$.

Table I.

τ	K_τ
0	+1.152
1	−2.135
2	+0.996
3	612
4	254
5	005
6	−0.127
7	169
8	160
9	128
10	093
11	062
12	039
13	023
14	013
15	007
16	004
17	002

Table II.

$-\log_{10}z$	B/r_0^3	C/r_0^3
0.0	−3.759	0.187
0.1	−2.490	945
0.2	−1.589	964
0.3	−0.9352	862
0.4	4545	777
0.5	0982	725
0.6	+0.1663	695
0.7	3621	677
0.8	5058	661
0.9	6096	643
1.0	6825	623
1.1	7315	598
1.2	7620	570
1.3	7780	539
1.4	7827	506
1.5	7788	473
1.6	7683	439
1.7	7527	405
1.8	7333	373
1.9	7113	342
2.0	6873	313

§ 4. Comparison with Experimental Results.

As already mentioned in the introduction, the calculated B agrees with the observed tmperature variation of the second virial coefficient, if two parameters r_0 and U_0 are given suitable values. Adopting these values, let us compare the calculated C with the observed third virial coefficients. The results for neon, argon, methane and nitrogen are given in the following 4 tables.

Table III.

Neon, $r_0 = 3.10$ Å, $U_0/k = 35.7°$,
observed values are due to Holborn-Otto.⁽⁴⁾

T(°K)	B(Å^3)		$C\times10^{-2}$(Å^6)	
	obs.	calc.	obs.	calc.
65.2	−34.8	−35.4	15.5	8.0
90.6	−13.6	−13.3	12.2	6.9
123	0.2	0.0	6.1	6.3
173	10.7	9.9	5.5	6.0
223	15.1	14.9	6.3	5.9
273	17.7	17.4	7.0	5.7
373	19.7	20.4	11.9	5.5
473	21.7	22.0	9.2	5.3
573	22.8	22.7		
673	22.8	23.1		

Table IV.

Argon, $r_0 = 3.82$ Å, $U_0/k = 119°$,
observed values are due to Holborn-Otto.

T(°K)	B(Å^3)		$C\times10^{-2}$(Å^6)	
	obs.	calc.	obs.	calc.
173	−106.8	−107.5	48	28
223	−62.7	−62.1	46	28
273	−36.7	−35.9	33	24
323	−18.3	−18.7	31	23
373	−7.1	−6.2	27	22
423	1.9	2.0	27	22
473	7.8	9.3		
573	18.6	18.3		

Table V.

Methane, $r_0 = 4.27$ Å, $U_0/k = 148°$.
observed values are due to Michels-Nederbragt.⁽⁵⁾

T(°K)	B(Å^3)		$C\times10^{-2}$(Å^6)	
	obs.	calc.	obs.	calc.
273	−89.6	−90.1	79	54
298	−72.1	−71.3	72	52
323	−57.6	−58.2	66	50
348	−46.1	−46.0	65	48
373	−35.9	−35.0	59	47
398	−27.2	−27.1	55	46
423	−19.3	−19.8	49	45

Table VI.

Nitrogen, $r_0 = 4.15$ Å, $U_0/k = 95°$,
observed values are due to Holborn-Otto.

T(°K)	B(Å^3)		$C\times10^{-2}$(Å^6)	
	obs.	calc.	obs.	calc.
143	−132.4	−128.0	73	50
173	86.0	−85.4	59	46
223	−43.8	−42.6	56	41
273	17.2	−17.6	46	38
323	−0.4	−1.1	36	36
373	10.2	10.7	35	36
423	19.1	18.7	30	35
473	25.5	25.5	28	35
573	34.3	34.1	24	34
673	39.0	39.9	31	33

Systematic disagreement is eminent, indicating that the assumed model does not agree sufficiently with the true intermolecular potential.

§ 5. Conclusion.

The present model⁽⁴⁾ requires modification: it is not suitable, however, to choose a number other than 12 as the exponent n of the repulsive term. Here we remember that the temperature variation of the third virial coefficient predicted by "box-potential":

$$U(r) = \begin{cases} \infty & r < \sigma \\ -U_0 & \sigma < r < g\sigma \\ 0 & g\sigma < r \end{cases}$$

with $1.8 < g < 2.0$ shows rather sufficiently the characteristic feature of the observed one. This value of g, $1.8 < g < 2.0$, corresponds to large width of the negative part of intermolecular potential $U(r)$. For these reasons we can anticipate that a more accurate model would have to be wider and harder than the present model, such as the dotted curve shown in Fig. 2.

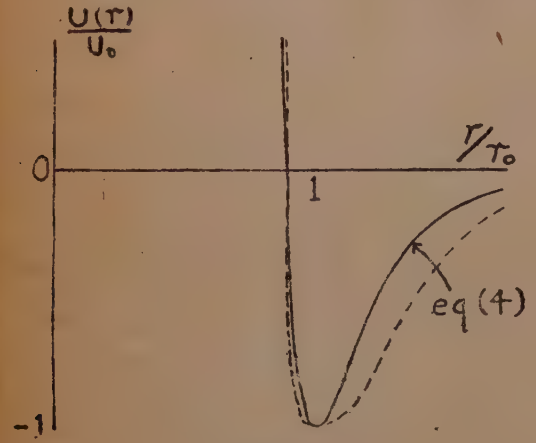

Fig. 2.

The author wishes to thank Prof. M. Kotani for his helpful discussions.

References.

(1) J. E. Mayer and M. G. Mayer: Statistical Mechanics (1940) Chap. 13.

(2) Lennard-Jones, Proc. Roy. Soc. A **106** (1924) 463, Proc. Phys. Soc. **43** (1931) 461.

(3) T. Kihara, Nippon Sugaku-Buturigakukaisi **17** (1943) 11.

(4) L. Holborn u. J. Otto, Zeits. f. Phys. **10** (1922) 367, **23** (1924) 77, **30** (1824) 320, **33** (1925) 1, **38** (1926) 359.

(5) A. Michels and G. W. Nederbragt, Physica **3** (1936) 569.

Short Notes.

Thermodynamics of Phase Change.

By Ryoichi KIKUCHI.

Institute of Physics, Faculty of Science, University of Tokyo.

(Received March 11, 1948).

In a recent paper, E. F. Lype(1) has reported his opinion on the phase change of higher orders, inducing criticisms by P. W. Bridgman(2) and R. Oldenburger(3). The author wants to add a few remarks to their discussions.

While the "second order transition" meant by Ehrenfest(4) occurs in the case where the order of transition remains unchanged along a curve in $p-T$ plane, Lype is dealing with the case in which the conditions for second order transition are satisfied only at a point P in the plane, as rightly pointed out by the critics. In the latter case, as shown by Lype, there generally lie two transition curves passing the point P, whose directions Dp/DT are to be determined by the equation(5)

$$\left(\left(\frac{\partial^2 Z}{\partial p^2}\right)\right)\left(\frac{Dp}{DT}\right)^2 - 2\left(\left(\frac{\partial^2 Z}{\partial p \partial T}\right)\right)\frac{Dp}{DT} + \left(\left(\frac{\partial^2 Z}{\partial T^2}\right)\right) = 0 \tag{1}$$

If these two curves do not degenerate into one, we can easily show that, along each of the transition curves, on the one side of P, we get $S_a > S_b$, and on the other side $S_a < S_b$(6). As the phase is more stable on the higher temperature side of the transition curve if $S_a > S_b$, the diagram of more stable phases for the four regions divided by the two curves must be such as in Fig. 1, in which the solid curves mean the portion on which $S_a > S_b$. In this case transition does not occur at the point P and on the curves except P, we have first order transitions.

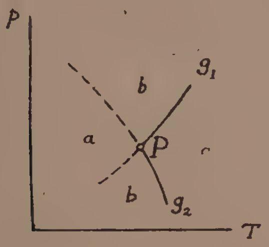

Fig. 1.

According to circumstances there may occur the case in which in one of the four regions, e. g., in the left region, the phase in Fig. 1, i. e., a cannot exist in equilibrium. Then in this region the phase b must be realized, and the phase diagram becomes such as in Fig. 2, giving really the second order transition at P and the first order ones on the portions Pg_1 and Pg_2 except the point P. One of the examples of Fig. 2 is the superconductor transition shown in Fig. 3, in which the transition is of the first order along the curve g except the point $P(H=0)$, where it is of the second order. In this case p in Eq. (1) should be replaced by the strength of magnetic field H, and the extensive variable correspouding to H is magnetization σ, so that

$$Z = -SdT - \sigma dH \qquad (2)$$

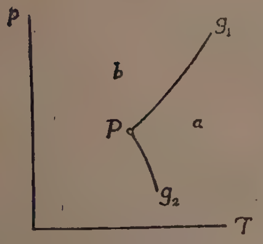

Fig. 2.

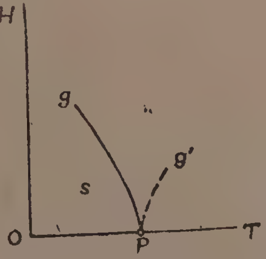

Fig. 3

Considering the peculiarity of superconductor, we have from Eq. (1)

$$\left(\left(\frac{\partial\sigma}{\partial H}\right)\right)\left(\frac{DH}{DT}\right)^2 + \frac{((C))}{T} = 0, \qquad (3)$$

which is the Rutger's equation(7) and was verified experimentally(8). It must be noted that in this case, out of the two roots of Eq. (3), only $DH/DT < 0$ is realized. This is explained by the possibility that the region in which the superconducting phase can exist in equilibrium stably or metastably disappears among the middle region between curves g and g' in Fig. 3.

In connection with the transition of Fig. 2 the author wants to add the following remark. After the above discussions we can easily conclude the non-existence of apparently probable phase diagram such as Fig. 4. which claims that along a smooth curve g the transition is of the first order except only a point P at which it is of the second order.

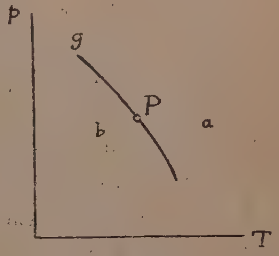

Fig. 4.

The author wants to express his cordial thanks to Messrs. H. Ichimura, A. Ishihara, and A. Miyake who introduced to him the papers by Lype and others and discussed earnestly on the problem with him.

References and Notes.

(1) E. F. Lype: Phys. Rev. **69**, 652 (1946).

(2) P. W. Bridgman: ditto, **70**, 425 (1946).

(3) R. Oldenburger: ditto, **70**, 433 (1946).

(4) P. Ehrenfest: Comm. Leiden, Suppl. 75b (1933).

(5) Notations in Eq. (1) is the same as used by Ehrenfest.

(6) a and b mean two possible phases on the opposite side of the transition curve. In the singular case $S_a = S_b$, the volumes of the two phases must be different along each of the transition curves and we can conclude the same result, Fig. 1, using the volume instead of the entropy.

(7) P. Ehrenfest: loc. cit.; A. J. Rutgers, Physica **1**, 1055 (1934).

(8) W. H. Keesom and J. A. Kok: Physica **1**, 175 (1934).

On the Effect of Mechanical Stress upon the Permittivity of Barium Titanate.

By Yutaka TAKAGI, Etsuro SAWAGUCHI and Tetsuo AKIOKA.

Second Faculty of Engineering, University of Tokyo.

(Recived March 16, 1948)

Barium titanate has nowadays become known as a new kind of ferroelectrics on account of many evidences. Among them hysteresis loops(1) found in cathode-ray oscillograms and the Curie-Weiss law(2) proved to hold at heigher temperatures may especially be mentioned. The temperature at which the sharp peak(3) of permittivity occurs has been identified with the Curie point of this ferroelectrics.

It has been confirmed that a structural transformation(4) accompanies with the dielectric transition; the lattice is cubic above the Curie temperature, while it becomes tetragonal in ferroelectric state in consequence of slight elongation of one axis parallel to the direction of intrinsic polarization. If, therefore, any alignment of the Weiss-domains(5) should occur under the influence of electric field, then some change of external dimensions of a piece of ceramic must be observed. In fact Mason(6) recently detected the existence of this effect, i.e. the electrostrictive strain, and from it he was able to estimate the amount of alignment of domains to be about 7.5%.

We have here investigated the inverse effect of hindering the alignment of domains by means of mechanical compression. A piece of barium titanate ceramic, silver-plated on both faces, was set between the compression discs of Amsler-type testing machine, and at the same time it was inserted in one branch of a capacitance bridge. The temperature was slowly raised at the rate of 0.5 deg/min. by an electric furnace set arround the specimen. 70 V/cm field strength of 3 KC/sec was used for measurements. The results are shown in Fig. 1. Just as expected, the decrease of permittivity is proved to be the case; the effect is especially notable near the Curie temperature. The

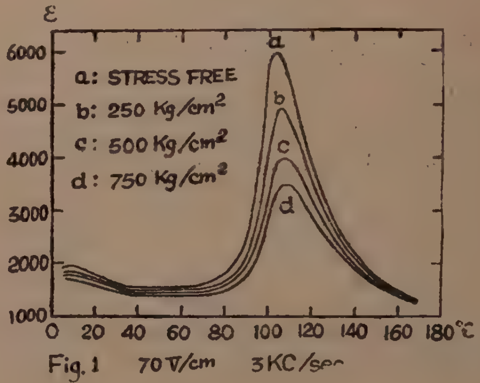

Fig. 1.

values are not corrected for the decrease of thickness, so the effect plotted here must be regarded as being somewhat under-estimated.

Apparently it may be seen from these curves that the Curie point is raised slightly as the stress is increased. This spurious aspect is removed in

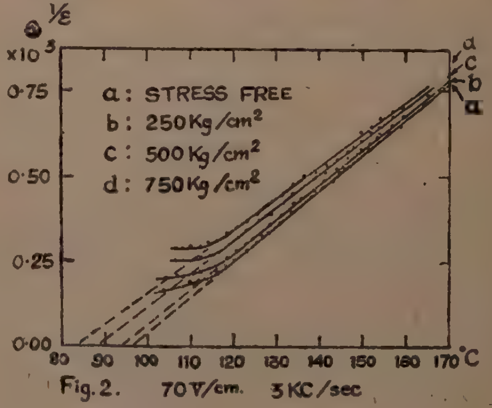

Fig. 2.

Fig. 2, which shows the results of plotting the inverse of permittivity against temperatures. The paraelectric Curie point at which the extrapolation of any straight line intersects the abscissa proves to be lowered by compression. Because the

Poisson's ratio(6) is 0.27 for this material, the compression means the contraction of lattice dimensions, and this lowering of the Curie point is quite reasonable.

Brown tube oscillograms were photographed at various temperatures during the course of the above measurements. 5000 V/cm swing of 50 cycles/sec was applied to the specimen in a circuit similar in principles to that used by Sawyer and Tower. With increasing stress a marked depression of dielectric saturation values is observed, and if the stress is unloaded the flattened hysteresis loop immediately recovers its original shape. Two typical examples among them, photographed at 8°C and 80°C respectively, are shown reproduced in Figs. 3 and 4.

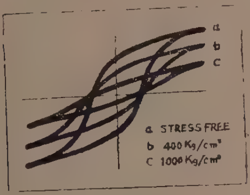

Fig. 3.

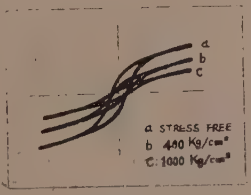

Fig. 4.

The effect of transverse compression was also investigated, and slight elevation of saturation polarization was perceived. The effect, however, was not so conspicuous as in the longitudinal case, and was somewhat errorneous on account of frequent fractures of test-pieces.

The authors wish to express their sincere thanks to Dr. H. Inuzuka and Mr. S. Sawada and Mr. G. Shirane for many fascilities generously endowed by them.

References.

(1) J. K. Hulm: Nature, **160** (1947), 127.

(2) S. Roberts: Phys. Rev., **71** (1947), 890.

(3) In our country, this peak was first discovered by Ogawa in January, 1944.

(4) S. Miyake and R. Ueda: J. Phys. Soc. Jap., **1** (1946), 32. M. G. Harwood, P. Popper and D. F. Rushman; Nature, **160** (1947), 58.

(5) H. F. Kay and R. G. Rhodes: Nature, **160** (1947), 126.

(6) W. P. Mason: Phys. Rev., **72** (1947), 869.

Theory of the Transition in KH_2PO_4. (I)*

By Yutaka Takagi.

Tokyo Institute of Technology.

(Received April 20, 1948)

The well-known "hydrogen-bond model" of potassium dihydrogen phosphate which was first introduced by Slater(1) has been discussed in another way. The method is essentially similar to that developed by the present writer in his paper(2) on "Statistical Theory of Binary Alloys. I." Slater's assumptions may be briefly summarized as follows: (1) each bond connecting the opposite oxygen atoms on the corners of neighbouring PO_4-radicals has always one and only one hydrogen, (2) each phosphate tetrahedron has always two hydrogens close to it, and (3) among the six probable kinds of H_2PO_4-configurations, two types which have both two H's either on the upper corners (let this be denoted by D_+) or on the lower corners (let this be denoted by D_-) are energetically more stable by an amount ε_0 than the other four configurations which have one H on an upper corner while the other on a lower corner (let these four be denoted by D_0).

Let us consider a piece of crystal containing N molecules of KH_2PO_4, then obviously we have**

$$D_+ + D_- + D_0 = N. \qquad (1)$$

Now, any bond shall be specified by b₊ and b₋ according to whether the H on it is localized near the lower PO_4 or the upper PO_4, respectively. The following identities hold

$$\left.\begin{aligned} 2b_+ &= 4D_+ + 2D_0, \\ 2b_- &= 4D_- + 2D_0. \end{aligned}\right\} \qquad (2)$$

If the b_+'s and b_-'s given by Eq. (2) were allowed to be arranged at random, the total number of configurations would be

$$(b_+ + b_-)!/b_+!\,b_-!. \qquad (3)$$

But from them we must pick up the satisfactory cases, because many undesirable configurations containing forbidden groups such as HPO_4, H_3PO_4 and etc. are also counted in (3). The writer has been able to prove, to an approximation just comparable with that of quasi-chemical theory(3) of superlattices, that if one multiplies (3) by the following expression,

$$\left(\frac{b_+}{b_+ + b_-}\right)^{4D_+}\left(\frac{b_-}{b_+ + b_-}\right)^{4D_-}\left\{4\left(\frac{b_+}{b_+ + b_-}\right)^2 \cdot \left(\frac{b_-}{b_+ + b_-}\right)^2\right\}^{D_0}\frac{N!}{D_+!\,D_-!\,D_0!}, \qquad (4)$$

undesirable cases will effectively be excluded.

Consequently,
$$W = \frac{b_+^{\,b_+} b_-^{\,b_-}}{(b_+ + b_-)^{b_+ + b_-}} \times \frac{4^{D_0} N!}{D_+!\,D_-!\,D_0!}. \qquad (5)$$

It is easy to verify that Eq. (5) agrees exactly with that(4) formerly obtained by Slater.

Along the line of this idea the writer has succesfully discussed a generalized case in which external electric field is not necessarily papallel to c-axis. The results obtained are as follows: (1) the susceptibility χ_a in the direction of a-axis is given by

$$\frac{\varepsilon_0}{N\mu_a^2}\chi_a = \frac{\varepsilon_0}{kT}\exp\left(-\frac{\varepsilon_0}{kT}\right), \qquad (6)$$

where μ_a denotes the dipole moment of a D_0-group in the plane perpendicular to c-axis, (see Fig. 1); (2) if a strong field is applied in the direction of a-axis the ferroelectric Curie point is lowered, although the general aspect of first order transition remaining unaltered: and (3) if a strong field is applied in the direction parallel to c-axis, the temperature range of transition becomes greatly broadened and shifted to the higher side. The curve, however, is of quite a different shape from the observed one(5) which, as known well, closely resembles a magnetization vs. temperature curve of ferromagnetics.

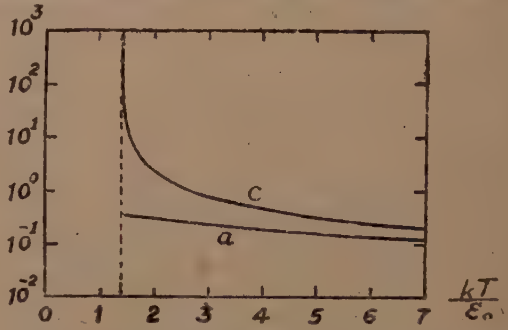

Fig. 1. Curve (a) represents $\varepsilon_0\chi_a/N\mu_a^2$, where χ_a is susceptibility in the direction of a-axis, and μ_a denotes the dipole moment of D_0-group in the same direction. Curve (c) represents $\varepsilon_0\chi_c/N\mu_c^2$, where χ_c is susceptibility in the direction of c-axis, and μ_c denotes the dipole mement of D_+ or D_- groups in the direction of c-axis.

References.

(*) A full text of this note was already published with 10 figures in "Nippon Sugaku-Buturi Gakkai-Si" **17** (1943), 280. (in Japanese).

(**) If printed in Roman type, the symbols stand for the individuals: while if printed in italic type they mean the total number of denoted species contained in a crystal.

(1) J. C. Slater: J. Chem. Phps. **9** (1941), 16.

(2) Y. Takagi: Proc. Phys.-Math. Soc. Jap. **23** (1941), 44.

(3) R. H. Fowler and E. A. Guggenheim: Proc. Roy. Soc. A, **174** (1940), 189.

(4) J. C. Slater: ibid. the formula (3.10).

(5) G. Busch: Helv. Phys. Acta, **11** (1938), 269.

Theory of the Transition in KH_2PO_4, (II)*.

By Yutaka TAKAGI.

Tokyo Institute of Technology.

(Received April 20, 1948)

For the purpose of explaining the second order transition observed in experiments, the restriction with regard to the number of H's around each phosphate tetrahedron mentioned in the preceding note, is tentatively loosened a little in this second note. Namely, it may be assumed that the following reaction,

$$D_+ + D_- + 2\varepsilon_\tau \rightarrow HPO_4 + H_3PO_4, \qquad (1)$$

will occur provided that a finite amount of energy $2\varepsilon_\tau$ is added to the crystal.

Let these newly admitted groups HPO_4 and H_3PO_4 be denoted by the symbols M and T respectively, and add to them suffixes + or — according to whether their dipole moments are in $+c$ or $-c$ direction. Then the following identities hold:

$$\left.\begin{aligned} 2b_+ &= 4D_+ + 2D_0 + 3M_+ + M_- + 3T_+ + T_-, \\ 2b_- &= 4D_- + 2D_0 + M_+ + 3M_- + T_+ + 3T_-. \end{aligned}\right\} \qquad (2)$$

According to the same idea as in the preceding note, the satisfactory configurations in which the number of each kind of atomic groups, i.e. D_+, D_-, D_0, M_+, M_-, T_+ and T_-, is just as many as given beforehand, can be enumerated as follows:

$$W = \frac{b_+^{\,b_+} b_-^{\,b_-}}{(b_+ + b_-)^{b_+ + b_-}} \times \frac{4^{D_0} 2^{(M_+ + M_- + T_+ + T_-)}\, N!}{D_+!\,D_-!\,D_0!\,M_+!\,M_-!\,T_+!\,T_-!}. \qquad (3)$$

The internal energy U is given by

$$U = -(D_+ - D_-)\mu E - (M_+ - M_- + T_+ - T_-)(\mu/2)E + D_0\varepsilon_0 + (M_+ + M_- + T_+ + T_-)\varepsilon_\tau. \qquad (4)$$

The temperature dependence of spontaneous polarization calculated from these equations is shown in Fig. 1, where the number beside each curve denotes the value of $\varepsilon_\tau/\varepsilon_0$. Thus, the purpose of the present treatment is fulfilled fairly well. Comparison with Busch's experiments⁽¹⁾ tells us that the best fit is obtainable when $\varepsilon_\tau/\varepsilon_0$ is about 5.

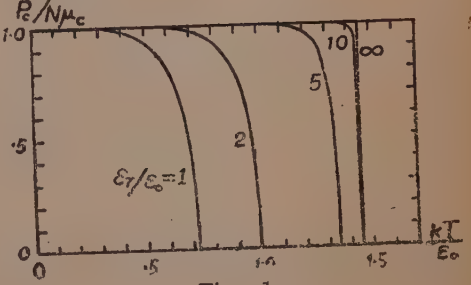

Fig. 1.

Fig. 1. P_c: spontaneous polarization along c-axis, and $N\mu_c$: saturation polarization along c-axis.

If it is assumed that the more easily M and T groups are generated the more remarkable becomes the depression of the ferroelectric critical temperature. The curve of Curie temperature T_c vs. $\varepsilon_\tau/\varepsilon_0$ is shown in Fig. 2. The reasonable value of ε_τ which is estimated from these two figures is about 1 kcal/mol. (The point marked with S corresponds to Slater's critical temperature⁽²⁾, i.e. the temperature which is to be expected when $\varepsilon_\tau/\varepsilon_0$ is ∞.

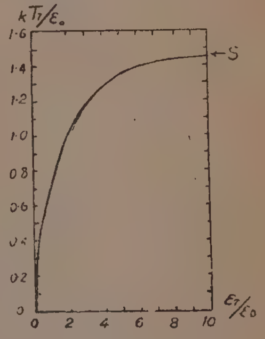

Fig. 2.

Configurational specific heat is shown in Fig. 3. As a consequence of the present reformation, λ-type peak, though it is extraordinary high and

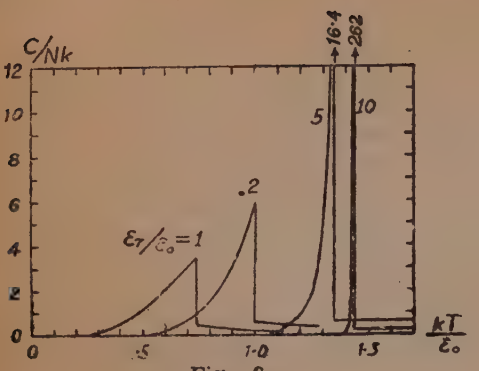

Fig. 3.

becomes almost undistinguishable from latent heat derived in the preceding note especially when $\varepsilon_\tau/\varepsilon_0$ is more than∼10, is thus predicted.

References.

* A full text of this note will soon be published with 9 figures in this Journal.

(1) G. Busch: Helv. Phys. Acta, **11** (1938), 269.

(2) J. C. Slater: J. Chem. Phys., **9** (1941), 16.

Theory of the Transition in KH_2PO_4.

By Gen SHIRANE And Takehiko OGUCHI.

The Second Faculty of Engineering, University of Tokyo. *Tokyo Institute of Technology*

(Received April 20, 1948)

There are two possibilities for the explanation of the second order transition in actual KH_2PO_4 crystal. One of which was examined by Takagi⁽¹⁾, while the other will be discussed here.

The writers assume that, if a finite amount of energy $2\varepsilon_T$ is added to the crystal, some bonds may have either two hydrogens (say b'_0) or none (say b_0), while the number of hydrogens around each phosphate remains strictly constrained to two. Thus the following reaction will occur:

$$b_+ + b_- + 2\varepsilon_T \leftrightarrows b_0 + b'_0$$

Since the crystal is neutral, b_0 is of course equal to b'_0. Therefore both b_0 and b_0' shall hereafter be denoted by b_0. Then the following identities hold:

$$b_+ + b_0 = 2D_+ + D_0$$

$$b_- + b_0 = 2D_- + D_0 .$$

With the method analogous to that used by Takagi⁽²⁾, the writers have succeeded in proving that the satisfactory configurations in which the number of each kind of atomic groups D₊, D₋ and D₀ and the number of each kind of bonds b_+, b_-, b_0 and b'_0 are given, can be enumerated as follows:

$$W = \frac{(b_+ + b_0)^{2(b_+ + b_0)}(b_- + b_0)^{2(b_- + b_0)}}{(b_+ + b_- + 2b_0)^{b_+ + b_- + 2b_0} b_+^{b_+} b_-^{b_-} b_0^{b_0}} \times \frac{4^{D_0} N!}{D_+!\,D_-!\,D_0!} .$$

The internal energy is

$$U = -(D_+ - D_-)\mu E_c + D_0\varepsilon_0 + 2b_0\varepsilon_T .$$

The temperature dependence of spontaneous polarization, configurational specific heat, etc. have been calculated from these equations for several values of $\varepsilon_T/\varepsilon_0$. Let the results be compared with those previously obtained by Takagi⁽¹⁾: (1) the relation between Curie temperature T_T and $\varepsilon_T/\varepsilon_0$ exactly coincides with that between T_τ and $\varepsilon_\tau/\varepsilon_0$, (see the preceding note, Fig. 2.), (2) if the value of $\varepsilon_\tau/\varepsilon_0$ is to be equated to the value of $\varepsilon_T/\varepsilon_0$, the temperature dependence of spontaneous polarization and configurational specific heat are similar to those of the preceding note, when especially $\varepsilon_T/\varepsilon_0$ becomes large.

The best agreement with experiments[3] is also obtained when $\varepsilon_T/\varepsilon_0$ is about 5, and the value of ε_T is found to be about 1 kcal/mol. ε_T is the energy required to cut off one hydrogen bond, the value of which has been estimated to be about 1 ~ 9 kcal/mol from various experiments. The present results may, therefore, be said quite reasonable.

The writers wish to express their sincere thanks to Prof. Takagi for his kind guidance in this work.(*)

References.

(*) A full text of this note will soon be published with 5 figures in this Journal.

(1) Y. Takagi: Note II in this issue.

(2) Y. Takagi: Note I in this issue.

(3) G. Busch: Helv. Phys. Acta. **11** (1938), 269.

Statistical Theory of the Ferromagnetic Superlattice.*

Part I. General Theory.

By Toshinosuke MUTO, Tetsuo EGUCHI and Motoichi SHIBUYA.

Institute of Science and Technology, University of Tokyo
& Institute of Physics, Kyushu University.

(Received December 15, 1947).

§ 1. Introduction.

The influence of order-disorder transformation upon the ferromagnetic properties of alloys has been extensively observed, through the peculiar heating processes of quenching and annealing, by many experimental investigators⁽¹⁾, although we have still hardly established the sufficiently confirmative evidence indicatve of the fact that the ordered structures in alloys are necessarily associated with the ferromagnetic state. Among a large number of alloys observed experimentally, however, a few of them, i. e., Ni_3Fe⁽²⁾, Ni_3Mn⁽³⁾, Heusler alloys⁽⁴⁾ and others may be considered safely to have ordered structure associated with the ferromagnetic state on the basis of the combined experimental results of thermal, electrical, magnetic, thermoelectcical and X-ray-measurements, although the X-ray data for the former class of alloys are now lacking owing to the similar electronic structures of constituent atoms involved. In view of the experimental situation mentioned above, it is highly desirable, for the detailed analysis and discussions of the experimental materials, to work out theoretically the relationships between the order of constituent atoms and ferromagnetic properties of alloys, giving the possible orientations in the field of experimental researches. In contrast to the ferromagnetism⁽⁵⁾ which can not be understood without a thorough quantum-mechanical investigation the theory of atomic arrangements in superlaltice is purely a classical statistics and it has been relatively simply worked out by Bragg and Williams⁽⁶⁾, Bethe⁽⁷⁾ and others⁽⁸⁾, assuming** for the interactions between constituent atoms in alloys the quantum-mechancal bond energy sensibly dependent upon the mutual distances of the atoms, although much remains to be done as regards quantitative results. As is well known, however, we are forced to meet with the unsolved difficulties connected with the many electron systems in the quantum theory of ferromagnetism. It, therefore, is hardly possible to work out quantum-mechanically the ferromagnetism of superlattice-alloys without introducing some plausible simplifications of the crystal-model or the Brillouin zone structure of alloys, thus enabling us to remove the above mentioned mathematical difficulties. Now the available statistical method of treatment of the order-disorder problom may be considered to throw much light on the other cooperative phenomena, i. e., the adsorption, the ferromagnetism and the melting. In fact, U. Firgau⁽⁹⁾ har recently succeeded in showing that an adequate phenomenological description of the ferromagnetism of pure metals may be given on the lines of the superlattice theory refined by Bethe, using the simplified model of Ising⁽¹⁰⁾. In this connection, therefore, we shall here develop the statistical theory of the ferromagnetism of superlattice-alloy along a similar way to that of Firgau in the case of pure metals in order to clarify the possible correlation between the atomic distribution in superlattice and the molecular magnet distribution responsible for the ferromagnetism of alloys. In spite of the approximate nature* involved in the assumption that there is no correlation between the bond energy of constituent atoms and the exchange energy responsible for the ferromagnetism, the statistical distributions of both constituent atoms in alloy and magnetic moments of molecular magnets situated at each lattice point of the crystal may be considered to be sensibly influenced with respect to each other, indicating the possible relationship between the order of the constituent atoms and the ferromagnetism of alloys, which fact shall be shown in the present paper. In Part I, the general theory of the ferromagnetic superlattice shall be dealt with, in Part II the obtained result shall be applied to the anomalous specific heat and the spontaneous magnetization and in Part III the elastic scattering of slow neutron by the ferromagnetic superlattice shall be worked out theoretically in close connection with the possible influence of the ferromagnetism of alloys upon the mentioned phenomena.

---

* The content of the paper was read already in the symposiums of magnetism held at University of Tokyo in November, 1945 and further, in tne annual meeting of the Physical Society of Japan held in May, 1946.

** Although the theory of cohesion of alloys has not quantum-mechanically been worked yet, the mechanism of cohesion of alloys will be taken approximately to be of intermediate type between the metallic and ionic binding on a simple theoretical consideration, which expectation shall be tested quantitatively in the detailed calculation of the binding energy of alloy by one of the authors in our institute.

§ 2. A Model of the Ferromagnetic Alloys Capable of Order-Disorder Transformations.

Along a similar way to Firgau's theory⁽¹¹⁾ of ferromagnetism of pure metals, we shall here adopt Ising's model of the ferromagnetic binary alloys, in which two kinds of molecular magnets associated with A-and B-atoms involved are distributed among all lattice points of the crystal lattice, the possible orientations of each of the molecular magnets being supposed to be parallel or antiparallel to a definite direction of the external magnetic field. According to the quantum theory of the electronic systems in alloys, the exchange interaction energies $-w_{AA}$, $-w_{AB}$ and $-w_{BB}$ ($w_{AA}>0$, $w_{AB}>0$, $w_{BB}>0$) are supposed approximately to exist only between a pair of nearest neighbours of molecular magnets with parallel orientations with respect to each other, allowing for the rapid decrease of the mentioned energies with the mutual distances separating them and, furthermore, the bond interaction energies of v_{AA}, v_{AB} and v_{BB} between constituent atoms are considered to play important roles in the atomic distribution in alloys in a similar way to the case of Bethe's theory⁽¹²⁾ of superlattice. The double suffices belonging to each of the interaction energies denote the kinds of pairs of constituent atoms concerned respectively. Since all the molecular magnets of the alloy are distributed to have parallel orientations with respect to each other at absolute temperature zero the alloy may be considered to become ferromagnetic in a similar way to that of the ferromagnetic metals owing to the exchange interaction energies of molecular magnets mentioned above.

In order to find the total energy of a given distribution of A- and B- atoms and their associated molecular magnets, we must know how many pairs of unlike neighbours with parllel or antiparallel magnetic moments occur in the crystal. Denoting the numbers of pairs of nearest neighbours mentioned above by $Q_{AB}=Q_{AB}^{\upuparrows}+Q_{AB}^{\updownarrows}$, $Q_{AA}=Q_{AA}^{\upuparrows}+Q_{AA}^{\updownarrows}$ and $Q_{BB}=Q_{BB}^{\upuparrows}+Q_{BB}^{\updownarrows}$ respectively, we obtain for the total energy of the crystal

$$\begin{aligned} E = E_0 &+ v_{AA}Q_{AA}+v_{AB}Q_{AB}+v_{BB}Q_{BB} \\ &-w_{AA}Q_{AA}^{\upuparrows}-w_{AB}Q_{AB}^{\upuparrows}-w_{BB}Q_{BB}^{\upuparrows}, \end{aligned} \tag{1}$$

where E_0 expresses the sum of the internal energies of each of the constituent atoms involved and their vibrational energies, which do not concern us for our problem under consideration. In dealing with the energy of the alloy it is convenient to take as zero the energy of the constituent metals for pure constituent metals only with antiparallel pairs of molecular magnets. After a simple calculation, the expression (1) may be reduced to the following form,

---

* In a more accurate treatment of the problem under consideration, we have to take into account quantum-mechanically the mutual interactions among the valency electrons mainly responsible for the cohesion of alloys and the $3d$ electrons which give rise to the ferromagnetism of alloys, on account of which some correlative behaviours in the crystal energy may be expected to appear. In the classical statistics of the problem considered here, however, we shall be permitted to neglect approximately such characteristic correlation in energy of both kinds of electrons in alloys.

$$E = E_0' - vQ_{AB} - w_{AA}Q_{AA}^{\upuparrows} - w_{AB}Q_{AB}^{\upuparrows} - w_{BB}Q_{BB}^{\upuparrows}, \tag{2}$$

where E_0' expresses the crystal energy* independent of the distributions of both the constituent atoms and the molecular magnets within the alloy and $v = (v_{AA}+v_{BB})/2 - v_{AB} > 0$.

§ 3. Statistical Theory of Both Atomic and Molecular Magnet Distributions in Alloys.**

The fundamental problem in the theory of the ferromagnetism of superlattice is to calculate the probability of the occupation of a lattice point by a given constituent atoms with its magnetic moment of a definite orientation as a function of both temperature T and mutual interaction energies introduced above. For this purpose we shall now proceed along a similar way to Bethe's theory of superlattice or Firgau's theory of the ferromagnetism of pure metals. For simplicity of the calculation, we shall here take a simple cubic lattice or a body-centred cubic one consisting of equal numbers of A- and B-atoms, the nearest neighbours of any atom situated at a lattice point being expressed by Z in number.

According to Bethe(13), we shall now calculate the partition function of a group of sites consisting of one site, arbitrarily selected, and its boundary sites of nearest neighbours, the statistical influence of ordering of all the remaining sites of the exterior upon the boundary ones of the group being taken into account, on the average, by introducing the statistical parameters ε_a and ε_s respectively. ε_a refers to the degree of ordered distribution of A- and B-atoms in alloys and ε_s to that of the possible orientations of the molecular magnets among the lattice sites of the crystal. From the consideration of the physical symmetry of lattice sites regarding both atomic and magnetic moment distributions, it is possible to establish two basic equations for determining ε_a and ε_s as functions of temperature T and mutual interaction energies v, w_{AA}, etc.

In a more accurate method of treatment, however, we have necessarily to introduce four statistical parameters ε_a, ε_a', ε_s and ε_s' corresponding to the combinations of the different kinds of atoms and the different orientations of the molecular magnets in order to take into account the statistical influence of ordering of all the exterior sites upon the boundary of the group and then four basic equations to determine the dependences of all the parameters upon temperature and mutual interaction energies are required to be established from the physical symmetry of lattic sites of the crystal. To a first approximation, however, we shall be permitted reasonably to take two statistical parameters ε_a and ε_s, instead of four, for a preliminary investigation of the problem in question, thus avoiding the laborious mathematical procedure unnecessary for a qualitative investigation of the physical characteristics of the phenomena.

Among Z neighbours of the centre site of the group, there are n wrong atoms and $Z-n$ right atoms with respect to the atomic distribution. Furthermore, m_A wrong atoms and m_B right atoms are supposed to have parallel magnetic moments with respect to an external magnetic field, while $n-m_A$ wrong atoms and $Z-n-m_A$ right atoms to have antiparallel magnetic moments respectively. Thus, a given distribution of both atoms and magnetic moments among the sites of the group under consideration may be considered to be specified uniquely with a triple numbers of n, m_A and m_B. In the computation of the partition function for each configuration, specified by n, m_A and m_B, or the group mentioned above, it is sufficient to take into account the following Boltzmann factors and statistical parameters weighting unfavourably the occurrence of a wrong pair compared to right pair in accordance with Bethe and Firgau:

For atomic distribution:

Boltzmann factor = 1 corresponding to a pair of unlike atoms,

,, $= \exp(-v/kT) = x_a$,, to a

---

* The influence of the atomic rearrangement upon the lattice vibrations is neglected approximately in our theory.

** The ferromagnetism of alloys has been discussed qualitatively by Bitter (Phys. Rev. **54**, 1938, 79) along a similar way to the procedure in Bragg-Wiliams' theory of superlattice alloys, but the detailed discussion has not been attempted.

pair of like atoms,

Statistical parameter $= \varepsilon_a$,, to a wrong atom on the boundary.

For magnetic moment distribution:

Boltzmann factor $= \exp(-w_{AA}/kT) = x_A$ corresponding to a pair of A atoms with antiparallel molecular magnets,

,, $= \exp(-w_{BB}/kT) = x_B$,, of B atoms ,, ,, ,,,

,, $= \exp(-w_{AB}/kT) = x_{AB}$,, of A- and B-atoms ,, ,,,

,, $= \exp(2\beta_A H/kT) = y_A$ }

,, $= \exp(2\beta_B H/kT) = y_B$ } ,, to an A- or B- atom with magnetic moment parallel to the external magnetic field respectively,

Statistical parameter $= \varepsilon_s$,, to a parallel magnetic moment of molecular magnet on the boundary,

where k denotes Boltzmann constant, T the absolute temperature, H the magnitude of the external magnetic field, and β_A and β_B represent the magnetic moments of A- and B-molecular magnets respectively.

For the partition functions (or relative probabilities) of specified configurations of the group under cosideration, therefore, it follows, by the similar reasonings of Bethe(14) and Firgau(15),

$$r^{\uparrow}{}_{n,m_A,m_B} = \binom{z}{n} x_a^n \varepsilon_a^n \cdot y_A \cdot y_A^{m_A} \binom{n}{m_A} \cdot x_A^{n-m_A} \varepsilon_s^{m_A} \cdot y_B^{m_B} \binom{z-n}{m_B} x_{AB}^{z-n-m_A} \varepsilon_s^{m_B}, \tag{3}$$

for the case of the right atom with parallel magnetic moment on a centre site of the group,

$$r^{\downarrow}{}_{n,m_A,m_B} = \binom{z}{n} x_a^n \varepsilon_a^n \cdot y_A^{m_A} \binom{n}{m_A} x_A^{m_A} \varepsilon_s^{m_A} \cdot y_B^{m_B} \binom{z-n}{m_B} x_{AB}^{m_B} \varepsilon_s^{m_B}, \tag{4}$$

for the case of the right atom with antiparallel magntic moment on a centre site of the group,

$$w^{\uparrow}{}_{n,m_A,m_B} = \binom{z}{n} x_a^{z-n} \varepsilon_a^n \cdot y_B \cdot y_A^{m_A} \binom{n}{m_A} x_{AB}^{n-m_A} \varepsilon_s^{m_A} \cdot y_B^{m_B} \binom{z-n}{m_B} x_B^{z-n-m_B} \varepsilon_s^{m_B}, \tag{5}$$

for the case of the wrong atom with parallel magnetic moment on a centre site of the group, and

$$w^{\downarrow}{}_{n,m_A,m_B} = \binom{z}{n} x_a^{z-n} \varepsilon_a^n \cdot y_A^{m_A} \binom{n}{m_A} x_{AB}^{m_A} \varepsilon_s^{m_A} \cdot y_B^{m_B} \binom{z-n}{m_B} x_B^{m_B} \varepsilon_s^{m_B}, \tag{6}$$

for the case of the wrong atom with antiparallel magnetic moment on a centre site of the group respectively.

Accordingly, the total relative probability for the centre atoms with parallel magnetic moment being right is

$$\begin{aligned} r^{\uparrow} &= \sum_{n=0}^{z} \sum_{m_A=0}^{n} \sum_{m_B=0}^{z-n} r^{\uparrow}{}_{n,m_A,m_B} \\ &= y_A\{x_{AB} + \varepsilon_a x_a x_A + \varepsilon_s y_B + \varepsilon_s \varepsilon_a x_a y_A\}^z, \end{aligned} \tag{7}$$

using the binomial theorem in algebra.

Similarly we get

$$\begin{aligned} r^{\downarrow} &= \sum_{n} \sum_{m_A} \sum_{m_B} r^{\downarrow}{}_{n,m_A,m_B} \\ &= \{1 + \varepsilon_a x_a + \varepsilon_s x_{AB} y_B + \varepsilon_s \varepsilon_a x_a x_A y_A\}^z, \end{aligned} \tag{8}$$

for the total relative probability for the centre atom with antiparallel magnetic moment being right,

$$\begin{aligned} w^{\uparrow} &= \sum_{n} \sum_{m_A} \sum_{m_B} w^{\uparrow}{}_{n,m_A,m_B} \\ &= y_B\{x_a x_B + \varepsilon_a x_{AB} + \varepsilon_s x_a y_B + \varepsilon_s \varepsilon_a y_A\}^z, \end{aligned} \tag{9}$$

and

$$\begin{aligned} w^{\downarrow} &= \sum_{n} \sum_{m_A} \sum_{m_B} w^{\downarrow}{}_{n,m_A,m_B} \\ &= \{x_a + \varepsilon_a + \varepsilon_s x_a x_B y_B + \varepsilon_s \varepsilon_a x_{AB} y_A\}^z, \end{aligned} \tag{10}$$

for the total relative probabilities for the centre atom with parallel and antiparallel magnetic moments being wrong respectively.

Hence, the normalized probabilities of the centre atom being right or wrong are

$$r = \frac{r^{\uparrow} + r^{\downarrow}}{r^{\uparrow} + r^{\downarrow} + w^{\uparrow} + w^{\downarrow}} \quad \text{or} \quad w = \frac{w^{\uparrow} + w^{\downarrow}}{r^{\uparrow} + r^{\downarrow} + w^{\uparrow} + w^{\downarrow}}, \tag{11}$$

respectively.

The probability of an atom in the boundary being wrong is given by the average number of wrong atoms in the boundary divided by z, which is equal to

$$w' = \frac{1}{z}\sum_{n}\sum_{m_A}\sum_{m_B} n(r^{\uparrow}{}_{n,\,m_A,\,m_B} + r^{\downarrow}{}_{n,\,m_A,\,m_B}$$
$$+ w^{\uparrow}{}_{n,\,m_A,\,m_B} + w^{\downarrow}{}_{n,\,m_A,\,m_B})/(r^{\uparrow}+r^{\downarrow}+w^{\uparrow}w^{\downarrow})$$
$$= \frac{1}{z}\left\{\varepsilon_a\frac{\partial}{\partial\varepsilon_a}(r^{\uparrow}+r^{\downarrow}+w^{\uparrow}+w^{\downarrow})\right\}/(r^{\uparrow}+r^{\downarrow}+w^{\uparrow}+w^{\downarrow}). \tag{12}$$

By the physical symmetry of lattice sites regarding atomic distribution, we must have $w = w'$ along similar reasoning to that of Bethe's theory[16], namely,

$$z(w^{\uparrow}+w^{\downarrow}) = \varepsilon_a\frac{\partial}{\partial\varepsilon_a}(r^{\uparrow}+r^{\downarrow}+w^{\uparrow}+w^{\downarrow}). \tag{A}$$

Next, the probability of a centre atom having parallel molecular magnet with respect to the external magnetic field is

$$\frac{r^{\uparrow}+w^{\downarrow}}{r^{\uparrow}+r^{\downarrow}+w^{\uparrow}+w^{\downarrow}},$$

while the probability of an atom in the boundary having parallel molecular magnet with respect to the external magnetic field is given by

$$\frac{1}{z}\sum_{n}\sum_{m_A}\sum_{m_B}(m_A+w_B)(r^{\uparrow}{}_{n,\,m_A,\,m_B}+r^{\downarrow}{}_{n,\,m_A,\,m_B}$$
$$+w^{\uparrow}{}_{n,\,m_A,\,m_B}+w^{\downarrow}{}_{n,\,m_A,\,m_B})/(r^{\uparrow}+r^{\downarrow}+w^{\uparrow}+w^{\downarrow})$$
$$= \frac{1}{z}\cdot\left\{\varepsilon_s\frac{\partial}{\partial\varepsilon_s}(r^{\uparrow}+r^{\downarrow}+w^{\uparrow}+w^{\downarrow})\right\}/(r^{\uparrow}+r^{\downarrow}+w^{\uparrow}+w^{\downarrow}),$$

along a similar consideration to the above

Accroding to the physical symmetry of lattice sites regarding the distribution of molecular magnets, the above mentioned probabilities must be equated with respect to each other, which leads to

$$z(r^{\uparrow}+w^{\downarrow}) = \varepsilon_s\frac{\partial}{\partial\varepsilon_s}(r^{\uparrow}+r^{\downarrow}+w^{\uparrow}+w^{\downarrow}), \tag{B}$$

which can now be used, together with the consistency equation (A), for determining both ε_a and ε_s as functions of temperature T and mutual interaction energies v, w_{AA}, w_{AB} and w_{BB}.

It is interesting to remark that the above consistency-equations (A) and (B) are easily shown to be reduced to that of Bethe's theory of superlattice in the limiting case of the external magnetic field H and the exchange interation energies w_{AA}, w_{AB} and w_{BB} being made equal to zero, and, furthermore, in the limiting case of the bond energy v being made to vanish and $w_{AA} = w_{AB} = w_{BB}$, they can be reduced to that of Firgau's theory for the ferromagnetism of pure metals. The statistical theory of the ferromagnetic superlattice developed above, therefore, may be considered to be a rational generalization of both Bethe's theory in superlattice and Firgau's theory in ferromagnetic metals. Since the products of ε_a and ε_s are contained in (A) and (B), the statistical correlation between atomic and magnetic moment distributions may be considered to occur in our theory of the ferromagnetic superlattice.

§ 4. Numerical Solution of the Basic Equations (A) and (B) for a Simple Cubic Lattice.

Substituting $z = 6$ valid for the simple cubic and putting $H = 0$ $(y_A = y_B = 1)$ in the equations (A) and (B) in order to obtain a detailed knowledge of the influence of spontaneous magnetization upon the physical properies of alloys, the basic equations (A) and (B) may be reduced to the following simultaneous algebraic equations of the 6th order in ε_a and ε_s.

$$(\varepsilon_s+x_B)(x_{AB}\varepsilon_a+x_a\varepsilon_s+\varepsilon_a\varepsilon_s+x_ax_B)^5$$
$$+(x_B\varepsilon_s+1)(\varepsilon_a+x_ax_B\varepsilon_s+x_{AB}\varepsilon_a\varepsilon_s+x_a)^5$$
$$=\varepsilon_a(\varepsilon_s+x_a)(x_ax_A\varepsilon_a+\varepsilon_s+x_a\varepsilon_a\varepsilon_s+x_{AB})^5$$
$$+\varepsilon_a(x_A\varepsilon_s+1)(x_a\varepsilon_a+x_{AB}\varepsilon_s+x_ax_A\varepsilon_a\varepsilon_s+1), \tag{A$'$}$$

$$(x_ax_A\varepsilon_a+x_{AB})[(x_ax_A\varepsilon_a+\varepsilon_s+x_a\varepsilon_a\varepsilon_s+x_{AB})^5$$
$$-\varepsilon_s(x_a\varepsilon_a+x_{AB}\varepsilon_B+x_ax_A\varepsilon_s\varepsilon_a+1)^5]$$
$$=\varepsilon_s(x_Ax_B+x_{AB}\varepsilon_a)(\varepsilon_a+x_ax_B\varepsilon_s+x_{AB}\varepsilon_a\varepsilon_s+x_a)^5$$
$$-(x_ax_B+x_{AB}\varepsilon_a)(x_{AB}\varepsilon_a+x_a\varepsilon_s+\varepsilon_a\varepsilon_s+x_ax_B)^5. \tag{B$'$}$$

Since it is quite difficult to solve analytically the algebraic equations (A)′ and (B)′ owing to the inclusion of the terms of the high order in ε_a and ε_s, we have evaluated them numerically along a rather laborious but elementary way, corresponding to each of the appropriate values assigned for the intearction energies involved, the resluts of which are described graphically in the accompanying figures (the plots of ε_a and ε_s against T). Now we shall here summarize the definitions of the various kinds of quantities which appear in the figures:

$$\theta_a = v/k, \quad \theta_s = (w_{AA}+w_{AB}+w_{BB})/3k,$$
$$\alpha_A = 3w_{AA}/(w_{AA}+w_{AB}+w_{BB}),$$
$$\alpha_B = 3w_{BB}/(w_{AA}+w_{AB}+w_{BB}),$$

$$\alpha_{AB} = 3w_{AB}/(w_{AA}+w_{AB}+w_{BB}).$$

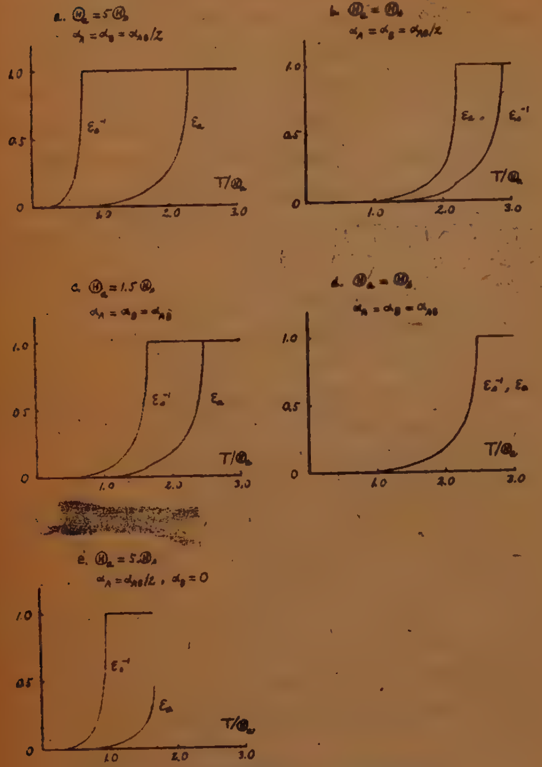

Fig. 1. Statistical Parameters versus Temperature.

where θ_a and θ_s will be taken to give approximately some measures of order-disorder and magnetic Curie points respectively. Since the physically permissible values of ε_a and ε_s are to be restricted to the intervals of $0 \leqq \varepsilon_a \leqq 1$ and $1 \leqq \varepsilon_s \leqq \infty$ respectively, the temperature dependences of ε_a and ε_s are found to be described by the peculiar curves with one or more kinks as seen clearly in the figures. The appearance of the curves with turning points (Fig. 1 (e)) is ascribed to such circumstances that there is no solution of (A)′ and (B)′ above the temperatures indicated by the turning points of the curves. At present it is not sufficiently clear without a careful examination of the free energy of the mentioned alloy, whether the mentioned (unfavourable) circumstances are due to the approximate nature in our method of treatment and to the unsuitable choices of the physical quantities or they correspond really to the physical situation, i. e., the limit of solubility of solid solution. The detailed discussion regarding the above point shall be reserved in later paper where the improvement of the theory is dealt with through the introduction of the four statistical parameters ε_a, ε_a', ε_s and ε_s' mentioned above.

§ 5. Long Distance- and Local-Orders.

For the evaluation of the directly measureable physical quantities, i. e., the anomalous specific heat, the spontaneous magnetization, etc., it is quite sufficient only to know the probabilities of a given kind of atom with a definite orientation of molecular magnet occupying one of the lattice sites involved, as clearly shown in Part II. For theoretical discussion of the phenomena, however, it is highly instructive to introduce the auxiliary quantities of both local- and long distance-orders defined in a suitable way. For this purpose, therefore, we shall here introduce the local- and long distance-orders regarding both atomic- and magnetic moment-distributions, defined as closely to Bethe's case of superlattice as possible, by the following equations.

Namely, we have

$$\sigma_a = \frac{q-q(\text{rand})}{q(\max)-q(\text{rand})}, \quad q = \frac{Q_{AB}}{Q}, \; (Q = Nz/2,$$

$$S_a = \frac{(r^{\uparrow}+r^{\downarrow})-(r^{\uparrow}+r^{\downarrow})_{\text{rand}}}{(r^{\uparrow}+r^{\downarrow})_{\max}-(r^{\uparrow}+r^{\downarrow})_{\text{rand}}},$$

for the local- and long distance-orders regarding atomic distribution, and, furthermore,

$$\sigma_m = \frac{p-p(\text{rand})}{p(\max)-p(\text{rand})}, \quad p = (Q^{\uparrow\uparrow}_{AA}+Q^{\uparrow\uparrow}_{AB}+Q^{\uparrow\uparrow}_{BB})/Q,$$

$$S_m = \frac{(r^{\uparrow}+w^{\uparrow})-(r^{\uparrow}+w^{\uparrow})_{\text{rand}}}{(r^{\uparrow}+w^{\uparrow})_{\max}-(r^{\uparrow}+w^{\uparrow})_{\text{rand}}},$$

for those regarding magnetic moment distribution respectively, where the suffices "max" or "rand" refer to the values at $T = 0$ or above the critical temperature of the mentioned distributions, and Q_{AB}, $Q^{\uparrow\uparrow}_{AB}$, $Q^{\uparrow\uparrow}_{BB}$ and $Q^{\uparrow\uparrow}_{AA}$ can be easily represented with $r^{\uparrow}$, $r^{\downarrow}$, $w^{\uparrow}$ and $w^{\downarrow}$ by the use of a simple probability consideration, as shown in Part II. Figures 2 (a) ~ (e) show the temperature-variations of σ_a, S_a, σ_m and S_m for some of the assigned values of the mutual interactoin energies, which results are to be taken into account in the discussions of both the anomalous specific heat and the spontaneous magnetization evaluated in

Part II. In the figures (b), the mutual correlations between the atomic- and magnetic moment-distributions are recognized expricitly in the appearance of the kinks on the curves, the atomic (or magnetic moment) disorder being accelerated, with the increase of temperature, by the magnetic moment (or atomic) disorder in the order-disorder transformations, while in the remaining figures, there 's no kinks although the mutual influences are considered to exist implicitly in the mentioned transformation. The degree of the mutual influences of both distributions, therefore, will be considered to depend sensibly upon each of the interaction energies of both bond- and exchange-type between constituent atoms.

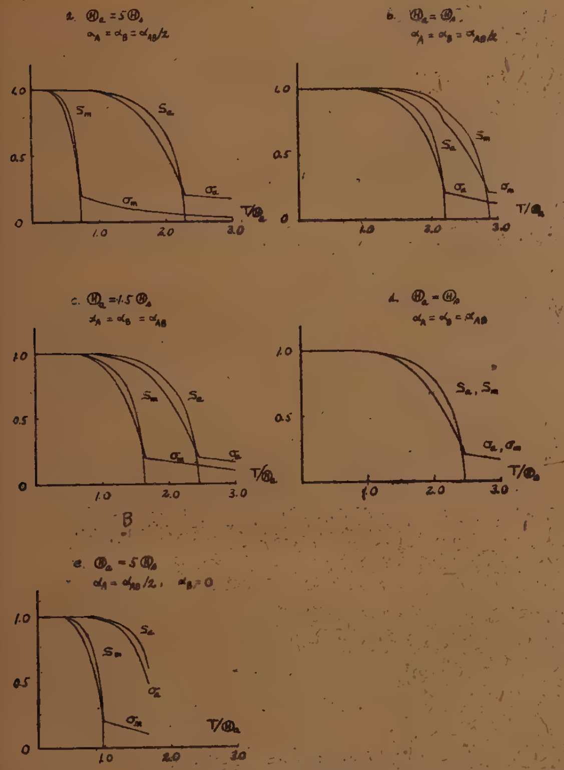

Fig. 2. Order-Parameters versus Temperature.

The authors are indebted to Special Resarch-Committee of Theoretical Physics, National Research Council of Educational Ministry for financial aid.

References.

(1) Nix and Shockley: Rev. Mod. Phys. **10** (1938) 60.

(2) Kaya and Kussmann; Zeits. f. Phys. **72** (1931) 293.
Kaya and Nakagawa: Proc. Phys.-Math. Soc. Japan **22** (1940) 126.
Thompson: Proc. Phys. Soc. **52** (1940) 217.

(3) Leech and Sykes: Phil. Mag. **27** (1939) 742.
Haworth: Phys. Rev. **56** (1939) 289.
Kaya: Sci. Pap. Hokkaido Imp. Univ. **2** (1939) 29.
Pan: Phys. Rev. **56** (1939) 933.
Kaya, Sato and Kumasaka; Nippon Kinzoku-gaku Kaisi **6** (1941) 188.

(4) Bradley and Rodgers; Proc. Roy. Soc. **A 144** (1934) 340.
Heusler; Ann. d. Phys. **19** (1934) 155.

(5) Seitz: Modern Theory of Solids, 1940.
Becker u. Döring: Ferromagnetism, 1937.
Bitter: Introduction to Ferromagnetism, (1937).

(6) Bragg and Williams: Proc. Roy. Soc. **A 145** (1934) 699.

(7) Bethe: Proc. Roy. Soc. **A 150** (1935) 552.

(8) Peierls: Proc. Roy. Soc. **A 154** (1936) 207.
Kirkwood: J. Chem. Phys. **6** (1938) 244.
Fowler and Guggenheim: Proc. Roy. Soc. A **174** (1940) 189.
Takagi: Proc. Phys.-Math. Soc. Japan **23** (1941) 44.
Bethe: J. Appl. Phys. **9** (1938) 244.
Nix: J. Appl. Phys. **8** (1937) 783.
Nix. and Shockley: loc. cit.

(9) Firgau: Ann. d. Phys.

(10) Ising: Zeits. f. Phys. **31** (1925) 253.

(11) Firgau: loc. cit.

(12) Bethe: loc. cit.

(13) Bethe: loc. cit.

(14) Bethe; loc. cit.

(15) Firgau: loc. cit.

(16) Bethe: loc. cit.

Statistical Theory of the Ferromagnetic Superlattice. Part II. Anomalous Specific Heat and Spontaneous Magnetization.

By Toshinosuke MUTO, Tetsuo EGUCHI and Motoichi SHIBUYA.

Institute of Science and Technology, University of Tokyo
& Institute of Physics, Kyushu University.

(Received December 15, 1947)

§ 1. Anomalous Specific Heat.

In order to obtain the anomalous specific heat we have to evaluate the internal energy (1) of Part I by the use of the probabilities of the occupation of any lattice points by a given atom of a definite orientation of molecular magnet, which have been worked out in chapters (3) and (4) of Part I.

Since Q_{AB} represents the number of pairs of unlike atoms, we have

Q_{AB} = (number of A-atoms on α-sites)
× (number of B-atoms on the neighbouring β-sites)
+ (number of B-atoms on α-sites)
× (number of A-atoms on the neighbouring β-sites),

where α- or β-sites mean the lattice-sites occupied by A- or B-atoms at absolute temperature zero respectively.

According to a simple probability consideration, it follows

$$Q_{AB}=\frac{N}{2}\frac{r^{\uparrow}+r^{\downarrow}}{r^{\uparrow}+r^{\downarrow}+w^{\uparrow}+w^{\downarrow}}\cdot\frac{\sum\limits_{n}\sum\limits_{m_A}\sum\limits_{m_B}(z-n)(r^{\uparrow}_{n,m_A,m_B}+r^{\downarrow}_{n,m_A,m_B})}{r^{\uparrow}+r^{\downarrow}}$$
$$+\frac{N}{2}\frac{w^{\uparrow}+w^{\downarrow}}{r^{\uparrow}+r^{\downarrow}+w^{\uparrow}+w^{\downarrow}}\cdot\frac{\sum\limits_{n}\sum\limits_{m_A}\sum\limits_{m_B}n(w^{\uparrow}_{n,m_A,m_B}+w^{\downarrow}_{n,m_A,m_B})}{w^{\uparrow}+w^{\downarrow}}$$
$$=\frac{N}{2}\Big\{z(r^{\uparrow}+r^{\downarrow})+\varepsilon_a\frac{\partial}{\partial\varepsilon_a}(-r^{\uparrow}-r^{\downarrow}+w^{\uparrow}+w^{\downarrow})\Big\}\cdot(r^{\uparrow}+r^{\downarrow}+w^{\uparrow}+w^{\downarrow})^{-1},\tag{1}$$

where N means the total number of lattice sites involved.

Similarly we get

$Q^{\upuparrows}_{AA}$ = (number of A-atoms with parallel molecular magnets on α-sites)
× (number of A-atoms with parallel molecular magnets on the neighbouring β-sites)
+ (number of A-atoms with antiparallel molecular magnets on α-sites)
× (number of A-atoms with antiparallel molecular magnets on the neighbouring β-sites),

$$Q_{AA}=\frac{N}{2}\Big\{y_A{}^2\frac{\partial}{\partial y_A}\Big(\frac{r^{\uparrow}}{y_A}\Big)+\Big(\varepsilon_a\frac{\partial}{\partial\varepsilon_a}-y_A\frac{\partial}{\partial y_A}\Big)r^{\downarrow}\Big\}\cdot(r^{\uparrow}+r^{\downarrow}+w^{\uparrow}+w^{\downarrow})^{-1},\tag{2}$$

$$Q^{\upuparrows}_{BB}=\frac{N}{2}\Big\{y_B{}^2\frac{\partial}{\partial y_B}\Big(\frac{w^{\uparrow}}{y_B}\Big)+\Big(z-\varepsilon_a\frac{\partial}{\partial\varepsilon_a}-y_B\frac{\partial}{\partial y_B}\Big)w^{\uparrow}\Big\}\cdot(r^{\uparrow}+r^{\downarrow}+w^{\uparrow}+w^{\downarrow})^{-1},\tag{3}$$

and

$$Q^{\upuparrows}_{AB}=\frac{N}{2}\Big\{y_B\frac{\partial}{\partial y_B}(r^{\uparrow})+\Big(z-\varepsilon_a\frac{\partial}{\partial\varepsilon_a}-y_B\frac{\partial}{\partial y_B}\Big)r^{\downarrow}+y_A\frac{\partial}{\partial y_A}(w^{\uparrow})+\Big(\varepsilon_a\frac{\partial}{\partial\varepsilon_a}-y_A\frac{\partial}{\partial y_A}\Big)w^{\downarrow}\Big\}\cdot(r^{\uparrow}+r^{\downarrow}+w^{\uparrow}+w^{\downarrow})^{-1},\tag{4}$$

Putting the above expressions (1)~(4) into the total energy E of Part I, eq. (2), we have, for the part of the energy due to atomic and molecular magnet-distributions,

$$E=\Big\{\frac{N}{2}\Big[-v\Big(z(r^{\uparrow}+r^{\uparrow})+\varepsilon_a\frac{\partial}{\partial\varepsilon_a}(-r^{\uparrow}-r^{\downarrow}-w^{\uparrow}-w^{\downarrow})\Big)$$
$$-w_{AA}\Big(y_A{}^2\frac{\partial}{\partial y_A}\Big(\frac{r^{\uparrow}}{y_A}\Big)+\Big(\varepsilon_a\frac{\partial}{\partial\varepsilon_a}-y_A\frac{\partial}{\partial y_A}\Big)r^{\downarrow}\Big)$$

$$-w_{BB}\left(y_B^2\frac{\partial}{\partial y_B}\left(\frac{w^{\uparrow}}{y_B}\right)+\left(z-\varepsilon_a\frac{\partial}{\partial\varepsilon_a}-y_B\frac{\partial}{\partial y_B}\right)w^{\downarrow}\right)$$

$$-w_{AB}\left(y_B\frac{\partial}{\partial y_B}r^{\uparrow}+\left(z-\varepsilon_a\frac{\partial}{\partial\varepsilon_a}-y_B\frac{\partial}{\partial y_B}\right)r^{\downarrow}\right.$$

$$\left.+y_A\frac{\partial}{\partial y_A}w^{\uparrow}+\left(\varepsilon_a\frac{\partial}{\partial\varepsilon_a}-y_A\frac{\partial}{\partial y_A}\right)w^{\downarrow}\right)\Big]$$

$$\div(r^{\uparrow}+r^{\downarrow}+w^{\uparrow}+w^{\downarrow})\Big\}_{y_A=y_B=1}, \tag{5}$$

where the various kinds of the relative probabilities involved in E may be considered to be dependent upon the absolute temperature T and the mutual interaction energies v, w_{AA}, w_{AB} and w_{BB}, in which the characteristic dependences of ε_a and ε_s upon the mentioned physical quantities are to be allowed for, as shown in the figures of the Chaper 4 in Part I.

Thus, for the anomalous specific heat of constant volume of the alloy, we get

$$C_v=\left(\frac{\partial E}{\partial T}\right). \tag{6}$$

In order to show the characteristic behaviours of the anomalous specific heat C_v and the total energy E, we have numerically computed, by using (5), (6) and the temperature dependences of the various quantities involved for each of the appropriate values of the mutual interaction energies assigned, which results shall be described graphically in the accompanying figures.

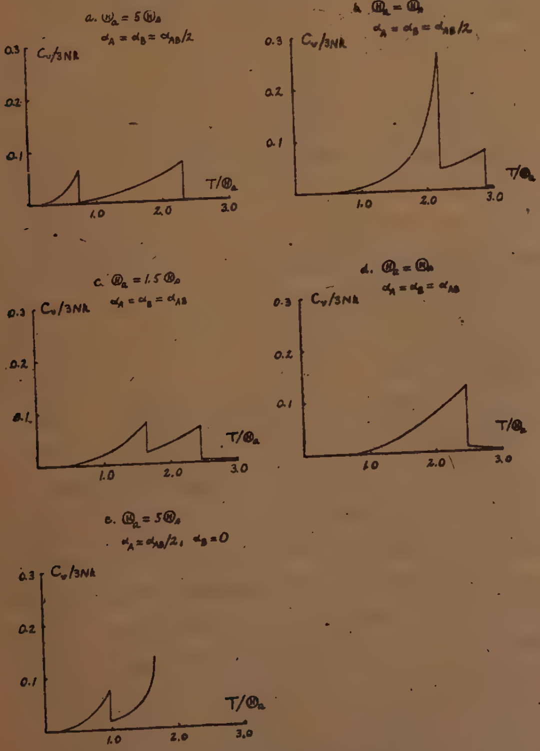

Fig 3. Anomalous Specific Heat versus Temperature.

§ 2. Spontaneous Magnetization (Saturation Value of Magnetization).

Along a similar consideration as above, we get, for the spontaneous magnetization of the alloys,

$$M=\frac{N}{2}\left\{\beta_A\frac{r^{\uparrow}-r^{\downarrow}+w^{\uparrow}-w^{\downarrow}}{r^{\uparrow}+r^{\downarrow}+w^{\uparrow}+w^{\downarrow}}\right.$$

$$\left.+\beta_B\frac{r^{\uparrow}+r^{\downarrow}+w^{\uparrow}-w^{\downarrow}}{r^{\uparrow}+r^{\downarrow}+w^{\uparrow}+w^{\downarrow}}\right\}_{y_A=y_B=1}, \tag{7}$$

after some processes of the computation regarding the numbers of molecular magnets with parallel orientations with respect to the external magnetic field, where

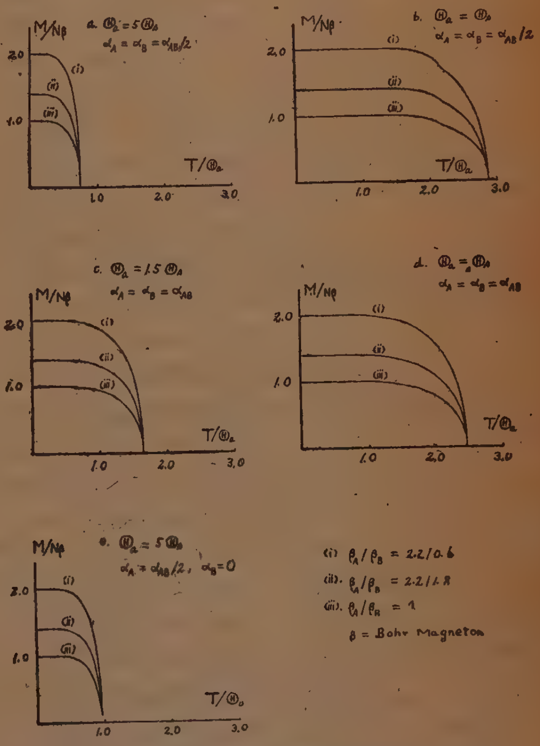

Fig. 4. Spontaneous Magnetization versus Temperature

$$\left.\begin{aligned}\bar{r}^{\uparrow}&=\frac{1}{z}y_B^2\frac{\partial}{\partial y_B}\left(\frac{w^{\uparrow}}{y_B}\right)+\frac{1}{z}y_B\frac{\partial}{\partial y_B}(r^{\uparrow}+r^{\downarrow}+w^{\downarrow}),\\ \bar{r}^{\downarrow}&=\frac{1}{z}y_B\left(z-\varepsilon_a\frac{\partial}{\partial\varepsilon_a}-y_B\frac{\partial}{\partial y_B}\right)\left(\frac{w^{\uparrow}}{y_B}\right)\end{aligned}\right|$$

$$\left.\begin{aligned}
&+\frac{1}{z}\left(z-\varepsilon_a\frac{\partial}{\partial\varepsilon_a}-y_B\frac{\partial}{\partial y_B}\right)(r^{\uparrow}+r^{\downarrow}+w^{\downarrow}),\\
\overline{w}^{\uparrow}&=\frac{1}{z}y_A^2\frac{\partial}{\partial y_A}\left(\frac{r^{\uparrow}}{y_A}\right)+\frac{1}{z}y_A\frac{\partial}{\partial y_A}(w^{\uparrow}+w^{\downarrow}+r^{\downarrow}),\\
\overline{w}&=\frac{1}{z}y_A\left(\varepsilon_a\frac{\partial}{\partial\varepsilon_a}-y_A\frac{\partial}{\partial y_A}\right)\left(\frac{r^{\uparrow}}{y_A}\right)\\
&+\frac{1}{z}\left(\varepsilon_a\frac{\partial}{\partial\varepsilon_a}-y_A\frac{\partial}{\partial y_A}\right)(w^{\uparrow}+w^{\downarrow}+r^{\downarrow}).
\end{aligned}\right\}\tag{8}$$

In a similar way to the case of anomalous specific heat, the temperature dependences of the spontaneous magnetization have been numerically evaluated for each of the assigned values of the mutual interaction energies, which results shall be described in the following figures.

§ 3. Discussion of the Results and Comparison with the Experiments.

As seen in the figures of the numerically evaluated results corresponding to each of the assigned values of the mutual interaction energies of bond and exchange types, the temperature variations of both anomalous specific heat and spontaneous magnetization will be found to show the characteristic behaviours sensibly dependent not only upon the ratios of both measures of Curie points θ_a and θ_s but also upon the relative magnitudes of the three kinds of exchange energies among the molecular magnets involved, although the general behaviours of the mentioned physical quantities dependent upon mutual interaction energies are now quite difficult to be predicted theoretically owing to the complicated forms of the algebraic equations (A') and $(B)'$ in Part I, which have not been controlled analytically as yet. Generally speaking, however, we shall be able to expect the existence of the complicated correlations of both atomic and magnetic moment-distributions among lattice points owing to the inclusion in a complex manner of ε_a and ε_s in the expression of the total energies and the saturation magnetizations of the crystals.

Regarding the anomalous specific heats, one or two maxima will be seen to occur with the temperature variations according to the relative magnitudes of mutual interaction energies, the origin of which is ascribed to the physically discontinuous change, associated with the atomic and magnetic Curie points, of the total energy of the crystal as a whole in which the distinction between the exchange and bond energies of the crystal can not be made as usual owing to the statistical correlation of both distributions in atomic and molecular magnet arrangement (see the figures in the text). As for the temperature variations of the spontaneous magnetization, we have rather monotonous curves qualitatively similar to those of the ferromagnetic, pure metals except for that shown in the figure 4 (b), where there appears a kink on the curve in spite of $\theta_a = \theta_s$, indicating the correlations between both distributions in constituent atoms and in molecular magnets. In view of the results obtained above, the appearance of the mutual correlations of both distributions may be considered to depend sensibly upon each of the mutual interaction energies of bond and exchange types between constituent atoms of the alloys. Whether the occurrence of the broken curves in Fig. 4 (e) may be ascribed to the approximate nature of our theory and to the unsuitable choice of the physical quantities or really to the physical situation of the phenomena shall be discussed in the later paper through introducing four statistical parameters together with a careful examination of the free energy of the alloys.

Now the anomalous specific heats of Ni_3Fe and Ni_3Mn have been observed⑴ experimentally to have two maxima on the curves of the temperature-variations (at the roughly estimated values of 540°C and 550°C for Ni_3Fe and at 490°C and 540°C for Ni_3Mn) in qualitative agreements with the theoretical results obtained above, although, in the latter alloys, there is a discrepancy between the experimental data due to Thompson⑵ and Kaya⑶, the latter of which has observed only a single but broad maximum in the specific heat versus temperature diagram. It, however, seems to us that the mentioned broad maximum observed by Kaya⑷ may be considered to be due to the experimentally unresolved overlapping of the two maxima of specific heat to be separated in the narrow range of temperatures. The temperature variations of spontaneous magnetization of the mentioned alloys, on the other hand, have been found experimentally to show the rather monotonous behaviours similar to that of the ferromagnetic pure metals, which results also are really the ones to be expected theoretically to occur. Owing to the complicated expressions of $(A)'$ and $(B)'$, however, the rather laborious procedures of numerical calculations will be required for determining the relative magnitudes of v, w_{AA}, w_{AB} and w_{BB} which give the best fitting to the available experimental results, which computation shall be attempted in later occasion. Furthermore, in the experimental result regarding FeCo alloy of Kussmann and others⁽⁵⁾, it is quite interesting to point out that the magnetization of the mentioned alloy is observed to make an abrupt change to zero with increasing temperatures owing to the occurrence of the solubility limit of the solid solution.

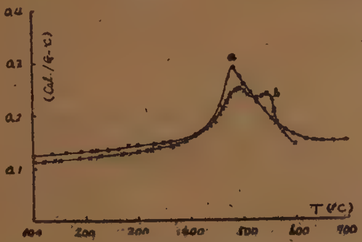

Fig. 5. a, b. Specific Heat of Ni₃Mn.
a. Kaya & Nakayama. b. Thompson.

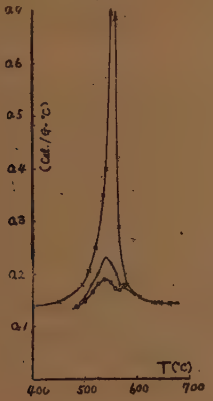

Fig. 5. c. Specific Heat of Ni₃Fe.
Each of the curves corresponds to the different way of heat treatment of materials.
(Kaya, Sato & Kumasaka)

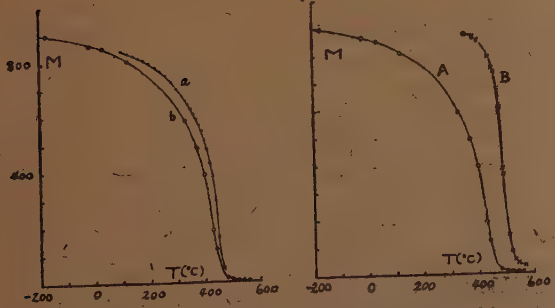

Fig. 6. Saturation Magnetization.
a. Kaya & Nakayama b. Thompson
c. Saturation Magnetization of Annealed (A) and Quenched (B) Ni₃Mn

§ 4. Extension of the Theory to Treat the Quenched Alloys.

In order to find experimentally the atomic Curie points in ferromagnetic superlattice, Thompson has made use of the magnetization data dependent upon the higher temperatures at which the alloy was kept in the annealing process just before the quenching one, the measurement of the spontaneous magnetization being carried out quickly at a constant temperature (ordinarily at room temperature) just in the quenched state. The Curie point of atomic rearrangement in superlattice may easily be estimated from the abruptly decreasing behaviours of the observed magnetization described as a function of temperature just before the quenching (Fig. 6 (c) B). Such experimental procedure for the determination of the atomic Curie point from the purely magnetic data, however, will actually be permitted to be taken only for the case of the relatively short relaxation-time regarding the reorientation of molecular magnets compared with that regarding the rearrangement of constituent atoms involved, which states of affairs will probably be realized in the ordinary superlattices. In the theoretical discussion of the mentioned case, we have to work theoretically the probabilities of the distributions of molecular magnets for a fixed atomic distribution specified by the temperatures just before the quenching process, which case will easily be handled by a trivial modification of the theory developed in Part I.

According to our theory developed in Part I, the statistical distributions of both constituent atoms and molecular magnet-orientations have been shown to be completely determined by the various kinds of relative probabilities $r^{\uparrow}$, $r^{\downarrow}$, $w^{\uparrow}$, $w^{\downarrow}$ and the consistency equations (A) and (B). By making use of the equations (3), (4), (5) and (6) in Part I, we are able to compute the average number n of wrong atoms around any lattice site in the crystal as follows.

$$\bar{n} = \sum_{n}\sum_{m_A}\sum_{m_B} n(r^{\uparrow}_{n,m_A,m_B} + r^{\downarrow}_{n,m_A,m_B} + w^{\uparrow}_{n,m_A,m_B} + w^{\downarrow}_{n,m_A,m_B})/(r^{\uparrow}+r^{\downarrow}+w^{\uparrow}+w^{\downarrow})$$

$$= \varepsilon_a\left\{\frac{\partial}{\partial\varepsilon_a}(r^{\uparrow}+r^{\downarrow}+w^{\uparrow}+w^{\downarrow})\right\}/(r^{\uparrow}+r^{\downarrow}+w^{\uparrow}+w^{\downarrow}). \quad (9)$$

The average number of right atoms around any lattice site in the crystal, therefore, will be given by $(z-\bar{n})$, z being the total number of nearest neighbours of any lattice site. The average distribution of constituent atoms in the annealing process just before the quenching one will be determined statistically by the quantities $\bar{n}$ and $z-\bar{n}$, which are dependent upon v, w_{AA}, w_{AB}, w_{BB} and T (temperature of the annealing process).

The statistical distribution at temperature T_0 for a fixed atomic distribution specified by $\bar{n}(T)$ may be written on a quite similar reasoning to that of Part I as follows.

$$\left.\begin{aligned}
r^{\uparrow}_{\bar n} &= (x_A+y_A\varepsilon_s)^{\bar n}(x_{AB}+y_A\varepsilon_s)^{z-\bar n}y_A\binom{z}{\bar n}\bar{x}_a^{-\bar n}\bar{\varepsilon}_a^{-\bar n},\\
r^{\downarrow}_{\bar n} &= (1+y_Ax_A\varepsilon_s)^{\bar n}(1+y_Bx_{AB}\varepsilon_s)^{z-\bar n}\binom{z}{\bar n}\bar{x}_a^{-\bar n}\bar{\varepsilon}_a^{-\bar n},\\
w^{\uparrow}_{\bar n} &= (x_{AB}+y_A\varepsilon_s)^{\bar n}(x_B+y_B\varepsilon_s)^{z-\bar n}y_B\binom{z}{\bar n}\bar{x}_a^{z-\bar n}\bar{\varepsilon}_a^{-\bar n},\\
w^{\downarrow}_{\bar n} &= (1+y_Ax_{AB}\varepsilon_s)^{\bar n}(1+y_Bx_B\varepsilon_s)^{z-\bar n}\binom{z}{\bar n}\bar{x}_a^{z-\bar n}\bar{\varepsilon}_a^{-\bar n},
\end{aligned}\right\} \quad (10)$$

where the various quantities involved in the equations have been defined in Part I, and the barred quantities refer to those specified by the temperature in the annealing process while the other to those for the temperature at which the measurement of spontaneous magnetization are carried out. Since the statistical distribution of molecular magnet is to be taken into consideration for a definite distribution of constituent atoms, we have, for the consistency equation of the problem under consideration,

$$z(r^{\uparrow}_{\bar n}+w^{\uparrow}_{\bar n}) = \varepsilon_s\frac{\partial}{\partial\varepsilon_s}(r^{\uparrow}_{\bar n}+r^{\downarrow}_{\bar n}+w^{\uparrow}_{\bar n}+w^{\downarrow}_{\bar n}). \quad (11)$$

In a similar way to the case in Part I, the spontaneous magnetization may be written as

$$M = \Bigg[\frac{N}{2}\Bigg\{\beta_A\Bigg(r^{\uparrow}_{\bar n}-r^{\downarrow}_{\bar n}+\bar{n}+2y_A\frac{\partial}{\partial y_A}\cdot\left(\frac{r^{\uparrow}_{\bar n}}{y_A}+r^{\downarrow}_{\bar n}+w^{\uparrow}_{\bar n}+w^{\downarrow}_{\bar n}\right)+\beta_B\Bigg(w^{\uparrow}_{\bar n}-w^{\downarrow}_{\bar n}+\bar{n}-z$$
$$+2y_B\frac{\partial}{\partial y_B}\left(r^{\uparrow}_{\bar n}+r^{\downarrow}_{\bar n}+\frac{w^{\uparrow}_{\bar n}}{y_B}+w^{\downarrow}_{\bar n}\right)\Bigg\}$$
$$\cdot(r^{\uparrow}_{\bar n}+r^{\downarrow}_{\bar n}+w^{\uparrow}_{\bar n}+w^{\downarrow}_{\bar n})^{-1}\Bigg]_{y_A=y_B=1} \quad (12)$$

which is easily found to depend upon T, T_0, v, w_{AA}, w_{AB} and w_{BB}. For the specified values of T_0, v, w_{AA}, w_{AB} and w_{BB}, the spontaneous magnetization M will be numerically computed for each value of T, i. e., the temperature just before the quenching. from which result the atomic Curie point may actually be determined as mentioned above.

Finally it should be mentioned that the theoretical results obtained here are readily applicable to the theories of electrical conductivity, thermoelectromotive force, paramagnetism above the magnetic Curie point and the elastic scattering of slow neutron in the ferromagnetic superlattice, whose theoretical discussions are our programme now in progress together with the improvement of the present theory through the introduction of four statistical parameters mentioned in Chap. 3 of Part I.

The authors are indebted to Special Research Committee of Theoretical Physics, National Research Council of Educational Ministry for financial aid.

References.

(1) Kaya: Sci. Pap. Hokkaido Imp. Univ. **2** (1939) 29.
Kaya and Nakagawa: Proc. Phys.-Math. Soc. Japan **22** (1940) 126.
Kaya, Sato and Kumasaka: Nippon Kinzokugaku Kaisi **6** (1941) 188.
Thompson: Proc. Phys. Soc. **52** (1940) 217.
(2) Thompson: loc. cit.
(3) Kaya and Nakagawa: loc. cit.
(4) Kaya and Kussmann: Zeits. f. Phys. **72** (1931) 293.
Kaya and Nakagawa: loc. cit.
Thompson: loc. cit.
Kaya: loc. cit.
(5) Kussman, Scharnkow and Schulze: Zeits. f. tech. Phys. **13** (1932) 57.

Statistical Theory of Rubber-like Elasticity.
(The Network Structure)

By Akira ISHIHARA.

Faculty of Science, University of Tokyo.

(Received January 16, 1948)

§ 1. Introduction.

Many papers have been published concerning the statistical theory of rubber-like elasticity(1). Most of them, however, treat only one representative molecular chain without referring to the network structure of vulcanized rubber. Recently two papers have been published for this problem, that is Flory-Rehner's(2) and Guth-James'(3). But the essential point of the Flory's paper is different from that of Kuhn(1), and moreover his theory is limited only to the particular structure of regular tetrahedron. Therefore, the theory is not satisfactory, though the treatment and the idea is very interesting. On the other hand the latter papers are very fine, but since they are using Gaussian functions for the configuration functions of network chains, the theoretical stress-strain relation is only applicable to small elongation. The relation applicable to somewhat higher extension can also be deduced, not using Gaussian functions explicitly.

§ 2. Theory of the Network Structure of Slightly Vulcanized Rubber.

Vulcanized rubber has a so-called network structure irregularly bonded by "sulfur-bridges" between molecules. But, in "ideal" vulcanized rubber, vulcanized slightly as in the experiment of Meyer and Ferry, all the molecules are not always bonded together; some of them may be completely free and others are bonded only at one end. But these latter molecules or molecular chain segments do not contribute to the stress arising from the retractive force of chains, but only contribute to it through internal pressure. Since the inclusion of these chains into consideration complicates the theory, we neglect it in the following treatment.

We idealize the network by assuming secondly that each chain has no steric hinderance or interaction, thirdly that the junctions—sulfur bridges—do not shift and the plastic properties do not appear, and finally that the network is "coherent" in the sense of James and Guth(3). The last condition is necessary to solve eq. (11) in the following treatment.

In this "ideal network" "micro-" and "macro-" Brownian motions take place, arising from the motion of the elements of the chains and that of chains themselves. But the ratio of the contribution of these two movements to the stress is the same in the order as the ratio of each molecular weight(4), and we neglect the latter in the following treatment.

Thus, each junction is "free" and is not fixed in the space, but some junctions locating on the surface of a sample are "fixed" and maintain the shape of the sample (Fig. 1.). Actually, at the surface, the outward push of internal pressure and the inward contraction of chains are in equilibrium, and the shape is maintained. We designate the former junctions by $i, j, k, \ldots.$ and the latter by $\alpha, \beta, \gamma, \ldots.$ and both junctions altogether by $a, b, c, \ldots..$

Now we consider neighbouring junctions a and b. The chain connecting these junctions is not always single. In this case we call these junctions $a_1, a_2, \ldots.$ and $b_1, b_2, \ldots.$ for instance. We designate the positions of the junctions by r_a and r_b, and the number of the elements of the chain connecting them by N_{ab}. Taking the direction of $r_a - r_b$ as a polar axis we designate by $n_{ab}(\omega)$ the number of the elements of the chain in $d\omega$ in the direction of solid angle ω, then the entropy of the

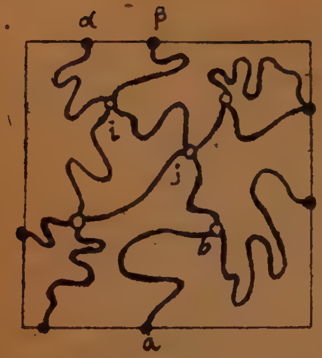

Fig. 1. Ideal network.

○ fixed junctions, ● free junctions.

whole system is given by(4)

$$S/k = -\sum_{a \neq b} \int n_{ab}(\omega) \log n_{ab}(\omega)\, d\omega + \text{const.}, \qquad (1)$$

where k is Boltzmann's constant and the summation extends over all the pairs of the network junctions. $n_{ab}(\omega)$ satisfies the following conditions:

$$\int n_{ab}(\omega) d\omega = N_{ab}, \qquad (2)$$

$$\int n_{ab}(\omega) \cos\theta_{ab}\, d\omega = |\boldsymbol{r}_a - \boldsymbol{r}_b|/l, \qquad (3)$$

where θ_{ab} is the polar angle of an element and l the length of an element.

In thermodynamical equilibrium, S must be maximum with respect to the variation of $n_{ab}(\omega)$, satisfying the above conditions. Accordingly, if we take λ_{ab} and μ_{ab} as Lagrange's multipliers, we can obtain the equilibrium distribution function of θ_{ab} from ordinary Euler's equation (It can be readily seen that the distribution is independent of azimuthal angle.):

$$\lambda_{ab} n_{ab}(\omega) = \exp(\mu_{ab} \cos\theta_{ab}). \qquad (4)$$

From the additional conditions,

$$\lambda_{ab} N_{ab} = 4\pi \sinh \mu_{ab}/\mu_{ab}, \qquad (5)$$

$$\lambda_{ab} |\boldsymbol{r}_a - \boldsymbol{r}_b|/l = 4\pi\{\cosh \mu_{ab}/\mu_{ab} - \sinh \mu_{ab}/\mu^2_{ab}\}. \qquad (6)$$

Accordingly, if we introduce Langevin's function $L(\mu_{ab})$

$$|\boldsymbol{r}_a - \boldsymbol{r}_b|/N_{ab} l = L(\mu_{ab}). \qquad (7)$$

Then the entropy of eq. (1) becomes

$$S/k = -\sum_{a \neq b} \{\mu_{ab} |\boldsymbol{r}_a - \boldsymbol{r}_b|/l - N_{ab} \log \lambda_{ab}\}. \qquad (8)$$

Moreover, the entropy must be maximum with respect to the coordinates of free junctions. This condition is given from eqs. (6) and (8) when $N_{ab} l \gg |\boldsymbol{r}_a - \boldsymbol{r}_b|$

$$\sum_b \left(\frac{x_a - x_b}{N_{ab} l}\right) \left\{1 + \frac{3}{5} \frac{|\boldsymbol{r}_a - \boldsymbol{r}_b|^2}{N_{ab}^2 l^2} + \cdots\right\} = 0. \qquad (9)$$

These equations just determine the equilibrium coordinates of free junctions. It must be noticed that these equations are not linear. Higher terms of $|\boldsymbol{r}_a - \boldsymbol{r}_b|/l$ arise from the network structure and characterize it. But, in the first approximation these terms may be neglected.

Then if we put, following James(3):

$$\left.\begin{aligned} r_{ii} &= \sum_{i \neq j} 1/N_{ij}, \\ r_{ij} &= -1/N_{ij}, \end{aligned}\right\} \qquad (10)$$

equation (9) becomes linear equations:

$$\sum_j r_{ij} x_j = -\sum_a r_{ia} x_a, \quad \text{etc.} \qquad (11)$$

These equations can be solved if the fourth condition of ideal network structure is satisfied, and the coordinates of free junctions are determined as a function of fixed junctions. If a unit cube of the sample is deformed by stretching into a rectangular parallelepiped whose sides correspond to L_x, L_y and L_z, they can be represented as follows:

$$\left.\begin{aligned} x_i &= x_i^0 L_x \\ y_i &= y_i^0 L_y \\ z_i &= z_i^0 L_z \end{aligned}\right\} \qquad (12)$$

where x_i^0 etc. are the equilibrium positions of x_i etc. before stretching and can be determined from eq. (11).

To the extent of deformation that the above approximation is fulfilled the volume of the sample does not change, and if the direction of the stretching is in x-direction of the parallelepiped,

$$L_x L_y^2 = L_x L_z^2 = 1. \qquad (13)$$

Then the stress σ can be readily calculated from the above equations, and is given as follows (noting that the sample is isotropic before stretching):

$$\frac{\sigma}{kT} = \sum_{i \neq j} N_{ij} \left[\frac{|\boldsymbol{r}_i^0 - \boldsymbol{r}_j^0|^2}{N_{ij}^2 l^2} \left(L_x - \frac{1}{L_x^2}\right) + \right.$$
$$\left. + \frac{9}{25} \frac{|\boldsymbol{r}_i^0 - \boldsymbol{r}_j^0|^4}{N_{ij}^4 l^4} \left(L_x^3 + \frac{1}{3} - \frac{4}{3L_x^3}\right) + \cdots \right]. \qquad (14)$$

This equation is essentially identical with that already given by us considering only one representative chain, and can reproduce the experimental *S* shape of the stress-strain relation. But the higher terms of eq. (14) will be different from them owing to the neglect of the higher terms of eq. (9). Actually, before the higher terms affect the result, crystallization will occur. Therefore, we must take internal energy into consideration before the calculation of these terms.

I am indebted to Prof. T. Sakai for his advice and interest in this work.

References.

(1) W. Kuhn: Koll. Zeits. **76** (1936), 258; Naturwiss. **24** (1936), 346; etc.,
E. Guth and H. Mark: Monats. f. Chem. **65** (1935), 93; Zeits. Elektrochem. **43** (1937), 353,
E. Guth: Kautschuk **13** (1937), 201,
E. Guth and H. James: Ind. Eng. Chem. **33** (1941), 1624; **34** (1942), 1365,
T. Sakai: Nippon Sugaku-Buturigakukai-shi **7** (1943), 226,
Y. Oti: ibid. **2** (1947), 182,
R. Kubo: J. Phys. Soc. Jap. **2** (1947), 47, 51,
M. S. Green and A. V. Tobolsky: J. Chem. Phys. **14** (1946), 80.
(2) P. J. Flory and J. Rehner: J. Chem. Phys. **11** (1943), 512.
(3) H. M. James and E. Guth: J. Chem. Phys. **11** (1943), 455,
H. M. James: J. Phys. **15** (1947), 651.
H. M. James and E. Guth: ibid. 669.
(4) T. Sakai ahd A. Ishihara: J. Phys. Soc. Jap. **3** (1948) 171.

Structure Viscosity of High Polymer Solutions.

By Akira Ishihara.

Faculty of Science, University of Tokyo.

(Read September 9, 1947; Received January 16, 1948).

§ 1. Introduction.

There are many investigations concerning the relation between the specific increase of viscosity of high polymer solutions and the molecular weight of the polymer. These papers aim mainly at testifying Staudinger's viscosity rule:

$$[\eta] = KM, \qquad (1)$$

which is introduced comparatively boldly. In eq. (1) $[\eta]$ represents the intrinsic viscosity, M the molecular weight of the suspension, and K is a numerical factor. This equation is not always suitable, but must be replaced as follows:

$$[\eta] = KM^{\alpha}, \qquad (2)$$

where α is a parameter varying from 0.5 to 1 for most suspensions; α is close to 0.5 for random flexible chains and to 1 for straight stiff chains(1).

However, according to the theoretical papers which are published lately by Huggins(2), Debye(3) and Kramers(4) etc., Standinger's rule holds for random chains ($\alpha = 1$), and does not hold for straight chains ($\alpha = 2$). In this respect the results obtained by Haller(5) and Kuhn(6) are more close to the experiments. According to these authors the above contradiction comes from the fact that the polymer does not consist of points and rods, but of elements which have finite volumes.

But there remains another incomplete point. Namely the model of the polymer-suspension in these theoretical papers is rigid and does not defrom by the effect of the stream. Therefore, the structure viscosity which is remarkable in the solutions of flexible polymer is out of question. These are hydrodynamical researches of this problem,(7) but in these treatments the structure viscosity comes from the orientation effect of the stream, and it seems that there is a structure viscosity arising from another source in high polymer solutions, i. e., the deformation of the molecules.

Staudinger(8) pointed out that the intrinsic viscosity $[\eta]_{C=0}$ of cellulose nitrate which is obtained merely as the limit of zero concentration manifests structure viscosity, and the effect becomes greater as the polymerization increases (Fig. 1). The appearance of the curves in Fig. 1 is also the feature of flexible chains such as rubber.(9) Therefore, the intrinsic viscosity must be a limiting value not only of zero concentration, but also of zero velocity gradient. This point is accentuated lately also by Lyms.(10)

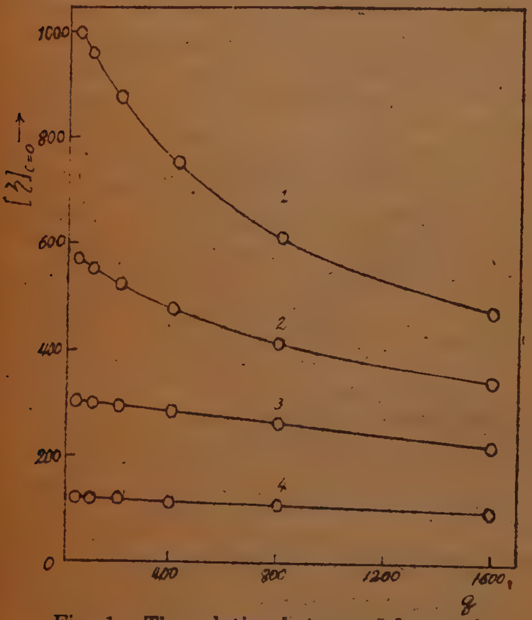

Fig. 1. The relation between $[\eta]_{C=0}$ and velocity gradient q for 4 species of cellulose nitrate(8).

Polymerization $\begin{cases} 1: 2650;\ 2: 1530 \\ 3: 870;\ 4: 310. \end{cases}$

The purpose of this paper is to advance the theories from the viewpoint of the deformation of the chains. But the problem becomes difficult if we consider the deformation from the beginning. Therefore, we consider the deformation to be very small and replace it by "micro-segment motion" around an equilibrium point, which in turn is determined by the rigidity of the chain and the magnitude of the velocity gradient.

§ 2. Rigid Suspension Model.

We take for polymer-suspensions the so-called "pearl-necklace" model. The suspensions are composed of N identical spheres connected by $N-1$ rods of length l. The radius of the spheres is a and the mass is m. As mentioned above, we consider first the rigid pearl necklace. The solution of the motion of these suspensions is given by several authors.(11) The centers of gravity of the suspensions flow with the solvent molecules. We take a coordinate system fixed to the center of gravity of a suspension, and represent the velocity of the flow by $(0, qx, 0)$; q is the velocity gradient. The polymer-suspension may rotate around its center of gravity. Therefore, we denote the rotation by $\Omega(w_1, w_2, w_3)$, the position of the ith sphere of the suspension by $\boldsymbol{R}(x, y, z)$, and the velocity of the flow at this point by $\boldsymbol{V}$ (For the purpose of convenience we omit the suffix of the particle in the notation.) Then the sphere is subjected to the Stokes' force:

$$\boldsymbol{K} = \kappa(\boldsymbol{V}-[\Omega, \boldsymbol{R}]). \tag{3}$$

Here κ is a proportional constant, and can be written for the present model:

$$\kappa = 6\pi\eta_0 a, \tag{4}$$

where η_0 is the viscosity of the solvent.

From eq. (3) we can calculate the rotatory moment $\boldsymbol{M}$:

$$\boldsymbol{M} = \sum[\boldsymbol{R}, \boldsymbol{K}]. \tag{5}$$

To consider the rotational motion of the polymer it is convenient to take a coordinate system referred to the principal axes of inertia of the suspension and represent the motion by Euler's equation of motion.(11) The equation is complicated in general, but in the case where the two of the principal moments of inertia coincide with each other, namely in the case where the arrangement of the spheres has an axial symmetry the equation is simplified and may be represented as follows:

$$\left.\begin{aligned} &A(\ddot\theta+\dot\varphi\dot\psi\sin\varphi)-(A-C)\dot\varphi\sin\theta(\dot\varphi\cos\theta+\dot\psi) \\ &\qquad = \kappa q(R-P)/4\cdot\sin 2\theta\sin 2\varphi-\kappa(P+R)\dot\theta, \\ &A(\dot\theta\dot\psi-\ddot\varphi\sin\theta-\dot\varphi\dot\theta\cos\theta)-(A-C)\dot\theta(\dot\varphi\cos\theta+\dot\psi) \\ &\qquad = -\kappa q\sin\theta(P\sin^2\varphi+R\cos^2\varphi) \\ &\qquad\quad +\kappa(P+R)\dot\varphi\sin\theta, \\ &C(\ddot\varphi\cos\theta-\dot\varphi j\sin\theta+\ddot\psi) \\ &\qquad = \kappa P\{q\cos\theta-2(\dot\varphi\cos\theta+\dot\psi)\}. \end{aligned}\right\} \tag{6}$$

Here θ, φ and ψ are Eulerian angles between the fixed coordinate axes and those referred to the principal axes of inertia, A and C the moments of inertia, and P and R are given by

$$P=\sum x^2,\quad R=\sum y^2=\sum z^2. \tag{7}$$

To solve these equations in general is still difficult, and the solution in the case of $m=0$ corresponding to the approximation of Stokes is usually used. In this case the solution can be obtained by equating the right side of the above equations to zero, and it can be shown that the motion of the polymer coincides with the motion obtained hydrodynamically.(11) But in the more special case where the configuration of the suspension is spherical, it can be readily seen that the following uniform rotation is possible:

$$\theta=\psi=\text{const.}, \tag{8}$$

$$\varphi=q/2.$$

This solution is identical with that obtained by Debye in an approximate method, and is physically plausible. Therefore, we use this solution in the following.

Then the mean energy loss W per 1 c.c. of solution in unit time which is induced by the presence of polymers is given by,

$$\begin{aligned} W &= n\sum\overline{(\boldsymbol{K},\ \boldsymbol{V}-[\Omega,\ \boldsymbol{R}])},\\ &= \frac{1}{36}\frac{1+C}{1-C}(n\kappa q^2N^2l^2), \end{aligned} \tag{6}$$

where n is the number of polymer in 1 c.c. of solution and c the cosine of the bound angle.

§ 3. The Effect of Deformation.

It can be conceived that the particles of a suspension are displaced by the centrifugal force induced by the above rotational motion and in general oscillate around a new equilibrium point. It is convenient to consider the motion in the coordinate system rotating with the angular velocity $q/2$. The particle originally situated at $(x_0,\ y_0,\ z_0)$ will be displaced into $(x_0+\xi_0,\ y_0+\eta_0,\ z_0+\zeta_0)$. In this position the centrifugal force and the elastic force must be in equilibrium. Therefore, if the elastic force obeys Hooke's law,

$$k\xi_0=mx_0(q/2)^2,\quad k\eta_0=my_0(q/2)^2.$$

Since $x_0/\xi_0,\ y_0/\eta_0$ may be considered to be approximately similar for all the particles, we can put

$$k=smq^2, \tag{10}$$

where s is a constant determined by the elastic nature of the polymer.

Then the elastic restoring force $\boldsymbol{S}$ when the particle is displaced by $(\xi,\ \eta,\ \zeta)$ from the above new equilibrium position is given by,

$$\boldsymbol{S}=-k\boldsymbol{s},$$

$$\boldsymbol{s}=(\xi,\ \eta,\ \zeta). \tag{11}$$

When the displacement is small and the influence of the neighbouring segments is neglected, the equation of motion in this moving coordinate system is given as follows

$$m\frac{d^2\boldsymbol{s}}{dt^2}=\boldsymbol{K}'+\boldsymbol{S}-m\begin{cases}(-q\dot{\eta}),\\(q\dot{\xi}),\\0.\end{cases} \tag{12}$$

where

$$\boldsymbol{K}'=\boldsymbol{K}-\kappa\frac{d\boldsymbol{s}}{dt}=\begin{cases}-\kappa\dot{\xi}+\kappa q/2\cdot r_0\sin(qt+\theta),\\-\kappa\dot{\eta}+\kappa q/2\cdot r_0\cos(qt+\theta),\\0.\end{cases} \tag{13}$$

$$r_0{}^2=x_0{}^2+y_0{}^2, \tag{14}$$

$$\tan\theta=y_0/x_0. \tag{15}$$

Therefore, eq. (12) becomes

$$\left.\begin{aligned} &m\ddot{\xi}+\kappa\dot{\xi}+k\xi-mq\dot{\eta}=f_\xi,\\ &m\ddot{\eta}+\kappa\dot{\eta}+k\eta+mq\dot{\xi}=f_\eta,\\ &m\ddot{\zeta}+\kappa\dot{\zeta}+k\zeta=0. \end{aligned}\right\} \tag{16}$$

where

$$\left.\begin{aligned} f_\xi &= \kappa q/2\cdot r_0\sin(qt+\theta),\\ f_\eta &= \kappa q/2\cdot r_0\cos(qt+\theta), \end{aligned}\right\} \tag{17}$$

Therefore, the polymer segment is subjected to forced vibration induced by the flow. It may be remarked here that the frequency of the vibration is twice the angular velocity. This is naturally to be expected, since the flow changes with period π. Moreover, the vibration is a damped one, and gives rise to energy loss.

If we consider a stationary state, among the solution of eq. (16) only the following motion remains.

$$\left.\begin{aligned} \xi &= \frac{r_0}{2\sqrt{1+s^2(mq/\kappa)^2}}\sin(qt+\theta-\theta_0),\\ \eta &= \frac{r_0}{2\sqrt{1+s^2(mq/\kappa)^2}}\cos(qt+\theta-\theta_0), \end{aligned}\right\} \tag{18}$$

where

$$\tan \theta_0 = \kappa / smq. \tag{19}$$

Therefore, the mean energy loss per 1 c.c of solution in unit time is given by,

$$w = \frac{qn}{2\pi}\int_0^{2\pi/q} \Sigma(\dot{\xi} f_\xi + \dot{\eta} f_\eta)dt,$$

$$= \frac{W}{1+s^2(mq/\kappa)^2} \tag{20}$$

Thus the total energy loss $(\eta-\eta_0)q^2$ is given from eqs. (9) and (20) by

$$(\eta-\eta_0)q^2 = \frac{n\kappa q^2}{36}\frac{1+C}{1-C}N^2 l^2\left[1+\frac{1}{1+s^2(mq/\kappa)^2}\right], \tag{21}$$

and the intrinsic viscosity obtained as a limit of zero concentration is

$$[\eta]_{C=0} = KN\left[1+\frac{1}{1+s^2(mq/\kappa)^2}\right], \tag{22}$$

where

$$K = \frac{\pi a}{6m}\frac{1+C}{1-C}l^2.$$

This equation can also be deduced by the physical method of Kramers(4) in the same approximation used in deriving eq. (12).

§ 4. Results.

The structure viscosity corresponding to eq. (22) is illustrated for several values of s in Fig. 2.

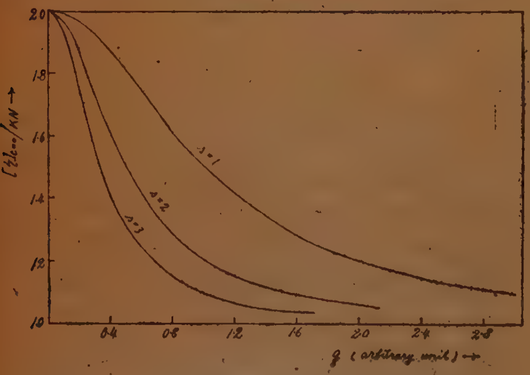

Fig. 2. The theoretical curves of $[\eta]_{C=0}$ according to eq. (22) for several values of s.

In the figure the abscissa is in an arbitrary scale. It can be seen that the theoretical curves reproduce the main features of the experimental curves in Fig. 1. The molecular constant s may be comparatively small in the sample of low degree of polymerization. The curves in Fig. 2 approach to the limiting value of Debye more rapidly than in the case of larger s. In the limit of infinite s, the suspension does not deform and the curves approach to the Debye's. This value is the same as Kramers', because his calculation corresponds to a rigid suspension as in the cases of Huggins(2) and Debye.(3) On the contary, if we consider the state when the influence of the flow upon the suspension is too small to be rigid, the viscosity of the solution diminishes as the velocity gradient increases.

In conclusion the author wishes to make an acknowledgement to Prof. T. Sakai and N. Saito.

References.

(1) R. Houwink: J. prak. Chem. **157** (1940), 15; I. Sakurada: Ka. Sen. Koensyu **5** (1940), 33; P. J. Flory: J. Am. Chem. Soc. **65** (1943), 372;
A. Bartovics and H. Mark: ibid. **65** (1943) 1901;
W. C. Carter, R. L. Scott and M. Magat: ibid. **68** (1946), 1480.
(2) M. L. Huggins: J. Phys. Chem. **42** (1938); 911; **43** (1939), 439;
J. App. Phys. **10** (1939), 700; **14** (1943), 246.
(3) P. Debye: J. Chem. Phys. **14** (1946), 636.
(4) H. A. Kramers: J. Chem. Phys. **14** (1946), 415.
(5) W. Haller: Koll. Zeits. **56** (1931), 256; **61** (1932), 26.
(6) W. Kuhn: Zeits. f. phys. Chem. A **161** (1932), 1. etc.
(7) J. M. Burgers: Second Report on Viscosity and Plasticity, Amsterdam 1938. pp. 113.
A. Peterlin: Zeits. f. Phys. **111** (1938), 232.
(8) H. Staudinger u. R. Mohr: Ber. **70** (1937), 2303.
H. Staudinger: Organische Kolloidchemie.
(9) B. Dogadkin u. D. Pewsner: Koll. Zeits. **53** (1930), 239; etc.
(10) W. J. Lyms: J. Chem. Phys. **13** (1945), 43.
(11) See (2)-(7) in the above references, and especially N. Saito: J. Phys. Soc. Jap., in press.

Note added in proof.

Recently N. Saito has proposed another attempt at the present subject on the line of hydrodynamical method.(7) His calculation corresponds to "überfluide Lösung", whereas the present calculation corresponds to "Elastische Löusung".

Crystallite Theory of Liquid, II. Solid-Liquid Transformation.

By Akiya OOKAWA.

Kobayashi Institute of Physical Research, Kokubunji, Tokyo.

(Received February 14, 1948.)

§ 1. Introduction.

In the previous paper[1)] the present author extended a molecular theory of liquid at low temperature based upon a newly proposed molecular model of liquid. This model is one which can be considered as representing the structure of both liquid and solid in common. In short the main feature of the model can be described as follows:

a) A structure of a mosaic of fine fragments which are in contact with each other on well-defined interfaces, each having a perfect crystalline pattern throughout its own domain (refer to Fig. 1);

b) Existence of an excess configurational energy, due to the misfit of the elements at the interfaces;

c) Dynamic rather than static equilibrium, accompanied by some degenerate translational degrees of freedom for each crystallites.

In the previous report on the theoretical consideration of the specific heat of liquid at low temperature, the misfit potential energy per unit interface area and the available volume of the centre of gravity of a crystallite was smoothed out in respect to both the translational and the orientational coordinates of the crystallite. This premise was made for the moment on the base of some experimental evidences concerning the X-ray scattering and non-rigid viscous flow of liquid, but it has no concrete foundation since the statistical stability of the random orientational distribution of the crystallites is not yet concluded theoretically.

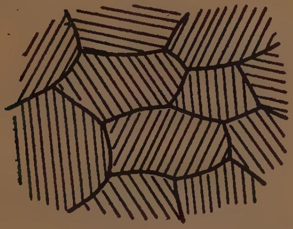

Fig. 1. A structure of a mosaic of fine fragments (foam structure).

In the case of solid, the crystallites in a single grain are oriented approximately parallel to each other. Such an orientational order of the crystallite realized in solid may be considered as the result of the fact that firstly the increase of the misfit potential energy accompanying the relative disorientation of crystallites is much larger than in liquid and that secondly there are co-operative couplings of neighbouring crystallites.

In the present paper a theory based on the crystallite model will be developed by adopting the view that the state of orientational disorder corresponds to the liquid and that of orientational order to the solid. It will be demonstrated that the state of perfect disorder (the liquid state) is in fact thermodynamically stable above the order-disorder transition point and the state of order (the solid state) below that point.

§ 2. General Formulation.

A general formulation of the theory on the proposed model is developed here, including the former conventional treatment as its special case.

The total degrees of freedom of a system of N elements consist of the translational, the orientational, and the internal degrees of freedom of the constituent crystallites. The partial partition function f_i for the internal degrees of freedom of the i-th crystallite is assumed to be separable from the others. The total partition function Ξ of the system is given by

$$\Xi = \sum_i \Pi f_i \sum_{x_i, p_{x_i}, o_i} \exp(-\varepsilon/kT) \Pi_i dx_i dp_{x_i} do_i . \quad (1)$$

x_i and o_i are the translational and the orientational coordinates respectively of the i-th crystallite, and p_{x_i} are the momentum coordinates corresponding to x_i. The momentum coordinates corresponding to o_i are not necessary to be considered, as o_i are not such an orientational coordinate of rigid rotors. The first summation is to be taken over all possible distributions of crystallite sizes with restriction

$$\sum n_i \alpha_i^3 = N, \tag{2}$$

where n_i is the number of crystallites of linear dimension α in the unit of lattice constant a(3).

The total energy ε of the system consists of the translational kinetic energy and the misfit potential energy, that is,

$$\varepsilon = \sum_i \frac{1}{2m_i}(p_{x_i}^2 + p_{y_i}^2 + p_{z_i}^2) + \varepsilon_p(\alpha_1, \alpha_2, \ldots; o_1, o_2, \ldots), \tag{3}$$

where m_i is the average mass of the i-th crystallite. In the strict sense the misfit potential energy ε_p depends on the translational as well as on the orientational coordinates of the crystallites, but for the moment it may be permissible to reserve the dependence upon the latter only, using the value smoothed over in respect to the former coordinates.

Integrating the equation (1), with ε as given by (3), with regard to $p_{x_i}, p_{y_i}, p_{z_i}, x_i, \ldots .$, we obtain

$$\Xi = \sum \prod_i \left[f_i \frac{(2\pi m_i kT)^{3/2}}{h^3} \right] \sum_{o_i} v_i(\alpha_1, \alpha_2, \ldots .; o_1, o_2, \ldots .) \exp(-\varepsilon_p/kT) \prod_i do_i, \tag{4}$$

where v_i denotes the available volume of the centre of gravity of the i-th crystallite.

The misfit potential energy ε_p is proportional to the total area of the internal surface of the system. Assuming uniform crystallite size distribution for the sake of brevity, that is, n crystallites of the same linear dimension α, then ε_p may be represented by

$$\varepsilon_p = n\alpha^2 \varepsilon_0(o_1, o_2, \ldots .), \tag{5}$$

where ε_0 is the misfit energy per unit interface area, depending on the orientational coordinates of the crystallites.

The relative shear movement of two crystallites with different orientations, accompanied by the Brownian motion of their interface, is illustrated schematically in Fig. 2, where the relative shear between A element and B element in each crystallite is obviously proportional to the growth or the decay of the crystallites I and II (compare with Fig. 1 in the discussion2) by Bragg). It is to be noted here that under a given external shearing force either of the upward or the downward movement of the interface will predominate to another, resulting in the macroscopic flow. The available volume v_i in any case goes in parallel with the range of allowed displacement of the crystallite boundary. The linear dimension of the latter being of the order of αa, we put

$$v_i = (\alpha a)^3 \beta_i(o_1, o_2, \ldots .), \tag{6}$$

β_i being of the available volume coefficient depending on orientations.

Substituting (5) and (6) into (4), it follows

$$\Xi = \sum_{n\alpha^3 = N} \left\{ \left[f \frac{(2\pi m_0 kT)^{3/2} a^3}{h^3} \right]^n \alpha^{(3/2 \times 3 + 3 + 2)n} \cdot \sum_{\omega_i} \exp(-n\alpha^2 \varepsilon_0/kT) \prod_i \beta_i \, d\omega_i \right\}, \tag{7}$$

where $m_0 = m/\alpha^3$ is the mass of an element and the number of discriminable orientational configuration of each crystallite is assumed to be α^2 in a unit solid angle, that is, $do_i = \alpha^2 d\omega_i$.

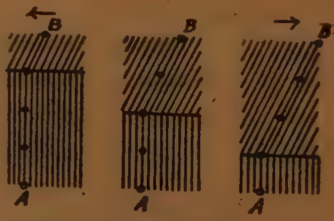

Fig. 2. Relative shear of two crystallites with different orientations, accompanied by Brownian motion of the interface.

The unit misfit potential energy ε_0 and the available volume coefficient β_i are the functions of the set of relative orientational coordinates of nearest neighbouring crystallites. The straightforward manipulation of such a many-body problem is prohibitively difficult. It may be, however, permissible to reduce the problem to a kind of one-body problem according to

$$\sum_{\omega_i} \exp(-n\alpha^2 \varepsilon_0/kT) \prod_i \beta_i d\omega_i$$

$$\equiv\left[\frac{1}{\sigma}\iiint\exp(-\alpha^2\bar{\varepsilon}_0/kT)\,\bar{\beta}\,d\omega\right].\tag{8}$$

The quantities $\bar{\varepsilon}_0$ and $\bar{\beta}$ in (8) are assumed to be functions of the absolute orientational coordinates of a specified crystallite only, but in such a way that they are dependent on the degree of order of the total system. The symmetry number σ of one crystallite is introduced, in order to extend the integration over all orientations of the cryatallite.

If we assume the internal degrees of freedom to be vibrational just as in Einstein model, equation (7) can be reduced approximately to

$$\Xi=\left[\frac{kT}{h\nu}\right]^{3N}\sum_{\alpha}[\xi(\alpha)]^N,\tag{9}$$

where

$$\xi(\alpha)=\left[\left(\frac{h\nu}{kT}\right)^3\frac{(2\pi m_0kT)^{3/2}a^3}{h^3}\,\alpha^{19/2}\cdot\frac{1}{\sigma}\iiint\exp(-\alpha^2\bar{\varepsilon}_0/kT)\bar{\beta}\,d\omega\right]^{\alpha^{-3}}.\tag{10}$$

ξ may be regarded to represent the thermodynamical probability per element of the system for a perfectly crystalline state.

§ 3 Cooperative Nature.

Now we are in stage to determine the functional form of orientational dependence of $\bar{\varepsilon}_0$ and $\bar{\beta}$. We assume a system of cubic symmetry for the perfectly crystalline state.

The angular variation of the unit misfit potential energy at interfaces between a specified crystallite and its nearest neighbours may be represented schematically as in Fig. 3, for a state of perfect orientational order and for a state of orientational disorder respectively.

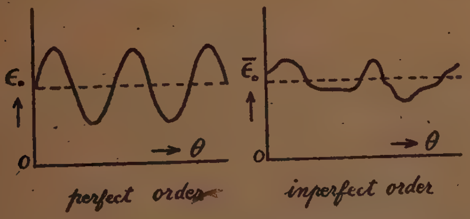

Fig. 3, The angular variation of the unit misfit potential energy.

In a state of perfect order, ε_0 varies according to

$$\varepsilon_0=k_0+k_1(s_1+s_2+s_3)+k_2p+\ldots,\tag{11}$$

where

$$\left.\begin{aligned}s_1&=\alpha_{11}^2\alpha_{12}^2+\alpha_{12}^2\alpha_{13}^2+\alpha_{13}^2\alpha_{11}^2,\\ s_2&=\alpha_{21}^2\alpha_{22}^2+\alpha_{22}^2\alpha_{23}^2+\alpha_{23}^2\alpha_{21}^2,\\ s_3&=\alpha_{31}^2\alpha_{32}^2+\alpha_{32}^2\alpha_{33}^2+\alpha_{33}^2\alpha_{31}^2,\\ p&=\alpha_{11}^2\alpha_{12}^2\alpha_{13}^2+\alpha_{21}^2\alpha_{22}^2\alpha_{23}^2+\alpha_{31}^2\alpha_{32}^2\alpha_{33}^2,\end{aligned}\right\}\tag{12}$$

and α_{11}, α_{12}, α_{13}, ..., α_{33} denote the direction cosines between the ξ-, η-, ζ-axes of the crystallite and the x-, y-, z-axes of the bulk system. In a state of imperfect order, we formulate the angular variation of the mean unit misfit energy $\bar{\varepsilon}_0$ by

$$\begin{aligned}\bar{\varepsilon}_0&=k_0+k_1(\bar{s}_1+\bar{s}_2+\bar{s}_3)+k_2p+\ldots.\\ &\quad+t[k_1(s_1+s_2+s_3-\bar{s}_1-\bar{s}_2-\bar{s}_3)+k_2(p-\bar{p})+\ldots].\end{aligned}\tag{13}$$

A new parameter t is introduced to specify the degree of orientational order of the system such that $t=1$ and $t=0$ correspond to the state of perfect order and that of perfect disorder*.

The angular variation of the available volume coefficient is assumed to be given by

$$\bar{\beta}=s_1s_2s_3,\tag{14}$$

which is in accordance with the requirement that $\bar{\beta}$ shall be zero for such a configuration as represented by $\alpha_{ij}=\delta_{ij}$ or its analogue in a state of perfect order (refer to Fig. 2). The necessary modification for the state of imperfect order is neglected here, merely for the sake of brevity.

If the energy constants k_2, etc. are sufficiently large, the system is substantially restrained from taking the configurations other than those corresponding to such a set of direction cosines as

$$\begin{pmatrix}1&0&0\\0&\cos\theta_1&\sin\theta_1\\0&-\sin\theta_1&\cos\theta_1\end{pmatrix},\quad\begin{pmatrix}\cos\theta_2&0&-\sin\theta_2\\0&1&0\\\sin\theta_2&0&\cos\theta_2\end{pmatrix},$$
$$\begin{pmatrix}\cos\theta_3&\sin\theta_3&0\\-\sin\theta_3&\cos\theta_3&0\\0&0&1\end{pmatrix}\tag{15}$$

In this case the estimation of the average values in equation (13) is easy, that is

---

* In the case of lower crystal symmetry, it is natural to introduce more than one parameter for the degree of order discriminative for each crystal axes, which seems to promise the possible existence of the so-called liquid-crystalline state.

$$\bar{s}_1+\bar{s}_2+\bar{s}_3=\frac{1}{2}\overline{(s_2+s_3)}+\frac{1}{2}\overline{(s_3+s_1)}+\frac{1}{2}\overline{(s_1+s_2)}$$

$$=\sum_{i}\frac{1}{2}\frac{1}{2\pi}\int_0^{2\pi}\sin^2\theta_i\cos^2\theta_i\,d\theta_i=\frac{3}{8}, \qquad (16)$$

and the expression (13) reduces, omitting the constant term k_0, to

$$\bar{\varepsilon}_0(t)=\frac{3}{8}(1-t)k_1+tk_1(s_1+s_2+s_3). \qquad (17)$$

By substitution of (14) and (17) into (10), we obtain

$$\xi_t(\alpha)=\left[\left(\frac{h\nu}{kT}\right)^3\frac{(2\pi m_0kT)^{3/2}a^3}{h^3}\alpha^{19/2}g_t(\alpha)\right]^{\alpha^{-3}}, \qquad (18)$$

where

$$g_t(\alpha)=e^{-3(1-t)\alpha^2k_1/8kT}\frac{1}{\sigma}\iiint e^{-(t\alpha^2k_1/kT)(s_1+s_2+s_3)}\cdot s_1s_2s_3\,d\omega. \qquad (19)$$

We approximate the expression $g_t(\alpha)$ by

$$g_t(\alpha)=g_{t1}(\alpha)g_{t2}(\alpha)g_{t3}(\alpha), \qquad (20)$$

where the expressions

$$\left.\begin{aligned}
g_{t1}(\alpha)&=e^{-(1-t)\alpha^2k_1/8kT}\sigma^{-1/3}\\
&\quad\cdot\int_0^{2\pi}e^{-(t\alpha^2k_1/2kT)(s_2+s_3)}s_2^{1/2}s_3^{1/2}d\theta_1\\
g_{t2}(\alpha)&=e^{-(1-t)\alpha^2k_1/8kT}\sigma^{-1/3}\\
&\quad\cdot\int_0^{2\pi}e^{-(t\alpha^2k_1/2kT)(s_3+s_1)}s_3^{1/2}s_1^{1/2}d\theta_2\\
g_{t3}(\alpha)&=e^{-(1-t)\alpha^2k_1/8kT}\sigma^{-1/3}\\
&\quad\cdot\int_0^{2\pi}e^{-(t\alpha^2k_1/2kT)(s_1+s_2)}s_1^{1/2}s_2^{1/2}d\theta_3
\end{aligned}\right\} \qquad (21)$$

correspond to the respective set of configurations given by (15), Strictly speaking, the configurations of the specified crystallite, each corresponding to one of the three sets of (15), are exclusive to each other, being incapable of simultaneous realization. The separation treatment, as assumed in (16) and (20), is not rigorous in this respect. But the average quantities $\bar{\varepsilon}_0$ and $\bar{\beta}$ being determined by the relative orientational coordinate of the specified crystallite in reference to its nearest neighbours, this treatment may be allowable through the reduction process (8), in the first step of approximating the angular variation of these quantities by the absolute coordinate of only one specified crystallite.

For the last we must characterize the parameter t, above introduced to specify the degree of orientational order of the system. As the expression $\xi_t(\alpha)$, as already remarked, gives the thermodynamical probability per element, the quotient

$$[\xi_0(\alpha)]^{\alpha^3}/[\xi_t(\alpha)]^{\alpha^3}=g_0(\alpha)/g_t(\alpha)=[g_{01}(\alpha)/g_{t1}(\alpha)]^3 \qquad (22)$$

represents the thermodynamical probability per crystallite for a state of perfect disorder relative to that for a state of the degree of order t, both being of the same crystallite size α. In order to determine the thermodynamical value of parameter t as the implicit function of the temperature, accordingly, we assume the functional relation

$$1-t=g_0(\alpha)/g_t(\alpha). \qquad (23)$$

§ 4. Approximate Estimation.

Integrating the expression (21), we obtain (σ is simply put to 4^3)

$$g_{t1}(\alpha)=g_{t2}(\alpha)=g_{t3}(\alpha)=\frac{\pi}{16}e^{-\alpha^2k_1/8kT}\cdot\left[I_0\left(\frac{t\alpha^2k_1}{8kT}\right)-I_1\left(\frac{t\alpha^2k_1}{8kT}\right)\right], \qquad (24)$$

where I_0 and I_1 are the modified Bessel functions. (23) then becomes

$$t=1-[I_0(z)-I_1(z)]^{-3};\quad z=t\alpha^2k_1/8kT, \qquad (25)$$

according to which $t(\alpha,T)$ can be solved graphically as the function of α and T. (Fig. 4).

It is evident that in the case

$$\alpha^2k_1/8kT>z_c/t_c$$

three states are possible, each corresponding to $t=0$, t_1, and t_2. The state of the largest $t(t=t_2)$ is, however, the most stable state, because g and therefore ξ is greatest for $t=t_2$. On the contrary, in the case

$$\alpha^2k_1/8kT<Z_c/t_c$$

the possible state is only that of $t=0$, the state of perfect disorder. This critical point represents the transition point between the states of order and this is the melting point or the freezing point, from the viewpoint of the present theory using the crystallite model.

The quantity $\xi(\alpha)$ in (9), as determined by substitution from (25) into (18), varies with α at constant temperature and we approximate the sum in (9) by the maximum term $\xi_{\max}(\alpha^*)$.

The parameter of the degree t for the state of nearly perfect order, above the transition point, has a value very nearly equal to unity. Therefore, t_2 may be considered to be equal to 1. At the same time, z being sufficiently great, I_0 and I_1 may be approximated with the first term of their asymptotic expansion

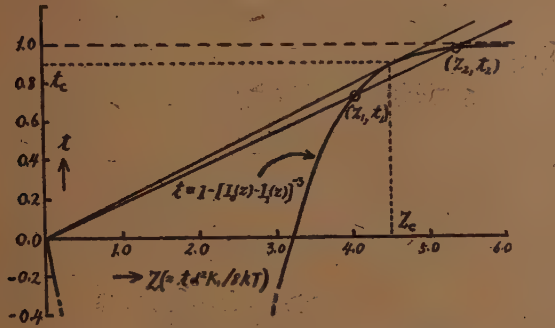

Fig. 4. Determination of t, according to eq. (25).

$$I_n(z) \sim \frac{1}{\sqrt{2\pi z}} e^z \left[1 - \frac{4n^2-1}{1!\,8z} + \frac{(4n^2-1)(4n^2-3)}{3!\,(8z)^2} + \cdots\right].$$

Then it follows

$$\xi_1(\alpha) = \left[\left(\frac{\sqrt{\pi}}{16}\right)^3 \left(\frac{h\nu}{kT}\right)^3 \frac{(2\pi m_0 kT)^{3/2} a^3}{h^3} \cdot \left(\frac{4kT}{k_1}\right)^{9/2} \alpha^{1/2}\right]^{\alpha^{-3}}. \tag{26}$$

The maximum term $\xi_{1,\max}$ is given by

$$\log \xi_{1,\max} = (1/6)(\alpha_1{}^*)^{-3}, \tag{27}$$

where $\alpha_1{}^*$ is determined according to

$$\alpha_1{}^* = e^{1/3}(\theta_1/T)^6 \tag{28}$$

with

$$\frac{1}{\theta_1} = \frac{\sqrt{\pi}}{16} \frac{h\nu}{k} \frac{(2\pi m_0 k)^{1/2} a}{h} \left(\frac{4k}{k_1}\right)^{3/2}. \tag{29}$$

The transition temperature T_0 is estimated according to

$$(\alpha_1{}^*)^2 k_1/8kT_0 = z_c/t_c \sim 4.5/0.9 = 5.0. \tag{30}$$

The excess value Δe_1, Δc_1 of the internal energy and the specific heat for the solid over those for the perfectly crystalline state are derived from (9) and (27), by the use of the thermodynamical equations, as follows:

$$\Delta e_1 = 3kT(\alpha_1{}^*)^{-3}, \tag{31}$$

$$\Delta c_1 = 57k(\alpha_1{}^*)^{-3}. \tag{32}$$

The treatment of the state of perfect disorder $t = 0$, below the transition temperature, is quite the same as in previous report. The maximum $\xi_{0,\max}$ is given by

$$\log \xi_{0,\max} = \left[\frac{19}{6} - \frac{(\alpha_0{}^*)^2 k_1}{4kT}\right](\alpha_0{}^*)^{-3}, \tag{33}$$

where $\alpha_0{}^*$ is determined according to

$$\log(\alpha_0{}^*)^2 = \frac{2}{3} + \frac{6}{19}\log\frac{T}{\theta_0} + \frac{1}{38}\frac{(\alpha_0{}^*)^2 k_1}{kT} \tag{34}$$

with

$$\theta_0 = \left(\frac{\pi}{16}\right)^2 \left(\frac{h\nu}{k}\right)^2 \frac{(2\pi m_0 k) a^2}{h^2}. \tag{35}$$

The excess value Δe_0, Δc_0 of the internal energy and the specific heat for the liquid over that for perfectly crystalline state are given by

$$\Delta e_0 = [(3/8)(\alpha_0{}^*)^2 k_1 - (3/2)kT](\alpha_0{}^*)^{-3}, \tag{36}$$

$$\Delta c_0 = -\frac{3}{2}k\left[1 + \frac{[(\alpha_0{}^*)^2 k_1/8kT - 3/2]^2}{[(\alpha_0{}^*)^2 k_1/8kT - 19/4]}\right](\alpha_0{}^*)^{-3} \tag{37}$$

Taking $h\nu/k = 200$, $m_0 = 100 \times 1.62 \times 10^{-24}$, and $a = 10^{-8}$ for the material constants, we obtain $\theta_0 \sim 500$°k. The calculated results for the transition temperature, the crystallite size and the specific heat at the point are shown in Table 1, assuming several values for k_1. The calculated behaviour of the specific heat is also shown in Fig. 5 in the vicinity of the transition point, which exhibits obvious characteristics of the λ-transition.

Table I. ($\theta_0 = 500$)

$\frac{k_1}{k}$	transition temperature	crystallite size		specific heat	
		$\alpha_1{}^{*3}$	$\alpha_0{}^{*3}$	c_1/k	c_0/k
500	97.8	21.5	1.66	5.65	2.10
1000	272	36.3	2.73	4.57	2.46
1500	486	47.4	3.41	4.20	2.57
2000	749	58.4	4.32	3.90	2.65
2500	1025	66.4	5.07	3.86	2.71

§ 5. Discussion.

The observed values of the specific heat of the solid monatomic metals at the melting point vary between $3.2\,k$ and $4.2\,k$, much greater than $3k$, which might be expected elementarily for the perfectly crystalline system. These discrepancies from the normal value support qualitatively the above concluded nature of the λ-transition of the melting phenomena. However, that the theoretical behaviour of the specific heat is apparently more drastic than the observation seems to disclose the inadequacy of either the present interpretation of the solid-liquid transformation or the approximate treatment of the proposed model.

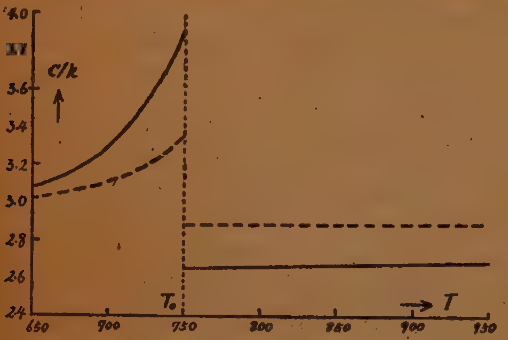

Fig. 5. Specific heat vs. temperature curve.

—— for $\theta_0 = 500$, $k_1/k = 2000$ (see Tab. 1).

- - - - for $\theta_0 = 500 \times 3^{-2}$, $k_1/k = 1000$ (see Tab. 2).

It is obvious that the conventional assumptions which is made in the above description concerning the procedure of reduction of the many-body problem and that of relating the parameter for the degree of order to the thermodynamical probability should be founded on much more unambiguous reasonings. But the drastic nature of the temperature dependence of the specific heat can yet be moderated by some modification of the included constants, k_1 and θ_0, even when the present crude assumptions are maintained. Another result of calculation, assuming $k_1/k = 1000$ and several smaller values than 500 for θ_0, is tabulated in Table II (compare Fig. 5).

Table II. ($k_1/k = 1000$)

θ_0	transition temperature	crystallite size		specific heat	
		α_1^{*3}	α_0^{*3}	c_1/k	c_c/k
500×1	272	36.3	2.73	4.57	2.46
500×2^{-2}	516	93.6	7.00	3.61	2.79
500×3^{-2}	751	163	12.4	3.35	2.88
500×4^{-2}	977	241	18.5	3.24	2.92
500×5^{-2}	1204	355	25.2	3.16	2.94

The assignment of the value of ν much smaller than that of the Debye temperature, which is regarded to be mainly responsible for the decrease of the value of θ_0, may be justified to some degree by the reasoning as follows:

The translational degrees of freedom of the crystallites are the result of degeneration of some vibrational degrees of freedom of the system, caused by the relaxation process of the rigid coupling of the crystallites at their interfaces. The thermal elastic wave of relatively lower frequency is likely to degenerate more easily than that of higher frequency[3]. Therefore, if we assume the distribution $g(\nu)d\nu$ for the number of modes of the thermal wave in the frequency range $\nu \sim \nu + d\nu$, the equation (9) shall be modified into

$$\Xi = \exp\left[\int_0^{\nu_0} g(\nu)\log(1-e^{-h\nu/kT})d\nu\right]$$

$$\cdot\sum_{\alpha}\exp\left[-\int_0^{\nu^*} g(\nu)\log(1-e^{-h\nu/kT})d\nu\right]$$

$$\cdot\left[\frac{(2\pi m_0 kT)^{3/2}a^3}{h^3}\alpha^{19/2}\frac{1}{\sigma}\iiint\exp(-\alpha^2\bar{\varepsilon}_0/kT)\bar{\beta}d\omega\right]^{\alpha^{-3}}$$

$$\sim\left[\frac{kT}{h\nu_D}\right]^{3N}\sum_{\alpha}\left[\left(\frac{h\nu^*}{kT}\right)\frac{3(2\pi m_0 kT)^{3/2}a^3}{h^3}\alpha^{19/2}\right.$$

$$\left.\cdot\frac{1}{\sigma}\iiint\exp(-\alpha^2\bar{\varepsilon}_0'/kT)\bar{\beta}d\omega\right]^{\alpha^{-3}}, \qquad (9')$$

where $\nu^*(\alpha, T)$ is determined relative to the characteristic relaxation time for a specified configuration at a given temperature.

In this way the experimental facts may be interpreted to support the conformability of the crystallite model, adopted in the present theory, at least approximately.

§ 6. Summary.

It is presented that the solid-liquid transformation phenomena in general can be formulated according to the crystallite theory. The order-disorder transition of the orientational distribution of the constituent crystallites corresponds to the solid-liquid transformation, the ordered (the solid) state being stable below the transition point and the disordered (the liquid) state above the transition point. In regard to the experimental data concerning the specific heat, it is suggested that the degenerating vibrational modes of the thermal wave are to correspond to those of much lower frequency, which is justified to some degree by the deliberation on the relaxational nature at the crystallite boundaries.

In conclusion the author wishes to express his

sincere thanks to Dr. S. Oka and Dr. S. Miyake for their hearty encouragement and the useful discussions. He is also indebted to the National Research Council, at the expenditure of which this study is persued.

References.

(1) A. Ookawa: J. Phys. Soc. Jap. **2** (1948) 108.
(2) W. L. Bragg: Proc. Phys. Soc. **52** (1940), 64.
(3) L. Brillouin: J. de Phys. Rad. **7** (1936), 153.

On the Active Centers of the Oxide-coated Cathode.

By

Hazimu KAWAMURA, Akira SHINOHARA, and Katsuya TAKAHASHI.

Mazda Research Laboratories, Tokyo-Shibaura El. Co., Kawasaki, Kanagawa.

(Received March 8, 1948).

The density of the excess barium atoms in the oxide-coated cathode have been measured by many authors[1] by chemical methods. Their results, however, seem to be not reliable, because of the roughness of these chemical methods. In the present report, we have measured this density by physical method, with satisfactory result. We have also investigated the difference between the density of these free barium atoms in the ordinary fine-grained oxide and that in the coarse-grained one having very low emission.

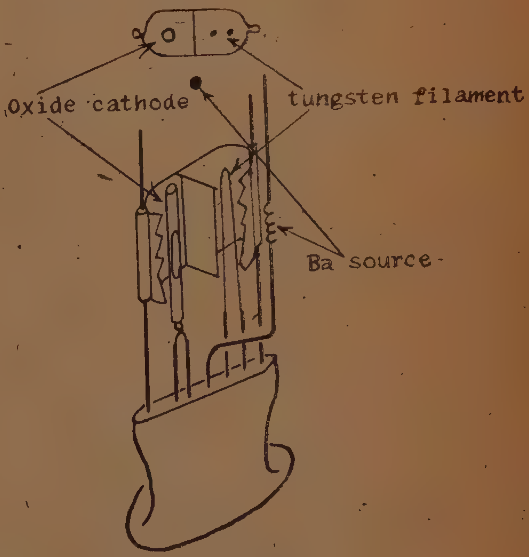

Fig. 1.

§ 1. Experimental Procedure.

The barium atoms evaporated from the "batalum" getter were deposited on the oxide-coated cathode and the tungsten filament of hair-pin type which are set side by side in the vacuum tube, as shown in Fig. 1. The one side of the nickel sleeve faced to the Ba source was coated with Ba-Sr carbonate. By the deposition of barium atoms, the thermionic emission from the tungsten filament increases rapidly to a maximum value as shown by the crosses in Fig. 2, which shows the completion of the monatomic film of Ba, whose desity is known* to be 2.5×10^{14} atoms/cm^2. Thus we can deposit a known quantity of the barium atoms on the oxide-coated cathode, the distances from the Ba source to the tungsten and to the oxide-coated cathode being made to be equal. After deposition of Ba, the oxide-coated cathode was heated to about 940°K for several minutes. Then, the thermionic emission measured at 700°K, increased to a constant value as shown by the circles in Fig. 2. By this procedure the deposited barium atom diffuses into the layer of the oxide, and therefore, the difference in the emission between A and B in Fig. 2, is due to the deposited barium atoms. By the heat treatment at higher temperature such as 1200°K, these excessive barium atoms evaporate off as shown in curve C.

---

* As the radius of Ba atom is about twice of that of W atom, the desity of Ba atoms adsorbed on the W surface is 1/4 of the density of W atoms arranged on the (110) surface of the tungsten which is 1.425×10^{15} atoms/cm^2. And as the surface density of the optimum emission is known to be about 0.7 times the complete monatomic film, the required density is $1.425\times0.7\times10^{15}/4=2.5\times10^{14}$ atmos/cm^2.

According to the theory of semicoductor, saturated thermionic emission from the oxide-coated cathode is proportional to the square root of the density of the free barium atoms, as expressed in the relation,

$$i = AT^{\frac{5}{4}} n^{\frac{1}{2}} \exp(-\Psi e/kT).$$

Hence, if we assume that the emission at A is i_0, and that at B is i, $i^2 - i_0^2$ should be proportional to the quantity of the depositied barium atoms. In the Fig. 3, were plotted $i^2 - i_0^2$, and the quantity of the deposited Ba, which was varied by changing the time of duriation of deposition, in the number

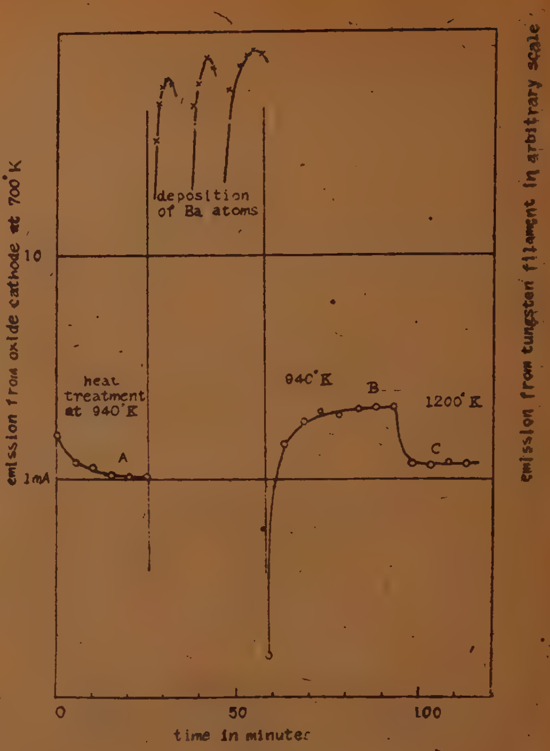

Fig. 2.

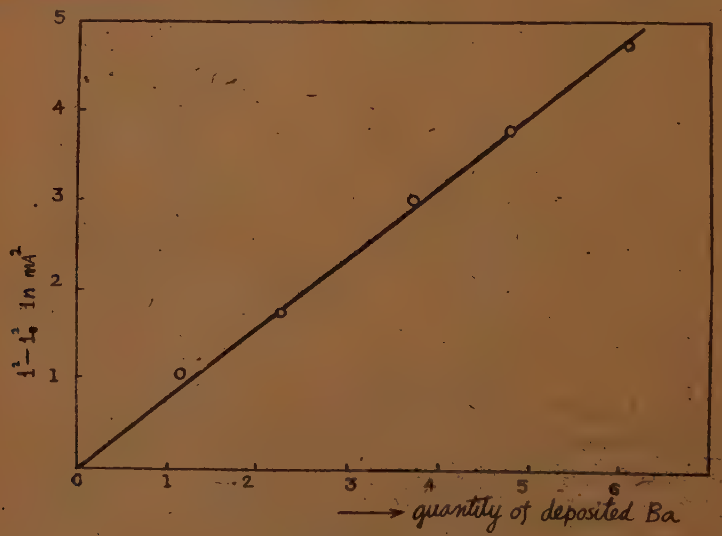

Fig. 3.

of monatomic film on the tungsten.

§ 2. The Results.

The above experiments were carried out with ordinary oxide-coated cathode of fine grained crystal and those of coarse-grianed which were treated by water or chlorine vapour during evacuation*, oxide, the water vapour of about a few mm Hg is introduced to change a part of the oxide to hydroxide. Afterward, this hydroxide is decomposed to oxide at about 1000°C. The crystal grains of the oxide grow remarkably in this process. The treatment by chlorine vapour was performed by etching the nickel anode by a drop of dilute HCl before mounting. The Cl vapour from the nickel chloride reacts upon the oxide during evacuation and promotes the grain growth of the oxide crystal.

---

* After the deposition of the carbonate to the

Table I

		i_0	i for $n=10^{-6}$	n_0	ϕ(eV)	A
1	fine grained	0.98 ma	0.54 ma	3.3×10^{-6}	1.15	6×10^{-7}
2		1.0 ma	0.54 ma	3.4×10^{-6}	1.08	3×10^{-7}
3		1.7 ma	1.3 ma	1.9×10^{-6}	1.01	3×10^{-7}
4	treated by H_2O	11 μa	0.12 ma	8.5×10^{-9}	1.36	3×10^{-6}
5	treated by Cl	10 μa	0.09 ma	1.2×10^{-8}	1.43	7×10^{-6}

whose thermionic emission were only about 10^{-2} times of the fine-grained one as shown in Table I. In

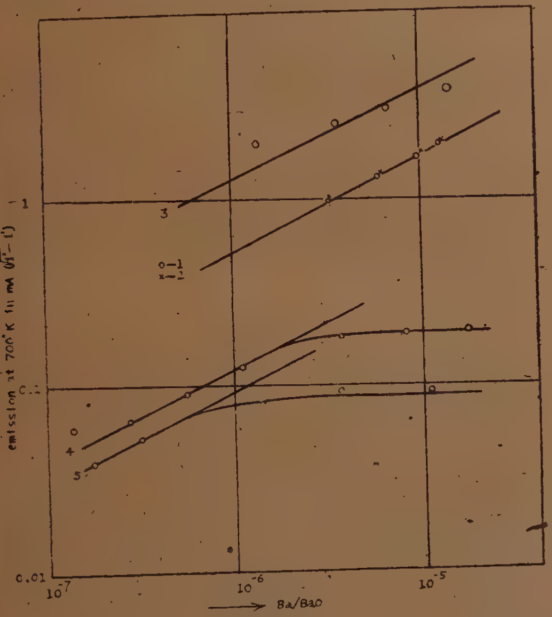

Fig. 4.

Fig. 4, we took the square root of $i^2-i_0^2$ as the ordinate and the ratio of excess barium atoms to BaO* as the abscissa on a log-log section paper. From these curves we obtain the results in Table I. As shown in the third column, the stationary emission i_0, that is, the emissionu nder the condition that the oxide was treated at 940°K for a sufficiently long time, is about one hundred times larger for the fine-grained than for the coarse-grained oxide, but the emission is much the same for the same density of the free Ba, as shown in the fourth column. n, the density of the free Ba in the stationary state, is about several hundred times larger for the fine-grained oxide than for the coarse-grained one, which can almost explain the difference in the stationary emission current i_0. But we can not neglect the small difference in the work function which should produce several times difference in the stationary emission. The Dushman constant A obtained from our experiment, is almost equal to the theoretical value 1.2×10^{-6}.

As shown in Fig. 2, the deposited Ba atoms evaporate off from the oxide at the higher temperature, and from this behaviour we can obtain the heat of evaporation of free Ba in the oxide. The rate of evaporation of the free Ba is proportional to the number n of free atoms and the proportionality constant α is considered to have the from.

$$\alpha = A\exp(-E/kT),$$

where A is a contant and E is the heat of evaporation. On the other hand, the free Ba is produced at a constant rate $v(T)$ by the reduction owing to the impurity in the core metal, or by the simple dissociation of BaO. Therefore, we obtain the relation,

$$-dn/dt = \alpha n - v.$$

Solving this equation, we get

$$\left.\begin{aligned} n &= n_0+\beta\exp(-\alpha t) \\ n_0 &= v/\alpha \end{aligned}\right\},$$

where β is a certain constant. Hence, the decrease of the emission, due to the evaporation of excess Ba, can be experessed by

$$\log(i^2-i_0^2) = -\alpha t + const.,$$

---

* The number of the Ba atoms deposited on the oxide, which correspond to the monatomic film of Ba on W, was $2.5\times10^{14}\times7\times10^{-2}=1.75\times10^{13}$ atoms, since the area of the oxide cathode was 7×10^{-2} cm². On the other hand, the number of the BaO molecules in the oxide, whose weight was 1.4 mg, was 6.6×10. The ratio Ba/BaO for the deposition corresponding to the monatomic film on the W was 2.65×10^{-6}.

where i_0 is the stationary value of the emission, or $i_0 \sim n_0$. From the slope of the curves in Fig. 5,

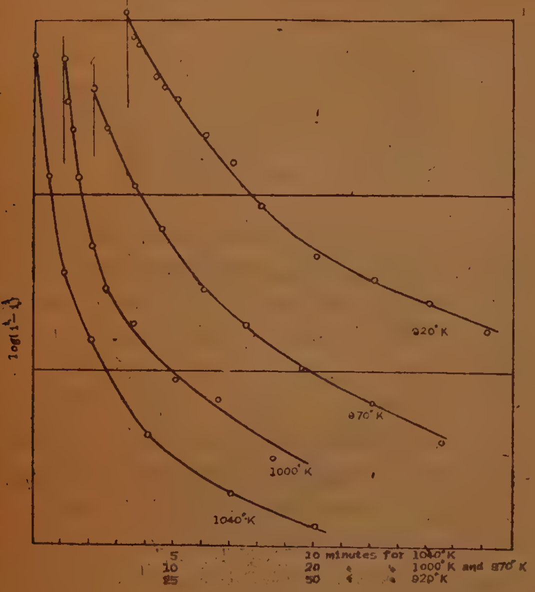

Fig. 5.

where $\log(i^2-i_0^2)$ is plotted against t, we can obtain the rates of evaporation $\alpha = A\exp(-E/kT)$ for the various temperatures. The fact, that the $\log(i^2-i_0^2)$ vs. t curves are not straight lines as expected from the above theory, may show that the heat of evaporation is not strictly constant but somewhat dependent upon n or i. Hence we must determine the heat of evaporation by plotting the logarithm of the slopes of the curves for a fixed value of i (or n) against temperatures. Thus we obtained the values in Table II, where we can say

Table II.

n	Heat of evaporation (eV)	
	fine grain	coarse grain
5×10^{-6}	2.28	
2×10^{-6}	2.32	2.24
1×10^{-6}	2.35	2.28
5×10^{-7}	2.39	2.33
2×10^{-7}	2.44	

that the heat of evaporation of free Ba is almost the same both for the fine-grained and the coarse-grained oxides, and is approximately equal to 2.3 eV.

§ 3. Discussion.

From the heat of evaporation of the free barium just determined we can compute the energy required to produce one active center—free Ba. Now we consider the next cycle:—

1) To produce one active center (free Ba) and half a molecule of oxygen in gaseous phase from one molecule of solid oxide, which require the energy ε,

2) To evaporate this active center, which require the heat of evaporation of the free Ba, E.

3) To condense the evaporated Ba atom to Ba metal. The required energy is the negative sign of the heat of evaporation of Ba metal; $-L$.

4) To compose BaO with this Ba metal and oxygen gas, where we get the heat of formation of BaO, H.

Thus we can obtain the energy relation, $\varepsilon+E-L-H=0$. Hence $\varepsilon = H+L-E$, where $E = 2.3$ eV as in the above result, and $L = 1.9$ eV, $H = 5.8$ eV. Therefore we get $\varepsilon = 5.4$ eV.

The heat of formation employed in this computation is for the ordinary coarse-grained crystal. As suggested by one of the presnt authors[2] from the experiment upon the sublimation of the oxide, the heat of dissociation of the fine-grained oxide is smaller than that of the coarse-grained by about 1 eV. Therefore, the heat of formation L for the fine-grained should be about 4.8 eV, and hence ε is reduced to about 4.4 eV, which may explain the values of n for the fine-grained crystal higher than that of the coarse-grained.

References.

(1) T. P. Berdennikowa: Phys. Zeits. U.S.S.R. **2** (1932) 77.
H. Fritz: Mikrochemie **17** (1935) 191.
C. H. Prescott & J. Morrison: J. Am. Chem. Soc. **60** (1938) 3047.
(2) H. Kawamura: J. Phys. Soc. Jap. **1** (1946) 8.

On the Specific Heat of the Natural Rubber.

By Hiroshi ICHIMURA.

Physics Department, Faculty of Science, University of Tokyo.

(Recieved February 26, 1948.)

§ 1. Abstract.

We calculate the constant volume specific heat of the natural rubber from the constant pressure specific heat which is measured experimentally, and show that the low temperature part of it is expressed by the combination of the Debye's and Einstein's formulae. After that, we attempt some theoretical considerations on the transition phenomena at 200°K.

§ 2. The Derivation of C_v from C_p.

A detailed measurement of the specific heat (C_p) at constant pressure of the natural rubber has been given by N. Bekkedahl.[1] For the purpose of the theoretical treatment, however, the specific heat (C_v) at constant volume is more convenient. Therefore, we caluculate C_v from C_p by the thermodynamical relation

$$C_p - C_v = v\alpha^2 T/\kappa \qquad (1)$$

where v is the specific volume, α is the volume thermal expansion coefficient and κ is the isothermal compressibility. The data of v and α is also given by Bekkedahl[2], but we cannot find the appropriate measurement of κ, so we extrapolate the experimental formula for the vulcanised rubber by A. Scott[3]. At the transition point at about 200°K, we use the Ehrenfest's formula.

$$\Delta C_p = T(\Delta\alpha)^2/v\Delta\kappa \qquad (2)$$

on the assumption that this transition is the transformation of the second order. Δ means the jump of those quantities at this point. Since ΔC_p and $\Delta\alpha$ are given in the data, $\Delta\kappa$ can be estimated by this formula.

At the temperature below 200°K we neglect the variation of α and κ. From these considerations we get C_v at the temperature from 20°K to 320°K. (Fig. 1)

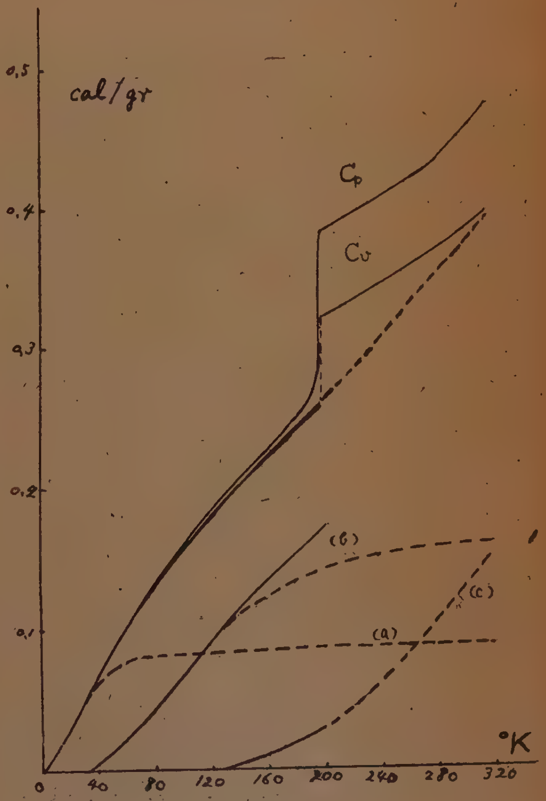

Fig. 1.

Below 200°K this curve can be approximated by the combination of the Debye's specific heat formula, choosing its characteristic temperature $\theta_D = 110$°K and two Einstein's formulae, choosing their characteristic temperatures $\theta_E^{(1)} = 340$°K, $\theta_E^{(2)} = 1380$°K and the number of oscilators 6, 21 (per. isoprene) respectively. Of course these numerical values are nothing but the very rough approximation. However, in comparison with the infra-red absorption, it may be considered that there are the groups of normal vibration which have their frequencies near the above estimated values.

If we extrapolate this approximate formula above 200°K, and subtract it from C_v in Fig. 1, we obtain the "additional specific heat" at the transition. (Fig. 3 solid line.) But since above 200°K some other vibrations may become excited, the ture additional heat curve must be steeper for the high temperature side, but their difference may be small near the transition point.

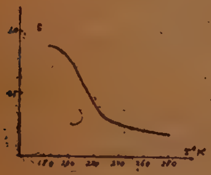

Fig. 2.

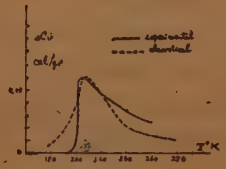

Fig. 3.

§ 3. The Theory For the Additional Specific Heat.

About the origin of the discontinuity of the specific heat of rubber at about 200°K, it has been thought that at this temperature the so-called micro-Brownian motion of the chain segment of the rubber molecule stops coöperatively, owing to some special properties of the intermolecular or intramolecular potentials acting between them, and it manifests itself as the transformation of the second order in the thermodynamical sense. Recently, however, Boyer and Spenser[4] in the U.S. have published the new idea. They consider this phenomena as the irreversible process, depending essentially on the time rate of heating and cooling, and the rapid increase of the internal viscosity.

Here, we think that at least in the case of the rubber, the former explanation is more preferable, and in the following, make a calculation of the additional specific heat due to the transition, according to this idea.

We assume that the unit volume of rubber contains N segments, vibrating as in the lattice model of liquids, (for the present problem, the configuration of the chain has not the important relation.) and at about 200°K, these segments change from the state (I) of the higher frequency to the state (II) of the lower frequency on raising the temperature. We think the state (II) as the state of the micro-Brownian motion and the vibration of the internal degrees of freedom remain unchanged. We set N_1 and N_2 for the number of the segments which are in the state (I) and (II) $(N_1+N_2=N)$, and consider that they are packed together like the lattice whose coordination number is γ. So we can make the analogous treatment as in the theory of the binary alloy. The total energy of the intermolecular attraction W is given approximately by

$$W=-2S_1\varphi_1-2S_2\varphi_2-2J\varphi_*$$

where $-2\varphi_1$ is the interaction energy of the segment pairs where both segments are in (I), s_1 is the number of those pairs, $-2\varphi_2$ and s_2 have similar meaning in (II), and $-2\varphi_*$ and J are the energy and the number of the pairs in which one segment is in (I) and the other in (II). We have the relations

$$2s_1=\gamma N_1-J,\qquad 2s_2=\gamma N_2-J,$$
$$\gamma N=2s_1+2s_2+2J,$$

so we get

$$W=-\gamma N\varphi_2-\gamma N_1\varphi+Jw,\quad \varphi=\varphi_1-\varphi_2,$$
$$w=\varphi_1+\varphi_2-2\varphi_* \tag{3}$$

The value of this W is specified by N_1 and J. The number of configurations consistent with this energy may be taken as

$$G(N_1,J)=h(N_1)\left(\frac{\gamma}{2}N\right)!\,2^J\left[J!\left(\frac{\gamma N_1-J}{2}\right)!\left(\frac{\gamma N_2-J}{2}\right)!\right]^{-1}$$

following Fowler and Guggenheim, the proportionality constant $h(N_1)$ being determined by the relation $\sum_J G(N_1,J)=N!/N_1!\,N_2!\doteqdot G(N_1,J_0)$, where J_0 is the value of J by which G has the maximum value. It may be written as

$$G(N_1,J)=\frac{N!}{N_1!\,N_2!}\cdot\frac{J_0!\left(\frac{\gamma N_1-J_0}{2}\right)!\left(\frac{\gamma N_2-J_0}{2}\right)!\,2^J}{J!\left(\frac{\gamma N_1-J}{2}\right)!\left(\frac{\gamma N_2-J}{2}\right)!\,2^{J_0}},$$
$$J_0=\gamma N_1N_2/N. \tag{4}$$

Hence, the part of the partition function of the present system, relating to the transition is given by

$$\Gamma(N_1, T) = \sum_J G(N_1, J) \exp\left[(\gamma N_1\varphi - Jw)/kT\right] \cdot (\Pi g_1)^{N_1}(\Pi g_2)^{N_2}, \tag{5}$$

where g_1 and g_2 are the partition functions for vibrations which partake in this transition.

The free energy change ΔF by this transition is obtained from the relation $-kT\log\Gamma$. We can evaluate the summation by its maximum term as usual, so we have

$$\begin{aligned}\Gamma(N_1, T) &= G(N_1, \bar{J}) \exp\left[(\gamma N_1\varphi - \bar{J}w)/kT\right] \cdot (\Pi g_1)^{N_1}(\Pi g_2)^{N-N_1}\\ \bar{J} &= \frac{\gamma N_1(N-N_1)}{N}\,\frac{2}{\beta+1},\\ \beta &= \left\{1+\frac{4N_1(N-N_1)}{N^2}(e^x-1)\right\}^{\frac{1}{2}},\\ x &= 2w/kT,\end{aligned} \tag{6}$$

and we can determine the equilibrium value of $s = N_1/N$ by the condition $(\partial\Delta F/\partial s)_T = 0$. The equation for determining s is

$$\frac{\gamma}{2}\log\frac{\beta+(1-2s)}{\beta-(1-2s)}+\left(1-\frac{\gamma}{2}\right)\log\frac{1-s}{s} = -\gamma\varphi/kT+3\log\frac{(1-\exp(-h\nu_1/kT))}{(1-\exp(-h\nu_2/kT))} \tag{7}$$

here we set $(\Pi g) = (1-\exp(-h\nu/kT))^{-1}$, assuming Einstein model for molecular vibrations.

The additional specific heat ΔC_v may be obtained from

$$\Delta C_v = -T\left(\frac{\partial^2\Delta F(s(T), T)}{\partial T^2}\right)\frac{\rho N_L}{mN} \tag{8}$$

where ρ is the density, N_L is the Loschmidt number and m is the molecular weight of the segment.

To solve s explicitly from (7) is not easy, so we caluculated the temperature variation of s, assuming the various constants as $\gamma = 10$ $\varphi = 2kT_0$, $w = 0{,}23\,kT_0$, $h\nu_1 = 2kT_0$, $h\nu_2 = 0{,}65\,kT_0$, $\rho = 1$, $T_0 = 200°\mathrm{K}$. (Fig. 2) The expression for ΔC_v is also very complicated, but the important terms are approximately

$$\begin{aligned}\Delta C_v \doteqdot \frac{\rho k N_L}{m}\Big\{\Big[&-\gamma\varphi/kT+3\left(\frac{h\nu_1}{k}\right)(\exp(h\nu_1/kT)-1)^{-1}\\ &-3\left(\frac{h\nu_2}{k}\right)(\exp(h\nu_2/kT)-1)^{-1}\Big]\left(\frac{\partial S}{\partial T}\right)\\ &+3s\left(\frac{h\nu_1}{kT}\right)^2\exp(h\nu_1/kT)(\exp(h\nu_1/kT)-1)^{-2}\\ &+3(1-s)\left(\frac{h\nu_2}{kT}\right)^2\exp(h\nu_2/kT)(\exp(h\nu_2/kT)-1)^{-2}.\end{aligned} \tag{9}$$

If we take $m = 500$, this gives the dashed line in Fig. 3. This value of m corresponds to seven isopren radicals. The value of w of the above magnitude is necessary to give the same tendency as in the experiment. Of course other choises of the constants may be considered, but in the order of the magnitude, they will not give difference from the above results.

Although our calculation is very rough, we may think from these results that in the transition some of the vibrations in the group $\Theta_E(1)$ in § 1 change to the micro-Brownian motion, raising the temperature.

§ 4. Conclusion.

By the above considerartions, it may be said that the additional specific heat is the λ type and not the step-like type as may be seen at first sight, and its origin is interpreted as the cooperative change of the vibrational state of the segments. We think, not only the present case, also the similar phenomena of the other high polymeric materials is explained in the same manner.

In conclusion, the author expresses his hearty thanks to Prof. T. Sakai for his kind guidance and to Mr. R. Kikuti and Mr. A. Ishihara for their valuable discussions.

References.

(1) N. Bekkedahl: J. Research N.B.S. **15** (1935), 509.
(2) N. Bekkedahl: J. Research N.B.S. **13** (1934), 411.
(3) A. H. Scott: J. Research N.B.S. **14** (1935), 99.
(4) R.E. Boyer & R.S. Spenser: J. Appl. Phys. **15** (1944), 398.; **16** (1945), 594. etc.

On the Theory of the High Polymer Solutions.

By Hirosi ICHIMURA.

Physics Department, Faculty of Science, University of Tokyo.

(Recieved February 26, 1948)

§ 1. Introduction.

The thermodynamical properties of the high polymer solutions has been investigated theoretically by several authors during these ten years.(1)-(4) Huggince(5) and Flory(7) have first applied the statistical mechanics on this problem and derived the osmotic pressure formula which agrees with experiments when the concentration of the polymer is high. Various extentions9)10) of these treatments have been attempted, and Flory8) has extended his theory to the dilute case. These, however, are all very rough approaches and the exact treatment seems to be encquntered with formidable difficulties.

In the present paper, we intend to make clearer the nature of approximations made in Flory's treatments8). After that an approximate treatment for the very dilute solutions will be attempted, considering the heat of mixing which is neglected in his papers.

§ 2. The Free Energy of Mixing.

We consider the system of N solvent molecules and p chain molecules which are composed of n segments, the size of the segment being assumed to be approximately equal to that of the solvent molecules.

The partition function Γ of this system can be written in the following form, using the idea of the phase integral of Gibbs.

$$\begin{aligned}\Gamma &= \exp(-\psi(N_1, p)/kT)\\ &= \frac{1}{N_1!\,p\,!}\, g_1{}^{N_1} g_p{}^{N_p} J_1{}^{N_1} J_p{}^{N_p}\\ &\quad\cdot\int \exp(-W(N_1,p)/kT)\,dq \qquad (1)\end{aligned}$$

where $\psi(N_1, p)$ is the free energy of the system, g_1 and g_p are the partition functions for the internal degrees of freedom of the solvent and polymer molecules respectively, J_1 and J_p are the momentum parts of the phase integral (the suffix 1 indicates the solvent and p the polymer throughout this paper), and the integral extends over all configurational coordinates of the molecules. $W(N_1, p)$ means the potential energy of this system, which is determined when we fix the configuration of all molecules.

When we neglect the difference in the forces for different pairs of molecules, the configuration integral reduces to the number of the ways of distributing these molecules in the container volume. Now we approximately estimate this number with the quasi-lattice model, that is, we enumerate the number of ways of packing N_1 solvents and p polymers among $N=N_1+pn$ lattice sites whose coordination number is τ.

The number of ways of setting the first polymer in the empty lattice is

$$NC \qquad (2)$$

where C is the number of configuration of this chain molecule when we fixed its one end.

The number of ways of setting the second polymer molecule can be taken approximately as

$$\underset{[1]}{(N-v')C}+\underset{[2]}{(v'-n)C'} \qquad (3)$$

where v' means the average number of sites contained in the domain around a polymer outside of which the other polymers are entirely free from the influences of the one in this volume and C' is the average number of configurations of the second chain molecule when it comes into the above v'. (Fig. 1).

For the third polymer we may write

$$\underset{[1\cdot1]}{(N-2v')C}+\underset{[1\cdot2]}{2(v'-n)C'}\ldots\ldots \text{when the second lies in the sites in [1]}$$

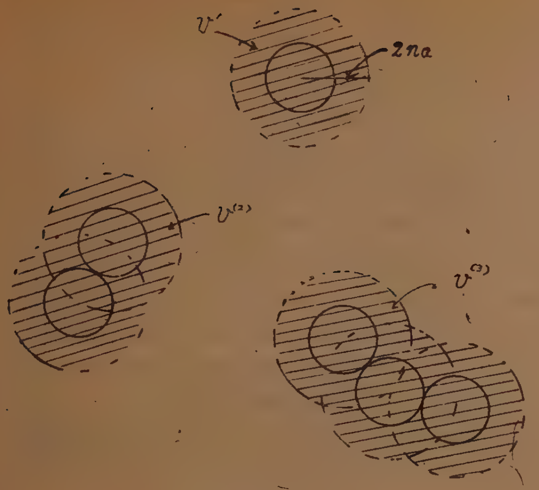

Fig. 1

$(N-v^{(2)})C+(v^{(2)}-2n)C^{(2)}$ .. ,, [2]
[2·1] [2·2] (4)

For the 4th

$(N-3v')C+3(v'-n)C'$ ....when the 2nd lies in [1] and the 3rd in [1·1],
$(N-v'-v^{(2)})C+(v'-n)C'$
$+(v^{(2)}-2n)C^{(2)}$,, [1] ,, [1·2],
$(N-v'-v^{(2)})C+(v^{(2)}-2n)C^{(2)}$
$+(v'-n)C'$,, [2] ,, [2·1],
$(N-v^{(3)})C+(v^{(3)}-3n)C^{(3)}$,, [2] ,, [2·2],
(5)

where the meanings of $v^{(2)}$, $v^{(3)}$, may be seen from Fig. 1, and $C^{(2)}$ is the average number of the configuration of the chain with the fixed one end when there are two chains in the volume $v^{(2)}$, etc. Proceeding in this manner to the p-th polymer, making the product of corresponding factors, and summing up all of them, we get a great number of terms. But, when the concentration of the polymer is very small we can arrange them as follows, assuming $N \gg pv'$, $v' \gg n$ and $v^{(2)} \doteqdot 2v'$,

$$\begin{aligned}&N(N-v')(N-2v')\ldots\ldots(N-(p-1)v')C^p\\&+\{N(N-v')\ldots\ldots(N-(p-2)v'\cdot(p-1)(v'-n)+\ldots\ldots\\&+N(v'-n)\cdot(N-2v')\ldots\ldots(N-(p-1)v')\}C^{p-1}C'\end{aligned} \tag{6}$$

The other terms which contain more than two v's in their factors may be neglected. The number of packing N_1 distinct molecules in remaining $N_1+pn=N$ sites is $N_1!$ So we obtain for the number of the system in question

$$\begin{aligned}G&=\frac{N^pC^p}{p!\,2^p}\left(1-\frac{v'}{N}\right)\left(1-\frac{2v'}{N}\right)\ldots\ldots\left(1-\frac{(p-1)}{N}v'\right)\\&\quad\times\left\{1+\frac{(v'-n)}{(N-v')}\frac{C'}{C}+\ldots\ldots+\frac{(p-1)(v'-n)}{N-(p-1)v'}\frac{C'}{C}\right\}\\&\doteqdot\frac{N^pC^p}{p!\,2^p}\left(1-\frac{p(p-1)}{2}\frac{v'}{N}\right)\\&\qquad\cdot\left(1+\frac{p(p-1)}{2}\frac{(v'-n)}{N}\frac{C'}{C}\right)\\&\doteqdot\frac{N^pC^p}{p!\,2^p}\left(1-\frac{p^2}{2}\frac{v'}{N}\left(1-\frac{C'}{C}\right)\right)\end{aligned} \tag{7}$$

and for the free energy

$$\begin{aligned}\phi(N_1p)&=-kT\Big[\log(g_1^{N_1}g_p^{N_p}J_1^{N_1}J_p^{N_p})\\&\quad-p\log 2-p\log p+p\log N+p\log C\\&\quad+\log\left(1-\frac{p^2}{2}\frac{v'}{N}\left(1-\frac{C'}{C}\right)\right)\Big].\end{aligned}$$

From this we can derive the free energy of mixing $\Delta\phi$,

$$\Delta\phi=-kT\left[p\log N-\frac{p^2}{2}\frac{v'}{N}\left(1-\frac{C'}{C}\right)\right] \tag{8}$$

Expanding the logarithm and differentiating this with respect to N_1, considering N_1 and $N_2=pn$ are independent, we get for the partial molal free energy of the solvent,

$$\Delta\overline{\phi}_1=-RT\left[\frac{p}{N}+\frac{p^2}{2}\frac{v'}{N^2}\left(1-\frac{C'}{C}\right)\right]. \tag{9}$$

If we denote by v_2 the volume fraction of the polymer, the equation (9) can be written as

$$\Delta\overline{\phi}_1=-RT\left[\frac{v_2}{n}+\frac{v_2^{\,2}}{2}\frac{v'}{n}\left(1-\frac{C'}{C}\right)\right], \tag{10}$$

where $\frac{v'}{n}\left(1-\frac{C'}{C}\right)$ depends on the nature of the polymer molecule. Flory's treatment[8)] is an attempt to connect this factor with the other experimental quantities.

The above derivation is merely the reformulation of Flory's ideas, but it will make clearer the meanings of the Flory's coefficient of v_2 in the formula. The theoretical estimation of v' and C' will be very difficult and we hope to consider it in future. From the manner of the above deduction, we may easily see that when the volume of the segment is β times that of the solvent molecule, we can simply modify the above equation as

$$\Delta\psi_1=-RT\left[\frac{v_2}{\beta n}+\frac{v_2^2}{2\beta^3}\frac{v'}{n}\left(1-\frac{C'}{C}\right)\right] \tag{11}$$

When the concentration of the polymer is increased, the terms negleted in (6) become dominant, and from the manner of counting shown above, we are led to assume that the most probable value of the number of ways of setting the $(x+1)$th polymer ($x>a=$ some fixed number) can be written as

$$(N-xn)\bar{C}^{(x)}$$

in which $\bar{C}^{(x)}$ means the average number of the configuration of the chain when there are x polymers in the container. Here we set for this number approximately as in Flory's paper,

$$C\left(1-\frac{\frac{xn}{N}}{v'}\cdot\frac{1}{v'}\right)^{n-1}\doteq C'\left(1-\frac{xn}{N}\right)^{n-1}. \tag{12}$$

So we obtain for the concentrated case

$$G=\frac{1}{2^p p!}N^a C^a\left\{1-\frac{a^2}{2}\frac{v'}{N}\left(1-\frac{C'}{C}\right)\right\}$$

$$\cdot\prod_{x=a}^{p}(N-xn)C\left(1-\frac{xn}{N}\right)^{n-1}$$

$$=\frac{1}{2^p p!}N^p C^p\left\{1-\frac{a^2}{2}\frac{v'}{N}\left(1-\frac{C'}{C}\right)\right\}$$

$$\prod_{x=a}^{p}\left(1-\frac{xn}{N}\right)^{n}, \tag{13}$$

where a may be very much smaller than p, so finally,

$$G\doteq\frac{1}{2^p p!}N^p C^p\prod_{x=1}^{p}\left(1-\frac{xn}{N}\right)^{n}. \tag{14}$$

This is essentially equal to the number of the configurations of the system in question given in Flory's paper.

§ 3. The Heat of Mixing of the Dilute Solutions.

When the difference between the molecular forces of both types cannot be neglected, we have the non-zero heat of mixing, and the evaluation of the partition function will become more complicated.

In this chapter we develop an approximate treatment for the dilute case by the method somewhat analogous to that of Fowler-Guggenheim. If no long range forces are acting, the polymer molecules in the sufficiently dilute solution can be treated independently when we consider the interaction with the solvent. This will easily be seen from the above considerations.

We consider as in § 2 the system of N_1 solvents and p polymers in a container, and assume that in the quasi-lattice arrangement all the polymer has n_1 solvent molecules in its nearest neighbours and the remaining nearest neighbour sites are occupied by the segments of its own, owing to the coiling up. The total potential energy of this system will have the following form, assuming that it can be approximated by the sum of the energies of the molecular pairs

$$E\doteq-2\varepsilon_1S_1-2\varepsilon_*S_*-2\varepsilon_2S_2,$$

where S_1 is the number of the nearest neighbour pairs of solvent-solvent type, S_* the solvent-segment type, S_2 the segment-segment type, and $-2\varepsilon_1$, $-2\varepsilon_*$, $-2\varepsilon_2$ are the energies of these pairs respectively. Assuming that the solvent has γ and the segment in the chain has δ nearest neighbours, it will easily be seen

$$2S_1=\gamma N_1-pn_1,\quad 2S_2=p(\delta n-n_1),\quad S_*=pn_1.$$

So we get

$$E=-\gamma N_1\varepsilon_1-\delta pn\varepsilon_2+pn_1(\varepsilon_1+\varepsilon_2-2\varepsilon_*).$$

The number of the configurations consistent with this energy can be considered approximately as

$$g(n_1)=h(N_1,p)\binom{\delta n}{n_1}^{p}\binom{\gamma N_1}{pn_1}, \tag{16}$$

where $h(N_1,p)$ is the proportionality constant, $\binom{\delta n}{n_1}$ means the number of distributing the solvent segment bonds among the total nearest neighbour sites of a polymer and $\binom{\gamma N_1}{pn_1}$ means the number of ways of choosing the solvent-molecular sites which make the pairs with the segment. The last two factors will be the corrections to C^p and $N_1!$.

We determine $h(N_1,p)$ by assuming that the total number of configurations without specifying n_1 is equal to G in § 2, and replacing the sum with its maximum term.

$$\sum_{n_1}g(n_1)=G\doteq g(n_{10}),\quad n_{10}=\delta n\cdot\gamma N_1/(\gamma N_1+\delta pn)$$

n_{10} makes g maximum. So we have

$$g(n_1) = \frac{N^pC^p}{2^pp\,!}\left\{1-\frac{p^2}{2}\frac{v'}{N}\left(1-\frac{C'}{C}\right)\right\}$$

$$\frac{(n_{10}!)^p(pn_{10})\,!\,\{\delta n-n_{10})\,!\}^p(\gamma N_1-pn_{10})\,!}{(n_1\,!)^p(pn_1)\,!\{(\delta n-n_1)!\}^p(\gamma N_1-pn_1)\,!} \qquad (17)$$

and the partition function which leads to the free energy of mixing is

$$Z = \exp(-\Delta\psi(N_1,\,p)/kT)$$

$$= \sum_{n_1} g(n_1)\exp(-pn_1w/kT),\quad w = \varepsilon_1+\varepsilon_2-2\varepsilon_*$$

We evaluate this $\sum$ as usual, so we get

$$Z = g(n_1)\exp(-pn_1w/kT)$$

where n_1 is the solution of the equation $(\gamma N_1/p-n)\cdot(\delta n-n_1)^2 = n_1{}^2\exp(w/kT)$ and it can be written as

$$n_1 = \frac{\delta n\cdot\gamma N_1}{(\delta n_p+\gamma N_1)}\frac{2}{\beta+1},$$

$$\beta = \left\{1+\frac{4\gamma N_1\cdot\delta np}{(\gamma N_1+\delta np)^2}(\exp(x)-1)\right\}^{\frac{1}{2}},\quad x = w/kT.$$

Therefore

$$\Delta\psi = -kT\log g(n_1)+pn_1\,w \qquad (18)$$

From this we can derive the partial molal free energy of mixing and the heat of mixing of the solvent, using the definition of n_{10} and n_1.

$$\Delta\bar{\phi}_1 = -RT\left\{\frac{p}{N}+\frac{1}{2}\frac{p^2}{N^2}v'\left(1-\frac{C'}{C}\right)-w(\partial pn_1/\partial N_1)/kT\right\} \qquad (19)$$

$$\Delta\bar{H}_1 = N_Lw(\partial pn_1/\partial N_1) = N_Lw\frac{\delta^2}{\gamma}\exp(w/kT)\frac{n^2p^2}{N^2} \qquad (20)$$

and the osmotic pressure formula is given by

$$\pi = -\frac{\Delta\phi_1}{V_1} = \frac{RT}{V_1}\left[\frac{v_2}{n}+v_2{}^2\left\{\frac{1}{2}\left(1-\frac{C'}{C}\right)\frac{v'}{n}-\frac{w}{RT}\frac{\delta^2}{\gamma}\exp(w/kT)\right\}\right] \qquad (21)$$

where v_1 is the molal volume of the solvent.

These are the approximate formula to the square term of v_2.* If we want to go further, it will be very complicate even in our rough treatments. The equation (20) has the same form as van Laar's formula. If we assume $\gamma = 12$, $\delta = 6$ (closest packing) and take $w = 10\,k$, we get $\Delta\bar{H}_1 = 60\,v_2{}^2$ cal/mol at 300°K as in Gee's[11] experiment for rubber-benzene system.

For the concentrated case, we can also intend the same approximate calculations, but before it we must investigate more exactly the numbers C, C', ..., v', and their changes by the interaction with the solvent. It will be very difficult and interesting problem.

Concluding this treatment, the author expresses his hearty thanks to Prof. T. Sakai for his kind guidance in the research and to Mr. R. Kikuti, Mr. A. Isihara and Mr. A. Miyake for their valuable discussions.

References.

(1) G.V. Schulz: Zeits f. phys. Chem. **A176** (1936), 317.

(2) K.H. Meyer: ,, **B44** (1939), 383.

(3) E. Hückel: Zeits f. Electrochemie **42** (1936), 753.

(4) M.L. Huggince: J. Chem. Phys. **9** (1941), 440.

(5) ,, : J. Phys. Chem. **46** (1942), 151.

(6) P. J. Flory: J. Chem. Phys. **9** (1941), 666.

(7) ,, : J. Chem. Phys. **10** (1442), 51.; **12** (1944), 425.

(8) ,, : ,, **13** (1945), 453.

(9) A.R. Miller: Proc. Camb. Phil. Soc. **39** (1943), 54, 131.
W.J.C. Orr: Trans. Faraday Soc. **40** (1944), 320.
E. A. Guggenheim: Proc. Roy. Soc. **183** (1944), 203, 213.

(10) P. M. Doty & T. Alfrey: J. Chem. Phys. **13** (1945), 77.

(11) G. Gee & L.R.G. Treloar: Trans. Faraday Soc. **38** (1942), 147.

---

* In the more concentrated solution, the terms corresponding to polymer-polymer interaction will appear from the correction to G in (14).

Large Elastic Deformation of Rubber.

By Ryogo KUBO.

Department of Physics, Faculty of Science, University of Tokyo.

(Read April 14, 1945. Received February 27, 1948)

Introduction.

The ordinary elastic theory based on the Hooke's law becomes naturally powerless for such large deformation as in the case of rubber. The functional form of the elastic potential can not be determined in an unambiguous way when the higher order terms of the strain are included.[1] For instance, we may assume the validity of Hooke's law. In spite of its apparent simplicity of such an assumption, the equation becomes fairly complicated. Moreover, it is not adequate for the case of rubber.

Experiments show that the rigidity of suitably vulcanized rubber is nearly independent of the stress for the simple shear up to such deformation as corresponds to about 300% elongation. In the case of the elongation, this simple proportionality does not hold between the stress and the strain. Statistical theories succeeded in the explanation of these properties in a brilliant way.

Based on these consideration we shall undertake to develop here mathematical theories of large deformation of rubber, giving first the fundamental equations and then some applications.

§ 1. Description of the Deformation.

We take the coordinate system (x, y, z) fixed in the space. Suppose that the elementary volume, which was at $r=(x, y, z)$ before the deformation, is displaced to $r'=(x', y', z')$ by some given elastic deformation. The displacement (u, v, w) are defined by

$$x'=x+u, \quad y'=y+v, \quad z'=z+w. \tag{1}$$

The deformation is described by the equation.

$$dr'=T dr, \tag{2}$$

where we have put

$$T=\begin{pmatrix} 1+u_x & u_y & u_z \\ v_x & 1+v_y & v_z \\ w_x & w_y & 1+w_z \end{pmatrix}, \quad u_x=\frac{\partial u}{\partial x}, \text{ etc.} \tag{3}$$

Then we get

$$dr^2=(T\,dr)^2=dr\,T^*T\,dr \tag{4}$$

where T^* is the transposed matrix of T.

Thus the principal values and the axes of the deformation $dr \to dr'$ will be obtained from the symmetric matrix T^*T. In particular, the principal values α_1^2, α_2^2, α_3^2 of T^*T give the magnification ratio α_1, α_2, α_3 in three orthogonal principal axes. For these we have

$$\begin{aligned} \alpha_1^2+\alpha_2^2+\alpha_3^2 &= \text{trace } T^*T, \\ \alpha_1\alpha_2\alpha_3 &= \det T. \end{aligned} \tag{5}$$

§ 2. The Elastic Potential.

We assume the elastic potential of $dm=\rho dV$ in the block of rubber to be

$$f\,dV=\left[\frac{\mu}{2}(\alpha_1^2+\alpha_2^2+\alpha_3^2) + \frac{\lambda+\mu}{2}\left(\alpha_1\alpha_2\alpha_3-\frac{\lambda+2\mu}{\lambda+\mu}\right)^2\right]dV, \tag{6}$$

where dV is the volume element before the deformation. The first term on the right hand side is the free energy due to the thermal motion of the net-work of rubber, which is derived by the statistical theories.[2] The second term is the change in cohesive energy caused by the volume dilatation.

In the case of simple shear we get at once

$$T=\begin{pmatrix} 1 & \gamma & 0 \\ 0 & 1 & 0 \\ 0 & 0 & 1 \end{pmatrix}, \quad T^*=\begin{pmatrix} 1 & 0 & 0 \\ \gamma & 1 & 0 \\ 0 & 0 & 1 \end{pmatrix}, \tag{7}$$

$$f=\frac{\mu}{2}\gamma^2+\text{const.}$$

so that the stress is given by

$$\frac{\partial f}{\partial \gamma} = \mu\gamma \qquad (8)$$

which shows the exact proportionality between the shearing stress and the strain.

For small deformation ($\alpha_1 = 1+l,\ \alpha_2 = 1+m,\ \alpha_3 = 1+n$) we have

$$f = f_0+\frac{\mu}{2}(l^2+m^2+n^2)+\frac{\lambda}{2}(l+m+n)^2.$$

Thus the constants λ and μ are the Lame's constants used in the ordinary theories of elasticity.

The characteristic property of rubber-like elasticity lies in the fact that,

$$\lambda \gg \mu \qquad (9)$$

which implies that

$$\det T \doteqdot 1 \qquad (10)$$

or the invariance of volume for ordinary deformation of rubber.

From Eqs. (3) and (5) we have

$$f = f_1+\frac{\lambda+\mu}{2}(\det T-1)^2-\mu(\det T-1)+\frac{\mu^2}{\lambda+\mu} \qquad (11)$$

where

$$f_1 = \frac{\mu}{2}\,\mathrm{trace}\ T^*T. \qquad (12)$$

For the elastic deforamtion of rubber in ordinary conditions, Eq. (10) may be considered as a subsidiary condition; thus we need only f_1 for the elastic potential.

§ 3. Fundamental Equation of Elastostatics.

Our static problems are mainly concerned with the equilibrium of a block of rubber of a given form when some surface-force $\boldsymbol{F}$ and the body-force $\boldsymbol{G}$ are applied to it. In ordinary cases $\boldsymbol{F}$ and $\boldsymbol{G}$ will be expressed in terms of the coordinates after the deformation. Here we assume, however, that they are given in relation to the volume element dV and the surface element dS before the deformation; that is, when the displacement $dS\to dS,'$ $dV\to dV'$ is caused by some deformation, we put the forces equal to $\boldsymbol{G}(\boldsymbol{r}')dV$ and $\boldsymbol{F}(\boldsymbol{r}')dS$ ($\boldsymbol{r}' = \boldsymbol{r}+\boldsymbol{u}(\boldsymbol{r})$).

Let $\boldsymbol{u}(\boldsymbol{r})$ be the displacement in the elastostatic equilibrium. If a small additional virtual displacement $\delta\boldsymbol{u}(\boldsymbol{r})$ is given, the virtual work δW will be

$$\delta W = \iiint\left(\frac{\delta f_1}{\delta \boldsymbol{u}}\right)\cdot\delta\boldsymbol{u}\,dV-\iiint \boldsymbol{G}(\boldsymbol{r}')\delta\boldsymbol{u}\,dV$$
$$-\iint \boldsymbol{F}(\boldsymbol{r}')\delta\boldsymbol{u}\,dS \qquad (13)$$

where the notation $\delta f_1/\delta\boldsymbol{u}$ means the functional derivative of f with regard to the function $\boldsymbol{u}(\boldsymbol{r})$. The integration must be taken over the region Ω occupied by the block before the deformation and its boundary surface Γ (cf. Fig. 1).

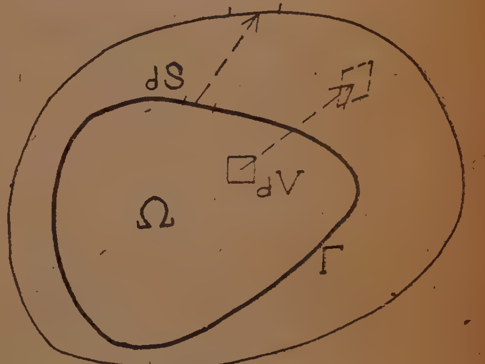

Fig. 1.

Eq. (10), on the other hand, makes a subsidiary condition given to this variation problem. Hence our problem becomes

$$\delta W+\delta\iiint p\det T dV = 0$$

where p is the undetermined multiplier.

Carrying out some elementary transformation, we arrive at the differential equations

$$\mu\Delta u+\begin{vmatrix} p_x & p_y & p_z \\ v_x & 1+v_y & v_z \\ w_x & w_y & 1+w_z \end{vmatrix}+G_x = 0,\quad \text{etc.,} \qquad (14)$$

and the boundary conditions

$$\mu\{(1+u_x)n_x+u_yn_y+u_zn_z\}+p\begin{vmatrix} n_x & n_y & n_z \\ v_x & 1+v_y & v_z \\ w_x & w_y & 1+w_z \end{vmatrix}-F_x = 0,\quad \text{etc.,} \qquad (11)$$

where $\boldsymbol{n} = (n_x, n_y, n_z)$ is the direction cosines of the outer normal to the boundary Γ.

These equations can be written in more concise forms;

$$\mu\Delta\boldsymbol{u}(\boldsymbol{r})+\boldsymbol{G}(\boldsymbol{r}+\boldsymbol{u})+T^{*-1}\,\mathrm{grad}\,p = 0, \qquad (14)$$

$$[\mu T+pT^{*-1}]\boldsymbol{n}(r) = \boldsymbol{F}(\boldsymbol{r}+\boldsymbol{u}) \qquad (15)$$

or

$$T^*[\mu\Delta\boldsymbol{u}(\boldsymbol{r})+\boldsymbol{G}(\boldsymbol{r}+\boldsymbol{u}))\}+\text{grad}\, p = 0 \qquad (14')$$

$$(\mu T^*T+p)\boldsymbol{n} = T^*\boldsymbol{F}(\boldsymbol{r}+\boldsymbol{u}). \qquad (15')$$

Our problem is now to solve these equations under the boundary condition, that is, for prescribed value of $\boldsymbol{u}(\boldsymbol{r})$ or $\boldsymbol{F}(\boldsymbol{r}+\boldsymbol{u})$ on the boundary Γ. It must be noticed here that $\boldsymbol{G}$, $\boldsymbol{F}$ and T involve the unknown function $\boldsymbol{u}(\boldsymbol{r})$.

§ 4. Uniform Strain.

We assume here that the body-force $\boldsymbol{G}$ can be neglected. When $\boldsymbol{u}(\boldsymbol{r})$ is a linear function of $\boldsymbol{r}$, Eq. (14) shows that $p = \text{const.} = p_0$.

In particular, for the deformation

$$u = a_1x, \quad v = a_2y, \quad w = a_3z,$$

the surface force F will be given by

$$\boldsymbol{F} = \begin{bmatrix} \mu(1+a_1)+\dfrac{p_0}{(1+a_1)} & 0 & 0 \\ 0 & \mu(1+a_2)+\dfrac{p_0}{1+a_2} & 0 \\ 0 & 0 & \mu(1+a_3)+\dfrac{p_0}{1+a_3} \end{bmatrix} \begin{bmatrix} n_x \\ n_y \\ n_z \end{bmatrix}$$

If $a_2 = a_3$, and $\boldsymbol{F} = 0$ on the boundary surfaces parallel to y- and z- planes, we get at once the surface force X acting parallel to the x-axis on the x-plane: i.e.

$$X = \mu\left\{(1+a_1)-\frac{1}{(1+a_1)^2}\right\} \qquad (16)$$

where X is related to the original cross section of the sample. This is the equation of state for the elongation of rubber well-known today.

§ 5. Deformation of a Spherical Shell.

As examples of the application of our fundamental equations, we shall treat the symmetric deformation of spherical shell and a hollow cylinder in this and the next paragraphs.

Suppose that a thin shell of radius r is expanded to the radius r' by a deformation. Then the condition (10) becomes

$$r^2dr = r'^2dr \qquad (17)$$

or

$$r'^3 = r^3+c^3 \qquad (18)$$

Thus we have

$$x' = (r^3+c^3)^{\frac{1}{3}}\frac{x}{r}, \quad \text{etc.}$$

The components of the tensor T are given by

$$T_{xx} = \frac{r'}{r}-\frac{c^3x^2}{r^3r'^2}$$

$$T_{xy} = T_{yx} = -\frac{c^3xy}{r^3r'^2}, \quad \text{etc.}$$

and the reciprocal tensor T^{-1} by

$$T_{xx}^{-1} = \frac{r}{r'}+\frac{c^3x^2}{r^4r'}, \quad \text{etc.}$$

$$T_{xy}^{-1} = T_{xy}^{-1} = \frac{c^3xy}{r^4r'}, \quad \text{etc.}$$

From Eq. (14) we have

$$\frac{\partial p}{\partial x} = 2\mu\frac{c^6x}{rr'^7},$$

and therefore,

$$\frac{dp}{dr} = 2\mu c^6/(r^3+c^3)^{\frac{7}{3}}$$

$$p(r) = 2\mu c^6\int\frac{dr}{(r^3+c^3)^{7/3}}$$

The direction cosines of the normals to the outer and inner surfaces of the shell are $(x, y, z)/r$ and $-(x, y, z)/r$ respectively. Hence, the surface forces acting on these surfaces are given by

$$|F(r)| = \mu r'^2r^{-2}\left\{r^4r'^{-4}+2c^6\int^r(r^3+c^3)^{-7/3}dr\right\}$$

We denote the radii of the outer and inner spheres of our shell by a and b in the natural state, and by a' and b' in the deformed state. Let P_i and P_0 be the pressures inside and outside the hollow sphere, which are related to the surface forces by

$$F(a) = -P_0a'^2/a^2, \quad F(b) = P_ib'^2/b^2$$

according to their definition. Thus we finally arrive at the equation

$$\frac{P_i-P_0}{\mu} = \frac{a^4}{a'^4}-\frac{b^4}{b'^4}+2c^6\int_b^a\frac{dr}{(r^3+c^3)^{7/3}}$$

$$= 2\left(\frac{a}{a'}-\frac{b}{b'}\right)+\frac{1}{2}\left(\frac{a^4}{a'^4}-\frac{b^4}{b'^4}\right), \qquad (18)$$

where

$$a'^3-a^3 = b'^3-b^3 = c^3.$$

For any given pressure difference P_i-P_0 these equations permit us to determine the expansion of

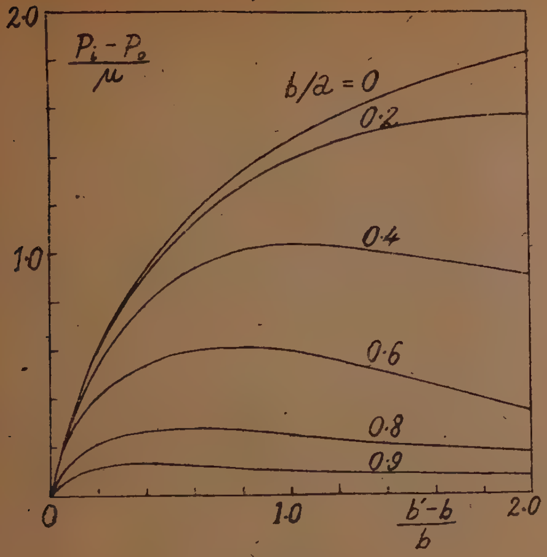

Fig. 2a.

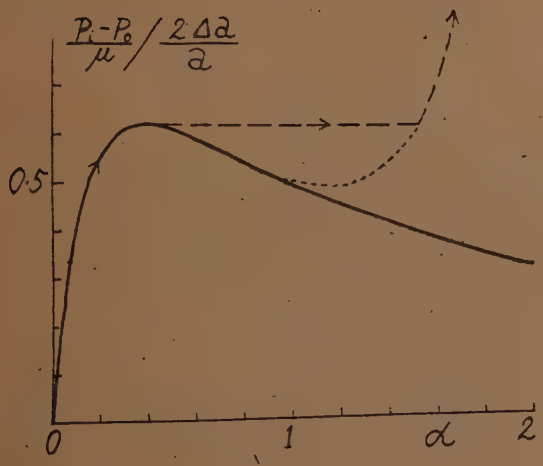

Fig. 2b.

the shell. The expression (18) shows a maximum at some value of b/b' for any given value of b/a except $b/a = 0$ (Fig. 2a).

If the shell is sufficiently thin ($\Delta a = a - b \ll a$), Eq. (18) can be approximated by

$$(P_i - P_0)/\mu = 2\frac{\Delta a}{a}\frac{a}{a'}\left(1-\left(\frac{a}{a'}\right)^6\right) \tag{19}$$

Fig. 2b shows the behaviour of the function at the right hand side of (19). The pressure difference $P_i - P_0$ has a maximum value

$$(P_i - P_0)_{\max} = 2\times 6\times 7^{-7/6}\mu\Delta a/a$$

for the magnification ratio

$$\alpha = a'/a = 7^{1/6} = 1.387.$$

If we rise the inner pressure by sending air into the thin shell, the static equilibrium will be labile as soon as P grows over the maximum value. Then the shell will yield under this pressure difference. In actual cases, however, the elastic law (8) will become invalid for too large strain; the rigidity will be larger, so that the shell will expand along such a curve as, shown schematically in Fig. 2b by the dashed curve.

If we close the shell and lower the outer pressure P_0, the shell will experience a limited expansion. Suppose that the inner pressure is given by

$$P_i = P_1 a^3/a'^3$$

for isothermal expansion $a \to a'$, that is, we have the inner and outer pressures equal to P_1 in the intial state. Then Eq. (19) becomes

$$P_1/\alpha^3 - P_0 = 2\mu\frac{\Delta a}{a}\frac{1}{\alpha}\left(1-\frac{1}{\alpha^6}\right).$$

As P_0 decreases to zero from P_1, the limit of the expansion α_m will be given by

$$\frac{P_1}{\mu}\Big/\frac{\Delta a}{a} = 2\alpha_m^2\left(1-\frac{1}{\alpha_m^6}\right).$$

If P_1 is large and $\Delta a/a$ is small sufficiently, we can see at once that

$$\alpha_m \backsim (P_1 a/\Delta a)^{1/2}$$

§ 6. Deformation of a Hollow Cylinder.

The deformation of a hollow cylinder can be treated in the similar manner. Using the cylindrical coordinate system the condition (10) will be

$$r'^2 = r^2 + c^2$$

Calculating T and T^{-1} from this equation, Eq. (14) gives

$$p = \frac{\mu}{2}\left\{-\frac{c^2}{r^2+c^2} + \log\frac{r^2}{r^2+c^2} + \text{const}\right\}$$

Thus we get

$$P_i - P_0 = \frac{\mu}{2}\left\{\frac{a^2}{a'^2} - \frac{b^2}{b'^2} + \log\frac{ab'}{a'b}\right\}$$

where the notations are of the similar meaning to those in § 5. In particular, this equation will be transformed into

$$P_i - P_0 = \frac{\mu \varDelta a}{a}\left(1 - \frac{1}{\alpha^4}\right), \quad (\alpha = a'/a)$$

for a thin-wall cylinder, and

$$P_i - P_0 = \frac{\mu}{2}\left\{\frac{c^2}{b^2+c^2} + \log\frac{b'}{b}\right\}$$

for an infinitely thick-wall cylinder ($a \to \infty$).

The expansion curve $P_i - P_0$ versus α has no maximum, so that the yielding does not occur in this case.

§ 7. Dynamical Equations.

In this section we shall derive the fundamental equations for the elasto-dynamics. If the internal viscosity can be put out of our consideration, we need only add the inertial term

$$\iiint \rho \frac{\partial^2 \boldsymbol{u}}{\partial t^2} \delta \boldsymbol{u} \, dV$$

to the virtual work, Eq. (13). Thus we get

$$\rho \frac{\partial^2 \boldsymbol{u}}{\partial t^2} = \mu \varDelta \boldsymbol{u} + \boldsymbol{G} + T^{*-1} \operatorname{grad} p \tag{20}$$

as the fundamental equation. The boundary condition remains the same as given by (15).

The nature of the internal viscosity is rather complicated. We shall proceed here only in a formal way. Now we assume that the rigidity μ in Eq. (20) is to be replaced by some time-dependent differential operator μ^*. This cannot be determined in an unambiguous way. The simplest assumptions will be as follows:*

$$\text{I.} \quad \mu^* = \mu + \eta \frac{\partial}{\partial t} \tag{21a}$$

$$\text{II.} \quad \mu^* = \mu \frac{\partial}{\partial t} \Big/ \left(\frac{\partial}{\partial t} + \frac{1}{\tau}\right) \tag{21b}$$

$$\text{III.} \quad \mu^* = \left(\mu_0 \frac{\partial}{\partial t} + \frac{\mu_\infty}{\tau}\right) \Big/ \left(\frac{\partial}{\partial t} + \frac{1}{\tau}\right). \tag{21c}$$

Thus the typical equations of our dynamics take the forms,

$$\rho \frac{\partial^2 \boldsymbol{u}}{\partial t^2} = \mu \varDelta \boldsymbol{u} + \eta \frac{\partial}{\partial t} \varDelta \boldsymbol{u} + T^{*-1} \operatorname{grad} p, \tag{22a}$$

$$\rho \left(\frac{\partial}{\partial t} + \frac{1}{\tau}\right) \frac{\partial^2 \boldsymbol{u}}{\partial t^2} = \mu \frac{\partial}{\partial t} \varDelta \boldsymbol{u} + \left(\frac{\partial}{\partial t} + \frac{1}{\tau}\right) T^{*-1} \operatorname{grad} p, \tag{22b}$$

$$\rho \left(\frac{\partial}{\partial t} + \frac{1}{\tau}\right) \frac{\partial^2 \boldsymbol{u}}{\partial t^2} = \left(\mu_0 \frac{\partial}{\partial t} + \frac{\mu_\infty}{\tau}\right) \varDelta \boldsymbol{u} + \left(\frac{\partial}{\partial t} + \frac{1}{\tau}\right) T^{*-1} \operatorname{grad} p. \tag{22c}$$

The boundary conditions are obtained by replacing μ in Eq. (15) by μ^* defined above.

Our assumption I. means the existence of the frictional resistance for the relative displacement of the substance. The assumption II states that the stress will relax in a sufficiently long time. The assumption III is the most general; it means the existence of both the internal friction and the relaxation of the stress, though the latter occurs only in a limited way in this case.

For the simple shear

$$u = \gamma y, \quad v = 0, \quad w = 0,$$

our boundary condition (15) gives the surface forces, namely

$$\boldsymbol{F} = \begin{pmatrix} \mu^* + p & \mu^* \gamma & 0 \\ -p\gamma & \mu^* + p & 0 \\ 0 & 0 & \mu^* + p \end{pmatrix} \boldsymbol{n}$$

provided that the acceleration terms of Eq. (22) can be neglected. Hence the shearing strain γ and stress S are related by the equation

$$\mu^* \gamma = S \tag{23}$$

the solution of which are:

$$\text{I.} \quad \gamma = \frac{S}{\mu}(1 - e^{-\mu t/\eta}) \quad \text{for constant } S,$$

$$\text{II.} \quad S = \mu \gamma e^{-t/\tau} \quad \text{for constant } \gamma,$$

$$\text{III.} \quad S = \{\mu_\infty + (\mu_0 - \mu_\infty) e^{-t/\tau}\} \gamma \quad \text{for constant } \gamma.$$

The case II corresponds to the well-known Maxwell's equation.

For the simple elongation, the elongation a_1 and the tensional force X are determined by the differential equation,

$$\mu^* \left\{1 + a_1 - \frac{1}{(1+a_1)^2}\right\} = X. \tag{24}$$

The assumptions I, II, and III give the following results:

$$\text{I.} \quad 1 + a_1 - \frac{1}{(1+a_1)^2} = \frac{X}{\mu}(1 - e^{-\mu t/\eta})$$

for constant S

---

* These are mere assumptions. More satisfactory theories of relaxation must be based on the statistical treatments of the network structure.

$$\text{II.}\quad X=\mu\left\{1+a_1-\frac{1}{(1+a_1)^2}\right\}e^{-t/\tau}$$

for constant a_1

$$\text{III.}\quad X=\{\mu_\infty+(\mu_0-\mu_\infty)e^{-t/\tau}\}$$
$$\times\left\{1+a_1-\frac{1}{(1+a_1)^2}\right\}\text{for constant } a_1.$$

So far we have neglected the acceleration terms in the dynamic equations. When these are taken into account, simple shear and elongation are no longer possible in non-static cases, because then p is not constant and the linear deformation does not satisfy the integrability condition of p, i.e.

$$\text{rot grad}\, p=\text{rot}\, T^*\left(\rho\frac{\partial^2 \boldsymbol{u}}{\partial t^2}-\mu^*\varDelta\boldsymbol{u}\right)=0.$$

§ 8. Transverse Waves.

When the displacement $\boldsymbol{u}$ is a function of $(\boldsymbol{kr}-ct)$, Eq. (20) gives

$$T^*(c^2\rho-\mu)\boldsymbol{u}''=\text{grad}\, p \tag{25}$$

On the other hand, the condition (10) becomes $(\boldsymbol{ku}')=0$, which is the condition of the transverse waves. Taking the direction of the wave vector as our x-axis and that of the displacement as our y-axis, Eq. (25) is transformed into

$$(c^2\rho-\mu)\begin{pmatrix} v'v'' \\ v'' \\ 0 \end{pmatrix}=\begin{pmatrix} p_x \\ p_y \\ p_z \end{pmatrix}$$

When $c^2\rho-\mu\neq 0$, the integrability condition of p is $v'''=0$, so that we have no wave motion in this case. Hence the necessary condition for the existence of wave motion is

$$c=\sqrt{\rho/\mu}$$

as in the ordinary theories of small vibration of shear modes. Our result, however, is valid for waves not only with small but also with large amplitudes, provided that the equation (25) is valid.

When the visco-elastic or elastoviscous properties are takan into account, the wave equation becomes $\left(\rho\frac{\partial^2}{\partial t^2}-\mu^*\frac{\partial^2}{\partial x^2}\right)v=0$ where μ^* is given by the assumptions (21). Since the equation is linear (in spite of finite amplitudes), one can easily obtain the solution by the substitution

$$v=B\exp\{i(\omega t-qx)\}$$

Thus the complex wave vector q gives us the dispersion and absorption of the transverse waves in rubber-like substances.

References.

(1) For example; M. Biot, Phil. Mag. (7) **27**, 468, (1939), R. Kappus, Zeits. angew. Math. Mech. **19**, 271, 344 (1939), M. Mooney, J. Appl. Phys. **11**, 582 (1940).

(2) R. Kubo, Kagaku, **15**, 43 (1945), **16**, 7 (1946), J. Phys. Soc. Japan. **2**, 51 (1947), J. Colloid Sci, **2**, 527 (1947). H.M. James and E. Guth, J. Chem. Phys. **11**, 455 (1943). There appeared during the war a considerable number of works which all reached the similar conclusions. Among them I refer here only a few, for I was hardly able to get any information about them at the time of the preparation of this paper in 1945.

Collective Electron Ferromagnetism, II.

By Hiroshi WATANABE.

Research Institute for Iron, Steel and other Metals, Tohoku University.

(Received March 9, 1948).

§ 1. Introduction.

Many attempts have been made to discuss ferromagnetism from the standpoint of the collective electron picture. In a previous paper[1] the author tried to establish a theory with the least possible arbitrariness. Using this method we can evaluate the width of the energy band, which is responsible for ferromagnetism. The exchange integral of the electrons in the band can also be obtained from the measured magnetic properties of metals or alloys using the theory of collective electron ferromagnetism based on Stoner-Hirone-Miyahara's statistics.

We shall proceed now to the problem of susceptibilities above the Curie point and the specific heat associated with ferromagnetism.

A part of the subject, which will be considered here, has already been discussed by Hori[1)], but Bloch-Slater's statistics were used therein which are insufficient when interactions between the electrons are strong. This renders his explanation of the phenomenon but is of a qualitative value.

In this paper the observed deviatien from the linear law between χ (susceptibility above the Curie point) and $\frac{1}{T-\theta}$ (θ: Curie point) was explained by the fact that the 4s band overlaps the 3d band. The specific heat due to spontaneous magnetization has already been worked out by Stoner[3)] with a comparison with experiment given for Ni, but as our model differs from Stoner's the results also deviates from his and approaches closer to the observation.

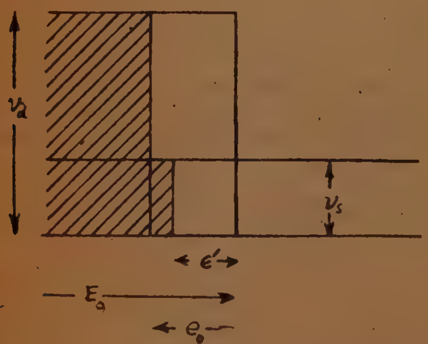

Fig. 1.

§ 2. Formulae of Magnetism for Overlapping Bands.

Fig. 1 is a schematic representation of the electronic structure of ferromagnetics which is the basis of the following calculations. This figure shows schematically the overlapping of the 3d and 4s band of Fe, Ni, Co or their alloys wherein the densities of the levels of both bands are assumed to be constant with respect to energy and are denoted as ν_d and ν_s. The top of the 3d band is E_0, which is its width, and the 4s band is assumed to have no upper limit. (Of course it is actually limited, but no serious change will be caused in the calculated result by this assumption). Taking into account the exchange integral of the 3d electrons, the Fermi-energies differ in the two bands. $E_0-\varepsilon_0$ is the Fermi-energy of the 3d band when the exchange integral is absent. $E_0-\varepsilon'$ is the Fermi-energy of the 4s-band. The number of holes in the 3d band is $2\nu_d\varepsilon_0$ and that of the 4s band below E_0 is $2\nu_s\varepsilon'$. In such a case, the relation between ε_0 and ε' can be determined by the condition that the energy of the system is a minimum.

Thus we can obtain easily

$$\varepsilon' = \left(2-\frac{J\nu_d}{L}\right)\varepsilon_0 . \; * \tag{1}$$

The saturation magnetization at absolute zero is $2\nu_d\varepsilon_0 = n$, so that

$$\frac{1}{2}h = \nu_d\varepsilon_0+\nu_s\varepsilon' = \frac{1}{2}n\left(1+\frac{2\nu_s}{\nu_d}-\frac{J\nu_s}{L}\right). \tag{2}$$

Now the energy of the system of electrons represented in Fig. 1, is given by

$$F = n'\eta kT+\Omega+J\sigma^2L, \quad n' = 2(E_0-\varepsilon_0)\nu_d+2(E_0-\varepsilon')\nu_s, \tag{3}$$

where $2\mu L\sigma = M$ is the magnetic moment of the system, and

$$\begin{aligned}\Omega = kT&\int_0^{E_0}\nu_d \log\left[1+\exp(\eta-x-\beta-\beta')\right]d\varepsilon\\ -kT&\int_0^{E_0}\nu_d \log\left[1+\exp(\eta-x+\beta+\beta')\right]d\varepsilon\\ -kT&\int_0^{\infty}\nu_s \log\left[1+\exp(\eta-x-\beta-\beta')\right]d\varepsilon\\ -kT&\int_0^{\infty}\nu_s \log\left[1+\exp(\eta-x+\beta+\beta')\right]d\varepsilon,\end{aligned} \tag{4}$$

and

$$x = \frac{\varepsilon}{kT}, \quad \beta = \frac{J\sigma}{kT}, \quad \beta' = \frac{\mu H}{kT}.$$

It is well known that M and n' are expressed by Ω as follows:

$$M = -\frac{\partial\Omega}{\partial H}, \quad n' = -\frac{1}{kT}\frac{\partial\Omega}{\partial\eta}.$$

---

* This is valid only when $\nu_d+2\nu_s-\frac{J\nu_d\nu_s}{L}>0$. This condition is satisfied in the following numerical examples.

These results can be simplified by the condition that the d band is nearly filled, i. e.

$$n' = kT\left\{\nu_d \log\left[\frac{1+\exp(\eta+\beta+\beta')}{1+\exp\left(\eta-\frac{E_0}{kT}+\beta+\beta'\right)}\cdot\frac{1+\exp(\eta-\beta-\beta')}{1+\exp\left(\eta-\frac{E_0}{kT}-\beta-\beta'\right)}\right]\right.$$
$$\left.+\nu_s\log[(1+\exp(\eta+\beta'))(1+\exp(\eta-\beta')]\right\}. \tag{5}$$

$$M = \mu kT\left\{\nu_d \log\left[\frac{1+\exp(\eta+\beta+\beta')}{1+\exp\left(\eta-\frac{E_0}{kT}+\beta+\beta'\right)}\cdot\frac{1+\exp\left(\eta-\frac{E_0}{kT}-\beta-\beta'\right)}{1+\exp(\eta-\beta-\beta')}\right]\right.$$
$$\left.+\nu_s\log\left[\frac{1+\exp(\eta+\beta')}{1+\exp(\eta-\beta')}\right]\right\}. \tag{6}$$

Solving (5) and (6) simultaneously, we can determine σ and η at any given temperature. Further, writing $\frac{E_0}{kT}-\eta$ for η, and remembering that $\frac{E_0}{kT} \gg 1$, we obtain from (6)

$$h = kT\{\nu_d\log[(1+\exp(\eta+\beta+\beta'))(1+\exp(\eta-\beta-\beta'))]$$
$$+2\nu_s\eta\}, \tag{7}$$

$$\frac{2L}{J}\beta = \nu_d\log\left[\frac{1+\exp(\eta+\beta+\beta')}{1+\exp(\eta-\beta-\beta')}\right]+2\nu_s(\beta+\beta), \tag{8}$$

The spontaneous magnetization is obtained from the above simultaneous eqnations by putting $\beta' = 0$. The Curie point is obtained by puting $\beta' = \beta = 0$ in (7), and taking limit $\beta' = 0$, $\beta \to 0$ in (8):

$$h = k\theta\{\nu_d\log[1+\exp(\eta_\theta)]+\nu_s\eta_\theta\}, \tag{9}$$

$$\frac{L}{J} = \frac{\nu_d}{1+\exp(-\eta_\theta)}+\nu_s \tag{10}$$

the latter two eqns. simultaneously giving the value of θ and η_θ. Hence the Curie point θ is given by

$$k\theta = \frac{n}{2}\left(1+2\frac{\nu_s}{\nu_d}-\frac{J\nu_s}{L}\right)$$
$$\cdot\left[\nu_d\log\left\{1\Big/\left(1+\frac{\nu_s}{\nu_d}-\frac{L}{J\nu_d}\right)\right\}\right.$$
$$\left.+\nu_s\log\left\{\left(1+\frac{\nu_s}{\nu_d}-\frac{L}{J\nu_d}\right)\Big/\left(\frac{L}{J\nu_d}-\frac{\nu_s}{\nu_d}\right)\right\}\right]^{-1} \tag{11}$$

§ 3. Susceptibilities above the Curie Point.

If we assume that in (6) M, β and β' are small, we obtain the limiting value of $\frac{M}{H}$ when $H \to 0$, whence the susceptibity χ becomes

$$\frac{1}{\chi} = \frac{L}{2L\mu^2}\,\frac{L/J-\nu_s-\nu_d/[1+\exp(-\eta_\theta)]}{\nu_s+\nu_d/[1+\exp(-\eta_\theta)]} \tag{12}$$

Now if we define the Curie-Weiss Constant C* by

$$\frac{1}{C} = d\left(\frac{1}{\chi}\right)\Big/dT, \tag{13}$$

then

$$C_\theta^* = (C^*)_{T=\theta}$$
$$= C_H\cdot\left(\frac{\theta}{Jh/2kL}\right)^2(1+\exp(\eta_\theta))\Big/\left(1-\frac{J\nu_s}{L}\right), \tag{13}$$

where

$$1+\exp(\theta_\theta) = 1\Big/\left(1+\frac{\nu_s}{\nu_d}-\frac{L}{J\nu_d}\right),$$
$$C_H = \frac{\eta\mu^2}{k}\left(1+2\frac{\nu_s}{\nu_d}-\frac{J\nu_s}{L}\right),$$

$\frac{\eta\mu^2}{k}$ being the Curie-Weiss constant in Hirone's theory.

Now we shall calculate χ from (12) for Ni. As the ratio of the low temperature specific heat to the temperature is proportional to $\nu_d+2\nu_s$, we can estimate as:

$$\nu_d+2\nu_s = 1.81\times10^{12}(\text{per atom erg}^{-1}) \tag{14}$$

And the ratio of the numbers of electrons in the 3d and 4s bands should be approximately equal to that of the densities of energy levels in the two bands,

$$\nu_d : \nu_s = 9.4 : 0.6 = 15.63. \tag{15}$$

From (14) and (15) we obtain

$$\nu_d = 1.605\times10^{12},\quad \nu_s = 0.103\times10^{12}. \tag{16}$$

On the other hand we can determine the value of J from (11), assuming that $n = 0.6$, the result being

$$J = 6.62\times10^{-13}\ \text{erg}. \tag{17}$$

(In the previous paper J was 6.63×10^{-13} erg, indicating that the effect of the overlapping of the bands does not effect much on the value of the exchange integral)

Using this value of J, and from (12) we can calculate $1/\chi\times 10^{-4}$ and plot as in Fig. 2.

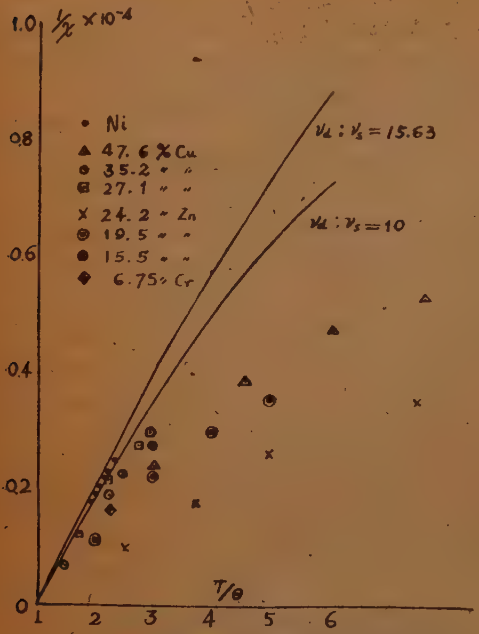

Fig. 2. High Temperature Susceptibility of Ni and its Alloys.

The theoretical curve is curved slightly downward at very high temperatures.

For comparison, the observed values by Sucksmith and Pearce[4]) are inserted in the figure.

The observed and theoretical values agree up to $T/\theta=2$, but at higher temperatures, experimental values are lower.

The present theory would assert that the behavior of the $1/\chi-T$ relation is the same for Ni-alloys too, assuming that the form of the band do not differ from Ni in these alloys, but experimental resluts do not confirm it, as shown by the examples[5]) inserted in the figure. Two points will be noted;

(1) $1/\chi$ decreases as the content of the additional element increases.

(2) For the same value of T/θ, $1/\chi$ is smaller for Zn than for Cu. From these points it may be concluded that the present model is too simple to explain the observed data; presumably the density of the levels at the top of the $3d$ band is not constant but is somewhat smaller than for the lower energies and hence the effect of the overlapping of the $4s$ band becomes more accentuated, as the holes in the $3d$ band become smaller.

§ 4. The Specific Heat for the Single Band Model. Conclusion.

We shall proceed to calculate the specific heat of our electron system. The calculation should be carried out with the overlapping band model, but since this is laborious and no justifying results can be expected from it, we shall content ourselves with a calculation for the single $3d$ band model. The total energy is given by

$$E=\int_0^{E_0}\left[\frac{kT\left(x-\frac{1}{2}\beta\right)\nu(\varepsilon)}{1+\exp(x-\eta-\beta)}+\frac{kT\left(x+\frac{1}{2}\beta\right)\nu(\varepsilon)}{1+\exp(x-\eta+\beta)}\right]d\varepsilon. \tag{18}$$

Remembering that $\frac{E_0}{kT}\gg 1$, E can be represented by

$$E=E_E+E_M,$$

where

$$E_E=\nu(kT)^2\left[\int_0^\infty\frac{xdx}{1+\exp(x-\eta-\beta)}+\int_0^\infty\frac{xdx}{1+\exp(x-\eta+\beta)}\right], \tag{19}$$

and

$$E_M=-\frac{1}{4}\frac{J}{L}n^2\zeta^2.\ * \tag{20}$$

Putting

$$G(\eta)=\int_0^\infty\frac{xdx}{1+\exp(x-\eta)}=\int_{-\infty}^{\eta}\log(1+\exp(\eta))d\eta, \tag{21}$$

then (19) reduces to

$$E_E=\nu(kT)^2[G(\eta+\beta)+G(\eta-\beta)]. \tag{22}$$

The funcition $G(\eta)$ can be developed in a series of powers of $\exp(\eta)$:

$$G(\eta)=\begin{cases}\exp(\eta)-\frac{1}{2^2}\exp(2\eta)+\frac{1}{3^2}\exp(3\eta)-\ldots\ldots & \text{for } \eta\leqq 0,\\[2ex] \frac{\eta^2}{2}+\frac{\pi^2}{6}-\left\{\exp(-\eta)-\frac{1}{2^2}\exp(-2\eta)\right.\\ \left.\quad+\frac{1}{3^2}\exp(-3\eta)-\ldots\ldots\right. & \text{for } \eta\geqq 0,\end{cases} \tag{23}$$

The specific heat of our system is given by

$$C=C_E+C_M\doteqdot\frac{dE_E}{dT}+\frac{dE_M}{dT}, \tag{24}$$

---

* $\zeta=\sigma/\sigma_0$, where σ_0 is the spontaneous magnetization at $T=0$. Cf. (1).

where the derivatives in the last eqn. can be calculated easily by the series (23). Especially, the specific heat at low temperature is obtained by using $\eta-\beta \ll 0$ and $\eta+\beta \gg 1$,

$$(E_E)_{T\to 0} = 2\nu\varepsilon_0{}^2 = n\varepsilon_0\,,$$

$$\gamma = \left(\frac{C_E}{T}\right)_{T\to 0} = \frac{\pi^2}{3}\nu k^2. \qquad (25)$$

If we use the value of ν for Ni obtained in the previous paper from the observed value θ and χ above the Curie point, namely

$$\nu = 1.683\times 10^{12},$$

then we can obtain:

$$\gamma = 1.508\times 10^{-3} \text{ cal mol}^{-1}\text{deg}^{-2}.$$

The observed ualue is

$$1.74\times 10^{-3} \text{ cal mol}^{-1}\text{deg}^{-2}.$$

For Co, calculating in the same manner, ν becomes 1.466×10^{12}, so that $\gamma = 1.31\times 10^{-3}$ cal mol^{-1} deg^{-2}, the corresponding observed value being 1.20×10^{-3} cal mol^{-1} deg^{-2}.

Just above the Curie point

$$(C_{\theta+0}) = 2\nu k^2\theta\left(2G-\frac{F^2}{F'}\right), \qquad (27)$$

where

$$F = \log(1+\exp(\eta_\theta)),\ G = G(\eta_\theta),\ F' = F'(\eta_\theta).$$

The value of (27) is for Ni 1.057 cal mol^{-1} deg^{-1}, the experimental value being 1.08. For Co no accurate measured value seems to exist. The above agreement with experiment is better than in Stoner's treatment but the curve $C = T/\theta$ or $E-T/\theta$ as a whole is as we see in Figs. 3–6, in obvious disagreement with observation. This must presumably be due to the following facts:

(1) The statistics used are not rigorous in evaluating the energy decrease due to spontaneous magnetization. Strictly speaking the exchange integral should not be common to all electrons in the d band, but should depend on their wave number vectors, so that the energy decrease can not simply be represented by $-J\sigma^2L$.

(2) The basic idea, the collective electron model, is not correct in discussing energies of ferromagnetic system: in other words, even in our constant energy density model, the electrons are considered perfectly free and correlation effects are neglected. As a result, $-\frac{d\zeta^2}{d\vartheta}(\vartheta = T/\theta)$ and hence the specific heat also becomes considerably smaller than those observed near the Curie point. Improvement along this line should be made in future.

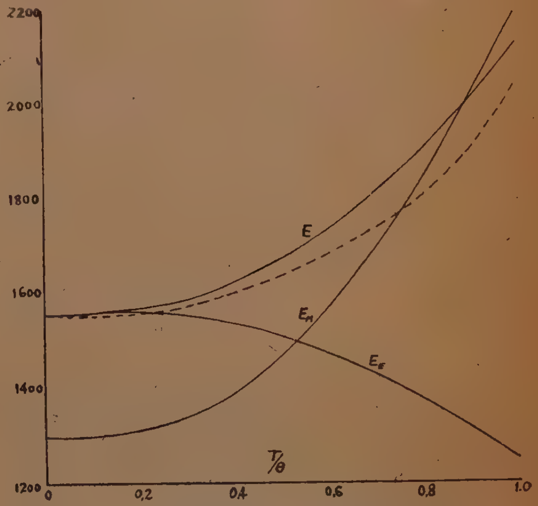

Fig. 3. Electronic Energy of Ni. The Curie point is assumed to be 650°K.
------ Observed E
———— Present calculation
The vertical axis are suitably shifted for energies.

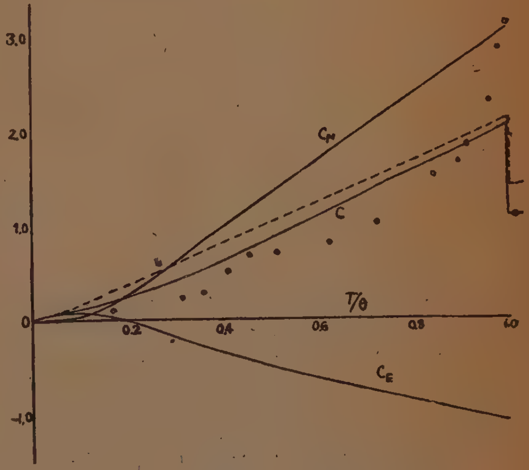

Fig. 4. Electric Specific Heat of Ni
● Observed C
———— Present calculation
------ Stoner's calculation

References.

(1) Watanabe: Phys. Soc. Jap. 3 (1948) 12,
(2) N. Hori: Bull. I. P. C. R. 19 (1940), 412 (in

Japanese).
(3) E. C. Stoner: Proc. Roy. Soc. A **169** (1939) 339,
(4) W. Sucksmith and R. R. Pearce: Proc. Roy. Soc. A **167** (1938), 189.
(5) C. Manders: Ann. d. Phys. (XI), **5** (1936), 167: A. Wheeler: Phys. Rev. **56** (1939), 1137.

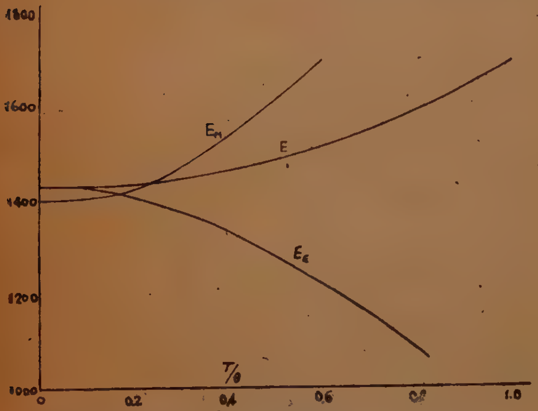

Fig. 5. Electronic Energy of Co. The Curie point is assumed to be 1410°K

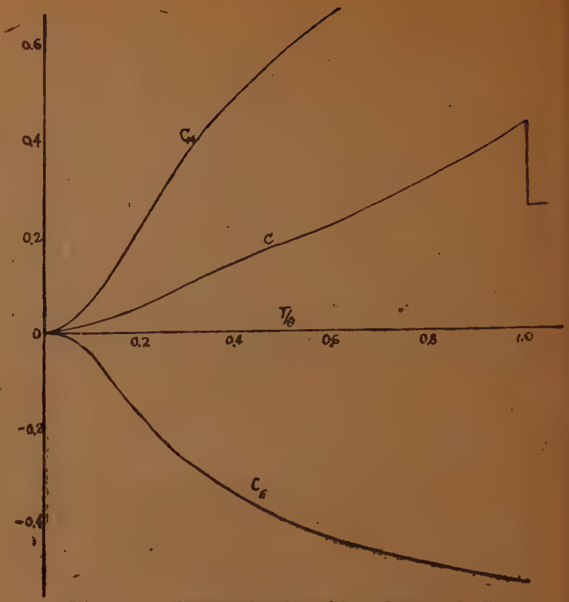

Fig. 6. Electronic Specific Heat of Co

On a Phenomenon Observed with Geiger-Müller Counters in Ultraviolet Measurement.

By Itaru NONAKA.

Matsuda Research Laboratory, Tokyo Shibaura Electric Co., Ltd,

(Read July 10, 1944. Received March 12, 1948)

§ 1. Introduction.

For a practical purpose we have tried to measure feeble near ultraviolet light by Geiger-Müller counters and have observed a very peculiar phenomenon that the sensitivity of the counter is very much increased during the continuous measurement.

The near ultraviolet light we used was that from an incandescent lamp filtered through two sheets of glass filters UV$-D_1$ (6 mm total thickness) and has a spectral distribution shown in Fig. 1.

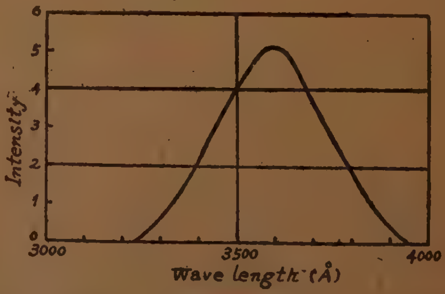

Fig. 1. Spectral distribution of the ultraviolet light used.

Up to the present, many investigators have tried to measure ultraviolet or visible light by Geiger-Müller counters, but they have not observed any phenomenon similar to that observed by us. Their counters, however, were all filled with CO_2, N_2, or H_2, and were, therefore, of the type so-called "slow counters". On the contrary, the counters we used in this experiment were filled with mixture of argon and alcohol vapour of ratio 10 to 1, and so the type so-called "fast counters" discovered by Trost⁽⁵⁾ and widely used in nuclear physics recently.

The constructions of the counters used are shown in Fig. 2 (A), (B), (C), and the total pressures of the gas filled were 8~15 cm Hg.

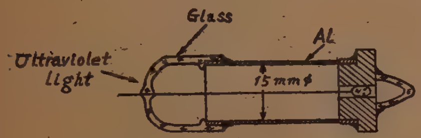

Fig. 2 (A). Al-[A] counter.

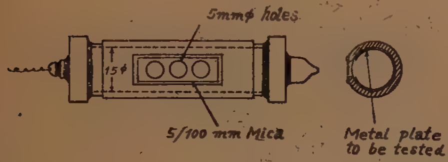

Fig. 2 (B). Counter of type [B], [C], [E].

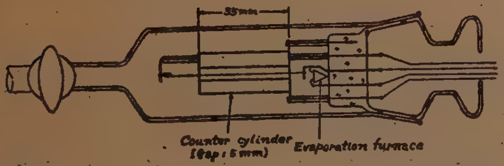

Fig. 2 (C). Counter of type [N] which has a evaporation furnace in it.

Pulses of the counters were amplified by a three stage amplifier and fed to a scale of 64 circuit or to a scale of 1024 circuit when necessary. A combination of the scale of 64 circuit and a "Riken" mechanical recorder was known by a test to lose several counts at above 60000/min. and to saturate at 80000/min..

§ 2. Discovery of the Phenomenon.

As aluminium is one of the metals which can emit photoelectrons by ultraviolet of wave length of the order of 3600 Å, at first we substituted a glass stopper for the micarex one of a thin aluminium counter used in nuclear physics as shown in Fig. 2 (A), and admitted the ultraviolet light obliquely through this glass stopper.

During the continuous measurement of the ultraviolet light the counting rate, which was initially 63/min. including the natural counts of about 15/min., increased at first gradually and then acceleratively to 2300/min. after about 100 minutes and to a number unable to be recorded by the scaling circuit after 120 minutes. These results are shown in Fig. 3, curve I. Then, at 121 minutes the continuous irradiation was stopped and the sensitivities were measured every 10 or 20 minutes by irradiating for a short time from 5 to 15 seconds. The sensitivity decayed with time as shown in Fig. 3, curve II. This increase and decay of the counting rate occurred only when ultraviolet light was measured, and, for example, when gamma-rays were measured continuosly there observed no increase as shown by curve III of Fig. 3.

Hereafter we shall denote the state of counters at which the sensitivities for ultraviolet light are much increased as "activiated state".

The fact was also ascertained that in its activiated state the counter has exactly the same sensitivity for gamma-rays and for natural counts as in the nonactiviated state. This phenomenon of activiation, therefore, is independent of the "Spontanentladung"⁽⁵⁾⁽⁶⁾ and the "Nachentladung"⁽⁵⁾ which are both undesirable phenomena of

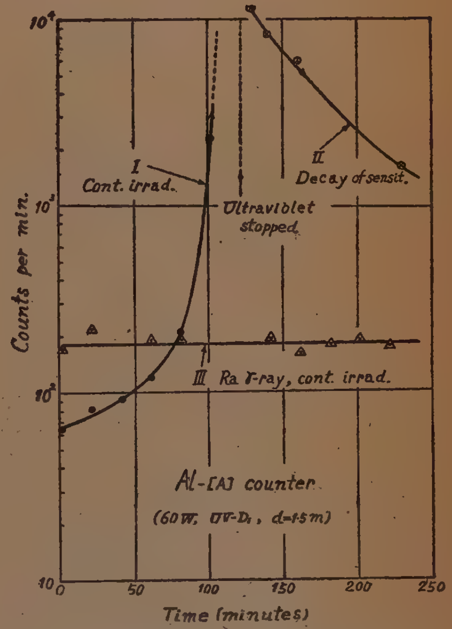

Fig. 3. Activiation by near ultraviolet and the case of Ra γ-rays (Al-[A] counter)

counters. Only the sensitivity for ultraviolet light increases or decays, so the photoelectron emissivity of the surface of the counter cylinder is considered to be changed by discharges of the counter. As the true character of the phenomenon has been known to some extent, we advanced to examine some other metals than aluminium.

§ 3. Activation of Several Metals.

We constructed counters of the type shown in Fig. 2 (B), in which the metal to be tested is inserted in a form of a cylinder with a gap. The windows of the counter are covered by a mica film of 5/100 mm in thickness.

(i) Al.

At first we tested Al which has purity of 99.7 % and was polished by sand papers. The results were the same as those of Al-[A] counter described in the preceding chapter.

Secondly, we tested Al surfaces which were through the process of "Zaponieren",(5) namely, coated with thin film of zabon-lacquer. In this case, too, the results were the same as those of the ordinary Al surface and are shown in Fig. 7.*

(ii) Mg.

Mg was evaporated in vacuum on a thin copper plate and was inserted in a counter of the type shown in Fig. 2 (B). This counter showed also an intense activation under continuous irradiation and counting, and the increased sensitivity decayed after continuous irradiation was stopped. The results are shown in Fig. 4.

(iii) Zn.

At first, Zn was also evaporated on a thin copper plate and was inserted in a counter of the type shown in Fig. 2 (B). The observed results are shown in Fig. 5. Contrary to the case of Al or Mg, the sensitivity decreased initially and then came to a constant value after 30 minutes under continuous irradiation. When the continuous irradiation was stopped the sensitivity recovered almost to its initial value after about 60 minutes. These decrease and increase of sensitivity can repeat many times, but after leaving the counter as it is for 20 days it was found that the circumstances were quite changed; the sensitivity became to increase under continuous irradiation as shown in the last part of Fig. 5.

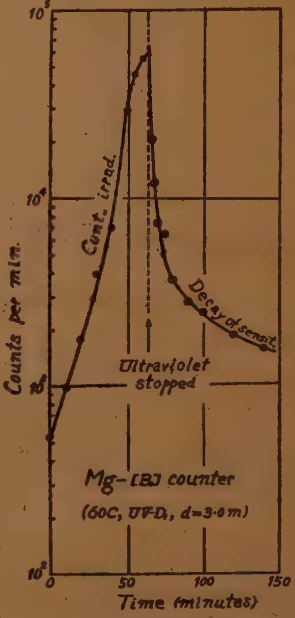

Fig. 4. Mg-[B$_1$] counter.

Generally speaking, in the case of Zn the sensitivity seems to increase or decrease under continuous irradiation according to its surface condition.

Secondly, to test a Zn surface which does never come in contact with air we constructed a counter having in it a furnace for evaporation of Zn metal, as shown in Fig. 2 (C). The Zn metal in the furnace was evaporated directly to the inner surface of the counter cylinder in high vacuum and then argon and alcohol vapour were let into.

When this counter was irradiated by the near ultraviolet light and continuous counting was performed, the sensitivity increased gradually and reached a constant value after scores of minutes. When the continuous irradiation was stopped, the sensitivity decayed to its initial value in the same

---

* The reason of the fact that the counting rates are horizontal at 80000/min. is due to the saturation property of the scale of 64 recorder, and when a scale of 1024 recorder was used the counting rates rose as high as 3.5×10^5/min., which is considered to be the maximum counting rate allowed to the counter because at this counting rate the average time interval of successive two pulses is of the order of the dead time of the counter.

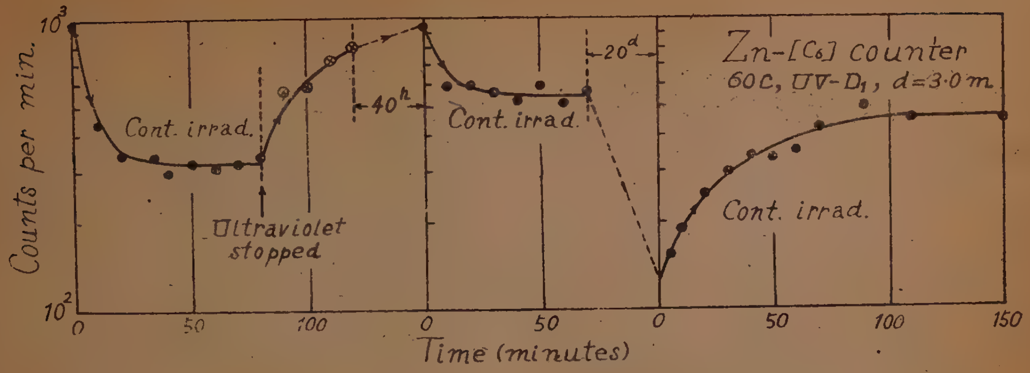

Fig. 5. The case of Zn which was once brought in contact with air. (Zn-[C₆]counter)

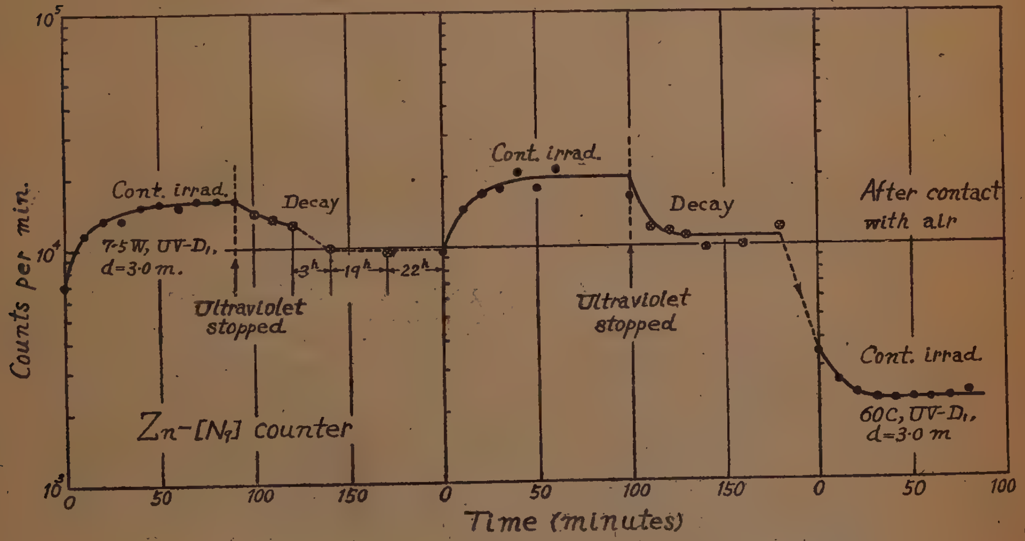

Fig. 6. The case of Zn which does never come in contact with air. (Zn-[N₉] counter).

way as in the case of Al or Mg and in opposition to the case of Zn in contact with air. An example is shown in Fig. 6. After air was let into this counter and pumped off again, the sensitivity became to decrease under continuous irradiation, agreeing well with the results shown in Fig. 5. The ratio of the initial sensitivities of the counter before and after being in contact with air was known to be 94.

§ 4. Effect of Wave Length of Ultraviolet Light.

The ultraviolet light used hitherto was the near ultraviolet light shown in Fig. 1. Al, Mg and Zn are considered to have their wave length limits of photoelectric effect in this region. When any ultraviolet light whose wave length is far shorter than the wave length limits is used, the activiation phenomenon may be considered to show any different aspects. To test this point we used a low pressure quartz mercury lamp of capillary type as the ultraviolet light source. It is known that about 80 per cent of the ultraviolet emitted by such a lamp consists of resonance line 2537 Å.

Under continuous irradiation by this 2537 Å ultraviolet no activiation phenomenon was observed in Al, Al(z) or Mg counters, one example of which is shown in Fig. 7 (the case of Al(z) counter). As seen in the figure, in the case of near ultraviolet of average wave length of 3600 Å the activiation phenomenon is obviously observed, but in the case of 2537 Å counting rate is almost constant after

3 hours' continuous irradiation.

There were, however, some exceptions observed in some cases of polished Al. For example, a counter was not activated by 2537 Å for four days after it was prepared, but on the fifth day it became to be activated. No such exception was observed in the cases of Al(z) and Mg.

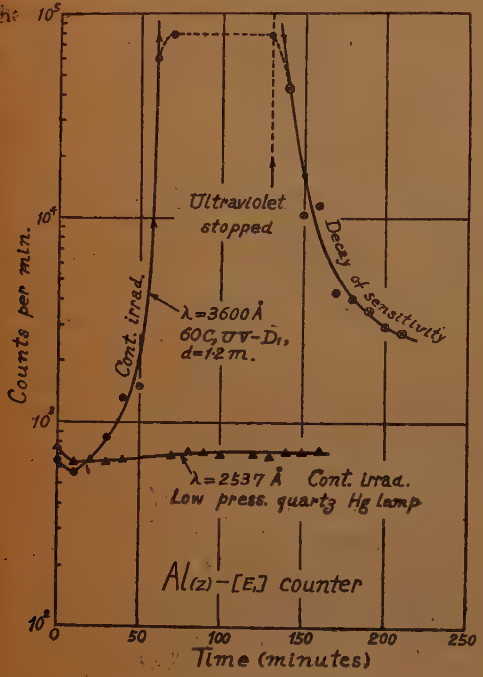

Fig. 7. Effect of the difference of wave length of ultraviolet. (Al(z)-[E_1] counter).

§ 5. Mechanism of the Activation Phenomenon.

The mechanism of the activation phenomenon may be considered as follows; positive ions (most of them are alcohol ions⁽⁷⁾) produced in every discharges of the counter are attached to the surface of the cathode cylinder and a layer of positive charge is formed there. This positive charge layer lowers the work function of photoelectrons and the sensitivity for the near ultraviolet becomes increased. When continuous irradiation is stopped, attachment of new positive ions ceases and the positive charge layer is neutralised gradually by the electrons emerging from the metal through the potential barrier by tunnel effect. This results in the decay of the sensitivity.

That the activation is produced by the positive ions and not by the direct action of the ultraviolet light is ascertained by the facts firstly that the counter shows no such phenomenon by mere irradiation when it is not working, and secondly that the time required for activation decreases as the counter potential becomes higher, as shown in Table I, number of positive ions produced in each discharge being a increasing function of the potential above threshold $U-U_0$.

Table I.

Time required to be activiated.

$U-U_0$ (in volts)	Time required to be activiated from 1000/min. to 70000/min.,
20	40 min.
40	23 min.
80	10 min.

"Spontanentladung" of counters is explained by Minakawa⁽⁶⁾ to be originated from the cold emission due to the strong field produced by a positive charge layer owing to the positive ion attachment on the cathode surface. In the case of the activation phenomenon no "Spontanentladung" was accompanied even in the very highly activated state, so it is considered that the degree of attachment of positive ions is lower than in the case of "Spontanentladung" and the cold emission into the gas space not caught by the positive charge layer is negligibly small.

The above mentioned mechanism is that of the increase and decay of the sensitivity for near ultraviolet light observed in Al or Mg. But, in the case of Zn brought in contact once with air, the sensitivity does not increase but decrease when continuously irradiated by near ultraviolet light. The attachment of positive ions is considered to occur also in this case, but, if the surface shows a selective photo-electric effect in its spectral sensitivity curve as frequently observed in thin film photo-cathodes, it may be considered to occur that the emission of photoelectrons at a fixed wave length (3600 Å in this case) decreases when the wave length limit is made longer by the positive ion attachment. Such a case is really observed in a platinum photo-cathode on which K atoms are adsorbed.

Finally the reason why the activation does not occur by the ultraviolet light of 2537 Å is considered to be that generally the spectral sensitivity curve at wave lengths far shorter than the wave length limit has a tendency to converge to a constant value as observed by Kreuchen(3)(4) or Schulze(9), and, therefore, the emission of photoelectrons at a fixed wave length far shorter than the limit does not change even if the work function of the surface is altered by the positive ion attachment.

§ 6. Formula of Decay.

The decay of the sensitivity of the counter in activated state is considered to follow the following formula

$$I(t)=\frac{I_0}{(1+\alpha t)^n}+I_\infty, \qquad (1)$$

Where $I(t)$ means the counting rate at time t, I_∞ that at $t=\infty$ or when not in activated state, and I_0, α and n are constants. I_∞ can be determined by the sensitivity before activation, and n is determined from the inclination of the curve on the graph of $\log_{10}(I-I_\infty)$ vs. $\log_{10}t$ at large t.

Three examples are shown in Fig. 8, where $I(t)$ is expressed in counts per min., and t is in min. Solid curves are those expressed by the formula (1) as follows,

$$\text{Al}-[\text{C}_1]\text{ counter,}\quad I=\frac{190\times10^4}{(1+1.2\,t)^{1\cdot6}}+390$$

$$\text{Al}-[\text{A}]\text{ counter,}\quad I=\frac{53500}{(1+0.28\,t)^{1\cdot2}}+82$$

$$\text{Mg}-[\text{B}_1]\text{ counter,}\quad I=\frac{36700}{(1+1.16\,t)^{0\cdot80}}+535.$$

The agreements between the formula and the experiment are very well in spite of the large variations of the value of $I(t)$.

Among the four constants in the formula I_∞ and n are the characteristic quantities of the decay curve, but I_0 and α are not, because they are transformed to another values when the origin of time t is displaced.

The values of n for different counters are generally not equal, even if the counter cylinders are of the same metal. The ranges of the values of n for Al, Mg, and Zn are shown in Table II.

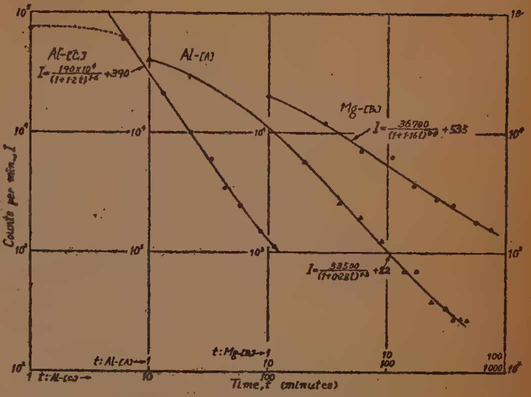

Fig. 8. Decay curves of the nessitivities.

Table II.
Values of n.

Cylinder metal	Range of n
Al	1.2 ∼ 1.9
Mg	0.6 ∼ 1.4
Zn	0.6 ∼ 1.0

The physical meanings of the formula (1) are not distinctly known at present, so it must be accepted as a mere experimental formula.

In conclusion, the author expresses his cordial thanks to Dr. M. Tanaka for his kind encouragement throughout this work, and also to Mr. K. Takahashi for his technical assistance.

References.

(1) G. L. Locher: Phys. Rev. **42** (1932), 525.
(2) W. Christoph: Ann. d. Phys. **23** (1935), 747.
(3) K. H. Kreuchen: Zeits. f. Phys. **94** (1935), 549.
(4) K. H. Kreuchen: Zeits. f. Phys. **97** (1935), 625.
(5) A. Trost: Zeits. f. Phys. **105** (1937), 399.
(6) O. Minakawa: Proc. Imp. Acad. Tokyo, **18** (1942), 644; **19** (1943), 246.
(7) O. Minakawa: Proc. Imp. Acad. Tokyo. **19** (1643), 19.
(8) O. Minakawa: Proc. Imp. Acad. Tokyo. **19** (1943), 246.
(9) R. Schulze: Zeits. f. Phys. **92** (1934), 212.

Crystal Structure of Ammonium Dihydrogen Phosphate $NH_4H_2PO_4$.

By Ryuzo UEDA.

Department of Applied Physics, Waseda University, Tokyo.

(Received March 22, 1948)

§ 1. Introduction.

Though ammonium dihydrogen phosphate is said to be isomorphous with the potassium salt(1), it behaves rather different in the manner of the phase transition and the electric properties(2): its temperature coefficients of dielectric constant parallel to c- and a-axes are reversed. It is the object of this paper to describe the detailed structure of this substance and show the difference in their structure which would account for the different properties of the two substances.

X-ray investigation of this substance has been carried out by Hassel(3) and Hendricks(4). Hendricks made precision measurements by using Siegbahn's spectrograph and obtained the following data:—

$$a = 7.51\ \text{Å},\ c = 7.53\ \text{Å},\ c/a = 1.0017$$
$$(c/a = 1.0076\ \text{Groth})$$

Hassel gave same space group with potassium salt, $D_{2d}^{12}-I-\bar{4}2d$. Atomic parameters have not been determined.

The crystals used here are formed in slow evaporation from water solution for a few days. Examining X-ray spectra, it is found that the crystal has a comparatively large extinction effect. This effect was eliminated in such a way that one specimen is prepared by grinding with the fine emery powder and the other by rapid cooling in the liquid air. As the mass absorption coefficient of this substance for MoK_α is 3.1, it seems unnecessary to make corrections for absorption in measuring the intensity of spectra.

§ 2. Lattice Constants and Space Group.

Lattice constants a and c are determined by the back-reflection method, using copper and chrome radiation. The results obtained are given by:—

$$a = 7.479 \pm 0.000\ \text{Å},\ c = 7.516 \pm 0.005\ \text{Å},$$
$$c/a = 1.005\ (\text{at } 25°\text{C})$$

It is found that four molecules are contained in the unit lattice.

A number of spectra for the oscillation about [100] and [001] are examined and their relative intensities are measured with a microphotometer using optical wedges. From the laws of missing spectra observed, the space group of this crystal is determined to be $D_{2d}^{12}-I-\bar{4}2d$, confirming the Hassel's results.

There are $4NH_4$, 4P, 8H and 16O in the lattice. Considering equivalent points from the crystal symmetry, atoms and radicals except eight acid hydrogen atoms must take the following positions:(5)

$$\text{P}\ldots\ldots 4(\text{a})\quad 000;\ \frac{1}{2}\,0\,\frac{1}{4}.$$

$$\text{NH}\ldots 4(\text{b})\quad 00\frac{1}{2};\ \frac{1}{2}\,0\,\frac{3}{4}.$$

$$\text{O}\ldots\ldots 16(e)\ xyz;\ y\bar{x}\bar{z};\ \bar{x}\bar{y}z;\ \bar{y}x\bar{z};\ \frac{1}{2}-x,\ y,$$
$$\frac{1}{4}-z;\ \frac{1}{2}-y,\ \bar{x},\ z+\frac{1}{4};\ x+\frac{1}{2},\ \bar{y},\ \frac{1}{4}-z;$$
$$y-\frac{1}{2},\ x,\ z+\frac{1}{4}\ \text{and these}\ +\frac{1}{2}\,\frac{1}{2}\,\frac{1}{2}.$$

Thus the parameters to be determined are x, y and z of the oxygen atom. These three parameters can also be expressed in the following way.

$$\theta_1 = 2\pi x,\quad \theta_2 = 2\pi y,\quad \theta_3 = 2\pi z.$$

§ 3. Determination of θ_1 and θ_2.

Approximate positions of oxygen atoms are determined from measuring the intensities of $(h00)$

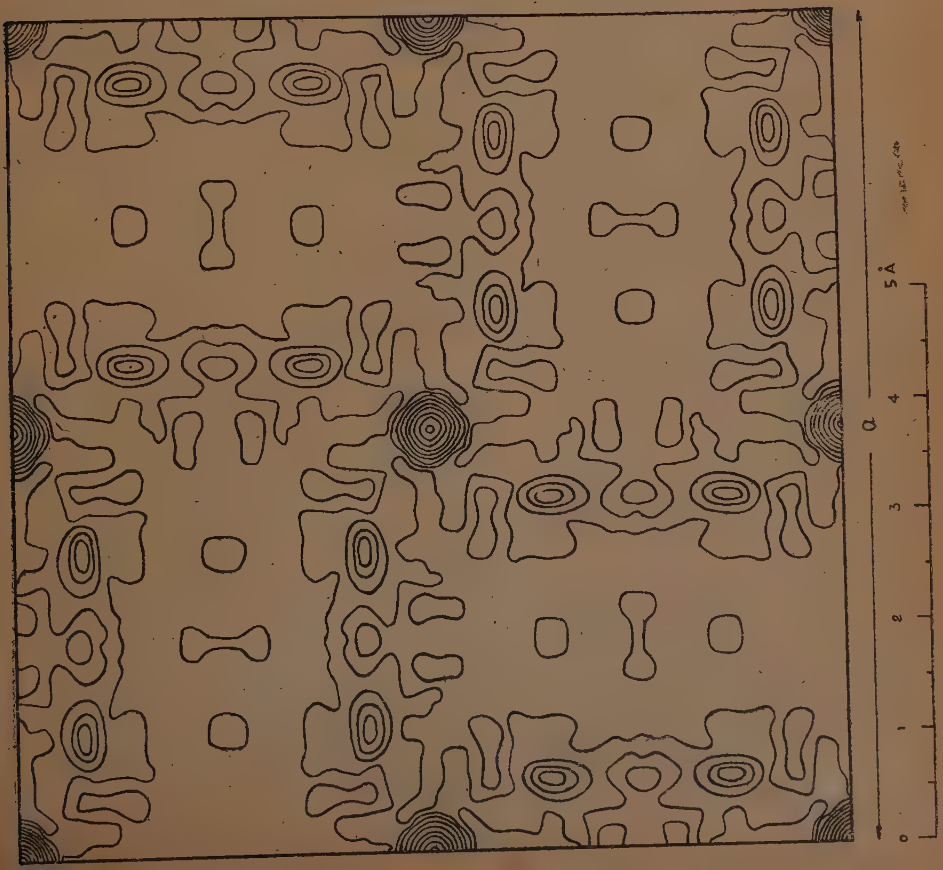

Fig. 1. Electron density, ρ_{xy}, projected upon (001)

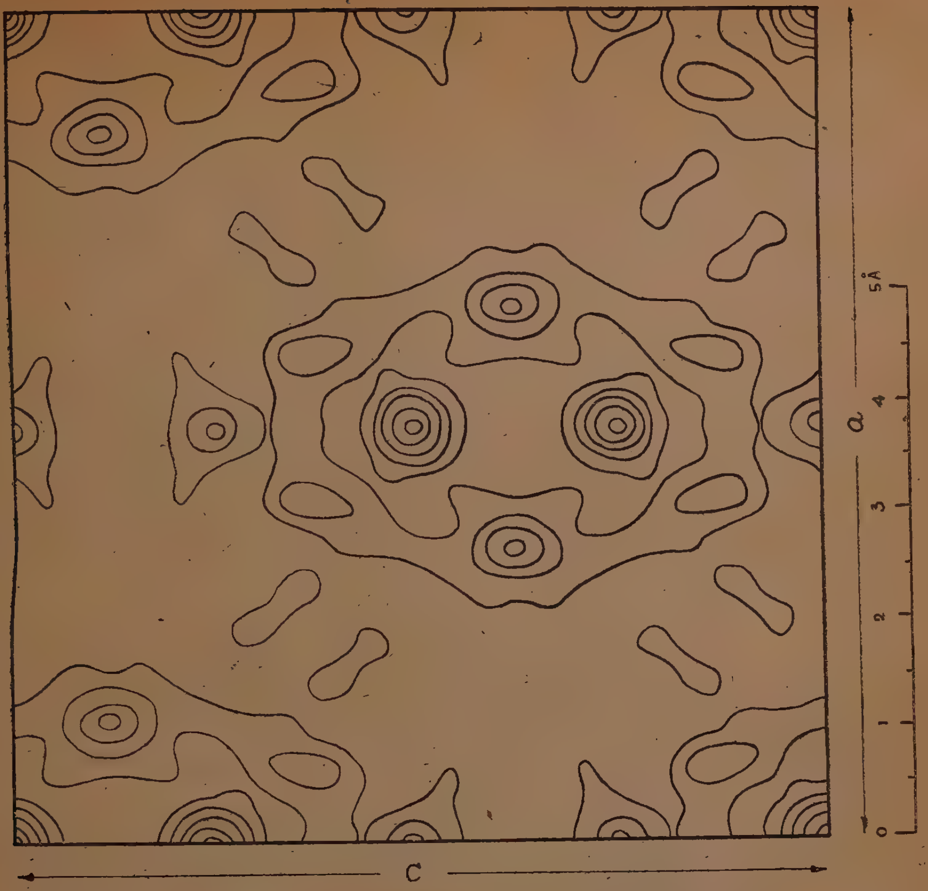

Fig. 2. Electron density, ρ_{xz}, projected upon (010)

reflections and from the properly assumed P-O distance. Then the parameter x, y and z can be expressed as a function of the angle φ between the X-axis and the projection of the P-O bond upon (*001*). The value of φ consistent with observed $F(h00)$ was found to be 30° or 60°, both being equivalent in this crystal. If φ is assumed to be 60° then θ_1 and θ_2 become

$$\theta_1 \simeq 29.8^\circ \quad \theta_2 \simeq 51.3^\circ$$

The atomic scattering factors in $F(h00)$ expressions are obtained from that of James-Brindley's results⁽⁶⁾ and the temprature factor is assumed to be almost the same as that of KH_2PO_4, which is determined from the difference between observed and calculated F values by West. Then, ρ_{xy}, electron density of the crystal projected upon (*001*) plane, becomes

$$\begin{aligned}\rho_{xy} = {} & \mathrm{F}(000)+2\sum_1^h \mathrm{F}(h00)\cos h\theta_1+2\sum_1^k \mathrm{F}(0k0)\cos k\theta_2 \\ & +4\sum_1^h\sum_1^k \mathrm{F}(hk0)\cos h\theta_1 \cos k\theta_2 \\ & -4\sum_1^h\sum_1^k \mathrm{F}(hk0)\sin h\theta_1 \sin k\theta_2\end{aligned}$$

In this expression, $|\mathrm{F}|$ values are provided from the observed intensities of spectra, and their signs are determined by the approximate positions of oxygen atoms preliminarily determined as above. The result is shown in Fig. 1. Structure factors are recalculated to find more accurate positions for oxygen atoms using following combinations of parameters, which would correspond to the most probable positions of the peak for oxygen atoms in this figure.

$$\begin{cases}\theta_1 = 30^\circ \\ \theta_2 = 51^\circ\end{cases} \begin{cases}\theta_1 = 30^\circ \\ \theta_2 = 52^\circ\end{cases} \begin{cases}\theta_1 = 30^\circ \\ \theta_2 = 53^\circ\end{cases} \begin{cases}\theta_1 = 29^\circ \\ \theta_2 = 51^\circ\end{cases}$$

$$\begin{cases}\theta_1 = 29^\circ \\ \theta_2 = 52^\circ\end{cases} \begin{cases}\theta_1 = 29^\circ \\ \theta_2 = 53^\circ\end{cases}$$

Of these positions, those which agree best to the observed F-values are :—

$$\theta_1 = 30^\circ, \qquad \theta_2 = 53^\circ$$

§ 4. Determination of θ_3.

If we shift the origin of the coordinate from the so far assumed position to $\left(00-\frac{1}{8}\right)$, then the expression for ρ_{xz} is given by

$$\begin{aligned}\rho_{xz} = {} & \mathrm{F}(000)-2\sum_1^h \mathrm{F}(h00)\cos h\theta_1+2\sum_1^h \mathrm{F}(00l)\cos l\theta_3 \\ & -4\sum_1^h\sum_1^l \mathrm{F}(h0l)\cos h\theta_1 \cos l\theta_3.\end{aligned}$$

The signs of F-values of the types $l = 8n$ and $l = 8n \pm 4$ can be given immediately, and we obtain $\theta_3 = 40^\circ \sim 45^\circ$ using these terms only by carrying out the Fourier synthesis.

On comparing the observed F($h0l$) values with the calculated F($h0l$) ones, it is found $\theta_3 = 43^\circ$ by the trial-error method. We recalculated the F($h0l$) valus and found that the signs of all terms remained unchanged. Fig. 2 shows the result of Fourier synthesis by using observed F($h0l$) whose signs are determined in the way above described. In this figure we find $\theta_3 = 45^\circ$ as the position of maximum electron density corresponding to the oxygen atom. Recalculating F($h0l$) values by taking $\theta_3 = 45^\circ$, it is found that the agreement between observed and calculated F values is best for almost all terms and their signs remain unchanged.

At the same time, from this figure θ_1 and θ_2 are found to be 30° and 53° respectively and they are accepted to be the most reliable values of these parameters. Now, three parameters θ_1, θ_2 and θ_3, and accordingly x, y and z are determined.

§ 5. Positions of Hydrogen Atoms.

The positions of hydrogen atoms cannot be determined directly by X-ray method. According to the consideration of the space group, there are the following two sets of positions for them ;

8(c) $(00u)$, $(00\bar{u})$, $\left(\frac{1}{2}\,0\,\frac{1}{4}\pm u\right)$

8(d) $\left(\frac{1}{4}\,u\,\frac{1}{8}\right)$. $\left(u\,\frac{3}{4}\,\frac{7}{8}\right)$, $\left(\frac{3}{4}\,\bar{u}\,\frac{1}{8}\right)$, $\left(\bar{u}\,\frac{1}{4}\,\frac{7}{8}\right)$

and these $+\frac{1}{2}\frac{1}{2}\frac{1}{2}$,

Where 8(c) set is the position lying on the line connecting P-atom (for example (000)) with N-atom $\left(00\frac{1}{2}\right)$ and it approaches too close to either N-atom or O-atom to be allowable. The positions, however, lying on the set 8(c) which lies on the two-fold rotation axes parallel to x- and y-coordinates, is more accomodating with other atoms in the structure.

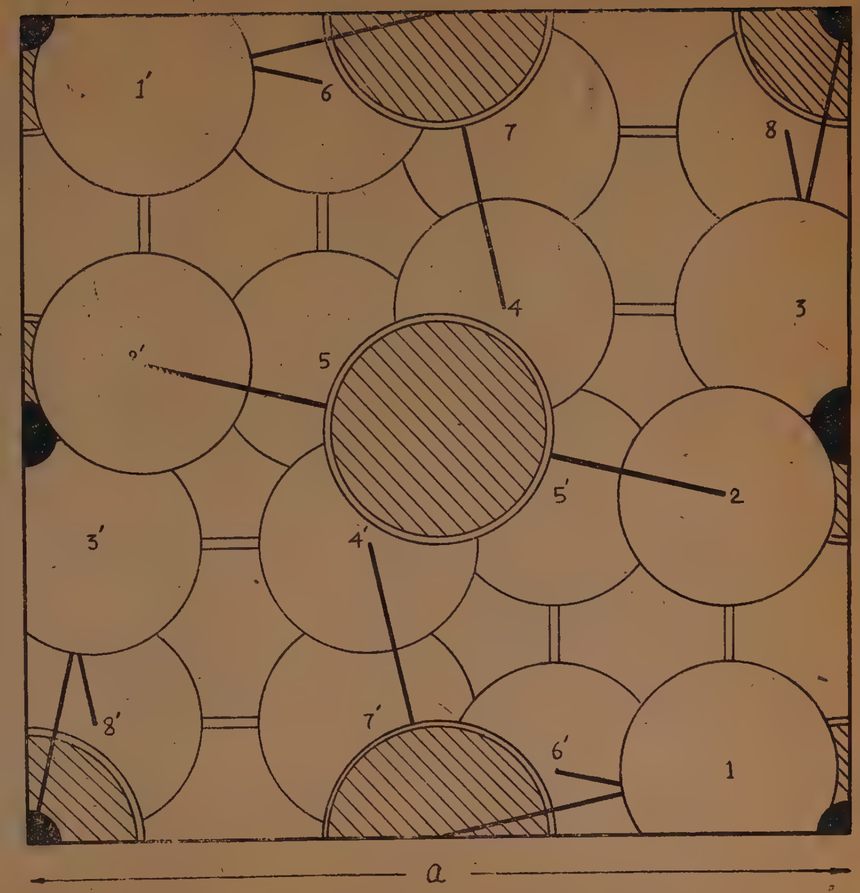

Fig. 3. Crystal structure projected upon (010). Numbers on the oxygen atoms in two figures correspond to each other.

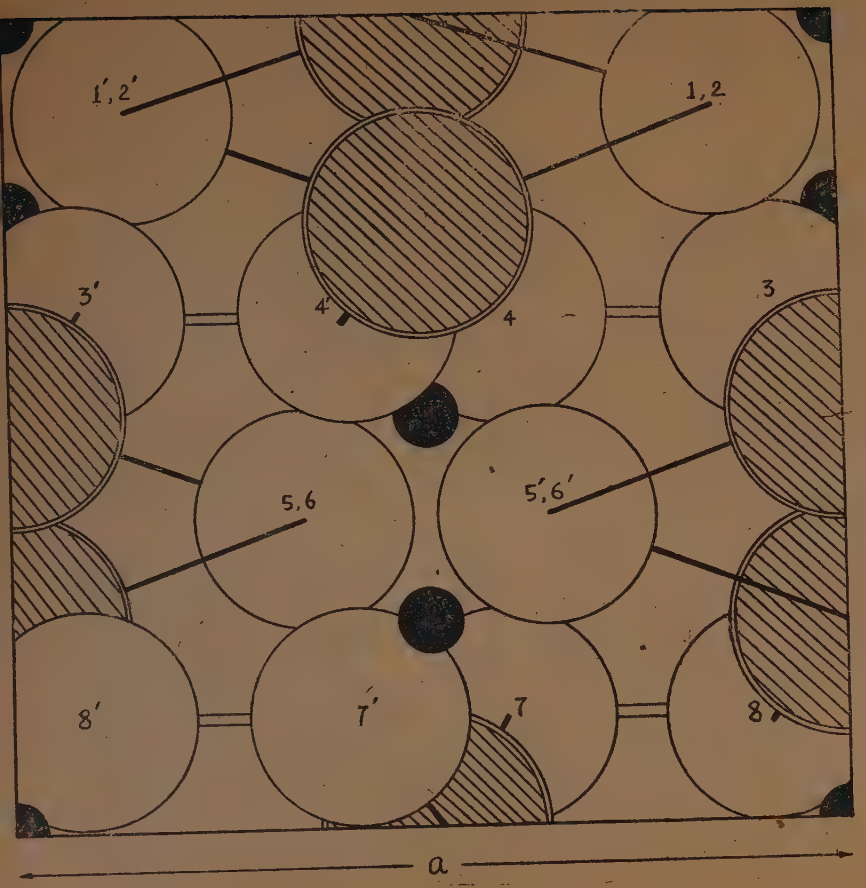

Fig. 4. Crystal structure projected upon (001).

▨ --- NH_4 ○ ----O ● ---- P

═ O-H--O — N-H--O

If it is assumed that $u = 0.147$ in 8(d), then the hydrogen atoms lie in the midway of the line connecting two oxygen atoms which belong to phosphate groups adjacent to each other and O-H distance is calculated to be 1.25 Å. It seems rather better for us to consider that the hydrogen atoms lie in general closer to one of the two adjacent oxygen atoms and take the middle position 8(d) with $u = 0.147$ as the statistical average. In fact, the transition of KH_2PO_4 can only be understood by using such a model.

Hydrogen atoms in NH_4 radicals will take the general positions and would form tetrahedrons about N-atoms.

§ 6. Crystal Structure.

As already mentioned, the crystal structure of this substance is analogous to that of KH_2PO_4. The schematic representations of the structure projected upon (001) and (010) planes are shown in the Figs. 3 and 4, which correspond to the Fourier patterns above reproduced. The parameters of each atom are shown in the Table I. From these results we can describe the details of the structure :—

Table I.

Atomic Parameters

Atoms or radicals	θ_1	θ_2	θ_3
NH_4	0°	0°	180°
P	0°	0°	0°
O	30°	53°	45°
H	90°	(53°)	45°

i) PO_4 tetrahedron

Each phosphorous atom is surrounded tetrahedrally by four oxygen atoms. Atomic distances and valence angles are as follows :—

$$P-O = 1.58\ \text{Å},\quad O-O = 2.53\ \text{Å},\quad O-O' = 2.59\ \text{Å}$$

$$\chi_1 = 106°\ 16',\quad \chi_2 = 110°\ 4',\quad \chi = (O\widehat{P}O')$$

ii) O–H...O bond

O–H...O = 2.49 Å. This value is smaller as compared with that of 2.54 Å found in potassium dihydrogen phosphate, and is considered to show somewhat stronger binding than in the latter. This bond lies in the plane perpendicular to c-axis, whereas in the case of KH_2PO_4 the same bond is inclined about 4° to this plane.

iii) N–H...O bond

$$NH_4-O = 2.87\ \text{Å},\qquad NH_4-O' = 3.09\ \text{Å},$$
$$O-O = 4.27\ \text{Å},\qquad O-O' = 5.42\ \text{Å}.$$

Each ammonium radical has tetrahedral four oxygen atoms around it with atomic distances shown above.

Since the hydrogen atoms in the ammonium radicals are so close to oxygen atoms which have high electronegativity, the formation of hydrogen bond is considered to be highly probable. The atomic distance between nitrogen and oxygen atoms obtained are comparable to that of substances which are considered to have a similar hydrogen bond such as :—

	N–H...O distances (Å)$^{(7)}$
Urea	2.98
Grycin	2.76, 2.88.
Diketopiperazine	2.85

iv) Comparison with KH_2PO_4.

Table II shows corresponding data of $NH_4H_2PO_4$ and KH_2PO_4, the latter being due to West. Distinguished differences in them are in short :—

Table II.

Lattice constants and Interatomic distances

	$NH_4H_2PO_4$ (Å)	KH_2PO_4 (Å)
a	7.479	7.43
c	7.516	6.97
P–O	1.58	1.56
O–O	2.53	2.46
O–O′	2.59	2.60
$(NH_4)K-O$	2.87	2.81
$(NH_4)K-O'$	3.09	2.79
O–H...O	2.49	2.54
N–H...O	2.87	—

a) In KH_2PO_4, a-axis is longer than c-axis, and it is reversed in $NH_4H_2PO_4$.

b) In KH_2PO_4, O–H··· O hydrogen bonds are inclined about 4° to the plane parallel to *(001)*, but in $NH_4H_2PO_4$ they are completely contained in the plane *(001)*.

c) N–H··· O hydrogen bonds are formed in $NH_4H_2PO_4$ crystal.

It is considered that these structural differences found in both crystals will be important factors which result in their different electric properties in spite of analogous structure.

§ 7. Summary.

The analysis of the crystal structure of $NH_4H_2PO_4$ is performed by using the method of double Fourier series.

Parameters of atoms and radicals in the crystal are determined by projecting electron densities upon *c*- and *a*-planes. From the axial and atomic parameters obtained, interatomic distances and valence angles are calculated and compared with that of KH_2PO_4.

In conclusion, the author wishes to express his sincere thanks to Prof. I. Nitta, Prof. T. Watanabé and their associates, especially to Mr. K. Sakurai who gave him cordial guidance throughout the study in the laboratory of Osaka University in the war time and also to Prof. H. Miyabe of Waseda University who permit him to carry out this investigation and to Dr. S. Miyake of Kobayashi Institute of Physical Research who kindly read this manuscript.

References.

(1) J. West: Zeits. f. Krist. **74** (1930) 306.

(2) J. C. Slater: J. Chem. Phys. **9** (1941) 16.
H. Takahashi: Proc. Phys. Math. Soc. Japan **23** (1941) 1069.
G. Bush: Helv. Phys. Acta **11** (1938) 269.

(3) O. Hassel: Zeits. f. Elektrochem. **31** (1925) 523.

(4) S. B. Hendricks: Amer. J. Sci. **14** (1927) 269.

(5) Internationale Tabellen zur Bestimmung von Kristallstrukturen II 179 (1935).

(6) ibid. II 571.

(7) L. Pauling: Nature of the Chemical Bond 2nd ed. 295 (1935).

On the Phase Transition of Barium Titanate (II).

By Ryuzo UEDA.

Kobayashi Intitute of Physical Research, Kokubunjimachi Tokyo, and Department of Applied Physics, Waseda University, Tokyo.

(Read November 27, 1947; Received March 22, 1948).

§ 1. Introduction.

In the previous papers,(1),(2) Miyake and the present author reported the experimental observation on the phase change of barium titanate $BaTiO_3$ by using X-ray, calorimetric and dilatometer methods. We confirmed the existence of a lattice transformation from tetragonal to cubic, and of anomalies in heat capacity and thermal expansion at the Curie point, about 110°C, which corresponds to the conspicuous peak in the dielectric constant. We also found the existence of a transitional region over a temperature interval of about 10°C below the Curie point. In this paper, the result of closer observations upon this transitional temperature range will be described.*

The sample used in the present study is the same one as in the previous studies.

§ 2. Dilatometer Masurements.

The measurements were made with a oil-in-glass dilatometer, which consists of a glass capillary stem, 0.510 mm in inner radius, and a glass bulb, about 1.3 cc in volume. A sample powder of ca. 1.8 gr. was inserted into the bulb, and the dilatometer was filled with paraffin oil whose meniscus in the capillary was read by using a cathetometer. The bulb of the dilatometer was dipped in a oil-bath thermostat controlled by means of an air-mercury regulater. The oil was stirred by a propellar fan, and the temperature control was sensitive to ±0.05°C. The method here employed was capable to detect volume changes of the order of 10^{-6} cc per gram. The measurement was performed in the following way: the thermostat was brought to the desired temperture and reading were taken at a few minutes' interval until two successive readings showed no change. The thermostat was then readjusted to another temperature and readings were taken in the similar way as before. We could always obtain reproducible results either on raising or lowering the temperature.

---

* A part of the result has already been reported briefly in a short note. J. Phys. Soc. Japan, **3** (1948) 177.

One of the results is reproduced in Fig. 1, in which the reading of dilatometer is taken in the ordinate. The latter, however, contains the volume change of glass and oil in addition to that of the sample itself. For the calculatation of the net volume change of the sample itself, it is necessary to know the accurate volume of the sample, paraffin oil and glass, and their respective thermal expansion coefficients. In order to know the net volume change without using these ambiguous quantities, however, the following procedure was adopted. That is, if the whole effective volume of the dilatometer is V and the temperature T, then the volume change with temperature is given by

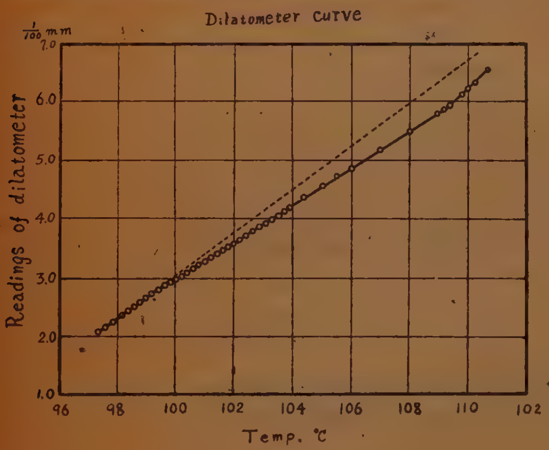

Fig. 1.

$$\frac{dV}{dT} = \alpha V_s + A$$

where α and V_s are the coefficient of thermal expansion and the volume of the sample powder respectively. A is a constant representing the rate of volume change of paraffin oil and glass, and it can be determined if we can know dV/dT from the dilatometer curve, V_s from the weight and the density of the sample, and α from the X-ray study. As reported in the previous paper α is known to take values $3.2\times10^{-5}/°C$ in the cubic region, and $1.9\times10^{-5}/°C$ in the tetragonal region. Corresponding to these numericals, we can obtain the following values for A; $A = 4.24\times10^{-5}$ cm^3/°C corresponding to the cubic region and $A = 4.54\times10^{-5}$cm^3/°C corresponding to the tetragonal region. We assume now $A = (4.39\pm0.15)\times10^{-5}$ cm^3/°C, the mean value of the above two. From these, we can calculate the net volume of the sample V_s, plus an undetermined constant, by the formula

$$V_s + \text{const.} = V - AT$$

Fig. 2 shows the change of the net volume of barium titanate, plus an unknown constant obtained by the above procedure.

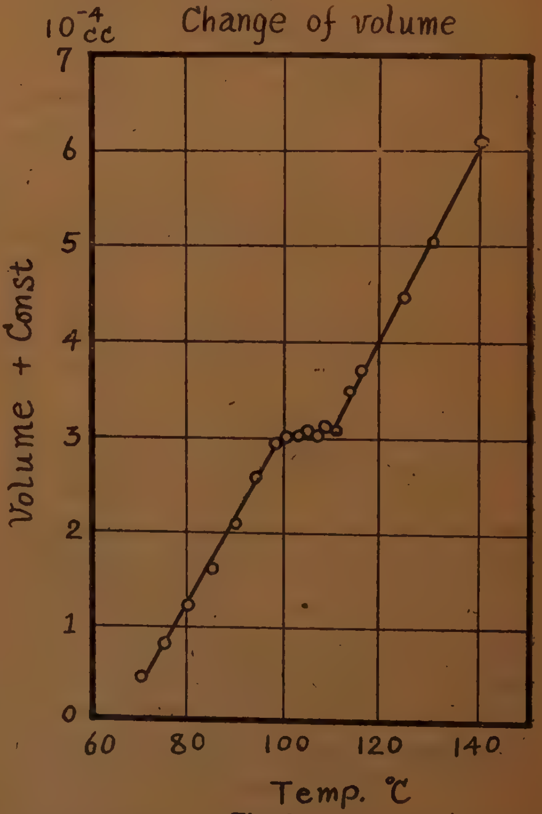

Fig. 2.

The volume of the sample increases linearly from room temperature to 99°C. From this temperature the curve almost stops to increase for an interval of about 10°C, but again it begins to ascend steeply at 110°C. The interval of about 10°C seems to correspond to a transitional region in the phase change of barium titanate.

Von Hippel and his co-workers(3) have found a similar anomalous region in thermal expansion of barium titanate over a range of +95°C ~ +120°C, confirming that in this interval α nearly equals to zero. But their temperature range is much wider than ours. The discrepancy may be attributed either to the difference in added impurities or to different temperature conditions of calcining the sample ceramics.

Von Hippel(3) and Wul(4) reported the existence of the second small peak in the dielectric constant at about +10°C, and that there is an anomaly in the thermal expansion, too. In order to confirm the existence of such an effect, the present author also performed the dilatometer measurement over the range of −10°C ~ +30°C, but it could not be observed any suspected anomaly at this temperature.

§ 3. X-ray Study.

As formerly reported, barium titanate transforms from tetragonal symmetry of low temperature form to cubic one of high temperature form at about 110°C, whereby $\left(\delta = \frac{c}{a} - 1\right)$, the deviation of axial ratio of the tetragonal lattice c/a from unity, is small positive quantity less than only 1%. The change of δ plotted against the temperature is represented in Fig. 3 of the previous paper.(2) It decreases gradually with temperature, but the detailed behavior of the curve in the transitional temperature range has not been determined yet.

It may be interesting to study the minute change of Debye lines near the Curie temperature, where the lines take a diffuse appearance as formerly reported.

To examine more closely about this point, a series of photographs was taken at temperatures 110°, 106°, 102°, 98°, 94°, 90°, 86°C and the room temperature. The sample was oscillated about its axis by nearly 30°. The change of the fine structure of the Debye lines of (510) (431) and (422) in the transitional temperature range were studied by the back reflection method, using CuKα radiation. The dispersion of the lines for these reflections are considerably high because of the large Bragg angle, that being almost 80° for (510) (431) reflection and 70° for (422) reflection. The times of exposure of photographs were about 3 hours.

Some special cares were paid to assure the determination of the accurate temperature of the sample in the high temperature camera. That is, the sample rod is set upon a small copper cylindrical block. The temperature at the upper end of the block was measured by the sensible thermocouple. This total system was inserted into a small electric furnace whose small window is allowed to pass X-ray pencils. The temperature constancy in the furnace during the exposure was within ± 0.05°C.

The photometer tracings of lines of photograms are reproduced in Fig 3. In the cubic region, namely above 110°C, two main peaks in Fig. 3 clearly correspond to the Kα_1 and Kα_2 lines of (510) (431) reflection. As soon as the temperature descends below 110°C, lines gradually begin to broaden (at 106°C) and the broadening reaches maximum at about 102°C. At about this temperature a small hump begins to appear outside

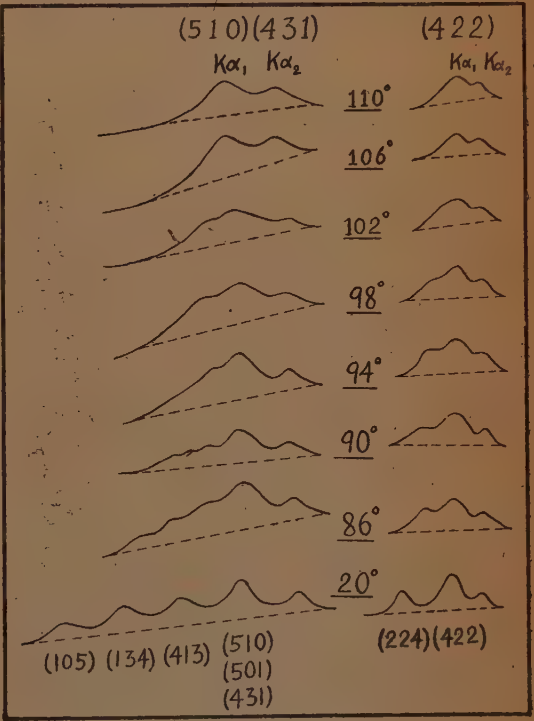

Fig. 3.

the main peaks. At 98°C the two main peaks begin to recover the sharpness again, and also the small hump become clearer. Lowering furthermore the temperature down to 86°C, the main lines get the sharpness completely and the small hump splits up into three peaks, which correspond to the (105), (134) and 413)—reflections due to the tetragonal lattice. At room temperature these peaks become more separated from each other. For the (422) line the circumstances are all similar to the above case of (510) (431)—reflection, except that there exists only one extra line outside the two main Kα reflections of (422), corresponding its small multiplicity.

In the transitional temperature range, (105), (134) and (413) lines become diffuse as will be seen in Fig. 3 and so we cannot estimate lattice constant c in this range. Lattice constant a, however, may be calculated on the degenerated main line, the (510), (501), (431)-reflections. It is reproduced in Fig. 4. In the cubic region a decreases linearly

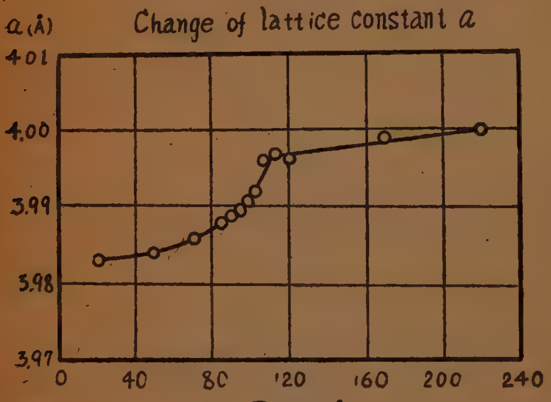

Fig. 4.

up to the Curie point, whereby it begins to contract suddenly but without appreciable discontinuity, and a comparatively rapid change continues in a temperature range of about 10°C. As shown in Table I, the change of a is rather steep between 106° and 102°C as compared with the rest. At these temperature range, the line broadening reaches maximum. δ on the third column of the table was calculated from the relation

$$\delta = \left(\frac{c}{a}-1\right) = \left(\frac{V}{a^3}-1\right),$$

where V represents the lattice volume. Since, as

Table I.

Temp. °C	a	δ
20	3.983	9.1
50	3.984	8.9
70	3.986	7.7
86	3.988	6.5
90	3.989	5.8
94	3.990	4.9
98	3.991	4.5
102	3.992	3.8
106	3.996	0.7
110	3.997	0.0

already shown in Fig. 2, V is known to be nearly constant between 99°-110°C, δ can be expressed in the following form,

$$\delta = \frac{a_0^3}{a_t^3}\{1-\alpha(t_l-t)\}-1,$$

where a_0 represents the lattice constant at the Curie point, α cubic expansion coefficient which is 1.9×10^{-5} in the lower temperatures. t_l is the lower temperature limit of the transitional range, that is 99°C, and a_t is a lattice constant at temperature t, which is known from Fig. 4 and Table I.

The change of δ with the temperature thus calculated is plotted by open circles in Fig. 5.

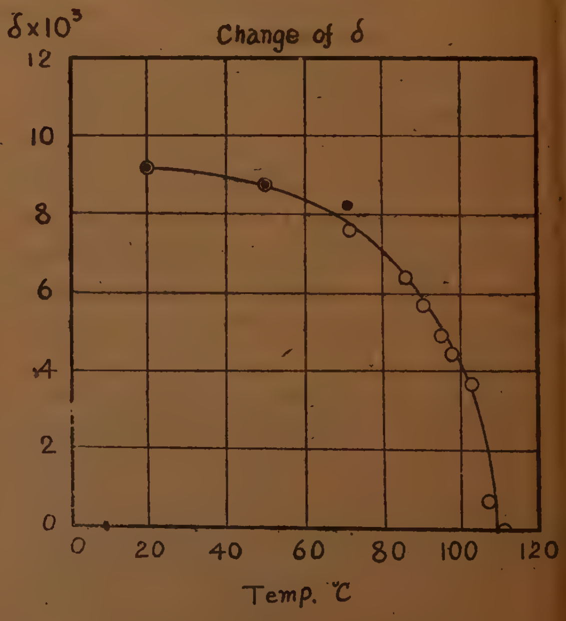

Fig. 5.

Solid circles in the figure, on the other hand, indicate the values newly calculated from the measurement of the separations of multiplet lines of (510) (431)-reflections. We can get a more detailed knowledge of δ than that formerly reported, including the transitional temperature range. The change of δ seems to be gradual, although it is somewhat steep between 106° and 102°C.

§ 4. Discussion.

The temperature ranges in which thermal expansion stops to increase and the lattice constant a varies appreciably and also Debye lines become diffuse are all agreeing with each other. Changes in the diffraction pattern here observed in this temperature interval may be explained in the following manner: at temperatures above the Curie point, each crystallite in the powder sample is considered as being a small crystal of a perfect cubic lattice of the perouskite type. Passing the temperature down the Curie point, each crystallite splits out into many domains, each of which is considered to possess a tetragonal lattice, having a spontaneous electric polarization along c-axis. Such a domain structure can be considered to be analogous to that found in Rochelle salt crystal.(5) As the result of the domain formation, the lattice in the crystallite becomes more or less deformed. This results in the inhomogeneity of lattice constant as well as the diminution of the size of coherent regions in the lattice. These effects will make the distribution of intensity of reflections broaden. Especially, it may be more pronounced in the neighbourhood of about 105°C on account of small size of domains. Below the transitional temperature range, each domain grows up into a large tetragonal crystallite and Debye lines of the multiplet will become sharper again. Domain structure above assumed can alternatively described as the twinned structure of the crystallite. In fact recently Kay and Rhodes(6) confirmed more directly the existence of the twinned structure on the single crystal of barium titanate.

In the recent papers, Kay and Rhodes(6) and Harwood, Popper and Rushmann(7) reported that there is the co-existence of the cubic and tetragonal lattices in some temperature range about the Curie point. Harwood also concluded that the axial ratio c/a has a large discontinuity in the transition. As far as our observation is concerned, we cannot detect the co existence of the two phases in any temperature range, and there seems to be no evidence for the distinct discontinuity in the axial ratio near the Curie point.

In conclusion, the author wishes to express his sincere thanks to Dr. S. Miyake who gave him a cordial guidance throughout the study, and to Mr. T. Ogawa who kindly gave him precious samples prepared in his laboratory.

References.

(1) S. Miyake and R. Ueda: J. Phys. Soc. Japan, **1** (1946) 32.

(2) S. Miyake and R. Ueda: *ibid.* **2** (1947) 93.

(3) A. von Hippel, R. G. Breckenridge, F. G. Chesley and L. Tisza: Ind. Eng. Chem. **38** (1946).

(4) B. Wul: Nature **156** (1945 480.

(5) S. Miyake: Proc. Phys.-Math. Soc. Japan., **23** (1941) 377, 810. J. Phys. Soc. Japan **2** (1947) 98.

(6) H. F. Kay and R. G. Rhodes: Nature **160** (1947) 126.

(7) M. G. Harwood, P. Popper and D. F. Rushman: Nature **160** (1947) 58.

On the Carriers of Electricity and Heat in Superconductors.

By Zirô MIKURA

Research Institute for Iron, Steel and Other Metals, Tôhoku University,

Sendai, Japan.

(Read December 16, 1944; Received March 30, 1948)

§ 1. The most striking and rather mysterious features of superconductivity are, firstly, that the electrical resistance of a superconductor is completely absent, and secondly, that the magnetic induction inside the body is always zero. The elucidation of the former property has been supposed to be difficult since the zero resistance seems to indicate a completely frictionless motion of electrons through a metal. On the other hand, the vanishing of the magnetic induction inside the body appears to contradict with the magnetic behavior predicted for a perfect conductor on the ordinary Maxwell's field equation. In one of his previous papers, however, the author(1) suggested that those peculiar properties of a superconductor might be explained if we assume that a superconductor is merely a conductor in which electrons have very few chances of being scattered by the lattice, and it is not necessarily requested for these chances to vanish. From this assumption it was deduced that the usual derivation of Ohm's law is not valid for superconductors. Hence, all the experiments, which have been made in order to estimate the order of magnitude of the electrical resistivity in a superconductor, should lose their original meaning, and thus the observed results of zero resistance becomes to be not so strange as appeared at first. It was also shown in that paper that such a conductor as we have assumed above, under a certain condition, might act as a perfectly diamagnetic body in magnetic field, though it has long been believed to behave itself in quite a different way in magnetic field. From those considerations the author concluded that superconductivity might be regarded as one type of metallic conduction, where electronic scatterings by the lattice field are so rare that the ordinary theory on metallic conduction is not applicable.

§ 2. Before entering into the main discourse, we shall consider first of all how the normal conduction of electricity is explained in the modern theory of metals. This can be reduced to the problem of the motion of electronic waves in a periodic potential field representing the lattice. When the potential field is perfectly periodic, the waves suffer no scattering: that is, the electrical resistivity is completely null. In the case of real metals, however, the lattice field is not perfectly periodic on account of the thermal motion of atoms and the lattice imperfections caused by impurities and mechanical distortions. Thus the normal resisitvity will be roughly divided into two parts: (1) the temperature dependent part due to thermal motion of the lattice (ideal resistivity); and (2) the temperature-independent part due to lattice imperfections (residual resistivity).

Let us now consider to what extent we may apply the above idea to the case of superconductivity. We know empirically that the applied electric and magnetic fields affect the motion of electron also in a superconductor. Thus it is reasonable to suppose that the conduction problem not only in a normal metal but also in a superconductor should be the problem on the motion of electrons in the periodic field representing the lattice. From this viewpoint we may assume that the mechanisms of electronic scatterings by the lattice field are the same in both cases of normal and superconducting states. At first sight, however, it seems difficult to explain, on the basis of this idea, the complete disapearance of the residual resistance during the process of transition from the normal to the superconducting state, because the lattice imperfections caused by impurities and the mechanical distortions seem unlikely to disappear abruptly at a certain temperature near the absolute zero--the transition point. As seen later, however, the difficulty will be avoided if we suppose that it is not the property of the lattice field itself but that of the carriers of electricity, that changes at the transition point.

§ 3. The object of this section is to find a reasonable model of a superconductor compatible with the following four empirical facts:

[Fact I] Between the electrical and thermal resistivities, ρ_r and w_r, due to scatterings of electronic waves by the lattice irregularities, the well-known Wiedemann-Franz law holds, which is given by

$$\frac{\rho_r}{w_r T} = \frac{\pi^2}{3}\left(\frac{k}{e}\right)^2, \tag{1}$$

where T is the absolute temperature, k the Boltzmann constant, and e the electronic charge(2)*

[Fact II] The electrical resistivity becomes too small to measure when the transition to the superconducting state takes place completely.

[Fact III] Contrary to the case of the electrical resistivity, the thermal resistivity is rather greater in the superconducting state than in the normal. For instance, the thermal resistivity of superconducting lead at a certain temperature a few degrees below the transition point was about five times larger than the value in the normal state at the same temperature(3). (The latter may be obtained when observations are made in a sufficiently large magnetic field).

[Fact IV] The specific charge q/μ (where q and μ are the charge and mass, respectively, of a carrier in a superconductor) is exactly identical with the ratio for an ordinary electron.(4) (Gyromagnetic experiment).

Considering that the most part of the electrical resistance at the temperature just above the transition point is the residual one, one may conclude that, in this temperature range the electronic scatterings due to the thermal motion of the lattice are negligibly rare compared with those due to impurities and lattice distortions. Thus the thermal resistance due to the thermal motion of the lattice may also be neglected. It may then be concluded from [Fact I] that even the whole electrical and thermal resistivities, ρ and w, in this temperature range should satisfy the Wiedemann-Franz law (1)**. On the other hand, the validity of this law means that we can apply the usual theory on metallic conduction, in which one and the same value of mean free path may be used in calculating both the electrical and the thermal resistivities. Thus we get the usual formulae

$$\rho = \frac{m^* v}{e^2 n l}, \tag{2}$$

and

$$\frac{1}{w} = \frac{\pi^2 k}{3}\frac{nl}{m^* v}\frac{1}{T}, \tag{3}$$

where m^*, v and l are the effective mass, the speed, and the mean free path of an electron on the top of the Fermi distribution, n the number of electrons per c.c. Of course, the combination of formulae (2) and (3) leads to the Wiedemann-Franz law (1).

As the process of the electronic scattering in superconductors, as already stated in § 2, is unlikely to differ essentially from that in normal metals, we can also define such quantities as the charge, the effective mass, the speed and the mean free path for the carrier in a superconductor. We shall designate those quantities by q, μ^*, v_s and l_s respectively, and the number of carriers per c.c. by n_s. In the case of superconductivity, however, we cannot apply a formula analogous to the equation (2), since the ordinary theory on electronic conduction and consequently Ohm's law do not hold here, and the definition of electrical resistivity given in the sense of Ohm's law loses its meaning.(1)

Nevertheless, we may conclude

---

* If we take, instead of ρ_r and w_r, the whole resistivities ρ and w, which involve the effect of electronic scatterings due to thermal motions of the lattice, this law holds no longer at low temratures considered here.

** We neglect here the thermal conduction by the lattice, too.

$$\frac{\mu^* v_s}{q^2 n_s l_s} \ll \frac{m^* v}{e^2 n l} \qquad (4)$$

from [Fact II] because in the present paper superconductivity interpreted as the limiting case of normal conductivity when the probability of scattering of electrons becomes small.

Now we shall discuss [Fact III], which tells us that the thermal resistance in the superconducting state is rather greater than that in the normal state. It seems to be out of question that this decrease in conduction of heat in the superconducting state is caused by the decrease of the part played by carriers in the metal, and the conduction by the lattice is not affected by the transition. We shall now discuss the two factors which determine the magnitude of conduction of heat by carriers: (1) the temperature gradient in the system of carriers for a definite temperature gradient impressed on the lattice; and (2) the amount of heat transported by carriers for a given temperature gradient in the carrier system. In the case of electronic heat conduction of a normal metal, the temperature gradient in the electronic system is plausibly assumed to be the same as that of the lattice: that is, the two systems are assumed to be in thermal equilibrium with each other. Equation (3) may only be derived under this condition. In a superconductor, however, it might be possible for the carrier system to have a smaller temperature gradient than that in the lattice itself, because the carriers are assumed to have little interactions with the lattice. It will then be possible to account for the low conduction of heat in the superconducting state on the basis of either of the following three assumptions:

[Assumption I] Carriers in a superconductor move quite freely through the lattice. But, in a superconductor whose temperature is not uniform, the carrier system is not in thermal equilibrium with the lattice and the temperature gradient in the carrier system is much smaller than that in the lattice. Hence, the carriers have rather less contribution to heat conduction.

[Assumption II] In the case of a superconductor, too, the carrier system is assumed to be in the thermal equilibrium with the lattice and consequently to have the same temperature gradient as in the lattice. But heat-carrying ability of the carriers in a superconductor is assumed to be small compared with the electrons in a normal metal, if the same temperature gradient in carrier system is assumed in both cases.

[Assumption III] In a superconductor both factors mentioned above act unfavorably for heat conduction.

The decrease of the thermal conductivity in the superconducting state has so far usually been explained in [Assumption I]. Under this assumption the equation 3) of course cannot be applied, and consequently we cannot deduce from [Fact III] the relation

$$\frac{n_s l_s}{\mu^* v_s} \lesssim \frac{nl}{m^* v}. \qquad 5)$$

But, if [Assumption II] is true, then the equation (3) holds also for a superconductor* and relation (5) follows from [Fact III]. (5) represents a relation which compares the amount of thermal energy carried by the carriers in both superconducting and normal states, when the carrier system in both cases have the same temperature gradient. Thus the relation (5) is independent of the different possible assumptions regarding the interaction between the lattice and the carriers. Accordingly, if relation (5) is valid under [Assumption II], it must hold as well under [Assumption III]. Therefore, the validity of relation (5) does depend upon whether [Assumption I] is false or not. It would be possible to settle this problem by the following experiment. In Fig. 1 let AE denote a superconducting rod placed in vacuum, the temperature of which is kept constant in such a manner that it may be lower than the normal transition temperature T_0 at A, but higher than this temperature at E. As a consequence, the rod may be supposed to be superconducting between A and C, and normal

---

* It was noted(1) that equation (2) becomes invalid in the case of highly conductive body on account of increasing effect of the magnetic field due to the electrical current itself. In deriving equation (3), however, we assume that there are neither electrical current nor external magnetic field, so the validity of this equation may be extended to the case of high conductivity.

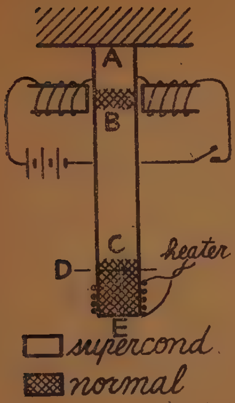

Fig. 1

between C and E. At a certain point B, near the end A, an electromagnet is placed as shown in the figure, in order to destroy superconductivity, if needed, at this point without affecting the temperature appreciably. Imagine that we measure the thermal conductivity between B and a certain point D, which lies between C and E. If [Assumption I] be true, then the thermal conductivity, expected when B is in the normal state, would be abnormally high compared with the value expected when B is in the superconducting state. The reason for this is as follows: under [Assumption I] a superconducting rod, both ends of which are normally conducting, would show a very large thermal conductivity, corresponding to the situation that the carriers are in thermal equilibrium with the lattice on both ends of the rod, and freely movable in the middle portion of it. Unfortunately, this sort of experiment has never been carried out, but de Haas and Rademakers' experiment on the thermal conductivity of a rod in the intermediate state under the influence of a transverse magnetic field suggests that such a large thermal conductivity would not appear in the experiment proposed above. The intermediate state is now generally believed to be such a state, where the metal is divided up into thin, alternatively superconducting and normal laminae parallel to the applied magnetic field.⁽⁵⁾ If [Assumption I] be true, the thermal conductivity of a metal in the intermediate state under the influence of a transverse magnetic field would be abnormally high, just as it would be expected in the experiment shown in Fig. 1 with the magnetic field applied. De Haas and Rademakers' experiment, however, has shown that the thermal conductivity of a metal in the intermediate state lies between those in the normal and superconducting states. Thus we may conclude that [Assumption I] does not hold and therefore relation (5) can be applied.

The consequence of the above considerations is that we have deduced relations (4) and (5) from [Fact I], [Fact II], and [Fact III], on the basis of the generally accepted ideas about the mechanism of metallic conduction and the structure of the intermediate state. The combination of these two relations (4) and (5) leads immediately to the result:

$$\frac{\mu^* v_s}{q^2 n_s l_s} \ll \frac{\mu^* v_s}{e^2 n_s l_s},$$

that is,

$$[q| \gg |e|. \tag{6}$$

On the other hand, from [Fact IV] we obtain*

$$\frac{q}{\mu} = \frac{e}{m} \tag{7}$$

From (6) and (7) we know that a carrier in a superconductor has a very large electric charge compared with the ordinary electron, and moreover, a large mass exactly proportional to this charge. This suggests that the electrons in a metal begin to condense (not necessarily in coordinate-space, but rather in momentum-space) into droplets as soon as superconductivity takes place in the metal, and that each of the droplets behaves like a "giant electron". The circumstances have some resemblance to the case of ferromagnetism. In ferromagnetism a large number of electrons have the same attitudes as regards the direction of spin; similarly we may say that a large number of electrons in a superconductor have the same attitudes as regards momentum. The suggestion of this type, however, is not new. The propositions presented by Frenkel, Kronig, and Stark may be considered to be along the same line. Among these, the author agrees with Frenkel,⁽⁷⁾ who suggested that the classical electromagnetic interaction between moving electrons may be the origin of the binding force for building a "giant electron". The electron condensation proposed in this paper, however, is different from those old ones in the point that it is derived, as a necessary result, from the experimental facts, by taking into account the generally accepted concepts on metallic conduction.

---

* μ and m are here the true masses. See reference (6).

References.

(1) Z. Mikura, Proc. Phys.-Math. Soc. Japan, **24** (1942), 899.

(2) E. Grüneisen und E. Goens, Zeits f. Phys., **44** (1927), 615.

(3) W. J. de Haas and A. Rademakers, Physica, **7** (1940), 992.

(4) I.K. Kikoin and S.V. Goobar, C.R Acad. Sci., URSS. **19** (1938), 249.

(5) See, for instance, D. Shoenberg, *Superconductivity*, Chapter III.

(6) C.G. Darwin, Proc. Roy. Soc., **154** (1936), 61.

(7) J. Frenkel, Phys. Rev., **43** (1933), 907.

Tables Useful for the Numerical Calculations of the Air Stream at High Speeds.

By Isao IMAI.

Department of Physics, Faculty of Science, University of Tokyo.

(Received April 4, 1948)

For treating problems in high speed flow, it is essential to consider the effect of compressibility of the fluid, and the mathematical difficulty with which we are confronted is known to be very great. Moreover, after having obtained the analytical solution, we are often compelled to make very tedious numerical calculations in order to get a clear view of the actual state of affairs which ought to be represented by the analytical results. It may be expected, however, that such numerical work can be reduced considerably by the use of suitably arranged tables. In fact, for the case of air, the present author prepared such numerical tables, which have been conveniently used in many of his theoretical studies on the air stream at high speeds. These tables will be given in this paper.

If we assume that the flow takes place adiabatically, we have by Bernoulli's theorem

$$\frac{p}{p_0}=\left(1-\frac{\gamma-1}{2}\frac{q^2}{c_0^2}\right)^{\frac{\gamma}{\gamma-1}}, \tag{1}$$

$$\frac{\rho}{\rho_0}=\left(1-\frac{\gamma-1}{2}\frac{q^2}{c_0^2}\right)^{\frac{1}{\gamma-1}}, \tag{2}$$

$$c^2=c_0^2-\frac{\gamma-1}{2}q^2, \tag{3}$$

where γ is the ratio of the specific heats, and p is the pressure, ρ the density, q the velocity, c the local velocity of sound, and also the suffix 0 refers to the state corresponding to the fluid at rest. From (3) it will readily be seen that the velocity at which the local velocity of sound is equal to the fluid velocity is given by

$$c_*=\sqrt{\frac{2}{\gamma+1}}c_0. \tag{4}$$

We may conveniently take c_* as the unit of velocity. Then (1), (2), (3) become

$$\frac{p}{p_0}=(1-\alpha^2q^2)^{\frac{\gamma}{\gamma-1}}, \tag{5}$$

$$\frac{\rho}{\rho_0}=(1-\alpha^2q^2)^{\frac{1}{\gamma-1}}, \tag{6}$$

$$c^2=\frac{\gamma+1}{2}-\frac{\gamma-1}{2}q^2, \tag{7}$$

with

$$\alpha^2=\frac{\gamma-1}{\gamma+1}. \tag{8}$$

Hence, the local Mach number is given by

$$M=\frac{q}{c}=\sqrt{\frac{2}{\gamma+1}}\frac{q}{\sqrt{1-\alpha^2q^2}}. \tag{9}$$

It is convenient to introduce two functions:

$$\mu = \sqrt{1-M^2} = \sqrt{\frac{1-q^2}{1-a^2q^2}}, \tag{10}$$

$$R = q\frac{\rho}{\rho_0} = q(1-a^2q^2)^{\frac{1}{\gamma-1}}. \tag{11}$$

Taking $\gamma = 1.4$ for air, we have prepared tables of p/p_0, ρ/ρ_0, M, μ, R against q, which are shown below. Although the method of application of the tables seems to be evident, it may not be superfluous to give a few remarks.

In the first place, let it be required to calculate the pressure coefficient, assuming the velocity to be already known. The pressure coefficient C_p is defined by

$$C_p = (p-p_1)/\frac{1}{2}\rho_1 q_1^2, \tag{12}$$

where the suffix 1 refers to a certain standard state, such as the stream at infinity in the case of uniform flow past an obstacle. Remembering that $c^2 = \gamma p/\rho$, we have

$$\frac{p_1}{\rho_1 q_1^2} = \frac{\gamma p_1}{\rho_1}\cdot\frac{1}{\gamma q_1^2} = \frac{c_1^2}{\gamma q_1^2} = \frac{1}{\gamma M_1^2},$$

so that

$$C_p = \frac{2}{\gamma M_1^2}\,\frac{p_0}{p_1}\cdot\frac{p}{p_0} - \frac{2}{\gamma M_1^2}. \tag{13}$$

For any particular value of M_1, we can find q_1 and hence p_1/p_0 by means of the table. On the other hand, values of p/p_0 corresponding to those of the velocity q can be immediately read off from the table. Thus (13) may be very conveniently used for our pursose.

Next, let us consider the air stream through a pipe with slowly varying cross section. Denoting the sectional area by S, we have, as the condition of continuity,

$$\rho q S = \text{const, so that } RS = \text{const.} \tag{14}$$

For a given pipe S is known, and so R is given by (14). Hence, by the use of the table of R, the velocity q can be found at any arbitrary section S.

Further, the table of R admits of another application of much importance. For a two-dimensional steady motion of a compressible fluid, we can define a stream function Ψ such that

$$\frac{\rho}{\rho_0}u = \frac{\partial\Psi}{\partial y}, \quad \frac{\rho}{\rho_0}v = -\frac{\partial\Psi}{\partial x}, \tag{15}$$

so that

$$R \equiv q\frac{\rho}{\rho_0} = \sqrt{\left(\frac{\partial\Psi}{\partial x}\right)^2 + \left(\frac{\partial\Psi}{\partial y}\right)^2} = \frac{\partial\Psi}{\partial n}, \tag{16}$$

where (u, v) are the velocity components and dn

q	M	μ	$\frac{\rho}{\rho_0}$	$\frac{p}{p_0}$	$q\frac{\rho}{\rho_0}$
0.00	0.0000	1.0000	1.0000	1.0000	0.0000
1	191	1.0000	1.0000	0.9999	100
2	183	0.9998	0.9998	9998	200
3	274	9996	9996	9995	300
4	365	9993	9993	9991	400
5	457	9990	9990	9985	499
6	548	9985	9985	9979	599
7	639	9980	9980	9971	699
8	731	9973	9973	9963	798
9	822	9966	9966	9953	897
10	914	9958	9958	9942	996
0.11	1005	9949	9950	9930	1094
12	1097	9940	9940	9916	1193
13	1188	9929	9930	9902	1291
14	1280	9918	9919	9886	1389
15	1372	9905	9907	9869	1486
16	1464	9892	9894	9851	1583
17	1556	9878	9880	9832	1680
18	1648	9863	9866	9812	1776
19	1740	9848	9850	9791	1872
20	1832	9831	9834	9769	1967
0.21	1924	9813	9817	9745	2062
22	2016	9795	9800	9721	2156
23	2109	9775	9781	9695	2250
24	2201	9755	9762	9668	2343
25	2294	9733	9742	9640	2435
26	2387	9711	9721	9611	2527
27	2480	9688	9699	9581	2619
28	2573	9663	9677	9550	2709
29	2666	9638	9653	9518	2799
30	2759	9612	9629	9485	2889
0.31	2853	9584	9604	9451	2977
32	2946	9556	9579	9415	3065
33	3040	9527	9552	9379	3152
34	3134	9496	9525	9342	3239
35	3228	9465	9497	9304	3324
36	3322	9432	9469	9264	3409
37	3417	9398	9439	9224	3493
38	3511	9363	9409	9183	3575
39	3606	9327	9378	9141	3658
40	3701	9290	9347	9097	3739
0.41	3796	9251	9314	9053	3819
42	3892	9212	9281	9008	3898
43	3987	9171	9247	8962	3976
44	4083	9128	9213	8916	4054
45	4179	9085	9178	8868	4130
0.46	4275	9040	9141	8819	4205
47	4372	8994	9105	8770	4279
48	4468	8946	9067	8719	4352
49	4565	8897	9029	8668	4424
50	4663	8847	8991	8616	4495

q	M	μ	$\frac{\rho}{\rho_0}$	$\frac{p}{p_0}$	$q\frac{\rho}{\rho_0}$
0.50	0.4663	0.8847	0.8991	0.8616	0.4495
51	4760	8794	8951	8563	4565
52	4858	8741	8911	8510	4634
53	4956	8686	8870	8455	4701
54	5054	8629	8829	8400	4768
55	5152	8570	8787	8344	4833
56	5251	8510	8744	8287	4897
57	5350	8448	8701	8230	4959
58	5450	8385	8657	8171	5021
59	5549	8319	8612	8112	5081
60	5649	8251	8567	8053	5140
0.61	5750	8182	8521	7992	5198
62	5850	8110	8474	7932	5254
63	5951	8036	8427	7870	5309
64	6053	7960	8380	7808	5363
65	6154	7882	8331	7745	5415
66	6256	7801	8283	7681	5467
67	6359	7718	8233	7617	5516
68	6462	7632	8183	7553	5565
69	6565	7544	8133	7487	5612
70	6668	7452	8082	7422	5657
0.71	6772	7358	8030	7355	5701
72	6876	7260	7978	7289	5744
73	6981	7160	7925	7221	5785
74	7086	7056	7872	7154	5825
75	7192	6948	7818	7085	5864
76	7298	6837	7764	7017	5901
77	7404	6721	7710	6948	5936
78	7511	6601	7654	6878	5971
79	7619	6477	7599	6808	6003
80	7727	6348	7543	6738	6034
0.81	7835	6214	7486	6668	6064
82	7944	6074	7429	6597	6092
83	8053	5928	7372	6526	6119
84	8163	5776	7314	6454	6144
85	8274	5617	7256	6382	6168
86	8384	5450	7197	6310	6190
87	8496	5274	7138	6238	6210
88	8608	5090	7079	6165	6229
89	8721	4894	7019	6092	6247
90	8834	4687	6959	6020	6263
0.91	8948	4466	6898	5946	6278
92	9062	4229	6838	5873	6291
93	9177	3973	6776	5800	6302
94	9292	3695	6715	5726	6312
95	9408	3388	6653	5652	6320
96	9526	3043	6591	5578	6327
97	9643	2647	6528	5505	6333
98	9761	2171	6466	5431	6336
99	9880	1542	6403	5357	6339
1.00	1.0000	0.0000	6339	5283	6339

q	M	μ	$\frac{\rho}{\rho_0}$	$\frac{p}{p_0}$	$q\frac{\rho}{\rho_0}$
1.00	1.0000	0.0000	0.6339	0.5283	0.6339
1	1.0120	1556	6276	5209	6339
2	1.0241	2211	6212	5135	6336
3	1.0363	2720	6148	5061	6333
4	1.0486	3155	6084	4987	6327
5	1.0609	3544	6020	4913	6320
6	1.0734	3900	5955	4840	6312
7	1.0858	4232	5890	4766	6302
8	1.0984	4545	5825	4663	6291
9	1.1111	4843	5760	4619	6278
10	1.1239	5129	5695	4546	6264
1.11	1.1367	5404	5629	4473	6248
12	1.1496	5671	5564	4400	6231
13	1.1627	5931	5498	4328	6213
14	1.1758	6184	5432	4255	6192
15	1.1890	6432	5366	4183	6171
16	1.2023	6675	5300	4111	6148
17	1.2157	6913	5234	4040	6124
18	1.2292	7148	5168	3969	6098
19	1.2428	7380	5102	3898	6071
20	1.2566	7609	5035	3827	6042
1.21	1.2704	7835	4969	3757	6013
22	1.2843	8059	4903	3687	5981
23	1.2984	8282	4837	3617	5949
24	1.3126	8502	4770	3548	5915
25	1.3269	8721	4704	3479	5880
26	1.3413	8939	4638	3411	5844
27	1.3558	9156	4572	3343	5806
28	1.3705	9371	4505	3275	5767
29	1.3853	9586	4439	3208	5727
30	1.4002	9801	4373	3141	5685
1.31	1.4153	1.0015	4307	3075	5643
32	1.4305	1.0229	4242	3010	5599
33	1.4458	1.0442	4176	2945	5554
34	1.4613	1.0655	4110	2880	5508
35	1.4769	1.0869	4045	2816	5461
36	1.4927	1.1083	3980	2753	5412
37	1.5087	1.1296	3915	2690	5363
38	1.5248	1.1511	3850	2628	5312
39	1.5410	1.1725	3785	2566	5261
40	1.5575	1.1940	3720	2505	5208
1.41	1.5741	1.2156	3656	2445	5155
42	1.5909	1.2373	3592	2385	5100
43	1.6078	1.2590	3528	2326	5045
44	1.6250	1.2809	3464	2267	4989
45	1.6423	1.3025	3401	2209	4931
46	1.6599	1.3248	3338	2152	4873
47	1.6776	1.3470	3275	2095	4814
48	1.6955	1.3692	3212	2040	4754
49	1.7137	1.3917	3150	1985	4694
50	1.7321	1.4142	3088	1930	4632

is the line element normal to the stream line. It is obvious from (16) that if Ψ is known as a function of (x, y), R and hence, by the use of the table, the velocity q can be found at any point in the stream.

Finally the author wishes to express his hearty thanks to Miss H. Tanaka and Miss Y. Tanaka for their assistance in the numerical work.

q	M	μ	$\frac{\rho}{\rho_0}$	$\frac{p}{p_0}$	$q\frac{\rho}{\rho_0}$
1.50	1.7321	1.4142	0.3088	0.1930	0.4632
51	1.7506	1.4369	3027	1876	4570
52	1.7695	1.4598	2965	1824	4507
53	1.7885	1.4828	2904	1771	4444
54	1.8078	1.5060	2844	1720	4380
55	1.8273	1.5294	2784	1669	4315
56	1.8471	1.5530	2724	1619	4249
57	1.8672	1.5768	2665	1570	4184
58	1.8875	1.6008	2606	1522	4117
59	1.9081	1.6251	2547	1474	4050
60	1.9290	1.6495	2489	1427	3982
1.61	1.9501	1.6742	2431	1381	3914
62	1.9716	1.6992	2374	1336	3846
63	1.9934	1.7244	2317	1291	3777
64	2.0155	1.7500	2261	1247	3708
65	2.0380	1.7758	2205	1204	3638
66	2.0608	1.8019	2150	1163	3569
67	2.0839	1.8283	2095	1121	3499
68	2.1074	1.8550	2041	1081	3429
69	2.1313	1.8821	1987	1041	3358
70	2.1555	1 9095	1934	1002	3288
1.71	2.1802	1.9373	1882	965	3218
72	2.2053	1.9655	1830	928	3148
73	2.2308	1.9941	1778	891	3076
74	2.2567	2.0231	1727	856	3005
75	2.2832	2.0525	1677	821	2935
76	2.3100	2.0824	1627	787	2864
77	2.3374	2.1127	1578	754	2793
78	2.3653	2.1435	1530	722	2723
79	2.3937	2.1749	1482	691	2653
80	2.4227	2.2067	1435	660	2853
1.81	2.4523	2.2391	1389	631	2514
82	2.4824	2.2721	1343	602	2444
83	2.5132	2.3057	1298	574	2375
84	2.5446	2.3399	1253	546	2306
85	2.5767	2.3747	1210	520	2239
86	2.6094	2.4102	1166	494	2169
87	2.6429	2.4465	1124	469	2102
88	2.6772	2.4834	1082	445	2034
89	2.7123	2.5212	1042	422	1969
90	2.7482	2.5598	1001	399	1902
1.91	2.7849	2.5992	962	377	1837
92	2.8226	2.6395	923	356	1772
93	2.8612	2.6807	885	336	1708
94	2.9008	2.7229	848	316	1645
95	2.9414	2.7662	812	297	1583
96	2.9832	2.8106	776	279	1521
97	3.0261	2.8560	741	262	1460
98	3.0702	2.9027	707	245	1400
99	3.1155	2.9507	674	229	1341
2.00	3.1623	3.0000	641	214	1282

q	M	μ	$\frac{\rho}{\rho_0}$	$\frac{p}{p_0}$	$q\frac{\rho}{\rho_0}$
2.00	3.1623	3.0000	0.0641	0.0214	0.1282
1	3.2104	3.0507	610	199	1226
2	3.2601	3.1030	579	185	1170
3	3.3114	3.1568	549	172	1114
4	3.3643	3.2123	520	159	1061
5	3.4190	3.2695	491	147	1007
6	3.4757	3.3287	464	136	956
7	3.5344	3.3899	437	125	905
8	3.5952	3.4533	411	115	855
9	3.6584	3.5190	386	105	807
10	3.7240	3.5872	361	96	758
2.11	3.7923	3.6580	338	87	713
12	3.8634	3.7317	315	79	668
13	3.9376	3.8085	294	72	626
14	4.0151	3.8886	273	65	584
15	4.0962	3.9722	253	58	544
16	4.1812	4.0598	233	52	503
17	4.2704	4.1516	215	46	467
18	4.3642	4.2481	197	41	429
19	4.4631	4.3496	180	36	394
20	4.5675	4.4567	164	32	361
2.21	4.6781	4.5699	149	28	329
22	4.7954	4.6900	135	24	300
23	4.9202	4.8175	121	21	270
24	5.0535	4.9536	108	18	242
25	5.1962	5.0991	97	15	218
26	5.3495	5.2552	85	13	192
27	5.5150	5.4236	75	11	170
28	5.6943	5.6059	65	9	148
29	5.8897	5.8041	56	7	128
30	6.1036	6.0211	48	6	110
2.31	6.3394	6.2601	41	5	95
32	6.6012	6.5250	34	3	79
33	6.8943	6.8214	28	3	65
34	7.2256	7.1561	23	2	54
35	7.6045	7.5385	18	1	42
36	8.0439	7.9815	14	1	33
37	8.5622	8.5036	10	1	24
38	9.1867	9.1321	7	0	17
39	9.9603	9.9100	5	0	12
40	10.9547	10.9090	3	0	7
2.41	12.3022	12.2614	2	0	5
42	14.2806	14.2455	1	0	2
43	17.6209	17.5925	0	0	0
44	25.3327	25.3129			

An Approximate Method of Calculating Compressible Fluid Flow Past a Thin Aerofoil.

By Isao Imai.

Department of Physics, Faculty of Science, University of Tokyo.

(Received April 15, 1948)

§ 1. Introduction.

As is well known, the uniform flow of a compressible fluid past a thin aerofoil of given shape can be successfully dealt with by the linear theory of Prandtl and Glauert, if the fluid velocity is everywhere well below the local velocity of sound. But, the theory gets less accurate as the critical Mach number is approached, at which the local velocity of sound is first attained by the fluid velocity at some point in the field of flow. Indeed, even the method of successive approximation, which has been developed by the present writer(2), starting with the Prandtl-Glauert theory as a first approximation, seems to be poorly convergent near the critical Mach number. On the other hand, the M^2-expansion method is obviously out of question for so high a Mach number as the critical in the case of a thin aerofoil. Also, the hodograph method is inadequate for the treatment of a profile of an arbitrarily given shape. It may be said that there is at present no available method of attack which gives us correct information concerning the flow conditions over a given aerofoil at or near the critical Mach number.

In view of this, we shall give, in the following, an approximate method of calculation, which is essentially a refinement of the Prandtl-Glauert approximation, and which is believed to give satisfactory results even near the critical Mach number.

§ 2. Fundamental Equations.

The two-dimensional irrotational motion of a compressible fluid is governed by the following equations. The condition for irrotational motion is

$$\frac{\partial u}{\partial y} = \frac{\partial v}{\partial x}, \tag{2.1}$$

where (u, v) are the component velocities at the point (x, y). The equation of continuity is

$$\frac{\partial}{\partial x}(\rho u) + \frac{\partial}{\partial y}(\rho v) = 0. \tag{2.2}$$

The density ρ is usually assumed to be a function of the pressure p only and is related to the resultant velocity q by Bernoulli's theorem:

$$q dq + dp/\rho = 0, \quad q = \sqrt{u^2+v^2}. \tag{2.3}$$

Now, (2.2) can also be written in the form:

$$\left(1-\frac{u^2}{c^2}\right)\frac{\partial u}{\partial x} + \left(1-\frac{v^2}{c^2}\right)\frac{\partial v}{\partial y} - \frac{uv}{c^2}\left(\frac{\partial u}{\partial y}+\frac{\partial v}{\partial x}\right) = 0, \tag{2.4}$$

where $c = \sqrt{dp/d\rho}$ is the local velocity of sound.

Let us consider a thin aerofoil set in a uniform flow which is parallel to the x-axis. It will be natural to suppose that the disturbance due to the presence of the aerofoil is so small that the component velocity v perpendicular to the undisturbed flow would be small everywhere in the field of flow. Thus, by substituting (2.1) and neglecting terms containing squares and higher powers of v, (2.4) reduces to

$$\left(1-\frac{u^2}{c^2}\right)\frac{\partial u}{\partial x} + \frac{\partial v}{\partial y} = 0. \tag{2.5}$$

Also, we may safely identify u with q, so that p, ρ, c may be regarded as functions of u only. Now, if we put

$$\mu = \sqrt{\left|1-\frac{u^2}{c^2}\right|}, \tag{2.6}$$

(2.1) and (2.5) become respectively

$$\frac{\mu \partial u}{\mu \partial y} = \frac{\partial v}{\partial x}, \quad \frac{\mu \partial u}{\partial x} = \mp \frac{\partial v}{\mu \partial y}, \tag{2.7}$$

where we have to use the upper or the lower sign according as $u < c$ or $u > c$, that is, the flow is subsonic or supersonic.

Let us now introduce the variables:

$$\int \mu\,du = \omega, \tag{2.8}$$

$$\xi = x, \quad \eta = \int \mu\,dy, \tag{2.9}$$

so that

$$\frac{\partial}{\partial x} = \frac{\partial}{\partial \xi} + \frac{\partial \eta}{\partial x}\frac{\partial}{\partial \eta}, \quad \frac{\partial}{\partial y} = \mu\frac{\partial}{\partial \eta}. \tag{2.10}$$

Now, remembering the assumption of small disturbance, it will readily be seen that $\partial\eta/\partial x$ is small, so that (2.7) reduce to

$$\frac{\partial \omega}{\partial \eta} = \frac{\partial v}{\partial \xi}, \quad \frac{\partial \omega}{\partial \xi} = \mp\frac{\partial v}{\partial \eta}, \tag{2.11}$$

which form the basis of our approximate method. In this paper we shall be solely concerned with the subsonic flow. Accordingly, we have only to deal with the Cauchy-Riemann equations, by taking the minus sign in (2.11).

§ 3. Procedure of Calculation.

Let the profile be given by the equation:

$$y = g(x), \tag{3.1}$$

where $g(x)$ is a two-valued function of small magnitude, whose two branches $g_1(x)$, $g_2(x)$ represent the upper and the lower surface respectively. Since μ has no physical significance inside the profile, we may define its value in an arbitrary manner, provided that $\partial\eta/\partial x$ should be small. Thus we may conveniently adopt either of the following definitions.

(a) Inside the profile: $g_2(x) < y < g_1(x)$, $\mu = 1$. Hence,

$$\eta = g(x) + \int_{g(x)}^{y} \mu\,dy, \tag{3.2}$$

so that $y = g(x)$ corresponds to $\eta = g(\xi)$. Thus the image profile in the $\xi\eta$-plane has the same shape as the original profile in the xy-plane.

(b) Inside the profile: $g_2(x) < y < g_1(x)$, $\mu = 0$. Hence

$$\eta = \int_{g(x)}^{y} \mu\,dy, \tag{3.3}$$

so that $y = g(x)$ corresponds to $\eta = 0$. Thus the image profile in the $\xi\eta$-plane is a flat plate lying on the ξ-axis.

The definition (b) has the great merit of being much simpler than the definition (a), but seems to be less accurate, in view of the fact that $\partial\eta/\partial x$ becomes large near the stagnation point.

Now our problem is to solve (2.11) with the following boundary conditions:

$$\left.\begin{array}{lll} \text{For} & y = g(x), & v = ug'(x). \\ \text{For} & (x, y) \to \infty, & u \to u_\infty, \; v \to 0. \end{array}\right\} \tag{3.4}$$

If we adopt the definition (a), these can be written, in the $\xi\eta$-plane as:

$$\left.\begin{array}{lll} \text{For} & \eta = g(\xi), & v = ug'(\xi). \\ \text{For} & (\xi, \eta) \to \infty, & \omega \to \omega_\infty, \; v \to 0, \end{array}\right\} \tag{3.5}$$

the suffix ∞ denoting the state in the undisturbed flow.

In the following we shall only deal with the subsonic flow. Then, it is obvious from (2.11), which are nothing but the Cauchy-Riemann equations for v, ω, that v and ω are harmonic functions conjugate to each other. Therefore, v and ω can, in principle, be determined, if the value of one of them, say v, is given on the boundary of the field of flow. In usual application, however, it is only required to find the velocity distribution on the surface of the aerofoil. For this purpose following procedures may be employed with success.

1. Determination of the analytic function which conformally maps the given aerofoil $y = g(x)$ on to a unit circle $Z = e^{i\theta}$ in the Z-plane. The profile will then be expressed as $x = x(\theta)$, $y = y(\theta)$, θ being the parameter. For such a calculation a numerical method due to the present writer(1)(5) seems to be convenient.

2. Assumption of plausible value of u on the surface.

3. Calculation of $v = ug'(x)$. It must be remembered that, in conformity with Joukowski's assumption, v should be put equal to zero at the trailing edge.

4. Calculation of $\omega(\theta)$. We have

$$\omega(\theta) = \omega_\infty - v^*(\theta), \tag{3.6}$$

where $v^*(\theta)$ is the conjugate Fourier series corresponding to $v(\theta)$, so that

$$v^*(\theta) = -\frac{1}{2\pi}\int_0^{2\pi} [v(\varphi+\theta) - v(\theta)] \cot\frac{\varphi}{2}\,d\varphi, \tag{3.7}$$

the numerical calculation of which may be effected, for instance, in the manner described in the writer's previous paper(4).

5. Determination of u from ω, by means of the numerical table of ω against u. The value of u thus found is a better approximation to the velocity on the surface.

The iterative process 3 to 5 should be repeated until the values are repeated sufficiently accurately.

If the undisturbed velocity is sufficiently high, supersonic region will appear. Strictly speaking, in such a case, the above procedure based upon the Cauchy-Riemann equations, (2.11) with the upper sign, will be invalidated. For an approximate calculation, however, the same procedure may be employed without serious error, provided that the local velocity of sound is only slightly exceeded by the fluid velocity. For, μ being then small, the second equation of (2.11) may be replaced by $\partial v/\partial \eta = 0$, and consequently the minus sign may be substituted for the plus sign.

Finally, a few words may be added concerning the relation of our method of approximation to that of Prandtl and Glauert. Their method is based on the assumption that the disturbance due to the presence of the aerofoil is small, so that not only the direction but also the magnitude of the velocity vector differ but little from those of the undisturbed flow. If we remember that we have, in this paper, only assumed the inclination to be small, it might be said that our method constitutes, in a sense, that is, with regard to the magnitude of the velocity, an infinitely high approximation of the method of thin-wing-expansion. Further, it is obvious that, on substituting μ by μ_∞, the value for the undisturbed flow, our approximation reduces to the Prandtl-Glauert approximation.

§ 4. Remarks concerning the Numerical Work.

In practical application of the above-mentioned procedure, the following remarks have been found of much use.

1. A first approximation to u may be obtained by the Prandtl-Glauert approximation. Thus, denoting by (u_0, v_0), the velocity at the surface for an incompressible fluid, we may conveniently use $u_\infty+\sqrt{1-M^2}(u_0-u_\infty)$ as a first approximation, M being the Mach number of the undisturbed flow.

2. Owing to the rapid variation in v near the leading and trailing edges, numerical calculation of v^* there cannot be made very accurately, This difficulty can be avoided by taking the following procedure. Remembering the relation $u_0 = u_\infty - v_0{}^*$, which ought to be exact for an incompressible fluid, we can write (3.6) in the form

$$\omega = u_0+(\omega-u_0) = u_0+\omega_\infty-u_\infty-(v-v_0)^*. \qquad (4.1)$$

Since $v-v_0$ is small, inaccuracies which may arise in the calculation of $(v-v_0)^*$ are expected to be small.

3. At each step of successive approximation we have $\omega_N = \omega_\infty - v_N{}^*$: Hence we can write

$$\omega_{N+1} = \omega_N-(v_{N+1}-v_N)^*. \qquad (4.2)$$

Since $v_{N+1}-v_N$ gets smaller as the iteration proceeds, numerical work becomes increasingly easier.

4. If u is already known for a Mach number M_1, we may take as a first approximation to ω, for a Mach number M_2,

$$\omega_1(M_2) = \omega_\infty(M_2)+\frac{u_\infty(M_2)}{u_\infty(M_1)}[\omega(M_1)-\omega_\infty(M_2)]. \qquad (4.3)$$

Then, on account of the equality:

$$\omega(M_1)-\omega_\infty(M_2) = -[v(M_1)]^* \doteq -[u(M_1)g']^*,$$

we have

$$\omega(M_2)-\omega_1(M_2)$$

$$= -\left[\left\{u(M_2)-\frac{u_\infty(M_2)}{u_\infty(M_1)}u(M_1)\right\}g'\right]^*. \qquad (4.4)$$

Since the right-hand side is in general small, numerical labour will be reduced considerably.

§ 5. Adiabatic Gas Flow.

So far we have made no specification of the functional relation between the pressure and the density. As is well known, when a gas is in steady motion the changes in density may, in general, be assumed to take place adiabatically, so that $p \backsim \rho^{-\gamma}$, γ being the ratio of the specific heats of the gas. In this case Bernoulli's theorem (2.3) gives

$$\frac{p}{p_0} = \left(1-\frac{\gamma-1}{2}\frac{q^2}{c_0{}^2}\right)^{\frac{\gamma}{\gamma-1}}, \qquad (5.1)$$

$$\frac{\rho}{\rho_0}=\left(1-\frac{\gamma-1}{2}\frac{q^2}{c_0^2}\right)^{\frac{1}{\gamma-1}}, \qquad (5.2)$$

$$c^2=\gamma\frac{p}{\rho}=c_0^2\left(1-\frac{\gamma-1}{2}\frac{q^2}{c_0^2}\right), \qquad (5.3)$$

where p_0, ρ_0, c_0 are respectively the pressure, density, and velocity of sound at the stagnation point: $q=0$. The critical velocity c_*, at which the velocity of the gas is coincident with that of sound, is readily obtained from (5.3) as

$$c_*=\sqrt{\frac{2}{\gamma+1}}\,c_0. \qquad (5.4)$$

If c_* is chosen as the unit of velocity, (5.1), (5.2), (5.3) become

$$\frac{p}{p_0}=(1-\alpha^2q^2)^{\frac{\gamma}{\gamma-1}}, \quad \frac{\rho}{\rho_0}=(1-\alpha^2q^2)^{\frac{1}{\gamma-1}}, \qquad (5.5,\ 6)$$

$$c^2=\frac{\gamma+1}{2}-\frac{\gamma-1}{2}q^2, \quad \alpha^2=\frac{\gamma-1}{\gamma+1}. \qquad (5.7)$$

Hence, remembering that q and u can be identified in our approximation, we have

$$\mu=\sqrt{\frac{1-u^2}{1-\alpha^2u^2}}, \qquad (5.8)$$

$$\omega=\int^u\mu\,du=\int_0^u\sqrt{\frac{1-u^2}{1-\alpha^2u^2}}\,du \qquad (5.9)$$

$$=\frac{1}{\alpha^2}\int_0^u\sqrt{\frac{1-\alpha^2u^2}{1-u^2}}\,du-\frac{1-\alpha^2}{\alpha^2}\int_0^u\frac{du}{\sqrt{(1-u^2)(1-\alpha^2u^2)}}$$

$$=\frac{1}{\alpha^2}E(u,\alpha)-\frac{1-\alpha^2}{\alpha^2}F(u,\alpha), \qquad (5.10)$$

where $F(u,\alpha)$ and $E(u,\alpha)$ are the elliptic integrals of the first and second kinds respectively.

Now, γ has the value 1.4 for air. For numerical calculation in the various problems concerning air flow, the writer(3) had already prepared the tables of p/p_0, ρ/ρ_0, q/c, μ against q, and therefore it was quite a simple matter to construct a table of ω against u, by making numerical integration (5.9) starting from $u=0$. The accuracy of the result was tested by comparing the value of ω for $u=1$ with that obtained by using (5.10); the agreement was found to be complete. The result is given in Table I.

§ 6. Application of the Method.

The above method has been applied to a number of profiles to calculate the distributions of the velocity and, hence, of the pressure on the surface. The result will be given here for two typical profiles only, an elliptic cylinder of thickness ratio 1/10 and an NACA 0015 aerofoil, each placed symmetrically in the air stream. Figs. 1 and 2 show the velocity distributions on the profiles for some values of Mach number. The part of the curve which corresponds to the supersonic state is shown by the broken line. The velocity distribution over the NACA 0015 at $M=0.65$, as calculated by the Prandtl-Glauert approximation is also included in Fig. 2 in order to compare with our result. It will be seen that the effect of compressibility makes its appearance more conspicuously in the region of maximum velocity, and that, with inceasing Mach number, the effect grows more and more rapidly as the critical Mach number is approached. These features seem to be in good agreement with reality, and moreover to be common to all commonly used aerofoils, but could not, of course, be predicted on the basis of the Prandtl-Glauert approximation. By using the electrolyte tank method, Taylor(7) has investigated the velocity distribution on the surface of an aerofoil of the generalized Joukowski type with thickness ratio 15%. He found that when $M=0.65$ the process of iteration converged rapidly and definite velocity distribution could be obtained, but that when $M=0.68$ the process yielded a divergent result. Since the profile is very similar to the NACA 0015, it will be interesting to compare the results with ours. It is true that for $M=0.65$ Taylor's result, which is also shown in Fig. 2, cannot be said to be in very good agreement with ours. However, the fact that his iterative process

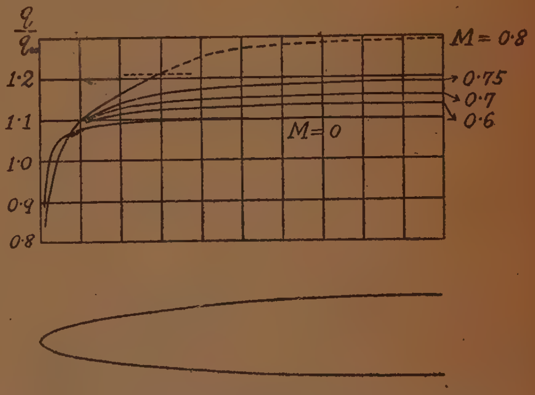

Fig. 1. Velocity distribution over an elliptic cylinder of 10% thickness.

Table I.

u	ω	u	ω	u	ω	u	ω	u	ω	u	ω
0.00	0.0000	0.50	0.4816	1.00	0.8029	1.50	1.2277	2.00	2.2777	0.950	0.7915
1	100	51	4904	1	8039	51	2410	1	3080	55	7932
2	200	52	4992	2	8058	52	2555	2	3387	60	7947
3	300	53	5079	3	8083	53	2702	3	3700	65	7962
4	400	54	5165	4	8112	54	2851	4	4019	70	7976
5	500	55	5251	5	8146	55	3003	5	4343	75	7988
6	600	56	5337	6	8183	56	3157	6	4673	80	8000
7	700	57	5421	7	8224	57	3314	7	5009	85	8010
8	799	58	5506	8	8268	58	3473	8	5351	90	8019
9	899	59	5589	9	8315	59	3634	9	5700	95	8025
10	999	60	5672	10	8365	60	3798	10	6055	1.000	8029
0.11	1098	0.61	5754	1.11	8417	1.61	3964	2.11	6417	5	8032
12	1198	62	5836	12	8473	62	4132	12	6787	10	8039
13	1297	63	5916	13	8531	63	4304	13	7164	15	8048
14	1396	64	5996	14	8591	64	4477	14	7548	20	8058
15	1495	65	6076	15	8654	65	4654	15	7941	25	8070
16	1594	66	6154	16	8720	66	4833	16	8343	30	8083
17	1693	67	6232	17	8788	67	5014	17	8753	35	8097
18	1792	68	6308	18	8858	68	5198	18	9173	40	8112
19	1890	69	6384	19	8931	69	5385	19	9603	45	8129
20	1989	70	6459	20	9006	70	5575	20	3.0044	50	0.8146
0.21	2087	0.71	6533	1.21	9083	1.71	5767	2.21	495		
22	2185	72	6606	22	9162	72	5962	22	958		
23	2283	73	6678	23	9244	73	6160	23	1433		
24	2381	74	6750	24	9328	74	6361	24	1922		
25	2478	75	6820	25	9414	75	6565	25	2424		
26	2575	76	6888	26	9502	76	6771	26	2942		
27	2672	77	6956	27	9593	77	6981	27	3476		
28	2769	78	7023	28	9685	78	7194	28	4027		
29	2865	79	7088	29	9780	79	7410	29	4597		
30	2962	80	7152	30	9877	80	7629	30	5188		
0.31	3058	0.81	7215	1.31	9976	1.81	7851	2.31	5802		
32	3153	82	7277	32	1.0077	82	8077	32	6441		
33	3249	83	7337	33	181	83	8306	33	7108		
34	3344	84	7395	34	286	84	8538	34	7807		
35	3439	85	7452	35	394	85	8774	35	8541		
36	3533	86	7508	36	504	86	9013	36	9316		
37	3627	87	7561	37	616	87	9256	37	4.0140		
38	3721	88	7613	38	730	88	9502	38	1021		
39	3815	89	7663	39	846	89	9753	39	1971		
40	3908	90	7711	40	964	90	2.0007	40	3010		
0.41	4000	0.91	7757	1.41	1085	1.91	264	2.41	4165		
42	4093	92	7800	42	1207	92	526	42	5483		
43	4185	93	7841	43	1332	93	792	43	4.7057		
44	4276	94	7880	44	1459	94	1063				
45	4367	95	7915	45	1588	95	1337				
46	4458	96	7947	46	1720	96	1616				
47	4548	97	7976	47	1853	97	1899				
48	4638	98	8000	48	1989	98	2187				
49	4727	99	8019	49	2127	99	2480				
0.50	0.4816	1.00	0.8029	1.50	1.2267	2.00	2.2777				

diverged for $M = 0.68$ seems to be in satisfactory agreement with our finding that the critical Mach number of the NACA 0015 aerofoil is slightly less than 0.675.

Further, it will be mentioned that Stanton(6) measured the pressure distribution round the same Joukowski profile of 0.8 inch chord in a small 3-inch high speed wind tunnel for some values of

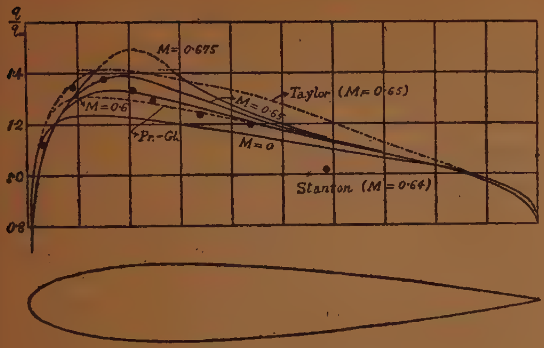

Fig. 2. Velocity distribution over an NACA 0015 aerofoil.

Mach number. His result for $M = 0.64$ is also included in Fig. 2. Considering the difficulty expected to be met with in such a delicate experiment, the agreement with our theoretical result may be regarded as fairly satisfactory.

§ 7. Summary.

In this paper, an approximate method is given for the calculation of a uniform flow of a compressible fluid past a thin aerofoil of arbitrary shape, on the assumption that the inclination of the velocity to the direction of the undisturbed flow is so small that its squares and higher powers may be neglected. Thus the method is essentially a refinement of the Prandtl-Glauert approximation, which, in addition to the above, makes the assumption that the magnitude of the velocity is only slightly different from that of the undisturbed flow.

The method has been successfully applied to a number of aerofoils, but the results are reported in this paper for only two profiles, that is, an elliptic cylinder of thickness ratio 10% and an NACA 0015 aerofoil. It has been found that the effect of compressibility is more pronounced in the region of minimum pressure, and that the effect grows more rapidly as the critical Mach number is approached. Further, for a commonly used aerofoil, the point of minimum pressure appears gradually to move downstream as the Mach number is increased.

This work was completed in 1944, but since has been left unpublished owing to the difficult conditions during and after the war. Meanwhile the writer has developed another new method of approximations for treating compressible fluid flow, which can be improved to allow application to thick profiles. Since comparison of the two methods seems to be of much interest, it has now been decided to report first the former method. The comparison will be made in a forthcoming paper.

In conclusion, I should like to express my hearty thanks to Miss H. Tanaka and Miss Y. Tanaka for their assistance in the numerical work.

References.

(1) Imai, I.: J. Soc. Aero. Sci. Nippon **9** (1942), 865.
(2) Imai, I.: Rep. Aeron. Res. Inst. Tokyo Imp. Univ., No. **294** (1944).
(3) Imai, I.: J. Phys. Soc. Japan, **3** (1948), 342.
(4) Imai, I. & Kawada, D.: Rep. Aeron. Res. Inst. Tokyo Imp. Univ., No. **325** (1945).
(5) Imai, I. & Satō, K.: J. Aeron. Res. Inst. Tokyo Imp. Univ., No. **247** (1945), 91.
(6) Stanton, T.E.: British A. R. C., R. & M., No. **1280** (1929).
(7) Taylor, G. I.: Proc. Fifth Volta Congress (1935), 198.

On a New Method of Approximation for Treating Compressible Fluid Flow.

By Isao IMAI.

Department of Physics, Faculty of Science, University of Tokyo.

(Received April 20, 1948)

§ 1. Introduction and Summary. In a previous paper(2) the present writer has given an approximate method of calculating compressible fluid flow past an arbitrary thin aerofoil, which is essentially a refinement of the Prandtl-Glauert linear theory. In the following will be given a new method of approximation, which is very similar in nature to the previous method, but requires considerably less numerical work in actual application. The method is based on the assumption that the flow is nearly parallel and thus the angle of inclination between the velocity vector and the direction of the undisturbed uniform flow is so small that its squares and higher powers may be safely neglected. By applying the method we calculate the velocity distribution round an NACA 0015 aerofoil and a symmetrical Joukowski aerofoil of thickness 11.7 % placed symmetrically in a uniform flow for various Mach numbers.

Finally comparison is made between the present and the previous methods.

§ 2. Fundamental Equations. Let us consider a two-dimensional irrotational flow of a non-viscous compressible fluid in the xy-plane. Then the conditions of continuity and irrotationality are respectively expressed in the form

$$\frac{\partial}{\partial x}(\rho u)+\frac{\partial}{\partial y}(\rho v)=0, \tag{2.1}$$

$$\frac{\partial u}{\partial y}-\frac{\partial v}{\partial x}=0, \tag{2.2}$$

where u, v are the component velocities and ρ is the density of the fluid. If we put

$$u=q\cos\theta,\quad v=q\sin\theta, \tag{2.3}$$

where q is the magnitude of the velocity and θ the angle between the x-axis and the velocity vector, (2.1) and (2.2) can be written as

$$\frac{\partial\theta}{\partial x}=\frac{\partial}{\partial y}\log q+\frac{1}{\rho}\frac{\partial\rho}{\partial x}\sin\theta\cos\theta+\frac{1}{\rho}\frac{\partial\rho}{\partial y}\sin^2\theta, \tag{2.4}$$

$$\frac{\partial\theta}{\partial y}=-\frac{\partial}{\partial x}\log(\rho q)-\frac{1}{\rho}\frac{\partial\rho}{\partial y}\sin\theta\cos\theta+\frac{1}{\rho}\frac{\partial\rho}{\partial x}\sin^2\theta. \tag{2.5}$$

For an incompressible fluid, (2.4) and (2.5) reduce respectively to

$$\frac{\partial\theta}{\partial x}=\frac{\partial}{\partial y}\log q,\quad \frac{\partial\theta}{\partial y}=-\frac{\partial}{\partial x}\log q, \tag{2.6}$$

which show that $\theta+i\log q$ is an analytic function of $x+iy$.

For a compressible fluid Bernoulli's theorem can be written in the differential form as

$$q\,dq+dp/\rho=0, \tag{2.7}$$

where the pressure, p, may, in general, be assumed to be a known function of the density, ρ, only. Thus (2.4), (2.5) can be regarded as a system of non-linear partial differential equations for q, θ with x, y as independent variables.

We now assume that the flow is nearly parallel to the x-axis, so that θ may be taken to be small everywhere in the field of flow. Then (2.4) and (2.5) may be approximated by

$$\frac{\partial\theta}{\partial x}=\frac{\partial}{\partial y}\log q,\quad \frac{\partial\theta}{\partial y}=-\frac{\partial}{\partial x}\log(\rho q). \tag{2.8}$$

On account of (2.7), we have

$$\begin{aligned}\frac{d\log(\rho q)}{d\log q}&=1+\frac{q}{\rho}\frac{d\rho}{dp}\frac{dp}{dq}\\&=1-q^2/c^2\equiv\mu^2,\end{aligned} \tag{2.9}$$

where $c=(dp/d\rho)^{1/2}$ is the local velocity of sound. Hence (2.8) become

$$\frac{\partial\theta}{\partial x}=\frac{\mu\partial(\log q)}{\mu\partial y},\quad \frac{\partial\theta}{\mu\partial y}=-\frac{\mu\partial(\log q)}{\partial x}. \tag{2.10}$$

Let us put

$$\tau = \int \mu d(\log q) = \int \mu q^{-1} dq, \qquad (2.11)$$

$$\xi = x, \quad \eta = \int \mu dy. \qquad (2.12)$$

Then we have

$$\frac{\partial}{\partial x} = \frac{\partial}{\partial \xi} + \frac{\partial \eta}{\partial x}\frac{\partial}{\partial \eta}, \quad \frac{\partial}{\partial y} = \mu \frac{\partial}{\partial \eta}, \qquad (2.13)$$

and hence (2.10) become

$$\frac{\partial \theta}{\partial \xi} - \frac{\partial \tau}{\partial \eta} = -\frac{\partial \eta}{\partial x}\frac{\partial \theta}{\partial \eta}, \quad \frac{\partial \theta}{\partial \eta} + \frac{\partial \tau}{\partial \xi} = -\frac{\partial \eta}{\partial x}\frac{\partial \tau}{\partial \eta}. \qquad (2.14)$$

From the assumption of nearly parallel flow, it may readily be inferred that $\partial\eta/\partial x$ would be small, so that we may further reduce (2.14) to the Cauchy-Riemann equations:

$$\frac{\partial \theta}{\partial \xi} = \frac{\partial \tau}{\partial \eta}, \quad \frac{\partial \theta}{\partial \eta} = -\frac{\partial \tau}{\partial \xi}, \qquad (2.15)$$

which form the basis of our approximate method.

Here we have assumed that the flow is everywhere subsonic, so that μ is real. If a supersonic region appears somewhere in the field of flow, we may proceed just as in the previous method in similar occasion. Thus (2.11), (2.12) and (2.15) should be replaced by

$$\tau = \int |\mu| q^{-1} dq, \quad \eta = \int |\mu| dy;$$

$$\partial\theta/\partial\xi = \partial\tau/\partial\eta, \quad \partial\theta/\partial\eta = \partial\tau/\partial\xi$$

respectively. But, as long as the local velocity of sound is only slightly exceeded by the fluid velocity, we may apply, without serious error, the following approximate method, which is strictly valid for purely subsonic flow only.

§ 3. Procedure of Calculation.

Let us consider a uniform flow past a thin profile at a small angle of attack. The profile may be given by the equation:

$$y = g(x), \qquad (3.1)$$

where $g(x)$ is a two-valued function of small magnitude, $g_1(x)$ and $g_2(x)$ giving the upper and lower surfaces of the profile respectively.

For convenience, let us define the value of μ as 1 inside the profile, though it has naturally no physical significance there. Then (2.12) can be written as

$$\eta = g(x) + \int_{g(x)}^{y} \mu dy, \qquad (3.2)$$

whence $\partial\eta/\partial x$ may be readily shown to be small.

Now the boundary conditions are clearly:

$$\left.\begin{array}{ll} \text{For } y = g(x): & \theta = \tan^{-1} g'(x) \equiv \theta_0(x). \\ \text{For } (x, y) \to \infty: & \theta \to 0, \; q \to q_\infty. \end{array}\right\} \qquad (3.3)$$

In terms of the variables ξ, η, these become

$$\left.\begin{array}{ll} \text{For } \eta = g(\xi): & \theta = \theta_0(\xi). \\ \text{For } (\xi, \eta) \to \infty: & \theta \to 0, \; Q \to Q_\infty, \end{array}\right\} \qquad (3.4)$$

where Q is a certain fixed function of q defined by

$$Q = Ce^{\tau} \quad \text{i.e.} \quad \tau = \log Q + \text{const}, \qquad (3.5)$$

C being a certain constant.

The flow of an incompressible fluid past a profile can be exactly dealt with by solving the equations (2.6) with the boundary conditions (3.3), while the flow of a compressible fluid may be approximately given by the equations (2.15) together with the boundary conditions (3.4). But it will readily be seen that the two problems are exactly the same in form, the quantities x, y, q in the former problem being replaced respectively by ξ, η, Q in the latter. Thus we may say that the compressible flow in the physical xy-plane corresponds to the incompressible fluid flow in the $\xi\eta$-plane, the magnitude and inclination of the velocity vector being (q, θ) in the xy-plane and (Q, θ) in the $\xi\eta$-plane. Hence, in order to calculate the field of compressible fluid flow past any arbitrary profile in the xy-plane, we may proceed as follows. Given the undisturbed velocity q_∞, we first find $Q_\infty = Q(q_\infty)$, by using the numerical table of the function $Q(q)$. Then we calculate, in the $\xi\eta$-plane, the flow of incompressible fluid past the same profile for the undisturbed velocity Q_∞, values of (Q, θ) at any point (ξ, η) being thus found. Finally, to return to the xy-plane, use may be made of the relations (2.12):

$$x = \xi, \quad y = \int_0^{\eta} \mu^{-1} d\eta, \qquad (3.6)$$

and of the numerical table of the function $Q(q)$. Thus the velocity (q, θ) at any point (x, y) will be completely determined.

Usually we require only the velocity distribution on the surface of the body. Then the necessary calculation becomes a very simple matter, since the result can be obtained without recourse to the numerical integration (3.6). In fact, we can even construct a numerical table giving the values of the velocity (or the pressure) at any point on the profile as a function of the Mach number, irrespective of the shape of the profile.

It should be added, however, that the above considerations are wholly based upon the assumption of nearly parallel flow, so that deviations from the facts may occur for thick profiles such as a circular cylinder.

§ 4. Adiabatic Gas Flow.

We are, in general, concerned with the flow of gas obeying the adiabatic law:

$$p \backsim \rho^{\gamma}, \tag{4.1}$$

As is well known, we have, in this case,

$$\frac{p}{p_0} = \left(1-\frac{\gamma-1}{2}\frac{q^2}{c_0^2}\right)^{\frac{\gamma}{\gamma-1}}, \tag{4.2}$$

$$\frac{\rho}{\rho_0} = \left(1-\frac{\gamma-1}{2}\frac{q^2}{c_0^2}\right)^{\frac{1}{\gamma-1}}, \tag{4.3}$$

$$c^2 = \gamma\frac{p}{\rho} = c_0^2\left(1-\frac{\gamma-1}{2}\frac{q^2}{c_0^2}\right), \tag{4.4}$$

where γ is the ratio of the specific heats and p_0, ρ_0, c_0 are respectively the pressure, the density, and the velocity of sound at the stagnation point $q=0$. The critical velocity, c_*, at which the velocity of fluid is equal to the local velocity of sound, is immediately obtained from (4.4) as

$$c_* = \left(\frac{2}{\gamma+1}\right)^{\frac{1}{2}} c_0. \tag{4.5}$$

For convenience, we shall take c_* as the unit of velocity. Then (4.2), (4.3), (4.4) become

$$\frac{p}{p_0} = (1-a^2q^2)^{\frac{\gamma}{\gamma-1}}, \quad \frac{\rho}{\rho_0} = (1-a^2q^2)^{\frac{1}{\gamma-1}}, \tag{4.6, 7}$$

$$c^2 = \frac{\gamma+1}{2}-\frac{\gamma-1}{2}q^2, \quad a^2 = \frac{\gamma-1}{\gamma+1}. \tag{4.8}$$

Hence we have

$$\mu = \left(1-\frac{q^2}{c^2}\right)^{\frac{1}{2}} = \left(\frac{1-q^2}{1-a^2q^2}\right)^{\frac{1}{2}}. \tag{4.9}$$

Putting this into (2.11) and integrating, we have

$$\tau = \frac{1}{2a}\log\frac{1+a\mu}{1-a\mu}-\frac{1}{2}\log\frac{1+\mu}{1-\mu}, \tag{4.10}$$

and

$$Q = Ce^{\tau} = C\left(\frac{1+a\mu}{1-a\mu}\right)^{\frac{1}{2a}}\left(\frac{1-\mu}{1+\mu}\right)^{\frac{1}{2}}$$

Table I.

q	Q	q	Q	q	Q	q	Q	q	Q
0.00	0.0000	0.20	0.1983	0.40	0.3865	0.60	0.5535	0.80	0.6856
1	100	21	2081	41	3954	61	5610	81	6910
2	200	22	2178	42	4043	62	5685	82	6962
3	300	23	2275	43	4132	63	5759	83	7013
4	400	24	2371	44	4220	64	5832	84	7063
5	500	25	2467	45	4307	65	5904	85	7111
6	600	26	2563	46	4393	66	5975	86	7157
7	699	27	2659	47	4479	67	6045	87	7201
8	799	28	2754	48	4565	68	6114	88	7244
9	899	29	2849	49	4650	69	6182	89	7285
10	998	30	2943	50	4734	70	6249	90	7324
0.11	1097	0.31	3037	0.51	4817	0.71	6315	0.91	7361
12	1196	32	3131	52	4900	72	6380	92	7396
13	1295	33	3224	53	4982	73	6444	93	7429
14	1394	34	3317	54	5063	74	6506	94	7460
15	1493	35	3410	55	5144	75	6568	95	7488
16	1591	36	3502	56	5223	76	6628	96	7513
17	1690	37	3593	57	5302	77	6687	97	7535
18	1788	38	3684	58	5381	78	6745	98	7554
19	1886	39	3775	59	5458	79	6801	99	7569
0.20	0.1983	0.40	0.3365	0.60	0.5535	0.80	0.6856	1.00	0.7576

$$= Cq(1-\alpha^2q^2)^{\frac{1-\alpha}{2\alpha}}(1+\alpha\mu)^{\frac{1}{\alpha}}(1+\mu)^{-1}, \qquad (4.11)$$

where C is an arbitrary constant. C can be conveniently determined by the requirement that $Q \to q$ as $q \to 0$. Thus

$$C = 2(1+\alpha)^{-1/\alpha}. \qquad (4.12)$$

Taking $\gamma = 1.4$ for air, we have constructed a numerical table of Q against q, which is given below.

§ 5. Numerical Examples. In illustrations of the application of the method, we have calculated, for some Mach numbers, the velocity distributions round an NACA 0015 aerofoil and symmetrical Joukowski aerofoil with $\varepsilon = 0.1$ (corresponding roughly to the thickness ratio 11.7 %), which are placed symmetrically in a uniform flow. Calculations have been carried out only for the subsonic region, where $q < 1$ and hence μ is real. The result for the NACA 0015 is shown in Fig. 1, where for comparison the result obtained by the use of the previous method is also shown by dotted lines. Fig. 2 gives the result for the Joukowski aerofoil. In both figures the horizontal dotted lines indicate the critical state $q = 1$, where the local velocity of sound coincides with the fluid velocity. It will be seen that the effect of compressibility is more pronounced in the region of maximum velocity and that the effect grows increasingly rapidly as the critical Mach number is approached. These features were also borne out by the previous method⁽²⁾.

The subsonic flow of a compressible fluid past a symmetrical Joukowski aerofoil has been investigated by Kaplan⁽³⁾ and by Tomotika and Umemoto⁽⁴⁾, by the use of Poggi's method. Thus the latter authors have obtained analytical expression, correct to the order of M^2, for the velocity distribution round the aerofoil; Kaplan's result involves unfortunately a slight error. Also the present author has dealt with the flow past general Joukowski aerofoils by employing the method of thin-wing-expansion developed by himself⁽¹⁾ and obtained various formulae which are essentially the second approximation starting from the Prandtl-Glauert linear theory. Velocity distributions for $M = 0.6$ calculated by the use of these analytical expressions are also shown in Fig. 2 by dotted lines. The result obtained by Poggi's method is less satisfactory than that by the method of thin-wing-expansion, as should naturally be expected. Moreover, it seems that near the critical Mach number the present approximate method would provide more satisfactory result than the method of thin-wing-expansion, in spite of its far less numerical labour.

§ 6. Comparison with the Previous Method. Now comparison will be made between the present and the previous approximate methods. Both methods are essentially the same in principle, but numerical labour is considerably less with the present method. Indeed, the velocity and hence the pressure on the surface of the aerofoil at any Mach number can be immediately calculated from an incompressible flow with the aid of a numerical table, irrespective of the shape of the aerofoil. It will be seen in Fig. 1 that the numerical results by the two methods are in very good agreement except for the region of maximum velocity.

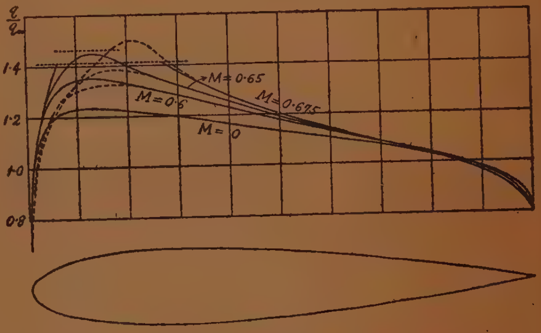

Fig. 1. Velocity distribution over NACA 0015 aerofoil.

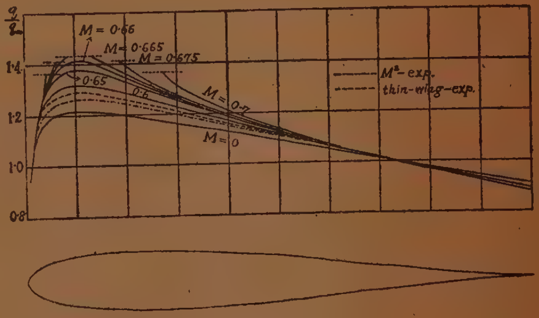

Fig. 2. Velocity distribution over symmetrical Joukowski aerofoil $\varepsilon = 0.1$.

According to the present method, however, the point of maximum velocity on the aerofoil is fixed when the Mach number is increased, though, in reality, more or less movement of the point seems to take place with increasing Mach number, as could be predicted by the previous method. Thus it would appear that the previous method presents better approximation to the reality than the present method. Presumably the reason may be found in the following fact.

(2.1) can be written in the form:

$$(c^2-u^2)\partial u/\partial x+(c^2-v^2)\partial v/\partial y-2uv\,\partial v/\partial x=0, \quad (5.1)$$

where (u, v) are the component velocities. The approximate nature of the previous method is due solely to neglect of $v^2\partial v/\partial y$ and $2uv\,\partial v/\partial x$ in (6.1), while that of the present mefhod is due to neglect of four terms in (2.4) and (2.5). Considering the order of magnitude of the neglected terms the above conclusion might perhaps be drawn.

However, from the theoretical point of view, the present method is preferable, since it permits of natural generalization to thick profiles. Indeed, the writer has recently developed a new method of dealing with the flow of a compressible fluid by applying the W.K.B. method, which is well known in quantum mechanics, and it has turned out that the present method of approximation is nothing but a limiting case, for thin aerofoils, of the general theory. This general theory based on the W.K.B. method as well as its application will be reported in the near future.

References.

(1) Imai, I.: Rep. Aeron. Res. Inst., Tokyo Imp. Univ., No. **294** (1944).

(2) Imai, I.: J. Phys. Soc. Japan **3** (1948), 346.

(3) Kaplan, C.: NACA Tech. Rep., No. **621** (1938).

(4) Tomotika, S. & Umemoto, H.: Rep. Aeron. Res. Inst., Tokyo Imp. Univ., No. **205** (1941).

On the Effect of Oxygen upon the Oxide-Coated Cathode.

Tetsuya ARIZUMI and Shin-ichiro NARITA.

Kawanishi Machine Works, Ltd., Kobe.

(Received April 5, 1948).

§ 1. Introduction.

The effect of the oxygen atmosphere upon thermionic emission from the oxide-coated cathode was studied by Kawamura,⑴ who has shown that the following relation holds between the emission current i and the partial pressure of oxygen p:

$$i=\alpha p^{-\frac{1}{m}} \quad (1)$$

where α and m are constants, depending upon the activated state of the cathode and the value of m ranges from 2.3 to 4.5. According to the theory of semi-conductor, it is concluded that m is equal to 4 in the best activated state, while it is equal to 2 in the unactivated state, in qualitative agreement with Kawamura's results. We repeated the similar experiments for the quantitative discussion on the theory and found new phenomena, described in the following paragraph.

§ 2. Procedure and Results.

All experiments were carried out in sealed-off tubes, shown schematically in Fig. 1. Three tubes A, B and C are operated as a diode for measuring the emission current, an ionization gauge and a pressure controlling chamber, including both an oxygen source and a batrum getter, respectively. The cathode of the diode is indirectly heated and the anode is divided into three parts, only one of which is used for the measurement of the emission current and the outside two are auxiliary electrodes, which are supplied with the same potential as the central anode (100V D. C.). The cathode temperature was measured by a thermocouple of the cathode nickel core and a tungsten wire of about

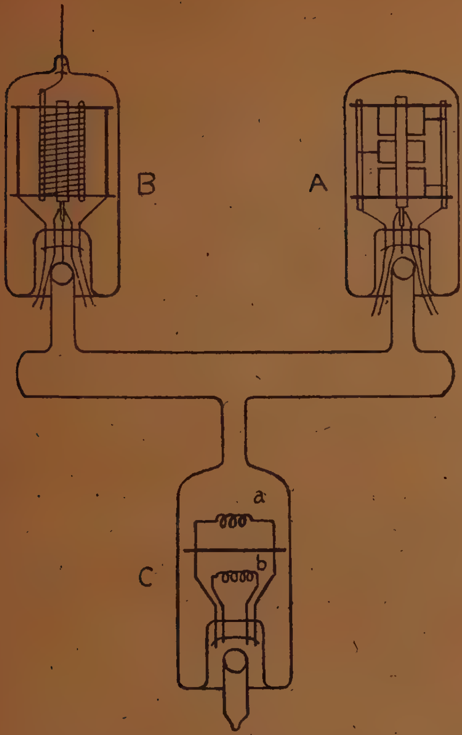

Fig. 1. Experimental tube
A : diode for measuring emission.
B : ionization gauge.
C : gas chamber. a : gas source
b : batrum getter

1 mm, welded to it. Both the thermo-couple and the ionization gauge were calibrated in advance of the measurements.

As the oxygen source, the following chemical reaction was utilized:

$$2CuO \rightarrow Cu_2O + O_2$$

A small amount of cupric oxide, inserted into a small tungsten coil is dissociated to increase the oxygen pressure by heating the coil electrically. To decrease the pressure, a proper amount of batrum getter is flashed. These procedures were very effective for the control of the partial pressure of oxygen.

Total tube was evacuated by a three stage oil diffusion pump, backed by a Cenco-type Megavac rotary pump. After the glass part was baked, all metal parts have been treated by H. F. and then a slight amount of getter had been flashed, the tube tipped off.

Free barium atoms, as impurity in the oxide-coated cathode, become to be contained through the dissociation,

$$2BaO \leftrightarrows 2Ba + O_2, \tag{2}$$

on account of which the amount of barium atoms depends upon the partial pressure of oxygen. However, it takes more or less long time to reach the equilibrium: Each point of the experimental results, shown in Fig. 2, was obtained after the equilibrium was established at the corresponding state. Fig. 2 shows that each curve in the log i vs. log p diagram is composed of two straight lines and each straiget part is nearly parallel to each other, differing from Kawamura's results.

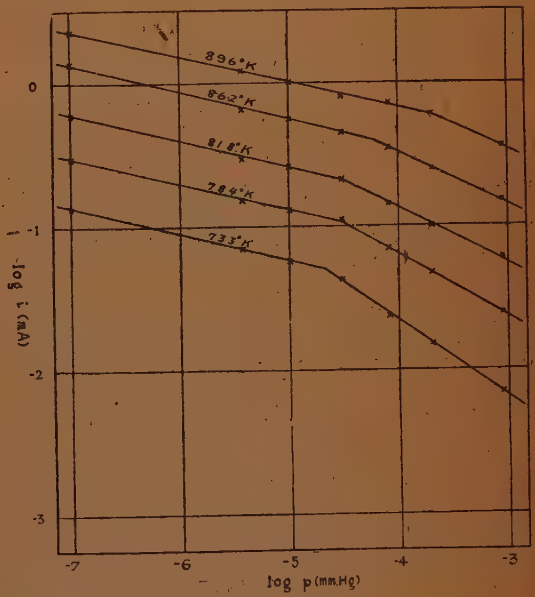

Fig. 2. The relation between emission and partial pressure of oxygen.

The values of m for two straight parts are approximately 5.5–6.0 and 2.0–3.0 respectively. The kink point of the curve moves to the higher pressure as the cathode temperature becomes higher.

For determining the work function, however, the above-mentioned procedure is inadequate, in which case the emission was measured in the following way. Usually the cathode is held at the higher constant temperature and only at the moment of measuring the emission current, the temperature of the cathode is lowered down rapidly to a definite temperature, at which the measurement is carried out. The Richardson diagram,

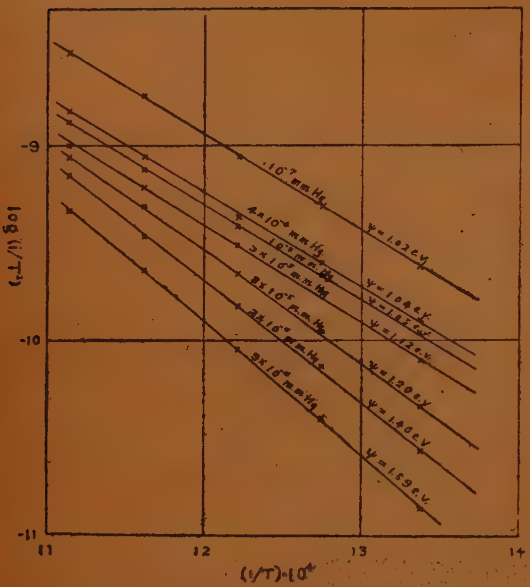

Fig. 3. The Richardson diagram.

shown in Fig. 3 were obtained by means of such procedure. If the partial pressure of oxygen is less than 10^{-7} m.m Hg, the Richardson line is straight and the work function is equal to about 1.0 e.v., but the Richardson lines become to be curved and the work function becomes the larger, as the oxygen pressure increases.

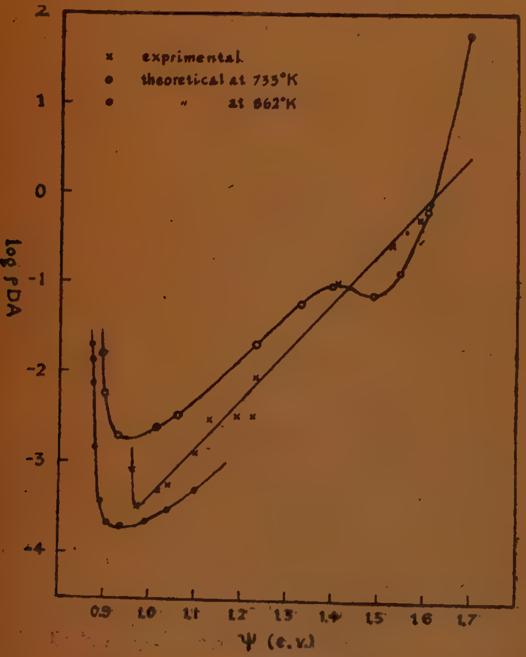

Fig. 4. The relation between Richardson constant and work function.

From these several diagrams, the relation between the work functions and the Richardson constants as shown in Fig. 4 is obtained. The logarithmic value of the Richardson constant decreases slightly at first and after passing through a minimum, it increases almost linearly with the increases of the work function.

§ 3. Discussion.

According to Nijboer's theory⁽²⁾ on semi-conductor, the number of conduction electrons, n is given by.

$$\frac{n(n+N)}{n_0-n}=\left(\frac{2\pi mkT}{h^2}\right)^{\frac{3}{2}}\exp\left(-\frac{eE}{kT}\right), \qquad (3)$$

where n_0 is the number of impurity levels, N that of "frozen-in" holes and the other notations are those customarily used. The thermionic emission of the semi-conductor is then written by

$$i=ne\rho D\left(\frac{kT}{2\pi m}\right)^{\frac{1}{2}}\exp\left(-\frac{e\phi}{kT}\right), \qquad (4)$$

where ρ is the roughness factor and D is transmission coefficient. If the relation $n \gg N$ holds, (4) becomes

$$i=D_1A_1n_0^{\frac{1}{2}}T^{\frac{5}{4}}\exp\left\{-\frac{e}{kT}\left(\frac{E}{2}+\phi\right)\right\}, \qquad (5)$$

which is also deduced from wilson's theory⁽³⁾ on the semi-conductor. On the other hand, if n is much less than N, (4) becomes

$$i=D_2A_2n_0T^2\exp\left\{-\frac{e}{kT}(E+\phi)\right\}. \qquad (6)$$

As the relation

$$n_0=Kp^{-\frac{1}{2}} \qquad (7)$$

holds due to the chemical equilibrium (2), (5) and (6) becomes

$$i=C_1p^{-\frac{1}{4}}\exp\left\{-\frac{e}{kT}\left(\frac{E}{2}+\phi\right)\right\} \qquad (8)$$

or

$$i=C_2p^{-\frac{1}{2}}\exp\left\{-\frac{e}{kT}(E+\phi)\right\} \qquad (9)$$

respectively, showing that in the unactivated state ($n \ll N$), where the oxygen pressure is large, the therminonic emission is proportional to $-1/2$ power

Table I.

Temperature (°K)	783	784	818	862	896
log N (cal. by (10))	11.72	12.03	12.25	12.49	12.67
log ρDN (cal. by (11))	9.97	10.09	10.31	10.54	10.61
log ρD	−1.73	−1.94	−1.94	−1.95	−2.06

of the pressure, while in the activated state ($n > N$), where the oxygen pressure is low, it is proportional to −1/4 power of its pressure. These theoretical predictions are in good agreement with the experimental results, described in the preceding paragraph.

Now we shall proceed to discuss quantitatively the theoretical expressions. The experimental fact that log i vs. log p curves are composed of two straight lines, shows that the emission formula (8) valid for $n > H$ holds in the region of the low pressure, while the formula (9) for $n < N$, holds for the higher pressure of oxygen, and accordingly n should become equal to N near the kink of the log i vs log p curves. Thus, the following expressions are obtained from (3) and (4) respectively, at these kink points:

$$\frac{2N^2}{n_0 - N} = \left(\frac{2\pi mkT}{h^2}\right)^{\frac{3}{2}} \exp\left(-\frac{eE}{kT}\right) \qquad (10)$$

and

$$i_c = Ne\rho D\left(\frac{kT}{2\pi m}\right)^{\frac{1}{2}} \exp\left(-\frac{e\phi}{kT}\right) \qquad (11)$$

where i_c is the emission current at the kink point. E and ϕ are found experimentally by Kawamura(4) to be 1.4 e.v. and 0.3 e.v. respectively and his recent work(5) shows that n_0 is of the order of 10^{16} at the best activated state. Accordingly it may well be assumed that n_0 is of the order of 10^{14} at the kink point. Thus N and ρDN can be evaluated by (10) and (11), the results of which are shown in Table I. As seen in the table, the values of N calculated by (10) and (11) individually coincide with each other, when ρD is assumed to be equal to 10^{-2}* and thus N is confirmed to be of the order of 10^{12}. Precisely speaking, N seems to increase slightly with the cathode temperature, but in the following calculation, it is assumed to be a constant, 10^{12}, for brevity.

Fig. 5 shows the Richardson diagram, plotted by making use of the calculated results and Fig. 6 the relation between log i and log p. If the equilibrium constant of the chemical reaction (2) is known, the values of n_0 corresponding to p are decided uniquely, but, to our regret, the exact value of the equilibrium constant has not been known up to the present. Thus, the correspondence of both quantities is selected to give the best fitting with the experimental results, that is to say, $n_0 = 10^{13}$ corresponding to $p = 10^{-7}$ mmHg, showing that the equilibrium constant (1/k) is equal to 6.5×10^{-28}. Although the inclinations of theoretical curves of log i vs log p are slightly larger than those of the experimental curves, the agreement of the theory with the experimental results seems to be rather satisfactory in both the Richard-

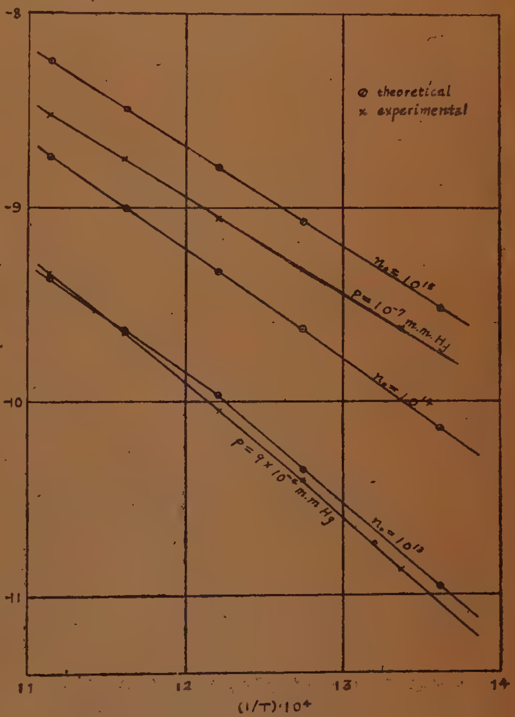

Fig. 5. Theoretical Richardson lines.

---

* Such small value of ρD is probably due to the patch effect. (See the reference (6)).

son diagram and the log i vs. log p curves.

The work function and the Richardson constant, obtained in the experiments are no other than the apparent values defined in the following equations.

$$\Psi = -\frac{k}{e}\frac{\partial\left(\log\frac{i}{T^2}\right)}{\partial\left(\frac{1}{T}\right)}, \tag{12}$$

and

$$\log \rho DA = \log\left(\frac{i_0}{T_0^2}\right)_e + \frac{e}{kT_0}(\Psi)_{T=T_0}, \tag{13}$$

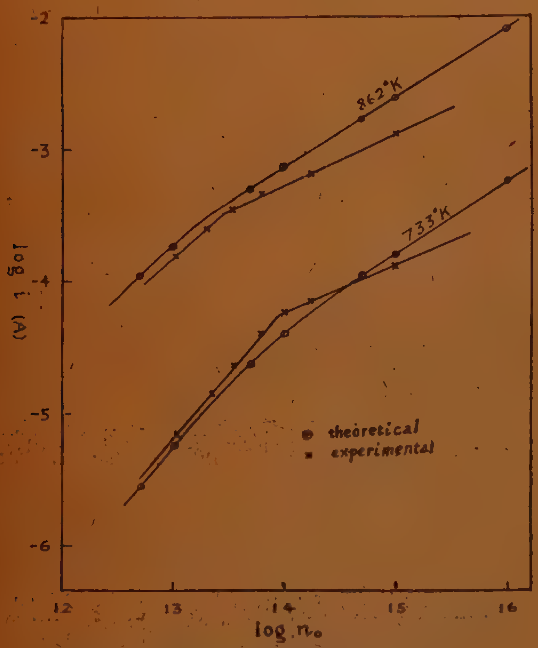

Fig. 6. Theoretical curves of log i vs. log n_0

where i_0 is the emission current at the cathode temperature T_0. As n_0 and N are assumed to be constants at a definite temperature, Ψ is expressed by

$$\Psi = \frac{3}{2}\frac{kT}{e} - \phi - \frac{\frac{3}{2}\frac{kT}{e}+E}{1+\frac{n}{N+n}+\frac{n}{n_0-n}}, \tag{14}$$

making use of (3) and (4). Theoretical values of log A (assuming $\rho D = 10^{-2}$) are also shown in Fig. 4 against work function, calculated by (14). The theoretical value of the work function at the best activated state is about 0.9 e. v., which is caused by plotting log (i/T²) instead of the exact expression of log (i/T$^{5/4}$). Although the theoretical curve shows a slightly anomalous behaviour, both the inclination and the absolute value of log A are in good agreemtnt with the experimental results.

§ 4. Conclusion.

In this paper, the effect of the oxygen atmosphere upon the thermionic emission from the oxide-coated cathode was studied experimentally, which results are summarized as follows.

(1) log i vs log p curves are composed of two straight lines.

and

(2) the Richardson line is a straight line at the lower pressure of oxygen, while it becomes curved as the pressure increases.

These experimental results have been shown to be quite well understood by the emission formula, deduced from Nijboer's theory on the semi-conductor, when ρD (roughness factor × transmission coefficient) is assumed to be equal to 10^{-2}. However, whether N and D are constants independent of both temperature and activated state of the cathode or not seems to be a future problem to be investigated.

References.

(1) H. Kawamura: Sugaku-Butsuri Gakkai-shi (in Japanese) **17**. (1943) 505.
(2) B. R. A. Nijboer: Proc. Phys. Soc., **51**, (1937) 575.
(3) A. H. Wilson: Proc. Roy. Soc., (A) **133** (1931) 458.
(4) E. Nishibori & H. Kawamura: Proc. Phys-Math. Soc. Japan. **22** (1940) 378.
(5) H. Kawamura: Lecture on Phys. Soc. Japan (1947).
(6) T. Arizumi: J. Phys. Soc. Japan **3** (1948) 191.

SHORT NOTE

On the low Pressure Gas Flow Conductance of a Tube Containing Vapors.

By Hiroo KUMAGAI, Kazuo YAMADA, Kenzo IWANAGA and Hideo SHIBATA.

Institute of Science and Technology, University of Tokyo.

(Received: July, 30, 1948).

The general definition of the speed of a vacuum pump was introduced by Langmuir⁽¹⁾ as follows:

$$S = -V\frac{dp}{(p-p_0)dt} \qquad (1)$$

where p_0 is the lowest pressure attainable by the pump and V the volume to be evacuated. The actual speed of the pump depends not only upon its design but also upon the conductance of the tubes connecting the pump and the vessel. Let S denote the speed of the pumping system, S_0 the speed of the pump itself and G_t the conductance of the tubes, then

$$\frac{1}{S} = \frac{1}{S_0} + \frac{1}{G_t}. \qquad (2)$$

By Knudson⁽²⁾, G_t is as follows;

$$G_t = G_0\bar{p} - G_k\frac{1+c_1\bar{p}}{1+c_2\bar{p}},$$

and at low pressure, $G_t = G_k$,

We measured the speed of the Cenco Rotary two-stage pump and the results are shown Fig. 1. In Fig. 1 (a), the curve I was obtained at room temperature with rotary pump oil A and the curve II with machine oil. In Fig. 1 (b), the curves I, II, III and IV were obtained with Cenco Hyvac oil at 30°C, 45°C, 60°C and 80°C respectively. Near the pressure of 10^{-1} mm Hg, the speed drops off remarkably and depends upon the kind of oils and their temperature. These facts cannot be explained away by the change of the conductance of the tubes, corresponding to the transition stage from the viscous flow to the molecular flow. Therefore, we must add $1/G_v$ to equation (2), where G_v is the conductance, $1/G_v$ the resistance, of oil vapors in the tubes. Then we have

$$\frac{1}{S} = \frac{1}{S_0} + \frac{1}{G_t} + \frac{1}{G_v} \qquad (3)$$

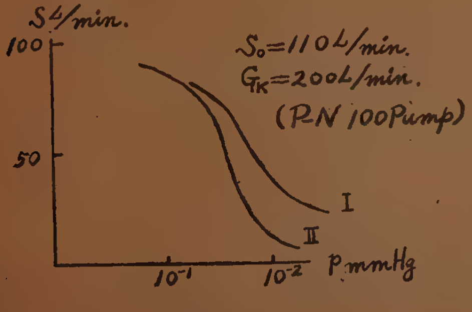

Fig. 1. *a*

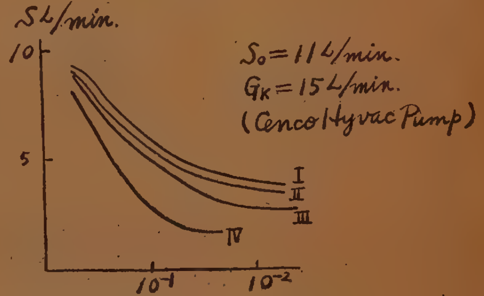

Fig. 1. *b*

In order to measure G_v; we used the apparatus shown in Fig. 2. U is a long tube of small diameter

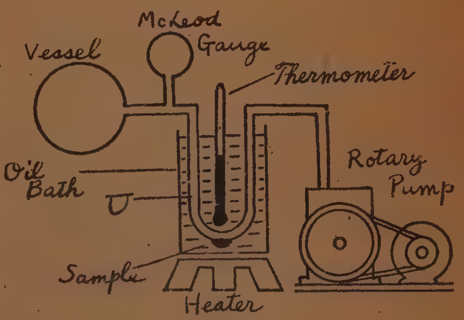

Fig. 2.

with a sample in its bottom. We measured the speed S of the system at various temperatures, which are shown in Fig. 3. If $2r$ and l are the diameter and the length of the tube respectively, P_T the pressure of saturated vapor of the sample at T°K, we have the relation from the kinetic theory of gases

$$G_v \backsim \frac{T}{P_T}\frac{\pi r^3}{l} \backsim \frac{\pi r^2}{l} T e^{\frac{L}{RT}} \tag{4}$$

where L is the latent heat of vaporization of the sample per mol. From equation (3), (4) and the measured speed S, we can calculate the conductance G_v of the vapor of the sample and the latent heat L. We obtained the latent heat of various sampleds as follows:

Hg ;	L≒19000 cal/mol (at 50°C~80°C)
diffusion pump oil ;	L≒17000 cal/mol (at 138°C~152°C)
rotary pump oil (A) ;	L≒10000 cal/mol (at 86°C~143°C)

From the conductance G_v obtained in this way and equation (3), we can explain quantitatively the results shown in Fig. 1. In our experiments, the pressure was measured with McLeod gauge.

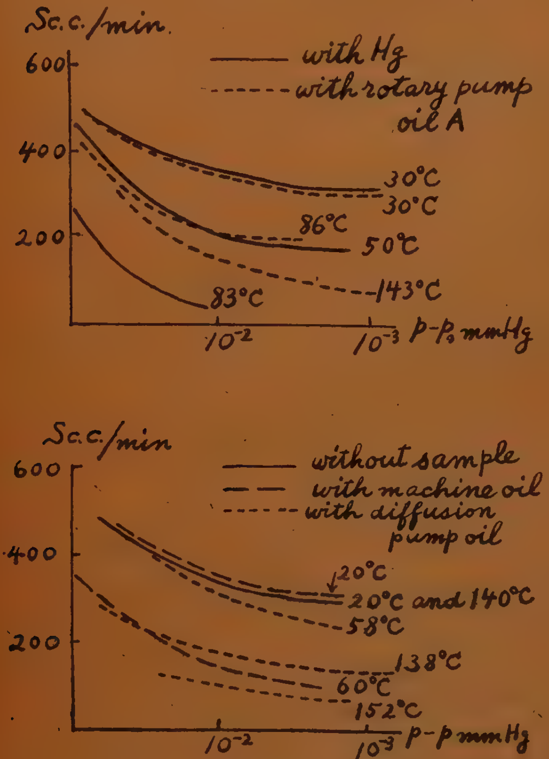

Fig. 3.

References.

(1) Gen. Elec. Rev. **19** (1916) 1060.
(2) Ann. d. Phys. **28** (1909) 75, 999.

AUTHOR INDEX

Akioka T.
Y. Takagi, E. Sawaguchi & ————; On the Effect of Mechanical Stress upon the permittivity of Barium Titanate 270
Arizumi T.; Thermionic Constants of the Polycrystalline Metal 1
On the Apparent Temperature Coefficient of Work Function 143
On the Thermionic Constants of the Polycrystalline Metal (II) 186
Thermionic Constants of the Oxide-Coated Cathode 191
———— & S. Narita; On the Effect of Oxygen upon the Oxide-Coated Cathode 356
Eguchi T.
T. Muto, ————, & M. Shibuya; The Statistical Theory of the Ferromagnetic Supperlattice, Part I. General Theory 277
Part II. Anomalous Specific Heat and Spontaneous Magnetization . 284
Hagiwara Y.; Application of Celestial Mechanics to the Theory of a Magnetron I 70
,, ,, II 76
,, ,, III 81
Harashima A.
————, T. Tanaka & K. Sakaoku; Cooperative Phenomena in Pd-H System I 208
T. Tanaka, K. Sakaoku & ————; Cooperative Phenomena in Pd-H System II 213
Hashimoto K.; Idea and Design of Wire-and-Plate Type Counter 151
Notes on the Production of Geiger-Müller. Counters and the Discharge Mechanism. 153
Three Ponit Spark Discharge Tube 156
Hirone T.
———— & N. Tsuya; On the Theory of Scattering of Hydrogen Atomic Ray by the Ferromagnetic Substance 260
Ichimura H.; On the Specific Heat of the Natural Rubber 305
On the Theory of the High Polymer Solutions 308
Imai I.; Tables Useful for the Numerical Calculations of the Air Stream at High Speed. 342
An Approximate Method of Calculating Compressible Fluid Flow Past a Thin Aerofoil 346
On a New Method of Approximation for Treating Compressible Fluid Flow 352
Ishiguro E.; On the Ground State of the Hydrogen Molecule 129
On the Value of the Electric Quadrupole Moment of the Deuteron 133
Ishihara A.; On Abnormal Melting of Raw Rubber 19
On Melting of Polymer Crystals 181
Statistical Theory of Rubber-like Elastisity (The Network Structure) 289
Structure Viscosity of High Polymer Solutions 291
T. Sakai & ————; On the Statistical Theory of Rubber-like Elasticity 171
Iwanaga K.
H. Kumagai, K. Yamada, ————, & H. Shibata; On the Low Pressure Gas Flow of a Tube Containing Vapors 361

KATAYAMA T.; On the Displacement Velocity of the Domain Boundary of Ferromagnetic Substance 202
KAWAI H.; The Influence of Temperature and Humidity on the Dielectric Constant and Piezoelectric Modulus of Rochelle Salt I 105
II 111
——— & M. MARUTAKE; The Dispersion of the Dielectric Constant In Rochell Salt Crystal at Low Frequencies 8
KAWAMURA H.
——— & J. SHIMAZU; On the Bombardment of Thorium Tungsten by the Alkali Metal Ions 126
———, A. SHINOHARA & K. TAKAHASHI; On the Active Centers of the Oxide-Coated Cathode 301
KIHARA T.; Determination of Intermolecular Forces from the Equation of State of Gases 265
KIKUCHI R.; Thermodynamics of Phase Change 268
KOBAYASHI A.; On the Crystal Rectifiers 41
KOTANI M.; On the Oscillation Mechanism of the Magnetron 36
KUBO M.
——— & S. MIYAKE; Electron Diffraction Study on Behaviors of Metals Deposited on Crystal Surface, Part III. Effect of Centers of Crystallization on Crystal Growth in Metal Films 114
KUBO R.; Statistical Theory of Linear Polymers, IV. Effects of Hinderance for Internal Rotation 119
Interaction between Electrons and Ions in Semiconductors, I. 254
Large Elastic Deformation of Rubber 312
KUMAGAI H.
———, K. YAMADA, K. IWANAGA & H. SHIBATA; On the Low Pressure Gas Flow Conductance of a Tube Containing Vapors 361
MARUTAKE M.
———, & H. KAWAI; The Dispersion of the Dielectric Constant in Rochelle Salt Crystal at Low Frequencies 8
MIKURA Z.; On the Carriers of Electricity and Heat in Superconductors 338
MIWA M.
———, & Y. WATANABE; On the Structure of Silver Sulphide and Silver Arsenic Alloy Grown on Silver Crystals 52
MIYAKE S.
M. KUBO & ———, Electron Diffraction Study on Behaviors of Metals Deposited on Crystal Surface, Part III. Effect of Centers of Crystallization on Crystal Growth in Metal Films 114
———; & R. UEDA; On Trasitional Region in Phase Change of Barium Titanate .. 177
MUTO T.
———, T. EGUCHI & MOTOICHI SHIBUYA; The Statistical Theory of the Ferromagnetic Superlattice Part I. General Theory 277

Part. II. Anomalous Specific Heat and Spontaneous Magnetization 284

NARITA S.
T. ARIZUMI & ———; On the Effect of Oxygen upon the Oxide-Coated Cathode ... 356

NOMOTO O.; On Schaeffer-Bergmann's Diffraction Diagrams of Vibrating Quartz Crystals, Produced when they are Observed in Directions not Parallel to any of the Crystallographic Axes ... 30
——— & S. OKUI; The Relation between the Intensity and the Action of Ultrasonic Waves ... 47

NONAKA I.; On a Phenomenon Observed with Gerger-Muller Counters in Ultraviolet Measurement ... 322

OGUCHI T.
G. SHIRANE & ———; Theory of the Transition in KH_2PO_4 ... 274

OKUI S.
O. NOMOTO & ———; The Relation between the Intensity and the Action of Ultrasonic Waves ... 47

ONO S.; The Radial Distribution Function in Liquid Argon ... 167

OOKAWA A.; Cryatallite Theory of Liquid, II. ... 295

OSHIDA I.; 'High Precision Nomogram ... 25
Graphical Solution of Wave Equations ... 219
On the Applications of Graphical Methods to the Problems of Heat Conduction .. 223
Graphical Treatment of Mechanical and Electrical Vibrations ... 232

SAKADI Z.
———, & E. TAKIZAWA; Mathematical Treatment on the Decay of a Vibrating System due to the Emission of Sound Wave into the Surrounding Medium ... 235

SAKAI T.
———, & A. ISHIHARA; On the Statistical Theory of Rubber-Like Elasticity ... 171

SAKAOKU K.
A. HARASHIMA, I. TANAKA & SAKAOKU; Cooperative Phenomena in Pd-H System, I. 208
T. TANAKA, ——— & A. HARASHIMA; Cooperative Phenomena in Pd-H System, II. 213

SAKURAI T.; Theory of Electromagnetic Oscillation on Plate Conductor ... 139
Approximate Evaluation of Electromagnetic Oscillating Modes on Plate Conductor with Slowly Curved Edge ... 241

SATO T.; Order-Disorder Transformation in the Alloy Ni_3Mn ... 198

SATO H.; On the Theory of Formation of the Ferromagnetic Superlattice ... 91

SAWAGUCHI E.
Y. TAKAGI, ———, & T. AKIOKA; On the Effect of Mechanical Stress upon the Permittivity of Barium Titanate ... 270

SHIBATA H.
H. KUMAGAI, K. YAMADA, K. IWANAGA & ———; On the Low Pressure Gas Flow Conductance of a Tube Containing Vapors ... 361

SHIBUYA M.

T. Muto, T. Eguchi & ———; The Statistical Theory of the Ferromagnetic Superlattice Part. I. General Theory 277
Part. II. Anomalous Specific Heat and Spontaneous Magnetization .. 284
Shimazu J.
H. Kawamura & ———; On the Bombardment of Thorium Tungsten by the Alkali Metal Ions 126
Shinohara A.
H. Kawamura, ———, & K. Takahashi; On the Active Centers of the Oxide-Coated Cathode 301
Shirane G.
———, & T. Oguchi; Theory of the Transition in KH_2PO_4 274
Sugamoto S.; Theory of Elasticity of Finite Displacement 90
Takagi Y.; Theory of the Transition in KH_2PO_4 (I) 271
" (II) 273
———, E. Sawaguchi, & T. Akioka; On the Effect of Mechanical Stress upon the Permittivity of Barium Titanate 270
Takahashi K.
H. Kawamura, A. Shinohara & ———; On the Active Centers of the Oxide-Coated Cathode 301
Takizawa E.
Z. Sakadi & ———; Mathematical Treatment on the Decay of a Vibrating System due to the Emission of Sound Wave into the Surrounding Medium 235
Tanaka T.
A. Harashima, ——— & K. Sakaoku; Cooperative Phenomena in Pd-H System, I. 208
———, K. Sakaoku & A. Harashima; Cooperative Phenomena in Pd-H System, II. 213
Tomonaga S.; Theory of Split-Anode Magnetron, I. 56
II. 62
A General Theory of Ultrashort Wave Circuits, II. 93
Tsuya N.; On the Theory of Antiferromagnetism 161
On the Structure of "90°—Magnetic Wall" in the Ferromagnetic Crystal 176
T. Hirone & ———; On the Theory of Scattering of Hydrogen Atomic Ray by the Ferromagnetic Substance 260
Tsuchihashi S.; Analytical Expression of Self-Consistent Wave Function for Lithium, Boron, Carbon & Oxygen 135
Doublet-Intervals of Lithium I, Boron I & Oxygen IV 137
Uchida S.; A New Approximate Solution in Boundary Value Problems by the Use of Orthogonal Curvilinear Coordinates 33
Ueda R.; Crystal Structure of Ammonium Dihydrogen Phosphate $NH_4H_2PO_4$ 323
On phase Transition of Barium Titanate (II) 333
S. Miyake & ———; On Transitional Region in Phase Change of Barium Titanate 177
Watanabe H.; Collective Electron Ferromagnetism, I. 12
II. 317

WATANABE Y.
M. MIWA & ———; On the Structure of Silver Sulphide and Silver Arsenic Alloy Grown on Silver Crystals 52
YAMADA K.
H. KUMAGAI, ———, K. IWANAGA & H. SHIBATA; On the Low Pressure Gas Flow Conductance of a Tube Containing Vapors 361
YAMANOUCHI T.; Tables Useful for Construction of Irreducible Representation of Symmetric Group 245
YOSHIDA S. On Electron Diffraction Study of Anodic Films Formed on Alminium 175

JOURNAL OF THE PHYSICAL SOCIETY OF JAPAN

VOL. 3, NO. 5~6, 1948

One Copy 150 yen

日本物理學會歐字報告

第3巻 第5~6號（昭和23年9~12月號）

編集兼發行者　清水武雄
東京都板橋區志村清水町375
印刷者　笠井重治
東京都中央區新富町3ノ17
印刷所　國際出版印刷社
東京都中央區新富町3ノ17

發行所　社團法人 日本物理學會
東京都文京區本富士町1 東京大學理學部內
日本出版協會會員 B-114032

昭和24年6月20日印刷・昭和24年6月25日發行

CONTENTS

Page

Toshinosuke MUTO, Tetsuo EGUCHI & Motoichi SHIBUYA: The Statistical Theory of Ferromagnetic Superlattice, Part I. General Theory 277

Toshinosuke MUTO, Tetsuo EGUCHI & Motoichi SHIBUYA: The Statistical Theory of Ferromagnetic Superlattice, Part II. Anam alous Specific Heat and Spontaneous Magnetization 284

Akira ISHIHARA: Statistical Theory of Rubber-like Elasticity (The Network Structure). 289

Akira ISHIHARA: Structure Viscosity of High Polymer Solutions 291

Akiya Ookawa: Crystallite Theory of Liquid. (II) Solid-Liquid Transformation 295

Hazimu KAWAMURA, Akira SHINOHARA & Katsuya TAKAHASHI: On the Active Centers of the Oxide-Coated Cathode 301

Hiroshi ICHIMURA: On the Specific Heat of Natural Rubber 305

Hiroshi ICHIMURA: On the Theory of the High-Polymer Solutions 308

Ryogo KUBO: Large Elastic Deformation of Rubber 312

Hiroshi WATANABE: Collective Electron Ferromagnetism. (II) 317

Itaru NONAKA: On a Phenomenon Observed with Geiger-Müller Counters in Ultraviolet Measurement 322

Ryuzo UEDA: Crystal Structure of Ammonium Dihydrogen Phosphate $NH_4H_2PO_4$ . . . 328

Ryuzo UEDA: On Phase Transition of Barium Titanate (II) 333

Ziro MIKURA: On the Carriers of Electricity and Heat in Superconductors 338

Isao IMAI: Tables Useful for the Numerical Calculations of the Air Stream at High Speeds 342

Isao IMAI: An Apppoximate Method of Calculating Compressible Fluid Flow Past a Thin Aerofoil 346

Isao IMAI: On a New Method of Approximation for Treating Compressible Fluid Flow . 352

Tetsuya ARIZUMI & Shin-ichiro NARITA: On the Effect of Oxygen upon the Oxide-Coated Cathode 356

SHORT NOTE

Hiroo KUMAGAI, Kazuo YAMADA, Kenzo IWANAGA & Hideo SHIBATA: On the Low Pressure Gas Flow Conductance of a Tube Containing Vapors 361